THE JOURNAL
OF
CHEMICAL PHYSICS

VOLUME 33, NUMBER 4 OCTOBER, 1960

Photolysis of Carbon Dioxide

BRUCE H. MAHAN

Department of Chemistry, University of California, Berkeley 4, California

(Received May 9, 1960)

The vacuum ultraviolet photolysis of carbon dioxide has been investigated. Kinetic data and quantum yield measurements indicate that electronically excited (^1D) oxygen atoms are produced in the primary process at 1470 A and 1236 A. Such a primary process is consistent with the tentative spectral assignments which have been made for carbon dioxide.

PREVIOUS investigations[1,2] of the photolysis of carbon dioxide have left the mechanism of the reaction in doubt. Groth[1] found the quantum yield of carbon monoxide at 1470 A to be near unity and suggested that oxygen atoms are formed in the primary process. Groth used a flow system and a gold-plated reaction vessel to prevent ozone formation, and thus his work cannot provide any indication of the detailed fate of the oxygen atom presumably produced in the primary process. Jucker and Rideal[2] state that the quantum yield of carbon monoxide is close to two, and conclude that no oxygen atoms are involved in the photolysis. They propose a mechanism which involves the reaction of a photoexcited carbon dioxide molecule with a normal molecule to give oxygen and carbon monoxide in one step. If this mechanism were to be correct, it would require a revision of the proposals that have been made for the fate of carbon dioxide molecules in the upper atmosphere.[3] We have re-examined the photolysis of carbon dioxide at 1470 A in an effort to make a choice between the two mechanisms, and also have extended the investigation to shorter wavelengths in order to test the effect of excitation energy on the primary photochemical process.

EXPERIMENTAL

The light source used in the early part of this research was a 60-cycle electrical discharge through xenon. A calcium fluoride window was placed in such a way that the reaction cell viewed the discharge axially. With a power dissipation of 1000 w this lamp delivered 10^{14} quanta of 1470 A radiation per sec through a window 25 mm in diam. The maximum intensity was obtained with a voltage drop of 500 v and a xenon pressure of 50 μ. This lamp was abandoned because the commercial neon sign electrodes gradually deteriorated.

The greater part of the work was done with microwave discharge lamps. A QK-61 magnetron (10-cm continuous wave) tuned to a cylindrical cavity was operated at a power input of 100 w. The discharge took place in a quartz tube of 25 mm diam located axially in the cavity. By adjusting the pressure in the tube to a few microns and by tuning the cavity the discharge could be brought to within a few millimeters of the window mounted on the end of the tube. The relatively short light path through unexcited gas minimized reabsorption of resonance radiation. A lithium fluoride window was used in conjunction with a pure krypton filling to obtain the 1236 A resonance line of krypton. A krypton discharge combined with a synthetic sapphire window had no photochemical effect on carbon dioxide, which indicates that the effective radiation from the krypton discharge was indeed confined to wavelengths less than 1450 A. A discharge through xenon together with a sapphire window provided essentially monochromatic radiation of 1470 A wavelength. Although a two-millimeter thickness of sapphire absorbs approximately one-half of the incident radiation at 1470 A, sapphire was used as a window in

[1] W. Groth, Z. physik. Chem. (Leipzig) **B37**, 307 (1937).
[2] H. Jucker and E. K. Rideal, J. Chem. Soc. **1957**, 1058.
[3] D. R. Bates, *The Earth as a Planet*, edited by G. P. Kuiper (University of Chicago Press, Chicago, Illinois).

Copyright © 1960 by the American Institute of Physics

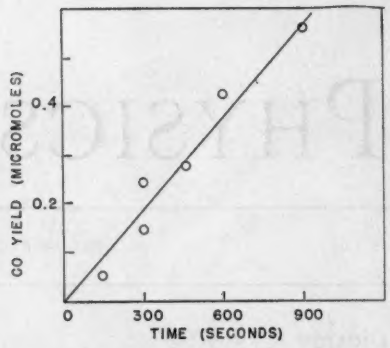

FIG. 1. The yield of carbon monoxide as a function of photolysis time at 1470 A. The pressure of carbon dioxide was 10 millimeters.

preference to calcium fluoride because of its superior mechanical properties.

The maximum output of the krypton lamp was 10^{15} quanta per sec through a window 25 mm in diam, and that of the xenon lamp was a factor of four lower. The lamps were often operated at less than maximum intensity in order to improve their stability. Various mixtures of helium with the heavier rare gases were tried as lamp fillings, but none improved the performance.

A cylindrical reaction vessel 25 mm in diam and 10 cm in length was fastened directly to the window of the lamp. The cell was serviced by a mercury free gas storage manifold. All pressures were measured with a thermocouple gauge or an electrically indicating spoon gauge. A conventional gas micro-analytical system which had provision for combustion of carbon monoxide and absorption of carbon dioxide completed the apparatus.

Mass spectrometric analyses were conducted with an instrument employing the Consolidated 21-620 analyzer tube.

All gases were purest available commercial grades, further purified by bulb to bulb distillation. Mass spectrometric analyses showed satisfactory purity in all cases except nitric oxide, which contained small amounts of nitrogen. This impurity was of no chemical consequence, and could easily be corrected for in the mass spectrometric analyses for carbon monoxide.

TABLE I. The photolysis of carbon dioxide at 1470 A.

Run	Time (sec)	CO_2 pressure (mm)	CO (micromoles)	O_2 (micromoles)
1	1200	35	0.22	0.0055
2	600	35	0.091	0.0046
3	900	35	0.15	0.0056
4	300	35	0.041	0.0040
5	150	35	0.041	0.0036
6[a]	600	10	0.42	0.0050
7	900	10	0.56	0.0049
8	300	10	0.15	0.0035
9	150	10	0.052	0.0022
10	450	10	0.27	0.0045
11	300	10	0.24	0.0042

[a] Runs at 10-mm pressure were made with a higher light intensity than those at 35 mm.

RESULTS AND DISCUSSION

I. Experiments with 1470 A Light

A preliminary set of experiments showed that the total yield of noncondensable material was independent of the pressure when essentially all the light was absorbed by carbon dioxide. Most of the data were then obtained at carbon dioxide pressures of 10 mm and 35 mm. Figure 1 and the data in Table I show that at both pressures the yield of carbon monoxide is a linear function of the illumination time. The extent of the decomposition of carbon dioxide ranged from 0.3% to 3% at the lower pressure, and from 0.1% to 0.4% at the higher pressure. These figures are somewhat misleading, since at 10 mm pressure one-half of the light is absorbed in the first three centimeters of the reaction cell, and at 35-mm pressure the corresponding distance is 0.83 centimeters. The effective percentage decompositions thus may be as much as a factor of 3 to 10 higher than those quoted above, but are still less than 10%.

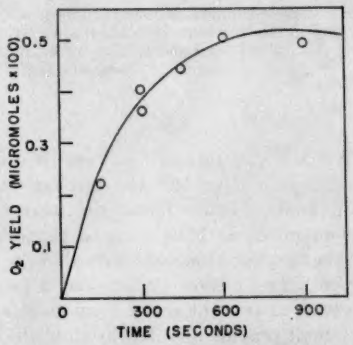

FIG. 2. The yield of oxygen as a function of photolysis time at 1470 A. The pressure of carbon dioxide was 10 mm.

The amount of oxygen produced and its time variation are shown in Fig. 2 and in Table I. The oxygen found both by mass spectral and chemical analysis is considerably less than one-half the amount of carbon monoxide produced. Furthermore, the data indicate that the amount of oxygen produced approaches a value which is time independent. This finding seems to correspond to the observations of Jucker and Rideal, who state that the photochemical yield as measured by pressure change decreased rapidly with time of illumination. Since it seemed likely that the missing oxygen should be present as ozone, an irradiated sample was collected in a quartz absorption cell without being allowed to come into contact with stopcock

grease. The ultraviolet spectrum showed the broad absorption band of ozone. Because of the breadth of this band and the small amount of products involved, no quantitative determinations of ozone were made.

It is convenient to discuss these results in terms of a mechanism involving oxygen atoms

$$CO_2+h\nu\rightarrow CO_2^* \qquad I_{abs}$$

$$CO_2^*\rightarrow CO+O \qquad (1)$$

$$2O+M\rightarrow O_2+M \qquad (2)$$

$$O+O_2+M\rightarrow O_3+M \qquad (3)$$

and the excited molecule reaction proposed by Jucker and Rideal augmented by a step in which ozone is produced.

$$CO_2+h\nu\rightarrow CO_2^* \qquad I_{abs}$$

$$CO_2^*+CO_2\rightarrow 2CO+O_2 \qquad (4)$$

$$CO_2^*+O_2\rightarrow CO+O_3. \qquad (5)$$

In addition to the indicated possibilities, ozone might be produced by the photolysis of molecular oxygen. However, since the experiments involve almost total absorption of the light by carbon dioxide, any absorption by the product molecules must decrease the yield of carbon monoxide. The fact that the carbon monoxide yield is a linear function of time suggests that absorption by the products is not important. To confirm this supposition, we may calculate the fraction of light absorbed by the molecular oxygen using the absorption coefficients[4] listed in Table II. In the runs done at 35 millimeters pressure, the amount of light absorbed by the molecular oxygen present at the end of the reaction would be 0.2% of the total incident radiation, if the products were to be uniformly distributed over the whole reaction vessel. Since most of the products are concentrated in the first two centimeters of the cell, a more reasonable estimate of the fractional light absorption of oxygen would be 1%. The concentration of ozone is expected to be slightly less than one third the concentration of carbon monoxide, with the consequence that ozone can absorb no more than 2 or 3% of the light incident on the reaction cell. Similar calculations show that the absorption of light by the products is also negligible in the runs done at 10 millimeters pressure. We can conclude that formation of ozone does not occur through photolysis of oxygen, and that no inner filter is to be expected either from oxygen or ozone.

TABLE II. Absorption coefficients.[a]

	1470 A	1236 A
CO_2	18	3.4
O_2	355	14
O_3	100	300
NO	10	56
CO	0.7	0.8

[a] Absorption coefficients are in units of cm^{-1} for gases at one atmosphere pressure and 25°C. The data refer to natural logarithms.

[4] K. Watanabe, M. Zelikoff, and E. Inn, "Absorption Coefficients of Several Atmospheric Gases," Air Force Cambridge Research Center Technical Report No. 52-23.

TABLE III. The effect of added oxygen.

Run	Time (sec)	CO_2 pressure (mm)	O_2 pressure (mm)	R[a]
12	600	35.0	0.17	0.96
13	600	35.0	0.16	0.95
14	600	35.0	0.20	1.00

[a] R is defined as the ratio of the amount of CO obtained by photolysis of the mixture to the amount obtained from the photolysis of pure carbon dioxide.

It is a consequence of the excited molecule mechanism that any variation in the rate of production of oxygen must result in a variation of the rate of formation of carbon monoxide. From a steady-state treatment of the excited molecule mechanism we obtain

$$d(CO)/dt=\frac{I_{abs}[2k_4(CO_2)+k_5(O_2)]}{k_4(CO_2)+k_5(O_2)}$$

for the rate of production of carbon monoxide and

$$d(O_2)/dt=\frac{I_{abs}[k_4(CO_2)-k_5(O_2)]}{k_4(CO_2)+k_5(O_2)}$$

for the rate of oxygen formation. These expressions show that when the oxygen concentration is essentially zero the initial rate of carbon monoxide formation is

$$[d(CO)/dt]_{initial}=2I_{abs}.$$

After the oxygen concentration has reached its steady value the rate of carbon monoxide production has fallen to

$$[d(CO)/dt]_{final}=1.5I_{abs}.$$

At the shortest irradiation times the oxygen produced corresponds to approximately one-half of the steady-state concentration. Therefore, the expected change in the rate of production of carbon monoxide over the range of decompositions investigated should amount to approximately 20% of the initial rate. Such a change should be detectable as a curvature in Fig. 1. Neither the data obtained at 10-mm pressure nor those obtained at 35 mm show any decreasing trend in the rate of formation of carbon monoxide.

To eliminate the possibility that any variation in the rate of production of carbon monoxide had gone undetected, oxygen was deliberately added to the reaction mixture and the yield of carbon monoxide compared with that occurring in the photolysis of pure carbon dioxide. The ratio of k_4 to k_5 was estimated from the value of the steady-state concentration of oxygen in the photolysis of pure carbon dioxide, and sufficient oxygen was added to the mixtures to insure that 99% of the excited carbon dioxide molecules would form

TABLE IV. The effect of added nitric oxide.

Run	Time (sec)	CO_2 pressure (mm)	NO pressure (mm)	O_2/CO	R[a]
15	600	13	0.005	0.17	1.0
16	600	14	0.016	0.19	1.1
17	600	26	0.080	0.40	1.0
18	600	40	0.080	0.35	1.1

[a] R is defined as in Table III.

ozone. At the same time, no more than one-tenth of the light incident on the mixtures was absorbed by oxygen. If the excited molecule mechanism is correct, the yield of carbon monoxide from the mixtures should be at least 30% lower than from the photolysis of pure carbon monoxide. As demonstrated by the data in Table III, the presence of considerable amounts of added oxygen does not affect the yield of carbon monoxide beyond that expected on the basis of the inner filter effect. Thus the experiments with added oxygen as well as the time dependence of the carbon monoxide yield are inconsistent with the excited molecule mechanism.

There is a further objection to the excited molecule mechanism. At the maximum concentrations of oxygen existing in the photolysis of pure carbon dioxide an electronically excited carbon dioxide molecule would encounter an oxygen molecule approximately every 10^{-4} second. Since the calculated radiative lifetime of carbon dioxide is 10^{-6} sec, formation of ozone by step 5 would seem very unlikely.

Runs 15–18 (Table IV) demonstrate that the addition of small amounts of nitric oxide definitely increases the oxygen to carbon monoxide ratio, presumably at the expense of the ozone yield. Furthermore, the absolute yield of carbon monoxide is unaffected by the addition of nitric oxide. These runs reinforce the conclusion that the mechanism by which carbon monoxide is produced is independent of the processes which produce oxygen or ozone. The atomic mechanism is consistent with such a conclusion.

The effect of nitric oxide on the oxygen yield may be explained by adding the steps

$$O+NO+M\rightarrow NO_2+M \qquad (6)$$

$$O+NO_2\rightarrow O_2+NO \qquad (7)$$

to the atomic mechanism. If the oxygen atoms involved are in the ^3P state, reactions (6) and (7) are extremely fast. Since it appears that the atoms involved in the photolysis of carbon dioxide are not in the ^3P state (*vide infra*) and since reactions (6) and (7) may not be fast for electronically excited atoms, the possibility that the reaction sequence

$$O+O_2+M\rightarrow O_3+M \qquad (3)$$

$$O_3+NO\rightarrow NO_2+O_2 \qquad (8)$$

is responsible for the increased oxygen yield must not be ignored. However, if nitrogen dioxide is formed in this way, the oxygen yield should be no greater than the original amount of nitric oxide in the mixture or no greater than 33% of the carbon monoxide yield, whichever is smaller. In runs 17 and 18 the oxygen yield is greater than 33% of the carbon monoxide yield, and in runs 15 and 16 the oxygen yield did exceed the original amount of nitric oxide in the mixture. The reactions of oxygen atoms therefore provide a more satisfactory explanation of the effect of nitric oxide addition.

Since the photolysis of carbon dioxide is a convenient reaction for estimating the intensities of vacuum ultraviolet light sources it is desirable to know the absolute quantum yield of the reaction. To determine the output of the lamp we photolyzed mixtures of carbon monoxide and oxygen and determined the amount of carbon dioxide produced. The primary photochemical process in oxygen at these wavelengths is without question the formation of a ^3P and a ^1D oxygen atom. Even though the rate of reaction of an oxygen atom with an oxygen molecule is approximately 40 times greater[5] than with a carbon monoxide molecule, exclusive formation of carbon dioxide will occur if the concentration of carbon monoxide is much greater than the concentration of oxygen. A difficulty in the design of the experiment arises because carbon monoxide absorbs 1470 A light. The carbon monoxide spectrum in this region consists of sharp bands, and possibly a weak underlying continuum. Watanabe and coworkers[4] state that this continuum may be due to an oxygen impurity in the carbon monoxide used in the spectral measurements. This is reasonable since the energy of a light quantum of 1470 A wavelength is insufficient to dissociate the carbon monoxide molecule, and a continuum is not to be expected. In any case, only a maximum possible value of the absorption coefficient is known. In our experiments the pressure of carbon monoxide was 22 mm and that of oxygen was in the range 0.040 to 0.060 mm. To determine whether absorption of light by carbon monoxide was a complicating factor at these concentrations, pure carbon monoxide was photolyzed and the amount of carbon dioxide determined. These experiments showed that in the experiments with oxygen-carbon monoxide mixtures, the contribution of reactions caused by photoexcited carbon monoxide to the carbon dioxide yield was negligible. By the comparison of four separate photolyses of the oxygen-carbon monoxide mixtures with four photolyses of pure carbon dioxide the quantum yield of carbon monoxide was found to be 1.1 ± 0.1. This result is consistent with the findings of Groth. It should be emphasized that due to the possibility of ozone formation in the actinometer this value is an upper limit. Finally, it should be realized that a quantum yield near unity is consistent with the atomic

[5] W. Groth, Z. physik. Chem. (Leipzig) **B37**, 315 (1937).

mechanism, but not with the excited molecule mechanism, which would predict a value greater than 1.5.

As a further test of the atomic mechanism, an attempt was made to detect the chemiluminescence of the reaction

$$O+NO\rightarrow NO_2+h\nu, \qquad (9)$$

which might occur during the photolysis of $NO-CO_2$ mixtures. For these experiments the ordinary reaction cell was replaced by a fluorescence cell consisting of two perpendicular Raman tubes. A photomultiplier and filter system permitted the detection of light emitted at right angles to the radiation from the lamp. Although the green chemiluminescence from reaction (9) could easily be detected in the photolysis of mixtures of O_2 and NO, N_2O and NO, and from the photolysis of pure NO, there was no indication of any emission from $NO-CO_2$ mixtures. These facts strongly suggest that ^3P oxygen atoms are in no way involved in the photolysis of carbon dioxide. Such a conclusion is consistent with the calculations which showed that molecular oxygen produced in the reaction did not undergo subsequent photolysis. The conclusion that ^3P oxygen atoms are not produced in the primary process is supported by the spectral assignments of Walsh[6] and Mulliken[7] who identify the 1470 A absorption band in CO_2 as a transition to a $^1\Delta_u-{}^1B_2$ state. Such an electronic state would correlate with the $^1\Sigma$ state of CO and the ^1D state of the oxygen atom. The dissociation to the excited oxygen atom is energetically allowed at these wavelengths since only 7.4 electron volts are required, while the energy of a 1470 A quantum corresponds to 8.3 electron volts. A mechanism involving ^1D oxygen atoms would thus appear to be consistent with available spectroscopic information, as well as the kinetic data presented here.

TABLE V. The photolysis of carbon dioxide at 1236 A.

Run	Time (sec)	CO_2 pressure (mm)	CO (micromoles)	O_2 (micromoles)
19	60	44	0.315	0.028
20	600	44	2.00	0.028
21	1200	44	3.25	0.018
22	300	44	1.14	0.055
23	900	44	2.57	0.020
24	20	44	0.125	0.013
25	600	10	1.89	0.005
26	300	10	0.87	0.0057
27	60	10	0.19	0.0071
28	20	10	0.059	0.0034
29	900	10	2.58	0.0045
30	300	10	0.90	0.0037
31	180	10	0.53	0.0070
32	60	10	0.125	0.0066

II. Experiments with 1236 A Light

The data obtained by using 1236 A radiation are displayed in Table V and Figs. 3 and 4. Although the results are similar to those obtained with 1470 A light, the dependence of carbon monoxide yield on irradiation time shows significant deviation from linearity. The fact that the oxygen yield reaches an approximately constant value is now more clearly demonstrated because the greater intensity of the krypton lamp permitted higher percentage decomposition within a reasonable time. Ozone was also detected as a reaction product at this shorter wavelength.

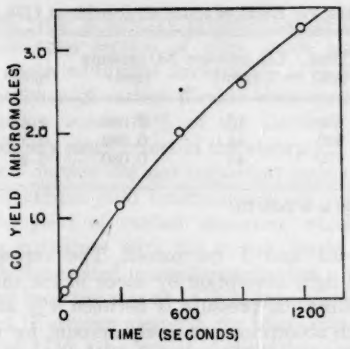

FIG. 3. The yield of carbon monoxide as a function of photolysis time at 1236 A. The pressure of carbon dioxide was 44 mm.

The nonlinear relation between carbon monoxide yield and time must either result from an inner filter effect or from a reaction between electronically excited carbon dioxide and oxygen molecules to form ozone. From the absorption coefficients in Table II and the oxygen yields one can calculate the fractional light absorption by the maximum amount of O_2 which is produced is 0.2% when the carbon dioxide pressure is 10 mm and 0.7% in those runs made at 44 millimeters pressure. It therefore is very unlikely that photolysis of oxygen is responsible for ozone formation or the nonlinear relationship between carbon monoxide and time. Ozone is more likely to cause an inner filter effect. At decompositions where the oxygen yield has reached its maximum, the amount of ozone is somewhere

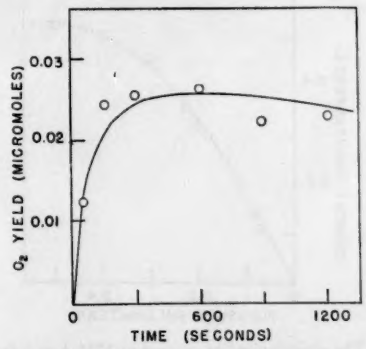

FIG. 4. The yield of oxygen as a function of photolysis time at 1236 A. The pressure of carbon dioxide was 44 mm.

[6] A. D. Walsh, J. Chem. Soc. **1953**, 2260.
[7] R. S. Mulliken, Can. J. Chem. **36**, 10 (1958).

TABLE VI. Effect of added nitric oxide at 1236 A.

Run	Time (sec)	CO_2 pressure (mm)	NO pressure (mm)	O_2/CO	R[a]
33	600	10	0.080	0.43	1.15
34	900	44	0.080	0.38	1.3
35	150	44	0.080	0.40	1.0

[a] R is defined as in Table III.

between 0.1 and 1 micromole. The corresponding fractional light absorption by ozone in the runs made at 44 millimeters pressure is between 4% and 40%. This much absorption can easily account for the time dependent rate of production of carbon monoxide.

To test this proposal, nitric oxide was introduced into the reaction mixture in an attempt to prevent ozone formation. The data in Table VI show that the ratio of oxygen to carbon monoxide increases upon addition of nitric oxide, which indicates that ozone formation is suppressed. Furthermore, it is clear that the addition of nitric oxide increases the carbon monoxide yield in experiments in which the irradiation time is relatively long, but does not affect the yield in experiments with short irradiation times. It would appear that the only way in which the yield of carbon monoxide may be increased by addition of nitric oxide is through elimination of ozone as an inner filter. Thus, both the effect of added nitric oxide and the calculations of the fractional light absorption of ozone present a consistent explanation of the decrease of the rate of carbon monoxide production with time.

The importance of the inner filter effect precludes a choice between the two mechanisms based only on the data obtained from the photolysis of pure carbon dioxide. The fact that when nitric oxide is added the carbon monoxide yield increases even though the oxygen concentration goes up is, however, some indication that reaction (5) is not important. Moreover, the calculated radiative lifetime of the electronic state of carbon dioxide excited by 1236 A light is slightly shorter than 10^{-6} sec, and collisions between excited carbon dioxide and oxygen molecules occur at most every 5×10^{-5} sec. On this basis the excited molecule mechanism does seem to offer a less satisfactory explanation of the facts than does the atomic mechanism.

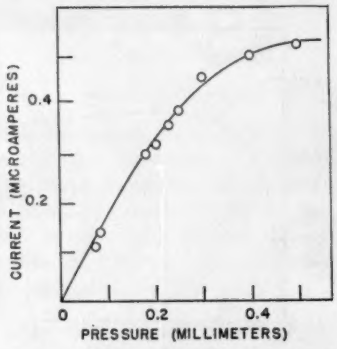

FIG. 5. The photoionization current at 1236 A as a function of nitric oxide pressure. The curvature is due to ion-electron recombination at the higher pressures.

In order to facilitate a choice between the two mechanisms, the quantum yield of carbon monoxide was determined. The photochemical reaction between oxygen and carbon monoxide can not be used as an actinometer at 1236 A. Most of the light incident on a mixture containing enough excess carbon monoxide to react with all oxygen atoms would be absorbed by the carbon monoxide itself. The fate of an electronically excited carbon monoxide molecule in such a mixture is not at all clear, and thus the amount of photolytically produced carbon dioxide cannot be used to measure light intensity. However, the photoionization current

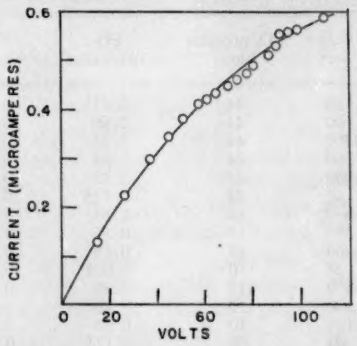

FIG. 6. The photoionization current in nitric oxide as a function of applied voltage. The nitric oxide pressure is 0.50 mm.

generated in the photolysis of nitric oxide can be used to estimate the light intensity, since the photoionization cross section of nitric oxide is known. Electrodes were inserted in the reaction cell, an appropriate potential was applied and the photocurrent measured with a galvanometer having a sensitivity of 5.0×10^{-9} amp/mm. Three different electrode geometries were used. In the first experiments a tungsten wire was located axially in the reaction cell and was surrounded by a cylindrical grid located at the wall. This arrangement had the advantage that the tungsten wire exposed a very small surface to the incident light, and therefore only very small photoelectric currents were produced even when the wire was biased at -100 v. However, because of the extremely high field at the central electrode sporadic electrical breakdown of the gas took place whenever more than 100 v were applied to the electrodes. The second and third electrode geometries consisted of two copper gauze electrodes located at opposite walls of the cell. In one case the electrodes extended the full length of the reaction cell, and in the other arrangement the electrodes were 2.0

cm long. The apparent efficiencies for electron-ion collection of the three systems varied slightly due to the fact that the light entering the reaction vessel was not collimated. To minimize errors due to this situation, the electrodes which were 2.0 cm long were used for the actinometry.

Figure 5 shows the photoelectric current as a function of nitric oxide pressure at a fixed electrode potential of 100 v. The curvature of the plot is more pronounced than would be expected from the equation

$$i \propto I_{abs} = I_0[1 - \exp(-klP)]$$

when the value of the absorption coefficient k reported by Watanabe[8] is used. Here i is the photocurrent, l is the length of the electrodes, and P is the pressure of nitric oxide in atmospheres. The exaggerated curvature indicates that a noticeable amount of ion-electron recombination occurs at pressures as low as 0.5 millimeter. This interpretation is substantiated by the fact that the photocurrent actually started to decrease when the pressure of nitric oxide was increased beyond 0.5 millimeter.

The variation of photocurrent with applied voltage at a pressure of 0.5 mm of nitric oxide is shown in Fig. 6. As is to be expected at this pressure, a saturation current is approached only at the highest applied voltage. At pressures of 0.01 mm saturation currents were obtained at approximately 45 v.

In the experiments in which the quantum yield was to be measured the lamp was deliberately run at reduced intensity in order to avoid high concentrations of ions and electrons which would favor recombination. A comparison of four runs in which carbon dioxide was photolyzed with four separate measurements of the photoionization current of nitric oxide resulted in a value of 1.2 ± 0.1 for the quantum yield of carbon monoxide. The most obvious systematic error in this determination would be failure to collect all ion pairs generated photolytically, which would result in a quantum yield which would be too large. The value of quantum yield is directly proportional to the photoionization cross section of nitric oxide and thus is subject to an additional uncertainty of $\pm 10\%$. Since the photolyses of carbon dioxide were carried out at pressures at which 80% of the incident light was absorbed, any small errors in the absorption coefficient of carbon dioxide are not important sources of error in the quantum yield determination. A value of the quantum yield of carbon monoxide which is near unity is consistent with the atomic mechanism, but not with the excited molecule mechanism.

As had been the case at 1470 A, it proved impossible to detect ^3P oxygen atoms in the photolysis of carbon dioxide at 1236 A by means of their chemiluminescent reaction with nitric oxide. Since the chemiluminescence could easily be observed in the photolysis of oxygen, nitrous oxide, and nitric oxide we are again forced to conclude that any oxygen atoms involved in the photolysis of carbon dioxide must be electronically excited. From an energetic point of view the atoms produced may be ^1S or ^1D. No definite identification of the excited electronic state of carbon dioxide which is involved here has been made, but Mulliken[7] has suggested that it may be related to a $^1\Delta g$ state of the linear molecule, which would imply dissociation to a ^1D atom is most probable. The similarities in the photolytic behavior at both wavelengths makes this conclusion seem reasonable.

In summary, it would appear that an atomic mechanism presents a consistent explanation of the quantum yield measurements and kinetic data obtained in this work. Since a photoexcited carbon dioxide molecule need not collide with another molecule in order to form carbon monoxide, the proposal of Bates[3] for the photolytic dissociation of carbon dioxide in the upper atmosphere seems reasonable.

ACKNOWLEDGMENT

The author would like to express grateful appreciation for support by the U. S. Air Force through AFOSR of the Air Research and Development Command.

[8] K. Watanabe, J. Chem. Phys. 22, 1564 (1954).

THE JOURNAL OF CHEMICAL PHYSICS VOLUME 33, NUMBER 4 OCTOBER, 1960

Quantitative Considerations Concerning Catalysis at a Semiconductor Surface

C. G. B. GARRETT

Bell Telephone Laboratories, Inc., Murray Hill, New Jersey

(Received January 11, 1960)

The theory of charge-transfer catalysis, originally proposed by Wagner and Hauffe, is set up in quantitative form. The objects of the treatment are to write down quantitative expressions for the absolute reaction rate, to show what are the consequences of the Wagner-Hauffe mechanism insofar as they concern the adsorption properties of the individual reacting materials, and to outline an experimental program for determining, by means of experiments on the semiconductor, alone and in association with each of the reacting substances in turn, the values prevailing in a practical case for the various parameters occurring in the theory.

I. INTRODUCTION

THE existence of a qualitative connection between the electrical properties of a semiconductor catalyst and its catalytic activity has been recognized for a number of years. The fundamental idea of charge-transfer catalysis was first advanced by Wagner and Hauffe[1] in 1938, and subsequently pursued by Garner, Gray and Stone,[2] by Vol'kenshtein,[3] by Hauffe,[4] and by Hauffe and Schlosser.[5] Experimental evidence indicative of the validity of the charge-transfer model is not lacking,[5–13] but most of it is quite qualitative in character, and there is lacking at the present time any precise, quantitative demonstration of the correctness of the model in any particular case.

In another field of research, the development of a variety of precise experimental tools for the study of the surfaces of single crystals of semiconductors—conspicuously germanium and silicon—has afforded the attainment of a good quantitative understanding of the electrical properties of a semiconductor surface.

In this paper we shall look into the quantitative implications of the charge-transfer theory of catalysis, with the object of seeing how these newly developed tools for the study of surfaces might be brought to bear on the problem. To do this it will be necessary to work out just what are the quantitative implications of the charge-transfer theory of catalysis, what physically meaningful parameters it involves, and how one would set about measuring the values for each one of these parameters in the laboratory. In presenting the theory we shall work out quantitative expressions for the absolute reaction rate, in terms of quantities that are familiar in semiconductor physics—capture cross sections, thermal speeds, etc.—and that can be measured by standard semiconductor techniques. In addition we shall pay attention to the problem of "saturation" (pre-emption of available sites), which seems hitherto to have been neglected in the development of models for semiconductor catalysis. To illustrate the predictions of the theory, we shall calculate graphs showing contours of constant reaction rate in a pressure diagram, with values arbitrarily assigned to the various parameters. Finally we shall turn to the most important question—that of deciding what techniques are available for the measurement of these parameters in a practical case.

The idea of charge-transfer catalysis is this. It is presumed that, at some stage, electrons are transferred to or from the semiconductor from or to some of the reacting materials. That is to say, some of the chemical substances appearing in the chemical equation behave as donors and some as acceptors. If some one of these materials were present by itself in contact with the semiconductor, we would have a case of "charge-transfer adsorption,"[14–17] in which electronic equilibrium would prevail between the adsorbed material and the semiconductor, with some fraction of the adsorbed atoms or molecules ionized. Under these circumstances, the rates of flow of electrons to and from the conduction band of the semiconductor will be equal, and the rates of flow of electrons to and from the valence band will be equal also. Some fixed amount of charge will have been transferred to or from the

[1] C. Wagner and K. Hauffe, Z. Elektrochem. **44**, 172 (1938).
[2] W. E. Garner, T. J. Gray, and F. S. Stone, Proc. Roy. Soc. (London) **A197**, 294 (1949).
[3] F. F. Vol'kenshtein, Uspekhi. Fiz. Nauk **60**, 249 (1956) and other references contained therein. See also Izvest. Akad. Nauk. S.S.S.R. Otdel Khim. Nauk **1957**, p. 916 and 924.
[4] K. Hauffe, *Semiconductor Surface Physics*, edited by R. H. Kingston (University of Pennsylvania Press, Philadelphia, Pennsylvania, 1956), p. 259.
[5] K. Hauffe and E. G. Schlosser, Z. Elektrochem. **61**, 506 (1957).
[6] For a general review, see J. T. Law, in *Semiconductors*, edited by N. B. Hannay (Reinhold Publishing Corporation, New York, 1959), p. 676.
[7] G. M. Schwab and J. Block, Z. Elektrochem. **58**, 756 (1954).
[8] A. Bielanski, J. Deren, and J. Haber, Nature **179**, 668 (1957).
[9] V. I. Lyashenko and I. I. Stepko, Izvest. Akad. Nauk S.S.S.R. Ser. Fiz. **21**, 201 (1957).
[10] I. A. Myasnikov, Izvest. Akad. Nauk S.S.S.R., Ser. Fiz. **21**, 192 (1957).
[11] N. P. Keier, S. Z. Roginskii, and I. S. Sazanova, Izvest. Akad. Nauk S.S.S.R., Ser. Fiz. **21**, 183 (1957).
[12] S. Z. Roginskii, Izvest. Akad. Nauk S.S.S.R., Ser. Fiz. **21**, 163 (1957).
[13] S. Z. Roginskii, Doklady Akad. Nauk S.S.S.R. **130**, 122 (1960).
[14] K. Hauffe and H.-J. Engell, Z. Elektrochem. **56**, 366 (1952).
[15] P. Aigrain and C. Dugas, Z. Elektrochem. **56**, 363 (1952).
[16] P. B. Weisz, J. Chem. Phys. **20**, 1483 (1952); **21**, 1531 (1953).
[17] H. J. Krusemeyer and D. G. Thomas, J. Phys. Chem. Solids **4**, 78 (1958).

semiconductor during the initial adsorption, and a surface dipole will exist. If now all of the reacting substances are present simultaneously, each separate charge-transfer equilibrium will be to some extent upset; in the steady state, there will be a continual draining-off of the substances appearing on the left-hand side of the chemical equation, and a continual production of the substances on the right-hand side, such that the net flow of charge to or from the semiconductor is zero. In addition, there will be steady-state fluxes of neutral atoms or molecules between the surface and the surrounding medium (a gas, let us say). In setting up analytical expressions for the rates of the various steps of the reaction, particular interest will attach to the processes of charge transfer to or from the semiconductor, since it is these, as Hauffe pointed out, that conspicuously depend on the electrical properties of the semiconductor. We shall, however, consider the other steps as well, with the object of setting up criteria for deciding when charge-transfer will be the rate-limiting step.

2. SURFACE DONORS AND ACCEPTORS. SURFACE STATES

The theory of charge transfer adsorption is presented in its most advanced and elegant form by Krusemeyer and Thomas.[17] We shall assume that the reader is familiar with this paper. Since, however, the ideas that are at the foundation of this theory are also implicit in the theory of charge-transfer catalysis, it is important to examine one or two of them rather critically.

It is assumed that, in the absence of adsorbed material, the surface of a crystal has associated with it "intrinsic" surface states, representing electron orbitals that are more or less precisely associated with the geometrical surface. Depending on the location of these states in an energy band diagram, the measurable surface electrical properties (volta potential, surface conductivity, etc.) may or may not be significantly affected by them. During the process of adsorption, these states disappear; fresh bulk electronic states are added to the crystal, and new electronic states, characteristic of the adsorbed material and again associated more or less precisely with the geometrical surface, come into existence. In the case that one and only one of these impurity levels lies within the forbidden gap of the semiconductor, one speaks of either a "donor level" or an "acceptor level," depending on whether the two states of charge of the impurity are 0 and $+1$ or -1 and 0. It is particularly to be noted that the foregoing remarks are true regardless of whether the binding of the impurity atom to the surface is covalent or ionic, or some compromise between the two. So long as the concentration of atoms on the surface is sufficiently small for the wave functions not to overlap one another, the "donor level" or "acceptor level" will be perfectly sharp and well defined, regardless of the type of binding. Only at high coverage, where overlapping inevitably occurs, will the system not be describable in this way; at high coverage, the impurity levels will broaden into a band, analogous to the "impurity band" in the bulk of a semiconductor.

For group III or V acceptors or donors in germanium or silicon, the position of the donor or acceptor level is given to a rough first approximation by the "hydrogenlike" model, and is independent of temperature. For surface donors and acceptors, it is clear that the "hydrogenlike" model is unlikely to be applicable. What is usually done instead is to start with the adsorbed atom at an infinite distance from the crystal, and ask how much work would be required to remove an electron from the atom and give it to the semiconductor (or conversely). The answer is clearly the difference between the ionization potential or electron affinity of the atom and the work function of the semiconductor, corrected by an amount corresponding to the energy difference between the Fermi level at the surface and the conduction or valence band edge. Unfortunately, these quantities often differ by several ev, so that one tends to come up with the answer that the donor or acceptor level lies well above the bottom of the conduction band or well below the top of the valence band. Now, of course, this may sometimes be the case; there is however a certain amount of experimental evidence that, more often than this argument would lead one to believe, the donor or acceptor level lies within the forbidden gap. The point must be this: the potential energy of the atom, in its neutral and in its ionized state, will be grossly affected by the proximity of the surface, so that the above calculation will not be very good. Evidence for this is offered, for example, by the Auger emission experiments of Hagstrum.[18] It is to be hoped that eventually it will be possible to calculate the proximity effect from first principles; for the moment, however, the best we can do is to regard the positions of the donor and acceptor levels as parameters open to experimental measurement.

The other point that it is necessary to discuss concerns the "intrinsic" surface states, which will be important (i) because their existence will affect the surface concentrations of carriers in the semiconductor; (ii) because they may affect the results of physical measurements on the surface. From the point of view of the semiconductor properties, the effect of such intrinsic states is to tend to clamp the surface potential at some particular value, independent of the existence or nonexistence of ionic charge; that is, to screen the space-charge region from the effect of such charge. In kinetic processes, of the sort which we shall discuss in the ensuing sections, the intrinsic states can also be important because of their ability to store electronic charge received from one atom on the surface, and return it to another. To take account of this in

[18] H. D. Hagstrum, Phys. Rev. 96, 336 (1954).

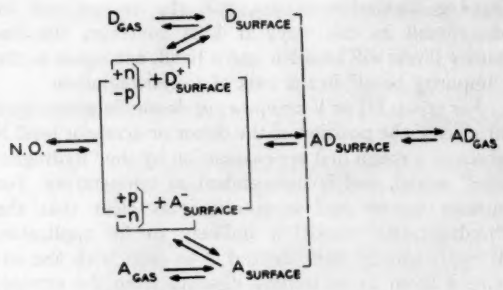

FIG. 1. Reaction scheme.

general terms would lead to an enormous complication of the analysis, and does not seem to be justified at the present time. We can however distinguish two extreme situations. If the intrinsic states are so few, or so remote in energy from the Fermi level, that, in some process wherein the surface potential is changed, the change in the charge density in intrinsic surface states is small in comparison with that in the space-charge region, the existence of the surface states may be neglected. In the contrary case, the intrinsic states will be of such overwhelming importance that the existence of the bulk semiconductor may be neglected. In this case, we would have to regard the assembly of intrinsic states as being itself a two-dimensional semiconductor, having its own one-electron energy surfaces in two-dimensional $\boldsymbol{k}$ space, and electrons distributed among the states that compose those surfaces according to Fermi-Dirac statistics. The theory to be developed in the ensuing sections could be taken over to such a system without requiring any substantial modification, except that carrier (volume) densities will be replaced by surface carrier densities and capture cross sections by capture perimeters.

3. BASIC PRINCIPLE. ORDERS OF MAGNITUDE

We shall now set up the theory of charge-transfer catalysis, according to the notions outlined in Sec. 1.

We write the reaction catalyzed by the semiconductor surface in the following form:

$$A+D\rightarrow AD, \tag{1}$$

where D stands for a singly-ionizable donor, and A for a singly-ionizable acceptor. The product species AD is supposed to behave neither as a donor nor as an acceptor. Other forms for the reaction could have been chosen instead; for example, we could write an equation with the donor species on the left-hand side and the acceptor on the right, or we could construct a more complicated equation with several donors and several acceptors on both sides. In the interest of brevity, we shall not consider these cases here: the modification required to fit the present analysis to other cases is quite straightforward.

The processes of adsorption, charge transfer, and reaction are shown schematically in Fig. 1. In this picture we allow for the possibility that un-ionized as well as ionized atoms can react, but we shall not take this possibility seriously in the present paper, since such a course will not in general lead to a rate that is sensitive to the electrical properties of the semiconductor. In the reaction scheme that invokes ionization, there are seven distinct steps, any one of which might be rate-limiting. We therefore concern ourselves in this section with making estimates of the rates at which the various steps can occur. For the sake of comparison, it will be worthwhile to keep in mind the order of magnitude of the rate at which a catalyzed reaction is actually observed to proceed. The quantity we want has the dimensions of molecules reacting per unit area per unit time, regardless of the "order of the reaction." It appears that, in practice, some simple inorganic reactions (such as the dissociation of molecular hydrogen on hot tungsten) can proceed as fast as 10^{21} cm^{-2} sec^{-1} or more, while at the other end of the scale, a catalyzed organic reaction may still be economic at a rate as low as 10^{12} cm^{-2} sec^{-1}.

Three of the steps shown in Fig. 1 involve exchange of ***neutral*** atoms with the gas. We shall treat this in a way consistent with the Krusemeyer-Thomas paper on charge-transfer adsorption[17]; that is, we shall assume that a molecule can evaporate only if it is un-ionized, and that the probability of its doing so is independent of whether neighboring sites are occupied or not. In equilibrium, the rates of exchange of some species of neutral atom between the semiconductor and the gas are given by $\frac{1}{4}N\bar{v}s$, where N is the density of atoms in the gas phase, $\bar{v}$ their mean thermal speed and s the sticking coefficient. At atmospheric pressure and room temperature $N\sim 3\times 10^{19}$ cm^{-3} and $\bar{v}\sim 10^{5}$ cm sec^{-1}. For

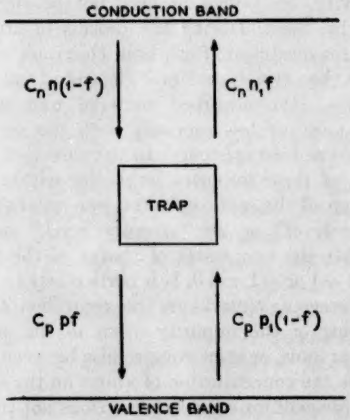

FIG. 2. Rates of transfer of electrons to and from the conduction and valence bands, according to the Shockley-Read trapping model.

s we shall choose 10^{-2}, as being representative of physical adsorption of any atom other than an atom of a rare gas. This gives a rate of exchange of the order of 10^{22} cm^{-2} sec^{-1}. If now we consider the maximum rate at which atoms can stick to the surface, if, once stuck, they are immediately removed; or, if we consider the maximum rate at which they can evaporate, if they are immediately pumped away, we shall arrive at a figure of the preceding order of magnitude—provided, or course, that the partial pressures (either the actual pressures, or the pressures that would prevail if the substances were allowed to accumulate) are all of the order of atmospheric. It is thus unlikely that this will very often be the limiting consideration in the catalyzed reaction.

Another of the steps shown in Fig. 1 is that in which the species A^- and D^+, once formed, react together on the surface to give AD. This rate is much more difficult to estimate *a priori*. The maximum rate at which the reaction can occur is that at which it is diffusion-limited. Unfortunately the theory of diffusion-limited surface reactions appears not to have been worked out, and there are certain difficulties in trying to extend the theory of diffusion-limited bulk reactions. If the surface diffusion constant is made small without limit, the rate will be determined instead by the probability of finding, on the sites on which they are formed, an A^- and a D sufficiently close to one another for reaction to occur *in situ*. In practice, this will probably mean the probability of finding them on neighboring sites. This we shall discuss in the next section.

We come now to the remaining steps shown in Fig. 1, all of which involve holes or electrons in the semiconductor. These are the things that will occupy us for most of the rest of the paper. As we shall show, the rates of charge transfer can generally be expressed as products of some sort of surface density, some sort of volume carrier concentration, a capture cross section, and a thermal speed of one of the carriers in the semiconductor. In a typical case the orders of magnitude of these quantities might be 10^{15} cm^{-2}, 10^{15} cm^{-3}, 10^{-17} cm^2, and 10^6 cm sec^{-1}. With these values, we shall have a rate of 10^{19} cm^{-2} sec^{-2}, which is very much in the range of interest. The last process to be considered is that involving the supply or disposal of hole-electron pairs in the semiconductor, which will only be important, as we shall see, under certain rather special circumstances. This quantity too can be of the order of 10^{10} cm^2 sec^{-1}, though it can be very much less.

We proceed now to a quantitative formulation of the foregoing ideas.

4. RATES OF CHARGE TRANSFER. DIFFUSION LIMITATIONS

In the nonequilibrium state, we must consider the four electron transfer processes shown in Fig. 2. The rates are most neatly and most generally written down by making use of the Hall-Shockley-Read[19,20] model for "trapping" in a semiconductor. This leads to a final result that is of the same form as that given by Hauffe, except that the unimolecular "reaction constants" are replaced by precisely defined physical quantities. (A "trap" is any center in a semiconductor crystal or on its surface, with the property that it can exist in two states of charge, differing by one electronic unit.)

The rates of the four transfer processes are also indicated on Fig. 2. Here, n and p stand for the electron and hole densities (in the present case, the values n_s and p_s that these quantities assume just below the surface); f is the fractional occupancy of the traps by electrons; n_1 and p_1 are the values that n and p would have if the Fermi level were to coincide with the trap level. C_n and C_p are products of the trap densities, the capture cross sections for holes or for electrons, whichever is indicated by the subscript, and the mean thermal speed for the respective carrier. The cross sections can, of course, be expressed in terms of the corresponding matrix elements, and could in principle be calculated *a priori* if the band structure of the semiconductor, and the wave functions of the impurity levels, were known.

If the trap is in equilibrium with the semiconductor, which is itself in equilibrium with respect to the reaction between electrons and holes, the rates of electron flow to and from the conduction band are equal, and the rates to and from the valence band are also equal. This condition leads to the following expressions for f:

$$f=n_s/(n_s+n_1)=p_1/(p_s+p_1)$$
$$=1/\{1+\exp[(E-E_F)/kT]\}, \quad (2)$$

which of course are precisely those one gets by applying Fermi-Dirac statistics directly, without considering the kinetics of the situation at all.

Let us now set

$$C_{pD}=N_D c_{pD}=\mathfrak{N}_D c_{pD}/f_D;$$
$$C_{nD}=N_D c_{nD}=\mathfrak{N}_D c_{nD}/f_D;$$
$$C_{pA}=N_A c_{pA}=\mathfrak{N}_A c_{pA}/(1-f_A);$$
$$C_{nA}=N_A c_{nA}=\mathfrak{N}_A c_{nA}/(1-f_A), \quad (3)$$

where the suffix (D or A) indicates whether the symbol to which it is attached refers to the donor or the acceptor species, the N's are the *total* surface densities (counting both ionized and un-ionized atoms) and the $\mathfrak{N}$'s are densities of the un-ionized species.

In the forward direction of the chemical reaction, there is a net rate of transfer of electrons *to* the semiconductor from the donor, and a net rate of transfer *from* the semiconductor to the acceptor, and these rates

[19] R. N. Hall, Phys. Rev. **83**, 228 (1951).
[20] W. Shockley and W. T. Read, Phys. Rev. **87**, 835 (1952).

are equal. Thus the rate of the reaction is given by

$$Q=\mathfrak{N}_D\left[c_{nD}\left(n_{1D}-\frac{1-f_D}{f_D}n_s\right)+c_{pD}\left(p_s-\frac{1-f_D}{f_D}p_{1D}\right)\right], \quad (4)$$

and also by

$$Q=\mathfrak{N}_A\left[c_{nA}\left(n_s-\frac{f_A}{1-f_A}n_{1A}\right)+c_{pA}\left(p_{1A}-\frac{f_A}{1-f_A}p_s\right)\right]. \quad (5)$$

Furthermore, if we assume that only ionized donors and acceptors can react, and if we further assume that the rate and the coverages are sufficiently low for bimolecular kinetics to hold, we can write a third expression for Q as follows:

$$Q=K[(1-f_D)/f_D][f_A/(1-f_A)]\mathfrak{N}_A\mathfrak{N}_D, \quad (6)$$

provided that the reaction product (the compound AD) is removes so fast that the back reaction can be neglected.

It will be convenient to tackle at this point a subject that we omitted in the previous section—the estimate of the order of magnitude of the "surface-diffusion-limited" reaction rate for the case that surface diffusion does not occur. Let us suppose that there are N_0 sites per unit area, so that, at low coverage, the density of ionized donor-acceptor pairs—that is, the density of ionized donors having ionized acceptors on neighboring sites—will be of the order of

$$\mathfrak{N}_A\mathfrak{N}_D f_A(1-f_D)/N_0(1-f_A)f_D,$$

apart from a numerical factor of the order of unity, dependent on the space group of the surface two-dimensional lattice. We now suppose that the probability per unit time of a pair reacting is given by some frequency factor ν_0, which will presumably be of the order of 10^{13} sec^{-1} if no "activated complex" is involved, and otherwise smaller than this by a Boltzmann factor. The rate of reaction is then given by Eq. (6), with a value of K of the order of ν_0/N_0. If N_0 is of the order of 10^{15} cm^{-2}, K will be around 10^{-2} cm^2 sec^{-1}, provided that no activated complex is involved. We may therefore say the following: where surface diffusion does not occur, the quantity K cannot be larger than 10^{-2} cm^2 sec^{-1}, and may in fact be considerably smaller; where surface diffusion can occur, the effect will be to allow K to be greater than the above argument would suggest.

If n_s, p_s, $\mathfrak{N}_A$, and $\mathfrak{N}_D$ are given, and also the fixed quantities that characterize the properties of the donors and acceptors (the positions of the donor and acceptor levels, and the capture cross sections), and if finally K is known, f_A and f_D may be eliminated from Eqs. (4), (5), and (6), and the rate Q is determined. But the quantities n_s, p_s, $\mathfrak{N}_A$, and $\mathfrak{N}_D$ are not those which are generally at the disposal of the experimenter. The experimental independent variables are the pressures P_A and P_D, the bulk doping of the semiconductor, and, sometimes, the fixed surface charge. It may also be possible to upset the hole-electron equilibrium within the semiconductor. What we have to do, therefore, is first to consider how the reaction rate depends on the quantities n_s, p_s, $\mathfrak{N}_A$, and $\mathfrak{N}_D$, and then to see, by methods that will be nothing more than straightforward generalizations of those used in considering equilibrium charge-transfer adsorption, how these quantities may be calculated when the experimental variables are known. This will occupy us during the next three sections.

5. DEPENDENCE OF THE REACTION RATE ON n_s, p_s, $\mathfrak{N}_A$, AND $\mathfrak{N}_D$

Let us begin by supposing that the reaction is not diffusion-limited. To do this, we set K in Eq. (6) large without limit. Then, so long as $\mathfrak{N}_A$ and $\mathfrak{N}_D$ are non-vanishing, either $(1-f_D)$ or f_A must be zero. The choice between these alternatives is made for us by the requirement that neither f_A nor f_D can be less than zero or greater than unity. Inspection of Eqs. (4) and (5) shows that the boundary between the two kinds of solution occurs where the surface concentrations of holes and electrons satisfy the equation

$$\mathfrak{N}_D(c_{nD}n_{1D}+c_{pD}p_s)/\mathfrak{N}_A(c_{nA}n_s+c_{pA}p_{1A})=1. \quad (7)$$

If the left-hand side of this equation exceeds unity, the surface has ionized acceptors on it but no ionized donors; we shall call this state of affairs *donor-limited*. In the contrary case there are ionized donors on the surface but no ionized acceptors, and the reaction will be called *acceptor-limited*. From Eqs. (4) and (5), the rates and the occupancy factors are given as follows:

Donor-limited Reaction $[\mathfrak{N}_D(c_{nD}n_{1D}+c_{pD}p_s) < (\mathfrak{N}_A c_{nA}n_s+c_{pA}p_{1A})]$

$$Q=\mathfrak{N}_D(c_{nD}n_{1D}+c_{pD}p_s) \quad (8)$$

$$(1-f_D)/f_D=0 \quad (9)$$

$$f_A/(1-f_A)=\frac{\mathfrak{N}_A(c_{nA}n_s+c_{pA}p_{1A})-\mathfrak{N}_D(c_{nD}n_{1D}+c_{pD}p_s)}{\mathfrak{N}_A(c_{nA}n_s+c_{pA}p_{1A})}. \quad (10)$$

Acceptor-limited Reaction $[\mathfrak{N}_D(c_{nD}n_{1D}+c_{pD}P_s) > \mathfrak{N}_A(c_{nA}n_s+c_{pA}P_{1A})]$

$$Q=\mathfrak{N}_A(c_{nA}n_s+c_{pA}p_{1A}) \quad (11)$$

$$f_A/(1-f_A)=0 \quad (12)$$

$$(1-f_D)/f_D=\frac{\mathfrak{N}_D(c_{nD}n_{1D}+c_{pD}p_s)-\mathfrak{N}_A(c_{nA}n_s+c_{pA}p_{1A})}{\mathfrak{N}_D(c_{nD}n_s+c_{pD}p_{1D})}. \quad (13)$$

We shall denote the values of n_s and p_s at which the reaction changes over from donor-limited to acceptor-limited by n_s^* and p_s^*.

So far we have supposed that the ionized species, once formed, can react limitlessly fast. Let us now go to

the case that the reaction constant K appearing in Eq. (6) is not infinite. From Eqs. (4)–(6) we get

$$Q^2-Q\{(n_s/n_{1A})\mathfrak{N}_A(c_{nA}n_{1A}+c_{pA}p_s)+(p_s/p_{1D})\mathfrak{N}_D(c_{nD}n_s+c_{pD}p_{1D})+(c_{nA}n_{1A}+c_{pA}p_s)(c_{nD}n_s+c_{pD}p_{1D})/K\}+\mathfrak{N}_A\mathfrak{N}_D(c_{nA}n_{1A}+c_{pA}p_s)(c_{nD}n_s+c_{pD}p_{1D})p_sn_s/p_{1D}n_{1A}=0. \quad (14)$$

In deriving this equation, we have ignored injection and extraction effects, and have therefore been entitled to use the relation $n_sp_s=n_i^2$. Equation (14) has two roots, but it may be shown that only one is consistent with the requirement that both f_A and f_D must lie between 0 and 1. If K is sufficiently small, we get the approximate solution

$$Q=K\mathfrak{N}_A\mathfrak{N}_D/n_{1D}n_{1A}. \quad (15)$$

Equation (15) gives a rate that depends on $\mathfrak{N}_A$ and $\mathfrak{N}_D$, but not on n_s or p_s explicitly. Physically, this is because the rate is proportional both to the concentration of ionized donors and to that of ionized acceptors, which, if the rate is so slow that the equilibrium occupancy factors hold, are proportional to $(1/n_s)$ and n_s, respectively.

6. INTRODUCTION OF THE PRESSURES. NUMBER OF AVAILABLE SITES

Here we proceed exactly as in the charge-transfer adsorption theory of Krusemeyer and Thomas. On the assumption of noninteracting adsorbed particles, the surface density of un-ionized donors ($\mathfrak{N}_D$) will be related to the pressure P_D of the component D in the gas phase by the equation

$$\mathfrak{N}_D=\lambda_DP_D, \quad (16)$$

so long as the pressure is so low that the surface is almost bare. The quantity λ_D will be some function of the temperature, depending, among other things, on the heat of adsorption of the neutral donor atoms. Similarly, the density of un-ionized acceptors on the surface will be given (again at low pressure) by

$$\mathfrak{N}_A=\lambda_AP_A. \quad (17)$$

When, however, the surface is extensively covered with ionized and un-ionized donors and acceptors, these expressions will no longer hold. We shall assume that the probability per unit time of an atom or molecule evaporating is still independent of whether neighboring sites are occupied, and that the probability of an impinging atom sticking is either some constant quantity s, if that site be empty, or zero, if it be filled. Then, denoting the total number of available sites per unit area by N_0, Eqs. (16) and (17) become

$$\mathfrak{N}_A=\lambda_AP_A\left[1-\frac{\mathfrak{N}_A}{N_0}\left(\frac{1}{1-f_A}\right)-\frac{\mathfrak{N}_D}{N_0}\left(\frac{1}{f_D}\right)\right] \quad (18)$$

$$\mathfrak{N}_D=\lambda_DP_D\left[1-\frac{\mathfrak{N}_A}{N_0}\left(\frac{1}{1-f_A}\right)-\frac{\mathfrak{N}_D}{N_0}\left(\frac{1}{f_D}\right)\right]. \quad (19)$$

Solving these equations for $\mathfrak{N}_A$ and $\mathfrak{N}_D$

$$\mathfrak{N}_A=\lambda_AP_A\Big/\left[1+\frac{\lambda_AP_A}{N_0}\left(\frac{1}{1-f_A}\right)+\frac{\lambda_DP_D}{N_0}\left(\frac{1}{f_D}\right)\right] \quad (20)$$

$$\mathfrak{N}_D=\lambda_DP_D\Big/\left[1+\frac{\lambda_AP_A}{N_0}\left(\frac{1}{1-f_A}\right)+\frac{\lambda_DP_D}{N_0}\left(\frac{1}{f_D}\right)\right]. \quad (21)$$

Now what do we in fact mean by "available sites?" If all the lattice points on some crystal surface are equivalent, then N_0 clearly means the density of such sites per unit area of exposed surface. There is often, however, the suspicion in catalysis that all sites are not equivalent, and we might wish to extend the validity of Eqs. (20) and (21) by allowing N_0 to be equal, not to the number of lattice points per unit area, but to some smaller number corresponding to those lattice points which are in some sense "active." There are difficulties in doing this, however, associated with the possibility that under these circumstances there will be a significant steady-state density of ions elsewhere than on "active sites." If this is the case, the charge density associated with them will have to be included specifically in the surface charge considerations of the next section.

7. FACTORS DETERMINING n_s AND p_s. THE ROLE OF THE SURFACE SPACE-CHARGE REGION

In this section we shall suppose that there is always hole-electron equilibrium within the semiconductor; the more general case is considered in Sec. 9.

For given bulk doping and for a given ionic surface charge, n_s and p_s are determined (in the absence of an applied electric field) by the neutrality condition

$$\sigma_{sc}+\sigma_{\text{ion}}+\sigma_{ss}=0, \quad (22)$$

where σ_{sc} is the charge density associated with the space-charge region in the semiconductor, σ_{ion} is that associated with the adsorbed ions, and σ_{ss} is that associated with the "intrinsic" surface states. As pointed out in Sec. 2, there is little advantage in taking explicit account of intrinsic surface states in the present theory, because, if they are sufficiently numerous to matter, they will displace the bulk semiconductor in its role as a source and sink of electrons. We shall therefore proceed on the supposition that the intrinsic states may be neglected.

In the notation of the preceding sections, the ionic charge density σ_{ion} is given by

$$\sigma_{\text{ion}}=e[\mathfrak{N}_D(1-f_D)/f_D-\mathfrak{N}_Af_A/(1-f_A)]. \quad (23)$$

It may be seen from Eqs. (9) and (12) that σ_{ion} is in fact a continuous, monotonically decreasing function of n_s, changing sign when $n_s=n_s^*$, $p_s=p_s^*$. Now, from the standard solutions of the space-charge problem, one knows that σ_{sc} is also a continuous, monotonically decreasing function of n_s, changing sign at the point at which $n_s=n_0$, the bulk electron concentration. Thus Eq. (22), for the case $\sigma_{ss}=0$, and for given $\mathfrak{N}_A$ and $\mathfrak{N}_D$, always has one solution and one only. Unfortunately, the exact expressions for σ_{sc}[21] involve integrals which cannot be expressed in terms of simple functions, so we shall have to introduce certain restrictions and approximations at this point. Let us restrict the discussion to the case that charge transfer occurs exclusively with the conduction band, which we can do by dropping terms in c_{pD} and c_{pA} from Eqs. (8) through (13). In this case n_s^* is given by

$$n_s^*=(\lambda_D P_D c_{nD})n_{1D}/(\lambda_A P_A c_{nA}), \tag{24}$$

an expression that holds whether there are saturation effects or not. Let us further restrict the problem by supposing that the semiconductor is extrinsic n type (as will generally be the case where charge transfer is entirely with the conduction band). It will be seen that the sign of the surface dipole now depends on whether n_s^* is greater or less than n_0. If $n_s^*<n_0$, the reaction will be donor-limited (or possibly diffusion-limited); the ionic charge will consist entirely (or at any rate mainly) of ionized acceptors, which carry a negative charge; and the compensating charge in the space-charge region will arise from the bulk donors that are exposed by the removal of electrons from the region close to the surface (a "depletion layer"). If $n_s^*>n_0$, the contrary statements are true, and the space-charge is of the "accumulation layer" type. In both cases, n_s must lie between n_s^* and n_0. We now proceed to a quantitative examination of these two configurations.

(i) $n_s^*>n_0$: *acceptor-limited reaction.* If the pressures are so small that the adsorbed ionized donors are insufficiently numerous to induce any appreciable space-charge layer in the semiconductor, we may set $n_s=n_0$ in Eq. (11) and use Eq. (17) for $\mathfrak{N}_A$, so getting

$$Q=\lambda_A P_A c_{nA} n_0. \tag{25}$$

As we increase the pressures (doing so always in such a way as to preserve $n_s^*>n_0$), we begin to develop an accumulation layer. We must then find n_s from the neutrality condition. From Eqs. (12), (13), and (24) we get

$$\sigma_{\text{ion}}=e\mathfrak{N}_D n_{1D}[(1/n_s)-(1/n_s^*)]. \tag{26}$$

To write down the space-charge, we make use of the following approximation,[21] holding where n_s is greater by a factor of e or more than n_0:

$$\sigma_{sc}=-e[\epsilon\epsilon_0 kTn_s/2\pi e^2]^{\frac{1}{2}}. \tag{27}$$

From (26) and (27) we get for n_s

$$n_s=\mathfrak{N}_D^{\frac{1}{2}}n_{1D}^{\frac{1}{2}}e^{\frac{1}{2}}(2\pi)^{\frac{1}{2}}/(\epsilon\epsilon_0 kT)^{\frac{1}{4}}$$
$$=\mathfrak{N}_D^{\frac{1}{2}}n_{1D}^{\frac{1}{2}}/\mathfrak{L}_{n1D}^{\frac{1}{2}}, \tag{28}$$

where $\mathfrak{L}_{n1D}$ means the "Debye length for a concentration n_{1D}." Even after an accumulation layer has developed, there will generally be an extensive region of pressure in which saturation effects may be neglected, so that we may write $\mathfrak{N}_A=\lambda_A P_A$ and $\mathfrak{N}_D=\lambda_D P_D$, and get

$$Q=(\lambda_A P_A)(\lambda_D P_D)^{\frac{1}{2}}n_{1D}^{\frac{1}{2}}c_{nA}/\mathfrak{L}_{n1D}^{\frac{1}{2}}. \tag{29}$$

Eventually, however, at sufficiently high pressure, these approximations for $\mathfrak{N}_A$ and $\mathfrak{N}_D$ cease to be adequate, and we must say instead

$$\mathfrak{N}_A=\lambda_A P_A/\left\{1+\frac{\lambda_A P_A}{N_0}+\frac{\lambda_D P_D}{N_0}\left[1+n_{1D}\left(\frac{1}{n_s}-\frac{1}{n_s^*}\right)\right]\right\} \tag{30}$$

$$\mathfrak{N}_D=\lambda_D P_D/\left\{1+\frac{\lambda_A P_A}{N_0}+\frac{\lambda_D P_D}{N_0}\left[1+n_{1D}\left(\frac{1}{n_s}-\frac{1}{n_s^*}\right)\right]\right\}, \tag{31}$$

which is the form that Eqs. (20) and (21) take in the present case. The behavior is now dependent on the magnitude of (n_{1D}/n_s), or, in effect of $\mathfrak{L}_{n1D}n_{1D}/N_0$. If this quantity is sufficiently large, the surface will become almost completely occupied by ionized donors, tending towards the exclusion of anything else. The reaction rate is then given by

$$Q=(\lambda_A P_A)c_{nA}N_0^5/(\lambda_D P_D)n_{1D}^3\mathfrak{L}_{n1D}^4. \tag{32}$$

In a practical case (with say $N_0=10^{15}$ cm^{-2}) the condition for this to hold is that the donor level lie some considerable distance above the edge of the conduction band. There is, of course, nothing at all to prevent this happening. Note, too, that if we were to use for N_0 some much smaller number (see remarks on "active sites" in the previous section), the condition on the position of the donor level would be less stringent.

If (n_{1D}/n_s) is not in fact large in comparison with 1, the surface tends instead to become saturated with un-ionized donors and un-ionized acceptors. The rate is then given by

$$Q=[\lambda_A P_A/(\lambda_A P_A+\lambda_D P_D)]N_0^{4/3}c_{nA}n_{1D}^{\frac{1}{2}}/\mathfrak{L}_{n1D}^{\frac{1}{2}}. \tag{33}$$

It will be noted that it is only in the region of low pressures, where the rate is given by Eq. (25), that the rate is affected by the bulk doping of the semiconductor at all. The upper limit to this region is given by equating the right-hand sides of Eqs. (25) and (29), and is given by

$$P_D=n_0^{\frac{1}{2}}\mathfrak{L}_{n1D}/\lambda_D n_{1D}^{\frac{1}{2}}. \tag{34}$$

For a given pressure product $P_A P_D$, the rate is highest in the region in which (25) holds. Thus it is in

[21] C. G. B. Garrett and W. H. Brattain, Phys. Rev. **99**, 376 (1955).

this region that diffusion limitations are most likely to come into effect. From Eq. (15) we get

$$Q=K(n_{1D}/n_{1A})(\lambda_A P_A)(\lambda_D P_D) \tag{35}$$

with the usual remark that the reaction will be diffusion-limited or transfer-limited according as to which rate is the slower.

(ii) $n_s^* < n_0$: *donor-limited reaction.* At low pressures, the rate is given, in accordance with Eqs. (8) and (16), by

$$Q=\lambda_D P_D c_{nD} n_{1D}, \tag{36}$$

independent of whether a substantial depletion layer exists or not. As we approach saturation, however, $\mathfrak{N}_D$ ceases to be given by $\lambda_D P_D$, and again the question arises of whether the surface becomes saturated first with atoms or ions. To investigate this, we must find n_s. The ionic charge, given by Eqs. (9), (10), and (23), is of the form

$$\sigma_{ion}=-e\mathfrak{N}_A(n_s-n_s^*)/n_{1A}, \tag{37}$$

while the charge in the space-charge region is given, to a good enough approximation,[21] by

$$\sigma_{sc}=en_0\mathfrak{L}_{n0}[\ln(n_s/n_0)]^{\frac{1}{2}}, \tag{38}$$

where $\mathfrak{L}_{n0}=[\epsilon\epsilon_0 kT/2\pi e^2 n_0]^{\frac{1}{2}}$, the "Debye length for a concentration n_0." By solving these two equations for n_s,

$$n_s=n_0\exp[-N_0^2/n_0^2\mathfrak{L}_{n0}^2]. \tag{39}$$

To bring in the pressures, we may write

$$\mathfrak{N}_A=\lambda_A P_A/\left\{1+\frac{\lambda_D P_D}{N_0}+\frac{\lambda_A P_A}{N_0}\left[1+\frac{n_s-n_s^*}{n_{1A}}\right]\right\} \tag{40}$$

$$\mathfrak{N}_D=\lambda_D P_D/\left\{1+\frac{\lambda_D P_D}{N_0}+\frac{\lambda_A P_A}{N_0}\left[1+\frac{n_s-n_s^*}{n_{1A}}\right]\right\}, \tag{41}$$

so that the question of whether neutral atoms or ions predominate depends on the magnitude of

$$(n_0/n_{1A})\exp[-N_0^2/n_0^2\mathfrak{L}_{n0}^2].$$

Here, however, we notice one departure from the acceptor-limited case. If N_0 is taken to be a number of the order of 10^{15} cm^{-2}, the requirement on n_0 is so severe that ions could only predominate if the semiconductor were highly degenerate—effectively, a metal. (Again, of course, the requirement ceases to be so strict if N_0 is taken to be some much smaller number. This would be so if only a small number of the sites were "active," *and if the steady state concentrations of ionized atoms on other sites were negligible.*) In view of the exponential dependence of n_s on $N_0^2/n_0^2\mathfrak{L}_{n0}^2$, we may simply say that, as soon as n_0 becomes equal to $2\pi e^2 N_0^2/\epsilon\epsilon_0 kT$, the surface will at once become entirely cluttered up with ionized acceptors, and the rate of the reaction will rapidly fall to zero. Otherwise, neutral atoms will predominate, and the rate will be given by

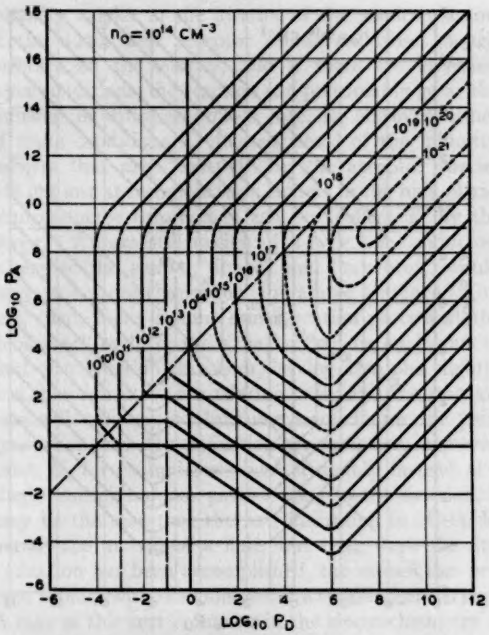

FIG. 3. Contours of constant reaction rate for the particular values for the parameters specified in the text. Each contour is labeled with the rate in molecules cm^{-2} sec^{-1}. The pressures are in mm. Electron concentration 10^{14} cm^{-3}.

$$Q=[\lambda_D P_D/(\lambda_A P_A+\lambda_D P_D)]N_0 c_{nD} n_{1D}. \tag{42}$$

Note that neither this expression nor that given by Eq. (36) depends on the bulk doping at all. The bulk doping thus affects only: (a) the boundary between the donor-limited and acceptor-limited region; (b) the acceptor-limited rate, in the case that no substantial accumulation layer exists; (c) the condition that the surface becomes saturated with ionized donors or acceptors before becoming saturated with un-ionized donors or acceptors.

8. NUMERICAL EXAMPLE

Let us take the case that charge transfer is with the conduction band. To give a numerical example, it is necessary to assign values to the following quantities:

$$\lambda_A,\ \lambda_D,\ n_{1D},\ n_{1A},\ c_{nD},\ c_{nA},\ \mathfrak{L}_{n1D},\ n_0,\ N_0,\ K.$$

Some of these quantities will not vary by more than a decade or two from system to system. For purposes of illustration, we make our choices as follows. The c's will generally be of the order of 10^{-10} cm^3 sec^{-1}, since capture cross sections are generally within an order of magnitude or two of 1 A^2, and thermal speeds of carriers around room temperature in wide band-gap semiconductors, where effective masses tend to be high, are of the order of 10^6 cm sec^{-1}. We therefore assign

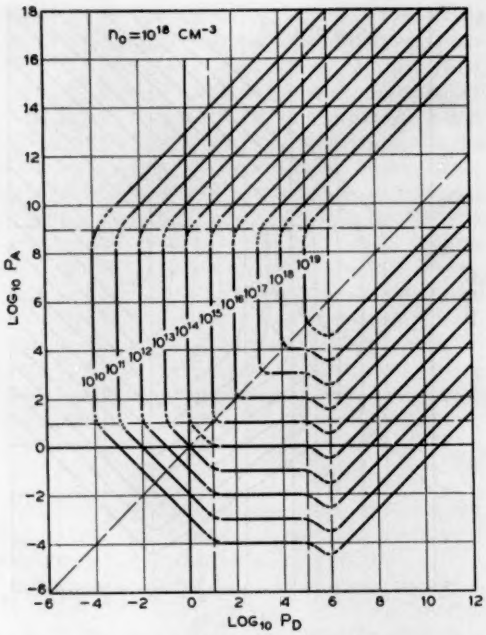

FIG. 4. The same as Fig. 3, but for an electron concentration of 10^{18} cm^{-3}.

$c_{nD}=10^{-11}$ cm^3 sec^{-1}, $c_{nA}=10^{-10}$ cm^3 sec^{-1}, just to have them different. N_0 we take as 10^{15} cm^{-2}, as representative of the density of lattice sites on a typical surface. No particular restrictions attach to the choice of n_{1D} and n_{1A}, except that the former must be greater than the latter (otherwise the reaction will presumably tend to go backwards), and that the ratio must not be greater than $\exp(\Delta G/kT)$, where ΔG is the (Gibbs) free energy of the reaction. We choose $n_{1D}=10^{16}$ cm^{-3}, $n_{1A}=10^{10}$ cm^{-3}, and are thereby committed to a value for $\mathfrak{L}_{n1D}$ in the vicinity of 10^{-5} cm. We choose $\lambda_A=10^6$ cm^{-2} (mm Hg)$^{-1}$, $\lambda_D=10^9$ cm^{-2} (mm Hg)$^{-1}$, for no particular reason, except that the pressure ranges in which the interesting things happen turn out to be reasonable. The remaining parameter is K, the diffusion-limited rate constant. This we pick as 10^{-8} cm^2 sec^{-1}, which probably is rather low; but, if we chose a much larger value, the diffusion-limited region would occur at pressures so low that we would have difficulty including it on the same diagram as the other regions. With these values, Figs. 3 and 4 have been constructed, with an electron concentration $n_0=10^{14}$ cm^{-3} in Fig. 3 and 10^{18} cm^{-3} in Fig. 4. In these figures are plotted contours of constant reaction rate (expressed in molecules reacting per cm^2 per sec); the ordinate is the pressure of the acceptor gas, in mm Hg, and the abscissa the pressure of the donor gas, in the same units. The dashed lines show the boundaries between the different pressure ranges in which Eqs. (15), (25), (29), (33), (36), and (42) hold; the reaction is donor-limited above and to the left of the 45° dashed line, acceptor-limited below and to the right of it. Where the contours have a slope of -1, the reaction is diffusion-limited (bottom left-hand corner); where the slope is 1, the surface is saturated with un-ionized donors or acceptors; where the contours are horizontal, the reaction is acceptor-limited, but there is no appreciable accumulation layer; where the slope is $-\frac{2}{3}$, the reaction is donor-limited and the accumulation layer is appreciable; where the contours are vertical, the reaction is donor-limited, and, in part of this region, there is an appreciable depletion layer. With these values for the parameters, saturation is always predominantly with the neutral atoms, so that the only effect of changing the electron concentration is in the low-pressure region and in changing the boundary between the donor- and acceptor-limited reaction. If we had chosen N_0 to have some considerably smaller value, in the vicinity of 10^{12} or 10^{13} cm^{-2}, the boundaries of the saturation regions would have depended on electron concentration as well.

9. INJECTION, EXTRACTION, AND TRANSISTOR EFFECTS

We turn next to the case that the hole-electron equilibrium at the surface is appreciably disturbed. Such a state of affairs can arise only if the carrier that in the bulk is the minority carrier is involved, either with one or with both of the reacting species. A quantitative analysis of the space-charge region in the presence of nonequilibrium effects has been given by Garrett and Brattain[21] but such a treatment will be of dubious validity when applied to wide band-gap semiconductors, such as we usually encounter in catalysis. We shall therefore content ourselves with a few qualitative remarks.

(i) Injection effects will occur when the donor species is in good contact with the conduction band and the acceptor species with the valence band; as the reaction proceeds, hole-electron pairs will be injected into the semiconductor, and must eventually be disposed of by recombination. In the opposite case—the donor species in good contact with the valence band and the acceptor with the conduction band—hold-electron pairs will be extracted, and the deficiency must be made up by thermal generation. In either case, the effect will usually be to change n_s or p_s or both in such a sense as to slow down the reaction. The rate-determining step, in fact, is no longer charge transfer, but pair creation or disposal. For narrow band-gap semiconductors, it is usually good enough to assume that the minority carrier diffusion length is large in comparison with the Debye length, so that the creation or disposal problem may be relegated to the space-charge-free region of the semiconductor. Under these circumstances, the maximum rate at which carrier pairs can be created or destroyed is of the order of $(D/\tau)^{\frac{1}{2}}$, where τ is the

minority carrier lifetime. The rate of the reaction can therefore be increased by decreasing τ, by introducing the right sort of chemical impurities or structural imperfections to act as recombination centres. If τ is reduced until the diffusion length is of the same order as the Debye length, we get, for germanium at room temperature, a maximum rate of the order of 10^{19} cm^{-2} sec^{-1}, which would correspond, if we made such material one side of a $p-n$ junction, to a saturation current of the order of 1 amp cm^{-2}.

(ii) Where extraction effects occur, the rate of the reaction could clearly be increased by illuminating the surface with light whose wavelength falls within the fundamental absorption band. This would then constitute a case of "photocatalysis." (Other reasons for photocatalysis are, however, imaginable.)

(iii) So far, throughout this paper, we have assumed that the surface of the semiconductor is electrically homogeneous. If, however, we have a patchy surface, some parts of which are n type and some p type, we shall be able to secure most rapid ionization of donors on the p regions and of acceptors on the n regions. (Remember, however, that a region must extend over a Debye length or so before we can safely say whether it is p type or n type, so that what we are considering here is inhomogeneity on a scale much larger than atomic.) Two problems then arise. It is necessary to turn an extra hole into a missing electron before the reaction can be regarded as complete, so that we have still to consider the flow of current between the n regions and the p regions, which of course depends again on the presence of recombination centers. Furthermore, there will now exist on the surface of the catalyst strong local electric fields, which may retard the movement of the ionized donors and acceptors toward one another. Tentatively we may say that this sort of catalytic surface will be most advantageous when the rates of ionization of donors and acceptors are exceptionally slow, for example, because the cross sections are very small. Perhaps catalysts composed of an intimate mixture of a metal and a semiconductor fall into this class.[22]

(iv) Injection and Extraction effects will probably be rather unimportant on wide band-gap semiconductors. There are no minority carriers to extract; and, as for injection, any reaction energetic enough to inject minority carriers will probably cause disruption of the semiconductor itself. For example, it is known for zinc oxide that, if holes are allowed to reach the surface, they discharge lattice oxygen.

(v) The remaining case to consider is the one in which both substances indeed negotiate with the same band, but in which that band corresponds to the minority carrier in the interior of the semiconductor. If the donor and acceptor atoms are close enough together on the surface, and if there are inversion layer conditions, the reaction can presumably go at the transfer- or diffusion-limited rate. If, however, either of these conditions is violated, some of the minority carriers that are "emitted" by the acceptor species will get lost at recombination centers in the bulk of the semiconductor before they can be "collected" by the donor. (We are still taking of n-type semiconductor; otherwise the words "donor" and "acceptor" would have to be interchanged in the above sentence.) Unless, then, there is some multiplication process at the "collector" surface, the situation will be analogous to that of a junction transistor, having an alpha slightly less than unity, with a floating base; and the reaction rate will only exceed by some small factor the pair-generation rate. Multiplication processes may, however, exist. If, for example, we have a doubly instead of a singly ionizable donor participating in the reaction, it may be the case that the first ionization in effect demands the arrival of a hole, but that, once the first ionization has been accomplished, the second can proceed rapidly with the emission of a conduction electron. A case of this sort is known in the electrochemistry of germanium.[23]

10. RELATION TO EXPERIMENT

A search of the literature shows that there are not lacking qualitative indications of a correlation between semiconductor surface and bulk properties and catalytic activity. Unfortunately, the theory of charge-transfer catalysis, as presented by Hauffe, or as developed by us in the present paper, is quite complicated, and contains quite a number of physical parameters. so that, if qualitative conclusions are all that are to be obtained, the theory will hardly recommend itself over earlier, purely descriptive models that purport to cover the same ground. If we had all the parameters required, for some particular system, to construct diagrams like Figs. 3 and 4, we would then be in a position to compare the predictions of the theory with actual measurements of the rate of the reaction, and to choose conditions for practical applications. But so long as we have no more information than is represented, for example, by a set of measurements of the reaction rate as a function of, let us say, the bulk doping of the semiconductor, it is clear that the number of adjustable parameters in the theory is sufficiently large to prevent one from concluding that it is unambiguously and uniquely right.

In view of these considerations, we shall consider each of the parameters in turn, and ask what experimental techniques are available for measuring it. In some cases, these techniques have indeed already been applied to systems of interest in catalysis, and, where

[22] One must, however, be careful to avoid supposing that a monolayer of oxide or nitride on the surface of a semiconductor is *ipso facto* a semiconductor. A three-dimensional semiconductive material must be at least a Debye length thick before it can be regarded as having the properties of bulk semiconductor.

[23] W. H. Brattain and C. G. B. Garrett, Bell System Tech. J. 34, 129 (1955).

this is the case, we shall give a reference to the literature. Unfortunately, however, there is no case in the literature in which a sufficient number of different techniques have been applied *to the same system under the same conditions* to permit a quantitative check on the predictions of the theory.

Before we proceed to the parameters themselves, it is first necessary to make a few remarks on general bulk and surface electrical measurements on semiconductors. To make much progress, it is clearly necessary to determine the effect of bulk impurities on the bulk conductivity and on the position of the Fermi level, since the ability to vary the position of the latter quantity is a valuable tool in the pursuit of equilibrium and non-equilibrium surface properties. The first point which has to be made is that, to this end, measurements on single crystals of controlled composition are greatly superior to measurements on powders. Measurements on powders, however, are only too common in the literature; sometimes the object is to determine the bulk conductivity, sometimes the effect of adsorbed gases on the surface conductivity. Unfortunately it is usually impossible to learn much about either quantity from such measurements. In one case for which a comparison between single crystal and powder measurements has now become possible—zinc oxide—it has turned out to be completely impossible to understand any of the numerous results on polycrystalline samples in the light of the single crystal measurements. The trouble presumably lies in the existence of space-charge barriers between the particles. A powder has one thing to recommend it, from the point of view of systems of interest in catalysis: large area. Unfortunately, the price one pays for this inability to make precise, meaningful electrical measurements is so high that the more widespread use of single crystal techniques is greatly to be desired.

A second point bearing on bulk properties must be mentioned at this point. The catalysis literature abounds with experiments in which various chemical impurities have been added to oxide semiconductor powders, in the hope of controlling thereby the position of the bulk Fermi level. Unfortunately, deviations from stoichiometry are also possible in these materials, so that, unless the pressure of oxygen at the time of incorporation of the impurity was carefully controlled, the concentrations of electrically active centers in the material remain quite unpredictable. A necessary preliminary, therefore, to a detailed study of the processes of catalysis at the surface of such a semiconductor is a series of careful measurements on the bulk properties of single crystals.

Turning from the bulk to the surface, it is worth considering briefly the question of the measurement of the surface carrier concentrations n_s and p_s. These are not, of course, constants of the system, since they will in general be sensitive to any of the experimental variables (the pressures, temperature, etc.) However, it will usually be convenient to measure them explicitly under each set of conditions, and a short discussion of how to do so will assist in the presentation of the proposed parameter-determining experiments.

The product $n_s p_s$ is equal (in equilibrium) to n_i^2, which is known if the bulk properties are known: it therefore suffices to determine one or the other of the two. From standard space-charge theory it is known that n_s and p_s are single-valued functions of the surface potential (the quantity usually called V_D in the German literature) so that any experiment that measures this quantity is sufficient to determine n_s and p_s. Of the various methods that have been used for determining the surface potential, the following are particularly noteworthy:

(i) *Determination of the Surface Conductivity.* The surface potential is a two-valued function of the surface conductivity—depending on whether the surface is hole-rich or electron-rich—so that it is necessary to know which of these is the case. Otherwise, *on a single crystal*, the measurement of surface conductivity is straightforward. The conductance of a thin slice is measured, and compared with what it would be if the surface potential were zero—a quantity calculable from the bulk conductivity and the dimensions of the slice. This technique has been extensively exploited in experiments on the surface properties of germanium and silicon[24] and has also been used for zinc oxide.[25]

One drawback of the surface conductivity method is that it requires a knowledge of the electron and/or hole mobilities, and of any changes in these quantities that may occur consequent on the imprisonment of the carriers in a narrow potential trough close to the surface. Measurements of the "surface Hall effect"[26] can be used to explore this matter: in any case, the variation in mobility is likely to be less troublesome in oxide semiconductors than in silicon or germanium, since the mean free paths in the bulk material are much smaller.

(ii) *Study of the Volta Potential.* Unfortunately, this technique is limited both by the fact that the volta potential is indeterminate to the extent of an additive constant, and by the possibility of the appearance of further dipole layers on top of the dipole formed by the semiconductor space-charge region and the adsorbed atoms. Changes in volta potential can, however, be measured with some certainty, so that (once a value for n_s or p_s has been found for some standard condition) the method can sometimes be of value.[27] It has, incidentally, the advantage that volta potential measurements on powders are free from the major objections to conductivity measurements discussed above.

---

[24] Several papers on this subject are to be found in *Semiconductor Surface Physics*, edited by R. H. Kingston (University of Pennsylvania Press, Philadelphia, Pennsylvania, 1955).

[25] H. J. Krusemeyer, Phys. Rev. **114**, 655 (1959).

[26] J. W. Zemel and R. L. Petritz, Bull. Am. Phys. Soc. **2**, 131 (1957).

[27] W. H. Brattain and C. G. B. Garrett, Bell System Tech. J. **35**, 1019, 1941 (1956).

(iii) *Measurement of the Surface Capacitance.* This method has been used only on germanium,[28] but it is straightforward, and has the advantage that no knowledge of the mobility of the carriers in the surface region is required.

We turn now to the determination of the system parameters.

A. n_{1A} and n_{1D}

It will be seen from Eq. (2) that a single measurement of the fractional ionization of the adsorbed species, at equilibrium at some particular coverage, suffices, together with a knowledge of n_s or p_s, to determine n_{1A} or n_{1D}. To determine the fractional ionization, we need to measure, for example, the total coverage (for which standard chemical techniques are available) and also the coverage by ions.

In the absence of intrinsic surface states, the coverage by ions is directly calculable from a knowledge of the surface potential, techniques for measuring which have been given previously. For, the ionic charge will then equal the change in the space-charge region [Eq. (22)], which is itself a known function of the charge in the space-charge region, given, in approximate form, by Eqs. (27) and (38).

If intrinsic surface states are present, one must do a little more. In the absence of adsorbed material, the distribution in energy and the density of the intrinsic surface states may be found, for example, by use of the field-effect technique, wherein one measures the fraction of some induced electronic charge that appears in the space-charge region and the fraction that is trapped in the intrinsic surface states. In the presence of adsorbed material, the result of repeating such a measurement will indicate the change, if any, that has occurred in the distribution and energy of the intrinsic states.[29] Thus a combination of these measurements will lead to a determination of the quantity σ_{ss} appearing in Eq. (22), and so, by subtraction, to a calculation of the ionic charge, whence n_{1A} or n_{1D} is found.

It was remarked previously that a single measurement of the fractional ionization suffices to determine n_{1A} or n_{1D}. However, it will usually happen that, with arbitrarily chosen conditions, an experiment of the above type will lead to the conclusion that the atoms are, within the experimental accuracy, either completely ionized or not ionized at all. To get an accurate determination of n_{1A} and n_{1D}, therefore, it is necessary to choose the conditions (for example, the bulk doping and the pressure) in such a way that the fractional ionization is somewhere near one-half.

B. λ_D and λ_A

To determine these quantities, one needs to measure some sort of equilibrium adsorption isotherm. If the quantities n_{1A} and n_{1D} have already been measured as described above, and a technique for determining n_s or p_s under the conditions of the experiment is to hand, the experimenter will be in a position to choose from the following techniques:

(i) Measure the total coverage as a function of the pressure, and make use of Eqs. (2), (3), (16), and (17).

(ii) Measure the surface conductivity, the volta potential or the surface capacity as a function of the pressure, translate the result into a determination of the surface potential (whence the ionic charge) and proceed as in the foregoing.

(iii) Perform the field effect experiment as a function of pressure, using frequencies low enough for substantial equilibrium to be reached within each cycle. The fraction of the charge that does not appear in the space charge region may then be used, together with a knowledge of n_{1A} or n_{1D}, to find λ_A and λ_D.

Since several methods are available, a quantitative check on the internal consistency of the data now becomes possible.

Techniques (i) and (ii) have been used to some extent in systems of interests in catalysis, but never where enough information is available to enable one to deduce λ_A and λ_D. Measurements on powder "conductivities" on the admission of gas to the system have often been reported, but, for reasons given above, these are at most of qualitative value. Volta potential measurements, which are not open to these objections, have also been reported in one or two cases. Thus, Lyashenko and Stepko[9] have reported changes in the "work function" of MnO_2, CuO, and NiO in the presence of various gases, but have not determined the pressure-dependence, and do not attempt any sort of quantitative comparison with the theory. With regard to the question of the temperature-dependence, which has occasionally been studied, both for the conductivity and for the volta potential, we shall have more to say later.

C. c_{nA}, c_{pA}, c_{nD}, and c_{pD}

These, being kinetic quantities, cannot be determined by equilibrium adsorption measurements, but are still accessible to experiment on one gas alone, without going to the full complexities of the catalyzed reaction. They can in fact be found by studying the kinetics of adsorption of each gas by itself, provided that the experiment is done under conditions in which n_s or p_s can be measured and the quantities discussed in the preceding paragraphs are known.

The simplest experiment would be one in which, starting at a condition of equilibrium between one of the

[28] W. H. Brown, W. H. Brattain, C. G. B. Garrett, and Montgomery, cited in footnote reference 24.

[29] There is a complication here arising from the possibility that, during the time of application of the field, the ionic charge may be changed. However, by performing the measurements at a sufficiently high frequency this process can be eliminated. See remarks on c_{nA}, etc. which follow later.

gases and the surface, some variable of the system (let us say, for the moment, the pressure) is suddenly changed by a small amount, and the subsequent approach to the new equilibrium is determined. By "small" one means that, after the sudden change, none of the chemical or electrochemical potentials of the system finds itself away from its final equilibrium value by an amount large in comparison with kT/e. Under these circumstances, it may easily be shown that the approach to equilibrium is always unimolecular, the relaxation times depending on some combination of the quantities c_{nA}.... To illustrate this, let us consider the gas to be the donor substance, so that only ionized and un-ionized donors are present on the surface. The kinetic equation can now be derived from Eq. (4), by setting the right-hand side equal to $(d/dt)\mathfrak{N}_D(1-f_D)f_D$. If we suppose that, during the relaxation, the pressure is held constant, and that there is always rapid equilibrium of the neutral atoms between the surface and the gas, this expression may be written $\mathfrak{N}_D d\Delta/dt$, where Δ is the departure of the quantity $(1-f_D)f_D$ from its equilibrium value. The right-hand side of Eq. (4) may then be written in terms of Δ, leading to an equation of the form $d\Delta/dt=-\Delta/\tau_1$. (It must be remembered that n_s itself will be changing during the relaxation process.) If, for example, we have an accumulation layer and the sample is n type, the time constant may be shown to be $1/3c_{nD}n_s$, so that a kinetic experiment will suffice to determine c_{nD}. To show the orders of magnitude involved, let us set $c_{nD}=10^{-10}$ cm^3 sec^{-1}. Thus, with n_s somewhere in the range of 10^{10} cm^{-3} to 10^{16} cm^{-3}, we shall expect time constants of the order of 1 to 10^{-6} sec. In this case, an abrupt change of pressure would hardly seem the best way of doing the experiment; we could, however, upset the equilibrium by suddenly applying a field to the surface of the semiconductor, and watching the relaxation electronically.

Experiments of this sort have not been carried out on single crystal samples in systems of interest in catalysis. Some experiments on polycrystalline samples of ZnO have been reported by Myaskinkov,[10] but, again, no attempt is made to extract anything quantitative from the experiments. (This would in any case be of dubious value, in view of the use of polycrystalline samples.)

D. $\mathfrak{L}_{n1D}$

This quantity is calculable from n_{1D}, provided that the dielectric constant of the material is known.

E. N_0

This quantity can be determined by extending the adsorption isotherm measurements (see remarks under "λ_A and λ_D" in the foregoing) to high pressures.

F. K

This, the last remaining quantity, cannot be determined without studying the catalysis itself. As was pointed out in a preceding section, it is expected that surface diffusion will not usually be the limiting factor, so that a knowledge of K will not usually be required. To put the matter another way: the determination of the parameters already enumerated suffice to enable one to predict the absolute reaction rate under all conditions except where, at extremely low pressures, the reaction rate is so low that the electronic factor in the catalysis has completely disappeared.

The reader may have noticed that, up to this point, no mention has been made of the usefulness of studying the temperature-dependence of any of the directly determinable quantities, such as the surface conductivity. The point is this. Each one of the parameters discussed in this paper will be expected to be, in greater or smaller degree, temperature-dependent. In consequence, all of the directly determinable quantities will have a temperature-dependence that bears no simple relation to that of any one of the parameters. Once all of the parameters have been determined as a function of the temperature, it will of course be possible to calculate the temperature-dependence of, for example, the surface conductivity under specified conditions: the contrary procedure, however, would hardly seem to be possible, without having at one's disposal all of the necessary information. Let us therefore conclude this section with the remark that it would be far better to concentrate on achieving an understanding of some catalysis system *at one temperature* in the first place. If we are to obtain a quantitative grasp of the process of catalysis at a semiconductor surface—to decide, for example, whether the charge-transfer model is, in some particular case, right or wrong—we must surely expose it to the discipline of a set of quantitative experiments sufficient to enable one to predict, without adjustable parameters, just what will be the absolute reaction rate under specified circumstances.

11. SUMMARY

In this paper we have attempted to set up the charge-transfer theory of catalysis at a semiconductor surface, as originally proposed by Wagner and Hauffe, in a quantitative manner, to the point at which numerical predictions of the absolute reaction rate are made, as a function of the variables that are at the disposal of the experimenter (the pressures, the bulk doping, and the surface charge) and parameters that are accessible to experiments carried out with each of the reacting substances by itself. Equations (8) and (11) give the rates, in terms of the densities of neutral atoms present on the surface, the positions in the energy band diagram of the donor and acceptor levels, the surface concentrations of carriers, and the capture cross sections. Equations (20) and (21) relate the densities of the neutral atoms present on the surface to the pressures, the density of available sites, and the electronic occupancy factors, which themselves are

given, where charge-transfer limitations are in force, by Eqs. (9), (10), (12), and (13), in terms of the positions of the donor and acceptor levels, the densities of neutral atoms and the surface concentrations of carriers. Equations (28) and (39) give, for the special case that there are no intrinsic surface states, that charge transfer occurs exclusively with the conduction band, and that the semiconductor is n type, expressions for the concentration of electrons at the surface in terms of the bulk electron concentration and other quantities mentioned in the foregoing, for the cases that the reaction is acceptor-limited and donor-limited, respectively. Other cases can be handled by the methods outlined in Sec. 7. Saturation effects are included in the theory, and diffusion-limited conditions are handled by means of a bimolecular reaction constant K, not related to any of the above quantities in any simple manner. Cases where injection, extraction or transistor effects may occur are discussed only qualitatively, but methods for their quantitative solution are indicated.

12. ACKNOWLEDGMENTS

I would like to express my appreciation to W. H. Brattain, N. B. Hannay, and J. T. Law for a number of helpful comments on the manuscript.

List of Symbols

A	A neutral acceptor atom or molecule.
A^-	An ionized acceptor atom or molecule.
C_{pD}, C_{nD}, C_{pA}, C_{nA}	Shockley-Read trapping coefficients (cm sec^{-1}).
c_{pD}, c_{nD}, c_{pA}, c_{nA}	Defined in Eq. 3. (cm^3 sec^{-1}).
D	A neutral donor atom or molecule.
D^+	An ionized donor atom or molecule.
E	Energy of a donor or acceptor level (ev).
E_F	Fermi level (ev).
e	Electronic charge (coulombs).
f	Electron occupancy factor.
f_A, f_D	Value of f for acceptors and donors, respectively.
$\mathbf{k}$	Crystal momentum.
k	Boltzmann's constant.
K	Surface reaction constant (mols^{-1} cm^2 sec^{-1}).
$\mathfrak{L}$	Debye length (for the carrier concentration indicated by the suffix; see Eqs. 27 and 28).
n	Density of electrons (cm^{-3}).
n_0	Density of electrons (cm^{-3}) in the bulk.
n_s	Density of electrons (cm^{-3}) just below the surface.
n_{1A}, n_{1D}	Value assumed by n_s when the Fermi level coincides with the acceptor or donor level, respectively.
n_i	Intrinsic carrier concentration (cm^{-3}).
N_A, N_D	Total superficial density (mols cm^{-2}) of acceptors and donors, respectively.
$\mathfrak{N}_A$, $\mathfrak{N}_D$	Superficial density (mols cm^{-2}) of un-ionized acceptors and donors, respectively.
N_0	Surface density (cm^{-2}) of available sites.
n_s^*	Value of n_s at which the reaction changes from donor-limited to acceptor-limited.
Q	Rate of the reaction (mols cm^{-2} sec^{-1}).
p	Density of holes (cm^{-3}).
p_0	Density of holes (cm^{-3}) in the bulk.
p_s	Density of holes (cm^{-3}) just below the surface.
p_{1A}, p_{1D}	Value assumed by p_s when the Fermi level coincides with the acceptor or donor level respectively.
p_s^*	Value of p_s at which the reaction changes from donor-limited to acceptor-limited.
T	Absolute temperature.
Δ	Departure of $(1-f_D)/f_D$ from its equilibrium value.
ϵ	Dielectric constant.
ϵ_0	Permittivity of free space (Far cm^{-1}).
λ_A, λ_D	Langmuir coefficients for un-ionized species. (Equation 16) [cm^{-2}, (mm Hg)$^{-1}$].
ν_0	Vibration frequency (sec^{-1}).
σ_{sc}, σ_{ion}, σ_{ss}	Superficial charge density (coulombs cm^{-2}) associated with, respectively, the space-charge region, the adsorbed ions, and the intrinsic surface states.
τ	Minority carrier lifetime.
τ'	Adsorption relaxation time.

Evidence for Internal Rotation in the Fine Structure of the Infrared Absorption of Oxygen in Silicon

H. J. HROSTOWSKI* AND B. J. ALDER†

Bell Telephone Laboratories, Inc., Murray Hill, New Jersey

(Received December 28, 1959)

Interpretation of the spectra of silicon saturated with oxygen highly enriched with O^{18} confirms that oxygen is located in an interstitial site. The over-all features of the absorption indicate that the oxygen is in a nonlinear Si_2O configuration. The fine structure in the asymmetric Si–O stretching vibration and its temperature dependence can be largely explained by motion of the oxygen in a potential barrier with sixfold symmetry. A symmetry analysis of this process predicts additional structure some of which has now been observed under higher resolution. The spectra of oxygen contaminated silicon containing 2% germanium corroborate our explanation of the fine structure.

The potential barrier hindering rotation of the oxygen about the axis joining its two bonded silicons has been ascribed to the surrounding silicon lattice. Calculation of the potential shows that as the oxygen rotates it can also wobble. Since the fine structure indicates that the ground-state splitting due to rotation is near 2 cm^{-1}, the barrier hindering rotation is about 200 cal/mole. Calculation of this barrier then indicates that the maximum wobble angle is 0.2° and the Si–O–Si angle near 150°.

INTRODUCTION

SMALL amounts of oxygen produce large variations in the optical properties of silicon.[1,2] The most pronounced change occurs in the 1100 cm^{-1} region which exhibits a strong absorption band whose intensity increases linearly with oxygen concentration. This absorption, which has been identified as an Si–O stretching vibration, exhibits an unusual temperature dependent fine structure. Understanding of this structure is complicated by conflicting evidence about the configuration of oxygen in silicon. A previous interpretation of the spectrum suggested that the oxygen is interstitial[2] while recent x-ray and density measurements favor a substitutional position.[3] To resolve this discrepancy, we have obtained the spectrum of the silicon-oxygen system highly enriched with O^{18}. The results are consistent with an interstitial site for oxygen. This configuration suggests that the fine structure results from tunneling of the oxygen atom through a barrier for restricted rotation. A group theoretical analysis of the problem confirms this in that it accounts for the main features of the fine structure. Observation of marked changes in the fine structure produced by altering the local environment gives further experimental verification of this interpretation.

These results suggest that the barrier is caused by the network of neighboring silicon atoms arranged about the Si_2O unit but not bonded to the oxygen atom. This network is highly ordered in the crystalline state and hence produces a barrier of high symmetry. The gross features of the spectrum show that the oxygen is in a nonlinear Si_2O configuration. Then the silicon atoms nearest but not bonded to the oxygen are in positions equivalent to those of the hydrogens in a staggered configuration of ethane. These silicons then give rise to a sixfold barrier as the oxygen rotates about the Si axis of Si_2O. Since the separations of various further distant silicon atoms can also be calculated, their influence on the barrier can be evaluated and possibly more insight into the origin of such barriers can be gained. Since such barriers might occur whenever a small amount of impurity is introduced in a solid lattice, it was thought worthwhile to make a detailed calculation of the barrier based on a simple model of interaction between nonbonded silicon and oxygen atoms. These considerations show a novel feature, namely that the oxygen also wobbles as it rotates. The potential for this behavior is formulated; however, the Schrödinger equation for it has not as yet been solved.

Another interesting aspect of such systems as this is that the temperature can be varied over a wide range. It is thus possible to go from the high-temperature limit of free rotation through restricted rotation to vibration in the potential minimum if the barrier is low. Observations can also be made at very low temperatures where narrower linewidths result in higher resolution. On the other hand, molecules which undergo tunneling or restricted rotation in the gas phase very frequently are locked in a given position on solidification and hence exhibit no fine structure in the solid state.

In the silicon-oxygen system it is possible to estimate the barrier restricting rotation from the temperature dependence of the intensities and the spacing of the fine structure. The position of the oxygen is then roughly fixed by the requirement that the calculated potential be consistent with the barrier deduced from experiment. Thus, the Si–O–Si angle and the extent of the wobble can be approximated.

* Present address: Atomics International, Canoga Park, California.

† Permanent address: Radiation Laboratory, University of California, Livermore, California.

[1] W. Kaiser, P. H. Peck, and C. F. Lange, Phys. Rev. **101**, 1264 (1956).

[2] H. J. Hrostowski and R. H. Kaiser, Phys. Rev. **107**, 966 (1957).

[3] A. Smakula and J. Kalnajs, J. Phys. Chem. Solids **6**, 46 (1958).

EXPERIMENTAL

A silicon rod with resistivity greater than 10^3 ohm cm was saturated with oxygen at the melting point of silicon (1.8×10^{18} atoms/cm^3) by the reduction of water vapor. The composition of the oxygen in the water was 55% O^{18}, 43.5% O^{16}, and 1.5% O^{17}. Spectra of this sample and an unsaturated oxygen-contaminated silicon sample containing 2% germanium were obtained as described previously.[2] Room temperature results for the 1100 cm^{-1} region are shown in Fig. 1 which also gives the spectrum of oxygen-free silicon for comparison. The Si_2O^{16} and Si_2O^{18} absorptions are clearly resolved. Figures 2 and 3 give the low-temperature spectra for both samples containing oxygen. Figure 2 shows that even an Si_2O^{17} absorption is easily detected below 50°K. This figure illustrates the peculiar behavior which concerns us. At room temperature (see Fig. 1) only one broad absorption is observed for

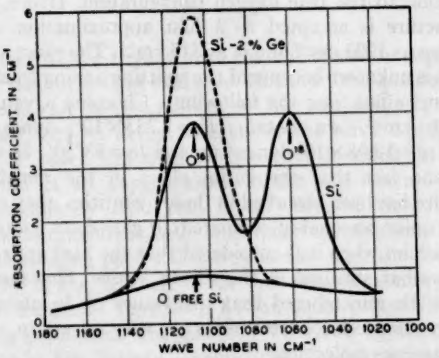

FIG. 1. Room temperature spectra in the 1100 cm^{-1} region.

each isotope. Cooling shifts this to higher energy and separates it into at least three distinct absorptions. The highest energy peak continues to increase in intensity down to 4.2°K. However, the remaining peaks show first an intensity increase followed by a decrease in intensity at lower temperatures. At 4.2°K only the highest energy peak is observed in most samples.

The wave numbers of the observed absorptions are listed in Table I. ν_1 and ν_3 are, respectively, the symmetric and asymmetric stretching motions of the Si_2O "molecule."[2] No isotopic shift was observed for ν_2, the symmetric bending vibration. However, the intensity ratio ν_3/ν_2 was identical with that obtained for samples with lower oxygen concentration. It is hence concluded that ν_2 is definitely an Si–O vibration, but its isotopic shift is less than 3 cm^{-1} which is too small to observe with our equipment. This is reasonable since there is very little motion of the oxygen atom in this vibration.

There is considerable evidence that oxygen may occur in different configurations in silicon. For instance, the major donor produced in oxygen-contaminated silicon by heat treatment[4] is a (distorted) tetrahedral SiO_4 complex.[5] In order to rule out the possibility that some of the behavior of ν_3 arises from absorption by SiO_4 this complex was purposely introduced. The silicon sample was heated at 450°C until a donor concentration, n, of 9×10^{16}/cm^3 was obtained. Although free charge carrier absorption and photoionization increased background absorption considerably, the temperature dependence of ν_3 was invariant within experimental error. The total intensity of the fine structure decreased by about 20% although n was only 5% of the original oxygen concentration. This result is in agreement with the conclusion that the main donor formed by heating is an SiO_4 complex.[5] No discrete vibrational absorptions of this complex were observed

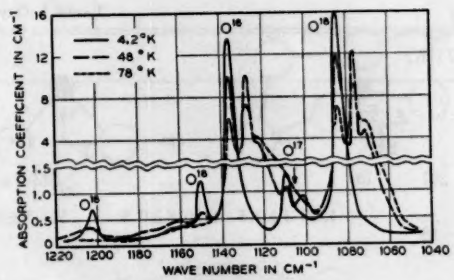

FIG. 2. Variation of ν_3 with temperature for silicon saturated with oxygen of composition 55% O^{18}, 1.5% O^{17}, and 43.5% O^{16}.

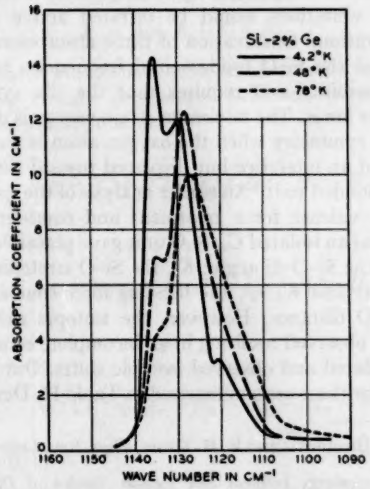

FIG. 3. Temperature variation of ν_3 for oxygen in silicon containing 2% germanium.

[4] C. S. Fuller, J. A. Ditzenberger, N. B. Hannay, and E. Buehler, Phys. Rev. **96**, 833 (1954) and Acta Met. **3**, 1 (1955).
[5] W. Kaiser, H. L. Frisch, and H. Reiss, Phys. Rev. **112**, 1546 (1958).

TABLE I. Oxygen absorptions in cm^{-1}.

T(°K)	Si						Si−2% Ge
	ν_1		ν_2	ν_3			ν_3
	O^{16}	O^{18}	O^{16}	O^{16}	O^{17}	O^{18}	O^{16}
297	...	...	513.5±2	1106±1	...	1058±1	1105±1
48	1203.3±0.5	1150.8±0.5	517.3±0.5	1136±0.3 1127.8±0.3 1122±1	1109±0.3 1101±0.3	1084.4±0.3 1076.7±0.3 1071±1	1135.3±0.3 1128.1±0.3
4.2	1203±0.3	1150.8±0.3	517.3±0.5	1136±0.3	1109±0.3	1084.4±0.3	1135.5±0.3 1129.5±0.3 1120.5±0.5

near 1100 cm^{-1} although numerous electronic bands occur below 500 cm^{-1}.[6]

In addition to the fine structure of ν_3, the important features of the new experimental results are: (1) observation of the 1150.8 cm^{-1} band, the isotopic ν_1 absorption for Si_2O^{18} which then identifies the 1203 cm^{-1} band as an Si–O vibration. (2) Addition of only 2% Ge radically changes the temperature dependence and spacings of the fine structure of ν_3 as shown in Fig. 3. (3) Although it is within the limits of experimental error, there appears to be a decrease in the separation of the subbands of ν_3 as the oxygen mass is increased.

OXYGEN CONFIGURATION

A substitution tetravalent oxygen would have to be in a site of tetrahedral symmetry. Only two fundamental vibrations would be infrared active for this configuration.[7] Observation of three absorptions in the region of the Si–O fundamental frequencies rules out this possibility and requires that the site symmetry be C_{2v} or lower. The minimum strain energy is obtained for this symmetry when the oxygen atom is not at the center of an interstice but displaced toward the silicon atoms bonded to it.[8] An earlier analysis of the spectrum[2] using a valence force treatment and considering the system as an isolated C_{2v} Si_2O unit gave plausible values for 2α, the Si–O–Si angle; K_1, the Si–O stretching force constant; and K_δ/r_0^2, the bending force constant; r_0 is the Si–O distance. However, the isotopic shift of ν_1 was not observed resulting in an incomplete comparison of calculated and observed isotopic shifts. Our present values for these are summarized in Table II. Deviations from the calculated values are less than 1% for 2α as small as 90°. However better agreement is obtained if 2α is quite a bit larger. These considerations indicate that this model, shown in Fig. 4(a), is a reasonable approximation to the true oxygen configuration. Hence, this structure is accepted as a first approximation. ν_1 is taken as 1203 cm^{-1} and ν_2 as 515 cm^{-1}. The exact value of ν_3 is unknown because of the splitting arising from the tunnel effect (see the following). Choosing a value of 1121 cm^{-1}, we obtain $K_1=7.233\times10^5$ dynes/cm, $K_\delta/r_0^2=1.608\times10^5$ dynes/cm, and $2\alpha=93°50'$. In spite of the fact that the entire effect of the remaining lattice has been absorbed in these quantities, they come out quite reasonably compared to gas-phase triatomic molecules when it is considered that the Si_2O system is somewhat strained in the silicon lattice. However, it must be remembered that the values of 2α obtained from valence force treatments are very uncertain, even for gaseous molecules.

When neighboring silicon atoms are considered, the equilibrium position of the oxygen atom is seen to be in the plane of four silicon atoms in a strained trans-cyclohexane configuration as illustrated in Fig. 4(b). Thus, the nature of the vibrational motions is more complicated than those obtained for Si_2O although three oxygen motions are still infrared active. One important difference is that in at least one normal mode the oxygen atom will have some component of its motion perpendicular to the Si_2O plane. It is the constraint on this motion which causes the tunneling of the oxygen atom. Since sufficient information to attempt the complicated vibrational analysis for the Si_6O structure is not available, in what follows only the simple Si_2O model is considered.

FINE STRUCTURE OF ν_3

In order to understand the fine structure, we note that there are six equivalent equilibrium positions for the oxygen atom as indicated schematically in Fig. 4(c). These are separated by potential barriers of height, V_0. When the oxygen atom is constrained to move only in the yz plane of Fig. 4, and only first nonbonded nearest neighbors are considered, the potential

[6] H. J. Hrostowski and R. H. Kaiser, Phys. Rev. Letters **1**, 199 (1958).

[7] G. Hertzberg, *Infrared and Raman Spectra of Polyatomic Molecules* (D. Van Nostrand Company, Inc., Princeton, New Jersey, 1945), p. 252.

[8] Divalent substitutional oxygen, a much less stable configuration, also has C_{2v} symmetry. However, this model is eschewed since the electronic activity expected from the two silicon electrons not used in bonding has not been observed. Furthermore, more precise x-ray measurements by W. Bond and W. Kaiser (to be published in J. Phys. Chem. Solids) contradict the earlier results[3] and favor an interstitial oxygen position.

energy V of the system can be approximated by

$$V=(V_0/2)(1-\cos 6\theta), \quad (1)$$

where θ is the angle of rotation about x. The resultant wave equation[9] is

$$d^2\Psi/d\theta^2+(2I/\hbar^2)[W-\tfrac{1}{2}V_0(1-\cos 6\theta)]\Psi=0, \quad (2)$$

where I is the appropriate moment of inertia. For internal energies W very much greater than V_0 the oxygen will rotate freely in the yz plane with energy levels

$$W_m=m^2\hbar^2/2I \qquad m=0, \pm 1, \pm 2, \cdots. \quad (3)$$

When W is very much less than V_0, the oxygen motion is an oscillation about a particular equilibrium position. In this case the oxygen atom may tunnel to an adjacent minimum through the barrier opposing rotation. The low temperature results can be interpreted by considering only the tunneling process. The temperature then must be

$$T<V_0/k. \quad (4)$$

Quantitative treatment of the fine structure requires information not yet available. However, the qualitative aspects can be determined by the methods of group theory without actual solution of the wave equation. For W much less than V_0 the wave function for the motion of an oxygen atom in the nth minimum is approximately H_v^n. This is the eigenfunction for a linear harmonic oscillator with quantum number v. The corresponding potential energy is shown by the dashed curves in Fig. 5. There is one such function centered at each minimum since each has an equal probability of being populated. The assumed V, shown by the solid curve in Fig. 5, has C_{6v} symmetry. The correct zeroth-order wave functions for this potential must form a basis for a representation of the point group C_{6v}. The characters of the reducible representations, $\Gamma_\pm$, formed by the H_v^n's for even (+) and odd (−) v are given in

TABLE II. Isotopic shifts for Si_2O.

Species	Obs			Calc	
T(°K)	297	48	4.2	$2\alpha=110°$	$2\alpha=90°$
$\nu_3(O^{16})/\nu_3(O^{18})$	1.045	1.047	1.047	1.042	1.038
$\nu_3(O^{16})/\nu_3(O^{17})$		1.024	1.024	1.021	1.019
$\nu_1\nu_2(O^{16})/\nu_1\nu_2(O^{18})$			1.046	1.045[a]	1.052[a]

[a] These quantities are independent of α. The value of 1.045 is for $\nu_2=\nu_2^1$; that of 1.052 for $\nu_2=\nu_2^1+3$ cm^{-1}.

[9] This treatment was introduced by L. Pauling, Phys. Rev. **36**, 430 (1930) for the rotation of small molecules in molecular crystals.

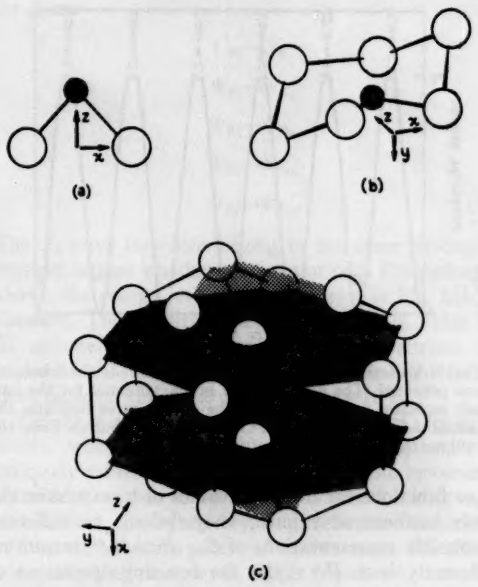

FIG. 4. Configuration of (a) Si_2O and (b) an equilibrium position of oxygen in the lattice; (c) illustrates schematically the oxygen atom in one of the six equivalent equilibrium positions. The first nearest neighbors lie in the dotted planes, the second neighbors in the solid planes.

Table III along with the characters of the irreducible representations of C_{6v}.[10] $\Gamma_\pm$ decompose into

$$\Gamma_+=A_1+B_1+E_1+E_2$$
$$\Gamma_-=A_2+B_2+E_1+E_2. \quad (5)$$

Thus, each vibrational state consists of two singly and two doubly degenerate sublevels whose wave functions are approximately

$$\Psi_{A_1}(v=0)=6^{-\frac{1}{2}}(H_v^1+H_v^2+H_v^3+H_v^4+H_v^5+H_v^6)$$
$$\Psi_{A_2}(v=1)$$

$$\Psi_{B_1}(v=0)=6^{-\frac{1}{2}}(H_v^1-H_v^2+H_v^3-H_v^4+H_v^5-H_v^6)$$
$$\Psi_{B_2}(v=1)$$

$$\Psi_{E_1}(v=0,1)=(12)^{-\frac{1}{2}}(2H_v^1+H_v^2-H_v^3-2H_v^4-H_v^5+H_v^6)$$

$$\Psi_{E_2}(v=0,1)=(12)^{-\frac{1}{2}}(2H_v^1-H_v^2-H_v^3+2H_v^4-H_v^5-H_v^6). \quad (6)$$

Only one function for each degenerate sublevel is listed since these are sufficient to determine the expected temperature dependence of the spectrum. Although

[10] Footnote reference 7, p. 114.

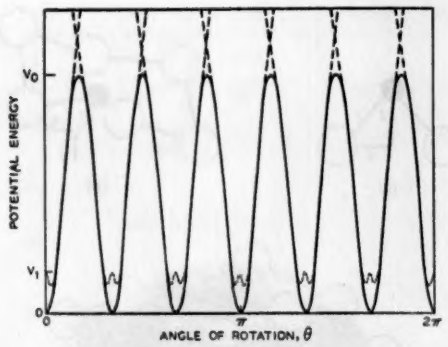

FIG. 5. Variation of V with θ. The solid curve is the schematic cosine potential. The dashed curve is the potential for the harmonic oscillator wave functions. The dotted curve indicates the potential if there were a small twelvefold contribution from the second nearest neighbors.

wave functions for different values of v may have the same mathematical form, they belong to different irreducible representations of C_{6v} since H_0^n transforms differently from H_1^n under the covering operations of the group. With these wave functions the approximate energy levels W_i for $v=0$, 1 are obtained from

$$W_i=\int \Psi_i^* H \Psi_i d\tau, \tag{7}$$

where H is the Hamiltonian operator. If the more improbable processes of tunneling to nonadjacent minima are ignored, the resultant W_i are

$$\begin{aligned} v&=0 & v&=1 \\ E_{A_1}{}^0&=W_{11}{}^0+2W_{12}{}^0 & E_{B_2}{}^1&=W_{11}{}^1-2W_{12}{}^1 \\ E_{E_1}{}^0&=W_{11}{}^0+W_{12}{}^0 & E_{E_2}{}^1&=W_{11}{}^1-W_{12}{}^1 \\ E_{E_2}{}^0&=W_{11}{}^0-W_{12}{}^0 & E_{E_1}{}^1&=W_{11}{}^1+W_{12}{}^1 \\ E_{B_1}{}^0&=W_{11}{}^0-2W_{12}{}^0 & E_{A_2}{}^1&=W_{11}{}^1+2W_{12}{}^1, \end{aligned} \tag{8}$$

where

$$W_{mn}{}^v=\int (H_v{}^m)^* H (H_v{}^n) d\tau. \tag{9}$$

TABLE III. Character table for the point group C_{6v} and the representations $\Gamma_\pm$.

Representation		Group element E	$2C_6$	$2C_3$	C_2	$3\sigma_v$	$3\sigma_d$
A_1	M_z	1	1	1	1	1	1
A_2		1	1	1	1	−1	−1
B_1		1	−1	1	−1	1	−1
B_2		1	−1	1	−1	−1	1
E_1	M_x, M_y	2	1	−1	−2	0	0
E_2		2	−1	−1	2	0	0
Γ_+		6	0	0	0	2	0
Γ_-		6	0	0	0	−2	0

The energy levels are ordered by noting that the most symmetric function, or that with the smallest number of nodes, has the lowest energy. Thus, $E_{A_1}{}^0$ lies lowest for $v=0$, $E_{B_2}{}^1$ for $v=1$. $W_{12}{}^0$ and $W_{12}{}^1$ are, respectively, negative and positive. Since in this approximation the $E_i{}^0$ differ only by the constant $W_{12}{}^0$ and the $E_i{}^1$ by a similar constant $W_{12}{}^1$, the energy level pattern is readily determined. The results are shown schematically in Fig. 6(a).

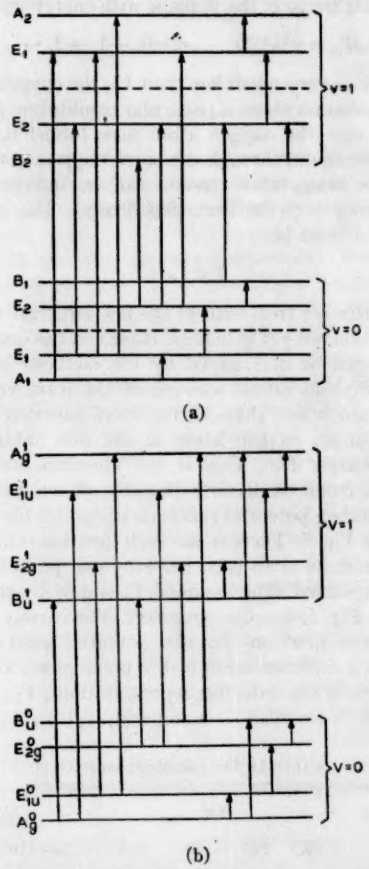

FIG. 6. Energy level patterns for $v=0$ and $v=1$ for (a) C_{6v} symmetry and (b) S_6 symmetry.

Transitions are allowed in the infrared when the direct product $\Psi_0{}^i\Psi_1{}^j$ contains an irreducible representation which transforms like one of the components of the dipole moment, M. The representations to which M_x, M_y, and M_z belong[10] are listed in Table III. Taking the direct products of the irreducible representations of Γ_+ and Γ_- it is found that

$$\begin{aligned} &A_1\times E_1=E_1\times A_2=E_2\times B_2=B_1\times E_2=E_1 \\ &E_1\times E_2=E_2\times E_1=E_1+B_1+B_2 \\ &E_1\times E_1=E_2\times E_2=A_1+A_2+E_2. \end{aligned} \tag{10}$$

Since the components of M belong to A_1 and E_1 (see Table III), fourteen possible transitions are allowed between the various levels for $v=0$ and $v=1$. Three are transitions between sublevels of the ground vibrational state, three between the sublevels for $v=1$. The eight remaining transitions, between levels of $v=0$ and $v=1$, might be observed in the infrared region as fine structure in those Si–O vibrations which most nearly approximate the tunneling motion. All the transitions are shown schematically in Fig. 6(a) and the corresponding energies listed in Table IV, in which

$$C=\int (H_0^n)^* H (H_1^n)\, d\tau.$$

In the preceding treatment it has been assumed that the oxygen is restricted to motion in the yz plane, but the six nearest nonbonded silicon atoms are arranged in a staggered configuration like the hydrogen atoms in an equilibrium position of ethane. As a result of this arrangement the oxygen will not stay in one plane but will wobble as it rotates. Wobbling means that the potential minimum of the oxygen will not always be in a plane perpendicular to the midpoint of the line joining the two bonded silicon atoms (the yz plane of Fig. 4). The angle between this perpendicular plane and the plane actually passing through the midpoint and the oxygen atom is designated by ϕ. The wobble is due to the repulsion between the oxygen and the particular silicon atom it approaches during rotation.

For very small values of ϕ the effective symmetry of the potential will not be changed. However, if ϕ is sufficiently large, the potential will have S_6 symmetry. The relations between the C_{6v} wave functions and those for S_6 are

$$\begin{aligned} &C_{6v}\rightarrow S_6\\ &\Psi_{A_1}\rightarrow\Psi_{A_g}\\ &\Psi_{B_1}\rightarrow\Psi_{B_u}\\ &\Psi_{E_1}\rightarrow\Psi_{E_{1u}}\\ &\Psi_{E_2}\rightarrow\Psi_{E_{2g}}. \end{aligned} \tag{11}$$

The S_6 wave functions belong to the same irreducible representations whether v is even or odd. Proceeding as above, the energy level diagram shown in Fig. 6(b) is obtained. The transition energies are given in Table IV. S_6 symmetry allows four transitions between the sublevels of a vibrational state and again eight transitions between the levels of $v=0$ and $v=1$.

The true symmetry of the potential or, in other words, whether the wobble is important, could be definitely established by observation of the low-energy transitions within a vibrational state. Lacking such information the symmetry might be established by noting that the S_6 potential allows more transitions when only the lowest level, A_g^0, is populated.

TABLE IV. Energies of allowed transitions.

C_{6v}		S_6	
Transition	Energy	Transition	Energy
$A_1^0\rightarrow E_1^0$	$-W_{12}^0$	$A_g^0\rightarrow E_u^0$	$-W_{12}^0$
$E_1^0\rightarrow E_2^0$	$-2W_{12}^0$	$A_g^0\rightarrow B_u^0$	$-4W_{12}^0$
$E_2^0\rightarrow B_1^0$	$-W_{12}^0$	$E_{1u}^0\rightarrow E_{2g}^0$	$-2W_{12}^0$
		$E_{2g}^0\rightarrow B_u^0$	$-W_{12}^0$
$A_1^0\rightarrow E_1^1$	$C+W_{12}^1-2W_{12}^0$	$A_g^0\rightarrow B_u^1$	$C-2W_{12}^1-2W_{12}^0$
$E_1^0\rightarrow E_2^1$	$C-W_{12}^1-W_{12}^0$	$A_g^0\rightarrow E_{1u}^1$	$C+W_{12}^1-2W_{12}^0$
$E_1^0\rightarrow E_1^1$	$C+W_{12}^1-W_{12}^0$	$E_{1u}^0\rightarrow E_{2g}^1$	$C-W_{12}^1-W_{12}^0$
$E_1^0\rightarrow A_2^1$	$C+2W_{12}^1-W_{12}^0$	$E_{1u}^0\rightarrow A_g^1$	$C+2W_{12}^1-W_{12}^0$
$E_2^0\rightarrow B_2^1$	$C-2W_{12}^1+W_{12}^0$	$E_{2g}^0\rightarrow B_u^1$	$C-2W_{12}^1+W_{12}^0$
$E_2^0\rightarrow E_2^1$	$C-W_{12}^1+W_{12}^0$	$E_{2g}^0\rightarrow E_{1u}^1$	$C+W_{12}^1+W_{12}^0$
$E_2^0\rightarrow E_1^1$	$C+W_{12}^1+W_{12}^0$	$B_u^0\rightarrow E_{2g}^1$	$C-W_{12}^1+2W_{12}^0$
$B_1^0\rightarrow E_2^1$	$C-W_{12}^1+2W_{12}^0$	$B_u^0\rightarrow A_g^1$	$C+2W_{12}^1+2W_{12}^0$
$B_2^1\rightarrow E_2^1$	W_{12}^1	$B_u^1\rightarrow E_{2g}^1$	W_{12}^1
$E_2^1\rightarrow E_1^1$	$2W_{12}^1$	$B_u^1\rightarrow A_g^1$	$4W_{12}^1$
$E_1^1\rightarrow A_2^1$	W_{12}^1	$E_{2g}^1\rightarrow E_{1u}^1$	$2W_{12}^1$
		$E_{1u}^1\rightarrow A_g^1$	W_{12}^1

COMPARISON WITH EXPERIMENT

Until the spectrum and its temperature dependence have been investigated under higher resolution, only preliminary conclusions can be drawn from the available data. However, one thing stands out clearly, namely, that W_{12}^0 is of the order of kT at 4.2°K, where k is the Boltzmann constant, since only one high energy absorption has been resolved at this temperature ($kT=2.9$ cm^{-1}). On heating, other higher sublevels of $v=0$ become populated and new absorptions appear. At higher temperatures thermal broadening merges these into one band.

The qualitative temperature variation of the intensities follows then from Boltzmann statistics. The intensity of the 1136 cm^{-1} peak observed at 4.2°K decreases steadily to some limiting value at high temperatures. The other absorptions at 1127.8 and 1122 cm^{-1} appear when kT approaches their energy separations from the ground state. Their intensities show first an increase on heating and then a decrease again as higher states of $v=0$ become populated. At high temperatures these too should reach limiting intensity values. The intensity maximum has been observed for the 1127.8 cm^{-1} peak. The 1122 cm^{-1} peak is resolved near 50°K. Measurements of this peak at higher temperatures are made difficult by thermal broadening and by the shifting of the bands to lower energy. This shift may arise from thermal expansion of the lattice which becomes appreciable near 120°K.[11]

Enough data are available to make a crude estimate of W_{12}^0 from the temperature variation of the intensity ratio of the 1136 and 1127.8 cm^{-1} peaks. It must be

[11] D. F. Gibbons, Phys. Rev. **112**, 136 (1958).

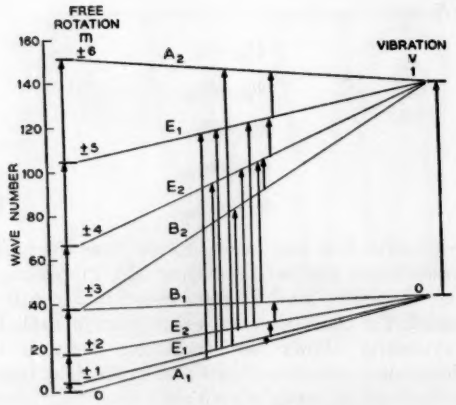

FIG. 7. Schematic variation of the energy levels and allowed transitions for C_{6v} symmetry.

assumed that the transition probabilities of these two absorptions are the same. That, in fact, they do not differ greatly is indicated by the essential temperature independence of the total intensity of ν_3. This calculation is also limited by the uncertainty in the assignment of these bands and by the inaccurate measurements of the intensities resulting from the limited resolution obtainable. Furthermore, the behavior of the 1127.8 cm^{-1} peak seems dependent on sample history.[12] The result of this calculation is that W_{12}^0 is about 5 cm^{-1} which is of the right order of magnitude in spite of the uncertainties mentioned above.[13]

It is not possible with the presently available data to decide which specific transitions correspond to the observed lines or whether the actual symmetry is C_{6v} or S_6. This is particularly so since preliminary results using a prism instrument with higher resolving power indicate still more fine structure. There is some evidence for another weak band below 1122 cm^{-1} near 50°K. Also at 4.2°K there are two pronounced shoulders on the low energy side of the 1136 cm^{-1} band. Previously, these shoulders have been indicated only by a slight asymmetry of the 1136 cm^{-1} absorption. However, in spite of these incomplete data, the fact that an energy of about 2 cm^{-1} is connected with the absorption allows one to estimate the barrier height and to locate the oxygen in the silicon lattice in an approximate way.

[12] The 1127.8 cm^{-1} absorption is sometimes observed at 4.2°K with intensity ranging up to 30% of the 1136 cm^{-1} band. However, this behavior varies considerably for different samples and appears to be dependent on the sample history as shown by H. J. Hrostowski and R. H. Kaiser, J. Phys. Chem. Solids **9**, 214 (1959). This behavior may result from symmetry effects caused by other nearby oxygen atoms which are not uniformly dispersed.

[13] The fact that the energy is so low obviates the possibility that the experimental results may be explained by interaction of the silicon lattice modes with Si_2O vibrations. B. N. Brockhouse, Phys. Rev. Letters **2**, 256 (1959) has found that the lowest energy (transverse acoustical) silicon mode occurs at 140 cm^{-1}. This is more than an order of magnitude too high to account for the temperature dependence of the fine structure.

Of further help would be the temperatures at which the various peaks appear, although these temperatures have not been precisely established.

THE FREE-ROTATION CASE

The earlier value of W_{12}^0 seems very high for a system involving such heavy atoms unless the moment of inertia is rather low. For this reason we consider the free-rotation case ($V_0=0$) which gives an upper limit to the splitting. The energy level scheme is obtained from Eq. (3) and is shown on the left side of Fig. 7. To calculate I it is first assumed that 2α is 90° as suggested by the valence force treatment and that the "normal" Si–O bond length, r_0, is shortened somewhat by the constraints of the silicon lattice. Taking $r_0=1.76$ A and assuming that only the oxygen atom rotates about the fixed Si axis of Si_2O, the value obtained for W_{01} is 0.7 cm^{-1}, which is less than the estimate of W_{12}^0. However, the nonbonded Si–Si distance, r_1, is only 2.48 A. This is extremely close to the normal Si–Si bond distance $r=2.35$ A. The expected repulsion between two nonbonded silicon atoms spaced so closely suggests that

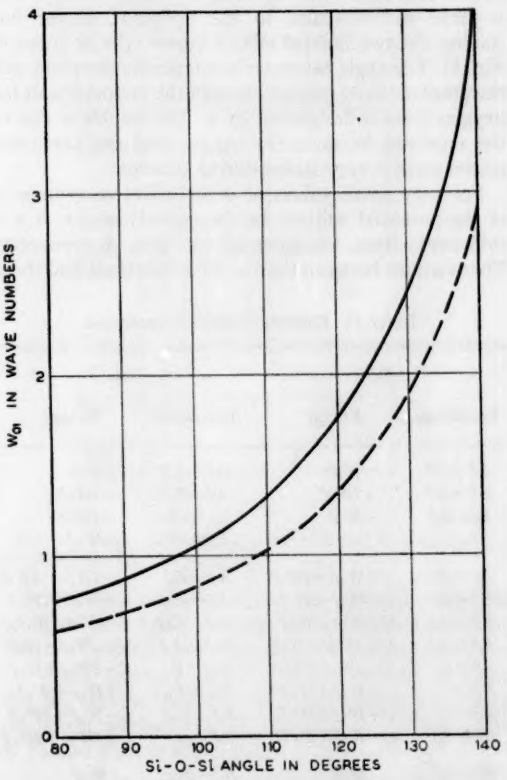

FIG. 8. The separation W_{01} of the lowest two rotational levels as a function of 2α. The dashed curve is for pure oxygen motion. The solid curve is for rotation of Si_2O about its center of mass in the oxygen direction.

r_1 and 2α should be much larger. Furthermore, a larger value of 2α causes less strain in the tetrahedral bond angles of the two silicon atoms bonded to the oxygen.

The dashed curve in Fig. 8 shows the dependence of W_{01} on 2α. W_{01} increases rapidly as 2α increases, reaching 2 cm^{-1} for $2\alpha=132°$. If on the other hand it is assumed that the whole Si_2O unit may rotate about its center of mass along $r_0\cos\alpha$, the solid curve of Fig. 8 is obtained and $W_{01}=2$ cm^{-1} for $2\alpha=124°$. Again W_{01} increases rapidly with 2α, but the motion of the silicon atoms helps to reduce the value of 2α for a given value of W_{01}. These approximations to free rotation are extremes since in the lattice the silicon atoms are neither rigidly restrained nor completely free. The true situation is a compromise. In any event W_{01} can be made larger than W_{12}^0 by stretching the Si–O–Si angle sufficiently. Since oxygen bond angles near 115° are not uncommon in simple molecules, it seems reasonable that a value near 130° could occur in the silicon lattice. For $2\alpha=130°$ and $r_0=1.76$ A, r_1 becomes 3.20 A and the repulsion between nonbonded silicon atoms is considerably reduced. The height h of the oxygen atom above the Si axis is then reduced to 0.83 A. It must be remembered that the actual value of 2α can be still larger since for restricted rotation the splitting would be less than 2 cm^{-1} for the above parameters as shown in Fig. 7.

THE POTENTIAL-RESTRICTING OXYGEN ROTATION

A quantitative treatment of the problem requires knowledge of the potential-restricting rotation. If for the adopted model [Fig. 4(c)] it is assumed that the oxygen is strongly bonded to two silicon atoms and interacts only by van der Waals forces with the remainder of the lattice, the potential can be calculated once the oxygen position is known. The assumption of van der Waals forces could be quite poor inasmuch as the oxygen atom has two unshared pairs of electrons in orbitals whose spatial distributions are not certain. These could give quite a directional character to the interaction with the rest of the silicon network. Because this effect is difficult to take into account quantitatively, one is forced to assume spherically symmetric interactions between the nonbonded silicon and oxygen atoms.

Because of the highly symmetric arrangement of the silicon lattice, the van der Waals interactions produce a symmetric potential V, opposing oxygen rotation about an axis joining the silicon atoms of Si_2O. The barrier to internal rotation can be estimated once the constants in the van der Waals forces are assumed. The oxygen is presumed to perturb only the positions of the silicons to which it is bonded. Those two silicons will have their separation increased so that r_0 and 2α are not too strained. Again it is assumed at first that 2α will be near 90° and that r_0 will be shortened relative to the normal distance by about half the increase in r, the normal Si—Si bond distance, as estimated from the force constants of the two bonds. Under these circumstances r_0 is decreased from 1.83 A to 1.76 A and r increased from 2.35 A to 2.48 A in the Si_2O unit.

The rotational potential, which in this approximation also causes the wobble, will be described by the Lennard-Jones potential. That potential V between two unlike atoms i and j is of the form[14]

$$V_{ij}(r)=4\epsilon[(\sigma^{12}/r_{ij}^{12})-(\sigma^6/r_{ij}^6)], \qquad (12)$$

where r_{ij} is the distance between the atoms, ϵ the depth of the potential, and σ the distance at which the potential is zero. σ estimated from the van der Waals radii of oxygen (1.40 A) and silicon (1.90 A) is $(1.40+1.90)/2^{1/6}=2.95$. The $2^{1/6}$ is the factor which relates the distance to the potential minimum to the distance at which the potential is zero. This value is reasonable judging from the atomic weights of oxygen and silicon since σ must be slightly greater than the neon-neon value (2.8 A) and somewhat smaller than argon-argon value (3.4 A). The value of ϵ must also lie between these two limits (24.5 and 84.0 cm^{-1}), and a value of 38.5 cm^{-1} was chosen. It remains to sum V_{ij} over all the nonbonded silicon atoms to get the total potential of interaction. The distances to the neighboring silicons were determined from the known crystal structure of the silicon lattice and the estimated position of the oxygen. This summation was carried out on an IBM 650 computer.

Seventy-eight neighbors were included in the summation. These comprise a spherical section of the lattice consisting of the first, second, and third neighbor atoms bonded to the Si_2O unit. Actually the number reduces to fifty-four since there are twenty-four coincidences in this section. The more neighbors that are considered, the nearer the center of mass of the system lies on the midpoint between the two bonded silicon atoms. The first six neighbors as already pointed out give rise to a potential with a periodicity of 60° if there is no wobble. The wobble angle ϕ, however, will only be the same every 120° since 60° apart it will have the same magnitude but opposite sign. The 12 second nearest neighbors give rise to no wobble but again to a sixfold barrier to rotation which is displaced by 30° relative to the barrier from the first six neighbors. The remaining atoms, as will be shown, contribute to a good approximation only a constant to the potential. Neglecting the wobble, the contribution of the first six neighbors has the form

$$V=A+B\cos 6\theta. \qquad (13)$$

Addition of the twelve next nearest neighbor contribution merely changes the values of A and B leaving a pure sixfold barrier to rotation.[15] The magnitude of the

[14] J. O. Hirschfelder, C. F. Curtiss, and R. B. Bird, *Molecular Theory of Gases and Liquids*, (John Wiley & Sons, Inc., New York, 1954), p. 32.

[15] If the potential law were such that the second nearest neighbors introduced maxima in the minima resulting from interaction with the first neighbors as shown by the dotted curve in Fig. 5, each vibrational state would consist of two widely spaced sets of sublevels similar to those in Table V if the $v=0$ level lies below the small maxima. ν_3 would then show two separated sets of fine structure contradicting the observed results.

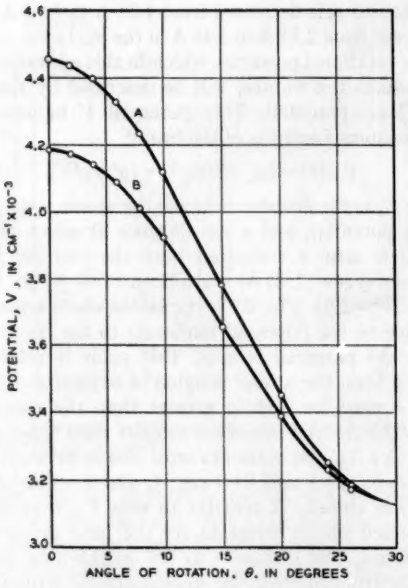

FIG. 9. The potential energy as a function of the angle of rotation. Curve A neglects oxygen wobble while B includes it.

coefficients and the effect of further neighbors were estimated from the parameters listed above with $r_0=1.83$ A and $\alpha=50°$; these are approximately the parameters derived from the valence force treatment for the Si_2O "molecule" in which the oxygen atom is 1.18 A above the Si–Si midpoint. The first 6 neighbors contribute then a potential of $3500+616\cos6\theta$ cm^{-1} or a barrier, V_0, of 1232 cm^{-1}. The second neighbors add an attractive potential—$175-35\cos6\theta$ cm^{-1} or a barrier of -70 cm^{-1}. The 36 further neighbors which have been summed contribute a potential independent of the angle θ of -157 cm^{-1}. This potential varies less than 5 parts in 10^4 with angle and is again attractive. Hence, all 54 neighbors would combine to give

$$V=3167+581\cos6\theta \text{ cm}^{-1} \qquad (14)$$

with $V_0=1162$ cm^{-1}.

The order of magnitude of this V_0 is in line with other known barriers for internal rotation; however, as has been seen, the chosen parameters do not lead to the proper splitting. For the chosen value of 2α the first 6 neighbors being closer than σ to the oxygen atom bring about a large repulsive potential while all further neighbors are far enough away to produce a net attractive potential. The potential of the second nearest neighbors is only 1/20 of the magnitude of the first neighbor contribution so that the effect of still further neighbors is quite small. In fact, the more further neighbors we take into account, the more independent of θ their contribution becomes since on the average they are spherically symmetrically distributed.

The wobble is opposed by a vibrational potential V_W since it involves the stretching of one Si—O bond and the shrinking of the other. V_W can be estimated from the Si_2O model. Since the tunneling is slow compared to the vibrations, the superposition of the symmetry coordinates[16] of the valence force treatment is justified. S_1 and S_2 are only affected to second order by the wobble while S_3 is affected to first order so that one can assume planar motion of the oxygen in the Si_2O plane. Hence to the order of keeping only harmonic terms, valid for small ϕ, the vibrational potential which resists wobbling is

$$V_W=K_1[1+2(M_{Si}/M_0)\sin2\alpha]^2(\Delta S_3)^2. \qquad (15)$$

The effect of the wobble will be to reduce the magnitude of the barrier since the wobble allows the oxygen an extra degree of freedom to find its potential minimum. This will be illustrated for the parameters that were originally proposed as being the most likely, namely $\epsilon=38.5$ cm^{-1}, $\sigma=2.95$ A, $r_0=1.76$ A, and $\alpha=45°$, so that the oxygen is 1.24 A above the midpoint. If no wobble were allowed, the potential from the 54 neighbors would be $3783+665\cos6\theta$ cm^{-1} while with the wobble it becomes

$$V=3657+528\cos6\theta+231(\phi-1.08\cos3\theta)^2 \text{ cm}^{-1}, \qquad (16)$$

that is, the barrier has been lowered from 1330 cm^{-1} to 1057 cm^{-1}. This is a much larger effect than the contribution of the second nearest neighbors. The maximum wobble angle for this configuration is 1.08° and hence quite small. The potential with and without wobble is plotted as a function of angle in Fig. 9. The potential including the wobble is plotted at the value of θ where the potential is a minimum. The variation of the value of ϕ with θ is given in Fig. 10.

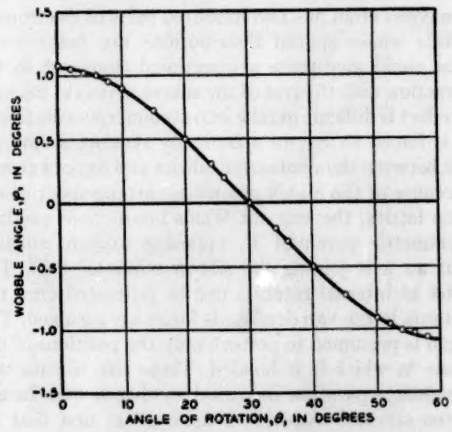

FIG. 10. Dependence of the wobble angle on the angle of rotation for $h=1.24$ A.

[16] Footnote reference 7, p. 149.

A comparison of the two potentials given so far without wobble shows that the barrier decreases with decreasing height h of the oxygen above the midpoint (1330 or 1162 cm^{-1} for h equal to 1.24 A and 1.18 A, respectively.) Reducing h to 1.09 A decreases the barrier to 552 cm^{-1}. This is as expected since the repulsion decreases. Furthermore, the maximum angle of wobble is, as expected, also smaller when the repulsion is weaker. This was learned by varying ϵ and σ in the potential over a range which is thought to include the extreme values they could assume in this general model. This study also shows that these extreme ranges of the parameters produce a change in the potential barrier and the maximum wobble angle of less than a factor of 2, which is surely comparable to the accuracy of the model. The formulas for V fit the results calculated from (12) to better than 70 cm^{-1} which is sufficient accuracy considering the crude basis of the theory.

Most of these results were obtained for structural parameters which maintained 2α near 90°. Information about the correct configuration can be obtained by assuming that the true reduced mass for the motion is the oxygen mass and by considering tunneling to an adjacent minimum. In this approximation the Dennison-Uhlenbeck[17] formula can be used to calculate the splitting. For $2\alpha=90°$ (that is, a barrier of 1057 cm^{-1}), the vibrational levels, calculated using a force constant determined from the slope of the cosine potential, are separated by 161 cm^{-1}. About six bound levels would be below the barrier. The separation of these is such that at 50°K (35 cm^{-1}) the first excited level is hardly populated, and the ground state splitting is negligible (2×10^{-10} cm^{-1}). These results contradict the experimental evidence and are not unexpected from the analysis of the free-rotation case. Thus, 2α must be increased. It is possible to estimate the true value by calculating the barrier which permits a splitting of about 2 cm^{-1} in the $v=0$ levels.

If it is assumed that 2α is 130° and $h=0.83$ A as indicated from the free-rotation case, the calculated barrier is 220 cm^{-1}. The separation of the harmonic oscillator levels is 110 cm^{-1}. The ground-state splitting is about 10^{-9} cm^{-1} and still too small. If the barrier is 56 cm^{-1} (160 cal), then the $v=0$ splitting is 2.3 cm^{-1}. The zero point energy puts the ground state at 46 cm^{-1}, so that the first excited vibrational state is well out of the barrier.[18] The height of the oxygen above the Si axis is about 0.5 A, and the maximum wobble angle would be about 0.15° and 2α about 150°. The lowest two free-rotor states for these parameters are separated by 4.2 cm^{-1}.

The above estimates of the small barriers from the adopted model are quite uncertain. A small barrier means [see Eq. (12)] that the repulsive and attractive forces nearly cancel, and hence the value of σ must be known with more precision then it is possible to estimate it. Furthermore, the nonbonded Si–Si distance is increased by about 1 A in the Si_2O unit. Hence, it is likely that the neighboring silicon network is also somewhat distorted. The energy is also small enough so that all sorts of spherically asymmetric forces could be of importance.

The conclusion one is led to then is that this case represents an intermediate case between free rotation and tunneling. If the wobbling can be neglected, the energy levels could be obtained in terms of Mathieu functions. If not, the Schrödinger equation for the problem has to be solved. Converting to spherical polar coordinates the energy levels are obtained from the equation

$$\{(\sin\theta)(\partial/\partial\theta)[\sin\theta(\partial/\partial\theta)]+(\sin^2\theta)^{-1}(\partial^2/\partial\phi^2) +(2I/\hbar^2)(W-V)\}\psi=0 \quad (17)$$

where V is of the form given by (16) and $I\leq M_0h^2$.

DISCUSSION

From the preceding considerations it seems likely that the fine structure in the 1100 cm^{-1} region arises from combination bands involving a normal mode of Si_2O and the ground-state energy levels of the tunneling motion. Thus, the $v=0$ to $v=1$ transitions shown in Figs. 6 and 7 have apparently not been observed. In any case, the observed fine structure is due to a sixfold potential in which only the lowest vibrational level lies below the barrier. If the barrier were larger, it would be impossible to get the observed splittings and temperature dependence of the intensities. The lack of structure in ν_1 and ν_2 indicates that these vibrations have very little motion in the direction required to permit tunneling. The low barrier and the lack of structure in ν_1 and ν_2 indicate that the Si–O–Si angle is very large. Furthermore, an increase in 2α to 130 degrees also lowers K_1 from 7.23 to 5.35×10^5 dynes/cm giving much closer agreement with the value of 5.0×10^5 dynes/cm estimated by other means.[19] Also, the isotopic ratio of the ν_3 frequency comes into better agreement with experiment for larger angles. The fact that the valence force treatment gives a poor value of the angle is not surprising from past experience.

More striking confirmation comes from the variation of ν_3 on addition of 2% germanium. It is known that germanium substitutionally replaces silicon in the lattice; thus the environment of a large fraction of the oxygen atoms is altered. For random substitution about 4% of the oxygen would exist in SiOGe units. These should absorb at lower energy (near 900 cm^{-1}) because of their higher reduced mass and the smaller value of

[17] D. M. Dennison and G. E. Uhlenbeck, Phys. Rev. **41**, 313 (1932).

[18] If we use an Si–O distance common in solids (1.62 A) this conclusion is not changed. In fact, this value makes it easier to obtain a low barrier.

[19] N. Wright and M. J. Hunter, J. Am. Chem. Soc. **69**, 803 (1947).

the Ge–O stretching force constant. Although the expected intensity is sufficiently high ($\alpha_{max} \approx 1$ at 4.2°K), no absorption attributable to this unit was detected. Furthermore, Kaiser and Thurmond,[20] in attempts to introduce oxygen into germanium rich germanium-silicon alloys, found that a two-phase system of SiO_2 and germanium resulted. They concluded that no Ge—O bonds are formed as long as silicon is present. Therefore, the absorption in Fig. 3 results from Si_2O units, and the environment of a large fraction of these is altered by the presence of germanium neighbors. For these oxygens the symmetry of the barrier is lowered, and also the magnitude of the barrier is changed. With the assumption of van der Waal's interactions the barrier height would increase as a silicon is replaced by a larger germanium atom. Since the magnitude of the barrier, as has been seen, is primarily affected only by the nearest nonbonded atoms, the results for germanium-doped silicon shown in Fig. 3 might then be interpreted as a superposition of the spectra of two species. The single peak at 1135.5 cm^{-1} is probably due to oxygen entirely surrounded by silicons, the two additional peaks to oxygens which have a single nonbonded germanium neighbor. This interpretation would be consistent with a higher barrier since the observation of more resolved bands at 4.2°K for the germanium doped sample could imply that more $v=0$ levels are occupied at this temperature. That the barrier is higher and consequently the splitting of the energy levels smaller is confirmed from spectra of oxygen-contaminated pure germanium samples. In such samples no fine structure could be resolved in the 860 cm^{-1} asymmetric Ge–O stretching vibration.[1] The most clear-cut evidence for the proposed model, however, is still the fact that by changing the environment the fine structure has been changed markedly.

Higher resolution spectra of both systems at more frequent temperatures will provide the confirming evidence needed for the proposed model. Numerical values of the masses and the potential barriers involved in the motion can then be obtained from comparison of the experimental spacings; particularly helpful would be the observation of transitions between different vibrational states of the actual tunneling motion. According to this treatment these should occur near 100 cm^{-1}. Furthermore, the true ground state separations can be deduced from the intensity variation of the fine structure. Experiments in the very low energy region (2 cm^{-1}) would also give such values from direct observation of the transitions within a given vibrational state.

[20] W. Kaiser and C. D. Thurmond, unpublished results.

ACKNOWLEDGMENTS

We are indebted to Dr. W. Kaiser for stimulating discussions and for providing many of the samples. We have also benefited from enlightening conversations with Professor W. D. Gwinn. Dr. R. G. Shulman has been helpful in suggesting important revisions of the manuscript. We also wish to acknowledge the assistance of Mr. R. H. Kaiser in obtaining the experimental results.

Cuprous Halide Films on Alkali Halide Crystals*

L. M. KRAEMER

Argonne National Laboratory, Argonne, Illinois, and The University of Chicago, Chicago, Illinois

(Received August 28, 1958)

Films of cuprous halides were formed by evaporation and condensation in a vacuum onto substrates of alkali halide crystals at room temperature. They were annealed for 15 min periods at temperatures between 60° and 150°C. Optical absorption spectra indicate that the annealing causes diffusion of CuCl and CuBr into KCl and KBr, but not into KI or NaCl, and of CuI into RbI, but not into KCl, KBr, KI, or NaCl. An interstitial mechanism for diffusion is consistent with the data but is not sufficient to account for the behavior of CuI.

INTRODUCTION

MONOVALENT copper in alkali halide crystals and in silver halide crystals is known to diffuse with unusual rapidity at temperatures above 200°.[1] A qualitative investigation of diffusion in alkali halide crystals at lower temperatures was made by taking advantage of differences in the optical absorption of cuprous halide and of cuprous ion dispersed in alkali halide. The optical absorption spectra at liquid nitrogen temperature of cuprous halide films deposited upon quartz plates are characterized by sharp peaks near 400 mμ (CuCl, 376.1 and 384.4 mμ; CuBr, 396.7 and 415.5 mμ; CuI, 335 and 405 mμ),[2] while those of cuprous ion dispersed in alkali halide single crystals consist of intense broad bands near 260 mμ (KCl–Cu, 263 mμ; KBr–Cu, 265 mμ; KI–Cu, 268 mμ; NaCl–Cu, 255 mμ) with no absorption in the region near 400 mμ.[3] When the cuprous halide film is deposited upon an alkali halide single crystal, transference of cuprous ion into the alkali halide substrate can be detected by appearance of the characteristic dispersed spectrum and reduction of the film absorption.

EXPERIMENTAL PROCEDURES

Apparatus and procedures used in the evaporation of thin films were those described by Delbecq and Yuster.[4] Heat for annealing was supplied by an element placed in the well of the Dewar; annealing temperatures were usually maintained for fifteen minutes with heating rates of 3° to 6° per minute. Optical spectra were taken at liquid nitrogen temperature with a Cary No. 11 spectrophotometer. Alkali halide crystals were grown by the Kyropoulos method or obtained from Harshaw Chemical Company Copper halides were prepared according to directions in *Inorganic Syntheses*[5] using the drying technique of Tubandt, *et al.*[6]

FILMS

The absorption spectra of cuprous halide films deposited upon alkali halide crystals at room temperature, before annealing, were the same as those of the films deposited upon quartz.

After annealing CuCl or CuBr films upon KCl or KBr for 15 min at 150°C, the absorption characteristic of the cuprous halide was much reduced and that of cuprous ion dispersed in potassium halide appeared.[7] At lower annealing temperatures this effect occurred most readily with CuCl on KCl (after 15 min at 60°) and least readily for CuBr on KBr (after 15 min. at 125° but not at 100°). See Fig. 1. Annealing a film of CuI on KI, even at 200°, and of CuI upon KCl and KBr produced no such change in the absorption but only some increase in the height and resolution of the peaks near 400 mμ, as was the case for CuI film on quartz upon similar treatment.[8] The spectrum of CuI on RbI also was essentially unchanged by annealing at 100° but 15 min at 150° resulted in a marked decrease in the absorption characteristic of CuI, while a high absorption band (presumed to arise from cuprous ion dispersed in RbI) appeared at 310 mμ. Annealing CuCl or CuBr films on KI produced absorption characteristic of CuI as well as of CuCl or CuBr, with no evidence of cuprous ion dispersed in KI.

When the halide of film and crystal were unlike, new absorption bands appeared upon annealing: at 292

* Based on work performed under the auspices of the U. S. Atomic Energy Commission.

[1] S. A. Arzybyschew and N. B. Borissaw, Phys. Z. Sowjetunion **10**, 44 (1936); S. A. Arzybyschew, Phys. Z. Sowjetunion **11**, 639 (1937); Tubandt, Reinhold, and Jost, Z. anorg. u. allgem. Chem. **177**, 268 (1928); C. Tubandt, Z. Elektrochem. **39**, 500 (1933).

[2] The observed maxima are in agreement with those reported by S. Nikitine and R. Reiss, Compt. rend. **242**, 1003 (1956), except for the lower wavelength maximum of CuBr which they give as 4116 A. The 405 mμ absorption in CuI is frequently, but not invariably, resolved into a doublet with maxima at 404 and 406 mμ.

[3] A. Smakula, Z. Physik **45**, 1 (1927); A. M. MacMahon, *ibid.* **52**, 336 (1928); M. Forro, *ibid.* **56**, 235 (1929). Absorption between 300 and 400 mμ appears after a time but, when the copper concentration is no more than 10^{-3} mole fraction, can easily be removed by heating the crystal at temperatures above 300°C.

[4] C. Delbecq and P. H. Yuster, J. Chem. Phys. **22**, 921 (1954).

[5] W. C. Fernelius, Editor, *Inorganic Syntheses* (McGraw-Hill Book Company, Inc., New York, 1946), p. 1.

[6] Tubandt, Rindtorff, and Jost, Z. anorg. u. allgem. Chem. **165**, 195 (1927). In the case of CuI, iodine was driven off and condensed in the cold trap; drying near the fusion temperature was continued until no further condensation could be seen.

[7] A small peak on the short wavelength side of the characteristic absorption near 260 mμ appeared in these spectra but not in those of crystals prepared by the Kyropoulos method.

[8] The change in height and resolution is attributed to reduction of lattice defects; cf. F. Fisher, Z. Physik **139**, 328 (1954).

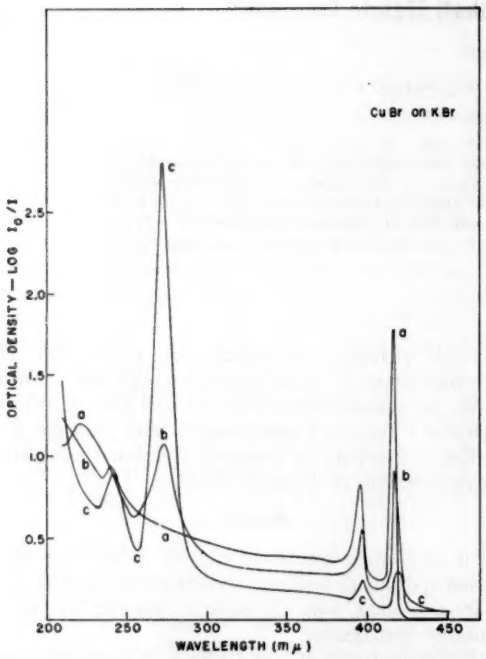

FIG. 1. Optical spectra at liquid nitrogen temperature of CuBr film on KBr crystal: (*a*) 15 min at 100°; (*b*) 15 min at 125°; (*c*) 10 min at 150°. Absorption of curve *a* is that of CuBr; absorption between 250 and 300 mμ corresponds to that of KBr–Cu.

mμ (CuCl on KBr), 282 mμ (CuCl on KI), 275 mμ (CuBr on KI). These disappeared when continued annealing removed the absorption characteristic of the original film; the absorption then was that of cuprous ion dispersed in the crystal lattice (e.g., CuCl on KBr→Cu^+ in KBr) or that of the cuprous halide corresponding to the alkali halide (CuCl on KI→CuI on KI). This new absorption (see Fig. 2) was not seen if the crystal was maintained at dry ice or liquid nitrogen temperature during the deposition of the film, but then would appear after warming to room temperature for about 5 min. It seems likely that this new absorption peaks arise from cuprous ion in a cuprous halide lattice with two kinds of halogen ions. The appearance of the 275 mμ absorption in CuBr on KI and the 282 mμ absorption in CuCl on KI supports this view, since CuI apparently does not diffuse into KI under the experimental conditions. The absence of such a peak for CuBr on KCl may be the result of more rapid diffusion of Cu^+ into KCl.

TABLE I. Atomic distances in cuprous and alkali halide crystals.[a]

Species	M-X distance (Observed)	Interstitial distance[b] (Calculated)	Cu-*X* distance with Cu^+ in the interstitial position (Calculated)		
			Na*X*	K*X*	Rb*X*
CuCl	2.35 A	...	1.99 A	2.22 A	...
CuBr	2.46	...	2.11	2.33	...
CuI	2.63	...	...	2.50	2.59 A
NaCl	2.81	0.35 A			
KCl	3.14	0.82			
KBr	3.29	0.75			
KI	3.53	0.67			
RbI	3.66	0.86			

[a] Copper halides from R. W. G. Wyckoff, *Crystal Structures* (Interscience Publishing Company, Inc., New York, 1948), Vol. I, Chap. III, p. 29. Alkali halides from Linus Pauling, *The Nature of the Chemical Bond* (Cornell University Press, Ithaca, New York, 1948), p. 352.

[b] *X*–*X* distance minus twice the halogen ion radius given by Pauling (see reference 9).

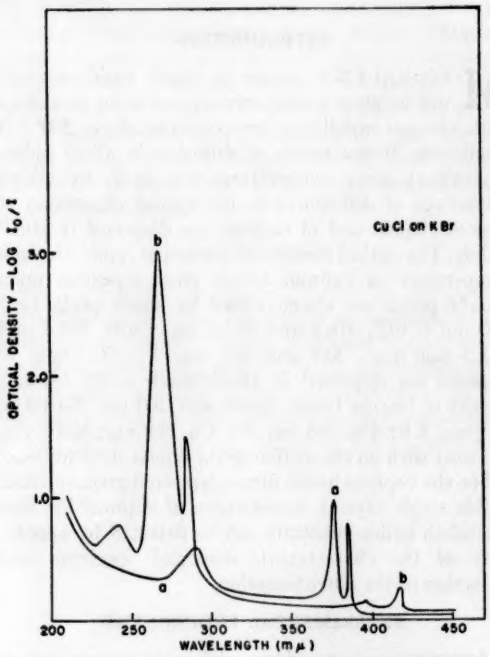

FIG. 2. Optical spectra at liquid nitrogen temperature of CuCl film on KBr crystal: (*a*) before annealing; (*b*) 10 min at 90°. Curve *a* shows absorption of CuCl and the new absorption referred to in the text.

Films of CuCl and CuBr were also deposited upon NaCl crystals. The spectra (see Fig. 3) of these, upon annealing, were modified only by the resolution into doublets of the larger of the peaks near 400 mμ—the 376 mμ band of CuCl on NaCl into 375 and 377.4 mμ and the 416 mμ band of CuBr on NaCl into 415.3 and 417.5 mμ. Repeated annealing at 150°C increased the resolution, but had no other effect. The resolution of these bands was never seen when the films were deposited upon quartz, potassium halides, or LiF, although the presence of two components was suggested by the flattening of the peaks (for CuCl or CuBr on KCl or KBr) after annealing had been continued until considerable diffusion into the crystal lattice occurred.

DISCUSSION

The different responses to annealing of CuCl films upon NaCl and upon KCl suggest that the dimensions of the underlying lattice are important in determining the diffusion from the film. The size of the cuprous ion is that of the sodium ion (0.95 A), while the ionic radius of potassium ion is 1.28 A[9]; thus one would anticipate that cuprous ion would readily substitute for Na^+ in the NaCl lattice but would produce considerable distortion in a positive ion position in the KCl lattice. Relatively high concentration of Cu^+ ion in NaCl–Cu crystals as compared with KCl–Cu crystals would then be predicted, and was observed experimentally upon preparation of these crystals by the Kyropoulos method.

The larger dimensions of the KCl lattice, however, would favor an interstitial position for Cu^+ in that lattice. (The anionic portion of the cuprous halide lattice—zincblende structure—is identical in arrangement to that of the corresponding face-centered cubic alkali halide lattice. The positions of cuprous ion and alkali metal ions in the respective lattices are interstitial to each other.) The atomic distances listed in Table I suggest that interstitial diffusion of cuprous ion from the copper halide film into alkali halide crystal is sterically possible for the potassium halides but doubtful for the sodium halides. The results of the annealing of copper halide films on alkali halide crystals are in agreement with a hypothesis of interstitial diffusion i.e., no diffusion of CuCl into NaCl, relatively ready diffusion of CuCl, CuBr, and CuI into KCl, KBr, and RbI, respectively.[10]

The increasing difficulty of diffusion in the potassium halide series—KCl, KBr, KI— is correlated with decreasing interstitial distance between halide ions (see Table I), but that alone is not enough to explain the behavior of CuI. If interstitial distance alone determined diffusion of Cu^+ from the film into base lattice, CuI would diffuse into KCl as readily as does CuCl; but CuI does not diffuse into KCl even at 150°, while it does so into RbI at 150° but not at 100°.

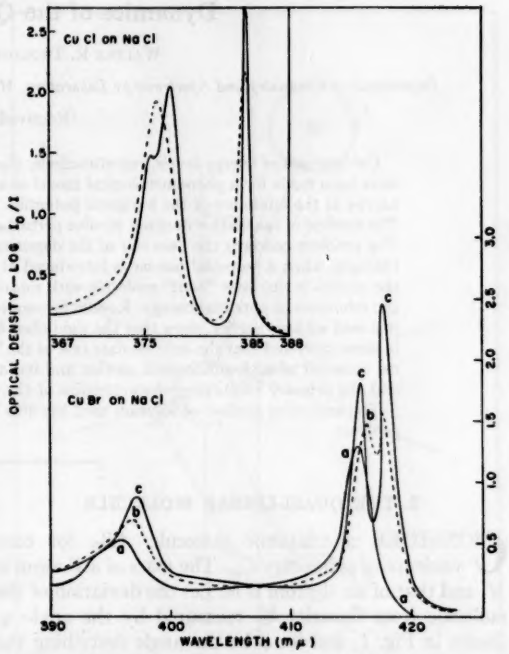

FIG. 3. Optical spectra at liquid nitrogen temperature of CuCl and CuBr films on NaCl crystals. For CuCl: Dashed curve, before annealing; solid, after two 15-min anneals at 100° and one 15-min anneal at 150°. For CuBr: (*a*) before annealing; (*b*) 15 min at 100°; (*c*) 15 min at 150°.

The resolution of the 376 mμ peak of CuCl film when on NaCl crystal and of the 416 mμ peak of CuBr when on NaCl suggest some interaction between cuprous ion and NaCl lattice even though no diffusion into the NaCl lattice seems to occur. Spectra of CuI film upon alkali halide crystals give no indication of interaction with the base lattice.

ACKNOWLEDGMENTS

The author is indebted to Dr. Charles J. Delbecq and to Dr. Philip H. Yuster for many stimulating discussions and numerous suggestions and to Elson Hutchinson for crystals grown by the Kyropoulos method.

[9] Linus Pauling, *The Nature of the Chemical Bond* (Cornell University Press, Ithaca, New York, 1948), p. 346.

[10] An interstitial mechanism cannot be the only one. Changes in the optical spectra of NaCl–Cu crystals (when Cu^+ concentration is greater than 10^{-4} mole fraction) occur at temperatures between 25° and 150°C. At 25° the initial change in the spectrum can be seen within an hour and, upon standing at room temperature for some months, the 376 and 384 mμ absorption peaks characteristic of CuCl at liquid nitrogen temperature appear, while the 255 mμ absorption of Cu^+ dispersed in NaCl is reduced. Heating NaCl–Cu crystals at 140° for several hours produces the same effect; the reverse process, rapid dispersion of cuprous ion, occurs when the temperature is raised above 300°C. Potassium halides, including KI–Cu, show corresponding behavior.

Dynamics of the Quasi-Linear Molecule

WALTER R. THORSON AND ICHIRO NAKAGAWA

Department of Chemistry and Spectroscopy Laboratory, Massachusetts Institute of Technology, Cambridge, Massachusetts

(Received April 7, 1960)

Calculations of energy levels, eigenfunctions, dipole transition moments, and other significant properties have been made for a phenomenological model of a two-dimensional harmonic oscillator with a superposed barrier at the minimum of the harmonic potential. A high-speed electronic digital computer was employed. The method of calculation does not involve perturbation theory and converges rapidly for all barrier heights. The problem concerns the behavior of the degenerate bending vibration of a linear triatomic molecule, for example, when a potential barrier is introduced at the linear configuration. In the limit of a high barrier, the motion is that of a "bent" molecule with rotational motion superposed on the bending vibration about the minimum of potential energy. Results for moderate to low barriers, and those for anharmonic vibration in a well with no barrier, show that the rigid classification of molecules as "linear" or "bent" is not possible in some cases and that the intermediate case of the "quasi-linear" molecule must be considered. The dynamical behavior of such anharmonic motion and its interaction with other vibrations have been investigated, and the primary identifying characteristics of the quasi-linear molecule delineated.

The analytical method of solution used has also been applied successfully to the one-dimensional barrier problem.

I. THE QUASI-LINEAR MOLECULE

CONSIDER a triatomic molecule AB_2, for convenience of symmetry C_{2v}. The mass of a B atom is M, and that of an A atom is m. Let the deviation of the molecule from linearity be measured by the angle α, shown in Fig. 1, and let ϕ be the angle describing the azimuthal direction of the AB_2 plane. Let the equilibrium A–B distance be R_0. This problem concerns the effects of a nonharmonic potential for the angle α. In any case, the potential is independent of ϕ. Further assume that the potential for the bond-stretching motions is essentially harmonic and that their frequencies are significantly higher than the frequency of bending motion. (This last assumption is sufficiently valid for every case in which the analysis in terms of a quasi-linear model is of interest.)

The generalized analysis of the dynamics of systems with some slowly varying coordinates has been made by Newton and Thomas.[1] They outline a method for writing the Hamiltonian in terms of "high-frequency" coordinates δ_k and the slowly varying coordinates q_α. (We already shall assume the center-of-mass translation is separated out.)

A. Dynamic Analysis

Let X, Y, Z be right-handed Cartesian coordinates of the atoms in a nonrotating system with origin at the center of mass, and x, y, z the right-handed Cartesian coordinates in a system rotating with the molecular frame. Let θ, ψ be the Eulerian angles fixing the relation of the z axis to the external Z axis. The plane of the molecule defines the xz plane; when the molecule is strictly linear only the z axis, the axis of symmetry, is defined. θ, ψ are thus the variables for rotation of the entire molecule. The remaining Eulerian angle ϕ is the angle measured counterclockwise from the line of nodes to the x axis and is the variable for rotation about the z axis.

The B atoms are labeled 1 and 3 as shown, and the atom A is 2. Small high-frequency displacements of the bond distances R_{12} and R_{23} from the equilibrium R_0 occur, and we call them Δ_{ij}. It is convenient to work with the symmetry coordinates $s=1/\sqrt{2}(\Delta_{12}+\Delta_{23})$ and $a=1/\sqrt{2}(\Delta_{12}-\Delta_{23})$, hereafter called symmetrical and asymmetrical stretching coordinates, respectively. The coordinates α and ϕ we shall treat as the slowly varying coordinates of the Newton-Thomas treatment. We define the "zero coordinates" $\mathbf{r}_i^0$ in terms of α

$$\begin{aligned} &z_1^0=R_0\cos\alpha=-z_3^0, \qquad z_2^0=0;\\ &x_1^0=(m/m+2M)\,R_0\sin\alpha=x_3^0,\\ &x_2^0=-(2M/m+2M)\,R_0\sin\alpha;\\ &y_i^0=0 \qquad i=1,2,3. \end{aligned} \tag{1}$$

We also define the instantaneous coordinates

$$\mathbf{r}_i=\mathbf{r}_i^0+\sum_\kappa \mathbf{r}_i^\kappa\delta_\kappa. \tag{2}$$

The vectors $\mathbf{r}_i^\kappa$ satisfy the following conditions and definitions:

$$\begin{aligned} &\sum_i m_i\mathbf{r}_i^\kappa=0; \qquad &&\sum_i m_i(\partial\mathbf{r}_i^0/\partial\alpha)\cdot\mathbf{r}_i^\kappa=0;\\ &\sum_i m_i[\mathbf{r}_i^0\times\mathbf{r}_i^\kappa]=0; \qquad &&\sum_i m_i(\mathbf{r}_i^\kappa\cdot\mathbf{r}_i^\lambda)=0, \quad \kappa\neq\lambda;\\ & && =1/V_k, \quad \kappa=\lambda. \end{aligned} \tag{3}$$

The components of the vectors $\mathbf{r}_i^\kappa$ are given in Table I. Furthermore,

$$\begin{aligned} &1/V_s=M/[1+(2M/m)\sin^2\alpha];\\ &1/V_a=\mu/2[1-(\mu/m)\sin^2\alpha], \end{aligned} \tag{4}$$

where μ is the reduced mass $\mu=2Mm/(m+2M)$.

[1] R. R. Newton and L. H. Thomas, J. Chem. Phys. **16**, 310 (1948).

The vibrational and rotational kinetic energy, in terms of the angular velocity ω of the rotating frame, and the time derivatives of the coordinates, is

$$T=\tfrac{1}{2}\sum_i m_i[\omega\times(\mathbf{r}_i^0+a\mathbf{r}_i^a+s\mathbf{r}_i^s)]^2$$
$$+\tfrac{1}{2}\sum_i m_i\left[\frac{\partial\mathbf{r}_i^0}{\partial\alpha}+a\frac{\partial\mathbf{r}_i^a}{\partial\alpha}+s\frac{\partial\mathbf{r}_i^s}{\partial\alpha}\right]^2\dot{\alpha}^2$$
$$+\tfrac{1}{2}\sum_i m_i[\mathbf{r}_i^a\dot{a}+\mathbf{r}_i^s\dot{s}]^2+\sum_i m_i[\omega\times\mathbf{r}_i]\cdot[\partial\mathbf{r}_i/\partial\alpha]\dot{\alpha}$$
$$+\sum_i m_i[\omega\times\mathbf{r}_i]\cdot[\mathbf{r}_i^a\dot{a}+\mathbf{r}_i^s\dot{s}]$$
$$+\sum_i m_i[\partial\mathbf{r}_i/\partial\alpha]\cdot[\mathbf{r}_i^a\dot{a}+\mathbf{r}_i^s\dot{s}]\dot{\alpha}. \quad (5)$$

The first term is the instantaneous kinetic energy of rotation, and the second and third terms are the simple vibrational kinetic energies. The fourth and fifth terms are vibration-rotation interactions, and the last term represents interactions between the rapid vibrations and the slow vibration in the coordinate α. For our purposes it is sufficient to use $\frac{1}{2}\sum_i m_i[\omega\times\mathbf{r}_i^0]^2$ for the first term, thus neglecting rotational distortion effects on the stretching motion. The third term is simplified to $(1/V_s)\dot{s}^2+(1/V_a)\dot{a}^2$. Since $\mathbf{r}_i^0$, $\mathbf{r}_i^a$, $\mathbf{r}_i^s$ all have vanishing y components, it is easily seen that only the terms dependent on ω_y make any contribution to the rotation-vibration interactions in the fourth and fifth terms. These complicated expressions may have significant interactions for high velocities of rotation around the y axis, but we ignore them in this simpler treatment. In fact, only the rotation about the z axis is retained for consideration; the fine structure arising from the large moments I_{xx} and I_{yy} is not studied. The moment I_{zz} is given by $\mu R_0^2\sin^2\alpha$.

Remaining terms have contributions which may be expanded in powers of the parameters (s/R_0), (a/R_0) and their time derivatives. Keeping only the lower-order terms, we obtain (rotational kinetic energy about the x and y axes is not included)

$$T=(\tfrac{1}{2}V_s)\dot{s}^2-2M^2/m(s\dot{s}/R_0^2)(r\dot{r})+(\tfrac{1}{2}V_a)\dot{a}^2$$
$$+\mu^2/2m(a\dot{a}/R_0^2)(r\dot{r})$$
$$+\tfrac{1}{2}\{\mu\dot{r}^2+[4M^2/(m+2M)](r/R_0)^2\dot{r}^2\}$$
$$+\tfrac{1}{2}\mu R_0^2\sin^2\alpha\dot{\phi}+\cdots, \quad (6)$$

where the variable $r=R_0\alpha$. At this point, the conjugate momenta are introduced

$$p_s=\partial T/\partial\dot{s},\quad p_a=\partial T/\partial\dot{a};\quad p_r=\partial T/\partial\dot{r},\quad p_\phi=\partial T/\partial\dot{\phi}, \quad (7)$$

and the kinetic energy is rewritten in terms of the momenta. The terms in s/R_0, a/R_0 may be shown to be small, since the relative amplitudes of the stretching vibrations are small. The remaining expression is then as follows:

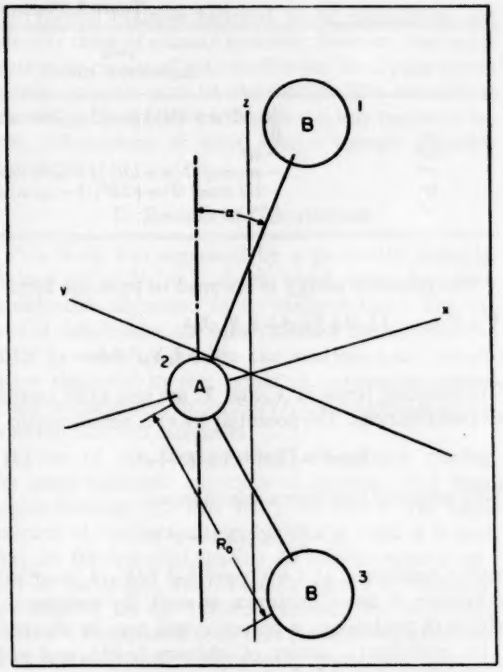

FIG. 1. Rotating coordinate system for dynamic analysis. The molecule lies in the xz plane.

$$T=\tfrac{1}{2}V_s p_s^2+\tfrac{1}{2}V_a p_a^2+[1/(2\mu R_0^2\sin^2\alpha)]p_\phi^2$$
$$+1/2\mu p_r^2-1/2\mu\{(2M/m)\alpha^2/[1+(2M/m)\alpha^2]\}p_r^2. \quad (8)$$

The last term has the effect of an additional anharmonicity in the bending potential, and will make a significant contribution if the bending amplitude is large. Its effect will be considered in some detail later.

When the expressions for V_a and V_s are written out, in powers of α^2, the resultant expression for the kinetic energy is

$$T=(1/2M)p_s^2+\mu^{-1}p_a^2+(1/2\mu)[p_r^2+p_\phi^2/r^2]$$
$$-1/\mu(\mu/m)\alpha^2p_a^2+(2M/m)\alpha^2p_s^2/2M$$
$$-\{(2M/m)\alpha^2/[1+(2M/m)\alpha^2]\}(p_r^2/2\mu)$$
$$+\{1/2\mu[(1/R_0^2\sin^2\alpha)-(1/r^2)]\}p_\phi^2. \quad (9)$$

The method to be employed is the treatment of the first three terms in (9) as the zero-order kinetic energy, and of the last four terms as perturbations. These perturbation terms are significant in producing characteristic properties of the quasi-linear molecule, since they only make an important contribution when the amplitudes of motion are large.

TABLE I. Displacement vector components.

r_i^κ	$\kappa=a$ Asymmetric stretch	$\kappa=s$ Symmetric stretch
x_1^κ	$[m/\sqrt{2}(m+2M)]\sin\alpha[1-(\mu/m)\sin^2\alpha]^{-1}$	$\sin\alpha/\sqrt{2}[1+(2M/m)\sin^2\alpha]$
x_2^κ	0	$-2M\sin\alpha/\sqrt{2}m[1+(2M/m)\sin^2\alpha]$
x_3^κ	$-x_1^a$	x_1^s
z_1^κ	$-m\cos\alpha/\sqrt{2}(m+2M)[1-(\mu/m)\sin^2\alpha]$	$\cos\alpha/\sqrt{2}[1+(2M/m)\sin^2\alpha]$
z_2^κ	$-2M\cos\alpha/\sqrt{2}(m+2M)[1-(\mu/m)\sin^2\alpha]$	0
z_3^κ	z_1^a	$-z_1^s$

The potential energy is assumed to have the form

$$V=V_0(r)+\tfrac{1}{2}k_a a^2+\tfrac{1}{2}k_s s^2+k_a X_a a^2\alpha^2 +k_s X_s s^2\alpha^2+\cdots. \quad (10)$$

The coupling terms in X_a and X_s are also to be treated as perturbations. The potential $V_0(r)$ is nonharmonic

$$V_0(r)=\tfrac{1}{2}k_r r^2+K_B/(c^2+r^2). \quad (11)$$

This potential possesses a minimum at

$$r_0=[(2K_B/k_r)^{\frac{1}{2}}-c^2]^{\frac{1}{2}}$$

and a maximum at $r=0$, provided $(2K_B/k_r)^{\frac{1}{2}}-c^2>0$; otherwise, it has a minimum at $r=0$. By varying the choice of parameters, a potential well may be obtained with or without a barrier, of arbitrary height, and with a minimum at any desired angle.

In the zero-order approximation, the Schrödinger equation is $H^0\Psi=E^0\Psi$, where the Hamiltonian H^0 is

$$H^0=[1/2M p_s^2+\tfrac{1}{2}k_s s^2]+[p_a^2/\mu+\tfrac{1}{2}k_a a^2] +1/2\mu[p_r^2+p_\phi^2/r^2]+\tfrac{1}{2}k_r r^2+K_B/(c^2+r^2). \quad (12)$$

The wave functions may be written in product form: $\Psi=\chi_{Ns}(s)\chi_{Na}(a)\psi(r,\phi)$. χ_{Na} and χ_{Ns} are wave functions of the one-dimensional harmonic oscillator, with natural frequencies $(2k_a/\mu)^{\frac{1}{2}}$ and $(k_s/M)^{\frac{1}{2}}$, respectively. $\psi(r,\phi)$ satisfies the Schrödinger equation

$$[1/2\mu(p_r^2+p_\phi^2/r^2)+\tfrac{1}{2}k_r r^2+K_B/(r^2+c^2)]\psi=\epsilon\psi. \quad (13)$$

B. Solution of the Equations for the Bending Motion

The variables in Eq. (13) are separated by the substitution $\psi=F_{nl}(r)\exp(il\phi)$, where $l=0,\pm1,\pm2,\pm3,\cdots$. Use of the dimensionless variable $u=(\mu\omega_0/\hbar)^{\frac{1}{2}}r$, where $\omega_0=(k_r/\mu)^{\frac{1}{2}}$, gives the following equation:

$$(d^2F/du^2)+(1/u)(dF/du)-(l^2/u^2)F+\lambda F-u^2F -[4G/(B+u^2)]F=0,$$

where

$$\lambda=2\epsilon/\hbar\omega_0; \qquad B=(\mu\omega_0/\hbar)c^2; \qquad G=K_B\mu/2\hbar^2; \qquad u_0=(\mu\omega_0/\hbar)^{\frac{1}{2}}r_0. \quad (14)$$

The substitution of the form

$$F_{nl}(u)=\exp(-u^2/2)u^l(B+u^2)\sum_{k=0}^{\infty}A(n,l;k)\mathfrak{L}_{l+k}^{\,l}(u^2), \quad (15)$$

where $\mathfrak{L}_{l+k}^{\,l}(u^2)$ is the normalized associated Laguerre polynomial,

$$\mathfrak{L}_{l+k}^{\,l}(u^2)=[l!/(l+k)!]^{\frac{1}{2}}[1/(l+k)!]L_{l+k}^{\,l}(u^2), \quad (16)$$

leads to an equation in the polynomials $\mathfrak{L}_{l+k}^{\,l}$. Multiplying by $\exp(-u^2/2)u^l\mathfrak{L}_{l+k'}^{\,l}$, and then integrating over variables u and ϕ, leads to a set of recursion relations for the coefficients $A(n,l;k)$

$$-A(n,l;k-1)[k(k+l)]^{\frac{1}{2}} +A(n,l;k)[B+l+2k+1-G/(\eta-k-l)] -A(n,l;k+1)[(k+1)(k+l+1)]^{\frac{1}{2}}=0; \quad k=0,1,2,\cdots. \quad (17)$$

Here the variable η contains the eigenvalue λ: $\eta=\tfrac{1}{2}[\lambda_{nl}/2+l-1]$. Equations (17) constitute a linear system in the coefficients $A(n,l;k)$; a solution exists if and only if the following infinite determinant vanishes:

$$\begin{vmatrix} c_{11}(\eta) & -c_{12} & 0 & 0 & \cdots \\ -c_{12} & c_{22}(\eta) & -c_{23} & 0 & 0 & \cdots \\ 0 & -c_{23} & c_{33}(\eta) & -c_{34} & 0 & 0 & \cdots \\ 0 & 0 & -c_{34} & c_{44}(\eta) & \cdots & & \\ & 0 & & & & & \\ \cdot & \cdot & \cdot & \cdot & \cdot & & \\ \cdot & \cdot & \cdot & \cdot & & \cdot & \\ \cdot & \cdot & \cdot & \cdot & & & \cdot \end{vmatrix} \quad (18)$$

$$c_{kk}(\eta)=B+l+2k-1-G/(\eta-l-k+1)$$

$$c_{k\,k+1}=[k(k+l)]^{\frac{1}{2}}.$$

The usefulness of the preceding analysis consists in the fact that roots of determinants of the form (18) may be rapidly calculated by finding the roots of continued fractions, $f_j(\eta)$

$$0=f_j(\eta)=c_{jj}(\eta) -\cfrac{c_{jj+1}^2}{c_{j+1j+1}(\eta)-\{c_{j+1j+2}^2/[c_{j+2j+2}(\eta)-(c_{j+2j+3}^2/\cdots)]\}} -\cfrac{c_{j-1j}^2}{c_{j-1j-1}(\eta)-\{c_{j-2j-1}^2/[c_{j-2,j-2}(\eta)-(\cdots/\cdots)]\}}. \quad (19)$$

All the fractions $f_j(\eta)$ have identical roots, regardless of the value of j. In general, for any given root, say, η_i, there is one particular value for j which affords the most convenient fraction for calculation. [The functions $f_j(\eta)$ have alternating roots and poles, and these tend to creep infinitesimally close together for most of the roots; only one or two roots are well separated from poles for each function]. The computer was programed to compute the functions $f_j(\eta)$ and find their roots η_i. In this way, the eigenvalues of determinants of minimum order 50 were rapidly computed. The 32 lowest eigenvalues were calculated for each set of values of the parameters. Subprograms were also written to calculate the normalized eigenfunctions, expectation values of μ^2 for each state, the dipole transition moments for fixed bond-dipole moment, $(n'l'/ue^{i\phi}/nl)$, and also the dipole matrix elements for a model in which the bond-dipole moment varies as a function of the angle.

C. Details of the Calculations

1. The eigenvalues are estimated to be accurate to five decimal places. The roots calculated were the following: $n=0$, $l=0$, 1, $\cdots 10$; $n=1$, $l=0$, 1, $\cdots 8$; $n=2$, $l=0$, 1, $\cdots 6$; $n=3$, $l=0$, 1, $\cdots 4$. These eigenvalues are the 32 lowest for molecules with near-linear structure.

2. The expression for F_{nl} generated by the recursion formulas is not a convergent series in the coefficients $A(n, l; k)$, but an asymptotic expansion. The expansion was truncated after the smallest $A(n, l; k)$, which always proved easily identifiable.

3. As has been indicated, in addition to the calculation of the dipole matrix elements for a fixed bond-dipole moment, another model was treated in which the magnitude of the A–B bond-dipole moment is a function of the angle. For mathematical convenience, the functional dependence chosen took the following form:

$$1/u\,|\,M_x\,| = (D_0+D_2u^2)/(B+u^2).$$

This function has the value D_0/B as u tends to zero, and the value D_2 as u tends to infinity. It is somewhat artificial in that it introduces a variation in the dipole moment that is closely correlated with the variation in potential energy, but such an assumed variation is not as unreasonable as it may at first appear. If, for example, the bent structure of B–A–B is the normally covalent one and the stable electronic structure when the molecule is linear is more ionic, then such a variation, correlated with the increasing potential energy and therefore with the degree of ionic character, is entirely plausible. In the calculations made, D_2 was chosen to be approximately $\frac{1}{2}D_0/B$. A moderate quantitative difference was found between the results for such a model and those for the constant bond-dipole model. Originally, such special behavior of the bond-dipole moment was invoked in order to explain the fact that the infrared absorption intensities of an experimental example believed to be quasi-linear are typically those of a linear molecule; however, the major qualitative results of both models for the dipole matrix elements support such an observation. The conclusions concerning the spectra of the quasi-linear molecule are thus independent of such special though plausible assumptions.

D. Results of Calculations

This work was suggested by a particular example, disiloxane $[(SiH_3)_2O]$, about which there has been considerable discussion as to configuration.[2] For the sake of definiteness, therefore, some of the assumptions made in order to develop the analysis bear quantitative similarity to the values of parameters appropriate to disiloxane. In particular, these special assumptions fall into two categories:

1. Size of the "unperturbed" vibrational spacing. For most triatomic molecules of interest, with bond angles between 135 and 160°, the size of the small moment of inertia associated with the angle ϕ is such that the fundamental spacing $2B$ falls between 6 cm^{-1} and 16 cm^{-1}, say, and one may expect a "rotation" spectrum in the far infrared, running up to perhaps 150 cm^{-1}. It appeared to us that the most sustained and complicated interactions should occur for cases in which the vibrational frequency for the quadratic well is low enough to permit large amplitudes of oscillation. Characteristically, for most molecules this bending frequency occurs between (150) cm^{-1} and 600 cm^{-1} (except for hydrogen-bending cases). We elected to sample behavior for the lower frequencies with larger amplitudes, and our calculations were made for a model with the masses and bond lengths of disiloxane and values for the "unperturbed" spacing corresponding to 200 cm^{-1} and 400 cm^{-1}. It should be mentioned that this special choice of masses, dimensions, and spacings is not at all atypical, and the results may be expected to possess entire generality for a large class of molecules; the use of smaller amplitudes would decrease rather than enhance any typical features.

2. Equilibrium bond angle. When the barrier to vibration through a linear configuration is substantially high, the equilibrium bond angle has a primary significance; but when this barrier becomes comparable to one or two vibrational spacings, such a parameter loses its primary significance, and what is important increasingly is the over-all amplitude of vibration, or the mean square displacement from the linear configuration. For example, one may readily imagine a linear molecule with a bending frequency such that its mean square displacement corresponds to a bond angle of 150°, but this certainly does not mean that we consider the equilibrium to occur at 150°. Therefore, what is characterized as the "equilibrium angle" for the bent

[2] R. C. Lord, D. W. Robinson, and W. C. Schumb, J. Am. Chem. Soc. 78, 1327 (1956).

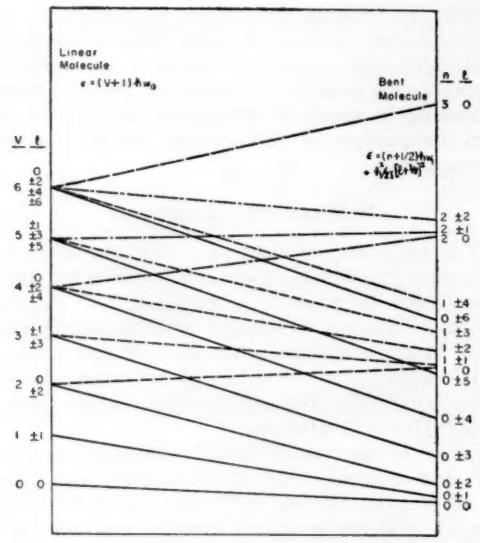

FIG. 2. Qualitative correlation diagram, showing the energy-level patterns for the linear molecule bending-vibration and for the bent molecule vibration-rotation.

molecule is best described as the "mean amplitude" for the linear *and quasi-linear* molecules. For this descriptive property we chose a value which approximated 150°. More acute angles would tend to make unrealistic requirements for very flat potentials, while models with angles closer to 180° would tend to resemble more closely typically linear features. A molecule with a 135° bond angle, such as NO_2, is bent enough to be definite, but 150° is so close to 180° that quasi-linear behavior is prejudicially likely, since it is improbable that large variation in potential energy from minimum 150° to maximum 180° would occur as a result of the types of electronic stabilization that determine directed valence in such cases. The authors are of the opinion that any kind of calculation on the electronic structures of such systems will support this notion. However, the initial reason for choosing 150° was that this value has been quoted in connection with disiloxane.[3,4]

It is important to point out that in addition to the masses of atoms and lengths of bonds three independent parameters must be specified in order to describe completely the potential for bending in our model. One of these is the force constant for the "unperturbed" harmonic well, and it determines the "unperturbed" spacing, $\hbar\omega_0$. We have sampled this parameter at two values, as previously indicated. The remaining two parameters describe the barrier, the constants B and G. Roughly speaking, these characterize the height and half-width of the barrier. The range of flexibility in their values provides variations in the location of the minimum, the "barrier height" ΔV (difference, in units $\hbar\omega_0$, between maximum and minimum), and the mean square amplitude of vibration. Because there are two parameters instead of one, there is no unique quantitative "correlation curve" between the bent-molecule and the linear-molecule energy levels. In order to mitigate this situation, we elected to impose the following conditions. At high barriers, the equilibrium angle was fixed at 150°. As the barrier height decreases, however, keeping the *minimum* at 150° leads to extraordinarily flat potentials with impossibly large amplitudes of vibration, because of the mathematical restrictions imposed by the Lorentzian shape of the barrier. Instead, therefore, the requirement was imposed that the absolute value of the potential at 150° have a fixed value; the relationship between B and G is then fixed, and the result is that as B increases the barrier height decreases, the location of the minimum moves very slowly in to more nearly linear positions, and the mean square amplitude is always approximately limited to 150° as an average bending displacement. This fixed value of the potential at 150° was chosen with the consideration in mind that a model with barrier height ΔV equal to 20 $\hbar\omega_0$, and a minimum at 150° is a good model of a "bent" molecule, and the value $V(u_0)$ at 150° for this case was used. Results

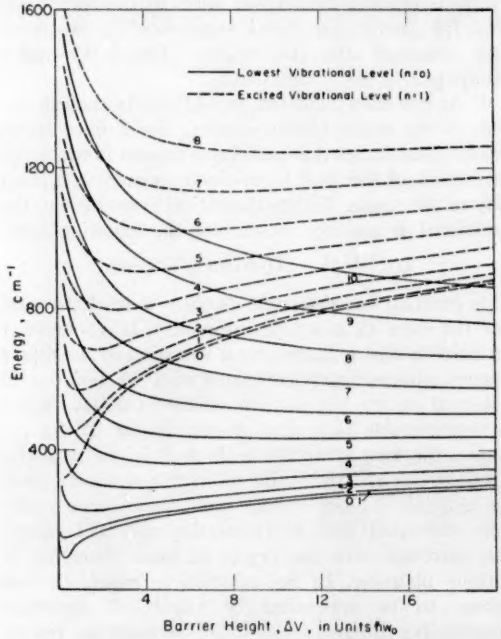

FIG. 3. Energy level diagram for moderate to high barriers (ΔV from $\hbar\omega_0$ to 20 $\hbar\omega_0$). The value of $\hbar\omega_0$ for this diagram is 400 cm^{-1}. (The behavior of the absolute energies below $\Delta V=1$ is not significant, as it depends on the curvature of the potential minimum.)

[3] J. R. Aronson, R. C. Lord and D. W. Robinson, J. Chem. Phys. **33**, 1004 (1960).
[4] R. F. Curl and K. S. Pitzer, J. Am. Chem. Soc. **80**, 2371 (1958).

prove to be insensitive to substantial variation in this choice; it is merely a device for restricting vibration amplitudes.

Figure 2 shows the qualitative correlation between the energy-level diagram for the degenerate bending vibration of the linear molecule, and that for the bending vibration of a bent molecule about a nonlinear equilibrium configuration, with superposed energy levels for different values of the angular momentum about the z axis. Here, l is the quantum number for this angular momentum; n is a quantum number for the energy for states of a given l; in the limit of the bent molecule it is the vibrational quantum number; v is the vibrational quantum number for the bending vibration of the linear molecule. Note that the states originating from a level of given v have lower energies for increasing angular momentum, since states of higher angular momentum are repelled from the center by the centrifugal potential, even for a flat-bottomed well, and consequently are less affected by changes in the potential near the center.

The correlation diagrams in Figs. 3 and 4 show the energy levels on the scheme described above, as a function of ΔV. Figure 3 shows the levels from 20 to 0, and Fig. 4 shows the expanded range from about 1.25 to 0. In Fig. 4, the diagram is *not* extended to the harmonic oscillator energy levels at $\Delta V=0$, because the limit $\Delta V=0$ occurs when the potential achieves zero curvature at $\alpha=0$; further increase in B then carries the model into that for a linear molecule with a "flat-bottomed" potential. The curvature increases steadily as B increases, and in the limit as $B\to\infty$ the potential approaches the simple harmonic form. (Incidentally, it

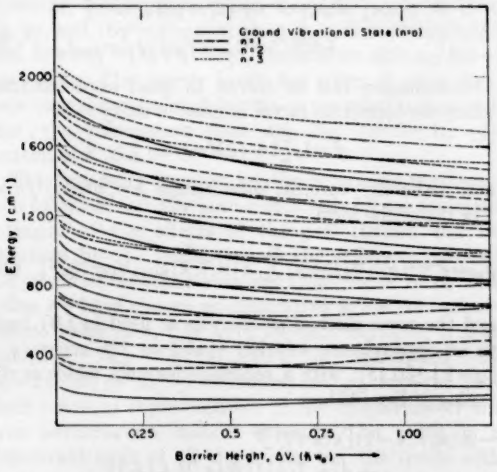

FIG. 4. Energy-level diagram for low barriers (ΔV from 0.05 $\hbar\omega_0$ to $\hbar\omega_0$; $\hbar\omega_0=400$ cm^{-1}). (Note that the energy levels do not approach those of the linear molecule when $\Delta V\to 0$; the limit when $\Delta V=0$ is a "flat-bottomed" well; in order to reach the harmonic oscillator potential one must pass through a range of anharmonic potentials with no barrier.)

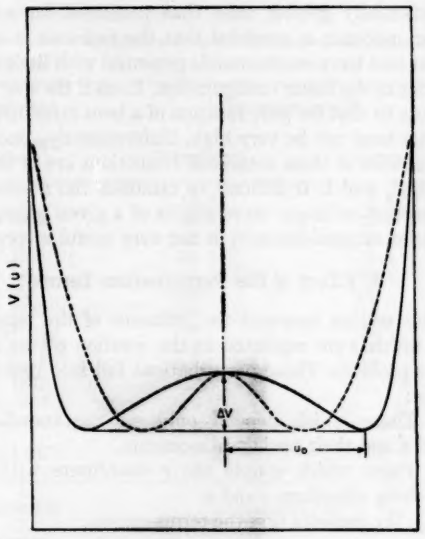

FIG. 5. Comparison of the potential employed in the computtation (dashed curve) with the potential most plausible for disiloxane. Note the decided asymmetry of the latter about its minimum.

is extremely instructive to consider the energy levels for a particle in a two-dimensional cylindrical box with their Bessel function solutions.)

Our model of the potential shows some shortcomings, which cannot be removed without a fourth parameter. The Lorentzian barrier produces potentials which are very nearly quadratically symmetric at their minima, but there is no reason that a realistic potential might not have quite different shape, asymmetric about its minimum, especially for low barriers. An example of this is illustrated in Fig. 5. Such differences are secondary, however, appearing in the quantitative results but not primarily affecting the qualitative features of the dynamics.

The most striking feature of Figs. 3 and 4 is that the energy levels, even for quite low barriers, resemble those of a bent molecule, with rotational levels superimposed on the vibrational-energy spacings. The rotational-energy levels correspond fairly well to those for a bent molecule with a bond angle corresponding to the location of the potential minimum; large amplitudes have the effect of centrifugal distortion. In general, the "rotation spectrum" $\Delta l=+1$, $\Delta n=0$ for any barrier height might be described by the formula

$$\nu=\nu_0''+B''(2l+1)-2D''(2l+1)^3+\cdots. \qquad (20)$$

The only difference between such a spectrum and a rotation spectrum is the presence of the constant term, ν_0''. Instead of occurring at B'', the first line would occur at $\nu_0''+B''$. This feature provides some indication of quasi-linearity: if a spectrum of the type described by formula (20) is found, with a lowest frequency

substantially greater than that predicted for a rigid rotor, evidence is provided that the molecule is quasi-linear and has a nonharmonic potential with little or no barrier at the linear configuration. Even if the spectrum is close to that for pure rotation of a bent structure, the barrier need not be very high. Unfortunately, since the frequencies of these rotational transitions are in the far infrared, and it is difficult to establish the absence of absorption to longer wavelengths of a given point, this criterion of quasi-linearity is not very useful at present.

E. Effect of the Perturbation Terms

This section concerns the influence of the terms in (9) which were neglected in the solution of the zero-order problem. These perturbations fall into two categories:

1. Those which depend only on the coordinates r and ϕ and their conjugate momenta.

2. Those which couple the r coordinate with the stretching vibrations s and a.

(a) We consider first the terms

$$-\{2M\alpha^2/m/[1+(2M/m)\alpha^2]\}p_r^2/2\mu + (1/2\mu R_0^2)[1/\sin^2\alpha - 1/\alpha^2]p_\phi^2. \quad (21)$$

The contribution of the last term in (21) depends on the difference between α^2 and $\sin^2\alpha$. Even for α as large as 30° corresponding to a bond angle of 120° the difference between α^2 and $\sin^2\alpha$ is only about 10%; we therefore ignore the contribution of this correction to the energy levels. The qualitative effect would be a slight shift of the rotational levels to a somewhat higher apparent moment of inertia.

The first term in the expression above produces a much more important effect. It makes an important constribution to the effective mass of the bending vibration, tending to lower the vibrational frequency. For strictly bent molecules, the angle does not deviate very much from the equilibrium value, α_0. Consequently, the above term then has the effect of merely creating a larger reduced mass; instead of the term $p_r^2/2\mu$ for the kinetic energy of bending, one must employ

$$[1+(2M/m)\alpha_0^2]^{-1}(p_r^2/2\mu).$$

For a bent molecule with a bond angle of 150°, α_0^2 is approximately 0.07; for our model, the effective correction factor is about 0.75. This implies a reduction in the vibrational energy quantum by a factor 0.87 from that obtained using the simple reduced mass valid for the linear configuration. The rotational spacings are only slightly affected for a bent molecule. In the actual calculation we have not included any such corrections.

The case in which this perturbation makes a significant alteration in the general features of the energy-level diagram is the case of the quasi-linear molecule when large amplitudes of oscillation and a low barrier at the linear configuration make it possible for different states to have widely different expectation values for α^2, which we denote hereafter by $\langle\alpha^2\rangle_{nl}$. We shall employ the perturbation theory to examine the consequences in such a case. In general, we may write

$$(p_r^2/2\mu)\psi_{nl}=[\epsilon_{nl}-\tfrac{1}{2}k_r r^2-K_B/(c^2+r^2)]\psi_{nl}, \quad (22a)$$

so that

$$-\{(2M\alpha^2/m)/[1+(2M\alpha^2/m)]\}(p_r^2/2\mu)\psi_{nl} = -\{(2M\alpha^2/m)/[1+(2M\alpha^2/m)]\} \times[\epsilon_{nl}-\tfrac{1}{2}k_r r^2-K_B/(c^2+r^2)]\psi_{nl}. \quad (22b)$$

The first-order perturbation corrections may be calculated by evaluation of the matrix elements

$$-\{nl|\{(2M/m)/[1+(2M\alpha^2/m)]\}[\epsilon_{nl}-V_0(\alpha)]|nl\}. \quad (23)$$

It may also be desirable to examine the case of a molecule which is quasi-linear but approaches in its behavior the case of a bent molecule. Under such circumstances, a better starting point for a zero-order Hamiltonian would be to use $\{1/[1+(2M\alpha_0^2/m)]\}(p_r^2/2\mu)$ for the bending vibrational kinetic energy in place of $p_r^2/2\mu$, where α_0 is, let us say, the equilibrium value of α. Then the residual perturbation is

$$\{(2M\alpha_0^2/m)[1-(\alpha^2/\alpha_0^2)]/[1+(2M\alpha^2/m)]\} \times\{1/2\mu[1+(2M\alpha_0^2/m)]\}p_r^2, \quad (24)$$

and its diagonal matrix elements would be computed instead of those of (22b), and the results added to the energies obtained from the solution of the zero-order problem with the Schrödinger equation

$$-\hbar^2/2\mu[1/1+(2M/m)\alpha_0^2] \times[(d^2\psi_{nl}/dr^2)+(1/r)(d\psi_{nl}/dr)] +\hbar^2l^2/2\mu r^2\psi_{nl}+V_0(r)\psi_{nl}=\epsilon_{nl}\psi_{nl}. \quad (25)$$

This equation can be solved to good approximation when the correction factor is close to unity: Let

$$q^2=1/[1+(2M\alpha_0^2/m)],$$

and make the variable substitution $\rho=[q(\mu k_r)^{\frac{1}{2}}/\hbar]r^2$. The use of the form

$$\psi_{nl}=e^{-\rho/2}(\rho)^{l/2q}(B+\rho)\sum_{s=0}^{\infty}A(n,l;k)\mathfrak{L}_{l+k}^{l}(q\rho^{1/q})e^{il} \quad (26)$$

and the same method of analysis as used in (B) leads to an approximate solution (valid to 2% accuracy if $|q-1|\leq 0.15$), with a recursion formula which is the analog of Eq. (17)

$$-A(n,l;k-1)[\kappa(k+l)]^{\frac{1}{2}} +A(n,l;k)\{(Bq+2k+l+1) -[(Gq^2+q^2-q)/(qn-k-l)]\} -A(n,l;k+1)[(k+1)(k+l+1)]^{\frac{1}{2}}=0 \qquad k=0,1,2,\cdots \quad (27)$$

TABLE II. The effect of perturbation on the rotation spectrum.

$\hbar\omega_0 = 400$ cm^{-1}; $\Delta V = 894$ cm^{-1}

		Uncorrected		Corrected	Frequencies (cm^{-1})	
n	l	$\epsilon_{nl}-\epsilon_{00}$ ($\hbar\omega_0$)	$[\langle\alpha^2\rangle_{nl}]^{\frac{1}{2}}$ (radians)	$\epsilon_{nl}-\epsilon_{00}$ ($\hbar\omega_0$)	Uncorrected	Corrected
0	0	...	0.1792	...	14.6	12.6
0	1	0.0366	0.1803	0.0316	42.0	36.2
0	2	0.1416	0.1835	0.1216	66.0	56.4
0	3	0.3064	0.1879	0.2628	86.5	74.5
0	4	0.5224	0.1927	0.4478	104	89.1
0	5	0.7828	0.1978	0.6692	120	101
0	6	1.0819	0.2025	0.9223	133	113
0	7	1.4150	0.2080	1.2044	146	122
0	8	1.7785	0.2128	1.5099	157	130
0	9	2.1693	0.2177	1.8357	167	138
0	10	2.5850	0.2227	2.1807	...	...
1	0	0.8420	0.1703	0.7574	...	...

$\hbar\omega_0 = 400$ cm^{-1}; $\Delta V = 421$ cm^{-1}

		Uncorrected		Corrected	Frequencies (cm^{-1})	
n	l	$\epsilon_{nl}-\epsilon_{00}$ ($\hbar\omega_0$)	$[\langle\alpha^2\rangle_{nl}]^{\frac{1}{2}}$ (radians)	$\epsilon_{nl}-\epsilon_{00}$ ($\hbar\omega_0$)	Uncorrected	Corrected
0	0	...	0.148	...	26.0	22.6
0	1	0.0649	0.153	0.0565	62.3	55.0
0	2	0.2206	0.161	0.1939	89.0	78.5
0	3	0.4431	0.168	0.3902	109.8	96.4
0	4	0.7177	0.1755	0.6313	127.0	111
0	5	1.0352	0.1825	0.9084	141.5	123
0	6	1.3889	0.189	1.2150	154	133
0	7	1.7739	0.195	1.5459	165	140
0	8	2.1867	0.202	1.9071	175	147
0	9	2.6241	0.207	2.2714	184	155
0	10	3.0838	0.213	2.6593	...	...
1	0	0.6349	0.134	0.5982	...	...

However, this formula differs from (17) only in that Bq, ηq, and (Gq^2+q^2-q) replace B, η, G in the calculation. Since $\eta q = \frac{1}{4}\lambda q + \frac{1}{2}(l-q)$, the final result is $\epsilon_{nl}/\hbar\omega_0 = 2\eta q - 2l + q$. The energy levels for given B, G, q, $\hbar\omega_0$, may then be calculated by the same program, except that the parameters used are Bq, $(q^2(G+1.)-q)$ instead of B, G.

The first-order energies for the remaining perturbation have not actually been computed. An approximate estimate of the effects of the perturbation can be obtained by the evaluation of the separate parts of the operator at some selected mean value of α. The value we have chosen as illustrative is the root-mean-square value of α, $[\langle\alpha^2\rangle_{nl}]^{\frac{1}{2}}$, for each state, n, l. The quantity $[\epsilon_{nl} - V_0([\langle\alpha^2\rangle_{nl}]^{\frac{1}{2}})]$ is multiplied by $[(-2M/m)\langle\alpha^2\rangle_{nl}]/[1+(2M/m)\langle\alpha^2\rangle_{nl}]$, and the product taken as representative of the magnitude of the true perturbation matrix element. The result is a downward shift of all the levels, but the levels with increasing angular momentum are affected most, since the value of $\langle\alpha^2\rangle_{nl}$ increases strikingly with angular momentum for most cases, particularly those cases in which there is either no barrier or an extremely low one. It is important to emphasize the effect of this perturbation, because although the simple zero-order calculations predict that the pure rotation spectrum ($\Delta n = 0$, $\Delta l = +1$) will converge eventually on the frequency corresponding to the unperturbed quantum of vibrational energy $\hbar\omega_0$, this perturbation invalidates that conclusion; instead, the convergence frequency of the rotation spectrum may easily be substantially lower. Calculations made from some exemplary models indicate that the magnitude of the downward shifts may be as much as 40% of $\hbar\omega_0$. Table II shows some levels for two typical barrier heights and their associated perturbation shifts computed in this way.

(b) We now consider the perturbations coupling the bending and stretching motions. Two terms appear in (9) which couple the motion of the bending coordinate r with the asymmetric and symmetric stretching vibrations. Only the case of the asymmetric stretch is considered here; the symmetric case is entirely analogous. The terms whose effect is to be treated by perturbation theory are then

$$-(\mu/m)(r/R_0)^2(p_a^2/\mu) + k_a X_a a^2 (r/R_0)^2. \quad (28)$$

The first-order perturbation energies will be computed.

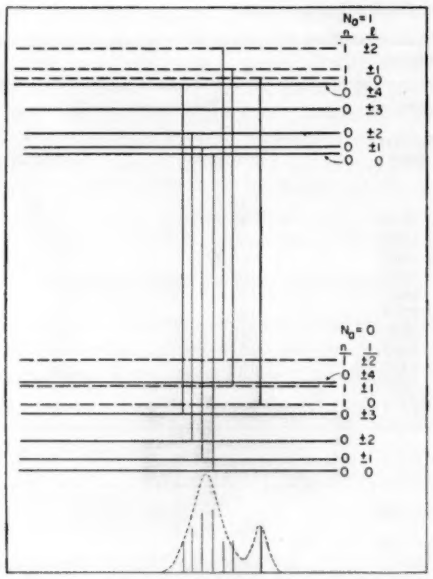

FIG. 6. Spectral interpretation of the side-band structure expected in the asymmetric stretch absorption band of a quasi-linear molecule with $\Delta V \approx \hbar\omega_0$.

Let the quantum number of the asymmetric stretching vibration be N_a, and the quantum numbers of the bending be, as usual, n, l. The diagonal matrix elements are then given by the expression

$$[-(\mu/m)(N_a \mid p_a^2 \mid N_a) + 2X_a(N_a \mid \tfrac{1}{2}k_a\alpha^2 \mid N_a)](nl \mid \alpha^2 \mid nl). \quad (29)$$

For the harmonic oscillator corresponding to the asymmetric stretch,

$$(N_a \mid p_a^2/\mu \mid N_a) = (N_a \mid \tfrac{1}{2}k_a\alpha^2 \mid N_a) = \tfrac{1}{2}(N_a+\tfrac{1}{2})\hbar\omega_a \quad (30)$$

Therefore the perturbation shifts for a state of given N_a, n, l are

$$-\tfrac{1}{2}(\mu/m+2X_a)(N_a+\tfrac{1}{2})\hbar\omega_a\langle\alpha^2\rangle_{nl}. \quad (31)$$

The expectation values of α^2 were computed in the calculations.

A difference in the observed frequency of the asymmetric stretch vibrational transitions $N_a=0$, n, $l \rightarrow N_a=1$, n, l, and $N_a=0$, n', $l' \rightarrow N_a=1$, n', l', arises out of a difference in the expectation values of α^2 in the different states, $\langle\alpha^2\rangle_{nl}$ and $\langle\alpha^2\rangle_{n'l'}$. This theory predicts large displacement effects of the various transitions if these expectation values are widely disparate, i.e., if there are large amplitudes of motion. (Such a situation can only arise if there is a low barrier or none at all.) A characteristic difference appears between (a) the case when the barrier height is negligible with respect to the vibrational quantum, and (b) the case when the barrier height is comparable to or slightly greater than the vibrational quantum, and the potential minimum occurs at a substantial value of α. In the first case, steadily progressive change occurs in the values for $\langle\alpha^2\rangle_{nl}$ in a manner reminiscent of the harmonic oscillator as the energy increases, and there is to be expected a series of bands somewhat closely spaced progressing to longer or shorter wavelengths, depending on whether $(-\mu/m+2X_a)$ is negative or positive. The spacing is proportional to the magnitude of this coefficient. A value of the coefficient X_a that is entirely comparable to values probable for normally harmonic oscillators may give rise to spacings from 10 to 20 cm^{-1}, because of the large amplitude.

A more peculiar situation arises in the case (b). If the barrier height is of a magnitude comparable to the vibrational quantum, the lowest vibrational level may have a fairly sharply localized probability distribution around the angle of minimum potential. Increases in the angular momentum on this level will result in mild, steady increase in the expectation values of α^2, $\langle\alpha^2\rangle_{0l}$. However, the first excited vibrational level $n=1$, $l=0$ is above the barrier or just below it, and consequently may have an expectation value for α^2 which is dramatically less than that for the lowest level. If X_a is negative (positive) and of the order of magnitude indicated earlier, there will result a shift of as much as 100 cm^{-1} to higher (lower) frequencies for the band with origin $n=1$, $l=0$, while the bands for $n=0$, l would be shifted to a much smaller extent to lower (higher) frequencies for increasing l. Calculations of the expectation values $\langle\alpha^2\rangle_{nl}$ were made and in fact, as Table II indicates, the value of $\langle\alpha^2\rangle_{\infty}$ can be significantly greater than $\langle\alpha^2\rangle_{10}$ only when the barrier height is low and of the order of magnitude of the vibrational spacing. Unfortunately, it is at just this point that the potential we have used, with its symmetrical minimum, proves inadequate to demonstrate the full possible effect. If the form shown by the solid curve in Fig. 5, with its abrupt rise in energy for values of α greater than the value at the minimum, were employed, instead of the more gradually curved form prescribed by the Lorentzian barrier shape, the results would be almost certainly as follows:

(a) The expectation values $\langle\alpha^2\rangle_{0l}$ would undoubtedly increase only slightly with increasing l and would be essentially the value at the minimum, α_0^2. Under such circumstances, the transitions from states $n=1$, increasing l, would move to lower (higher) frequencies more rapidly, thus enhancing the apparent intensity of the band with $n=0$. The diagrammatic scheme for the asymmetric stretch spectrum is shown in Fig. 6.

We have seen that the phenomenon of a side band or a series of side bands on the asymmetric stretch transition is almost certain evidence of a low barrier and large amplitudes. The barrier may not be higher than perhaps two vibrational quanta. When two side bands are found, it may be taken as evidence that there is a barrier comparable to the vibrational quantum.

TABLE III. Typical frequencies and relative intensities of electric dipole transitions, bending motion of the quasi-linear molecule.

Quantum numbers Initial		Final		$\hbar\omega_0=400$ cm^{-1} $\Delta V=1620$ cm^{-1}		$\hbar\omega_0=400$ cm^{-1} $\Delta V=706$ cm^{-1}		$\hbar\omega_0=200$ cm^{-1} $\Delta V=473$ cm^{-1}		$\hbar\omega=200$ cm^{-1} $\Delta V=177$ cm^{-1}	
n	l	n'	l'	ν (cm^{-1})	I	ν (cm^{-1})	I	ν (cm^{-1})	I	ν (cm^{-1})	I
0	0	0	1	9.1	23.4	17.1	14.0	13.4	9.22	28.4	5.74
0	1	0	2	27.0	22.6	47.6	13.4	36.4	9.08	54.8	6.03
0	2	0	3	44.4	20.2	72.9	11.3	54.6	8.40	72.3	5.42
0	3	0	4	60.9	16.5	93.9	8.50	69.2	6.80	85.3	4.38
0	4	0	5	76.4	12.6	112	5.73	81.1	5.25	95.6	3.25
0	5	0	6	90.8	8.95	127	3.58	91.1	3.82	104	2.27
0	6	0	7	104	5.91	140	2.05	99.6	2.63	111	1.50
0	7	0	8	117	3.70	152	1.10	107	1.75	117	0.95
0	8	0	9	128	2.18	163	0.57	113	1.11	123	0.58
0	9	0	10	139	1.21	172	0.28	119	0.68	127	0.34
1	0	1	1	11.0	2.70	373	2.51	28.3	2.89	71.0	2.23
1	1	1	2	32.4	2.60	75.0	2.38	54.7	2.88	83.6	2.24
1	2	1	3	52.4	2.25	100	1.87	71.4	2.52	93.8	1.83
1	3	1	4	71.0	1.75	119	1.27	83.9	1.97	102	1.36
1	4	1	5	87.0	1.30	134	0.78	93.8	1.57	109	0.94
0	1	1	0	423	0.32	292	0.54	193	0.42	128	0.82
0	2	1	1	417	0.33	282	0.55	185	0.48	144	0.62
0	3	1	2	405	0.30	284	0.43	185	0.40	155	0.42
0	4	1	3	396	0.25	290	0.28	187	0.30	164	0.26
0	5	1	4	391	0.19	297	0.17	190	0.21	171	0.16
0	6	1	5	387	0.13	304	0.09	193	0.13	176	0.10

This side-band effect may also be predicted for the symmetric-stretch transition in the Raman spectrum. At this point it may also be worth remarking that the results of electron diffraction on a quasi-linear molecule with such a low barrier should give the bent configuration with evidence of large amplitudes of vibration.

F. Intensities of Electric Dipole Transitions

The characteristic features of the infrared spectrum of a quasi-linear molecule are intermediate between those of the linear and the bent molecules. Intensities tend to resemble those of the linear molecule. It is necessary to consider two categories in the problem of intensities, intensities of transitions in the bending mode alone, and, intensities of other transitions.

1. The calculations made for the quasi-linear molecule show that the intensities of transitions resemble those for the linear molecule, although the frequencies begin to approach those of a bent molecule. It is important to understand the character of the spectrum in order to make this interpretation. The selection rule $\Delta l=\pm 1$ for all electric dipole transitions involving the x-component is rigorous. In the linear molecule, allowed transitions in absorption are $\Delta l=\pm 1$, $\Delta V=+1$. If we consider the series of transitions $\Delta l=+1$, $\Delta V=+1$, these become the strong "pure rotation spectrum" $\Delta l=+1$, $\Delta n=0$ of the bent molecule. Their intensities are quite large, because essentially they involve the "permanent moment." There are also the transitions $\Delta l=-1$, $\Delta V=+1$ of the linear molecule, and these become the transitions $\Delta l=-1$, $\Delta n=+1$ of the bent molecule, the "P-branch" of the vibration-rotation spectrum. As may be seen from the calculations, (Table III), these transitions are always of substantially smaller intensity than those for the pure rotation. Furthermore, their frequencies occur in the same general range as those in the higher frequency end of the rotation spectrum. The transitions forming the "R-branch" of the vibration-rotation spectrum correspond to transitions $\Delta l=+1$, $\Delta V=+3$ of the linear molecule, and are only very weakly allowed. Their frequencies are typically about two or three times those of the higher frequency rotational lines. This combination of circumstances explains the absence of a noticeable bending vibration absorption band in a quasilinear molecule; the absorption is distributed over a wide range of frequencies, and its strongest lines occur in a spectra region overlapped by the stronger pure rotational spectrum.

2. As an example of a transition other than those involving only the bending mode, we consider the symmetrical stretch. The symmetrical stretching transition is strictly forbidden in the linear molecule. In fact, however, it is forbidden for all configurations; there must be a simultaneous change in the angular momentum about the z axis, $\Delta l=\pm 1$, i.e., some "rotational" structure, to make it allowed. This means that the transition corresponding to the symmetric stretch in a bent molecule becomes a *combination band*, $\nu_s\pm\nu_a$, in the linear molecule; the intensity is much lower because the major contribution to the dipole moment does not arise from coupling between the stretching and bending coordinates. Without additional information on such coupling it is not possible to calculate explicitly the intensity of these "combina-

tions," since the critical quantity is the dipole derivative, $(\partial\mu_z/\partial s)$. In the quasi-linear molecule it is possibly very small, so that if the band appears at all it will be very weak. This appears to be the case for disiloxane.

A further consideration which renders the band weaker yet is that the many different transitions from different origin states will be widely distributed in frequency, because of the wide variations in rotational-energy-level differences. Therefore, if the symmetrical stretching band is observed, it will be weak and very widely distributed in frequency; observation would provide extremely valuable information about the spacing of the rotational levels, provided proper consideration be given to the effect of the perturbations discussed in Sec. E2.

II. SOME OTHER ANALOGOUS PROBLEMS

The analytical method used in this two-dimensional barrier problem may be extended to three dimensions or to one dimension. The latter problem is well known (the umbrella vibration in NH_3). The method is attractive in that it is exceedingly accurate (determinants of order 50×50 may be solved in seconds), and converges for all barrier heights. For the case of one dimension one merely replaces the Laguerre functions by Hermite functions, and proceeds entirely analogously to the solution for two dimensions. We have obtained calculations in this way, for all barrier heights, in the one-dimensional case; should the three-dimensional problem become of interest, it is potentially possibly for it to be solved in this way as well.

ACKNOWLEDGMENTS

This work was done in part at the M.I.T. Computation Center, Cambridge, Massachusetts, to which we are grateful for the use of the high-speed digital computer. One of us (I.N.) wishes gratefully to acknowledge the support of the United States National Institutes of Health.

We thank Professor R. C. Lord for stimulation of our interest in the problem, and for valuable discussion and criticism.

THE JOURNAL OF CHEMICAL PHYSICS VOLUME 33, NUMBER 4 OCTOBER, 1960

Far Infrared Spectrum and Structure of Disiloxane

J. R. Aronson,* R. C. Lord, and D. W. Robinson†

Spectroscopy Laboratory, Massachusetts Institute of Technology, Cambridge 39, Massachusetts

(Received April 7, 1960)

Study of the infrared absorption of gaseous disiloxane in the range 50–150 cm^{-1} shows that significant absorption is confined to the lower part of the range. A broad band with five rather flat maxima at about 56.4, 69.2, 80.1, 90.5, and 100 cm^{-1} is interpreted as the spectrum of the mixed vibrational and rotational transitions of a quasilinear triatomic molecule. The consequences of this model of disiloxane for the vibrational spectra of the molecule at higher frequencies are discussed and various unusual features of the spectra explained on the basis of the model.

THE valence angle of the Si—O—Si bond in disiloxane, $H_3SiOSiH_3$, is so large that the vibrational spectra of this molecule—infrared absorption of the vapor[1] and Raman spectrum of the liquid[1,2]—obey the selection rules of a D_{3d} structure. This is in contrast to the spectra of dimethyl ether, disilyl sulfide[2,3] and disilyl selenide,[2] which show clear-cut coincidences between strong Raman lines arising from skeletal vibrations and infrared frequencies in the vapor state. Our interest in studying the far infrared absorption of disiloxane was based on the hope of observing the bending vibration of the Si—O—Si skeleton, which our earlier work,[1,4] at frequencies above 180 cm^{-1}, had not revealed. The bending vibration is of especial importance because its frequency depends on the potential function for the displacement of the oxygen atom perpendicular to the Si—Si line. In view of the expected short distance (<0.5 A) of the potential minimum from this line, the potential function should be highly anharmonic unless the skeleton is strictly linear. In any event the frequency and structure of the infrared absorption due to the bending motion should be informative as to the nature of the potential function. This has indeed proved to be the case.

* Present address: Arthur D. Little, Inc., Acorn Park, Cambridge 40, Massachusetts.

† Present address: Department of Chemistry, The Johns Hopkins University, Baltimore 18, Maryland.

[1] R. C. Lord, D. W. Robinson, and W. C. Schumb, J. Am. Chem. Soc. **78**, 1327 (1956).

[2] (a) D. C. McKean, R. Taylor, and L. A. Woodward, Proc. Chem. Soc. (London) **1959**, 321. (b) E. A. V. Ebsworth, R. Taylor, and L. A. Woodward, Trans. Faraday Soc. **55**, 211 (1959).

[3] H. R. Linton and E. R. Nixon, J. Chem. Phys. **29**, 921 (1958).

[4] D. W. Robinson, J. Am. Chem. Soc. **80**, 5924 (1958). (See note added in proof.)

EXPERIMENTAL DETAILS AND RESULTS

The absorption of gaseous disiloxane, prepared as described earlier,[1] was investigated at a pressure of about 1 atm in a 10-cm cell with polyethylene windows. Gratings of 6.4 grooves/mm (blaze at 120 cm^{-1}) and 8 grooves/mm (blaze at 90 cm^{-1}) were used in a small spectrometer. All spectra were taken in the first order, the techniques for removal of higher orders being those described previously.[5,6]

No appreciable absorption was observed in the range 120–150 cm^{-1} at 1 atm pressure. Below 120 cm^{-1}, however, strong absorption was found, as shown in the top curve of Fig. 1. The absorption extended down to 50 cm^{-1}, the lower limit of the investigation. Upon reduction of the sample's pressure, a series of rather broad maxima appeared, located at about 56.4, 69.2, 80.1, 90.5, and ~100 cm^{-1}. The difficulty in locating the maxima of the rather broad peaks leads us to ascribe an error of about ±1 cm^{-1} to these values. The peak absorption coefficients implied by the curves of Fig. 1, which are not quantitatively reliable because of spectral impurity of the radiation and drift in background, are of the order of 2×10^3 cm^2/mol.

INTERPRETATION OF SPECTRA

At first sight the structure, low frequency, and broad range of the absorption of Fig. 1 are surprising, as is the fact that absorption is not found at higher frequencies. Except for their breadth, the series of peaks is reminiscent of the series observed for pure rotation in nitrogen dioxide,[7] ozone,[8] and sulfur dioxide.[6] If in fact one assumes a bent form of the Si—O—Si skeleton and neglects rotational interaction between the skeleton and the SiH_3 groups, one can use the equation for the pure rotational transitions of a centrifugally distorted approximate symmetrical top to evaluate a rotational constant for the skeleton.[8]

The rotational constant $A-(B+C)/2$ determined in this way is 6.5 cm^{-1} and the centrifugal distortion constant D_k is -4×10^{-3} cm^{-1}. The latter is about twice as large as the D_k value in NO_2, which is reasonable in view of the considerably larger Si—O—Si angle. Moreover the values of B and C are very small compared to A and may be estimated quite well as 0.1 cm^{-1}. Hence A is 6.6 cm^{-1} and I_A is 4.24×10^{-40} g-cm^2. With the assumption that this refers only to the moment of inertia of the skeleton about the axis of least inertia, one can calculate the bond angle if the Si—O distance is known. It turns out to be 148° (Si—O taken as 1.629 A), in good though perhaps somewhat fortuitous agreement with recent electron diffraction work on disiloxane.[9] The resultant value of the distance of the oxygen atom from the Si—Si line is 0.45 A.

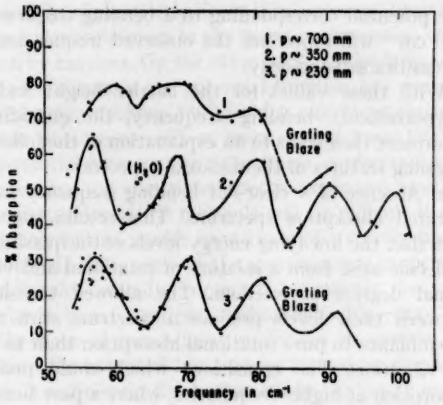

FIG. 1. Far infrared absorption of disiloxane.

INTERPRETATION OF THE SPECTRA ON THE QUASI-LINEAR BASIS

The short distance by which the equilibrium position of the oxygen atom appears to be removed from the Si—Si line implies that the potential function must be strongly anharmonic, since it must possess a maximum in between two minima separated by less than 1 A. Therefore in addition to the unusually large spacing of the energy levels for rotation about the axis of least inertia, we expect the levels for the bending vibration to be unusually close together. The separation of rotational and vibrational degrees of freedom implicit in the treatment of the preceding paragraph is thus not possible and the skeletal motions must be treated with due consideration of the special shape of the potential surface on which the oxygen atom is moving.

A treatment of the quasi-linear molecule has been given by Thorson and Nakagawa.[10] We believe the results of their treatment lead to an understanding of the far infrared spectrum of disiloxane and of other unusual features of the rotation-vibration spectra of the molecule. An important finding of their study for present discussion is that the kind of far infrared absorption shown in Fig. 1 is to be expected for a quasilinear molecule even if the potential maximum separating the minima is very low, in fact even when it is comparable to the zero-point energy of the bending motion. The inaccuracy of the experimental peak frequencies, the limited range ($\nu>50$ cm^{-1}) of the data and the relative insensitivity of the spectrum to the precise barrier height[10] make it impossible to give a reliable figure for this height at present. However, a barrier of the order of 400–500 cm^{-1} and a curvature of the *outer part* of

[5] R. C. Lord and T. K. McCubbin, Jr., J. Opt. Soc. Am. **47**, 689 (1957).
[6] A. Danti and R. C. Lord, J. Chem. Phys. **30**, 1310 (1959).
[7] G. R. Bird, A. Danti, and R. C. Lord, Spectrochim. Acta **12**, 247 (1958).
[8] Cf. Eq. 4 of footnote reference 7.
[9] Private communication from Professor O. Bastiansen gives 145°.
[10] W. R. Thorson and I. Nakagawa, J. Chem. Phys. **33**, 1 (1960).

the potential corresponding to a bending frequency of 200 cm^{-1} will reproduce the observed frequencies and intensities satisfactorily.

With these values for the barrier height and the (hypothetical) bending frequency, the quasi-linear-treatment then leads to an explanation of the following puzzling features of the disiloxane spectra:

a. Absence of a clear-cut bending frequency in the infrared absorption spectrum. This results from the fact that the low-lying energy levels of the quasi-linear molecule arise from a mixture of rotational and vibrational degrees of freedom. The allowed transitions between these levels produce a spectrum with more resemblance to pure rotational absorption than to that of vibration. The transitions which could produce absorption at higher frequencies, where a pure bending vibration frequency would be expected, are much weaker than those of a bent molecule since they are correlated with forbidden transitions in the linear oscillator. The intensity of the bending vibration in a strictly linear oscillator thus goes over into something like that of pure rotation in the quasi-linear oscillator. The amount of intensity remaining in those transitions which fall in the usual region of bending vibrations depends on the shape of the potential function and is smaller for a broad flat potential than for a steep one with the same angle of the minimum.

One of the cases calculated by Thorson and Nakagawa,[10] using a barrier height and zero-order frequency of 473 and 200 cm^{-1}, respectively, gave weighted frequencies (relative intensities) in the range 50–100 cm^{-1} of 54.6 (11.3), 70.0 (9.3), 82.0 (7.2), 91.8 (5.4), 100 (3). These agree satisfactorily with the frequencies and qualitatively with the intensities of the peaks shown in Fig. 1. An interesting aspect of the calculated frequencies is that the next lower peak is predicted at about 35 cm^{-1} on the quasi-linear model, and at about 44 cm^{-1} on the basis of the pure rotational picture. It is hoped to check these predictions experimentally in the near future.

b. Complex infrared absorption associated with the antisymmetric Si—O—Si stretching vibration. The absorption bands for this vibration in disiloxane and disiloxane-d_6 show evidence of multiple components, the most prominent of which is a high-frequency satellite separated by about 100 cm^{-1} from the main band. These components wash out the $P-R$ parallel structure of the band, a structure which is clearly shown by the nearby bands due to the nondegenerate SiH_3 and SiD_3 deformation. The satellite and the other components of the antisymmetric stretching are interpreted as upper-stage transitions which, in the case of the satellite particularly, have frequencies considerably shifted by a change in the mean Si—O—Si angle. This point has been treated in detail by Thorson and Nakagawa.

Evidence in support of the interpretation of the satellite as an upper-stage band appears to be furnished by its disappearance from the spectrum of disiloxane trapped in a rare-gas matrix at very low temperature.[11] At 20°K one would expect all the disiloxane molecules to be in the ground vibrational state and thus the mean distance of the oxygen atom from the Si—Si line would approach the value of 0.45 A. At higher temperatures the population of the higher levels increases, which produces a *decrease* in the mean distance of oxygen atom from the Si—Si line for one or two of the low-lying levels. In these states the skeleton would be more nearly linear on the average. This gives a reasonable basis for the appearance of the satellite at 1200 cm^{-1}, whose high frequency is a natural consequence of the larger effective Si—O—Si angle in certain excited states.[10] This satellite, incidentally, is not a unique feature of disiloxane, but appears in the spectra of various siloxane derivatives.

c. Adherence of the infrared spectrum of the vapor and the Raman spectrum of the liquid to vibrational selection rules for a linear skeleton. As was stated above, the vibrational spectra of disiloxane appear to obey D_{3d} (i.e., linear skeleton) selection rules. The antisymmetrical stretching vibration does not appear in the Raman effect and the symmetrical stretching is absent from the infrared, in contrast to dimethyl ether,[12] disilyl sulfide[3,4] and disilyl selenide,[4] in all of which the skeletal bond angle is reported to be much smaller than in disiloxane. The contrast with dimethyl ether is particularly marked in that the symmetrical stretching vibration of this molecule, which is strong and polarized at 918 cm^{-1} in the Raman effect of the liquid, also appears strongly in the infrared of the vapor (type-B band centered at about 932 cm^{-1}).

If the amplitude of the bending vibration in the quasi-linear molecule is sufficiently large, the nuclear motions are essentially the same as they would be in an excited state of the analogous vibration of a strictly linear skeleton. The spectrum of such a vibrating molecule should thus be that of a linear structure. The far infrared spectrum, taken together with the theory of Thorson and Nakagawa, indicates that the energy levels corresponding to an excited bending vibration are low. Hence at room temperature a large fraction of the molecules should be expected to obey the selection rules of a linear skeleton, with the additional complication of satellites of the antisymmetric stretching band as discussed above. Only at very low temperatures would one expect departure from the D_{3d} selection rules. An analogous explanation has been given of the behavior of a certain band at 750 cm^{-1} in the vapor spectrum of cyclobutane.[13] The intensity of this band is said to be less at high temperatures than at low because excitation of the low-frequency ring-bending vibration carries the molecule from a low symmetry

[11] R. F. Curl, Jr., and K. S. Pitzer, J. Am. Chem. Soc. **80**, 2371 (1958).

[12] A. Hadni, Compt. rend. **239**, 349–51, (1954).

[13] G. W. Rathjens, Jr., N. K. Freemen, W. D. Gwinn, and K. S. Pitzer, J. Am. Chem. Soc. **75**, 5634 (1953).

(D_{2d}), in which the band is allowed, to a high symmetry (D_{4h}), in which it is forbidden.

In a strictly linear skeleton, the symmetrical stretching vibration should be forbidden in the infrared (as is apparently the case) and sharp and polarized in the Raman effect. The Raman line reportedly[2] has a half-width of 9 cm^{-1} in liquid disiloxane. Though such a half-width is not unusual, even for a polarized line, some of it may arise from the same kind of influence as that described above for the antisymmetric vibration. Since most of the kinetic energy of the latter resides in the oxygen atom, while in the former the oxygen moves very little, the symmetric stretching vibration should be much less susceptible to such influence. However, there should be some influence, which should also make itself felt on replacement of O^{16} by O^{18}.

The observed extra broadening of the Raman line in an equimolar mixture of disiloxane and disiloxane-O^{18} is not given explicitly[2] but must be about 2 cm^{-1}, since the increase is interpreted to mean a downward shift in the O^{18} frequency of 3–4 cm^{-1}. This amount of broadening might well arise from the effect of the decreased amplitude of the O^{18} bending vibration on the symmetric stretching frequency. It should be pointed out especially that it is the anharmonicity of the bending vibration which is important for this effect in the quasi-linear molecule rather than the anharmonicity of the symmetric stretching. It also appears that calculations of the Si—O—Si bond angle based on harmonic force field treatments[2,14] should be regarded with reservation in view of the anharmonic nature of the potential function.

Finally we would like to comment on the concept of a "quasi-linear" molecule. There is surely no question that a molecule is strictly linear if its potential function shows a clear minimum in the linear configuration with no nearby maxima. On the other hand, as the foregoing discussion shows, if the potential function has minima at angles approaching 180° (which can mean quite a number of degrees—30° or more—away from 180° if the potential maximum at the linear configuration is low enough), the vibrational spectroscopic and possibly other properties of the molecule will be difficult if not impossible to distinguish from those of a strictly linear molecule. In fact, some of the spectroscopic properties of molecules usually regarded as strictly linear—disilylacetylene, cyanogen, carbon suboxide—may resemble those of quasi-linear molecules in certain respects, if the potential function for transverse displacements is sufficiently flat-bottomed. In the linear molecule disilyl acetylene,[15] the parallel band of SiH_2 deformation shows a clear-cut $P-R$ doublet, while the band due to the antisymmetric Si—C stretching vibration (analogous to the Si—O—Si motion) also has numerous components. These are probably due to the effect of excitation of the bending vibrations on the antisymmetric stretching frequency, and they produce a band contour which is strikingly similar to that of the Si—O—Si antisymmetric stretching band. No satellite is present, however, which is consistent with a strictly linear skeleton for disilyl acetylene.

ACKNOWLEDGMENTS

Discussions with Professor W. R. Thorson have been very helpful. The U. S. Air Force and the National Science Foundation gave financial assistance for which we express thanks.

[14] D. C. McKean, Spectrochim. Acta **13** 38 (1958).

[15] R. C. Lord, D. W. Mayo, H. E. Opitz, and J. S. Peake, Spectrochim. Acta **12**, 147 (1958).

Light-Induced *cis-trans* Isomerization of Nitrous Acid Formed by Photolysis of Hydrazoic Acid and Oxygen in Solid Nitrogen

JOHN D. BALDESCHWIELER* AND GEORGE C. PIMENTEL
Department of Chemistry, University of California, Berkeley, California

(Received May 6, 1960)

Photolysis of hydrazoic acid in solid nitrogen at 20°K with oxygen present yields both *cis-* and *trans-*nitrous acid. The identification is based on infrared detection of features of the isotopically substituted species HONO, DONO, and $HO^{18}NO^{18}$. The nitrous acid probably results from the reaction of imidogen with oxygen

$$NH+O_2=HONO.$$

Isomerization of nitrous acid occurs in the matrix at 20°K under the influence of irradiation. Ultraviolet radiation causes the *trans-* to *cis-* reaction, probably by electronic excitation to give a random mixture of the two forms. Near-infrared radiation reverses the reaction but the role of the radiation is not known. Bulk heating of the sample is not involved and a broad range of near-infrared frequencies is effective. No isomerization of DONO could be detected and $HO^{18}NO^{18}$ seemed to isomerize more slowly than did HONO. Only speculative interpretations of this phenomenon can be made at this time.

THE formation of nitrous acid during photolysis of hydrazoic acid in a nitrogen matrix containing some oxygen was proposed by Pimentel.[1] Two infrared features were observed which correspond reasonably well to the O—N stretching modes of the *cis-* and *trans-*isomers of HONO(856 and 794 cm^{-1}). Most surprising was the gradual disappearance of the band at 868 cm^{-1} and the growth of the band at 818 cm^{-1} during the spectroscopic study of the solid nitrogen sample. This behavior at 20°K furnished a basis of interest for further study and, as well, a basis for doubt concerning the identification of nitrous acid. The kinetic behavior, as interpreted by Pimentel, led to a low activation enthalpy for *cis-trans* isomerization (1.5 kcal) which is inconsistent with the best estimate of this barrier in gaseous nitrous acid, 12 kcal.[2] We report here studies directed toward the positive identification of the species causing the two absorptions and toward the elucidation of the process responsible for the kinetic behavior.

The spectroscopic studies of Jones, Badger, and Moore[2] and of D'Or and Tarte[3] furnish reliable data concerning gaseous nitrous acid. The *trans-* form is more stable than the *cis-* form by 506±250 calories[2] and the frequencies assigned to the torsional modes permit the estimate of the 12-kcal barrier to isomerization. The interpretations of the rotational structure furnish estimates of the molecular dimensions.[2] Palm[4] has made a normal coordinate analysis for nitrous acid, aiding the frequency assignment and the estimate of the isomerization barrier.

The electronic spectrum of nitrous acid in the spectral region 3000 to 4000 A was examined by D'Or and Tarte[5] and by Porter.[6] There is a system of diffuse bands extending from 3175 to 3835 A with a spacing of about 1100 cm^{-1} which is common to the spectra of HONO and of DONO.

The photolysis of hydrazoic acid in the gas phase has been reviewed briefly by Thrush.[7] At this time there seems to be no reason to doubt that the primary event in the photolysis is the reaction proposed by Beckman and Dickinson[8]:

$$HN_3+h\nu\rightarrow NH+N_2. \quad (1)$$

Becker and co-workers assume this reaction occurs when HN_3 is photolyzed in solid matrices at 20°K and it furnishes the basis for the interpretation of their experiments.[9]

We have found no literature reference to the mechanism of reaction between NH and O_2.

EXPERIMENTAL

The apparatus and technique for the matrix isolation study of nitrous acid have been described earlier.[9,10] A gaseous mixture of hydrazoic acid, oxygen, and nitrogen was deposited on a CsBr window held at 20°K, 16°K, or 4°K. The rate of sample deposition was a few cc (STP) per minute, i.e., 100–200 micromoles per minute. The base section of the cold cell permitted irradiation of the sample (after deposition) through a LiF window. The photolysis source was a medium pressure mercury arc (AH-4) focused onto the sample with a fused quartz lens. The radiation was filtered in some experiments with one of the filters listed in Table I. These filters are "cutoff" filters roughly characterized by the cutoff frequencies (or wavelengths) shown in

* Present address: Chemistry Department, Harvard University, Cambridge, Massachusetts.

[1] G. C. Pimentel, J. Am. Chem. Soc. **80**, 62–64 (1958).
[2] L. H. Jones, R. M. Badger, and G. E. Moore, J. Chem. Phys. **19**, 1599–1604 (1951).
[3] L. D'Or and P. Tarte, Bull. Soc. Roy. Sci. Liège **20**, 478–496 (1951).
[4] A. Palm, J. Chem. Phys. **26**, 855–859 (1957).
[5] L. D'Or and P. Tarte, Bull. Soc. Roy. Sci. Liège **20**, 685–692 (1951).
[6] G. Porter, J. Chem. Phys. **19**, 1278–1281 (1951).
[7] B. A. Thrush, Proc. Roy. Soc. (London) **A235**, 143 (1956).
[8] A. O. Beckman and R. G. Dickinson, J. Am. Chem. Soc. **50**, 1870 (1928).
[9] E. D. Becker, G. C. Pimentel, and M. Van Thiel, J. Chem. Phys. **26**, 145–150 (1957).
[10] E. D. Becker and G. C. Pimentel, J. Chem. Phys. **25**, 224–228 (1956).

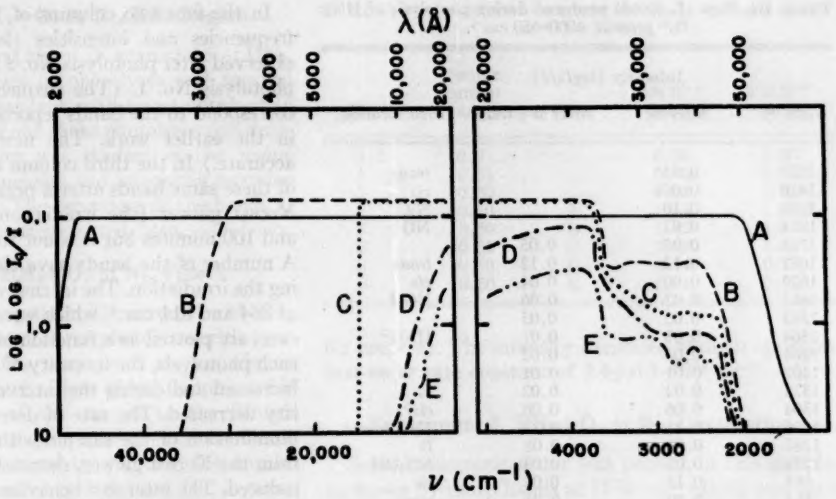

FIG. 1. Transmission properties of the filters shown in Table I.

the last two columns of Table I. The detailed transmission properties of these filters are shown in Fig. 1.

Spectra were recorded in the region 4000–650 cm^{-1} with a Perkin-Elmer model 21 Spectrophotometer (NaCl optics), in the region 700–400 cm^{-1} with a Perkin-Elmer model 12C Spectrometer (KBr optics), and in the near infrared and visible spectral regions (to 6000 A) with a Cary model 14 Spectrophotometer (quartz optics). Frequency accuracy is ± 2 cm^{-1} in the region 400–1000 cm^{-1}, ± 5 cm^{-1} to 2000 cm^{-1}, and about ± 10 cm^{-1} from 2000 to 4000 cm^{-1}.

Hydrazoic acid, HN_3, and DN_3 were prepared by the methods described by Van Thiel and Pimentel.[11] The desired amount of hydrazoic acid was mixed with oxygen (Stuart) at mole ratios O_2/HN_3 in the range between 1 and 7. To this mixture the matrix gas, nitrogen (Stuart), was added at a mole ratio N_2/HN_3 in the range between 250 and 500. Isotopically substituted oxygen was prepared by electrolysis of enriched H_2O^{18} (Weizmann Institute, Israel) using platinum electrodes. The isotopic composition of the water was 81% O^{18}, 2% O^{17}, 17% O^{16}, and the H/D ratio was about unity. A few crystals of anhydrous sodium sulfate were added to the electrolysis cell to provide an electrolyte.

TABLE I. Filters and spectral region excluded.

	Filter	uv-visible cutoff: λ below	Infrared cutoff: ν below
No filter	KBr (0.5 cm)	2000 A	400 cm^{-1}
A	LiF (0.5 cm)+ KBr (0.5 cm)	2000 A	1600 cm^{-1}
B	Slide glass	3000 A	2200 cm^{-1}
C	Corning 2460 RG5	6650 A	2300 cm^{-1}
D	Corning 2460 RG5 + Corning 27426 BG7	12 500 A	3150 cm^{-1}
E	Corning 2460 RG5 + Corning 22571 BG5	17 500 A	3650 cm^{-1}

[11] M. Van Thiel and G. C. Pimentel, J. Chem. Phys. **32**, 133–140 (1960).

RESULTS

Over 30 separate experiments were conducted. Only seven of these experiments will be described in detail but almost every conclusion presented has been corroborated in two or more experiments. The conditions of these seven experiments are presented in Table II.

Experiment 1. HN_3+O_2 in N_2

The sample, containing about 41 micromoles of HN_3, was deposited onto a CsBr window held at 16°K. The spectrum after deposition was similar to that reported by Becker *et al.* and it showed that most of the hydrazoic acid was present as monomer.

The sample was photolyzed for 60 minutes (photolysis No. 1) and the infrared spectrum was reexamined.

TABLE II. Experimental conditions.

Expt. No.	Sample	N_2/HN_3	O_2/HN_3	Deposition temp. (°K)	Temp. during spectral study (°K)
1	HN_3+O_2 in N_2	410	6.7	16	16, 20
2	HN_3+O_2 in N_2	410	6.7	20	20
3	HN_3+O_2 in N_2	410	6.7	20	20
4	HN_3+O_2 in N_2	455	6.5	20	4
5	DN_3+O_2 in N_2	340	1.2	20	20
6	$HN_3+O_2^{18}$ in N_2	294	?	20	20
7	$HN_3+O_2^{16}$, O_2^{18} in N_2	294	?	20	20

TABLE III. Expt. 1. Bands produced during photolysis of HN_3: O_2^{16} present. 4000–650 cm^{-1}.

	Intensity ($\log I_0/I$)		
ν(cm^{-1})	After $h\nu$	After $h\nu$+wait	Identification
3551	0.04		*trans*
3410	0.005		*cis*
2238	0.10		N_2O
1874	0.02		NO
1718	0.05	0.05	
1682	0.12	0.12	*trans*
1629	0.06	0.04	*cis*
1613	0.07	0.06	NO_2?
1583	0.05	0.05	
1564	0.01	0.01	HNO?
1464	0.03	0.02	
1402	0.01	0.01	
1323	0.02	0.02	E
1304	0.06	0.06	*cis*?
1296	0.21	0.22	N_2O, *trans*?
1287	0.09	0.08	D
1134	0.03	0.03	NH_2OH
864	0.12	0.05	*cis*
814	0.20	0.23	*trans*
662	0.04	0.03	*cis*

The intensity of the HN_3 absorption at 1273 cm^{-1} showed that about 50% of the HN_3 had been decomposed. Many new infrared absorptions were present. The sample was then exposed continuously for 104 minutes to the focused radiation of the Nernst glower source of the spectrometer with a glower current of 0.5 ampere. No measurable temperature rise was caused by this irradiation. During this period the intensities of some of the new bands were recorded repetitiously. Still at 16°K, the sample was photolyzed for an additional 60 minutes (photolysis No. 2). Again the spectral region 900–800 cm^{-1} was examined repetitiously over a period of 98 minutes but with the glower current reduced to 0.4 ampere. After photolysis No. 3 (30 minutes) the sample was studied in this limited region for 62 minutes with the glower current reduced to 0.34 ampere. The temperature of the sample was then raised to 20°K for the remainder of the experiment. The sample was photolyzed again (photolysis No. 4, 30 minutes) and the 900–800 cm^{-1} region was examined over a period of 69 minutes during which the sample was exposed to the glower radiation (0.5 ampere) for as short a period as possible (9 minutes). For most of this period the sample was left in the dark. For the following 67 minutes this procedure was repeated, 11 minutes exposed to the full radiation of the Nernst glower (0.5 ampere) and 56 minutes exposed to the portion of this radiation transmitted by a 5-mm lithium fluoride plate (filter A). The sample was photolyzed again (photolysis No. 5, 45 minutes) and the spectrum was recorded repetitiously for a period of 115 minutes with continuous glower irradiation (0.5 ampere). The last photolysis (photolysis No. 6, 32 minutes) was followed by spectral study during continuous glower irradiation (0.34 ampere).

In the first two columns of Table III are listed the frequencies and intensities ($\log I_0/I$) of the bands observed after photolysis No. 5 but not present prior to photolysis No. 1. (The frequencies 864 and 814 cm^{-1} correspond to the bands reported at 868 and 818 cm^{-1} in the earlier work. The new frequencies are more accurate.) In the third column are listed the intensities of these same bands after a period of irradiation by the Nernst glower (the irradiation period is between 50 and 100 minutes but it is not the same for each band). A number of the bands have changed in intensity during the irradiation. The intensity behaviors of the bands at 864 and 814 cm^{-1}, which were examined with special care, are plotted as a function of time in Fig. 2. During each photolysis, the intensity of the feature at 864 cm^{-1} increased and during the intervening periods the intensity decreased. The rate of decrease depends upon the illumination of the sample with the focused radiation from the Nernst glower, decreasing as glower current is reduced. The intensity behavior of 814 cm^{-1} was opposite that of 864 except during photolysis No. 2. The data are completely consistent with the interpretation that after photolysis No. 2 the intensity changes are due to conversion during glower irradiation of the compound causing the 864 cm^{-1} band into the compound causing the 814 cm^{-1} and the reverse conversion during photolysis. The behavior is different during photolysis No. 2 because decomposition of HN_3 is still an important process but thereafter the amount of HN_3 remaining is not sufficient to add noticeably to the products. The data indicate that the absorption coefficient at 864 cm^{-1} is larger than that at 814 cm^{-1} by a factor near 2.0. This is corroborated by the constancy (after photolysis No. 2) of the sum of the intensity of the band at 814 cm^{-1} plus one half that of the band at 864 cm^{-1}, as shown by the dashed line in Fig. 2.

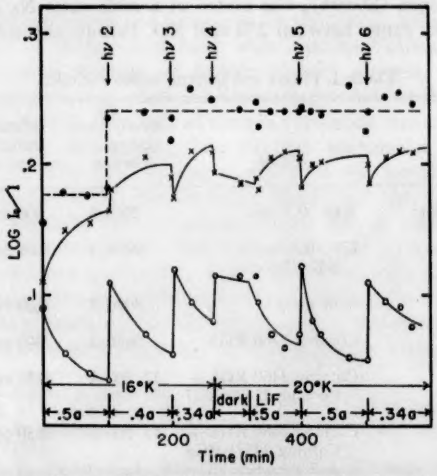

FIG. 2. Expt. 1. Intensities of bands at 864 and 814 cm^{-1}. ⊙ $\log I_0/I$(864 cm^{-1}). × $\log I_0/I$(814 cm^{-1}). ● $\log I_0/I$(814 cm^{-1})+½ $\log I_0/I$(864 cm^{-1}).

Experiment 2. HN_3+O_2 in N_2, KBr Region

This sample, containing about 28 micromoles of HN_3, was subjected to a series of photolyses and spectral studies with results consistent with those obtained in Expt. 1. Before and after one of the photolyses (photolysis No. 4) the spectrum was studied in the region 700–400 cm^{-1}. The frequencies and intensities recorded are shown in Table IV. The behaviors of the bands at 864 and 814 cm^{-1} were measured also, as shown.

Experiment 3. HN_3+O_2 in N_2, Filters

This sample, containing about 33 micromoles of HN_3, was subjected to a series of three photolyses with spectral studies between. The purpose of the experiment was to determine the rate of loss of the feature at 864 cm^{-1} during exposure of the sample to the focused radiation of the Nernst glower with various filters.

The results were analyzed by plotting the natural logarithm of optical density against time, i.e., in terms of first-order kinetics. The data are reasonably consistent with this assumption though they are of insufficient accuracy to verify positively the order.

TABLE IV. Expt. 2. Bands produced during photolysis of HN_3: O_2^{16} present. 700–400 cm^{-1}.

ν(cm^{-1})	Intensity ($\log I_0/I$) Before $h\nu$	After $h\nu$	After $h\nu$ + wait	Identification
864	...	0.09	0.04	*cis*
814	...	0.14	0.16	*trans*
662	0.04	0.05	0.03	*cis*
627	0.10	0.11	0.13	*cis, trans?*
585	0.10	0.11	0.10	*cis, trans?*

Table V lists the first-order rate constants, k, together with rate constants determined in Expt. 1. The results cannot be compared directly because the filters transmit only partially even in their most transparent spectral regions. Accordingly the experimental values, k, have been increased by dividing by the fraction of the light transmitted in the most transparent region. These derived values, k', are given in the last column of Table V. They show that the rate of the process causing the loss of the band at 864 cm^{-1} is reduced rather smoothly as the spectral region transmitted is narrowed. Furthermore, a significant rate of loss is caused by the focused radiation of the Nernst glower in the near-infrared region.

Experiment 4. HN_3+O_2 in N_2, Temperature

This sample, containing about 24 micromoles of HN_3, was deposited at 20°K and then the sample temperature was lowered to 4°K. The intensity of the band at 864 cm^{-1} was measured over a period of 43 minutes with constant illumination by the Nernst glower (current, 0.5 ampere). The intensity decreased with an apparent first-order rate constant of $2.4\pm0.5\cdot10^{-4}$ sec^{-1}.

TABLE V. First-order rate constants for loss of the band at 864 cm^{-1}. $T=20°K$.

Expt.	Source current (amp)	Filter	$k\times10^{+4}$ (sec^{-1})	$k'\times10^{+4}$ (sec^{-1})
1, 2	0.0	...	0.00	0.00
1	0.34	...	0.78	0.78
1	0.50	...	1.98	1.98
1	0.50	A	1.43	1.80
3	0.50	B	1.45	1.82
3	0.50	C	0.89	1.12
3	0.50	D	0.54	0.76
3	0.50	E	0.36	0.72

Experiment 5. DN_3+O_2 in N_2, Deuteration

Some monomeric water was present in this sample, as shown by sharp bands at 1179 cm^{-1} (D_2O) and 1404 cm^{-1} (HDO). This impurity gives probably the most reliable estimate of the percent deuteration (assuming exchange equilibrium between hydrazoic acid and water), 89%±5%.

This sample was exposed to three photolyses totaling 120 minutes, more sample was deposited and then a fourth photolysis of 45 minutes was conducted. Only the infrared spectra following the last photolysis need be reported here. Furthermore the results are consistent with those of two other experiments containing somewhat lower deuterium contents. Table VI shows the bands observed after but not prior to photolysis. The bands at 864 and 814 cm^{-1} were barely detectable and only two distinct new bands appeared in the spectral region 900–650 cm^{-1}. These bands, at 829 and 769 cm^{-1},

TABLE VI. Expt. 5. Bands produced during photolysis of DN_3 (89%). 4000–400 cm^{-1}.

ν(cm^{-1})	Intensity ($\log I_0/I$) After $h\nu$	Identification
2725	0.04	
2682	0.03	
2585	0.02	DONO *trans?*
2242	0.03	N_2O
1673	0.02	DONO *trans*
1614	0.01?	DONO *cis?*
1583	0.005?	
1295	0.01	N_2O
1289	0.01	D
1129	0.01	
1031	0.05	DONO *trans*
1023	0.02	DONO *cis?*
947	0.05	D
924	0.02	
917	0.06	ND_2OD
864	0.01?	HONO *cis*
829	0.08	DONO *cis*
814	0.01	HONO *trans*
769	0.03	DONO *trans*
617	0.06	DONO?
585	0.01?	DONO?
467	0.04	DONO?

TABLE VII. Expts. 6 and 7. Bands produced during photolysis of HN_3: O_2^{18} or $O_2^{18}+O_2^{16}$ present. 4000–650 cm^{-1}.

$\nu(cm^{-1})$	Intensity ($\log I_0/I$) Expt. 6	Expt. 7	Identification
3536	0.04	0.02	$HO^{18}NO^{18}$ *trans*
3404	0.005?	0.005?	$HO^{18}NO^{18}$ *cis*?
2238	0.05	0.025	N_2O
1689	0.025	0.02	
1682	...	0.02	$HO^{16}NO^{16}$ *trans*
1678	0.02	0.02	$HO^{18}NO^{16}$ *trans*
1663	...	0.01	
1641	0.06	0.03	$HO^{18}NO^{18}$ *trans*
1627	...	0.01	$HO^{16}NO^{16}$ *cis*
1589	0.04 (sh)[a]	0.02?	$HO^{18}NO^{18}$ *cis*?
1322	0.01	0.01	E
1296	...	0.03	$HO^{16}NO^{16}$ *trans*, N_2O^{16}
1287	0.06 (sh)	0.04 (sh)	D
1283	0.11	0.06	$HO^{18}NO^{18}$ *trans*
1256	0.03	0.01	N_2O^{18}
859	...	0.01	$HO^{16}NO^{18}$, $HO^{18}NO^{16}$ *cis*
850	0.04	0.02	$HO^{18}NO^{18}$ *cis*
814	...	0.01	$HO^{16}NO^{16}$ *trans*
810	0.03	0.01	$HO^{16}NO^{18}$, $HO^{18}NO^{16}$ *trans*
804	0.07	0.04	$HO^{18}NO^{18}$ *trans*
783	...	0.02	

[a] (sh)=shoulder.

are undoubtedly the counterparts of 864 and 814 cm^{-1}. It is true that 829 cm^{-1} is in coincidence with absorption by the species NHD_2, a product of photolysis in absence of oxygen.[11] The presence of oxygen, however, virtually eliminates ammonia, as seen in Expts. 1 through 4 and as verified in this experiment by the presence of at most a trace of absorption at 758 cm^{-1}, the most intense absorption of ND_3 in solid nitrogen.[11]

The next most prominent features were found at 917, 947, and 1031 cm^{-1}. The first two of these are produced in absence of O_2, and are assigned as species D and deuterated hydroxylamine, consistent with Van Thiel and Pimentel.[11] Assignments in the spectral region 650–400 cm^{-1} are not definite; the data are of lower reliability.

The spectral region 1100–700 cm^{-1} was examined repetitiously for 125 minutes with continuous irradiation by the Nernst glower (0.5 amp). None of the bands in this region changed intensity by more than the uncertainty in photometry, ± 0.01, though the weak absorption at 864 cm^{-1} seemed to disappear.

Experiments 6 and 7. $HN_3+O_2^{18}$ in N_2, Oxygen Isotopic Substitution

These samples were deposited at 20°K. In Expt. 6 the oxygen had the isotopic composition of the isotopically substituted H_2O (81% O^{18}). In Expt. 7, O_2 of this isotopic composition was mixed with an equal pressure of O_2^{16}. The bands produced during photolysis in each of these experiments are listed in Table VII.

In Expt. 6 the spectral region 925–650 cm^{-1} was examined repetitiously over a period of 180 minutes. The spectral feature at 850 cm^{-1} decreased in intensity during this time. The intensity of the feature was too low (0.04) to permit a quantitative specification of the apparent first-order rate constant. Qualitatively the disappearance of the band at 850 cm^{-1} seemed to be slower than that of the band at 864 cm^{-1} under comparable irradiation (see Expt. 1), possibly by as much as a factor of two or three.

DISCUSSION

Identification of HONO

In Expt. 1 there are a number of bands which can be assigned to the two forms of nitrous acid. These bands are in good agreement with the gas phase assignments,[2,3] as shown in Table VIII. The most distinct corroboration is, no doubt, provided by the bands at 1682 and 1629 cm^{-1}, undoubtedly the ν_2 modes, and the bands at 3551 and 3410 cm^{-1}, undoubtedly the ν_1 modes. The ν_3 modes could not be identified positively but there are indications that these vibrations absorb near 1300 cm^{-1}, in near-coincidence with bands due to other species such as D (at 1288 cm^{-1}), E (at 1325 cm^{-1}), N_2O (at 1296 cm^{-1}), and HN_3 (at 1273 cm^{-1}). The spectra do not permit distinction between the absorptions assignable to ν_5 and ν_6 but absorptions are found in the appropriate spectral region. Surely the spectral features produced during the photolysis in Expt. 1 are consistent with the postulate that photolysis of HN_3 in the presence of oxygen in solid nitrogen gives nitrous acid in both *cis*- and *trans*- forms.

The data of Expts. 5, 6, and 7 provide corroboration of the identification. Reasonable isotopic shifts are observed for the bands assigned to ν_2 and ν_4, shifts appropriate to modes which are predominantly N=O and N—O stretching motions. Though the assignments of bands to the other modes are less complete and less certain, no serious discrepancy is present.

There remains no doubt that the photolysis of hydrazoic acid in solid nitrogen in the presence of oxygen produces cis- and trans-nitrous acid.

Reaction of Formation of Nitrous Acid

If the primary photolytic process is the formation of NH by reaction (1), then nitrous acid is either formed through reaction (2) or reactions (3) and (4):

$$NH+O_2=HONO \qquad (2)$$

or

$$HN_3+h\nu=HN_3^* \qquad (3)$$

$$HN_3^*+O_2=HONO+N_2. \qquad (4)$$

The reactions (3) and (4) cannot be ignored since the photolytic excitation occurs under matrix conditions. As discussed by Pimentel,[1] the exact nature of the cage effect in matrix photolysis is not yet clear. It is conceivable that the constraints of the matrix cage alter the potential function for bond rupture in a fashion which permits reaction without the preliminary forma-

TABLE VIII. Vibrational frequencies of nitrous acid. *mx*=nitrogen matrix, 20°K.

	$HO^{16}NO^{16}$ (gas)		$HO^{16}NO^{16}$ (*mx*)	$DO^{16}NO^{16}$ (*mx*)	$HO^{15}NO^{15}$ (*mx*)
	D'O, T[a]	J, B, M[2]	Expt. 1	Expt. 5	Expts. 6, 7
trans					
ν_1 O—H str.[a]		3590	3551	2585	3536
ν_2 N=O str.	1700	1696	1682	1673	1641
ν_3 N—O—H bend	1267	1260	1296 (?)	1031	1283 (?)
ν_4 N—O str.	793	794	814	769	804
ν_5 O—N—O bend	598	598			
			627, 585	617, 585, 467(?)	
ν_6 O—H tors.[a]		543			
cis					
ν_1		3426	3410		3404
ν_2	1639		1629	1614 (?)	1589 (?)
ν_3			1304 (?)	1023 (?)	
ν_4	855	856	864	829	850
ν_5	525				
			662, 627, or 585		
ν_6	638	637			

[a] str.=stretch; tors.=torsion.

tion of NH (e.g., see the hypothetical curve *c* in Fig. 1 of footnote reference 1).

If reaction (2) is responsible, as seems more likely, this is probably the first direct evidence of this process. Wolfhard and Parker [12] have studied the ammonia-oxygen diffusion flame, and have shown that NH is an important reactant. Other spectral studies[13] of this flame have followed, including infrared methods.[14,15] Nitrous acid was detected in none of these experiments. However, the imidogen species, NH, is formed in a flame zone at a temperature above 2000°C and in the presence of hydroxyl radicals and oxygen atoms, so that other reactions are likely.[16]

Conditions more comparable to the matrix experiment would be the photolysis of gaseous HN_3 in the presence of oxygen. If the reaction occurs in the gas phase, recognition of reaction (2) would be difficult. Secondary reactions, including the disproportionation of HONO, would prevent accumulation of much nitrous acid. The interruption of such secondary reactions is a unique capability of the matrix method.

Isomerization of Nitrous Acid

The behaviors of the ν_4 bands of *cis*- and *trans*- HONO in Expt. 1 verify the occurrence of the isomerization reaction under matrix conditions, as proposed by Pimentel.[1] Figure 2 shows that the intensities of these two features behave in a complementary way, one increasing when the other decreases. The constancy of the sum of log I_0/I at 814 cm^{-1} and half that at 864 cm^{-1} indicates that the isomerization reaction is responsible and that the absorption coefficient of *cis*-HONO at 864 cm^{-1} is about double the absorption coefficient of *trans*-HONO at 814 cm^{-1}.

Two features of this isomerization process which were not recognized by Pimentel[1] are revealed in Fig. 2. First, the irradiation of the matrix sample containing nitrous acid with an AH-4 mercury lamp causes the formation of *cis*-HONO by the isomerization of *trans*-HONO. These photolysis periods always restore the ratio of the intensity at 814 cm^{-1} to that at 864 cm^{-1} to approximately 1.5. Using the absorption coefficients deduced above, this implies a mole ratio *trans*-/*cis*- near 3. The second feature is concerned with the intensity changes which occur between the photolysis periods. In Expt. 1, the rate of loss of the band at 864 cm^{-1} decreased as the Nernst glower current was lowered and practically no isomerization occurred during the wait period following photolysis No. 4 when the sample was not irradiated at all. The data prove that the disappearance of *cis*-HONO and growth of *trans*-HONO depend upon the irradiation of the sample by the light from the Nernst glower of the infrared spectrometer.

Ultraviolet-Induced Isomerization

The first of these light-induced reactions is undoubtedly caused by the absorption of ultraviolet light by nitrous acid. In the excited electronic state the loss of the inhibition of internal rotation would not be surprising. Presumably the ultraviolet light-induced reaction merely randomizes the *cis*- and *trans*- forms, the final

[12] H. G. Wolfhard and W. G. Parker, Proc. Phys. Soc. (London) **62**, 722 (1949); **65**, 2 (1952).

[13] M. Farber and A. J. Darnell, J. Chem. Phys. **22**, 1261–1263 (1954).

[14] D. A. Dows, E. Whittle, and G. C. Pimentel, J. Chem. Phys. **23**, 499–502 (1955).

[15] R. C. Lord and C. H. Sederholm, Spectrochim. Acta **1959**, 605–626.

[16] A remote piece of evidence is provided by the experiments of McKinley. On the basis of convincing chemical evidence, McKinley has proposed nitrous acid is present in the aqueous solution formed by dissolving the flame product gases of an H_2—O_2 flame containing small amounts of N_2 [J. D. McKinley, Jr., J. Chem. Phys. **22**, 1258 (1954)].

steady-state concentrations depending upon the relative absorption coefficients and the relative stabilities of the two species.

Infrared-Induced Isomerization

The second of these light-induced reactions is more unique and it has been studied in detail. The reaction seems to be approximately first-order insofar as our photometry accuracy permits a decision. Consequently the rates of isomerization are conveniently discussed in terms of the apparent first-order rate constants.

The first variable of interest is the frequency range which is effective. Filter A, lithium fluoride, has negligible transmission in the far infrared. Since the isomerization rate constant is affected very little by filter A, this isomerization is surely not caused by excitation of the ν_6 torsional mode in the spectral region in which the ν_6 fundamental mode absorbs. In fact the retention of a substantial rate of isomerization with filter E (see Table V) guarantees that the isomerization cannot be attributed to specific absorption in any of the fundamental vibrational modes of nitrous acid. Though filter E transmits less than 3% of the infrared radiation beyond 3500 cm^{-1}, the rate constant is still greater than 20% of its value with no filter.

These same filters eliminate the possibility that the isomerization should be attributed to a specific absorption in the visible or photographic infrared region. Filter E has negligible transmission at wavelengths below 17 500 A (frequencies above 5700 cm^{-1}). There remains the possibility that there is a specific absorption in the near-infrared region transmitted by filter E, 5700–3650 cm^{-1}. This is also inconsistent with the data, however. First, the near-infrared spectrum of the sample shows no distinct absorption bands. Second, the rate constants given in Table V are not in accord with this interpretation. In the last column are shown the rate constants, k', adjusted in accordance with the partial transmissions of the filters in this infrared region. If only frequencies in the range 5700–3650 cm^{-1} are effective, the adjusted k's should be constant. The trend shows that some of the isomerization process must be attributed to the spectral regions which have been excluded by the filters. *The data of Table V show that the isomerization process is induced by near-infrared light but over an extremely broad range of frequencies.*

This absence of frequency specificity leads to the obvious suggestion that the isomerization is caused by a bulk temperature rise in the sample. The absence of a measurable temperature rise in the salt window support could be blamed on poor thermal contact with the solid nitrogen film. This explanation can be ruled out as well. First, there is the difficulty that near-infrared light is apparently not absorbed by the sample. More compelling is the spectral evidence provided by the presence of small amounts of H_2O and NO in the sample of Expt. 1 (the former as an impurity, the latter as a photolysis product). These molecules provide monitors on the diffusion process. Water is known to diffuse rapidly in solid nitrogen at temperatures above 30–35°K[10,17] and nitric oxide at temperatures above 30°K.[18] The spectral features of these two molecules show conclusively that no diffusion occurs during the isomerization process. Hence any temperature rise caused by the Nernst glower irradiation must be less than 10°. This implies that cooling the sample to 4°K would be enough to keep the sample temperature below 20°K even during irradiation. If a bulk temperature rise caused the isomerization, then cooling to 4°K should stop the process completely. On the contrary, the result of Expt. 4 shows that the rate of isomerization is unaffected by cooling the sample to 4°K (within the experimental uncertainty). *The isomerization process cannot be attributed to a bulk-heating of the nitrogen matrix film.*

One other facet of the infrared-induced isomerization is revealed by Expts. 5, 6, and 7. Isotopic substitution causes a pronounced effect on the rate of isomerization. No isomerization of deuterated nitrous acid could be detected in Expt. 5, the time of study implying that the rate constant is lower than that for HONO by more than an order of magnitude. Even the oxygen eighteen substitution seemed to have a large effect on the rate (in Expt. 6), though this substitution causes an extremely small change in the reduced moment of inertia for the internal rotation associated with isomerization. This extreme mass-sensitivity of the isomerization rate is not compatible with an explanation based on the zero-point energy change of the effective activation energy. Rather it is reminiscent of the large mass effects expected for tunnelling processes.

In summary, the most obvious interpretations of the isomerization process seem to be ruled out. The simple kinetic picture offered earlier by Pimentel[1] must be discarded, since it predicts a very different isotopic substitution effect. The role of the infrared irradiation cannot be simply bulk-heating nor excitation of fundamental vibrations by absorption. We can offer only speculative proposals at this time. The absence of bulk-heating does not necessarily imply that there is no local heating. Perhaps the nitrous acid molecules are locally heated by some process such as absorption in the overtone region (the near infrared) or by Raman-like scattering processes. In either case, large amounts of vibrational energy could be placed in the nitrous acid, either to cause isomerization directly or indirectly through degradation of the energy into lattice heat in the immediate neighborhood of the nitrous acid. It is also possible that the phenomenon is somehow connected with the imperfect lattice arrangement of the matrix at an impurity site. Perhaps irradiation induces

[17] M. Van Thiel, E. D. Becker, and G. C. Pimentel, J. Chem. Phys. **27**, 486–490 (1957).

[18] J. D. Baldeschwieler, Ph.D. thesis, University of California, Berkeley, 1959.

a local annealing which could facilitate the isomerization. With any one of these possible roles of the irradiation, the isomerization could involve a barrier penetration mechanism. This feature is suggested by the mass-sensitivity of the rate. A more definite explanation will require more data. It does seem, however, that the infrared-induced isomerization is an unusual process, possibly of a type not observed before.[19]

CONCLUSIONS

The distinct identification of nitrous acid displays once again the unique potentialities of the matrix method for the study of interrupted chemical processes.[20] The direct study of the photolytic formation of nitrous acid from hydrazoic acid plus oxygen would be difficult and direct study of the light-induced isomerization of the *cis-* and *trans-* forms would be impossible with normal, gas phase conditions.

With respect to the kinetics of isomerization, the dilemma raised by Pimentel's simple rate interpretation[1] (i.e., the extremely low activation energy) was spurious but it has been replaced by another. It is now clear that under matrix conditions the isomerization reaction is induced by light. The "randomization" of the two forms under ultraviolet irradiation through electronic absorption is a reasonable explanation of the *trans*→*cis* change. However, the role of light in the *cis*→*trans* change, as brought on by near infrared irradiation, is not at all understood. The process responsible is characterized by an apparent absence of frequency sensitivity and a large isotopic effect.

Perhaps an unusual phenomenon has been detected—an infrared Raman scattering or a local annealing around a lattice impurity site are two possibilities.

ACKNOWLEDGMENTS

Grateful appreciation is expressed for research support by the American Petroleum Institute Research Project 54 and the United States Air Force through the AFOSR of the Air Research and Development Command. We would like to thank the National Science Foundation for predoctoral fellowship support (to J.D.B.).

[19] Though the process seems to be unusual, it cannot be called unique, for we have observed another infrared-induced matrix process which is also considered to involve rotational isomerization. The significance is less clear, however, since the spectral features under study are assigned to an isomeric form of N_2O_4, a species whose structure remains in some doubt. These results are described in footnote 18 and will be the subject of a separate publication. It is perhaps pertinent to add that the *cis-trans* isomerization of methyl nitrite suspended in solid nitrogen at 20°K could not be induced with infrared radiation. Mr. Yanis Abolinsch prepared such a sample in our laboratory. He found no measurable change in the spectral features of either *cis-* or *trans-*methyl nitrite after exposure of the sample to the focused radiation of the Nernst glower for a period of four hours.

[20] G. C. Pimentel, Spectrochim. Acta **12**, 94–96 (1958).

THE JOURNAL OF CHEMICAL PHYSICS VOLUME 33, NUMBER 4 OCTOBER, 1960

Study of Molecular Integrals. I. Two-Center Exchange Integrals*

R. C. SAHNI AND C. D. LABUDDE†

Institute for Mathematical Sciences, New York University, New York, New York

(Received September 4, 1959)

The evaluation of the two-center two-electron exchange integrals using prolate spheroidal coordinates and spherical coordinates is discussed. Estimates for the convergence rates of the infinite series which arise when both coordinate systems are used to evaluate the integrals are obtained.

INTRODUCTION

IN the theoretical determination of the electronic structure of molecules, several kinds of integrals arise which must be evaluated. The calculation of these integrals has been studied by several authors.[1–6] (The reader may consult these references for other literature on molecular integrals.) The hardest of these are the two-center two-electron integrals, the three-center one- and two-electron integrals, and the four-center two-electron integrals, as they give rise in general to infinite series. If these integrals are to be computed numerically, it becomes necessary to obtain

* The research reported in this paper was supported by the National Aeronautic and Space Administration.

† Present address: Department of Mathematics, Wayne State University, Detroit 2, Michigan.

[1] C. C. J. Roothaan, J. Chem. Phys. **19**, 1445 (1951).

[2] K. Rüdenberg, J. Chem. Phys. **19**, 1459 (1951).

[3] M. P. Barnett and C. A. Coulson, Phil. Trans. Roy. Soc. London **A243**, No. 864 (1951).

[4] M. Kotani, A. Amemiya, E. Ishiguro, and T. Kimura, *Table of Molecular Integrals* (Maruzen Company, Ltd., Tokyo, Japan, 1955).

[5] K. Rüdenberg, C. C. J. Roothaan, and W. Jaunzemis, J. Chem. Phys. **24**, 201 (1956).

[6] C. C. J. Roothaan, J. Chem. Phys. **24**, 947 (1956).

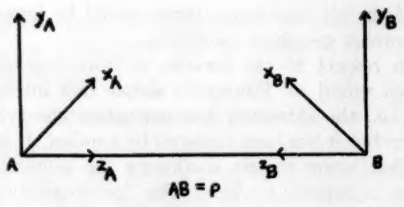

FIG. 1.

estimates of the convergence rates of these series so that appropriate cutoff criteria may be developed. The authors have carried out a systematic study of all the integrals involving $1s$, $2s$, and $2p$ functions. This paper will report the work on the two-center two-electron exchange integrals. Subsequent papers will report the work on the three- and four-center integrals.

1. TWO-CENTER TWO-ELECTRON EXCHANGE INTEGRALS

These integrals may be represented by:

$$\int_2\int_1 \chi_A^{(1)}(1)\chi_B^{(2)}(1)r_{12}^{-1}\chi_A^{(3)}(2)\chi_B^{(4)}(2)dV_1dV_2. \quad (1.1)$$

r_{12} is the distance from electron one to electron two. dV_δ, $\delta=1, 2$ are volume elements and the regions of integration are all of three-dimensional space. A, B represent the location of two nuclei in space. $P=AB$ (see Fig. 1). The functions $\chi_\mu^{(i)}(\delta)$, $i=1, 2, 3, 4$; $\mu=A, B$; $\delta=1, 2$ are among the five Slater functions given by

$$C(n, l, m; k)r_{\mu\delta}^{n-1}e^{-kr_{\mu\delta}}P_l^{|m|}(\cos\theta_{\mu\delta})\Phi_m(\phi_{\mu\delta}),$$

where k is a positive real number; n, l, m are integers satisfying

$$0\leq l<n\leq 2, \qquad 0\leq |m|\leq l;$$

$$C(n, l, m; k)=(2k)^{n+\frac{1}{2}}\left(\frac{(2l+1)(l-|m|)!}{2\pi(l+|m|)!(2n)!}\right)^{\frac{1}{2}};$$

and $\Phi_m(\phi)=\cos m\phi$ for $m>0$, $\Phi_0(\phi)=1/\sqrt{2}$, and $\Phi_m(\phi)=\sin|m|\phi$ for $m<0$.

2. METHODS FOR EVALUATING THE INTEGRALS

Two methods have been commonly considered for the evaluation of these integrals: one using prolate spheroidal coordinates and the other using spherical coordinates. In this paper we shall apply both of these methods to the evaluation of integrals (1.1) to determine the relative advantages and disadvantages of the methods. In particular, when infinite series are obtained, we shall derive estimates for the convergence rates of those series.

3. THE METHOD USING PROLATE SPHEROIDAL COORDINATES

In this coordinate system the integrals (1.1) take the form[5]

$$KC_1C_2C_3C_4\sum_{l=0}^{\infty}\sum_{m=0}^{l}C_{lm}\int_1^\infty\int_1^\infty\int_{-1}^1\int_{-1}^1\int_0^{2\pi}\int_0^{2\pi}[1+\xi_1\eta_1]^{l_1-|m_1|}[1-\xi_1\eta_1]^{l_2-|m_2|}[(\xi_1^2-1)(1-\eta_1^2)]^{(|m_1|+|m_2|)/2}$$

$$\times(\xi_1+\eta_1)^{n_1-l_1}(\xi_1-\eta_1)^{n_2-l_2}\exp(-\alpha_1\xi_1)\exp(-\beta_1\eta_1)Q_l^m(\xi_>)P_l^m(\xi_<)$$

$$\times P_l^m(\eta_1)P_l^m(\eta_2)[1+\xi_2\eta_2]^{l_3-|m_3|}[1-\xi_2\eta_2]^{l_4-|m_4|}[(\xi_2^2-1)(1-\eta_2^2)]^{(|m_3|+|m_4|)/2}(\xi_2+\eta_2)^{n_3-l_3}(\xi_2-\eta_2)^{n_4-l_4}$$

$$\times\exp(-\alpha_2\xi_2)\exp(-\beta_2\eta_2)\Phi_{m_1}(\phi_1)\Phi_{m_2}(\phi_1)\cos m(\phi_1-\phi_2)\Phi_{m_3}(\phi_2)\Phi_{m_4}(\phi_2)d\phi_1d\phi_2d\eta_1d\eta_2d\xi_1d\xi_2. \quad (3.1)$$

Here $C_{l0}=2(2l+1)$, $C_{lm}=4(-1)^m(2l+1)[(l-m)!/(l+m)!]^2$, $m\neq 0$, $\alpha_1=(\frac{1}{2})(k_1+k_2)$, $\alpha_2=(\frac{1}{2})(k_3+k_4)$, $\beta_1=(\frac{1}{2})(k_1-k_2)$, $\beta_2=(\frac{1}{2})(k_3-k_4)$, k_i, C_i, are the quantities associated with the Slater functions $\chi^{(i)}i=1, 2, 3, 4$ respectively, $K=\frac{1}{2}(\rho/2)^{n_1+n_2+n_3+n_4+1}$, and ρ is the internuclear distance.

Beginning with the variables ϕ_1, ϕ_2 we expand $\Phi_{m_1}\Phi_{m_2}$ and $\Phi_{m_3}\Phi_{m_4}$ as linear combinations of sines and cosines. The integral (3.1) will vanish unless the same functions occur in both the expansions for $\Phi_{m_1}\Phi_{m_2}$ and $\Phi_{m_3}\Phi_{m_4}$. If this is the case, the integrations over ϕ_1, ϕ_2 are immediate and the integral (3.1) may be written as a finite linear combination of integrals of the form

$$\sum_{l=M}^{\infty}C_{lM}\left[\int_1^\infty\int_1^\infty(\xi_1^2-1)^{M/2}\xi_1^{\tau_1}\exp(-\alpha_1\xi_1)Q_l^M(\xi_>)P_l^M(\xi_<)(\xi_2^2-1)^{M/2}\xi_2^{\tau_3}\exp(-\alpha_2\xi_2)d\xi_1d\xi_2\right]$$

$$\times\left[\int_{-1}^1(1-\eta_1)^{M/2}\eta_1^{\tau_2}\exp(-\beta_1\eta_1)P_l^M(\eta_1)d\eta_1\right]\left[\int_{-1}^1(1-\eta_2^2)^{M/2}\eta_2^{\tau_4}\exp(-\beta_2\eta_2)P_l^M(\eta_2)d\eta_2\right]. \quad (3.2)$$

Here the τ's are small, fixed integers and $M=0, 1, 2$ only.

We now note that if either $\beta_1=0$ or $\beta_2=0$, the series (3.2) will have only a finite number of terms different from zero. This will be the case in nearly three-quarters of the two-center exchange integrals involving Slater functions with major quantum numbers one or two. Hence, insofar as the convergence rate of the series is concerned, we need only consider the case where $\beta_1\neq 0$ and $\beta_2\neq 0$.

We further note that by the standard interchange of order of integration arguments, and the definitions of $\xi_<$, $\xi_>$ the series (3.2) may be written as a sum of two series of the form

$$\sum_{l=M}^{\infty} C_{lM}\left[\int_1^{\infty}\int_1^{\xi_2}(\xi_1^2-1)^{M/2}\xi_1^{\tau_1}\exp(-\alpha_1\xi_1)\,P_l^M(\xi_1)Q_l^M(\xi_2)\,(\xi_2^2-1)^{M/2}\xi_2^{\tau_3}\exp(-\alpha_2\xi_2)\,d\xi_1 d\xi_2\right]$$

$$\times\left[\int_{-1}^{1}(1-\eta_1^2)^{M/2}\eta_1^{\tau_2}\exp(-\beta_1\eta_1)\,P_l^M(\eta_1)\,d\eta_1\right]\left[\int_{-1}^{1}(1-\eta_2^2)^{M/2}\exp(-\beta_2\eta_2)\,\eta_2^{\tau_4}P_l^M(\eta_2)\,d\eta_2\right]. \quad (3.3)$$

We now expand $(\xi_1^2-1)^{M/2}\xi_1^{\tau_1}P_l^M(\xi_1)$; $(\xi_2^2-1)^{M/2}\xi_2^{\tau_3}Q_l^M(\xi_2)$; $(1-\eta_1^2)^{M/2}\eta_1^{\tau_2}P_l^M(\eta_1)$; $(1-\eta_2^2)^{M/2}\eta_2^{\tau_4}P_l^M(\eta_2)$ as linear combinations of functions $P_{l+\tau_5}(\xi_1)$, $Q_{l+\tau_6}(\xi_2)$, $P_{l+\tau_7}(\eta_1)$, $P_{l+\tau_8}(\eta_2)$ with coefficients, $G_{l\tau_1Mj_1}$; $G_{l\tau_3Mj_3}$, $G_{l\tau_2Mj_2}$; $G_{l\tau_4Mj_4}$, respectively, using the expansions given in Appendix A. Here $\tau_5=-M-\tau_1+2j_1$, $\tau_6=-M-\tau_3+2j_2$, $\tau_7=-M-\tau_2+2j_3$, $\tau_8=-M-\tau_4+2j_4$. If we define

$$A_{l_1i_2i_3i_4}=G_{l\tau_1Mj_1}G_{2\tau_3Mj_2}G_{2\tau_2Mj_3}G_{2\tau_4Mj_4}[(l-M)!/(l+M)!]^2 \quad (3.4)$$

then it can easily be shown from the properties of the G's that for all allowable values of the j's, the τ's and M,

$$\lim_{l\to\infty} A_{l_1i_2i_3i_4}\neq 0, \quad \pm\infty. \quad (3.5)$$

The number of different $A_{l_1i_2i_3i_4}$'s is bounded by some positive integer which is independent of l. Hence the convergence rate of the series (3.3) will be identical to that of a series of the form

$$\sum_{l=M}^{\infty}(2l+1)\left[\int_1^{\infty}\int_1^{\xi_2}\exp(-\alpha_1\xi_1)\,P_{l+\tau_5}(\xi_1)\,\exp(-\alpha_2\xi_2)Q_{l+\tau_6}(\xi_2)\,d\xi_1 d\xi_2\right]\left[\int_{-1}^{1}\exp(-\beta_1\eta_1)\,P_{l+\tau_7}(\eta_1)\,d\eta_1\right]$$

$$\times\left[\int_{-1}^{1}\exp(-\beta_2\eta_2)\,P_{l+\tau_8}(\eta_2)\,d\eta_2\right]. \quad (3.6)$$

We shall now derive an estimate for the convergence rate of series (3.6).

Starting with the last factor of a term in series (3.6) we write that factor as an infinite series

$$\int_{-1}^{1}\exp(-\beta_2\eta_2)\,P_{l+\tau_8}(\eta_2)\,d\eta_2=\sum_{i=0}^{\infty}[(-\beta_2)^i/i!]\int_{-1}^{1}\eta_2^iP_{l+\tau_8}(\eta_2)\,d\eta_2. \quad (3.7)$$

The integrals on the right-hand side of Eq. (3.7) were evaluated by M.P. Barnett and C. A. Coulson[3] and their values are as follows:

$$\int_{-1}^{1}\eta_2^iP_{l+\tau_8}(\eta_2)\,d\eta_2=\frac{2^{l+\tau_8+1}(i!)\,[(l+\tau_8+i)/2]!}{[(i-l-\tau_8)/2]!(i+l+\tau_8+1)!}, \quad (3.8)$$

if $i-l-\tau_8\geq 0$ and is even; otherwise, the integral (3.8) is equal to zero. Thus, we can readily deduce:

$$\int_{-1}^{1}\exp(-\beta_2\eta_2)\,P_{l+\tau_8}(\eta_2)\,d\eta_2=2^{l+\tau_8+1}\sum_{\substack{i=l+\tau_8\\ i-l-\tau_8\text{even}}}^{\infty}\frac{(-\beta_2)^i[(l+\tau_8+i)/2]!}{[(i-l-\tau_8)/2]!(i+l+\tau_8+1)!} \quad (3.9)$$

$$=2(-2\beta_2)^{l+\tau_8}\sum_{j=0}^{\infty}\frac{\beta_2^{2j}(l+\tau_8+j)!}{j!(2j+2l+2\tau_8+1!)}$$

$$=2(-2\beta_2)^{l+\tau_8}\frac{(l+\tau_8)!}{(2l+2\tau_8+1)!}\left[1+\frac{\beta_2^2}{2(2l+2\tau_8+3)}+\cdots\right].$$

Thus, for large l:

$$\int_{-1}^{1}\exp(-\beta_2\eta_2)\,P_{l+\tau_8}(\eta_2)\,d\eta_2\sim 2(-2\beta_2)^{l+\tau_8}\frac{(l+\tau_8)!}{(2l+2\tau_8+1)!}. \quad (3.10)$$

Similarly

$$\int_{-1}^{1}\exp(-\beta_1\eta_1)\,P_{l+\tau_7}(\eta_1)\,d\eta_1\sim 2(-2\beta_1)^{l+\tau_7}\frac{(l+\tau_7)!}{(2l+2\tau_7+1)!}. \quad (3.11)$$

To estimate the asymptotic behavior for large l of the double integral factors in the terms of series (3.6), we first use the recurrence relation

$$P_{l+1}(\xi)=[(2l+1)/(l+1)]\xi P_l(\xi)-[l/(l+1)]P_{l-1}(\xi) \tag{3.12}$$

to lower the index of $P_{l+\tau_5}(\xi)$ so that the double integral can be written as a linear combination of integrals of the form

$$\int_1^\infty\int_1^{\xi_2}\xi_1^{\tau_9}\exp(-\alpha_1\xi_1)P_{l+\tau_{10}}(\xi_1)\exp(-\alpha_2\xi_2)Q_{l+\tau_6}(\xi_2)d\xi_1d\xi_2, \tag{3.13}$$

where $l+\tau_6>l+\tau_{10}+1$. Now we can readily deduce the following inequalities, using the relations given in Appendices A and B:

$$\int_1^\infty\int_1^{\xi_2}\xi_1^{\tau_9}\exp(-\alpha_1\xi_1)P_{l+\tau_{10}}(\xi_1)\exp(-\alpha_2\xi_2)Q_{l+\tau_6}(\xi_2)d\xi_1d\xi_2\leq(\tau_9/\alpha_1)^{\tau_9}\exp(-\tau_9-\alpha_2)\int_1^\infty\int_1^{\xi_2}P_{l+\tau_{10}}(\xi_1)Q_{l+\tau_6}(\xi_2)d\xi_1d\xi_2$$

$$=(\tau_9/\alpha_1)^{\tau_9}\exp(-\tau_9-\alpha_2)(1/(2l+2\tau_{10}+1))\int_1^\infty Q_{l+\tau_6}(\xi_2)[P_{l+\tau_{10}+1}(\xi_2)-P_{l+\tau_{10}-1}(\xi_2)]d\xi_2$$

$$=(\tau_9/\alpha_1)^{\tau_9}\exp(-\tau_9-\alpha_2)(2l+2\tau_{10}+1)^{-1}\{[(\tau_6-\tau_{10}-1)(2l+\tau_6+\tau_{10}+1)]^{-1}-[(\tau_6-\tau_{10}+1)(2l+\tau_6+\tau_{10}^{-1})]^{-1}\}. \tag{3.14}$$

Thus, the double integral factors in the terms of series (3.6) approach zero as l approaches infinity at least as rapidly as C/l^2 (C=constant).

Finally, we may conclude that the absolute convergence rate of the series (3.6) will be at least as rapid as that of a series of the form

$$C\sum_{l=M}^\infty\frac{(2\beta_1)^{l+\tau_7}(2\beta_2)^{l+\tau_8}(l+\tau_7)!(l+\tau_8)!}{l(2l+2\tau_7+1)!(2l+2\tau_8+1)!}. \tag{3.15}$$

4. THE METHOD USING SPHERICAL COORDINATES

In this coordinate system the integrals (1.1) take the form

$$\int_2\int_1\chi_A^{(1)}(1)\chi_B^{(2)}(1)r_{12}^{-1}\chi_A^{(3)}(2)\chi_B^{(4)}(2)dV_1dV_2$$

$$=C_1C_2C_3C_4\sum_{l=0}^\infty\sum_{m=0}^l D_{lM}\int_0^\infty\int_0^\infty\int_0^\pi\int_0^\pi\int_0^{2\pi}\int_0^{2\pi}r_{A1}^{n_1+1}\exp(-k_1r_{A1})r_{B1}^{n_2-1}$$

$$\times\exp(-k_2r_{B1})(r_{A<}^l/r_{A>}^{l+1})r_{A2}^{n_3+1}\exp(-k_3r_{A2})r_{B2}^{n_4-1}\exp(-k_4r_{B2})P_{l_1}^{|m_1|}(\cos\theta_{A1})$$

$$\times P_{l_2}^{|m_2|}(\cos\theta_{B1})P_l^m(\cos\theta_{A1})P_l^m(\cos\theta_{A2})P_{l_3}^{|m_3|}(\cos\theta_{A2})P_{l_4}^{|m_4|}(\cos_{B2})$$

$$\times\sin\theta_{A1}\sin\theta_{A2}\Phi_{m_1}(\phi_1)\Phi_{m_2}(\phi_1)\cos m(\phi_1-\phi_2)\Phi_{m_3}(\phi_2)\Phi_{m_4}(\phi_2)d\phi_1d\phi_2d\theta_{A1}d\theta_{A2}dr_{A1}dr_{A2}, \tag{4.1}$$

where $D_{l0}=1$; $D_{lm}=2[(l+m)!/(l+m)!]$ $m\neq0$.

The analysis of the variables ϕ_1, ϕ_2 is identical to that given in the previous section. The integrations of these variables transform (4.1) into a linear combination of at most two series of the form

$$\sum_{l=M}^\infty D_{lM}\int_0^\infty\int_0^\infty\int_0^\pi\int_0^\pi r_{A1}^{n_1+1}\exp(-k_1r_{A1})r_{B1}^{n_2-1}\exp(-k_2r_{B1})(r_{A<}^l/r_{A>}^{l+1})$$

$$\times r_{A2}^{n_3+1}\exp(-k_3r_{A2})r_{B2}^{n_4-1}\exp(-k_4r_{B2})P_{l_1}^{|m_1|}(\cos\theta_{A1})P_{l_2}^{|m_2|}(\cos\theta_{B1})P_l^M(\cos\theta_{A1})$$

$$\times P_l^M(\cos\theta_{A2})P_{l_3}^{|m_3|}(\cos\theta_{A2})P_{l_4}^{|m_4|}(\cos\theta_{B2})\sin\theta_{A1}\sin\theta_{A2}d\theta_{A1}d\theta_{A2}dr_{A1}dr_{A2}. \tag{4.2}$$

Again, $M=0$, 1, 2 only.

Next, we expand $r_{B1}^{l_2}P_{l_2}^{|m_2|}(\cos\theta_{B1})$ and $r_{B2}^{l_4}P_{l_4}^{|m_4|}(\cos\theta_{B2})$ in terms of r_{A1}, ρ, $P_{l_5}^{|m_5|}(\cos\theta_{A1})$ and r_{A2}, ρ, $P_{l_6}^{|m_6|}$

$(\cos\theta_{A2})$, respectively, by the formulas given in footnote reference 3. Here $0\leq|m_5|\leq l_5\leq 1$ and $0\leq|m_6|\leq l_6\leq 1$. Then, we expand $r_{B1}^{n_3-l_3-1}e^{-k_3r_{B1}}$ and $r_{B2}^{n_4-l_4-1}e^{-k_4r_{B2}}$ in terms of r_{A1}, ρ, $P_{i_1}(\cos\theta_{A1})$ and r_{A2}, ρ, $P_{i_2}(\cos\theta_{A2})$, respectively, also by the formulas given in footnote reference 3. These expansions transform the series (4.2) into a linear combination of at most four series of the form

$$\sum_{l=M}^{\infty}\sum_{i_1=0}^{\infty}\sum_{i_2=0}^{\infty}D_{lM}(2i_1+1)(2i_2+1)\int_0^{\infty}\int_0^{\infty}\int_0^{\pi}\int_0^{\pi}r_{A1}^{\tau_1+1}\exp(-k_1r_{A1})f_{i_1}(k_2,r_{A1},\rho)(r_A{}^l</r_A{}^{l+1}>)$$
$$\times r_{A2}^{\tau_2+1}\exp(-k_3r_{A2})f_{i_2}(k_4,r_{A2},\rho)P_{i_1}(\cos\theta_{A1})P_{l_1}{}^{|m_1|}(\cos\theta_{A1})$$
$$\times P_{l_3}{}^{|m_3|}(\cos\theta_{A1})P_l{}^M(\cos\theta_{A1})P_l{}^M(\cos\theta_{A2})P_{l_3}{}^{|m_3|}(\cos\theta_{A2})$$
$$\times P_{l_4}{}^{|m_4|}(\cos\theta_{A2})P_{i_2}(\cos\theta_{A2})\sin\theta_{A1}\sin\theta_{A2}d\theta_{A1}d\theta_{A2}dr_{A1}dr_{A2}. \quad (4.3)$$

Here the τ's are small fixed integers and $f_i=p_i$ or q_i defined in footnote reference 3.

By analyzing each of the three cases $M=0$, 1, 2 separately, we find that we can expand $P_l{}^M(\cos\theta_{A1})P_{l_1}{}^{|m_1|}(\cos\theta_{A1})P_{l_5}{}^{|m_5|}(\cos\theta_{A1})$ and $P_l{}^M(\cos\theta_{A2})P_{l_3}{}^{|m_3|}(\cos\theta_{A2})P_{l_4}{}^{|m_4|}(\cos\theta_{A2})$ each as a linear combination of Legendre polynomials with the G's as coefficients by the expansions given in Appendix A. Then the integrations over the variables θ_{A1}, θ_{A2} can be performed using the orthogonality relations among the Legendre polynomials. The general result in all three cases $M=0$, 1, 2 is

$$D_{lM}(2i_1+1)(2i_2+1)\int_0^{\pi}\int_0^{\pi}P_{i_1}(\cos\theta_{A1})P_{l_1}{}^{|m_1|}(\cos\theta_{A1})P_{l_5}{}^{|m_5|}(\cos\theta_{A1})$$
$$\times P_l{}^M(\cos\theta_{A1})P_{i_2}(\cos\theta_{A2})P_{l_3}{}^{|m_3|}(\cos\theta_{A2})P_{l_4}{}^{|m_4|}(\cos\theta_{A2})P_l{}^M(\cos\theta_{A2})$$
$$\times\sin\theta_{A1}\sin\theta_{A2}d\theta_{A1}d\theta_{A2}=\sum_{j_1}\sum_{j_2}A_{lj_1j_2}, \quad (4.4)$$

where $A_{lj_1j_2}$ is a rational function of l, the degree of the numerator equaling the degree of the denominator. The summations over the indices j_1, j_2 arise from expanding $P_l{}^M(\cos\theta_{A1})P_{l_1}{}^{|m_1|}(\cos\theta_{A1})P_{l_5}{}^{|m_5|}(\cos\theta_{A1})$ and $P_l{}^M(\cos\theta_{A2})P_{l_3}{}^{|m_3|}(\cos\theta_{A2})P_{l_4}{}^{|m_4|}(\cos\theta_{A2})$ as linear combinations of Legendre polynomials, respectively. The number of different values for the j_1, j_2 is bounded by an integer independent of l. Because of the orthogonality properties of the Legendre polynomials, the i_1, i_2 are no longer independent but become linear functions of l. Thus, we have the general result:

$$\lim_{l\to\infty}A_{lj_1j_2}\neq 0, \quad \pm\infty. \quad (4.5)$$

Hence, the convergence rate of the series (4.2) will be identical to that of the series

$$\sum_{l=M}^{\infty}\int_0^{\infty}\int_0^{\infty}r_{A1}^{\tau_1+1}\exp(-k_1r_{A1})f_{l+\tau_3}(k_2,r_{A1},\rho)(r_A{}^l</r_A{}^{l+1}>)r_{A2}^{\tau_2+1}\exp(-k_3r_{A2})f_{l+\tau_4}(k_4,r_{A2},\rho)dr_{A1}dr_{A2}. \quad (4.6)$$

Now the $f_{l+\tau}$'s in (4.6) must equal either $p_{l+\tau}$ or $q_{l+\tau}$ as defined in footnote reference 3. Since

$$q_l=-k^{-1}p_l+[\text{higher order terms in } l] \quad (4.7)$$

we need consider only the case $f_{l+\tau}=p_{l+\tau}$ insofar as the convergence rate of (4.6) is concerned. We now write the $p_{l+\tau}$'s in (4.6) in terms of the $\gamma_{l+\tau}$'s defined in footnote reference 3 and note that the series (4.6) becomes a linear combination of at most four series of the form

$$\sum_{l=M}^{\infty}[(2+2\tau_3+1)(2+2\tau_4+1)]^{-1}\int_0^{\infty}\int_0^{\infty}r_{A1}^{\tau_1+1}\exp(-k_1r_{A1})\gamma_{l+\tau_5}(k_2,r_{A1},\rho)$$
$$\times(r_A{}^l</r_A{}^{l+1}>)r_{A2}^{\tau_2+1}\exp(-k_3r_{A2})\gamma_{l+\tau_6}(k_4,r_{A2},\rho)dr_{A1}dr_{A2} \quad (4.8)$$

where $\tau_5=\tau_3\pm 1$, $\tau_6=\tau_4\pm 1$.

Using the definitions of $r_{A<}$ and $r_{A>}$ and the standard interchange of order of integration argument, we may

write the series (4.8) as a sum of two series of the form

$$\sum_{l=M}^{\infty}[(2l+2\tau_3+1)(2l+2\tau_4+1)]^{-1}S_l=\sum_{l=M}^{\infty}[(2l+2\tau_3+1)(2l+2\tau_4+1)]^{-1}\int_0^{\infty}\int_0^{x}$$
$$\times y^{l+\tau_1+1}\exp(-k_1y)\gamma_{l+\tau_5}(k_2,y,\rho)x^{-l+\tau_2+1}\exp(-k_2y)\gamma_{l+\tau_6}(k_4,x,\rho)dydx \quad (4.9)$$

where $x=r_{A2}$, $y=r_{A1}$.

We shall now estimate the convergence rate of the series (4.9). First, we note that the integrands of S_l are nonnegative over the region of integration. Then we split up the integrals S_l into a sum of three integrals

$$S_l=S_l^1+S_l^2+S_l^3 \quad (4.10)$$

by splitting up the region of integration into three regions

$$\int_0^{\infty}\int_0^{x}=\int_0^{\rho}\int_0^{x}+\int_{\rho}^{\infty}\int_0^{\rho}+\int_{\rho}^{\infty}\int_{\rho}^{x}. \quad (4.11)$$

We may use the inequalities of Appendix B to derive the following inequalities for the S_l^j, $j=1, 2, 3$, and thereby determine their asymptotic behavior for large l.

$$S_l^1\geq\frac{\rho^{\tau_1+\tau_2+4}\exp[-(k_1+2k_2+k_3+2k_4)\rho]}{(2l+2\tau_5+1)(2l+2\tau_6+1)(2l+\tau_1+\tau_5+3)(2l+\tau_1+\tau_2+\tau_5+\tau_6+5)} \quad (4.12)$$

$$S_l^1\leq\frac{\rho^{\tau_1+\tau_2+4}\exp[(|k_4-k_3|+|k_2-k_1|)\rho]}{(2l+2\tau_5+1)(2l+2\tau_6+1)(2l+\tau_1+\tau_5+3)(2l+\tau_1+\tau_2+\tau_5+\tau_6+5)} \quad (4.13)$$

$$S_l^2\leq\frac{\rho^{\tau_1+\tau_2+4}\exp[(|k_4-k_3|+|k_2-k_1|)\rho]}{(2l+2\tau_5+1)(2l+2\tau_6+1)(2l+\tau_1+\tau_5+3)(2l+\tau_2+\tau_6-1)} \quad (4.14)$$

$$S_l^3\leq\frac{\rho^{\tau_1+\tau_2+4}\exp[(|k_4-k_3|+|k_2-k_1|)\rho]}{(2l+2\tau_5+1)(2l+2\tau_6+1)(2l+\tau_2+\tau_6-1)(2l+\tau_1-\tau_2+\tau_5+\tau_6+3)}. \quad (4.15)$$

From these inequalities we may infer that S_l behaves as K/l^4 for large l. Hence the series (4.9) converges at the same rate as does the series:

$$K\sum_{l=M}^{\infty}(1/l^4),\ K \text{ const.} \quad (4.16)$$

5. CONCLUSIONS

The results of this study show that the method using prolate spheroidal coordinates is preferable for the evaluation of the two-center exchange integrals to the method using spherical coordinates for two reasons. (1) Nearly three-quarters of the number of exchange integrals involving Slater functions with major quantum numbers one and two will give rise to finite series when the former method is used. The other method gives rise to infinite series in all cases. (2) The convergence rate of the infinite series in the former case have been shown to be much more rapid than that of the series obtained in the latter case.

ACKNOWLEDGMENTS

The authors wish to express their thanks to Professor Wilhelm Magnus for many helpful discussions in connection with this work.

APPENDIX A

EXPANSION FORMULA FOR THE LEGENDRE FUNCTIONS

We wish to give expansion formulas for $\cos^M\theta\sin^N\theta P_n^N(\cos\theta)$ and for $\xi^M(\xi^2-1)^N R_n^N(\xi)$ in terms of linear combinations of simpler functions where N, M, n are nonnegative integers, $1\leq\xi<+\infty$ and $R_n^N(\xi)=P_n^N(\xi)$ or $Q_n^N(\xi)$, the standard Legendre functions. The expansion formulas can easily be derived from the recurrence relations for Legendre functions and their differential equations.[7]

The expansion formulas are

$$\cos^M\theta\sin^N\theta P_n^N(\cos\theta)=\sum_{i=0}^{M+N}G_{nMNi}P_{n-N-M+2i}(\cos\theta) \quad (A.1)$$

$$\xi^M(\xi^2-1)^{N/2}R_n^N(\xi)=(-1)^N\sum_{i=0}^{M+N}G_{nMNi}R_{n-N-M+2i}(\xi), \quad (A.2)$$

where the G_{nMNi} (written G for short) are rational functions of n. In these formulas we take $P_{M-N-M+2i}$, $R_{n-N-M+2i}=0$ whenever $n-N-M-2i<0$. The first

[7] See E. W. Hobson, *Spherical and Ellipsoidal Harmonics* (Cambridge University Press, Cambridge, 1951).

thirteen G's are given below:

$$G_{n100}=[n/(2n+1)];$$
$$G_{n101}=[(n+1)/(2n+1)] \quad \text{(A.3)}$$
$$G_{n010}=[n(n+1)/(2n+1)];$$
$$G_{n011}=-[n(n+1)/(2n+1)] \quad \text{(A.4)}$$
$$G_{n200}=\frac{(n-1)n}{(2n-1)(2n+1)};$$
$$G_{n201}=\frac{2n^2+2n-1}{(2n-1)(2n+3)}; \quad \text{(A.5)}$$
$$G_{n202}=\frac{(n+1)(n+2)}{(2n+1)(2n+3)}$$
$$G_{n110}=\frac{(n-1)n(n+1)}{(2n-1)(2n+1)};$$
$$G_{n111}=\frac{n(n+1)}{(2n-1)(2n+3)} \quad \text{(A.6)}$$
$$G_{n112}=\frac{-n(n+1)(n+2)}{(2n+1)(2n+3)}$$
$$G_{n020}=\frac{(n-1)n(n+1)(n+2)}{(2n-1)(2n+1)};$$
$$G_{n021}=-2\frac{(n-1)n(n+1)(n+2)}{(2n-1)(2n+3)}; \quad \text{(A.7)}$$
$$G_{n022}=\frac{(n-1)n(n+1)(n+2)}{(2n+1)(2n+3)}.$$

In addition, we shall use the following formulas.[8]

$$\sin\theta P_n^{N+1}(\cos\theta)+2N\cos\theta P_n^N(\cos\theta)+(n-N+1)(n+N)\sin\theta P_n^{N-1}(\cos\theta)=0 \quad \text{(A.8)}$$

$$\cos\theta P_n^N(\cos\theta)=G_{n100}P_{n-1}^N(\cos\theta)+G_{n101}P_{n+1}^N(\cos\theta)-N\sin\theta P_n^{N-1}(\cos\theta) \quad \text{(A.9)}$$

$$\int_1^\infty P_v(\xi)Q_u(\xi)d\xi=[1/[(u-v)(u+v+1)]], \quad Re(u)>Re(v)>0. \quad \text{(A.10)}$$

APPENDIX B

SOME INEQUALITIES FOR THE BESSEL FUNCTIONS. $I_{n+\frac{1}{2}}$ AND $K_{n+\frac{1}{2}}$

The following inequalities for $I_{n+\frac{1}{2}}(x)$, $K_{n+\frac{1}{2}}(x)$ may be readily derived, using the integral representations[9] for $I_{n+\frac{1}{2}}$ and $K_{n+\frac{1}{2}}$, and integration by parts:

$$\frac{(2x)^{n+\frac{1}{2}}e^{-x}n!}{\sqrt{\pi}(2n+1)!}\leq I_{n+\frac{1}{2}}(x)\leq\frac{(2x)^{n+\frac{1}{2}}e^{x}n!}{\sqrt{\pi}(2n+1)!} \quad \text{(B.1)}$$

$$\frac{\sqrt{\pi}(2n)!e^{-x}}{(2x)^{n+\frac{1}{2}}n!}\leq K_{n+\frac{1}{2}}(x)\leq\frac{\sqrt{\pi}(2n)!}{(2x)^{n+\frac{1}{2}}n!}. \quad \text{(B.2)}$$

From the definition of $\gamma_n(k, x, \rho)$, (see footnote reference 3), $\rho>0$, $x\geq 0$ we can easily derive the following:

$$[(e^{-k(x+\rho)})/(2n+1)](x/\rho)^{n+\frac{1}{2}}\leq\gamma_n(k, x, \rho)\leq[e^{kx}/(2n+1)](x/\rho)^{n+\frac{1}{2}} \quad \text{for } 0\leq x\leq\rho \quad \text{(B.3)}$$

$$[(e^{-k(x+\rho)})/(2n+1)](\rho/x)^{n+\frac{1}{2}}\leq\gamma_n(k, x, \rho)\leq[e^{k\rho}/(2n+1)](\rho/x)^{n+\frac{1}{2}} \quad \text{for } x>\rho. \quad \text{(B.4)}$$

In addition, we will make use of the following inequalities:

$$\frac{e^{-kz}x^{n-1}}{n+1}\leq\int_0^x e^{-kv}y^n dy\leq[(x^{n+1})/(n+1)] \quad \text{(B.5)}$$

$$[x^{n+1}/(n+1)]\leq\int_0^x e^{kv}y^n dy\leq[(e^{kz}x^{n+1})/(n+1)] \quad \text{(B.6)}$$

$$\int_x^\infty e^{-kv}y^{-n}dy\leq[e^{-kz}/(n-1)x^{n-1})], \quad n\neq 1 \quad \text{(B.7)}$$

$$x^n e^{-kz}\leq(n/k)^n e^{-n}. \quad \text{(B.8)}$$

Here n is a positive integer, and k, x are positive real numbers.

---

[8] See Bateman Project, *Higher Transcendental Functions* (McGraw-Hill Book Company, Inc., New York, 1953).

[9] See G. N. Watson, *Bessel Functions* (Cambridge University Press, Cambridge, 1944).

Study of Molecular Integrals. II. Three-Center One-Electron and Two-Electron Integrals*

C. D. LaBudde† and R. C. Sahni

Institute for Mathematical Sciences, New York University, New York, New York

(Received September 4, 1959)

The evaluation of the three-center one-electron and two-electron integrals using spherical coordinates is discussed. Estimates for the convergence rates of the infinite series which arise in all cases are derived.

1. INTRODUCTION

IN paper I of this series, the authors discussed the evaluation of the two-center two-electron exchange integrals by two different methods and the convergence rates of the infinite series which arise in both cases.

In this paper we consider the problem of evaluating the three-center one- and two-electron integrals which arise in the theoretical determination of the electronic structure of triatomic molecules. These integrals are of the following three forms:

$$\int_1 \chi_A^{(1)}(1) r_{C1}^{-1} \chi_B^{(2)}(1)\, dv_1 \quad \text{(three-center potential energy integrals)} \tag{1.1}$$

$$\int_2 \int_1 \chi_A^{(1)}(1) \chi_B^{(2)}(1) r_{12}^{-1} \chi_A^{(3)}(2) \chi_C^{(4)}(2)\, dv_1 dv_2 \quad \text{(three-center hybrid exchange integrals)} \tag{1.2}$$

$$\int_2 \int_1 \chi_B^{(1)}(1) \chi_B^{(2)}(1) r_{12}^{-1} \chi_A^{(3)}(2) \chi_C^{(4)}(2)\, dv_1 dv_2 \quad \text{(three-center Coulomb exchange integrals).} \tag{1.3}$$

The χ's are among the Slater functions with major quantum number one or two. dV_δ $\delta=1, 2$ are volume elements and the integrations are over all of three-dimensional space. r_{12} is the distance from electron one to electron two. A, B, C, represent the locations of the three nucleii in space. $\rho_B = AB$, $\rho_C = AC$, and $<CAB = \alpha$. A, B, C are assumed to be noncolinear (see Fig. 1).

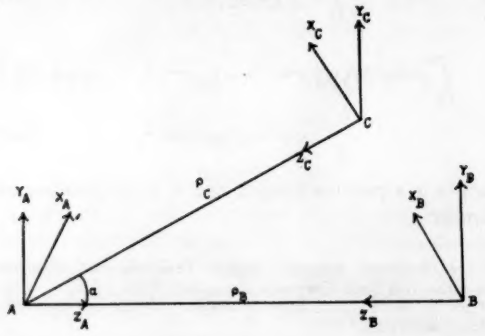

FIG. 1. Cartesian coordinates for a tri-atomic molecule.

2. METHOD FOR EVALUATING THE INTEGRALS

We shall employ the method using spherical coordinates to evaluate the integrals (1.1)–(1.3). The general procedure is identical to one used by the authors to evaluate the two-center exchange integrals.[1] The variables θ, ϕ are integrated explicitly. The results of these integrations are that integral (1.1) becomes an infinite series of one-dimensional integrals and integrals (1.2), (1.3) become infinite series of two-dimensional integrals. We then use the inequalities given in an earlier paper[1] to derive estimates for the convergence rates of these series.

* The research reported in this paper was jointly supported by the National Advisory and Space Administration and the Geophysical Research Directorate of the Air Force Cambridge Research Center, Air Research and Development.

† Present address: Department of Mathematics, Wayne State University, Detroit 2, Michigan.

[1] See R. C. Sahni and C. D. LaBudde, J. Chem. Phys. **32**, 1015 (1960), preceding article.

3. POTENTIAL ENERGY INTEGRALS

These integrals take the form

$$\int_1 \chi_A^{(1)}(1) r_{C1}^{-1} \chi_B^{(2)}(1) d\tau_1 = C_1 C_2 \sum_{i_1=0}^{\infty} \sum_{j=0}^{i} E_{i_1}' P_{i_1}^{j}(\cos\alpha) \int_0^{\infty}\int_0^{\pi}\int_0^{2\pi} r_{A1}^{n_1+1} e^{-k_1 r_{A1}}$$

$$\times r_{B1}^{n_2-1} e^{-k_2 r_{B1}} (\rho_{C<}^{i_1}/\rho_{C>}^{i_1+1}) P_{i_1}^{j}(\cos\theta_{A1}) P_{l_1}^{|m_1|}(\cos\theta_{A1}) P_{l_2}^{|m_2|}(\cos\theta_{B1}) \sin\theta_{A1}$$

$$\times \Phi_{m_1}(\phi_{A1}) \Phi_{m_2}(\phi_{A1}) \cos j\phi_{A1} d\phi_{A1} d\theta_{A1} dr_{A1}, \quad (3.1)$$

where $E'_{i0}=1$; $E'_{ij}=2(k-j)!/(i+j)!\, j\neq 0$: and $\rho_{C<}=\min(\rho_C, r_A)$: $\rho_C=\max(\rho_C, r_A)$.

The integrations of the variables ϕ, θ may be analyzed and performed in the same manner in which the integrations were analyzed and performed by the authors in the case of the two-center exchange integrals.[1] As a result of these integrations the series of integrals (3.1) is transformed into a finite linear combination of series of the form

$$\sum_{i=M}^{\infty} P_{i+\tau_1}(\cos\alpha)[1/(2i+2\tau_3+1)]S_i = \sum_{i=M}^{\infty} P_{i+\tau_1}(\cos\alpha)[1/(2i+2\tau_3+1)] \int_0^{\infty} x^{\tau_2+3/2} e^{-k_1 x} \gamma_{i+\tau_4}(k_2, x, \rho_B)(\rho_C^{i}/\rho_C^{i+1})\, dx, \quad (3.2)$$

where $x=r_{A1}$, and the τ's are small, fixed integers and $M=0, 1, 2$ only. The convergence rate of the series (3.2) is equivalent to that of the series (3.1).

We shall now proceed to investigate the absolute convergence rate of the series (3.2). We first note that the integrands of S_i are nonnegative. We then split up S_i into a sum of three integrals

$$S_i = S_i^1 + S_i^2 + S_i^3 \quad (3.3)$$

by splitting up the region of integration into three parts

$$\int_0^{\infty} = \int_0^{\rho_<} + \int_{\rho_<}^{\rho_>} + \int_{\rho_>}^{\infty}, \quad (3.4)$$

where $\rho_<=\min(\rho_B, \rho_C)$, $\rho_>=\max(\rho_B, \rho_C)$.

We must now consider three cases: $\rho_C<\rho_B$, $\rho_C>\rho_B$, and $\rho_C=\rho_B$. In each of the three cases separately we may use the inequalities given by the authors in an earlier paper[1] to derive inequalities for the S_i^j; $j=1, 2, 3$.

Case 1. $\rho_C<\rho_B$

Here we can derive the following inequalities for the S_i^j; $j=1, 2, 3$.

$$S_i^1 \geq \frac{e^{-k_2\rho_B-(k_1+k_2)\rho_C}\rho_B^{-\tau_4-1}\rho_C^{2+\tau_2+\tau_4}}{(2i+\tau_2+\tau_4+3)(2i+2\tau_4+1)}\left(\frac{\rho_C}{\rho_B}\right)^i \quad (3.5)$$

$$S_i^1 \leq \frac{e^{|k_2-k_1|\rho_C}\rho_B^{-\tau_4-1}\rho_C^{2+\tau_2+\tau_4}}{(2i+\tau_2+\tau_4+3)(2i+2\tau_4+1)}\left(\frac{\rho_C}{\rho_B}\right)^i \quad (3.6)$$

$$S_i^2 \geq \frac{e^{-k_2\rho_B}\rho_B^{-\tau_4-1}}{(2i+2\tau_4+1)}\left(\frac{\rho_C}{\rho_B}\right)^i \int_{\rho_C}^{\rho_B} x^{\tau_2+\tau_4+1} e^{-(k_1+k_2)x} dx \quad (3.7)$$

$$S_i^2 \leq \frac{\rho_B^{-\tau_4-1}}{(2i+2\tau_4+1)}\left(\frac{\rho_C}{\rho_B}\right)^i \int_{\rho_C}^{\rho_B} x^{\tau_2+\tau_4+1} e^{(k_2-k_1)x} dx \quad (3.8)$$

$$S_i^3 \leq \frac{e^{|k_2-k_1|\rho_B}\rho_B^{\tau_2+3/2}}{(2i+\tau_4-\tau_2-1)(2i+2\tau_4+1)}\left(\frac{\rho_C}{\rho_B}\right)^i. \quad (3.9)$$

If we take into account the coefficient of S_i, we can readily deduce that the over-all absolute convergence rate of the series (3.2) is the same as that of a series of the form

$$K\sum_{i=M}^{\infty}(1/i^{5/2})(\rho_C/\rho_B)^i \quad k=\text{const.} \tag{3.10}$$

Case 2. $\rho_C>\rho_B$

Here we can deduce the following inequalities:

$$S_i^1\geq\frac{e^{-(k_1+2k_2)\rho_B}\rho_B{}^{-\tau_2+5/2}\rho_C{}^{-1}}{(2i+2\tau_4+1)(2i+\tau_4+\tau_2+3)}\left(\frac{\rho_B}{\rho_C}\right)^i \tag{3.11}$$

$$S_i^1\leq\frac{e^{|k_2-k_1|\rho_B}\rho_B{}^{-\tau_2+5/2}\rho_C{}^{-1}}{(2i+2\tau_4+1)(2i+\tau_4+\tau_2+3)}\left(\frac{\rho_B}{\rho_C}\right)^i \tag{3.12}$$

$$S_i^2\geq\frac{e^{-k_2\rho_B}\rho_B{}^{\tau_4+1}\rho_C{}^{-1}}{(2i+2\tau_4+1)}\left(\frac{\rho_B}{\rho_C}\right)^i\int_{\rho_B}^{\rho_C}x^{\tau_2-\tau_4+1}e^{-(k_1+k_2)x}dx \tag{3.13}$$

$$S_i^2\leq\frac{e^{k_2\rho_B}\rho_B{}^{\tau_4+1}\rho_C{}^{-1}}{(2i+2\tau_4+1)}\left(\frac{\rho_B}{\rho_C}\right)^i\int_{\rho_B}^{\rho_C}x^{\tau_2-\tau_4+1}e^{-k_1x}dx \tag{3.14}$$

$$S_i^3\leq\frac{e^{k_2\rho_B-k_1\rho_C}\rho_B{}^{\tau_4+1}\rho_C{}^{\tau_2-\tau_4+1}}{(2i+2\tau_4+1)(2i+\tau_4-\tau_2-1)}\left(\frac{\rho_B}{\rho_C}\right)^i. \tag{3.15}$$

If we again take into account the coefficients of S_i, we see that in this case also, the absolute convergence rate is the same as that of the series (3.11).

We summarize the results of both cases in Fig. 2.

Case 3. $\rho_B=\rho_C$

Here $S_i^2=0$ and the absolute convergence rate of series (3.2) is the same as that of a series of the form

$$K\sum_{i=M}^{\infty}\frac{1}{i^{7/2}}. \tag{3.16}$$

4. HYBRID-EXCHANGE INTEGRALS

These integrals take the form

$$\int_2\int_1\chi_A{}^{(1)}(1)\chi_B{}^{(2)}(1)r_{12}{}^{-1}\chi_A{}^{(3)}(2)\chi_C{}^{(4)}(2)dv_1dv_2=C_1C_2C_3C_4\sum_{l=0}^{\infty}\sum_{m=0}^{l}D_{l_m}\int_0^{\infty}\int_0^{\infty}\int_0^{\pi}\int_0^{\pi}\int_0^{2\pi}\int_0^{2\pi}$$

$$r_{A1}{}^{n_1+1}e^{-k_1r_{A1}}r_{B1}{}^{n_2-1}e^{-k_2r_{B1}}(r_{A<}{}^l/r_{A>}{}^{l+1})r_{A2}{}^{n_3+1}e^{-k_3r_{A2}}$$

$$\times r_{C2}{}^{n_4-1}e^{-k_4r_{C2}}P_{l_1}{}^{|m_1|}(\cos\theta_{A1})P_{l_2}{}^{|m_2|}(\cos\theta_{B1})P_l{}^m(\cos\theta_{A1})$$

$$\times P_l{}^m(\cos\theta_{A2})P_{l_3}{}^{|m_3|}(\cos\theta_{A2})P_{l_4}{}^{|m_4|}(\cos\theta_{C2})\sin\theta_{A1}\sin\theta_{A2}$$

$$\times\Phi_{m_1}(\phi_{A1})\Phi_{m_2}(\phi_{B1})\cos m(\phi_{A1}-\phi_{A2})\Phi_{m_3}(\phi_{A2})\Phi_{m_4}(\phi_{C2})d\phi_{A1}d\phi_{A2}d\theta_{A1}d\theta_{A2}dr_{A1}dr_{A2}, \tag{4.1}$$

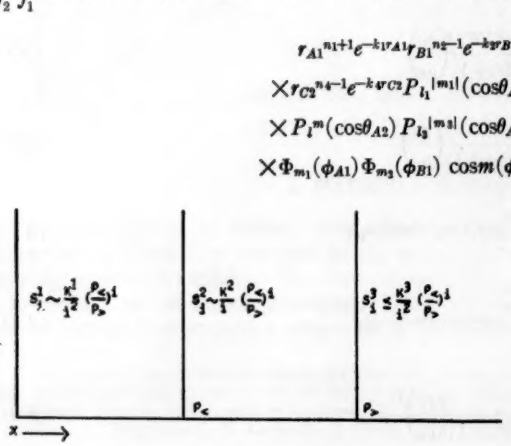

FIG. 2. k^1, k^2, k^3 are fixed constants.

where

$$D_{l_0}=1; \qquad D_{l_m}=2[(l-m)!/(l+m)!], \qquad m\neq 0.$$

If we carry out the analysis and integration of the variables ϕ_1, ϕ_2, θ_1, θ_2 as before, we may transform the series (4.1) into a finite linear combination of series of the following type:

$$\sum_{l=M}^{\infty}\frac{P_{l+\tau_7}(\cos\alpha)}{(2l+2\tau_3+1)(2l+2\tau_4+1)}S_l=\sum_{l=M}^{\infty}\frac{P_{l+\tau_7}(\cos\alpha)}{(2l+2\tau_3+1)(2l+2\tau_4+1)}\int_0^{\infty}\int_0^{z}y^{l+\tau_1+3/2}e^{-k_1y}$$

$$\times\gamma_{l+\tau_5}(k_2,y,\rho_B)x^{-l+\tau_2+\frac{1}{2}}e^{-k_3x}\gamma_{l+\tau_6}(k_4,x,\rho_C)dydx, \quad (4.2)$$

where $x=r_{A2}$, $y=r_{A1}$, the τ's are small fixed integers and $M=0$, 1, 2 only. The convergence rate of the series (4.2) is equivalent to that of the series (4.1).

We shall now investigate the absolute convergence rate of series (4.2). As before, the integrands of S are non-negative in the region of integration. We first split up the integrals S_l into sums of six integrals

$$S_l=\sum_{j=1}^{6}S_l^j \quad (4.3)$$

by splitting up the region of integration into six regions

$$\int_0^{\infty}\int_0^{z}\cdot dydx=\int_0^{\rho_<}\int_0^{z}\cdot dydx+\int_{\rho_<}^{\rho_>}\int_0^{\rho_<}\cdot dydx+\int_{\rho_<}^{\rho_>}\int_{\rho_<}^{z}\cdot dydx+\int_{\rho_>}^{\infty}\int_0^{\rho_>}\cdot dydx+\int_{\rho_>}^{\infty}\int_{\rho_<}^{\rho_>}\cdot dydx+\int_{\rho_>}^{\infty}\int_{\rho_>}^{z}\cdot dydx. \quad (4.4)$$

We must again consider three cases: $\rho_B<\rho_C$, $\rho_B>\rho_C$, and $\rho_B=\rho_C$. In each of the three cases, we apply the inequalities given in an earlier paper[1] to derive the inequalities for the S_l^j, given subsequently.

Case 1. $\rho_B<\rho_C$

Here we may easily derive the following inequalities for the S_l^j:

$$S_l^1\geq\frac{e^{-(k_1+2k_2+k_3+k_4)\rho_B-k_4\rho_C}\rho_B^{9/2+\tau_1+\tau_2+\tau_5}\rho_C^{-\tau_5-\frac{1}{2}}}{(2l+2\tau_5+1)(2l+2\tau_6+1)(2l+\tau_1+\tau_5+3)(2l+\tau_1+\tau_2+\tau_5+\tau_6+5)}\left(\frac{\rho_B}{\rho_C}\right)^l \quad (4.5)$$

$$S_l^1\leq\frac{e^{|k_4-k_3|\rho_B+|k_2-k_1|\rho_B}\rho_B^{9/2+\tau_1+\tau_2+\tau_5}\rho_C^{-\tau_5-\frac{1}{2}}}{(2l+2\tau_5+1)(2l+2\tau_6+1)(2l+\tau_1+\tau_5+3)(2l+\tau_1+\tau_2+\tau_5+\tau_6+5)}\left(\frac{\rho_B}{\rho_C}\right)^l \quad (4.6)$$

$$S_l^2\geq\frac{e^{-(k_1+2k_2)\rho_B-k_4\rho_C}\rho_B^{\tau_1+5/2}\rho_C^{-\tau_5-\frac{1}{2}}}{(2l+2\tau_5+1)(2l+2\tau_6+1)(2l+\tau_1+\tau_5+3)}\left(\frac{\rho_B}{\rho_C}\right)^l\int_{\rho_B}^{\rho_C}x^{\tau_2+\tau_5+1}e^{-(k_3+k_4)x}dx \quad (4.7)$$

$$S_l^2\leq\frac{e^{|k_2-k_1|\rho_B}\rho_B^{\tau_1+5/2}\rho_C^{-\tau_5-\frac{1}{2}}}{(2l+2\tau_5+1)(2l+2\tau_6+1)(2l+\tau_1+\tau_5+3)}\left(\frac{\rho_B}{\rho_C}\right)^l\int_{\rho_B}^{\rho_C}x^{\tau_2+\tau_5+1}e^{(k_4-k_3)x}dx \quad (4.8)$$

$$S_l^3\geq\frac{e^{-k_2\rho_B-k_4\rho_C}\rho_B^{\tau_5+\frac{1}{2}}\rho_C^{-\tau_5-\frac{1}{2}}}{(2l+2\tau_5+1)(2l+2\tau_6+1)}\left(\frac{\rho_B}{\rho_C}\right)^l\int_{\rho_B}^{\rho_C}\int_{\rho_B}^{z}y^{\tau_1-\tau_5+1}e^{-(k_1+k_2)y}x^{\tau_2+\tau_5+1}e^{-(k_3+k_4)x}dydx \quad (4.9)$$

$$S_l^3\leq\frac{\rho_B^{\tau_5+\frac{1}{2}}\rho_C^{-\tau_5-\frac{1}{2}}}{(2l+2\tau_5+1)(2l+2\tau_6+1)}\left(\frac{\rho_B}{\rho_C}\right)^l\int_{\rho_B}^{\rho_C}\int_{\rho_B}^{z}y^{\tau_1-\tau_5+1}e^{(k_2-k_1)y}x^{\tau_2+\tau_5+1}e^{(k_4-k_3)x}dydx \quad (4.10)$$

$$S_l^4\leq\frac{e^{|k_4-k_3|\rho_C+|k_2-k_1|\rho_B}\rho_B^{\tau_1+\frac{1}{2}}\rho_C^{\tau_2+\frac{1}{2}}}{(2l+2\tau_5+1)(2l+2\tau_6+1)(2l+\tau_6-\tau_2-1)(2l+\tau_1+\tau_5+3)}\left(\frac{\rho_B}{\rho_C}\right)^l \quad (4.11)$$

$$S_l^5\leq\frac{e^{k_2\rho_B+|k_4-k_3|\rho_C}\rho_B^{\tau_5+\frac{1}{2}}\rho_C^{\tau_2+\frac{1}{2}}}{(2l+2\tau_5+1)(2l+2\tau_6+1)(2l+\tau_6-\tau_2+1)}\left(\frac{\rho_B}{\rho_C}\right)^l\int_{\rho_B}^{\rho_C}y^{\tau_1-\tau_5+1}e^{-k_1y}dy \quad (4.12)$$

$$S_l^6\leq\frac{e^{k_2\rho_B+(k_4-k_1-k_2)\rho_C}\rho_B^{\tau_5+\frac{1}{2}}\rho_C^{\tau_1+\tau_2-\tau_5+7/2}}{(2l+2\tau_5+1)(2l+2\tau_6+1)(2l-\tau_2+\tau_6+1)(2l+\tau_6-\tau_2+\tau_5-\tau_1-3)}\left(\frac{\rho_B}{\rho_C}\right)^l. \quad (4.13)$$

The asymptotic behaviors of the S_l^j for large l are summarized in Fig. 3.

In this case, then, the over-all absolute rate of convergence of the series (4.2) is the same as that of a series of the form

$$K\sum_{l=M}^{\infty}(1/l^{9/2})(\rho_B/\rho_C)^l \quad K=\text{const.} \tag{4.14}$$

Case 2. $\rho_B > \rho_C$

Here we may derive the following inequalities for the S_l^j:

$$S_l^1 \geq \frac{e^{-k_2\rho_B-(k_1+k_2+k_3+2k_4)\rho_C}\rho_B^{-\tau_5-\frac{1}{2}}\rho_C^{\tau_1+\tau_2+\tau_5+9/2}}{(2l+2\tau_5+1)(2l+2\tau_6+1)(2l+\tau_1+\tau_5+3)(2l+\tau_1+\tau_2+\tau_5+\tau_6+5)}\left(\frac{\rho_C}{\rho_B}\right)^l \tag{4.15}$$

$$S_l^1 \leq \frac{e^{|k_4-k_3+|k_2-k_1||\rho_C}\rho_B^{-\tau_5-\frac{1}{2}}\rho_C^{\tau_1+\tau_2+\tau_5+9/2}}{(2l+2\tau_5+1)(2l+2\tau_6+1)(2l+\tau_1+\tau_5+3)(2l+\tau_1+\tau_2+\tau_5+\tau_6+5)}\left(\frac{\rho_C}{\rho_B}\right)^l \tag{4.16}$$

$$S_l^2 \geq \frac{e^{-(k_3+2k_4)\rho_B-(k_1+2k_2)\rho_C}\rho_B^{-\tau_5-\frac{1}{2}}\rho_C^{9/2+\tau_1+\tau_2+\tau_5}}{(2l+2\tau_5+1)(2l+\tau_1+\tau_5+3)(2l+2\tau_6+1)(2l+\tau_6-\tau_2-1)}\left(\frac{\rho_C}{\rho_B}\right)^l \tag{4.17}$$

$$\times\left[1-\left(\frac{\rho_C}{\rho_B}\right)^{2l+\tau_6-\tau_2-1}\right]$$

$$S_l^2 \leq \frac{e^{(|k_2-k_1|+k_4-k_3)\rho_C}\rho_B^{-\tau_5-\frac{1}{2}}\rho_C^{9/2+\tau_1+\tau_2+\tau_5}}{(2l+2\tau_5+1)(2l+\tau_1+\tau_5+3)(2l+2\tau_6+1)(2l+\tau_6-\tau_2-1)}\left(\frac{\rho_C}{\rho_B}\right)^l\left[1-\left(\frac{\rho_C}{\rho_B}\right)^{2l+\tau_6-\tau_2-1}\right] \tag{4.18}$$

$$S_l^3 \geq \frac{e^{-k_4\rho_C-(k_1+2k_2+k_3+k_4)\rho_B}\rho_C^{\tau_6+\frac{1}{2}}\rho_B^{-\tau_5-\frac{1}{2}}}{(2l+2\tau_5+1)(2l+2\tau_6+1)(2l+\tau_1+\tau_5+3)}\left(\frac{\rho_C}{\rho_B}\right)^l$$

$$\times\left[\frac{\rho_B^{\tau_2+\tau_5+\tau_2-\tau_6+4}-\rho_C^{\tau_1+\tau_5+\tau_2-\tau_6+4}}{(\tau_1+\tau_5+\tau_4-\tau_6+4)}-\frac{\rho_C^{\tau_1+\tau_2+\tau_5-\tau_6+4}}{(2l+\tau_2-\tau_6-1)}\left[\left(\frac{\rho_C}{\rho_B}\right)^{2l-\tau_2+\tau_6-1}-1\right)\right] \tag{4.19}$$

$$S_l^3 \leq \frac{e^{(|k_4-k_3|+|k_2-k_1|)\rho_B}\rho_C^{\tau_6+\frac{1}{2}}\rho_B^{-\tau_5-\frac{1}{2}}}{(2l+2\tau_5+1)(2l+2\tau_6+1)(2l+\tau_1+\tau_5+3)}\left(\frac{\rho_C}{\rho_B}\right)^l\left[\frac{\rho_B^{\tau_1+\tau_5+\tau_2-\tau_6+4}-\rho_C^{\tau_1+\tau_5+\tau_2-\tau_6+4}}{(\tau_1+\tau_5+\tau_4-\tau_6+4)}-\frac{\rho_C^{\tau_1+\tau_2+\tau_5-\tau_6+4}}{(2l+\tau_2-\tau_6-1)}\right.$$

$$\left.\times\left[\left(\frac{\rho_C}{\rho_B}\right)^{2l-\tau_2+\tau_6-1}-1\right]\right] \tag{4.20}$$

$$S_l^4 \leq \frac{e^{-k_2\rho_B+(k_4+|k_2-k_1|)\rho_C}\rho_C^{\tau_1+\tau_5+\tau_6+7/2}\rho_B^{-\tau_6+\tau_2+\frac{1}{2}}}{(2l+2\tau_6+1)(2l+\tau_6-\tau_2-1)(2l+2\tau_5+1)(2l+\tau_1+\tau_5+3)}\left(\frac{\rho_C}{\rho_B}\right)^{2l} \tag{4.21}$$

$$S_l^5 \leq \frac{e^{k_4\rho_C+(|k_2-k_1|-k_2)\rho_B}\rho_C^{\tau_6+\frac{1}{2}}\rho_B^{\tau_1+\tau_2-\tau_5-\tau_6+\frac{1}{2}}}{(2l+2\tau_5+1)(2l+\tau_1+3)(2l+2\tau_6+1)(2l+\tau_6-\tau_2-1)}\left(\frac{\rho_C}{\rho_B}\right)^l\left[1-\left(\frac{\rho_C}{\rho_B}\right)^{2l+\tau_1+\tau_5+3}\right] \tag{4.22}$$

$$S_l^6 \leq \frac{e^{(k_2-k_1-k_3)\rho_B+k_4\rho_C}\rho_B^{\tau_1+\tau_2-\tau_6+5/2}\rho_C^{\tau_6+\frac{1}{2}}}{(2l+2\tau_5+1)(2l+2\tau_6+1)(2l-\tau_2+\tau_6-1)(2l+\tau_6+\tau_5-\tau_1-\tau_2-3)}\left(\frac{\rho_C}{\rho_B}\right)^l. \tag{4.23}$$

The asymptotic behaviors of S_l^j for large l are summarized in Fig. 4.

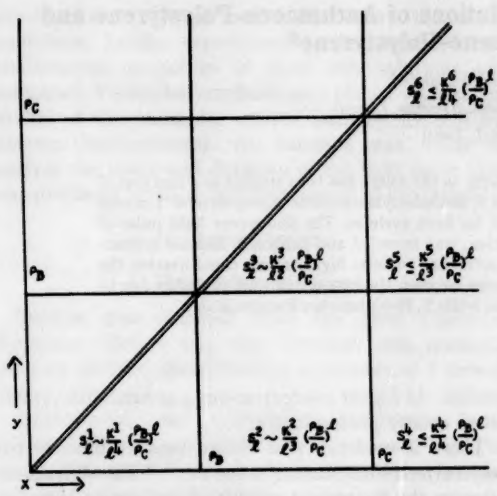

FIG. 3. The k^i are constants. The double lines bound the region of integration; $0 \leq y \leq x$, $0 \leq x < +\infty$.

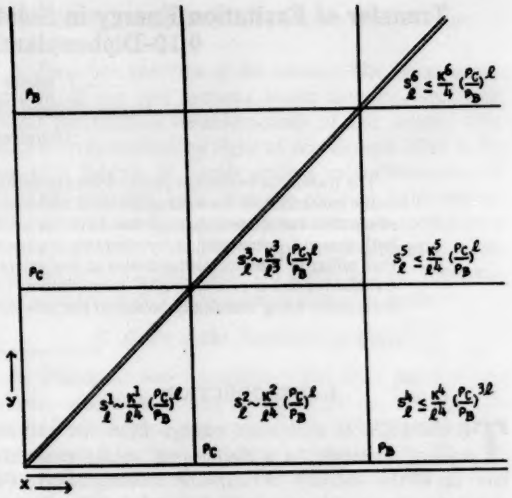

FIG. 4. The k^i are constants. The double lines bound the region of integration; $0 \leq y \leq x$, $0 \leq x < +\infty$.

In this case the absolute convergence rate of the series (4.2) is the same as that of a series of the form

$$k\sum_{l=M}^{\infty}(1/l^{11/2})(\rho_C/\rho_B)^l \quad k=\text{const.} \tag{4.24}$$

Case 3. $\rho_B=\rho_C$

Here $S_l^2=S_l^3=S_l^5=0$. In this case, the absolute convergence rate of the series (4.9) is the same as that of a series of the form

$$k\sum_{l=M}^{\infty}(1/l^{13/2}) \quad k=\text{const.} \tag{4.25}$$

5. COULOMB EXCHANGE INTEGRALS

$$\int_2\int_1 \chi_B^{(1)}(1)\chi_B^{(2)}(1)r_{12}^{-1}\chi_A^{(3)}(2)\chi_C^{(4)}(2)dv_1dv_2. \tag{5.1}$$

The analysis of these integrals and the results of that analysis are identical to those of the hybrid exchange integrals except in the one case where $\chi_B^{(1)}(1)=\chi_B^{(2)}(1)=\chi_{2.0,0;B}(1)$; the Slater function commonly referred to as $2S$. In this case the function of r_{B1} does not equal p_l or q_l but equals ζ_{3l},[2] when ζ_{3l} is written as a linear combination of functions γ_l, an extra factor of $1/(2l+2\tau+1)$ is introduced, where τ is a small fixed integer. We summarize the absolute asymptotic behavior of the series, in this case as follows:

Case 1. $\rho_B<\rho_C$

$$k\sum_{l=M}^{\infty}(1/l^{11/2})(\rho_B/\rho_C)^l. \tag{5.2}$$

Case 2. $\rho_B>\rho_C$

$$k\sum_{l=M}^{\infty}(1/l^{13/2})(\rho_C/\rho_B)^l. \tag{5.3}$$

Case 3. $\rho_B=\rho_C$

$$k\sum_{l=M}^{\infty}(1/l^{15/2}) \tag{5.4}$$

$k=\text{const.}$

[2] See M. P. Barnett and C. A. Coulson, Phil. Trans. Roy. Soc. London **A243**, No. 864 (1951), for definitions of these functions.

ACKNOWLEDGMENTS

The authors wish to express their thanks to Professor Wilhelm Magnus for many helpful discussions in connection with this work.

Transfer of Excitation Energy in Solid Solutions of Anthracene-Polystyrene and 9,10-Diphenylanthracene-Polystyrene*

L. J. BASILE AND A. WEINREB†
Argonne National Laboratory, Argonne, Illinois

(Received June 7, 1960)

The transfer of excitation energy from the excited solvent to the solute has been studied as a function of solute concentration for solid solutions of anthracene and 9,10-diphenylanthracene in polystyrene. Transfer efficiencies and fluorescence spectra have been obtained for both systems. The fluorescent light pulse of both systems, when excited by electrons and uv radiation, was recorded and analyzed. Results indicate that radiative transfer predominates at low solute concentration, while at higher solute concentration the transfer process is predominantly nonradiative. Differences between the two systems are probably due to anthracene being chemically bound to the polymer chain while 9,10-diphenylanthracene is not.

I. INTRODUCTION

TRANSFER of excitation energy from an excited solvent molecule to a fluorescent solute molecule has been the subject of various investigations. Of particular interest is the use of plastic solid solution scintillators.[1-8] The solvent, a noncrystalline heterogeneous mixture of randomly oriented long-chain molecules, makes up the rigid medium. A fluorescent solute is incorporated in this medium. Since the medium is rigid, Brownian motion of the molecules is very limited. Energy transfer by diffusion and collisions of accepting and donating molecules can be neglected.

The rigidity of the solvent medium is an important physical difference between plastic solid solution and liquid solution scintillators. An equally important difference between the two types of solutions is that polystyrene, the solvent used in this study, has a higher fluorescent quantum yield than most solvents used in liquid scintillating solutions. This facilitates the occurrence of a radiative transfer process in plastic solid solutions. In discussing the polystyrene-anthracene system, Koski suggests a radiative transfer mechanism involving fluorescence of polystyrene followed by absorption by anthracene.[1] The excited anthracene molecule then emits its characteristic radiation. Swank and Buck investigated a number of solutes in polystyrene.[2] They concluded that, while radiative transfer does contribute to the over-all process, the major fraction of energy is transferred by some nonradiative process. Krenz investigated the polystyrene-anthracene system in detail.[3] His evidence indicates that a radiative transfer process does take place at low solute concentration. At higher concentrations a nonradiative transfer of energy predominates.

There is evidence that shows that anthracene copolymerizes with styrene monomer.[9,10] The differences between the fluorescent spectra of anthracene that has been copolymerized with polystyrene and anthracene that has been imbedded after polymerization have been studied by Hinrichs.[11] Krenz suggests that in the case of copolymerization of anthracene in polystyrene the nonradiative transfer of energy is perhaps an intramolecular process involving the polymer chain. Avivi and Weinreb have shown that although anthracene is part of the polymer chain nonradiative energy transfer may still be an intermolecular process.[4] Such a process would involve polystyrene segments of one chain transferring energy to an anthracene molecule of some neighboring chain. These experiments necessarily involved differences in preparation of the solutions or changes in their physical properties. To provide further information on the effect that solute attachment exerts on luminescent properties of plastic scintillators, it seems appropriate to compare two systems which are prepared under the same conditions. In one system the solute is part of the polymer chain, in the other the solute is not attached. In other respects the systems should be reasonably similar. The systems chosen for this investigation were anthracene in polystyrene, in which the solute is part of the polymer chain, and 9, 10-diphenylanthracene in polystyrene, in which the solute is not part of the polymer chain.[12] Both plastic solid

* Work performed under the auspices of the U. S. Atomic Energy Commission.

† On leave from The Hebrew University, Jerusalem, Israel.

[1] W. S. Koski, Phys. Rev. **82**, 230 (1951).

[2] R. K. Swank and W. L. Buck, Phys. Rev. **91**, 927 (1953).

[3] F. H. Krenz, Trans. Faraday Soc. **51**, 1 (1955).

[4] P. Avivi and A. Weinreb, J. Chem. Phys. **27**, 716 (1957).

[5] I. M. Rozman, Izvest. Akad. Nauk. **22**, 1, 36 (1958).

[6] T. P. Belikova and M. D. Galanin, Izvest. Akad. Nauk. **22**, 1, 48 (1958).

[7] F. H. Brown, M. Furst, and H. Kallmann, Discussions Faraday Soc. **27**, 43 (1959).

[8] J. B. Birks and K. N. Kuchela, Discussions Faraday Soc. **27**, 57 (1959).

[9] E. V. Anufriyeva, M. V. Volkenshtein, and M. M. Koton, Zhur. Fiz. Khim. **31**, 1532 (1957).

[10] C. S. Marvel and B. D. Wilson, J. Org. Chem. **23**, 1479 (1958).

[11] H. Hinrichs, Z. Naturforsch. **9a**, 617 (1954).

[12] Extensive experiments carried out in this laboratory confirm this. The average molecular weight of plastic scintillators was determined by the intrinsic viscosity method. Five different solutes were studied, by varying the concentration in the original plastic. In four of the solute systems investigated, including 9,10-diphenylanthracene, the average molecular weight of the polymer turned out to be independent of the solute and solute concentration. For anthracene the average molecular weight of the polymer decreased with increasing concentration. These results support the assumption that anthracene is attached to the polymer chain and they show that 9,10-diphenylanthracene is not attached. Other investigations have shown more conclusively that anthracene does copolymerize with styrene monomer.

solutions are prepared and tested under the same conditions. In the experiments to be described the luminescence properties of these two solutions are compared. Particular emphasis was placed on lifetime studies of the molecules excited both by uv and by electron bombardment. An attempt was made to analyze the shape and duration of the light pulse that was produced by these different modes of excitation.

II. EXPERIMENTS

A. Preparation of Sample

Styrene was obtained from the Dow Chemical Company. Before use, the monomer was carefully vacuum distilled three times at a pressure of 5 mm of Hg.

Anthracene and 9,10-diphenylanthracene were obtained commercially from Pilot Chemicals, Inc. The compounds were of sufficiently high purity to be used without further purification.

The technique used in preparation of the plastic samples has been described previously.[13,14] Solutions of the solute in the monomer were thermally polymerized at 145°C in a constant-temperature oil bath for a period of 10 days.

B. Measurements

1. Intensity Measurements

a. Intensity measurements made under β excitation.—The measurements of light output were made in a manner described previously.[14] All intensities are expressed relative to that of a standard anthracene crystal having the same dimensions as the plastic sample.

b. Intensity measurements under ultraviolet excitation; determination of transfer efficiencies.—The transfer efficiencies of the solutions of anthracene-polystyrene and that of 9,10-diphenylanthracene in polystyrene were determined by the method described by Cohen and Weinreb.[15] Essentially it consists of comparing the fluorescent intensity that is obtained by excitation of the transferring solvent to the intensity obtained by direct excitation of the solute.

The measurements were made on a Beckman DU spectrophotometer. A Hanovia mercury lamp was the source of excitation. The reference solution was 1 gm per liter of aesculin in distilled water. Wavelengths for polystyrene excitation were chosen in the region of minimum absorption of the solute. For the anthracene samples, the polystyrene was excited with the 2650 A mercury line. For the samples containing 9,10-diphenylanthracene, the polystyrene was excited with the 2890 A mercury line. In both cases the solute was directly excited with 3340 A mercury line for which polystyrene is practically transparent. The plastic samples were 12 mm thick.

c. Emission spectrum of the solute.—The fluorescence spectra of the two systems under investigation were taken for various concentrations of the solute. The solutes were excited by light of wavelength 3340 A by use of a Bausch & Lomb grating monochromator. A Hanovia mercury lamp was the exciting light source. The transmitted fluorescence spectra were recorded on a Beckman DK-2 recording spectrophotometer. The samples were 12 mm thick. No correction for the spectral sensitivity of the photomultiplier was made.

2. Study of the Scintillation Pulse

a. Pulsed electron excitation.—The light pulse of the plastic scintillators was investigated by exciting the sample with a pulsed electron beam. The experimental apparatus has been described elsewhere.[16] The apparatus consists of an electron accelerating tube capable of accelerating electrons to an energy of approximately 75 kev. The duration of the electron pulse is less than 1 mμsec. The scintillator is placed at the exit window of the tube. Beneath the scintillator is a 1P28 phototube. The output of the phototube is fed directly into a traveling-wave oscilloscope. The pulse produced on the oscilloscope is automatically reproduced on graph paper by an apparatus developed at this laboratory.[17] The instrument is capable of drawing either a linear or a logarithmic plot of the pulse.

The light pulse was investigated for samples of two different sizes. One size, referred to as "thick," measured 2 cm in diameter and 12 mm thick. The other size, referred to as "thin," measured approximately 0.5 mm thick and 5 mm in diameter. The latter thickness was the minimum convenient for our work. It was estimated that a plastic sample having a thickness of 0.25 mm was more than sufficient to stop the electron beam completely.

It must be emphasized that before any measurements were taken a fresh surface was cut on the plastic samples. The measurement was then made as rapidly as possible, usually within 15 minutes. It was found that samples left exposed to air for at least 24 hours had lifetimes as much as 20% longer. This is probably due to some type of surface deterioration.

b. Ultraviolet excitation.—The photofluorescent lifetimes of anthracene and 9,10-diphenylanthracene in polystyrene were determined in the following manner. A *p*-terphenyl-polystyrene plastic was placed directly against the plastic sample to be measured, thick samples being enclosed in an aluminum sleeve to prevent *p*-terphenyl radiation from by-passing the plastic. A Kodak 2A gelatin filter between the plastic and the phototube cut off all wavelengths below 4000 A. When the *p*-terphenyl plastic was excited by electrons

[13] R. K. Swank and W. L. Buck, Nucleonics **11**, 48 (1953).
[14] L. J. Basile, J. Chem. Phys. **27**, 801 (1957).
[15] S. G. Cohen and A. Weinreb, Proc. Phys. Soc. (London) **B69**, 593 (1956).
[16] R. K. Swank, B. Phillips, W. L. Buck, and L. J. Basile, IRE Trans. Nuclear Sci. NS-5 No. 3-4, 183 (1958).
[17] R. K. Swank and E. A. Mroz, Rev. Sci. Instr. **30**, 880 (1959).

from the accelerator, the emitted p-terphenyl radiation excited the solute in the plastic directly below it.

This procedure is a modification of an earlier experiment in which Swank and Buck used α particles as a source of excitation. It proved feasible in our experiment because the mean lifetime of the p-terphenyl in polystyrene is less than 2.5 mμsec. This time interval is considerably shorter than the lifetimes of the solute systems being investigated. The p-terphenyl plastic acts as a pulsed source of uv. Since polystyrene is practically transparent to the fluorescence emitted by p-terphenyl, the solute molecules are excited directly. Such an arrangement eliminates the transfer of energy from the solvent to the solute.

The system is not without faults. It would be desirable to use a uv source that produces pulses of shorter duration. A monochromatic beam of exciting radiation would also be more desirable. A serious fault of this procedure is that the decay of the uv pulse emitted by a p-terphenyl plastic is nonexponential.[16] The slow component of this pulse may affect the results. The emission spectrum of p-terphenyl does extend beyond 4000 A. When only the p-terphenyl plastic with the gelatin filter was used, we were not able to obtain a measurable pulse on the oscilloscope unless we used a very intense electron beam. In measuring our samples the electron beam was of much lower intensity. The suspicion, however, remains that at the low solute concentrations some p-terphenyl radiation may have penetrated the samples and reached the phototube.

In a later phase of the work, the photofluorescence pulse of the solute was obtained by exciting the samples with light emitted from pure polystyrene. The arrangement was the same as that using the p-terphenyl plastic as a pulsed source of uv. In this case also, all excitation of the solute is direct—at least to the extent that reabsorption by polystyrene can be neglected.

III. RESULTS AND DISCUSSION

A. Intensities, Transfer Efficiencies, and Emission Spectra

The fluorescent intensity, plotted for the two systems as a function of solute concentration, is shown in Fig. 1 for the case of β excitation. In this case the energy is principally absorbed by the solvent (polystyrene). The intensity of the 9,10-diphenylanthracene samples is much higher than that of the corresponding anthracene samples. Figure 2 shows the fluorescent intensity of the two systems when the solute (9,10-diphenylanthracene or anthracene) is excited directly by uv of too long a wavelength to excite the polystyrene. Since transfer is not involved in the latter case, it is evident that in plastic solid solutions the quantum yield of anthracene is considerably lower than that of 9,10-diphenylanthracene. This explains most of the large difference between the fluorescent intensities of the two systems when excited by β rays.

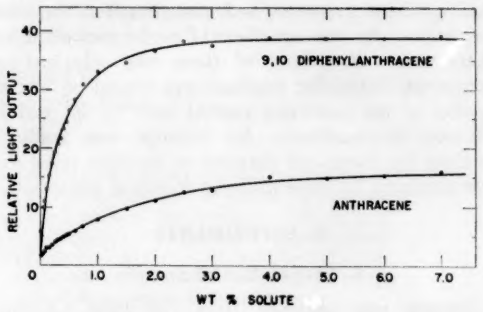

FIG. 1. Light output versus concentration of anthracene and 9,10-diphenylanthracene in polystyrene. Excitation was by the beta rays from a Cs^{137} source. All light outputs are relative to a standard anthracene crystal uncorrected for the spectral response of the photomultiplier.

The curves of Fig. 2 also show another interesting and important difference between the two systems studied. The fluorescence intensity of 9,10-diphenylanthracene decreases with increasing concentration. This is what would normally be expected if one assumes that self-absorption and some type of concentration quenching process takes place.

The intensity of the anthracene fluorescence increases with increase in concentration, although increasing self-absorption is certainly taking place. It is felt, therefore, that the observed increase in anthracene fluorescence is only a lower limit for the actual increase in the quantum yield of anthracene in polystyrene. We tend to believe that this increase is related to the fact that anthracene is attached to the polymer chain.[18] This effect has also been observed by Krenz.[3]

The emission spectra of the two systems, for transmitted fluorescence, are shown in Fig. 3. For low solute concentrations of 9,10-diphenylanthracene, there is an increase in the intensity. This is due to an increase in the absorption of the exciting radiation. The small difference in intensity observed between the spectra for concentrations of 0.05% and 0.07% indicates that the absorption of exciting radiation is practically complete. At higher concentration the intensity is much lower. This is what one would expect as a result of the processes of self-absorption and concentration quenching. The effect of re-emission is seen by the enhancement of the longer wavelength part of the spectrum.

The behavior of the emission spectra of the anthracene-polystyrene system is different. The initial increase in intensity, at low solute concentration, can also be interpreted as a consequence of increased absorption of

[18] Another possible explanation is that not all of the anthracene is part of the polymer chain, some part of it may form microcrystals which are distributed throughout the polymer. This would lead to an increase in light output, since the quantum yield of anthracene in the crystalline state is much greater than when it is dissolved. However, recent results of Broude and Medvedev [V. L. Broude and V. L. Medvedev, Doklady Akad. Nauk. S.S.S.R. **129**, 533 (1959)] seem to rule out this explanation.

the exciting radiation. However, the continued increase in intensity, as the concentration is greatly increased, clearly shows the previously mentioned effect of increased quantum yield (see Fig. 2). Once again part of the differences between the two systems can be due to the anthracene being chemically bound to the polymer chain.

The transfer efficiencies in the two systems are shown as functions of solute concentration in Fig. 4. The transfer efficiency for the 9,10-diphenylanthracene samples rises much faster with concentration than that for the corresponding anthracene samples. At higher concentrations the transfer efficiencies become similar. One would conclude from these results that the probability for energy transfer is greater in one system than in the other, or that there is a difference in the processes which compete with energy transfer. According to current theory on energy transfer, it is difficult to explain the large difference between the transfer probabilities of the two systems. The difference in the energy levels

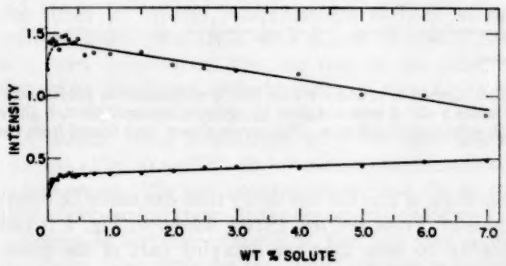

FIG. 2. Fluorescence intensity of anthracene and 9,10-diphenylanthracene in polystyrene. The solutes were directly excited by uv at 3340 A.

of the two solutes as observed from their absorption spectra seem too small to cause a large difference in the interaction with the solvent. It is felt that a large part of the observed difference in transfer efficiencies is due to the attachment of anthracene to the polymer chain. This may affect the transfer properties of the solvent, the solute, or both in a way that is not yet understood. Shimizu *et al.* have shown that the transfer efficiency in the system polystyrene *p*-terphenyl decreases with the temperature of polymerization.[19] This is attributed to the decrease in the average length of the polymer chain as the temperature of polymerization increases. Thus it would follow that shorter chains are less efficient for transferring energy. A similar effect has been observed by Funt and Hetherington.[20] These authors have shown that the light output for plastic scintillators with an average molecular weight less than 50 000, decreases with a decrease in molecular weight. Since the introduction of anthracene decreases the average molecular weight of the polymer the difference between the transfer efficiencies of the two systems being reported may be partly due to the differences in the length of the polymer chain.

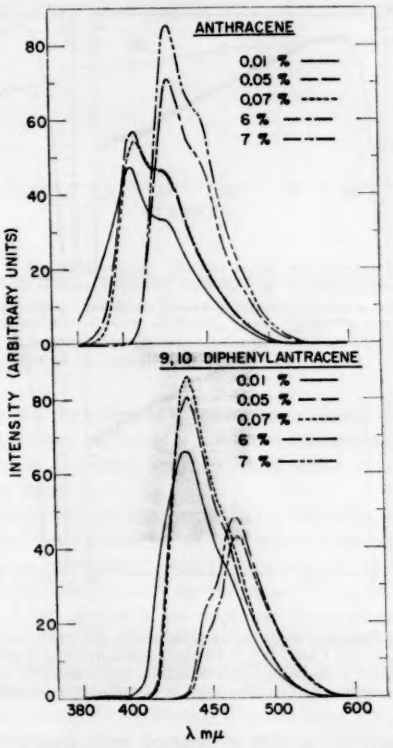

FIG. 3. Fluorescent spectra of anthracene and 9,10-diphenylanthracene in polystyrene. Excitation was by filtered Hg radiation near 3340 A.

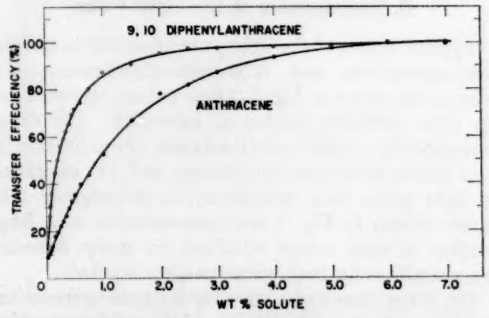

FIG. 4. Transfer efficiency vs concentration of the solutes. In the polystyrene-anthracene system, the polystyrene was excited with 2650 A radiation; in the 9,10-diphenylanthracene system the polystyrene was excited with 2890 A radiation. In both cases the solute was excited with 3340 A radiation. The curves are not corrected for the direct excitation of the solute taking place along with excitation of the solvent.

[19] S. Shimizu, F. Hirayama, and S. Okamoto, Ann. Rept. Research of Artificial Radioactive Isotopes in Japan **3**, 48 (1956).

[20] B. L. Funt and A. Hetherington, Appl. Radiation and Isotopes **4**, 189 (1958/59).

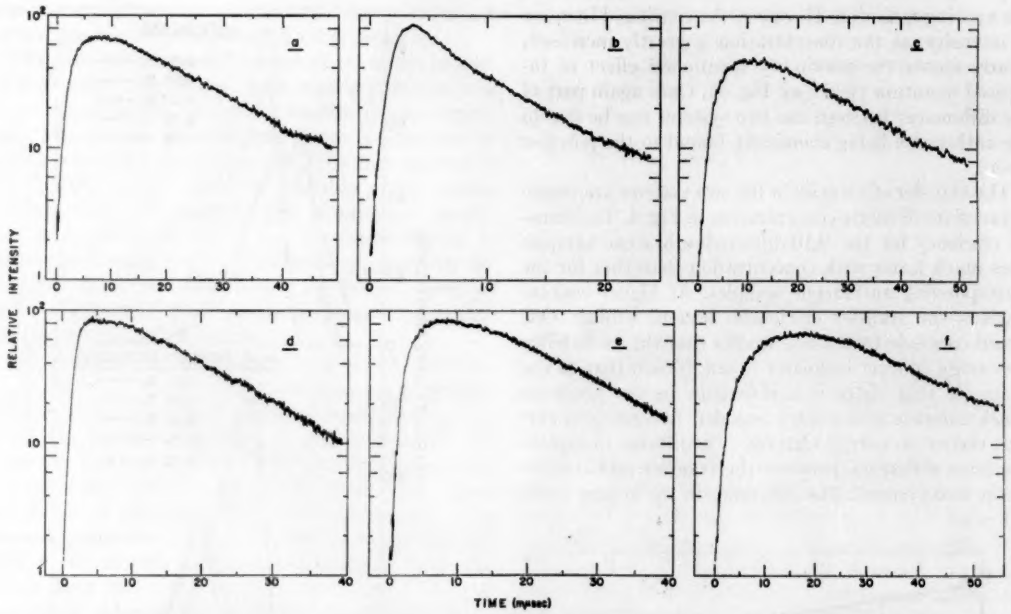

FIG. 5. Shapes of light pulses obtained by different modes of excitation. Curves a, b, and c are for 0.05% anthracene in polystyrene; curves d, e, and f for 7.0% 9,10-diphenylanthracene in polystyrene. Curves a and d were obtained by electron bombardment, b and e by excitation with *p*-terphenyl radiation, and c and f by excitation with polystyrene radiation. The curves shown were traced from the original recordings. The time scale is in millimicroseconds.

A word of caution is inserted with regard to the magnitude of the transfer efficiencies shown in Fig. 4. At higher concentration the transfer efficiencies approach 100%. No correction was made for the direct excitation of the solute, which accompanies ultraviolet excitation of the solvent (polystyrene). This direct excitation decreases with decreasing concentrations and is negligible at the low concentrations at which the differences between the two solute systems studied were most pronounced.

B. Investigation of the Light Pulse

Typical shapes of the light pulse observed in anthracene-polystyrene and 9,10-diphenylanthracene-polystyrene are shown in Fig. 5. These pulses were obtained by three different modes of excitation: (1) direct excitation by a pulsed electron beam, (2) excitation by light pulses from pure polystyrene, and (3) excitation by light pulses from *p*-terphenyl in polystyrene. The curves shown in Fig. 5 are representative of a large number of such curves obtained for many different concentrations for both solute systems studied.

The decay time τ of a pulse for instantaneous excitation is usually defined as the time interval during which the intensity decreases by a factor of e. This concept of decay time assumes that the intensity I can be adequately described as a function of time by an equation of the form $I=A\exp-t/\tau$. Hence a semilogarithmic plot of intensity vs time yields a straight line. From the slope of this line the decay time can easily be determined.[21] From the few curves shown in Fig. 5 it can readily be seen that the decaying part of the pulse, when displayed on a semilogarithmic plot, is not always a straight line. In this case, the determination of "decay times" by simply fitting a straight line to the decaying part of the pulse is not adequate. However, as a first step towards the analysis of these curves, the decay times obtained from the slope of the straight lines that best approximated the decay of the pulses were recorded systematically. Results are shown in Figs. 6 to 9.

Figure 6 shows the decay time τ_e for electron excitation, plotted as a function of the concentration of anthracene in polystyrene. The same function for 9,10-diphenylanthracene in polystyrene is shown in Fig. 7. These samples were excited by a pulsed beam of 75-kev electrons. The photofluorescent decay time τ_l of the same samples is shown in Figs. 8 and 9 for the case in which the samples were excited by electron-excited light pulses from a 3% *p*-terphenyl-polystyrene plastic. Table I gives results on the decay time τ_p and

[21] Even if the decay of the light pulse is strictly exponential, the pulse which is practically observed does not reach its maximum instantaneously, however fast the excitation, but increases gradually. This is due to the finite response time of the detecting device. For times which are long in comparison to the response time of the detector (in our case <2 mμsec) the pulse again decreases. In investigating the curves, only times which exceed the response time of the detector were given the full weight of consideration.

TABLE I. Decay times of solid solutions of anthracene and 9,10-diphenylanthracene in polystyrene.

Wt. % solute in polystyrene	Excitation by 75-kev electrons		Excitation by polystyrene radiation	
	Decay time	Rise time	Decay time	Rise time
		Anthracene		
	τ_e		τ_p	
0.0	13.5	2.2		
0.01	17.8	3.7	18.3	5.4
0.05	19.2	3.8	20.5	5.9
0.07	19.5	3.9	22.1	6.8
6.0	12.6	1.9	23.3	7.0
7.0	12.8	1.7	22.5	7.4
		9,10-Diphenylanthracene		
0.01	18.7	6.0	18.7	7.1
0.05	19.9	4.9	20.5	6.7
0.07	20.0	4.7	20.3	7.5
6.0	14.9	2.2	23.9	9.5
7.0	14.8	2.2	24.1	9.8

rise times for several concentrations of both solute systems, when the samples were excited by light pulses from pure polystyrene. The rise time of the pulse is defined as the time for the intensity to increase from 10% to 90% of its maximum value.

A similar trend is observed in τ_e for both solute systems (Figs. 6 and 7). At low solute concentrations, τ_e increases rapidly and becomes longer than the decay time of pure polystyrene. As the concentration increases, τ_e begins to decrease—sharply at first and then more gradually. The curve for the "thin" samples is similar to that for the "thick," except that the decay times are somewhat shorter. Also, the decrease in τ_e is more abrupt in the thin samples than in the thick one.

A different behavior is observed with the photofluorescent lifetime τ_l (Figs. 8 and 9). In this case only the solute molecule is being excited. At low concentrations the values of τ_l are very much lower than the corresponding values of τ_e. As the concentration increases, τ_l increases monotonically until τ_l is very close in value to τ_e.

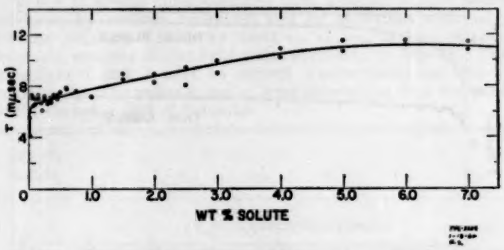

FIG. 7. Photofluorescent lifetime τ_l of anthracene in polystyrene vs concentration of anthracene. The anthracene was excited by the uv emission from a p-terphenyl plastic excited by a pulsed beam of 75-kev electrons. Open circles represent data from thick samples, closed circles represent data from thin samples. Values obtained by straight line fitting.

These results are interpreted in the following manner. For electron excitation, at low solute concentration, energy is transferred mainly via absorption of the polystyrene fluorescence by the solute. This, as will be shown later, results in an apparent decay time which is longer than the decay time of pure polystyrene. As the concentration of solute increases, a nonradiative transfer process becomes predominant. By such a process, energy is transferred directly from the excited polystyrene to the accepting solute. It is assumed that the time for energy transfer to take place decreases as the acceptor concentration increases. Eventually the transfer time becomes so short that the measured decay time is effectively the fluorescent decay time of the accepting solute.

The assumed transition, with increasing concentration, from a predominantly radiative transfer to a nonradiative transfer is qualitatively supported by the

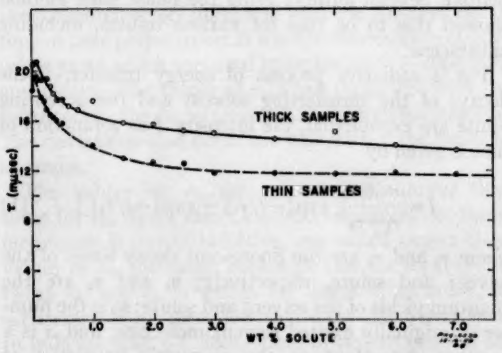

FIG. 6. Decay time of τ_e of anthracene in polystyrene versus concentration of anthracene. The samples were excited with a pulsed beam of 75-kev electrons. The thick sample was 12 mm thick by 2 cm in diameter; the thin sample was $\frac{1}{2}$ mm thick by 5 mm diameter. Values obtained by straight line fitting.

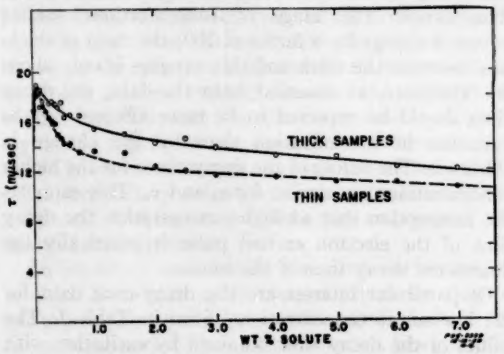

FIG. 8. Decay time τ_e of 9,10-diphenylanthracene in polystyrene versus concentration of 9,10-diphenylanthracene. The samples were excited with a pulsed beam of 75-kev electrons. The thick sample was 12 mm thick by 2 cm in diameter; the thin sample was $\frac{1}{2}$ mm thick by 5 mm in diameter. Values obtained by straight line fitting.

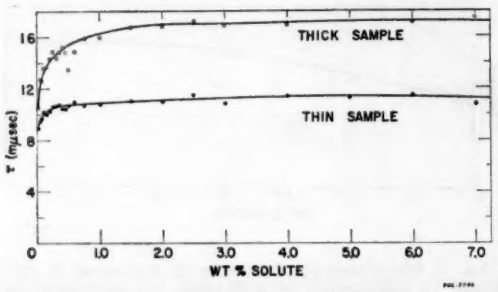

FIG. 9. Photofluorescent lifetime τ_l of 9,10-diphenylanthracene in polystyrene versus concentration of 9,10-diphenylanthracene. The solute was excited by the uv emission from a p-terphenyl-polystyrene plastic. Values obtained by straight line fitting.

data in Table I. For electron excitation, the rise time decreases with increasing concentration.

A closer comparison of Figs. 6 and 7 shows that the decreasing part of the curve is steeper in the case of 9,10-diphenylanthracene than for anthracene. This might indicate that the concentrations that are necessary for the occurrence of nonradiative transfer are lower for solutions of 9,10-diphenylanthracene than for anthracene. This explanation is supported by the difference in transfer efficiency of the two systems as shown in Fig. 4.

The differences in τ_e between the "thin" and "thick" samples for a given solute system are due to self-absorption and re-emission of the solute fluorescence. This effect, which increases with the thickness of the sample, tends to increase the observed decay time. This same effect causes the pronounced shift in the maximum of the fluorescence spectrum with changing concentration, which is seen from the curves of Fig. 3.

The results shown in Figs. 8 and 9 support and supplement the above interpretation. The increase in the decay time to a constant value is explained by the increasing contribution of reabsorbed and re-emitted fluorescence. The range of concentrations studied covers a change by a factor of 700; the ratio of thickness between the thick and thin samples is only about 30. Therefore, as observed from the data, the decay time should be expected to be more affected by the variation in concentration than by the change in thickness. The values of the decay times for the higher concentrations are similar for τ_e and τ_l. This supports the assumption that at high concentration the decay time of the electron excited pulse is practically the fluorescent decay time of the solute.

Of particular interest are the decay-time data for the low solute concentrations given in Table I. The values of the decay time obtained by excitation with polystyrene radiation are very close to the respective values of τ_e obtained by excitation with electrons. This supports the assumption that a radiative transfer process is taking place at low solute concentrations. At the high solute concentrations the decay time measured with polystyrene excitation is much longer than the corresponding τ_e. This indicates that, at high solute concentrations for electron excitation, a nonradiative transfer of energy becomes the dominant factor in the systems we studied. The nonradiative transfer process is much faster than the radiative transfer process.

The above results and interpretations are based on decay times which were obtained by applying the best straight line to the decaying section of the pulses. No doubt there are some quantitative inconsistencies. For example, there is no obvious reason why the difference in τ_l for "thick" and "thin" samples should be greater than the corresponding difference in τ_e, particularly when only the highest concentrations are considered (Figs. 6 and 8). It was felt that a more rigorous analysis of the pulse shape should be attempted. This, a rather elaborate study, was carried out for only a limited number of curves. The results however are sufficient to show that the above assumptions are reasonable. The method of analysis seems to be justified by the self-consistency of the results.

This analysis is based on the assumption that when pure polystyrene is excited by a pulsed electron beam the fluorescent decay is exponential, as shown by Swank *et al.*[16] Recently Kilin and Rozman claimed to have shown by the phase-shift method that the decay of polystyrene under electron excitation is nonexponential.[22] The measurements of Swank *et al.* were repeated many times and it was found that over one cycle on a semilogarithmic plot the decay is exponential. Beyond this the decay time seems to become longer. There are obvious reasons to believe that the method of Swank *et al.*, which was followed throughout this work, allows a much closer examination of the pulse shape than does the phase shift method. For the evaluation of the results given here, we may therefore assume the decay of polystyrene to be practically exponential. A second assumption is that the decay of the solutes, anthracene and 9,10-diphenylanthracene, is also exponential. Several authors using the phase shift method showed this to be true for various solutes, including anthracene.

For a radiative process of energy transfer, if the decays of the transferring solvent and the accepting solute are exponential, the intensity I as a function of time is given by

$$I=\frac{\alpha n_0\eta_1\eta_2}{\tau_1-\tau_2}[\exp(-t/\tau_1)-\exp(-t/\tau_2)], \qquad (1)$$

where τ_1 and τ_2 are the fluorescent decay times of the solvent and solute, respectively; η_1 and η_2 are the quantum yields of the solvent and solute; n_0 is the number of originally excited solvent molecules; and α is a constant dependent on the geometric properties of the system.[23]

[22] S. F. Kilin and I. M. Rozman, Optics and Spectroscopy **4**, 37 (1959).

[23] H. Kallmann, Phys. Rev. **117**, 36 (1960).

Equation (1) applies to the case of instantaneous excitation. This is practically fulfilled in our experiment in which the measured decay times are considerably longer than the exciting electron pulse.[21]

Equation (1) could apply to a nonradiative transfer process provided that the decay of the solvent is exponential. The only necessary modification would be to multiply the expression by τ_1/τ_T where τ_T is the reciprocal of the probability for nonradiative energy transfer under the given conditions. The decay time τ_1 of the solvent will now be shorter than that in the case of a radiative process of energy transfer. For both modes of energy transfer the intensity would be given by the expression

$$I=A[\exp(-t/\tau_1)-\exp(-t/\tau_2)], \qquad (2)$$

where A is a constant independent of time. Several of our curves were analyzed by use of Eq. (2). The object was to determine what magnitudes of τ_1 and τ_2 give the best fit to the observed pulses. The least-squares fitting of the theoretical curve to the experimental curve was accomplished by the computer George. The actual computer program was set to fit a function of the type

$$I=A_1\exp(-t/\tau_1)-A_2\exp(-t/\tau_2), \qquad (3)$$

a more general program used in several other problems. The best fit of the theoretical curve included the fulfillment of the additional condition of $A_1=A_2$. Some of the values τ_1, τ_2 obtained by this procedure are shown in Table II.

The values of τ_e and τ_p given in Table II are the same values as those given in Table I. The other values listed in Table II are those obtained from the computer. The indices 1 and 2 designate the solvent and solute, respectively. The indices e and p relate to direct electron excitation and excitation by polystyrene fluorescence, respectively. For low solute concentrations of 9,10-diphenylanthracene, the value of τ_{1p} obtained from the computer agrees quite well with the observed decay time of pure polystyrene. It was the fluorescence of pure polystyrene which was used to excite the 9,10-diphenylanthracene. The values of τ_{2e} agree quite well with the values of τ_{2p}; the decay time of 9,10-diphenylanthracene. The deviations that occur are well within the limits of accuracy.

The values for τ_{1e} are systematically lower than those for τ_{1p}. If for direct electron excitation the transfer process is purely radiative, one would expect these values to be the same. Although this discrepancy between τ_{1e} and τ_{1p} is within the limits of accuracy, its occurrence at all three low solute concentrations seem to indicate that the decay time of polystyrene, in the case of electron excitation, may be somewhat shorter than that for pure polystyrene. This may be partly due to the fact that self-absorption and re-emission in pure polystyrene may tend to lengthen the decay time. When a solute is added to the polystyrene, competition for the polystyrene fluorescence enters in. The solute may well absorb the polystyrene fluorescence at the point of origin and thus reduce the amount of self-absorption by the polystyrene. At a concentration of 0.07% of 9,10-diphenylanthracene, a nonradiative transfer process may already be active. This would tend to shorten the fluorescence decay time of polystyrene.

TABLE II. Decay times obtained from analyses of light pulses produced by electron excitation and by excitation with polystyrene radiation. The decay times τ_{1e}, τ_{2e}, τ_{1p}, and τ_{2p} resulted from the analysis of the light pulse according to Eq. (2). The subscripts 1 and 2 refer to solvent (polystyrene) and solute, respectively. The values τ_e and τ_p were determined from the slope of the decaying part of the pulse.

Wt. % solute	τ_e	τ_{1e}	τ_{2e}	τ_p	τ_{1p}	τ_{2p}
			9,10-Diphenylanthracene			
0.00	13.5			13.5		
0.01	18.7	12.4	9.8	18.9	13.4	10.6
0.05	19.9	12.2	10.5	20.5	13.7	11.7
0.07	20.0	11.5	10.0	20.3	13.4	10.4
6.0	14.9	7.6	6.8	25.9	16.7	14.3
7.0	14.8	7.8	6.5	24.1	16.3	15.5
			Anthracene			
0.00	13.5			13.5		
0.07	19.5	17.1	9.6	22.1	14.9	8.2
6.0	12.6	5.5	5.0	23.3	14	12
7.0	12.8	5.4	4.9	22.5	16	11.4

At high concentrations of 9,10-diphenylanthracene the assignment of the values τ_{1p} and τ_{2p} becomes rather difficult. The decay times of the solvent and solute are rather close in magnitude and it becomes difficult to decide which of the values obtained from the computer is τ_1 and τ_2.[24] The assignment of the values given in Table II was made in view of the close correspondence of the values of τ_{2p} and τ_{2e} at low solute concentration. If this is so then at high concentrations the value of τ_{2p}, obtained from the computer, would correspond closely to the value of τ_e, the measured value obtained by fitting the best straight line to the decaying part of the curve. The fact that the decay time τ_{1p} of polystyrene is slightly longer than the experimental 13.5 mμsec is not too surprising. At high concentrations the pulse obtained by polystyrene excitation has a broad maximum. This tends to reduce the accuracy of the analysis considerably.

An important result of this analysis is the breakdown of Eq. (2) at high solute concentrations for electron excitation. The numerical results obtained from the computer seem to defy any interpretation. The generally poor fit between the theoretical and experimental pulse shape confirm the fact that a relation of the type

[21] For the case $\tau_1=\tau_2$, Eq. (1) breaks down altogether and the shape of the pulse is given by $I=At\epsilon^{-t/\tau}$, where $\tau_1=\tau_2=\tau$.

of Eq. (2) is unable to adequately describe the experimentally observed pulse shape. This seems to be a general feature of the nonradiative transfer process in plastic solutions.

The results for anthracene are similar to those for 9,10-diphenylanthracene although the results are not as self-consistent. This is largely due to the considerably lower intensities of the anthracene samples. As a result there are considerably greater statistical fluctuations in the plotted pulses. This results in a poorer fit between the experimental and theoretical curves. Again, at high concentrations, the complete divergence between the values of τ_{2e} and τ_{2p} is obvious. Once again this indicates the inapplicability of Eq. (2) to the nonradiative transfer process. The values of τ_{2p} for high anthracene concentrations agree well with the value of τ_e, the decay time of anthracene, obtained by the straight line method. This agreement tends to confirm the interpretation given earlier. At low concentration the discrepancy between the values of τ_{1e} and τ_{1p} seems somewhat larger than would be expected from purely statistical error. It may be that the presence of anthracene, which is attached to the polymer chain, and the resulting decrease in the average chain length result in an increase in the decay time of polystyrene.

SUMMARY

Some fluorescence properties of solid solutions of anthracene and of 9,10-diphenylanthracene in polystyrene are investigated.

Measurements of intensity and of fluorescence spectra confirm former results which show that the quantum yield of anthracene in polystyrene increases with concentration.[3] The intensity of 9,10-diphenylanthracene decreases with concentration. This difference in behavior is attributed to the attachment of anthracene to the polymer chain.

The transfer efficiency at low concentrations of anthracene is considerably less than that at the corresponding concentrations of 9,10-diphenylanthracene. This may be a consequence of the attachment of anthracene to the chain or of the resulting decrease in the average length of the polymer chain.

The results of the decay time measurements seem to confirm the observed differences in the transfer efficiencies of the two systems.

The effect of chain attachment on the chain length may be the reason for an increase in the decay time of polystyrene when it is copolymerized with anthracene. This assumption has still to be verified by a direct investigation of the relation between chain length and the decay law of polystyrene.

The similarity between the light pulse obtained by electron excitation and excitation by polystyrene fluorescence for low solute concentrations shows that at this concentration the transfer of energy from polystyrene to the solute is almost exclusively radiative. At high solute concentrations the transfer process is predominantly nonradiative. The analysis of the light pulse seems to indicate that in the presence of this process the decay of polystyrene is nonexponential.

ACKNOWLEDGMENTS

The authors are particularly indebted to R. Marema for much technical help and assistance throughout the entire study, to E. Mroz for assistance in the operation of the electron accelerator, to T. Tisue for measuring the transfer efficiencies, and to S. Zawadski for running the computer. The authors would also like to express appreciation to W. Buck and I. Berlman for many helpful discussions throughout the entire study.

Metal-Metal Bonding in Dicobalt Hexacarbonyl Diphenylacetylene

DAVID A. BROWN

Department of Chemistry, University College, Dublin, Ireland

(Received May 6, 1960)

The nature of the bonding between the two cobalt atoms in dicobalt hexacarbonyl diphenylacetylene is discussed in terms of simple molecular-orbital theory. It is shown that, in addition to bonding via the π orbitals of the acetylene residue, it is essential to consider direct overlap between the $4p$ orbitals of the cobalt atoms. Master formulas and numerical tables are derived for the integrals $S(4p_s 4p_s)$, $S(4p_s 4p_\pi)$.

THE past few years have witnessed a rapid development in the chemistry of transition-metal complexes and in particular of π complexes.[1,2] It is perhaps noteworthy, however, that recent x-ray examination[3] of some binuclear complexes has revealed some rather surprising structures. The number of binuclear complexes, and indeed compounds, of transition metals which contain direct-metal bonds is very limited, examples being manganese and rhenium carbonyls,[4] $Mn_2(CO)_{10}$, $Re_2(CO)_{10}$, and complexes such as $(C_5H_5Mo)_2(CO)_6$ and $(C_5H_5W)_2(CO)_6$.[5] There are in addition more numerous examples of compounds in which it is necessary to assume weak bonds between the metal atoms in order to explain the observed diamagnetism; a well-known example of this situation is provided by iron enneacarbonyl. In view, therefore, of the relatively small number of binuclear complexes of known structure, it seemed interesting to consider the nature of the metal-metal bonding in dicobalt hexacarbonyl diphenylacetylene,[6] especially since in this compound the possibility of both direct interaction between the metal atoms and indirect interaction via the acetylene residue may occur. It was also hoped that an investigation of the bonding in the above complex might provide some insight into the nature of the bonding in more complicated cases.[7]

A detailed x-ray investigation[8] of the above complex has revealed the following salient features: a sixfold coordination about each cobalt atom with distorted octahedral symmetry, the carbon-carbon bond of the acetylene residue approximately normal to the cobalt-cobalt axis, an approximately tetrahedral symmetry about the carbon atoms of the acetylene, and an approximate molecular plane of symmetry if one neglects the twisting of the phenyl groups. Sly advances two approximate views of the structure; first, that each cobalt atom is in a d^2sp^3 hybridized state and that the bonds from the carbon atom are approximately tetrahedral (sp^3) in arrangement and second, that it is possible to consider the above structure as derived from the cobalt atom in a dsp^3, trigonal bipyramidal, hybridized state; in this case one of the hybrids (sp^2) is directed in the trigonal plane and toward the mid point (X) of the C—C bond (see Fig. 1). We shall reject the former model since it predicts an essential single C—C bond in the acetylene residue, a prediction

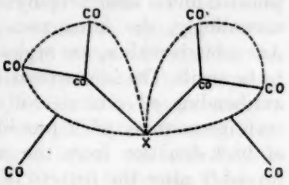

FIG. 1. Schematic structure of the complex (reproduced with the kind permission of Dr. Sly and the editor of the American Chemical Society.)

which is incompatible with the observed distance[9] of 1.46 A. The second model is more realistic and it will be adopted in the subsequent discussion. It should be emphasized at this juncture that the above model is only an approximation; however, the deviations which occur may well be due to steric effects of the bulky phenyl groups and, to date, no structural information is available on analogous complexes of acetylene. Nevertheless, the deviations are still small, since if we consider the triangle O_1O_2X, made up of the Co—Co axis and the distances of the respective cobalt atoms from the mid point of the C—C bond, it is found that the angles of the above triangle differ by at most 4° from $\pi/2$ and $\pi/4$. It seems, therefore, that our assumption of a symmetrical model is quite reasonable.

SYMMETRY CLASSIFICATION OF INTERACTIONS

The interactions between the metal orbitals and π orbitals of the acetylene residue are symmetrical with respect to the two cobalt atoms, so, for simplicity, we shall give a diagram for the interaction of only one

[1] E. O. Fischer and H. P. Fritz, Advances in Inorganic & Radiochemistry **1**, 55 (1959).
[2] F. A. Cotton and G. Wilkinson, Progr. Inorg. Chem. **1**, 1 (1959).
[3] A. A. Hock and O. S. Mills, Proc. Chem. Soc. **1958**, 233.
[4] L. F. Dahl, E. Ishishi and R. E. Rundle, J. Chem. Phys. **26**, 1750 (1957).
[5] F. C. Wilson and D. P. Shoemaker, Naturwissenschaften **43**, 57 (1956).
[6] H. W. Sternberg, H. Greenfield, R. A. Friedel, J. Wotiz, H. R. Markby, and I. Wender, J. Am. Chem. Soc. **76**, 1457 (1954).
[7] W. Hübel, E. H. Braye, A. Clauss, E. Weiss, U. Krüerke, D. A. Brown, G. S. D. King, and C. Hoogzand, J. Inorg. & Nuclear Chem. **9**, 204 (1959).
[8] W. G. Sly, J. Am. Chem. Soc. **81**, 18 (1959).
[9] Dr. Sly has subsequently informed me that on refinement this distance is reduced to 1.369 A; the new distance is even more incompatible with the first model above.

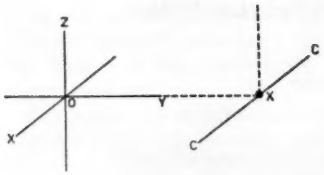

FIG. 2. System of axes of coordinates.

cobalt atom with the π orbitals. Consider the cobalt atom to be situated at the origin of a Cartesian coordinate system with axes as shown (Fig. 2); the C—C axis of the acetylene is assumed parallel to the x axis. A comparison is made with Fig. 1 if the z axis is considered to be perpendicular to the plane of the left-hand circle in the diagram. In this manner we may classify the interactions between the π orbitals of the acetylene and the cobalt orbitals according to the local-symmetry planes σ_{xy} and σ_{yz} as shown in Table I. Those orbitals which are involved only in the bonding of the carbonyl groups are neglected.

The symbol t_y denotes the cobalt sp^2 hybrid directed along the y axis toward the midpoint (X) of the C—C bond. It is obvious that a large number of interactions are possible and the problem becomes unduly complicated unless some simplifying assumptions are made; accordingly, the interaction of the $3d_{x^2-y^2}$ and the $3d_{z^2}$ orbitals with π_y are neglected since these are likely to be small. The interactions involving the empty and antibonding π^* orbitals will also be neglected since such interactions, while providing a satisfactory means of back-donation from the metal atom, do not appreciably alter the pattern of the bonding orbitals in the complex.

The discussion will be limited therefore to the following orbitals:

$$\mathrm{Co_1}(t_y)\cdots\pi_y$$

$$\mathrm{Co_1}(d_{yz})\cdots\pi_z$$

$$\mathrm{Co_1}(p_z)\cdots\pi_z.$$

TABLE I. Symmetries of orbitals responsible for metal-metal bonding.

σ_{xy}	σ_{yz}	Metal orbitals	π orbitals
+	+	t_y, $d_{x^2-y^2}$, d_{z^2}	π_y
−	+	d_{yz}, p_z	π_z
+	−	d_{xy}	π_y^*
−	−	d_{xz}	π_z^*

However, the symmetrical model which we have assumed for this complex as a result of the x-ray analysis requires that the orthogonal component of a given π orbital will interact in an identical manner with the same type metal orbital on $\mathrm{Co_2}$ as does the original π orbital with that of $\mathrm{Co_1}$; for example, in the first case given it follows that a symmetrical interaction of the type

$$\mathrm{Co_1}(t_y)\cdots\pi_y$$
$$\pi_z\cdots\mathrm{Co_2}(t_y')$$

must be considered for the complete complex. The general form of the interactions between the filled π orbitals and the t_y, d_{yz}, and p_z atomic orbitals on both cobalt atoms is as shown in Fig. 3, where β, γ, and δ denote the resonance integrals between the respective orbitals and H denotes the total Hamiltonian of the system, e.g.,

$$\beta = H_{14} = H_{58} = \int \psi_1 H \psi_4 d\tau = \int \psi_5 H \psi_8 d\tau.$$

Similarly, the Coulomb terms H_{ii} take the normal definition

$$H_{ii} = \int \psi_i H \psi_i d\tau.$$

With this notation, the secular determinant for the above set of interactions takes the form

$$\begin{vmatrix} H_{11}-E & 0 & 0 & \beta & 0 & 0 & 0 & 0 \\ 0 & H_{22}-E & 0 & 0 & \gamma & 0 & 0 & 0 \\ 0 & 0 & H_{33}-E & 0 & \delta & 0 & 0 & 0 \\ \beta & 0 & 0 & H_{44}-E & 0 & \delta & \gamma & 0 \\ 0 & \gamma & \delta & 0 & H_{44}-E & 0 & 0 & \beta \\ 0 & 0 & 0 & \delta & 0 & H_{33}-E & 0 & 0 \\ 0 & 0 & 0 & \gamma & 0 & 0 & H_{22}-E & 0 \\ 0 & 0 & 0 & 0 & \beta & 0 & 0 & H_{11}-E \end{vmatrix} = 0.$$

By simple manipulation this can be expressed as

$$\begin{vmatrix} f(E) & 0 \\ 0 & f(E) \end{vmatrix} = 0,$$

where

$$f(E) = \prod_{i=1}^{4}(H_{ii}-E) - \beta^2(H_{22}-E)(H_{33}-E)$$

$$-\gamma^2(H_{11}-E)(H_{33}-E) - \delta^2(H_{11}-E)(H_{22}-E) = 0.$$

The region in which the roots of this equation lie is readily obtained. We assume

$$|H_{44}| > |H_{22}| > |H_{11}| > |H_{33}|,$$

since this order is indicated by the observed ionization potentials and term values for the cobalt atom.[10] Let us

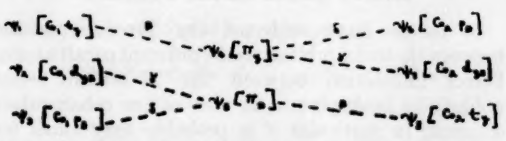

FIG. 3. General form of interactions between filled π orbitals and the t_y, d_{yz}, and p_z atomic orbitals on cobalt atoms.

now consider the variation of the function $f(E)$ with E:

$$f(0) = H_{11}H_{22}H_{33}H_{44} - \beta^2H_{22}H_{33} - \gamma^2H_{11}H_{33}$$

$$-\delta^2H_{11}H_{22} > 0$$

$$f(H_{33}) = -\delta^2(H_{11}-H_{33})(H_{22}-H_{33}) < 0$$

$$f(H_{11}) = -\beta^2(H_{22}-H_{11})(H_{33}-H_{11}) > 0$$

$$f(H_{22}) = -\gamma^2(H_{11}-H_{22})(H_{33}-H_{22}) < 0$$

$$f(H_{44}) = -\beta^2(H_{22}-H_{44})(H_{33}-H_{44})$$

$$-\gamma^2(H_{11}-H_{44})(H_{33}-H_{44})$$

$$-\delta^2(H_{11}-H_{44})(H_{22}-H_{44}) < 0$$

$$f(\infty) = +\infty.$$

The roots of $f(E)$ lie, therefore, as shown in Fig. 4. It is seen that the preceding type of interaction will lead to a stabilization of the lowest orbital and destabilization of the other orbitals. It will be shown later by calculation of group-overlap integrals and estimation of the Coulomb terms and resonance integrals that the net effect in the above case is bonding. The relative magnitude of the different interactions β, γ, and δ are most easily assessed by evaluating the group-overlap integrals between the relevant orbitals.

OVERLAP BETWEEN t_y AND π_y

In this case the trigonal hybrid (t_y) takes the form

$$\psi(t_y) = (1/\sqrt{3})\psi_{4s} + (2/\sqrt{3})\psi_{4p_y}$$

[10] D. C. Moore, *Atomic Energy Levels* (National Bureau of Standards, Washington, D. C., 1952), Vol. II.

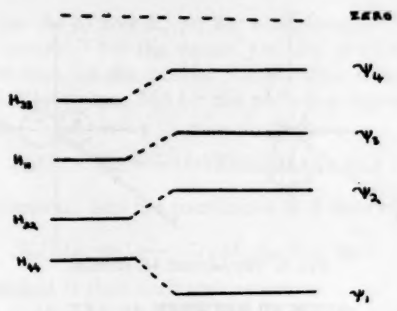

FIG. 4. Roots of $f(E)$.

where the y axis is directed toward the midpoint (X) of the C—C bond of the acetylene residue. The group-overlap integral is readily shown to be

$$S(t_y, \pi_y) = [2/(6)^{\frac{1}{2}}]S(2p_\sigma, 4s)\cos\phi$$

$$+(2/\sqrt{3})S(2p_\sigma, 4p_\sigma)\cos^2\phi,$$

where ϕ is the mean angle between the Co—C distances and the Co—X distance and takes the value of about 22°. Tables of $S(2p_\sigma, 4s)$ and $S(2p_\sigma, 4p_\sigma)$ are available as a result of two independent studies on the use of Slater orbitals of principal quantum number four.[11,12] The tables are not, however, always satisfactory for interpolation and we have calculated the required integrals for the nearest values of the parameters p and t for which values of the incomplete gamma function $A_n(p)$ for nonintegral n are available.[11–13] The value of the group integral $S(t_y, \pi_y)$ is given in Table II.

OVERLAP BETWEEN $3d_{yz}$ AND π_z

This overlap is of a simple $d_\pi - p_\pi$ type and takes the form

$$S(3d_{yz}, \pi_z) = \sqrt{2}\,S(2p_\pi, 3d_\pi)\cos\phi.$$

The value of $S(2p_\pi, 3d_\pi)$ was evaluated directly from the master formula given by Jaffé[14] with the use of the Swedish tables[15] for the numerical values of the auxiliary functions $A_n(p)$ and $B_m(pt)$ for integral n and m.

TABLE II. Group overlap integrals.

$S(t_y, \pi_y)$	0.239
$S(3d_{yz}, \pi_z)$	0.134
$S(4p_z, \pi_z)$	0.274

[11] L. Leifer, F. A. Cotton, and J. R. Leto, J. Chem. Phys. **28**, 364 (1958).

[12] D. A. Brown, J. Chem. Phys. **29**, 1086 (1958).

[13] There is a typographical error in the ADI Document Number 5481 of Cotton[11] for the master formula for $S(2p_\sigma, 4p_\sigma)$; a factor of one-half is omitted although the tabulated values of the integral are correct.

[14] H. H. Jaffe, J. Chem. Phys. **21**, 258 (1953).

[15] S. Flodmark, *Table of Molecular A & B Functions* (Institute of Theoretical Physics, Stockholm, 1957).

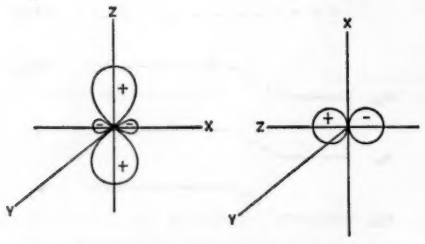

FIG. 5. The $3d_{z^2}$ and $4p_z$ orbitals.

OVERLAP BETWEEN $4p_z$ AND π_z

This interaction is closely related to the preceding and takes the form

$$S(4p_z, \pi_z) = \sqrt{2}\, S(2p_\pi, 4p_\pi) \cos\phi.$$

The integral $S(2p_\pi, 4p_\pi)$ was evaluated from the table and formula previously published.[13] The results of these calculations are given in Table II. These calculations show, therefore, that quite reasonable overlap does occur in the three types of interaction which we have considered before. If numerical values are now assigned (in point of fact it would be more accurate to say "guessed") for the different Coulomb terms on the basis of observed ionization potentials and spectroscopic promotion energies,[10] and if the proportionality constant between S_{ij} and H_{ij} is assigned a value previously found to be reasonable,[12] then it is possible to perform a numerical solution of the quartic equation. On solution it is found that the stabilization of ψ_1 is much greater than the destabilization of ψ_2 and this conclusion is generally valid for a reasonable range of the above Coulomb terms and resonance integrals. However, such calculations of the energy levels in complexes have only a limited value and so details are not given; the important point which emerges is that for a reasonable set of parameters the net effect of the above type of interactions is bonding. Further arguments are merely tendentious.

We must now consider the filling of the orbitals $\psi_1 \cdots \psi_4$. It is, of course, obvious that since we have been able to reduce the secular determinant from an order eight to one of order four, the solution of the quartic gives rise to a set of doubly degenerate orbitals. This fact is also a consequence of the symmetrical nature of the interactions which are under consideration. The neutral cobalt atom possesses the electron configuration $3d^7 4s^2$ and in the case of the complex it may assume the configuration

$$\mathrm{Co}[t_1^0 t_2^0 t_3^1 (d_{z^2})^0 (d_{xz})^2 (d_{yz})^2 (d_{xy})^2 (d_{x^2-y^2})^2 (p_z)^0].$$

The hybrids t_1 and t_2 and the orbital d_{z^2} will be directed toward three carbonyl groups and must, by necessity, be regarded as empty. We assume that the remaining d orbitals are filled (neglecting back-donation to the carbonyl ligands) and the problem of the remaining electron then arises. It is obvious that whatever the orbital in which we choose to place this remaining electron, since the given interaction leads to a set of doubly degenerate orbitals, the resulting ground state for the complex will be $\psi_1^4\psi_2^4\psi_3^2$. It follows, therefore, that irrespective of the magnitudes of β, γ, and δ, the completely symmetrical interaction so far considered is incapable of explaining the observed diamagnetism of the complex. This conclusion is equally valid if we choose to place the odd electron in one of the remaining d orbitals and thereby obtain a configuration $\psi_1^4\psi_2^4\psi_3^4$ since one unpaired electron will remain on each cobalt atom. In other words, metal-metal bonding via the acetylene residue is insufficient to explain the properties of dicobalt hexacarbonyl diphenylacetylene; we must consider, therefore, the possibility of direct metal-metal bonding.

DIRECT METAL-METAL BONDING

So far we have neglected any direct interaction between the metal orbitals on the different cobalt atoms. Direct interaction between the $3d$ orbitals seems unlikely to be important in view of the cobalt-cobalt distance; in particular it is probably very small for any but the $3d_{z^2}$ orbitals which are oriented along the z axis and some overlap might then be expected. It will in fact be shown below that this overlap is considerably smaller than that of the $4p_z$ orbitals which are also well oriented for direct interaction. Anticipating the detailed calculations given later, it is evident that if the overlap of the $4p_z$ orbitals is sufficient to remove some of the degeneracy of the symmetrical case, then the much smaller direct interaction of the $3d$ orbitals may be neglected. Moreover, since these orbitals are then fully occupied on each cobalt atom, their interactions cannot lead to any net increase in bonding energy. We are left, therefore, with a consideration of the interaction of the $3d_{z^2}$ and $4p_z$ orbitals centered on each cobalt atom.

The $3d_{z^2}$ and $4p_z$ orbitals are directed along the z axes which are perpendicular to the planes of the circles in Fig. 1; on the symmetrical model we assume that the z axes make angles of 45° with the Co—Co axis. With this model it can be shown that the group overlap integral takes the form

$$\begin{aligned} S(3d'_{z^2}/4p'_z;\, 3d''_{z^2}/4p''_z) &= [S(4p_\sigma, 4p_\sigma)\cos^2\Theta + S(4p_\pi, 4p_\pi)\sin^2\Theta] \\ &+ [S_{zz}(3d_{z^2}, 3d_{z^2})\cos^2\Theta + S_{xx}(3d_{z^2}, 3d_{z^2})\sin^2\Theta \\ &+ 2S_{xz}(3d_{z^2}, 3d_{z^2})\sin\Theta\cos\Theta] \\ &+ [2S_{xz}(3d_{z^2}, 4p_z)\cos^2\Theta + 2S_{zz}(3d_{z^2}, 4p_z)\sin\Theta\cos\Theta]. \end{aligned}$$

The notation $S_{xz}(3d_{z^2}, 4p_z)$ implies overlap along the x and z axes, respectively, of normally oriented $3d_{z^2}$ and $4p_z$ orbitals, as shown in Fig. 5. With this notation, it follows from symmetry that terms such as $S_{xz}(3d_{z^2}, 4p_z)$ are identically zero. The above summation involves

three types of overlap: (a) integrals between $3d_{z^2}$ orbitals only; (b) integrals between $3d_{z^2}$ and $4p_z$; and (c) integrals involving only $4p$ orbitals. Let us consider each type in turn.

The integral $S_{zz}(3d_{z^2}, 3d_{z^2})$ is simply $S(3d_\sigma, 3d_\sigma)$ for which the master formula is given by Jaffé.[16] It may be evaluated from the formula with the aid of the Swedish tables[15] for the appropriate parameters ($p=10.70$, $t=0$). Similarly, the integral $S_{zz}(3d_{z^2}3d_{z^2})$ is $S_{\sigma\sigma}$ symbatic for which the master formula is given by Craig *et al.*[17] and is again readily evaluated. However, to evaluate the cross integral $S_{zz}(3d_{z^2}, 3d_{z^2})$ it is convenient to replace $3d_{z^2}$ by the auxiliary (but *not* independent) functions[16]

$$3d_{z^2}=(1/\sqrt{3})\,(3d_{x^2-z^2}+3d_{z^2-y^2})$$

whence

$$S_{zz}(3d_{z^2}, 3d_{z^2}) = \tfrac{1}{3}[S_{zz}(3d_{z^2-y^2}, 3d_{z^2-y^2}) + S_{zz}(3d_{z^2-x^2}, 3d_{z^2-x^2}) + S_{zz}(3d_{z^2-x^2}, 3d_{z^2-y^2}) + S_{zz}(3d_{z^2-y^2}, 3d_{z^2-x^2})].$$

By means of the results deduced in the paper of Jaffé,[16] it is possible to simplify the above integral in terms of the type $S(3d_\sigma, 3d_\sigma)$ and $S(3d_\delta 3d_\delta)$, where the latter term denotes the integrals $S_{yy}(3d_{z^2-x^2}, 3d_{z^2-x^2})$ and equivalent terms. The final result is then

$$S_{zz}(3d_{z^2}, 3d_{z^2}) = -\tfrac{1}{2}S(3d_\sigma, 3d_\sigma)+\tfrac{1}{3}S(3d_\delta, 3d_\delta),$$

and from the master formulas given in the preceding references it is possible to evaluate this integral also.

The integrals involving the $3d_{z^2}$ and $4p_z$ atomic orbitals also require some manipulation of the $3d_{z^2}$ term but in addition require the derivation of a master formula for the integral $S_{zz}(3d_{z^2}, 4p_z)$ which is given in the Appendix. The integral $S_{zz}(3d_{z^2}, 4p_z)$ is thus evaluated from the master formula by means of the tables for $A_n(p)$ and $B_n(pt)$ for n nonintegral[11,12] and for m integral,[15] for the values $p=7.50$, $pt=2.82$. In order to evaluate the integral $S_{zz}(3d_{z^2}, 4p_z)$ it is again necessary to replace $3d_{z^2}$ by the preceding expression, whence

$$S_{zz}(3d_{z^2}, 4p_z) = -(1/\sqrt{3})\,S_{zz}(3d_{z^2-x^2}, 4p_z)$$

and integration over the coordinates Θ, ϕ shows that

$$S_{zz}(3d_{z^2}, 4p_z) = -(1/2\sqrt{3})\,S_{zz}(3d_{z^2}, 4p_z).$$

The integral is then evaluated as before.

The integrals $S(4p_\sigma, 4p_\sigma)$ and $S(4p_\pi, 4p_\pi)$ require the derivation of master formulas which are given in the Appendix. The evaluation of these integrals for the appropriate parameters $p=5.0$, $t=0$ is then a simple matter in terms of the new range of incomplete gamma functions $A_n(p)$ for nonintegral indices $j+0.4$ and integral j. The results of these calculations are given in Table III.

It follows from Table III that direct interaction between the $4p_z$ orbitals is considerably greater than that between $3d_{z^2}$ or between the $3d_{z^2}$ and $4p_z$; the group-overlap integral between the $4p_z$ orbitals situated on each cobalt atom has the value 0.3478. We shall take into account, therefore, only direct interaction of this type. It is of course possible to consider that the $3d_{z^2}$ and $4p_z$ orbitals are combined together to give one orbital directed toward the carbonyl group and the other away from the carbonyl group; if so, it is merely necessary to multiply the integral by one-half. From either point of view, it is still evident that it is the $4p$ orbitals which will be largely responsible for direct metal-metal interaction. If we return now to the case of general interaction, it is possible as a result of the calculations of overlap to assign to the matrix elements $H_{36}(=H_{63}$ a finite value, say v. The secular determinant then takes the form

$$\begin{vmatrix}
H_{11}-E & 0 & 0 & \beta & 0 & 0 & 0 & 0 \\
0 & H_{22}-E & 0 & 0 & \gamma & 0 & 0 & 0 \\
0 & 0 & H_{33}-E & 0 & \delta & \epsilon & 0 & 0 \\
\beta & 0 & 0 & H_{44}-E & 0 & \delta & \gamma & 0 \\
0 & \gamma & \delta & 0 & H_{44}-E & 0 & 0 & \beta \\
0 & 0 & \epsilon & \delta & 0 & H_{33}-E & 0 & 0 \\
0 & 0 & 0 & \gamma & 0 & 0 & H_{22}-E & 0 \\
0 & 0 & 0 & 0 & \beta & 0 & 0 & H_{11}-E
\end{vmatrix} = 0.$$

[16] J. L. Roberts and H. H. Jaffé, J. Chem. Phys. **27**, 883 (1957).
[17] D. P. Craig, A. Maccoll, R. S. Nyholm, L. E. Orgel, and L. E. Sutton, J. Chem. Soc. **1954**, 332.

TABLE III. Overlap integrals of metal-metal interactions.

$S(4p_\sigma, 4p_\sigma)$	0.2376
$S(4p_\pi, 4p_\pi)$	0.4578
$S_{zz}(3d_{z^2}, 3d_{z^2})$	0.0787
$S_{xz}(3d_{z^2}, 3d_{xz})$	0.0248
$S_{zz}(3d_{xz}, 3d_{xz})$	−0.0065
$S_{zz}(3d_{z^2}, 4p_z)$	0.0363
$S_{zz}(3d_{z^2}, 4p_z)$	−0.0105

By manipulation similar to that employed earlier it is possible to reduce this determinant to the form

$$\begin{vmatrix} f(E) & 0 \\ 0 & g(E) \end{vmatrix} = 0,$$

where $f(E)$ and $g(E)$ are polynomials of order four in E:

$$\left.\begin{matrix} f(E) \\ g(E) \end{matrix}\right\} = \prod_i (H_{ii} - E) \mp \epsilon(H_{11} - E)(H_{22} - E)(H_{44} - E)$$

$$-\beta^2(H_{22} - E)(H_{33} - E) - \gamma^2(H_{11} - E)(H_{33} - E)$$

$$-\delta^2(H_{11} - E)(H_{22} - E) \pm \beta^2\epsilon(H_{22} - E) \pm \gamma^2\epsilon(H_{11} - E).$$

We may now examine both $f(E)$ and $g(E)$ separately in exactly the same manner as adopted for the previous case of the doubly degenerate equation. Unfortunately it is possible to make unambiguous predictions of the positions of the roots in a few cases only. First, let us consider $f(E)$. It is readily shown that for this equation one root will lie below H_{44}, no root will occur between H_{44} and H_{22} and one root will lie between H_{22} and H_{11}. It can also be shown that for a reasonable range of parameters a third root will lie between H_{11} and H_{33}, and the final root above H_{33}. Nevertheless, the position of the latter roots is less certain that than of the first pair. In the case of $g(E)$ the algebraic prediction of the roots is even more difficult. Only with the assumption of reasonable values for the parameters can it be shown that $g(E)$ will possess one root below H_{44} and none between H_{44} and H_{22}; further prediction is impossible. It is necessary, therefore, to resort to numerical solution of the above polynomials. On substitution of the same numerical values of $H_{11} \cdots H_{44}$, β, γ, and δ and on estimation of ϵ by the same procedure as that adopted for the determination of the other interaction terms, it is a simple matter to obtain the roots of both $f(E)$ and $g(E)$. The roots of $f(E)$ lie as predicted and it is found that $g(E)$ possesses one root below H_{44}, two roots between H_{22} and H_{11} and one root between H_{11} and H_{33}.

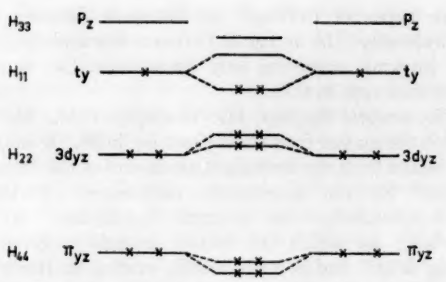

FIG. 6. Approximate energy levels for metal-metal bonding.

The condition for the presence of two roots of $g(E)$ lying between H_{22} and H_{11} is that $|\epsilon| > |H_{33} - H_{11}|$, in other words, that direct metal–metal interaction is large. The consequence of the presence of these roots is, of course, that the highest occupied orbital is bonding. The complete scheme of the occupation of the orbitals involved in metal-metal bonding now takes the form shown in Fig. 6. The constitution of the above orbitals is rather complicated. The lowest pair of bonding orbitals (which are almost degenerate) is composed presumably mainly of the acetylene π orbitals with smaller amounts of the metal orbitals ($3d_{yz}$ and t_y). The next pair of orbitals, again nearly degenerate, is largely composed of the metal $3d_{yz}$-orbitals while the remaining occupied orbital is largely a bonding combination of t_y and p_z orbitals with small contributions from the π-orbitals.

It must be realized, of course, that the preceding treatment is very approximate since it neglects a number of interactions, for example, the direct overlap of the $3d_{yz}$ orbitals. However, inclusion of effects of this order would, to be consistent, require a discussion of the back-donation effects in the carbonyl bonds. It is felt, therefore, that the relatively simple treatment developed here is to be preferred since it provides a satisfactory explanation of the diamagnetism of the complex.

If the energy-level scheme shown is generally valid then it is interesting to consider similar complexes of iron and nickel. It follows from the diagram that both an iron and a nickel complex might be less stable than the known cobalt compound, the iron compound because of the absence of the filled upper bonding orbital, and the nickel compound through the presence of a filled upper antibonding orbital. In view, however, of the difficulties of making detailed calculations for such systems these conclusions are liable to modification.

APPENDIX

The overlap intergrals $S_{zz}(3d_{z^2}, 4p_z)$, $S(4p_\sigma, 4p_\sigma)$, and $S(4p_\pi, 4p_\pi)$ are required. We shall evaluate these later in exactly the same manner as that used for integrals such as $S(2p_\sigma, 4p_\sigma)$.[11,12] The Slater-type

functions are used and have the form

$$\psi(3d_z^2)=(2\alpha_{3d})^{3.5}/(6!)^{\frac{1}{2}}(5/16\pi)^{\frac{1}{2}}r^2 \times\exp(-\alpha_{3d}r)(3\cos^2\theta-1),$$

$$\psi(4p_\sigma)=(2\alpha_{4p})^{4.2}/(7.4!)^{\frac{1}{2}}(3/4\pi)^{\frac{1}{2}}r^{2.7}\exp(-\alpha_{4p}r)\cos\theta,$$

$$\psi(4p_\pi)=(2\alpha_{4p})^{4.2}/(7.4!)^{\frac{1}{2}}(3/4\pi)^{\frac{1}{2}}r^{2.7} \times\exp(-\alpha_{4p}r)\sin\theta\cos\phi.$$

The method of evaluation follows that described by Mulliken *et al.* in terms of the spheroidal coordinates ξ, η, ϕ. For example, the integral $S_{zz}(3d_z^2, 4p_z)$ is given by the expression

$$S_{zz}(3d_z^2, 4p_z) =N_{34}\int_1^\infty\int_{-1}^{+1}(\xi-\eta)^{1.7}(\xi^2-\eta^2)(\xi\eta-1) \times(3\xi^2\eta^2+4\xi\eta+3-\xi^2-\eta^2)\exp(-p\xi)\exp(-pt\eta)d\xi d\eta,$$

where the parameters p and t have the usual significance and N_{34} is a normalizing constant, defined later. By means of a binominal expansion of the term with a nonintegral power it is a simple matter to obtain the following series expansion for $S_{zz}(3d_z^2, 4p_z)$:

$$S_{zz}(3d_z^2, 4p_z)=N_{34}\sum_{i=0}^{\infty}\binom{1.7}{i}(-1)^i[A_{6.7-i}(3B_{3+i}-B_{1+i}) +A_{5.7-i}(B_{2+i}+B_i)-A_{4.7-i}(3B_{5+i}+B_{1+i}) -A_{3.7-i}(B_{4+i}+3B_i)+A_{2.7-i}(B_{3+i}+B_{5+i}) +A_{1.7-i}(3B_{2+i}-B_{4+i})],$$

where

$$A_n(p)=\int_1^\infty\xi^n\exp(-p\xi)d\xi$$

$$B_m(pt)=\int_{-1}^{+1}\eta^m\exp(-pt\eta)d\eta,$$

$$N_{34}[p^{7.7}(1+t)^{3.5}(1-t)^{4.2}]/[16\sqrt{3}(7.4!)^{\frac{1}{2}}].$$

The incomplete gamma functions $A_n(p)$ required in the above formula are identical with those tabulated previously.[11,12]

The Integrals $S(4p_\sigma, 4p_\sigma)$ and $S(4p_\pi, 4p_\pi)$

The evaluation of these integrals is carried out in exactly the same manner as that given before and we shall give, therefore, only the master formulas.

$$S(4p_\sigma, 4p_\sigma)=N_{44}\sum_{i=0}^{\infty}\binom{1.7}{i}(-1)^i[A_{7.4-2i}B_{2+2i} -A_{5.4-2i}(B_{2i}+B_{4+2i})+A_{3.4-2i}B_{2+2i}],$$

$$S(4p_\pi, 4p_\pi)=\tfrac{1}{2}N_{44}\sum_{i=0}^{\infty}\binom{1.7}{i}(-1)^i[A_{7.4-2i}(B_{2i}-B_{2+2i}) +A_{(5.4-2i}(B_{4+2i}-B_{2i})+A_{3.4-2i}(B_{2+2i}-B_{4+2i})],$$

where

$$N_{44}=3p^{5.4}(1-t^2)^{4.2}/(2\times7.4!).$$

In these cases, however, the evaluation of the overlap integrals involved the calculation of a new range of the incomplete gamma functions $A_n(p)$ for the nonintegral indices $j+0.4$, with integral j. These were calculated on an IBM 602A computer as described previously.[12]

Values of $A_n(p)$ for $n=-7.6(1)$ to $+7.4$ and $(p)=2.0(0.5)$ to 8.0, and the values of $S(4p_\sigma, 4p_\sigma)$ and $S(4p_\pi, 4p_\pi)$ for $p=2.0$ (0.5) to 8.0, $t=0$ (0.1) 0.5 have been deposited as Document Number 6413 with the ADI auxiliary Publications Project, Photoduplication Service, Library of Congress, Washington 25, D.C. A copy may be obtained by citing the Document number and by remitting \$1.25 for photoprints, or \$1.25 for 35 mm microfilm. Advance payment is required. Make checks or money orders payable to: Chief, Photoduplication Service, Library of Congress.

ACKNOWLEDGMENTS

I should like to thank Dr. H. Tompa and J. de Meulenaer for evaluating the required overlap integrals and incomplete gamma functions. The numerical calculations were carried out on the IBM 602A computer of European Research Associates, Brussels.

This work is part of a project sponsored by European Research Associates, Brussels, and the Union Carbide Corporation, New York, New York, and I wish to take this opportunity to acknowledge with thanks this support.

Method for Investigating the Order of Chemiluminescent Reactions, the Diffusion Coefficient of the Labile Reactants, and the Catalytic Efficiency of Surfaces

ROBERT A. YOUNG*

Boeing Airplane Company, Seattle, Washington

(Received February 3, 1960)

A method is proposed for investigating the order of chemiluminescent reactions, the diffusion coefficient, and the catalytic efficiencies of surfaces for gas phase labile species. This method utilized the change in the decay rate of the labile reactants and of the light intensity. The decay rate of the labile species is controlled through adjustment of their diffusion loss to a catalytic surface.

INTRODUCTION

PRELIMINARY to measuring the rate of reactions involving labile species, one must find the reaction order. This is often difficult or tedious. We wish to discuss a method which, under proper circumstances, will allow the diffusion coefficient, the catalytic efficiency of surfaces, and the order of reactions involving labile species to be measured. For definiteness and ease of exposition we shall limit ourselves to chemiluminescent reactions of free radicals in the gas phase with particular emphasis on those occurring in active nitrogen. However, the labile particles need not be restricted to chemically reactive species, but may be atoms or molecules in metastable states in which case the catalytic surface would be considered an energy-transfer deactivating surface.

METHOD

In this section we shall first simplify the problems to be discussed by adopting several assumptions which will be analyzed later in terms of their experimental realizability.

1. The Diffusion Coefficient of Labile Spectra

Consider a closed volume V to which a long cylindrical diffusion tube of cross-sectional area A has been attached. Assume initially that the only loss of particles is by diffusion down the tube to a movable catalytic surface located at a distance L from its entrance. The situation is depicted in Fig. 1. Further assume that the rate of loss by such diffusion to the catalytic surface is slow enough that only a negligible gradient exists in the volume V. The diffusion problem is now one dimensional and the density gradient in the tube is independent of the position along the tube. These remarks and the continuity of mass flow lead to the equation

$$-V\frac{dn(0)}{dt}=\frac{AD}{L}[n(0)-n(L)]=\frac{Av\gamma n(L)}{4}, \quad (1)$$

where D is the diffusion coefficient, v is the mean thermal velocity at the catalytic surface, γ is the catalytic efficiency of the surface defined as the fraction of the labile particles striking the surface that react, $n(0)$ and $n(L)$ are the concentrations of the active species at the entrance of the diffusion tube and at the catalytic surface, respectively, and the catalytic surface is assumed to fill the cross section of the diffusion tube. The surface reaction is assumed to be of the first order which is in accord with the experimental facts pertaining to atomic nitrogen, oxygen, and hydrogen,[1-5]

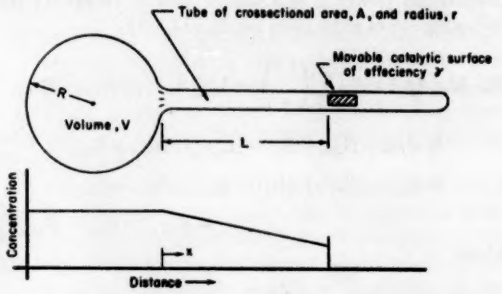

FIG. 1. A schematic description of the situation described by Eqs. (1) to (3). Atoms are lost from volume through diffusion to the catalytic surface located a distance L down the diffusion tube.

and with theoretical expectations.[6] Though the structure of the surface will effect its catalytic efficiency it is often disregarded for gaseous free radical surface reactions.[1-4] The concentration at the catalytic surface can be found relative to that at the entrance by solving the last equality. Substituting this $n(L)$ in the first equality gives

$$-dn(0)/dt=\{Avn(0)/4V[1+(\gamma vL/4D)]\}. \quad (2)$$

Since no gradient exists in the volume, the concentration of atoms in V is $n(0)$ and decays exponentially

* Now at Stanford Research Institute, Menlo Park, California.

[1] J. C. Greaves and J. W. Linnett, Trans. Faraday Soc. **54a**, 1323 (1958); **55**, 1338, 1346, 1355 (1959).
[2] K. D. Shuler and K. J. Laidler, J. Chem. Phys. **17**, 1212 (1949).
[3] R. A. Young, J. Chem. Phys. (to be published).
[4] W. V. Smith, J. Chem. Phys. **11**, 110 (1946).
[5] R. A. Young, J. Chem. Phys. (to be published).
[6] K. J. Laidler, J. Phys. Chem. **53**, 712 (1949).

with a time constant of

$$\tau=(V/A)[(L/D)+(4/\gamma v)]. \quad (3)$$

By measuring the decay of the atom concentration in V with the catalytic surface at several positions we may find

$$\partial\tau/\partial L=V/AD \quad (4)$$

and, knowing V/A, D may be computed. We can compute γ from the intercept of the graph of τ vs L.

2. The Reaction Order

The most important reactive systems generally involve only one or two labile reactants. If these participate in a chemiluminescent reaction of such a nature that the light intensity, I_1, is related to the reactants in the following way:

$$I_1=k_1 n_a^{\alpha} n_b^{\beta} d_a^{\delta} f_b^{\epsilon}\cdots, \quad (5)$$

where f_a, f_b, $\cdots$ are the concentrations of stable reactants which are not appreciably affected by the small loss represented by Eq. (5), then at sufficiently low concentrations of n_a and n_b these quantities will decay exponentially with a time constant given by Eq. (3). The light intensity will also decay exponentially with a time constant τ related to that of the components a and b by

$$\tau^{-1}=(\alpha/\tau_a)+(\beta/\tau_b). \quad (6)$$

Measuring τ_a, τ_b, and τ at two positions of the catalytic surface will suffice for the computation of α and β when these values of τ_a and τ_b are substituted in Eq. (6). Note that α and β cannot be found by measuring the decay of n_a and n_b and I_1 under only one set of conditions.

Equation (6) may be written in terms of the position L of the catalytic surface along the diffusion tube as

$$\tau=C(V/A)\left\{\frac{L^2+L(D_a\mu_a+D_b\mu_b)+\mu_a\mu_b D_a D_b}{(\alpha D_a^{-1}+\beta D_b^{-1})L+\alpha\mu_b+\beta\mu_a}\right\}$$

$$=(V/A)b_1\left\{\frac{L^2+b_2L+b_3}{b_4L+b_5}\right\}, \quad (7)$$

where $\mu_a=4/\gamma_a v_a$, $\mu_b=4/\gamma_b v_b$, and $c=(D_aD_b)^{-1}$.

If the experimental plot of τ vs L is fitted with the function shown in Eq. (7), the quantities of interest will be related to the fitting parameters b_n in the following manner:

$$(D_aD_b)^{-1}=b_1 \qquad D_aD_b\mu_a\mu_b=b_3$$

$$\alpha D_a^{-1}+\beta D_b^{-1}=b_4$$

$$\mu_aD_a+\mu_bD_b=b_2 \qquad \alpha\mu_a+\beta\mu_b=b_5. \quad (8)$$

Knowing or separately measuring one of the quantities D_a, D_b, μ_a, μ_b, α, β, allows the others to be found through Eq. (8).

PRACTICAL CONSIDERATION OF THE METHOD

There remains, however, the important question of the experimental feasibility of this method. There are two important groups of considerations that bear on this: the experimental realization of the conditions implicit in the derivation of Eqs. (1) to (3), and the actual detection of very small ($\sim 10^{12}$/cc) atom concentrations with adequate time response and negligible effect on their loss rate.

1. The Experimental Conditions Necessary that Eq. (3) Applies

First let us analyze the assumptions which lead to Eq. (3). This can conveniently be done by utilizing the results of Wise and Ablow,[7] who present solutions of the diffusion problem under discussion when the tube walls and end surface have catalytic efficiencies γ' and γ, respectively. Using this solution one can obtain the integrated loss on all surfaces and from this the exponential rate constant k. Using the fact that γ' is generally quite small[1-4] while γ can be made quite large[1-5] only the lowest diffusion mode need be retained. Upon expanding $k^{-1}=\tau$ as a power series in a suitable reduced variable one obtains Eq. (3) when the inequalities

$$\gamma' v r/2D<(r/L)^2$$
$$\gamma'/\gamma<(r/L) \quad (9)$$

are satisfied.

We shall now discuss the realization of these inequalities in the light of experimental measurement or extrapolated values of the parameters occurring in Eq. (9). For the particular case of atomic nitrogen, recent evidence[3] indicates that $\gamma\approx 10^{-5}$ and Eq. (9) becomes $10^{-3}<L^{-2}$ at about 1 mm Hg pressure when $v\approx 10^4$ cm/sec and, $r=1$ cm, $D\approx 200p^{-1}$ cm^2/sec. Thus at 1.0 mm Hg the decay time would be 10–100 sec, and follows Eq. (3). At lower pressures the first inequality in Eq. (9), is satisfied for larger L as D increases. Of course one must not reduce the pressure so low that the mean free path becomes comparable to r. The second inequality in Eq. (9) is easily satisfied under most conditions.[1-5]

The loss to the walls of the volume V must not be larger than the loss to the catalytic surface (already small) if accurate measurements are to be made. For a spherical bulb of volume V and area S of catalytic efficiency γ'' the decay constant is simply found as

$$k=v\gamma'' S/4V=v\gamma'' R/12 \quad (10)$$

and for a 3 liter bulb is $\approx 10^5\gamma''$. Thus γ'' must be 10^{-6}–10^{-7} for this loss to be relatively unimportant. Such values have been observed for a properly treated surface, for instance those covered with metaphosphoric acid.[3]

The very slow decay caused by diffusion down the tube (even if L is 10 cm) if compared to the charac-

[7] H. Wise and C. Ablow, J. Chem. Phys. **24**, 634 (1958).

teristic relaxation time of a diffusion mode in the bulb $\approx R^2D^{-1}\approx 1$ implies that a negligible gradient is produced in the bulb by the flux to the diffusion tube.

There are other complications that one may consider. In moving the catalytic surface along the diffusion tube the total volume available to the atoms has been altered. This effect is easily corrected. The pressure gradient generated by the reflux of molecules from the catalytic surface[1] is, under these circumstances, of negligible importance. One may conclude that the conditions on which the simple Eqs. (1) to (3) were founded are experimentally realizable.

2. Methods of Measuring Small Atom Concentrations

Perhaps a more difficult task is detecting the necessarily small concentrations ($\approx 10^{12}$/cc) of the labile species even though absolute measurements are unnecessary. There are a few special cases when this can easily be done (active nitrogen is one[8]). In collaboration with Mr. Sharpless and Dr. Clark of the University of Washington, there has been developed a fast response (1-sec) high-sensitivity (10^{-5} mm Hg partial pressure of atoms) Wrede gauge,[9] suitable to the method under discussion. Preliminary investigations using vacuum ultraviolet resonance absorption to detect N, O, H atoms indicate that this method, implemented by the recent development in photon Geiger counters and ion chambers[10] may be most fruitful. Such methods as paramagnetic[11,12] are becoming sensitive enough for this purpose. Catalytic probes have not as yet been sufficiently developed for this application, and would probably contribute significantly to the decay rate of the labile species.[4] Though mass spectrometers have recently been described with adequate sensitivity[13] the necessary leak rates into the ionization chamber may strongly effect the decay time. Optical pumping[14,15] with electron exchange between, for instance, Rb and a paramagnetic reactant has sufficient sensitivity in some cases. However, because of interaction of the molecular rotational moment with the electron spin moment the characteristic spectrum of the free radical may not be observed.[16] This technique may be of greater value in detecting paramagnetic metastable molecular states and may open up a relatively unexplored field of investigation.

It is to be anticipated that several experimental difficulties will occur. For instance, clustering between a reactant and an impurity would produce very scattered diffusion coefficient measurements, and catalytic surfaces often have a variable catalytic efficiency. In some cases the surface may catalyze the production of a new reactant which may contribute significantly to the loss of those species under study. However, one may expect, with sufficient gas purity and the proper choice of catalytic surfaces, that this method would be successful in determining the diffusion coefficient of reacting species, the catalytic efficiency of surfaces or their energy transfer efficiency, and the order of chemiluminescent reactions or other reactions whose flux may be measured.

[8] Berkowitz, Chupka, and Kistiakowsky, J. Chem. Phys. **25**, 457 (1956).
[9] R. A. Young and R. Sharpless, Bull. Am. Phys. Soc. **3**, 320 (1958).
[10] T. A. Chubb and H. Friedman Rev. Sci. Instr. **26**, 493 (1955). Brackmann, Fite, and Hagen, *ibid.* **29**, 125 (1959).
[11] S. Krongelb and M. W. P. Strandberg, J. Chem. Phys. **31**, 1196 (1959).
[12] Hildebrandt, Barth, and Booth, Progress Report No. 20–371 Jet Propulsion Laboratory, Pasadena, California.
[13] J. T. Herron and V. H. Dibeler, J. Chem. Phys. **31**, 1662 (1959).
[14] A. Kastler, J. phys. radium **11**, 255 (1950).
[15] H. G. Dehmelt, Phys. Rev. **103**, 1125 (1950).
[16] R. Bersohn, *The Ann Arbor Conference on Optical Pumping*, edited by P. Franken and R. Sands (The University of Michigan, Ann Arbor, Michigan, 1959), page 24.

THE JOURNAL OF CHEMICAL PHYSICS VOLUME 33, NUMBER 4 OCTOBER, 1960

Kinetic Theory of the Moderately Dense Rigid-Sphere Fluid. IV. Fluxes of Matter, Momentum, and Energy in a Mixture

ROBERT A. HARRIS AND STUART A. RICE*

Department of Chemistry, and Institute for the Study of Metals, University of Chicago, Chicago 37, Illinois

(Received January 26, 1960)

The perturbation solution of the modified Boltzmann equation is used to obtain the fluxes of matter, momentum, and energy. The fluxes are evaluated to first order in the gradients of density, flow velocity, and temperature, and are left in terms of the Sonine polynomial expansion coefficients. As an example, the calculation of the isothermal diffusion coefficient is carried out for the general case of unequal masses and radii. In the limit of identical particles, D is proportional to $(2kT/m)^{\frac{1}{2}}(N/v\sigma^2)\{[1/g(\sigma)]+(\text{const}/v)+\cdots\}$.

I. INTRODUCTION

In a previous paper[1] we have derived and obtained the formal solution to the modified Boltzmann equation descriptive of the rate of change of the singlet distribution function in a moderately dense rigid-sphere mixture. It is the purpose of the present paper to complete the solution of the transport equation, derive the fluxes of matter, momentum, and energy, and, therefrom, obtain the coefficients of diffusion, thermal diffusion, viscosity, and thermal conductivity.

For the purposes of brief review, it will be recalled that if the singlet distribution function is of the form

$$\bar{f}^{(1)}(1\alpha)=\bar{f}_0^{(1)}(1\alpha)(1+\Phi_{1\alpha}) \tag{1}$$

$$\bar{f}_0^{(1)}(1\alpha)=[(2\pi m_\alpha kT)^{-\frac{1}{2}}/v_\alpha]\exp\{-[\mathbf{p}_{1\alpha}-m_\alpha\mathbf{u}]^2/2m_\alpha kT\} \tag{2}$$

and the perturbation $\Phi_{1\alpha}$ is taken to be of the form

$$\Phi_{1\alpha}=\mathbf{C}_{1\alpha}\cdot\chi_{1\alpha}-\mathbf{A}_{1\alpha}\cdot\nabla_{R_{1\alpha}}\ln T-\mathbf{B}_{1\alpha}:\nabla_{R_{1\alpha}}\mathbf{u} \tag{3}$$

$$\chi_{1\alpha}=(1/\rho)(2m_\alpha/kT)^{\frac{1}{2}}\nabla_{R1\alpha}p-(2kT/m_\alpha)^{\frac{1}{2}}\nabla_{R1\alpha}\ln v_\alpha, \tag{4}$$

then the linearized Boltzmann equation may be solved by series expansion in Sonine polynomials. In Eqs. (1)–(4), the symbol 1α refers to the selected molecule "one" of species α, ρ is the density, m_α, $p_{1\alpha}$, v_α are respectively the mass, momentum, and volume per molecule of species α, $\mathbf{u}$ the mean velocity, p is the pressure, and the coefficients $\mathbf{C}_{1\alpha}$, $\mathbf{A}_{1\alpha}$, and $\mathbf{B}_{1\alpha}$ are to be determined. The evaluation of the coefficients of the gradients leads to a set of linear equations sufficient in number to fix all variables uniquely. The coefficients obtained in this manner are most easily expressed as ratios of determinants, the elements of which are integral brackets.[2] One of the major aims of this paper is the evaluation of a class of these integral brackets and, as an example, the complete theoretical calculation of the diffusion coefficient. The general statistical formulation of Bearman and Kirkwood[3] will be extensively used in the following analysis, and the concept of partial stress tensor will be found appropriate. In general, we shall evaluate all integrals only to terms linear in the gradients, a procedure consistent with the linear form of the transport equation as well as the linear form of the macroscopic laws of heat and matter flux.

By way of illustration of the general theory, we shall evaluate the diffusion coefficient for an arbitrary ratio of masses and sizes. Chapman and Cowling[4] attribute to Thorne the result that the zeroth-order approximation to the diffusion coefficient in the dense fluid is simply the dilute-gas diffusion coefficient divided by the pair-correlation functions evaluated at the point of contact. This result has also been obtained by Longuet-Higgins and Pople[5] by the use of an assumed analytic form for the velocity autocorrelation function. Our results are much more general than those just referred to in that we have evaluated the density dependence of the diffusion coefficient through terms of order v^{-2}. The result which is embodied in Eq. (42) should be valid to a much higher density than the zeroth-order calculations.

II. GENERAL EXPRESSIONS

Bearman and Kirkwood[3] have derived formal relations for the heat flux, matter flux, and stress tensor in a multicomponent system from the Liouville equation and general considerations of the statistical theory of

* Alfred P. Sloan Fellow.

[1] R. A. Harris and S. A. Rice, J. Chem. Phys. **32**, 538 (1960).

[2] For properties of these integral brackets, see J. O. Hirschfelder, C. F. Curtiss, and R. B. Bird, *The Molecular Theory of Gases and Liquids* (John Wiley & Sons, Inc., New York, 1954).

[3] R. J. Bearman and J. G. Kirkwood, J. Chem. Phys. **28**, 136 (1958).

[4] S. Chapman and T. G. Cowling, *The Mathematical Theory of Non-Uniform Gases* (Cambridge University Press, New York, 1953), pp. 292–294. We can find no other evidence of Thorne's work in the literature.

[5] H. C. Longuet-Higgins and J. Pople, J. Chem. Phys. **25**, 884 (1956).

transport. The results are

$$\mathbf{j}=\sum_\alpha\int\{\sum_{i=1}^{N\alpha}\langle\delta(\mathbf{R}_{i\alpha}-\mathbf{r}_1)\delta(\mathbf{p}_{i\alpha}-\mathbf{p}_1);\bar{f}^{(N)}\rangle[(\mathbf{p}_1/m_1)-\mathbf{u}]\}d^3p_1 \tag{5}$$

$$\mathfrak{d}_k=-\sum_\alpha\langle\sum_{i=1}^{N\alpha}m_\alpha[(\mathbf{p}_{1\alpha}/m_\alpha)-\mathbf{u}][(\mathbf{p}_{1\alpha}/m_\alpha)-\mathbf{u}]\delta(\mathbf{R}_{i\alpha}-\mathbf{r}_1);\bar{f}^{(N)}\rangle \tag{6}$$

$$\mathfrak{d}_v=-\sum_\alpha\sum_\gamma\int\langle\mathbf{r}\sum_{i=1}^{N\alpha}\sum_{j=1}^{N\gamma}\nabla V_{\gamma\alpha}\delta(\mathbf{R}_{i\alpha}-\mathbf{r}_1)\delta(\mathbf{R}_{i\gamma}-\mathbf{r}_2);\bar{f}^{(N)}\rangle d^3r \tag{7}$$

$$\mathbf{q}_k=\sum_\alpha\sum_{i=1}^{N\alpha}\langle\tfrac{1}{2}m_\alpha[(\mathbf{p}_{1\alpha}/m_\alpha)-\mathbf{u}]^2[(\mathbf{p}_{1\alpha}/m_\alpha)-\mathbf{u}]\delta(\mathbf{R}_{i\alpha}-\mathbf{r}_1);\bar{f}^{(N)}\rangle \tag{8}$$

$$\mathbf{q}_v=\sum_\alpha\sum_\gamma\tfrac{1}{2}\int\{[V(r)\mathbf{1}-\mathbf{r}\nabla_r V(r)]\cdot[\sum_{i=1}^{N\alpha}\sum_{j=1}^{N\gamma}\langle(\mathbf{p}_{1\alpha}/m_\alpha)\delta(\mathbf{R}_{i\alpha}-\mathbf{r}_1)\delta(\mathbf{R}_{j\gamma}-\mathbf{r}_2);\bar{f}^{(N)}\rangle$$
$$-\mathbf{u}\langle\delta(\mathbf{R}_{i\alpha}-\mathbf{r}_1)\delta(\mathbf{R}_{j\gamma}-\mathbf{r}_2);\bar{f}^{(N)}\rangle]\}d^3r, \tag{9}$$

where we have used the convenient notation

$$\langle\alpha;\bar{f}^{(N)}\rangle=\tau^{-1}\int_0^\tau\int\alpha f^{(N)}d^3R^{(N)}d^3p^{(N)}ds \tag{10}$$

for the expectation value of the dynamical variable α at the time t. Explicit evaluation of the flux vectors requires the introduction of the proper distribution function as well as the reduction of Eqs. (5)–(9) to tractable form by use of the dynamics of the collision process. With the use of methods identical to those employed by Rice, Kirkwood, Ross, and Zwanzig[6] it may be shown that in the limit of isolated binary encounters, the fluxes of matter, momentum, and energy for species α are, respectively,

$$\mathbf{j}_\alpha=N_\alpha\int[(\mathbf{p}_{1\alpha}/m_\alpha)-\mathbf{u}]\bar{f}^{(1)}(1\alpha)d^3p_{1\alpha} \tag{11}$$

$$(\mathfrak{d}_\alpha)_k=-N_\alpha m_\alpha\int[(\mathbf{p}_{1\alpha}/m_\alpha)-\mathbf{u}][(\mathbf{p}_{1\alpha}/m_\alpha)-\mathbf{u}]\bar{f}^{(1)}(1\alpha)d^3p_{1\alpha} \tag{12}$$

$$(\mathfrak{d}_\alpha)_v=\tfrac{1}{2}\sum_\gamma N_\alpha N_\gamma\int\mathbf{r}\nabla_r V(r)\,\bar{f}^{(2)}(1\alpha,2\gamma)d^3p_{1\alpha}d^3p_{2\gamma}d^3r \tag{13}$$

$$(\mathbf{q}_\alpha)_k=\tfrac{1}{2}(N_\alpha m_\alpha)\int[(\mathbf{p}_{1\alpha}/m_\alpha)-\mathbf{u}]^2[(\mathbf{p}_{1\alpha}/m_\alpha)-\mathbf{u}]\bar{f}^{(1)}(1\alpha)d^3p_{1\alpha} \tag{14}$$

$$(\mathbf{q}_\alpha)_v=\tfrac{1}{2}\sum_\gamma N_\alpha N_\gamma\int\left\{[V(r)\mathbf{1}-\mathbf{r}\nabla_r V(r)]\cdot\left[\int\left(\frac{\mathbf{p}_{1\alpha}}{m_\alpha}-\mathbf{u}\right)\bar{f}^{(2)}(1\alpha,2\gamma)d^3p_{1\alpha}d^3p_{2\gamma}\right]\right\}d^3r. \tag{15}$$

Note that the symbols $\mathbf{p}_{1\alpha}$ and $\mathbf{p}_{2\alpha}$ refer, respectively, to particles of species α and γ with momenta $\mathbf{p}_1$ and $\mathbf{p}_2$.

III. THE MASS FLUX

In the preceding paper[1] it was shown that the perturbation to the distribution function could be written in the form

$$\Phi_{1\alpha}=\sum_m C_m^{(1\alpha)}S_{\frac{1}{2}}^{(m)}(W_{1\alpha}^2)\mathbf{W}_{1\alpha}\cdot\chi_{1\alpha}-\sum_m a_m'^{(1\alpha)}S_{\frac{1}{2}}^{(m)}(W_{1\alpha}^2)\mathbf{W}_{1\alpha}\cdot\nabla_{r1}\ln T-\sum_m a_m''^{(1\alpha)}S_{\frac{1}{2}}^{(m)}(Z_{1\alpha}^2)\mathbf{Z}_{1\alpha}\cdot\nabla_{r_1}\ln T$$
$$-\sum_m b_m'^{(1)(1\alpha)}S_{5/2}^{(m)}(W_{1\alpha}^2)(\mathbf{W}_{1\alpha}\mathbf{W}_{1\alpha}-\tfrac{1}{3}W_{1\alpha}^2\mathbf{1}):\nabla_{r_1}\mathbf{u}$$
$$-\sum_m b_m''^{(1)(1\alpha)}S_{5/2}^{(m)}(Z_{1\alpha}^2)(\mathbf{Z}_{1\alpha}\mathbf{Z}_{1\alpha}-\tfrac{1}{3}Z_{1\alpha}^2\mathbf{1}):\nabla_{r_1}\mathbf{u}$$
$$-\sum_m b_m'^{(2)(1\alpha)}S_{\frac{1}{2}}^{(m)}(W_{1\alpha}^2)\nabla_{r_1}\cdot\mathbf{u}-\sum_m b_m''^{(2)(1\alpha)}S_{\frac{1}{2}}^{(m)}(Z_{1\alpha}^2)\nabla_{r_1}\cdot\mathbf{u}, \tag{16}$$

[6] S. A. Rice, J. G. Kirkwood, J. Ross, and R. W. Zwanzig, J. Chem. Phys. **31**, 575 (1959).

where the coefficients a, b, c are determined by the use of the orthogonality properties of the Sonine polynomials $S_\alpha^{(m)}$, and the reduced peculiar velocities $\mathbf{W}_{1\alpha}$ and $\mathbf{Z}_{1\alpha}$ are defined by

$$\mathbf{W}_{1\alpha}=(m_\alpha/2kT)^{\frac{1}{2}}[(\mathbf{p}_{1\alpha}/m_\alpha)-\mathbf{u}] \tag{17}$$

$$\mathbf{Z}_{1\alpha}=\sum_l \gamma_{\alpha l}(m_l/2kT)^{\frac{1}{2}}[(\mathbf{p}_{1\alpha}/m_l)-\mathbf{u}] \tag{18}$$

$$\gamma_{\alpha l}=0 \quad \text{if} \quad \alpha=l$$

$$\gamma_{\alpha l}=1 \quad \text{if} \quad \alpha\neq l. \tag{19}$$

By direct substitution of Eq. (17) into Eq. (11), the relation describing the mass current flow takes the form

$$\mathbf{j}_\alpha=\pi^{-\frac{3}{2}}(N_\alpha/v_\alpha)(2kT/m_\alpha)^{\frac{1}{2}}\int \exp(-W_{1\alpha}^2)(1+\Phi_{1\alpha})\mathbf{W}_{1\alpha}d^3W_{1\alpha}. \tag{20}$$

The first term in the integrand of Eq. (20) is an odd function integrated with an even weighting factor and therefore vanishes by virtue of the over-all symmetry properties of the integral. Thus, the only terms which give rise to a finite contribution to $\mathbf{j}_\alpha$ are those for which $\Phi_{1\alpha}$ is odd in $\mathbf{W}_{1\alpha}$. When all terms of this form which are simultaneously linear in the gradients and/or the mean velocity $\mathbf{u}$, are collected, the integral is easily evaluated to yield

$$\mathbf{j}_\alpha=(N_\alpha/v_\alpha)(2kT/m_\alpha)^{\frac{1}{2}}\Bigg\{(C_0^{(1\alpha)}/2)\chi_{1\alpha}-\nabla_{r_1}\ln T\Bigg\{(a_0'^{(1\alpha)}/2)+\Bigg[\sum_l \gamma_{\alpha l}(m_\alpha/m_l)^{\frac{1}{2}}\Bigg]$$
$$\times\Bigg[(a_0''^{(1\alpha)}/2)+(5a_1''^{(1\alpha)}/4)\Bigg(1-\sum_{\phi,\rho}[m_\alpha/(m_\phi m_\rho)^{\frac{1}{2}}]\gamma_{\alpha\rho}\gamma_{\alpha\phi}\Bigg)\Bigg]\Bigg\}\Bigg\}. \tag{21}$$

For a binary mixture with the components labeled α and β, Eq. (21) reduces to the simpler form

$$\mathbf{j}_\alpha=(N_\alpha/v_\alpha)(2kT/m_\alpha)^{\frac{1}{2}}\Bigg\{C_0^{(1\alpha)}\chi_{1\alpha}-\nabla_{r_1}\ln T\Bigg[a_0'^{(1\alpha)}+(m_\alpha/m_\beta)^{\frac{1}{2}}\Bigg(a_0''^{(1\alpha)}-\tfrac{5}{2}a_1''^{(1\alpha)}\frac{m_\alpha-m_\beta}{m_\beta}\Bigg)\Bigg]\Bigg\}. \tag{22}$$

IV. THE KINETIC CONTRIBUTION TO THE STRESS TENSOR AND ENERGY FLUX

Proceeding in the manner outlined in the previous section, the kinetic contribution to the stress tensor is seen to be given by the relation

$$(\mathfrak{s}_\alpha)_k=-(N_\alpha m_\alpha/\pi^{\frac{3}{2}}v_\alpha)(2kT/m_\alpha)\int \mathbf{W}_{1\alpha}\mathbf{W}_{1\alpha}\exp(-W_{1\alpha}^2)(1+\Phi_{1\alpha})d^3W_{1\alpha}. \tag{23}$$

The first term is readily integrated by the use of the identity

$$\int F(\mathbf{W})\mathbf{W}\mathbf{W}d^3W=\frac{1}{3}\int F(W)W^2dW. \tag{24}$$

By the same arguments that were advanced in the preceding section, only those terms in $\Phi_{1\alpha}$ which are even in the reduced peculiar velocity will contribute to the integral. Thus,

$$(\mathfrak{s}_\alpha)_k=-(N_\alpha m_\alpha/\pi^{\frac{3}{2}}v_\alpha)(2kT/m_\alpha)^{\frac{1}{2}}\Bigg((\pi/2)^{\frac{1}{2}}\mathbf{1}-\int \mathbf{W}_{1\alpha}\mathbf{W}_{1\alpha}\exp(-W_{1\alpha}^2)\Bigg\{\Bigg[b_0'^{(1)(1\alpha)}-b_0''^{(1)(1\alpha)}\sum_{l,\rho}\gamma_{\alpha l}\gamma_{\alpha\rho}\frac{m_\alpha}{(m_\rho m_l)^{\frac{1}{2}}}\Bigg]$$
$$\Bigg(\mathbf{W}_{1\alpha}\mathbf{W}_{1\alpha}-\tfrac{1}{3}W_{1\alpha}^2\mathbf{1}\Bigg):\nabla_{r_1}\mathbf{u}\Bigg)-\Bigg[(b_0'^{(2)(1\alpha)}+\tfrac{3}{2}b_1'^{(2)(1\alpha)}+\tfrac{15}{8}b_2'^{(2)(1\alpha)}+b_0''^{(2)(1\alpha)}+\tfrac{3}{2}b_1''^{(2)(1\alpha)}+\tfrac{15}{8}b_2''^{(2)(1\alpha)})$$
$$-(b_1'^{(2)(1\alpha)}+\tfrac{5}{2}b_2'^{(2)(1\alpha)}+b_1''^{(2)(1\alpha)}+\tfrac{5}{2}b_2''^{(2)(1\alpha)})\{\sum_{l,\rho}\gamma_{\alpha l}\gamma_{\alpha\rho}[m_\alpha/(m_l m_\rho)^{\frac{1}{2}}]\}W_{1\alpha}^2$$
$$+\Bigg(\tfrac{1}{2}b_2'^{(2)(1\alpha)}+\tfrac{1}{2}b_2''^{(2)(1\alpha)}\sum_{l,\rho,\psi,\phi}\prod_{s=1}^{\phi}\gamma_{\alpha s}\frac{m_\alpha^2}{m_s^{\frac{1}{2}}}\Bigg)W_{1\alpha}^4\Bigg]\nabla_{r_1}\cdot\mathbf{u}\mathbf{1}\Bigg\}d^3W_{1\alpha}\Bigg). \tag{25}$$

The identity,

$$\int F(W)\mathbf{WW}(\mathbf{WW}-\tfrac{1}{3}W^2\mathbf{1}):\nabla_{r_1}\mathbf{u}d^3W=\tfrac{2}{15}[\tfrac{1}{2}(\nabla\mathbf{u}+\nabla\mathbf{u}^+)-\tfrac{1}{3}\nabla\cdot\mathbf{u}\mathbf{1}]\int F(W)W^4d^3W, \tag{26}$$

may be employed to integrate Eq. (25). In the general multicomponent case the result is

$$(\mathfrak{d}_\alpha)_k=-(2N_\alpha kT/v_\alpha)\Big[\tfrac{1}{2}\mathbf{1}-\{\tfrac{1}{2}(\nabla\mathbf{u}+\nabla\mathbf{u}^+)-\tfrac{1}{3}\nabla\cdot\mathbf{u}\}\{b_0'^{(1)(1\alpha)}+b_0''^{(1)(1\alpha)}\sum_{l,\rho}\gamma_{\alpha l}\gamma_{\alpha\rho}[m_\alpha/(m_lm_\rho)^{\frac{1}{2}}]\}$$
$$-\tfrac{1}{2}\nabla\cdot\mathbf{u}\mathbf{1}\Big\{b_0'^{(2)(1\alpha)}+b_0''^{(2)(1\alpha)}-b_1'^{(2)(1\alpha)}+b_1''^{(2)(1\alpha)}\{\tfrac{3}{2}-\tfrac{5}{2}\sum_{l,\rho}\gamma_{\alpha l}\gamma_{\alpha\rho}[m_\alpha/(m_lm_\rho)^{\frac{1}{2}}]\}$$
$$-\tfrac{35}{4}b_2'^{(2)(1\alpha)}+b_2''^{(2)(1\alpha)}\Big(\tfrac{15}{8}-\tfrac{25}{4}\sum_{l,\rho}\gamma_{\alpha l}\gamma_{\alpha\rho}\frac{m_\alpha}{(m_lm_\rho)^{\frac{1}{2}}}-\tfrac{35}{8}\sum_{l,\rho,\psi,\phi}\prod_{s=1}^{4}\gamma_{\alpha s}\frac{m_\alpha^2}{m^{\frac{1}{2}}}\Big)\Big\}\Big]. \tag{27}$$

For the special case of the two component mixture with species α and β, Eq. (27) reduces to

$$(\mathfrak{d}_\alpha)_k=(N_\alpha kT/v_\alpha)\Big[[\mathbf{1}-\{\tfrac{1}{2}(\nabla\mathbf{u}+\nabla\mathbf{u}^+)-\tfrac{1}{3}\nabla\cdot\mathbf{u}\mathbf{1}\}\{m_\beta b_0'^{(1)(1\alpha)}+m_\alpha b_0'^{(2)(1\alpha)}\}m_\beta^{-1}$$
$$-\nabla\cdot\mathbf{u}\mathbf{1}\{b_0'^{(2)(1\alpha)}+b_0''^{(2)(1\alpha)}-b_1'^{(2)(1\alpha)}+\tfrac{1}{2}b_1''^{(2)(1\alpha)}[(3m_\beta-5m_\alpha)/m_\beta]$$
$$-\tfrac{35}{4}b_2'^{(2)(1\alpha)}-\tfrac{5}{8}b_2''^{(2)(1\alpha)}[(14m_\alpha^2+10m_\alpha m_\beta-3m_\beta^2)/m_\beta^2]\}\Big]. \tag{28}$$

Since the procedures used are of the same type, we merely quote the result of the evaluation of the kinetic contribution to the heat current

$$(\mathbf{q}_\alpha)_k=(5N_\alpha/8v_\alpha)[(2kTm_\alpha)^{\frac{1}{2}}/m_\alpha^2]\Big[\chi_{1\alpha}(C_0^{(1\alpha)}-C_1^{(1\alpha)})-\nabla_{r_1}\ln T(a_0'^{(1\alpha)}-a_1'^{(1\alpha)})+\sum_l\gamma_{\alpha l}(m_\alpha/m_l)^{\frac{1}{2}}$$
$$\times\{a_0''^{(1\alpha)}+a_1''^{(1\alpha)}(\tfrac{5}{2}-\tfrac{7}{2}\sum_{\rho,\phi}\gamma_{\alpha\rho}\gamma_{\alpha\phi}[m_\alpha/(m_\phi m_\rho)^{\frac{1}{2}}])\}\Big]. \tag{29}$$

IV. INTERMOLECULAR FORCE CONTRIBUTION TO THE STRESS TENSOR

It is convenient to rewrite Eq. (13) in a form which explicitly displays the course graining in time, i.e.,

$$\lim_{\tau\to+0}(\mathfrak{d}_\alpha)_v=\tfrac{1}{2}\sum_\gamma N_\alpha N_\gamma\lim_{\tau\to+0}\tau^{-1}\int_0^\tau\int\mathbf{r}\nabla_r Vf^{(2)}(1\alpha,2\gamma)d^3p_{1\alpha}d^3p_{2\gamma}d^3rds. \tag{30}$$

In the indicated limit, wherein only binary encounters occur, it is easily seen that

$$\mathbf{r}=\sigma_{\alpha\gamma}\mathbf{k};$$
$$d^3r=(p_{\alpha\gamma}/\mu_{\alpha\gamma})b_{\alpha\gamma}db_{\alpha\gamma}d\epsilon\tau, \tag{31}$$

where $\mathbf{k}$ is a unit vector along the line of centers when the rigid spheres are in contact, $\mu_{\alpha\gamma}$ the reduced mass of species α and γ, $b_{\alpha\gamma}$ the collision parameter, and ϵ the azimuthal angle specifying the binary encounter. With the use of Eq. (31) and the mechanical relations,

$$\nabla V(r)=-d\mathbf{p}_{\alpha\gamma}/ds$$
$$\Delta\mathbf{p}_{\alpha\gamma}=2\mathbf{k}(\mathbf{p}_{\alpha\gamma}\cdot\mathbf{k}), \tag{32}$$

Eq. (30) may be rewritten in the condensed form

$$\lim_{\tau\to+0}(\mathfrak{d}_\alpha)_v=\sum_\gamma N_\alpha N_\gamma\int\mathbf{kk}(\mathbf{p}_{\alpha\gamma}\cdot\mathbf{k})g^{(2)}(\sigma_{\alpha\gamma})\bar{f}^{(1)}(1\alpha)\bar{f}^{(1)}(2\gamma)\sigma_{\alpha\gamma}(p_{\alpha\gamma}/\mu_{\alpha\gamma})b_{\alpha\gamma}db_{\alpha\gamma}d\epsilon d^3p_{2\gamma}d^3p_{1\alpha}. \tag{33}$$

To obtain Eq. (33) in terms of the pair-correlation function $g^{(2)}(\sigma_{\alpha\gamma})$ requires no assumptions about the nature of the distribution function. However, in order to integrate Eq. (33) some specification must be made of the dependence of $g^{(2)}(\sigma_{\alpha\gamma})$ on momentum and time. As in the preceding papers, we shall assume that $g^{(2)}(\sigma_{\alpha\gamma})$ is determined by the local thermodynamic variables T, p, and concentration, and that any dependence on momentum may be neglected. The time dependence of $g^{(2)}(\sigma_{\alpha\gamma})$ is thereby contained explicitly in the time dependence of the local thermodynamic variables. Explicit integration of Eq. (33) over angles yields

$$(\delta_\alpha)_v=\sum_\gamma[2\pi g^{(2)}(\sigma_{\alpha\gamma})/15\mu_{\alpha\gamma}]\sigma_{\alpha\gamma}{}^3N_\alpha N_\gamma\int(2\mathbf{p}_{\alpha\gamma}\mathbf{p}_{\alpha\gamma}+p_{\alpha\gamma}{}^2\mathbf{1})\bar{f}^{(1)}(1\alpha)\bar{f}^{(1)}(2\gamma)d^3p_{1\alpha}d^3p_{2\gamma}, \tag{34}$$

whereupon expansion of the dyadic $2\mathbf{p}_{\alpha\gamma}\mathbf{p}_{\alpha\gamma}+p_{\alpha\gamma}{}^2\mathbf{1}$ in terms of $\mathbf{W}_{1\alpha}$ and $\mathbf{W}_{2\alpha}$ followed by introduction of the distribution functions leads to

$$\begin{aligned}(\delta_\alpha)_v=\sum_\gamma\frac{2N_\alpha N_\gamma\sigma_{\alpha\gamma}{}^3g^{(2)}(\sigma_{\alpha\gamma})}{15\mu_{\alpha\gamma}v_\alpha v_\gamma\pi^2}\int\exp(-W_{1\alpha}{}^2)\exp(-W_{2\gamma}{}^2)[1+\Phi_{1\alpha}+\Phi_{2\gamma}]d\mathbf{W}_{1\gamma}d\mathbf{W}_{2\gamma}\\ \times[(m_\gamma-m_\alpha)^2(2\mathbf{uu}+u^2\mathbf{1})+2m_\gamma kT(2\mathbf{W}_{2\gamma}\mathbf{W}_{2\gamma}+W_{2\gamma}{}^2\mathbf{1})\\ +2m_\alpha kT(2\mathbf{W}_{1\alpha}\mathbf{W}_{1\alpha}+W_{1\alpha}{}^2\mathbf{1})+2(m_\gamma-m_\alpha)(2m_\gamma kT)^{\frac{1}{2}}(\mathbf{uW}_{2\gamma}+\mathbf{W}_{2\gamma}\mathbf{u}+\mathbf{W}_{2\gamma}\cdot\mathbf{u}\mathbf{1})\\ +2(m_\alpha-m_\gamma)(2m_\alpha kT)^{\frac{1}{2}}(\mathbf{uW}_{1\alpha}+\mathbf{W}_{1\alpha}\mathbf{u}+\mathbf{W}_{1\alpha}\cdot\mathbf{u}\mathbf{1})\\ -2(2m_\alpha kT)^{\frac{1}{2}}(2m_\gamma kT)^{\frac{1}{2}}(\mathbf{W}_{1\alpha}\mathbf{W}_{2\gamma}+\mathbf{W}_{2\gamma}\mathbf{W}_{1\alpha}+\mathbf{W}_{1\alpha}\cdot\mathbf{W}_{2\gamma}\mathbf{1})].\end{aligned} \tag{35}$$

Examination of the structure of the integrand of Eq. (35) reveals that the only terms which are first order in gradients or in the mean velocity $\mathbf{u}$ are the terms in $\nabla\mathbf{u}$. Integration of Eq. (35), therefore, yields to order linear in the gradients and $\mathbf{u}$ the relation

$$\begin{aligned}(\delta_\alpha)_v=\sum_\gamma\frac{2\pi\sigma_{\alpha\gamma}{}^3N_\alpha N_\gamma g^{(2)}(\sigma_{\alpha\gamma})}{15\mu_{\alpha\gamma}v_\alpha v_\gamma}\Big\{&5kT(m_\alpha+m_\gamma)\mathbf{1}\\ &+\tfrac{1}{2}\{\tfrac{1}{2}(\nabla\mathbf{u}+\nabla\mathbf{u}^+)-\tfrac{1}{3}\nabla\cdot\mathbf{u}\mathbf{1}\}\{2m_\alpha kT\{b_0{}'^{(1)(1\alpha)}+b_0{}''^{(1)(1\alpha)}\sum_{l,\rho}\gamma_{\alpha\rho}\gamma_{\alpha l}[m_\alpha/(m_lm_\rho)^{\frac{1}{2}}]\}\\ &+2m_\gamma kT\{b_0{}'^{(1)(2\gamma)}+b_0{}''^{(1)(2\gamma)}\sum_{\gamma,\rho}\gamma_{\gamma\rho}\gamma_{\gamma l}[m_\gamma/(m_\rho m_l)^{\frac{1}{2}}]\}\}\\ &-\tfrac{5}{2}\nabla\cdot\mathbf{u}\mathbf{1}\Big[2kT\{(m_\alpha+m_\gamma)(b_0{}'^{(2)(1\alpha)}+b_0{}'^{(2)(2\gamma)}+b_0{}''^{(2)(1\alpha)}+b_0{}''^{(2)(2\gamma)})-m_\alpha b_1{}'^{(2)(1\alpha)}-m_\gamma b_1{}'^{(2)(2\gamma)}\}\\ &+b_1{}''^{(2)(1\alpha)}(m_\alpha kT\{3-5\sum_{l,\rho}\gamma_{\alpha l}\gamma_{\alpha\rho}[m_\alpha/(m_lm_\rho)^{\frac{1}{2}}]\}+3m_\gamma kT\{1-\sum_{l,\rho}\gamma_{\alpha l}\gamma_{\alpha\rho}[m_\alpha/(m_lm_\rho)^{\frac{1}{2}}]\})\\ &+b_1{}''^{(2)(2\gamma)}(3m_\alpha kT\{1-\sum_{l,\rho}\gamma_{\gamma l}\gamma_{\gamma\rho}[m_\gamma/(m_lm_\rho)^{\frac{1}{2}}]\}+m_\gamma kT\{3-5\sum_{l,\rho}\gamma_{\gamma l}\gamma_{\gamma\rho}[m_\gamma/(m_lm_\rho)^{\frac{1}{2}}]\})\\ &+b_2{}''^{(2)(1\alpha)}\Big(\tfrac{1}{2}m_\alpha kT\{\tfrac{15}{2}-25\sum_{l,\rho}\gamma_{\alpha l}\gamma_{\alpha\rho}[m_\alpha/(m_lm_\rho)^{\frac{1}{2}}]+\tfrac{35}{2}\sum_{l,\rho,\psi,\phi}\gamma_{\alpha l}\gamma_{\alpha\rho}\gamma_{\alpha\psi}\gamma_{\alpha\phi}\}\frac{m_\alpha{}^2}{(m_lm_\rho m_\psi m_\phi)^{\frac{1}{2}}}\\ &+\tfrac{1}{2}m_\gamma kT\Big\{\tfrac{15}{2}-15\sum_{l,\rho}\gamma_{\gamma l}\gamma_{\gamma\rho}[m_\gamma/(m_lm_\rho)^{\frac{1}{2}}]+\tfrac{15}{2}\sum_{l,\rho,\psi,\phi}\gamma_{\gamma l}\gamma_{\gamma\rho}\gamma_{\gamma\psi}\gamma_{\gamma\phi}\frac{m_\gamma{}^2}{(m_lm_\rho m_\psi m_\phi)^{\frac{1}{2}}}\Big\}\Big)\\ &+b_2{}''^{(2)(2\gamma)}\Big(\tfrac{1}{2}m_\alpha kT\{\tfrac{15}{2}-15\sum_{l,\rho}\gamma_{\alpha l}\gamma_{\gamma\rho}[m_\alpha/(m_lm_\rho)^{\frac{1}{2}}]+\tfrac{15}{2}\sum_{l,\rho,\psi,\phi}\gamma_{\alpha l}\gamma_{\alpha\rho}\gamma_{\alpha\psi}\gamma_{c\phi}[m_\alpha{}^2/(m_lm_\rho m_\psi m_\phi)^{\frac{1}{2}}]\}\\ &+\tfrac{1}{2}m_\gamma kT\Big\{\tfrac{15}{2}-25\sum_{l,\rho}\gamma_{\gamma l}\gamma_{\gamma\rho}[m_\gamma/(m_lm_\rho)^{\frac{1}{2}}]+\tfrac{35}{2}\sum_{l,\rho,\psi,\phi}\gamma_{\gamma l}\gamma_{\gamma\rho}\gamma_{\gamma\psi}\gamma_{\gamma\phi}\frac{m_\gamma{}^2}{(m_lm_\rho m_\psi m_\phi)^{\frac{1}{2}}}\Big\}\Big)\Big]\Big\}.\end{aligned} \tag{36}$$

V. THE INTERMOLECULAR FORCE CONTRIBUTION TO THE HEAT FLUX

Examination of the structure of the integrand of Eq. (15) reveals that the intermolecular force contribution to the heat flux depends upon a difference between two terms. By the definition of the rigid sphere potential $V(r)$

is zero when $r>\sigma$ and indefinitely large when $r\leq\sigma$. Since the pair correlation function depends exponentially upon the potential of mean force, and the potential of mean force is also indefinitely large when $r\leq\sigma$, it is seen that the first term in the integrand of Eq. (15) does not contribute to the heat flux. For, when $g^{(2)}$ does not vanish $V(r)$ is identically zero, and when $V(r)$ does not vanish, the product $g^{(2)}V(r)$ is zero by virtue of the exponential nature of $g^{(2)}$. To evaluate the second term in the integrand Eqs. (30), (31), and (32) are used to transform Eq. (15) to the form

$$(\mathbf{q}_\alpha)_v=-\sum_\gamma N_\alpha N_\gamma\frac{2\pi\sigma_{\alpha\gamma}{}^3g^{(2)}(\sigma_{\alpha\gamma})}{15\mu_{\alpha\gamma}}\int[2\mathbf{p}_{\alpha\gamma}\mathbf{p}_{\alpha\gamma}+p_{\alpha\gamma}{}^2\mathbf{1}]\cdot\left[\frac{\mathbf{p}_{1\alpha}}{m_\alpha}-\mathbf{u}\right]\bar{f}^{(1)}(1\alpha)\bar{f}^{(1)}(2\gamma)d^3p_{1\alpha}d^3p_{2\gamma}. \tag{37}$$

Substitution of the perturbation expansion and subsequent examination of the structure of the equation reveals that only those terms in χ and ∇T contribute to $(\mathbf{q}_\alpha)_v$ to the first order. The result of explicit integration is

$$\begin{aligned}(\mathbf{q}_\alpha)_v=-\sum_\gamma N_\alpha N_\gamma\frac{2\pi\sigma_{\alpha\gamma}{}^3g^{(2)}(\sigma_{\alpha\gamma})}{15\mu_{\alpha\gamma}v_\alpha v_\gamma}\left(\frac{2kT}{m_\alpha}\right)^{\frac{1}{2}}\Big[&-2(m_\gamma-m_\alpha)(2m_\alpha kT)^{\frac{1}{2}}\mathbf{u}\\
&+\chi_{1\alpha}[(5/2)kTC_0{}^{(1\alpha)}(m_\gamma+3m_\alpha)-(15/2)C_1{}^{(1\alpha)}m_\alpha kT]-\chi_{2\gamma}[3kTC_0{}^{(2\gamma)}(m_\alpha m_\gamma)^{\frac{1}{2}}+(15/4)kTC_1{}^{(2\gamma)}(m_\alpha m_\gamma)^{\frac{1}{2}}]\\
&-\nabla_r\ln T\Big((5/2)kTa_0{}'^{(1\alpha)}(m_\gamma+3m_\alpha)-(15/2)a_1{}'^{(1\alpha)}m_\alpha kT-35kTa_0{}'^{(2\alpha)}(m_\alpha m_\gamma)^{\frac{1}{2}}\\
&+(5/2)kT(m_\gamma+3m_\alpha)a_0{}''^{(1\alpha)}\sum_l\gamma_{\alpha\gamma}(m_\alpha/m_l)^{\frac{1}{2}}+a_1{}''^{(1\alpha)}\sum_l\gamma_{\alpha l}(m_\alpha/m_l)^{\frac{1}{2}}\\
&\times\{15m_\gamma kT+\tfrac{75}{4}m_\alpha kT-\tfrac{25}{4}m_\gamma kT\sum_{\phi,\rho}\gamma_{\alpha\phi}\gamma_{\alpha\rho}[m_\alpha/(m_\phi m_\rho)^{\frac{1}{2}}]-\tfrac{105}{4}m_\alpha kT\sum_{\phi,\rho}\gamma_{\alpha\phi}\gamma_{\alpha\rho}[m_\alpha/(m_\phi m_\rho)^{\frac{1}{2}}]\}\\
&+\sum_l\gamma_{\gamma l}(m_\gamma/m_l)^{\frac{1}{2}}\{-3kTa_0{}''^{(2\gamma)}(m_\gamma m_\alpha)^{\frac{1}{2}}-\tfrac{15}{2}kTa_1{}''^{(2\gamma)}(m_\alpha m_\gamma)^{\frac{1}{2}}\sum_{\phi,\rho}\gamma_{\gamma\phi}\gamma_{\gamma\rho}[m_\gamma/(m_\phi m_\rho)^{\frac{1}{2}}]\}\Big)\Big].\end{aligned} \tag{38}$$

VI. DIFFUSION COEFFICIENT

By way of illustration we shall now calculate the diffusion coefficient in a binary rigid-sphere mixture. Examination of Eq. (21) shows that the coefficient $C_0{}^{(1\alpha)}$ must be determined to calculate D and that the coefficients $a_0{}'^{(1\alpha)}$, $a_0{}''^{(1\alpha)}$ are required for the determination of the coefficient of thermal diffusion. Further, reference to Eq. (53) of a previous paper[1] shows that the expansion coefficient $C_0{}^{(1\alpha)}$ is determined by the relation

$$\begin{aligned}\sum_m\sum_\gamma[(N_\gamma-\delta_{\alpha\gamma})/(N_\alpha-1)][g^{(2)}(\sigma_{\alpha\gamma})/v_\alpha v_\gamma][\{S_{\frac{1}{2}}{}^{(k)}(W_{1\alpha}{}^2)\mathbf{W}_{1\alpha};\ S_{\frac{1}{2}}{}^{(m)}(W_{1\alpha}{}^2)\mathbf{W}_{1\alpha}\}_{1\alpha,2\gamma}C_m{}^{(1\alpha)}\\
+\{S_{\frac{1}{2}}{}^{(k)}(W_{1\alpha}{}^2)\mathbf{W}_{1\alpha};\ S_{\frac{1}{2}}{}^{(m)}(W_{2\gamma}{}^2)\mathbf{W}_{2\gamma}\}_{1\alpha,2\gamma}C_m{}^{(2\gamma)}]=\int W_{1\alpha}{}^2\bar{f}_0{}^{(1)}(1\alpha)\,S_{\frac{1}{2}}{}^{(k)}(W_{1\alpha}{}^2)d^3p_{1\alpha}.\end{aligned} \tag{39}$$

For the case of a binary mixture, Eq. (39) leads to four equations in four unknowns after account is taken of the symmetry introduced by the identity of some of the colliding molecules with the molecule of species α. The integration of the right-hand side of Eq. (39) gives just $(3/2)\delta_{0k}v^{-1}(2kT/m_\alpha)^{\frac{1}{2}}$, where δ_{0k} is a Kronecker delta. The bracket integrals which appear on the left-hand side of Eq. (39) may be found in the tabulation of Hirschfelder, Curtiss, and Bird,[2] and in the case of mixtures one must follow the precautions suggested by these authors. For a molecule of species α we find

$$\sum_m\sum_\gamma G(\alpha\gamma)[I_{km}{}^{1\alpha1\alpha}(1\alpha,\,2\gamma)C_m{}^{(1\alpha)}+I_{km}{}^{1\alpha2\gamma}(1\alpha,\,2\gamma)C_m{}^{(2\gamma)}]=(3\delta_{0k}/2v)(2kT/m_\alpha)^{\frac{1}{2}} \tag{40}$$

$$G(\alpha\gamma)=[g(\sigma_{\alpha\gamma})/v_\alpha v_\gamma][(N_\gamma-\delta_{\alpha\gamma})/(N_\alpha-1)]$$

where β is the second species of molecule present in the mixture and

$$\begin{aligned}I_{km}{}^{1\alpha1\alpha}(1\alpha,\,2\gamma)&=\{S_{\frac{1}{2}}{}^{(k)}(W_{1\alpha}{}^2)\mathbf{W}_{1\alpha};\ S_{\frac{1}{2}}{}^{(m)}(W_{1\alpha}{}^2)\mathbf{W}_{1\alpha}\}_{1\alpha,2\gamma}\\
I_{km}{}^{1\alpha2\gamma}(1\alpha,\,2\gamma)&=\{S_{\frac{1}{2}}{}^{(k)}(W_{1\alpha}{}^2)\mathbf{W}_{1\alpha};\ S_{\frac{1}{2}}{}^{(m)}(W_{2\gamma}{}^2)\mathbf{W}_{2\gamma}\}_{1\alpha,2\gamma}.\end{aligned} \tag{41}$$

To conclude the calculation of $C_0^{(1\alpha)}$ two 4- by 4 determinants must be evaluated. The relevant values of I will be found in the Appendix. Since the computations are straightforward but extremely tedious we only quote the result for $C_0^{(1\alpha)}$. By interchanging the superscripts the coefficient $C_0^{(2\beta)}$ is immediately obtained.

$$C_0^{(1\alpha)}=\frac{\mathfrak{A}}{\mathfrak{B}}$$

$$\mathfrak{A}=[3/8\pi^{\frac{1}{2}}\sigma_{\alpha\beta}^2\mu_{\alpha\beta}^{\frac{1}{2}}vg(\sigma_{\alpha\beta})]\Big[\frac{8g(\sigma_{\alpha\alpha})g(\sigma_{\alpha\beta})g(\sigma_{\beta\beta})\sigma_{\alpha\alpha}^2\sigma_{\beta\beta}^2N_\beta}{v_\alpha v_\beta N_\alpha}m_\alpha^5m_\beta^{9/2}$$

$$+\frac{8g(\sigma_{\alpha\alpha})g(\sigma_{\alpha\beta})g(\sigma_{\beta\beta})\sigma_{\alpha\alpha}^2\sigma_{\beta\beta}^2N_\alpha}{v_\alpha v_\beta N_\beta}m_\beta^5m_\alpha^{9/2}$$

$$+\frac{\sqrt{2}g(\sigma_{\alpha\alpha})g(\sigma_{\alpha\beta})\sigma_{\alpha\alpha}^2\sigma_{\alpha\beta}^2}{v_\alpha^2}\mu_{\alpha\beta}^{5/2}\{15m_\alpha^5m_\beta^2+30m_\alpha^3m_\beta^4+16m_\alpha^4m_\beta^3$$

$$+(N_\alpha/N_\beta)^2(15m_\alpha^{9/2}m_\beta^{5/2}+30m_\beta^{9/2}m_\alpha^{5/2}+16m_\alpha^{7/2}m_\beta^{7/2})\}$$

$$+\frac{\sqrt{2}g(\sigma_{\beta\beta})g(\sigma_{\alpha\beta})\sigma_{\beta\beta}^2\sigma_{\alpha\beta}^2}{v_\beta^2}\mu_{\alpha\beta}^{5/2}\{15m_\beta^5m_\alpha^2+30m_\alpha^4m_\beta^3+16m_\alpha^3m_\beta^4$$

$$+(N_\beta/N_\alpha)^2(15m_\alpha^{5/2}m_\beta^{9/2}+30m_\beta^{5/2}m_\alpha^{9/2}+16m_\alpha^{7/2}m_\beta^{7/2})\}$$

$$+\tfrac{1}{2}\cdot\frac{g(\sigma_{\alpha\beta})g(\sigma_{\alpha\beta})\sigma_{\alpha\beta}^4}{v_\alpha v_\beta}\mu_{\alpha\beta}^5\{(N_\beta/N_\alpha)[185(m_\alpha^{9/2}+m_\beta^4m_\alpha^{\frac{1}{2}})+288m_\alpha^{5/2}m_\beta^2+1344(m_\alpha^{7/2}m_\beta+m_\beta^3m_\alpha^{\frac{1}{2}})]$$

$$+(N_\alpha/N_\beta)[185(m_\beta^{9/2}+m_\beta^{\frac{1}{2}}m_\alpha^4)+288m_\alpha^2m_\beta^{5/2}+1344(m_\beta^{7/2}m_\alpha+m_\alpha^3m_\beta^{\frac{1}{2}})]\}\Big] \quad (42a)$$

$$\mathfrak{B}=(1/v_\alpha v_\beta)\{[16g(\sigma_{\alpha\alpha})g(\sigma_{\alpha\beta})/v_\alpha v_\beta]\sigma_{\alpha\alpha}^2\sigma_{\beta\beta}^2(m_\alpha^{9/2}m_\beta^{9/2}+m_\alpha^5m_\beta^4)$$

$$+[4\sqrt{2}g(\sigma_{\alpha\alpha})g(\sigma_{\alpha\beta})\sigma_{\alpha\alpha}^2\sigma_{\alpha\beta}^2N_\alpha/v_\alpha^2N_\beta]\mu_{\alpha\beta}^{5/2}(6m_\alpha^{9/2}m_\beta^2+15m_\alpha^{5/2}m_\beta^4+8m_\alpha^{7/2}m_\beta^3+6m_\alpha^5m_\beta^{\frac{1}{2}}+15m_\alpha^3m_\beta^{7/2}+8m_\alpha^4m_\beta^{5/2})$$

$$+[2\sqrt{2}g(\sigma_{\beta\beta})g(\sigma_{\alpha\beta})\sigma_{\beta\beta}^2\sigma_{\alpha\beta}^2N_\beta/v_\beta^2N_\alpha]\mu_{\alpha\beta}^{5/2}(13m_\beta^{9/2}m_\alpha^2+30m_\alpha^4m_\beta^{5/2}+15m_\alpha^3m_\beta^{7/2}$$

$$+13m_\beta^4m_\alpha^{5/2}+30m_\alpha^{9/2}m_\beta^2+15m_\alpha^{7/2}m_\beta^3)$$

$$+[g(\sigma_{\alpha\beta})g(\sigma_{\alpha\beta})\sigma_{\alpha\beta}^4/v_\alpha v_\beta]\mu_{\alpha\beta}^5[343(m_\alpha^3m_\beta+m_\alpha^{7/2}m_\beta^{\frac{1}{2}})+297(m_\alpha^2m_\beta^2+m_\alpha^{5/2}m_\beta^{\frac{1}{2}})$$

$$+329(m_\beta^3m_\alpha+m_\alpha^{\frac{1}{2}}m_\beta^{5/2})+180(m_\alpha^4+m_\alpha^{9/2}m_\beta^{-\frac{1}{2}})+195(m_\beta^4+m_\alpha^{\frac{1}{2}}m_\beta^{7/2})]$$

$$+[16g(\sigma_{\alpha\alpha})g(\sigma_{\alpha\beta})/v_\alpha v_\beta]\sigma_{\alpha\alpha}^2\sigma_{\beta\beta}^2(m_\alpha^{9/2}m_\beta^{9/2}+m_\alpha^4m_\beta^5)$$

$$+(4\sqrt{2}g(\sigma_{\beta\beta})g(\sigma_{\alpha\beta})\sigma_{\beta\beta}^2\sigma_{\alpha\beta}^2N_\beta/v_\beta^2N_\alpha)\mu_{\alpha\beta}^{5/2}(6m_\alpha^2m_\beta^{9/2}+15m_\alpha^4m_\beta^{5/2}+8m_\alpha^3m_\beta^{7/2}$$

$$+6m_\alpha m_\beta^5+15m_\alpha^{7/2}m_\beta^3+8m_\alpha^{5/2}m_\beta^4)$$

$$+[2\sqrt{2}g(\sigma_{\alpha\alpha})g(\sigma_{\alpha\beta})\sigma_{\alpha\alpha}^2\sigma_{\alpha\beta}^2N_\alpha/v_\alpha^2N_\beta]\mu_{\alpha\beta}^{5/2}(13m_\alpha^{9/2}m_\beta^2+30m_\alpha^{5/2}m_\beta^4+15m_\alpha^{7/2}m_\beta^3$$

$$+13m_\alpha^4m_\beta^{5/2}+30m_\beta^{9/2}m_\alpha^2+15m_\alpha^3m_\beta^{7/2})$$

$$+[g(\sigma_{\alpha\beta})g(\sigma_{\alpha\beta})\sigma_{\alpha\beta}^4/v_\alpha v_\beta]\mu_{\alpha\beta}^5[343(m_\alpha m_\beta^3+m_\beta^{7/2}m_\alpha^{\frac{1}{2}})+297(m_\alpha^2m_\beta^2+m_\alpha^{\frac{1}{2}}m_\beta^{5/2})$$

$$+329(m_\alpha^3m_\beta+m_\beta^{\frac{1}{2}}m_\alpha^{5/2})+180(m_\beta^4+m_\beta^{9/2}m_\alpha^{-\frac{1}{2}})+195(m_\alpha^4+m_\alpha^{7/2}m_\beta^{\frac{1}{2}})]\}. \quad (42b)$$

The diffusion of a given species is conveniently measured in a coordinate system in which the total flux of matter is zero. This coordinate system moves with the velocity of the center of mass. The isothermal mass flux of species α is given by the phenomenological relation

$$\mathbf{j}_\alpha=-D\nabla_r v_\alpha, \quad (43)$$

an equation to be compared with the statistical result embodied in Eq. (21). By direct comparison of coefficients,

$$D=(N_\alpha/2v_\alpha^2)(2kT/m_\alpha)C_0^{(1\alpha)}. \quad (44)$$

In the limit when all particles are identical it is easily seen that D is proportional to $(2kT/m_\alpha)^{\frac{1}{2}}[N_\alpha/v_\alpha\sigma^2 g^{(2)}(\sigma)]$. Note that $C_0^{(1\alpha)}$ is proportional to m_α. Owing to the complex nature of the coefficient $C_0^{(1\alpha)}$ little purpose is served by combining Eqs. (42a) and (44).

The purpose of this paper has been to obtain explicit relations for the fluxes of matter and energy and for the stress tensor and to completely evaluate the simplest of the transport coefficients, the diffusion constant. The general procedure to be followed for the evaluation of the thermal conductance and the viscosity is the same as that indicated herein. In all cases the expansion coefficients in the Sonine polynomial series must be evaluated and the resultant flux equation compared with the phenomenological relations. The comparison of terms provides an unambiguous determination of the transport coefficients.

APPENDIX I.

$$I_{00}^{1\alpha 1\alpha}(1\alpha 1\alpha)=4A \qquad I_{00}^{1\beta 1\beta}(1\beta 2\beta)=4B \qquad I_{00}^{1\alpha 2\alpha}(1\alpha 2\alpha)=-4A$$

$$I_{01}^{1\alpha 1\alpha}(1\alpha 2\alpha)=-A \qquad I_{01}^{1\beta 1\beta}(1\beta 2\beta)=-B \qquad I_{01}^{1\alpha 2\alpha}(1\alpha 2\alpha)=A$$

$$I_{11}^{1\alpha 1\alpha}(1\alpha 2\alpha)=\tfrac{59}{4}A \qquad I_{11}^{1\beta 1\beta}(1\beta 2\beta)=\tfrac{59}{4}B \qquad I_{11}^{1\alpha 2\alpha}(1\alpha 2\alpha)=-\tfrac{27}{4}A$$

$$I_{00}^{1\beta 2\beta}(1\beta 2\beta)=-4B \qquad I_{00}^{1\beta 2\alpha}(1\beta 2\alpha)=-\frac{8(m_\alpha m_\beta)^{\frac{1}{2}}}{(m_\alpha+m_\beta)}C=I_{00}^{1\alpha 2\beta}(1\alpha 2\beta)$$

$$I_{01}^{1\beta 2\beta}(1\beta 2\beta)=B \qquad I_{01}^{1\beta 2\alpha}(1\beta 2\alpha)=\frac{4(m_\alpha m_\beta)^{\frac{1}{2}}m_\beta}{(m_\alpha+m_\beta)^2}C=(m_\beta/m_\alpha)I_{01}^{1\alpha 2\beta}(1\alpha 2\beta)$$

$$I_{11}^{1\beta 2\beta}(1\beta 2\beta)=-\tfrac{27}{4}B \qquad I_{11}^{1\beta 2\alpha}(1\beta 2\alpha)=\frac{-54(m_\alpha m_\beta)^{\frac{1}{2}}}{(m_\alpha+m_\beta)^3}C=I_{11}^{1\alpha 2\beta}(1\alpha 2\beta)$$

$$I_{00}^{1\alpha 1\alpha}(1\alpha 2\beta)=\frac{8m_\beta}{(m_\alpha+m_\beta)}C=\frac{m_\beta}{m_\alpha}I_{00}^{1\beta 1\beta}(1\beta 2\alpha)$$

$$I_{01}^{1\alpha 1\alpha}(1\alpha 2\beta)=\frac{-4m_\beta^2}{(m_\alpha+m_\beta)^2}C=\frac{m_\beta^2}{m_\alpha^2}I_{01}^{1\beta 1\beta}(1\beta 2\alpha)$$

$$I_{11}^{1\alpha 1\alpha}(1\alpha 2\beta)=\frac{2m_\beta}{(m_\alpha+m_\beta)^3}(13\gamma_{\alpha\beta}m_\beta^2+30m_\alpha^2+16m_\alpha m_\beta)C$$

$$I_{11}^{1\beta 1\beta}(1\beta 2\alpha)=\frac{2m_\alpha}{(m_\alpha+m_\beta)^3}(13\gamma_{\alpha\beta}m_\alpha^2+30m_\beta^2+16m_\alpha m_\beta)C$$

$$A=(\pi kT/m_\alpha)^{\frac{1}{2}}\sigma_{\alpha\alpha}^2$$

$$B=(\pi kT/m_\beta)^{\frac{1}{2}}\sigma_{\beta\beta}^2$$

$$C=(\pi kT/2\mu_{\alpha\beta})^{\frac{1}{2}}\sigma_{\alpha\beta}^2$$

APPENDIX II.

Recently, the validity of the modified Boltzmann equation derived by Rice, Kirkwood, Ross, and Zwanzig has been questioned.[7] A detailed examination of the arguments used reveals that the difference between the Enskog equation and the Rice-Kirkwood-Ross-Zwanzig equation is due to the difference in the point at which the hard-sphere potential is introduced. In the RKRZ analysis the computation is carried as far as possible without explicit introduction of the nature of the potential. Thus, in the region where higher-order collisions may be neglected RKRZ Eq. (17) is valid for any potential that is continuous. The hard-sphere potential is first used in RKRZ Eq. (22). In contrast, the Enskog treatment introduces the discontinuous potential at the very outset of the calculation. With this choice, the integration of the Liouville equation must be performed carefully, since $f^{(2)}$ is discontinuous in the region of integration. The fact that two different equations arise when the nature of the potential is discontinuous and the discontinuity is introduced at two different points is reminiscent of the differences between the Kirkwood and the Born-Green formulations for the calculation of $g_0^{(2)}$ at equilibrium in a liquid. In that case the use of the superposition approximation at different points in the analysis leads to two different final equations.

The question of which equation is to be preferred is

[7] J. O'Toole and J. Dahler, J. Chem. Phys., **32**, 1097 (1960); C. Curtiss and H. Hollinger, private communication.

largely a matter of taste. First, we note that the computed transport coefficients are little affected by the difference.[6] Second, although the Enskog equation is consistent in that the hard-sphere potential is used at all times, the RKRZ equation has the advantage that, since no real hard-sphere fluids exist, the transport equation derived is the logical limit as $n \to \infty$ when the potential is of the form $V = (\sigma/R)^n$. This corresponds to a definite physical picture and classification scheme for fluids.

THE JOURNAL OF CHEMICAL PHYSICS VOLUME 33, NUMBER 4 OCTOBER, 1960

Kinetic Theory of the Moderately Dense Rigid-Sphere Fluid. V. Relaxation in Momentum Space

ROBERT A. HARRIS AND STUART A. RICE*

Department of Chemistry and Institute for the Study of Metals, University of Chicago, Chicago 37, Illinois

(Received February 5, 1960)

We consider the problem of a dense rigid-sphere fluid at equilibrium in configuration space but perturbed in momentum space. The relaxation time for the return to equilibrium is computed analytically and shown to correspond to very few collisions—about four at gas densities and about one at liquid densities. This result is in good agreement with machine computations by Alder and Wainwright and shock-tube measurements by Greene, Cowan, and Hornig. The results indicated that correlated successive binary collisions need not be considered to first order in the finite dense rigid-sphere fluid.

I. INTRODUCTION

THE theory of transport processes is concerned in part with two related physical processes. These are the transfer of energy or momentum under steady-state conditions and the unconstrained return to equilibrium from a nonequilibrium state. The first classification includes the calculation of the usual transport coefficients, the thermal conductance, shear viscosity, bulk viscosity, and diffusion constants. If a macroscopic system specified by the gross variables temperature, density, and composition is displaced slightly from equilibrium, the return to equilibrium follows an exponential decay with the time constant defined by the transport coefficients specified above. Thus, in the macroscopic description, these two classifications are not distinct and little extra is learned by solving the separate aspects of the problem.

When the microscopic theory of transport is considered, the two classifications become more important. We note that most microscopic theories are based on the solution of a transport equation. It is usually true that the derivation of the transport equation involves physical assumptions which can in part be checked by calculation of the relaxation time for the return to equilibrium after a suitable perturbation has been applied. In recent papers[1–4] there has been developed a modified Boltzmann equation suitable for the description of the singlet distribution function in a moderately dense fluid of rigid spheres. This equation, which refers to the case of uncorrelated binary encounters, may be regarded as the first term in an expansion in terms of the number of successive correlated binary encounters. If the expansion is to be useful, the series should converge rapidly, and if the relaxation to equilibrium can be shown to require but a small number of collisions, the utility of the first term as an approximation is markedly enhanced. It is the purpose of this paper to attack just this problem, the calculation of the relaxation time in momentum space for the moderately dense rigid sphere fluid.

The procedure we shall use is to solve the modified Boltzmann equation suitable for the moderately dense rigid sphere fluid for the case in which the singlet distribution function corresponds to equilibrium in configuration space. The method of solution is similar in spirit to that of Phillips,[5] but the techniques differ somewhat.[6] The perturbation to the equilibrium distribution in momentum space is expanded in terms of an orthonormal set of functions. The resulting equation is minimized with respect to the expansion co-

* Alfred P. Sloan Fellow.

[1] S. A. Rice, J. G. Kirkwood, J. Ross, and R. W. Zwanzig, J. Chem. Phys. **31**, 575 (1959).

[2] S. A. Rice, J. Chem. Phys. **31**, 584 (1959).

[3] R. A. Harris and S. A. Rice, J. Chem. Phys. **32**, 538 (1960).

[4] R. A. Harris and S. A. Rice, J. Chem. Phys. (to be published).

[5] N. J. Phillips, Proc. Phys. Soc. **73**, 800 (1959).

[6] The equation which determines the relaxation time is derived from a variational principle enunciated by Phillips.[5] Phillips has calculated the relaxation time by the method of successive approximations. The procedure which we use, as embodied in Eq. (7), is the explicit solution of Phillips' variational principle. In this manner we are able to determine any number of eigenvalues by increasing the number of terms in the trial solution. It is important to note that Phillips' method, as it is applied by him, does not apply to mixtures. Phillips assumes that the lowest eigenvalue is the same for both components but there is no *a priori* reason as to why this should be true.

efficients and a secular equation is obtained. The eigenvalues determined by solution of the secular determinant are the reciprocal relaxation times. Because of the minimization, these will be the longest relaxation times. Suitable combination of these relaxation times with other considerations leads to a computation of the number of collisions required to reach equilibrium. The theoretical result is in excellent agreement with both the machine calculations of Alder and Wainwright[7] and the shock-wave studies of Greene, Cowan, and Hornig.[8]

II. RELAXATION TIME

In the case of equilibrium in configuration space, the modified Boltzmann equation for the singlet distribution function, $\bar{f}^{(1)}$, derived by Rice, Kirkwood, Ross, and Zwanzig,[1] may be written

$$\partial\bar{f}^{(1)}/\partial t = g(\sigma)\int[\bar{f}^{(1)}(\mathbf{p}_1^*;t)\bar{f}^{(1)}(\mathbf{p}_2^*;t) - \bar{f}^{(1)}(\mathbf{p}_1;t)\bar{f}^{(1)}(\mathbf{p}_2;t)](p_{12}/\mu)\,bdbd\epsilon d^3p_2, \quad (1)$$

where $g(\sigma)$ is the equilibrium pair correlation function evaluated at the point of contact, σ is the rigid-sphere diameter, and the asterisk refers to the momenta after collisions. The integrand is to be evaluated for all possible collisions specified by the impact parameter b and the azimuthal angle ϵ. Note that the normalization of the distribution function appearing in Eq. (1) has been modified to conform with the later papers[3,4] of this series. Equation (1) is related to the ordinary Boltzmann equation (Phillips' starting point) by what is effectively a scaling of time. This time-scaling correspondence carries through all calculations. That is, Eq. (1) has the form of the dilute-gas Boltzmann equation, except for the modifying factor of $g(\sigma)$. We seek a perturbation solution with explicit time dependence of the form $\exp(-\Lambda t)$. It is convenient, therefore, to write the distribution function as

$$\bar{f}^{(1)}(\mathbf{p}_1;t) = \bar{f}_0^{(1)}(\mathbf{p}_1)[1+e^{-\Lambda t}\psi(p_1^2)]$$
$$\bar{f}_0^{(1)}(p_1) = [(2\pi mkT)^{-\frac{1}{2}}/v]\exp-[\mathbf{p}_1-m\mathbf{u}]^2/2mkT, \quad (2)$$

with v the volume per molecule and $\mathbf{u}$ the mean velocity of the fluid. The perturbation function $\psi(p_1^2)$ is restricted to an even dependence on momentum as is indicated by the argument. Neglecting terms of second order, the substitution of Eq. (2) into Eq. (1) gives the relation

$$\Lambda\bar{f}_0^{(1)}(1)\psi(p_1^2) = -g(\sigma)\int\bar{f}_0^{(1)}(1)\bar{f}_0^{(1)}(2) \times[\psi(p_1^{*2})+\psi(p_2^{*2})-\psi(p_1^2)-\psi(p_2^2)](p_{12}/\mu)\,bdbd\epsilon d^3p_2, \quad (3)$$

where the condition

$$\bar{f}_0^{(1)}(p_1)\bar{f}_0^{(1)}(p_2) = \bar{f}_0^{(1)}(p_1^*)\bar{f}_0^{(1)}(p_2^*) \quad (4)$$

has been used. Equation (3) is suggestive of an eigenvalue problem. To utilize this observation, we expand the perturbation function ψ in a set of functions orthonormal with respect to the weighting factor $\bar{f}_0^{(1)}$. Let the functions of this set be denoted ω_m, so that

$$\psi(p_1^2) = \sum_m b_m\omega_m(p_1^2)$$
$$\int\omega_m(p_1^2)\omega_n(p_1^2)\bar{f}_0^{(1)}(p_1)\,d^3p_1 = C\delta_{nm}/v, \quad (5)$$

with C a normalization constant. Direct substitution of Eq. (5) into Eq. (3) followed by multiplication by $\sum_n b_n\omega_n(p_1^2)$ and integration with respect to $\mathbf{p}_1$ gives

$$\Lambda\int\bar{f}_0^{(1)}(1)\sum_{m,n}b_mb_n\omega_m(p_1^2)\omega_n(p_1^2)\,d^3p_1 = -g(\sigma)\int\bar{f}_0^{(1)}(1)\bar{f}_0^{(1)}(2)\sum_n b_n\omega_n(p_1^2)[\sum_m b_m\{\omega_m(p_1^{*2}) + \omega_m(p_2^{*2})-\omega_m(p_1^2)-\omega_m(p_2^2)\}](p_{12}/\mu)\,bdbd\epsilon d^3p_1d^3p_2. \quad (6)$$

By use of the orthogonality conditions, the left-hand side of Eq. (6) vanishes unless $m=n$,

It is the purpose of this calculation to determine the longest relaxation time, corresponding to the minimum value of Λ. In the usual manner, the minimum value of Λ is determined by variation of the expansion coefficients. Thus, performing the variation with respect to b_k, and using the condition $(\partial\Lambda/\partial b_k)=0$, $(k=0, 1, \cdots)$ gives the secular equation

$$\sum_m b_m[-g(\sigma)\{m,k\}-\Lambda(m,m)\delta_{mk}]=0 \quad k=0, 1, \cdots, \quad (7)$$

Both the values of Λ and the expansion coefficients b_m are determined by the normalization conditions and the roots of the determinant

$$||-g(\sigma)\{m,k\}-\Lambda(m,m)\delta_{mk}||=0, \quad (8)$$

with $\{m,k\}$ and (m,m) defined by

$$\{m,k\} = \int\bar{f}_0^{(1)}(1)\bar{f}_0^{(1)}(2)[\omega_m(p_1^{*2})+\omega_m(p_2^{*2}) - \omega_m(p_1^2)-\omega_m(p_2^2)]\omega_k(p_1^2)\,(p_{12}/\mu)\,bdbd\epsilon d^3p_1d^3p_2, \quad (9)$$

$$(m,m) = \int\bar{f}_0^{(1)}(1)\omega_m^2(p_1^2)\,d^3p_1. \quad (10)$$

A most convenient set of functions satisfying Eq. (5)

[7] B. J. Alder and T. Wainwright, J. Chem. Phys. **31**, 459 (1959). *Transport Processes in Statistical Mechanics*, edited by I. Prigogine (Interscience Publishers, Inc., New York, 1958), p. 97.

[8] E. F. Greene, R. Cowan, and D. Hornig, J. Chem. Phys. **19**, 427 (1951).

is the set of Sonine polynomials, defined by

$$S_n^{(m)}(\zeta)=\sum_{j=0}^{m}(-)^j\frac{(m+n)!\zeta^j}{j!(n+j)!(m-j)!}, \tag{11}$$

We have already indicated that the argument of the perturbation function must be symmetric in the momentum. The variable argument, ζ, of the set of Sonine polynomials will therefore be taken to be the reduced peculiar velocity W^2, where

$$W^2=(m/2kT)[(\mathbf{p}/m)-\mathbf{u}]^2, \tag{12}$$

Now, in a binary collision, the number of particles, the momentum and the energy are conserved. By direct expansion, it is seen that if $m=0$, or 1, the brackets $\{m, k\}$ vanish identically using the conservation conditions mentioned. We therefore choose for the trial function the simple form

$$\psi(p^2)=b_3S_{\frac{1}{2}}^{(2)}(W^2)+b_3S_{\frac{1}{2}}^{(3)}(W^2) \tag{13}$$

containing two nonvanishing contributions. Evaluation of the brackets $\{m, k\}$ is tedious and only the results are quoted herein. The explicit calculation of $\{3, 3\}$ is given in the Appendix. It is found that[9]

$$(2, 2)=35/8v \tag{14}$$

$$(3, 3)=105/16v \tag{15}$$

$$\{2, 2\}=-(4/v^2)(\pi kT/m)^{\frac{1}{2}}\sigma^2 \tag{16}$$

$$\{2, 3\}=\{3, 2\}=-(3/v^2)(\pi kT/m)^{\frac{1}{2}}\sigma^2 \tag{17}$$

$$\{3, 3\}=-(2709/10v^2)(\pi kT/m)^{\frac{1}{2}}\sigma^2. \tag{18}$$

Using Eqs. (14) through (18), we find that the roots of the determinant are given by[10]

$$\Lambda_+=41.19[\sigma^2g(\sigma)/v](\pi kT/m)^{\frac{1}{2}}$$

$$\Lambda_-=1.008[\sigma^2g(\sigma)/v](\pi kT/m)^{\frac{1}{2}}, \tag{19}$$

with Λ_- clearly the smaller of the two. The longest relaxation time is thereby seen to be

$$\tau_-=[0.992v/\sigma^2g(\sigma)](m/\pi kT)^{\frac{1}{2}} \tag{20}$$

$$\tau_-\leqq[0.992v/\sigma^2](m/\pi kT)^{\frac{1}{2}}[1-\tfrac{5}{12}(\pi\sigma^3/v)+\cdots] \tag{21}$$

where Eq, (21) follows from the use of the well-known virial expansion for $g(\sigma)$. The magnitude of this relaxation time is, for liquid argon at 90°K of order 5×10^{-13} sec,[11] and for gaseous argon at 300°K of order 10^{-9} sec.

[9] The bracket (2, 2) is correct as printed above. A slight error led Phillips to give the value $15/8v$. This error was carried through into the relaxation time which agrees with our Eq. (19) when the correct value for (2, 2) is used.

[10] The inclusion of higher-order terms in the trial function has very little effect on the computed relaxation time. This finding is in agreement with the earlier work of Phillips.

[11] For the purposes of numerical calculation the radial distribution function on contact was evaluated from experimental data. Essentially identical results are obtained if the calculations of Kirkwood, Maun, and Alder [J. Chem. Phys. **18**, 1040 (1950)] or the calculations of Reiss, Frisch, and Lebowitz [J. Chem. Phys. **31**, 369 (1959)] are used.

III. DISCUSSION

The calculations of the preceding section show that the longest relaxation time in a rigid-sphere fluid is short enough to correspond to but a few collisions. There are a number of ways of estimating the number of collisions in the time τ_-. If the number of collisions per second for a dilute rigid-sphere gas is written

$$Z_1^0=4(\pi kT/m)^{\frac{1}{2}}(\sigma^2/v) \tag{22}$$

then $Z_1^0\tau_-$ is in the dilute gas approximation independent of both temperature and density. The product of Eqs. (20) and (22) corresponds to four collisions. To make an approximate calculation of Z, for a dense fluid, we *define*[12]

$$Z_1=\frac{128\sigma^2}{15v}\left(\frac{kT}{m\pi}\right)^{\frac{1}{2}}\left[\frac{1}{g(\sigma)}+\frac{8\pi\sigma^3}{15v}+\left(\frac{4\pi\sigma^3}{15v}\right)^2g(\sigma)\right]^{-1}, \tag{23}$$

which combines the calculated shear viscosity of the dense rigid-sphere fluid[2] with the mean-free-path relation for the shear viscosity. We regard this relation as a definition of the collision frequency Z_1. The product of Eqs. (23) and (20) gives

$$Z_1\tau_-=2.70\Big/\left\{1+\frac{8\pi\sigma^3}{15v}g(\sigma)+\left(\frac{4\pi\sigma^3}{15v}\right)^2[g(\sigma)]^2\right\}. \tag{24}$$

For the case of liquid argon, Eq. (24) corresponds to about one collision. Thus the number of collisions required to relax $1/e$ towards the equilibrium is indeed small.

In the derivation of Eq. (1) an essential hypothesis is that the evolution in time of a two-body subset is given by the pair Liouville equation for the transformation or distribution function; i.e., the dynamics of the system is determined by binary collisions only, with the exclusion of correlated binary, triple, etc., collisions. This hypothesis, essential for dilute gas theory, may be expected to hold at finite densities for the particular model of hard spheres in the limit as the time interval $\tau\to+0$. It would appear from naive considerations that at finite τ, the dynamics would be influenced by higher-order collisions. That is, in a dense fluid we might anticipate considerable correlation between successive collisions. If the collisions were completely uncorrelated, on the average there would be a loss of half the hot-particle momentum at each collision. After n collisions, the particle would remember only a fraction $(\frac{1}{2})^n$ of the initial momentum. The calculations of this paper show that the average collision frequency in a dense medium is large enough and the longest relaxation time short enough that successive collisions are largely uncorrelated. Thus in a dense medium, to relax $1/e$ towards equilibrium requires only one collision—quite close to the simple factor $\frac{1}{2}$ mentioned above.

[12] This is equivalent to the definition used in the second of footnote reference 7, p. 110.

There are two pieces of experimental evidence which can be compared with our deductions. Alder and Wainwright[7] studied the dynamics of a system of hard spheres (between 8 and 256 spheres constitute the system) by numerical integration of the equations of motion. A detailed computation of the velocity autocorrelation function revealed that equilibrium was attained in of the order of three collisions. This compares favorably with our computed relaxation time. Turning to the case of real gaseous systems, Greene, Cowan, and Hornig[8] have deduced from shock-tube measurements that translational degrees of freedom come to equilibrium in less than ten collisions, again in agreement with the calculations of this paper.

We believe it fair to conclude that the conjecture that correlated successive binary (triple) collisions, etc., need not be taken into account for hard spheres in a finite fluid has been verified by the considerable concordance between our analysis and experiment.

APPENDIX

As an example of the calculation of the bracket integrals, $\{m, k\}$, we shall evaluate $\{3, 3\}$. Now, by definition

$$\{3,3\}=\int\bar{f}_0^{(1)}(1)\bar{f}_0^{(1)}(2)[\omega_3(p_1^{*2})+\omega_3(p_2^{*2})-\omega_3(p_1^{2})-\omega_3(p_2^{2})]\omega_3(p_1^{2})\,(p_{12}/\mu)\,bdbd\epsilon d^3p_1d^3p_2. \quad (A1)$$

The evaluation of the integral is facilitated by a change of variables and by symmetrization. For the set of functions ω_m we choose the Sonine polynomials defined in Eq. (11). By explicit expansion

$$S_{\frac{1}{2}}^{(3)}(W^2)=\tfrac{105}{16}-\tfrac{63}{8}W^2+\tfrac{9}{4}W^4-\tfrac{1}{6}W^6, \quad (A2)$$

whereby, with the expression of the distribution functions in terms of the reduced variables W_i, Eq, (A1) becomes

$$\{3,3\}=-(4\pi^3v^2)^{-1}\int\exp(-W_1^2)\exp(-W_2^2)\,[\tfrac{9}{4}(W_1^{*4}+W_2^{*4}-W_1^4-W_2^4)-\tfrac{1}{6}(W_1^{*6}+W_2^{*6}-W_1^6-W_2^6)]^2(p_{12}/\mu)\,bdbd\epsilon d^3W_1d^3W_2 \quad (A3)$$

where the factor $\frac{1}{4}$ and the square are obtained by adding the four equal terms obtainable by interchange of $\mathbf{p}_1$, $\mathbf{p}_1^*$, $\mathbf{p}_2$, $\mathbf{p}_2^*$ and then factoring the resultant expression. The peculiar velocities may be written in terms of the velocity of the center of mass and the relative velocity, viz.

$$\begin{aligned}\mathbf{W}_1&=2^{-\frac{1}{2}}[\mathbf{G}-\boldsymbol{\gamma}]\\ \mathbf{W}_1^*&=2^{-\frac{1}{2}}[\mathbf{G}-\boldsymbol{\gamma}+2(\mathbf{k}\cdot\boldsymbol{\gamma})\mathbf{k}]\\ \mathbf{W}_2&=2^{-\frac{1}{2}}[\mathbf{G}+\boldsymbol{\gamma}]\\ \mathbf{W}_2^*&=2^{-\frac{1}{2}}[\mathbf{G}+\boldsymbol{\gamma}-2(\mathbf{k}\cdot\boldsymbol{\gamma})\mathbf{k}]\\ p_{12}/\mu&=(4kT/m)^{\frac{1}{2}}\gamma. \end{aligned} \quad (A4)$$

The vector $\mathbf{k}$ is of unit length and lies along the line of centers of the two rigid spheres when in contact. It is convenient to express $\mathbf{k}$ in spherical polar coordinates with the z axis chosen to lie along $\mathbf{p}_{12}/\mu$. Thus

$$\mathbf{k}=-\sin\phi\cos\epsilon\mathbf{i}+\sin\phi\sin\epsilon\mathbf{j}+\cos\phi\mathbf{h}. \quad (A5)$$

The substitution of (A4) and (A5) into (A3) followed by some algebraic rearrangement yields

$$\{3,3\}=-(\pi^2v^2)^{-1}\int(4\pi kT/m)^{\frac{1}{2}}\gamma\exp(-\gamma^2)\exp(-G^2)\times[81-18G^2-18\gamma^2+G^4+\gamma^4]\times[(\mathbf{k}\cdot\boldsymbol{\gamma})^2(\mathbf{k}\cdot\mathbf{G})^2-(\mathbf{k}\cdot\boldsymbol{\gamma})(\mathbf{k}\cdot\mathbf{G})(\boldsymbol{\gamma}\cdot\mathbf{G})]^2bdbd\epsilon d^3\gamma. \quad (A6)$$

In the same spherical polar system used to express the vector $\mathbf{k}$ in Eq. (A5), $\mathbf{G}$ makes an angle θ with the z axis and a longitudinal angle η. Thus, since $\boldsymbol{\gamma}$ and $\mathbf{p}_{12}/\mu$ are colinear

$$\begin{aligned}\boldsymbol{\gamma}\cdot\mathbf{G}&=\gamma G\cos\theta\\ \boldsymbol{\gamma}\cdot\mathbf{k}&=\gamma\cos\theta\\ \mathbf{k}\cdot\mathbf{G}&=G(\cos\epsilon\cos\phi+\sin\theta\sin\phi\cos\epsilon)\\ d^3G&=G^2\sin\theta dGd\theta d\eta. \end{aligned} \quad (A7)$$

The limits of integration with respect to the angles are: $0\le\epsilon\le2\pi$, $0\le\eta\le2\pi$, $0\le\theta\le\pi$, and there is no integration with respect to the angle ϕ. Direct substitution of (A7) into (A6) and integration with respect to η, ϵ, θ, and G gives

$$\{3,3\}=-(1/v^2)(4\pi kT/m)^{\frac{1}{2}}\int[\tfrac{135}{4}-18\gamma^2+\gamma^4]\times[7\cos^2\phi-5\cos^4\phi+6\cos^8\phi]\gamma^7e^{-\gamma^2}bdbd^3\gamma. \quad (A8)$$

If we make a substitution for ϕ in terms of the collision angle χ,

$$\phi=\tfrac{1}{2}(\pi-\chi)$$

and note that $\boldsymbol{\gamma}$ is restricted to be positive, then the decomposition of $\cos^n\phi$ into terms of the form $(1-\cos^l\chi)$ and integration of $d^3\gamma$ over angles permits (A8) to be written in the form

$$\begin{aligned}\{3,3\}=&-(135/4v^2)[\tfrac{5}{2}\Omega^{(1,2)}-\Omega^{(2,2)}+\tfrac{3}{2}\Omega^{(3,2)}-\tfrac{3}{8}\Omega^{(4,2)}]\\ &+(18/v^2)[\tfrac{5}{2}\Omega^{(1,3)}-\Omega^{(2,3)}+\tfrac{3}{2}\Omega^{(3,3)}-\tfrac{3}{8}\Omega^{(4,3)}]\\ &-(1/v^2)[\tfrac{5}{2}\Omega^{(1,4)}-\Omega^{(2,4)}+\tfrac{3}{2}\Omega^{(3,4)}-\tfrac{3}{8}\Omega^{(4,4)}]. \end{aligned} \quad (A9)$$

Fos the case of hard spheres, it may be shown that

$$\Omega^{(l,s)}=(4\pi kT/m)^{\frac{1}{2}}\int\gamma^{2s+3}(1-\cos^l\chi)\exp(-\gamma^2)bdbd\gamma=(kT/\pi m)^{\frac{1}{2}}\tfrac{1}{2}(s+1)!\left[1-\tfrac{1}{2}\frac{1+(-)^l}{1+l}\right]\pi\sigma^2, \quad (A10)$$

and thereby

$$\{3,3\}=-(2709/10v^2)(\pi kT/m)^{\frac{1}{2}}\sigma^2. \quad (A11)$$

THE JOURNAL OF CHEMICAL PHYSICS VOLUME 33, NUMBER 4 OCTOBER, 1960

New Solution of the Ising Problem for a Rectangular Lattice

C. A. HURST AND H. S. GREEN

University of Adelaide, South Australia

(Received April 5, 1960)

A new solution of the Ising problem for a rectangular lattice is derived from first principles. The solution, which is obtained algebraically, can be presented in a determinantal form different from though related to that found by Kac and Ward. By connecting the algebraic approach with the combinatorial solution, the latter is freed from dependence on topological conjectures. The new solution is considered to be fundamentally simpler than the others.

INTRODUCTION

TODAY there are two main approaches to the solution of the Ising problem, whose principal applications are to the thermodynamics of order-disorder phenomena, especially in ferromagnetic materials and binary alloys. The first solution of the problem for a rectangular lattice was obtained by Onsager and Kaufmann[1] by a spinor algebraic method which most people find long and difficult. A combinatorial solution of the problem, found by Kac and Ward,[2] appears much simpler and more direct; but it is not easy to demonstrate rigorously the relation between the partition function and the determinant, on which the combinatorial method depends. Kac and Ward based this relationship on a topological conjecture which is now known to be oversimplified. It is reported[3] that Feynman has advanced a new and more satisfactory conjecture.

In the present paper, we outline a new solution of the problem, which serves as a bridge between the algebraic and combinatorial solutions and is, we believe, simpler fundamentally than either. The solution can be presented combinatorially, in terms of a Pfaffian, whose square is an antisymmetric determinant with real elements, most of which are contained in the diagonal blocks. It can be seen that the Pfaffian and the associated determinant count closed polygons on the lattice, but in a different way from the Kac-Ward determinant. In spite of this difference, a relationship can be established between the two determinants which enables us to give an algebraic derivation of the Kac-Ward solution, as well as our own, which does not depend on any topological conjecture for its validity.

THE PFAFFIAN SOLUTION

We consider a rectangular lattice whose points are numbered from 1 to $N=mn$ in such a way that if

$$k=(k_2-1)m+k_1(1\leqslant k_1\leqslant m,\quad 1\leqslant k_2\leqslant n),$$

the kth point is in the k_1th column and the k_2th row. Assuming nearest-neighbor interactions, which depend only on the value of a "spin" parameter σ_k at each lattice site, the energy of the rectangular Ising lattice is

$$E(\mathfrak{d})=\sum_{k=1}^{N}(J\sigma_k\sigma_{k+1}+J'\sigma_k\sigma_{k+m}), \tag{1}$$

where $\pm J$ and $\pm J'$ are the energies of neighboring pairs situated east-west and north-south, respectively, relative to one another. The above expression neglects edge effects, which are known to be important,[4] or assumes the lattice to be wound on a torus in such a way that points numbered $(k_2-1)m$ and $(k_2-1)m+1$ are neighbors, and points numbered k and $N+k$ are identical.

If the σ_k's are represented by independent matrices with the eigenvalues -1 and $+1$, (requiring a representation in 2^N dimensions), the partition function is

$$\begin{aligned}Z&=Tr\{\exp[-\beta E(\mathfrak{d})]\}\\&=[2\cosh(\beta J)\cosh(\beta J')]^N Z_1,\end{aligned} \tag{2}$$

where $Tr\{\cdots\}$ denotes the trace of the matrix to which it is applied, and

$$Z_1=2^{-N}Tr[\prod_k(1-x\sigma_k\sigma_{k+1})(1-y\sigma_k\sigma_{k+m})],$$

$$x=\tanh(\beta J),\quad y=\tanh(\beta J'). \tag{3}$$

It is well known that Z_1 counts the number of ways of attaching closed polygons with nonoverlapping sides to a lattice, a polygon with $2a$ "westerly" sides and $2b$ "southerly" sides receiving the weight $x^{2a}y^{2b}$. This results from the fact that, on taking the trace, terms containing the powers σ_k and σ_k^3 of σ_k disappear, leaving only terms independent of σ_k (representing configurations in which no polygon passes through the kth point), quadratic in σ_k (representing configurations in which a polygon passes once through kth point) or quartic in σ_k (representing configurations in which a polygon passes twice through the kth point).

Instead of (3), we shall find it convenient to proceed from an equivalent expression, containing a set of "emission" matrices $(a_k^*,\ b_k^*)$ and corresponding "absorption" matrices $(a_k,\ b_k)$. Geometrically, the matrix a_k^* may be associated with the emission of the side of a polygon drawn from the kth point to the $k-1$th point, and b_k^* may be associated with the emission of the side of a polygon drawn from the kth

[1] L. Onsager, Phys. Rev. **65**, 117 (1944); B. Kaufman, *ibid.* **76**, 1232 (1944); B. Kaufman and L. Onsager, *ibid.* **76**, 1244 (1949).

[2] M. Kac and J. C. Ward, Phys. Rev. **88**, 1332 (1952).

[3] S. Sherman, Preprint, Princeton Institute for Advanced Study, Princeton, N. J.

[4] R. B. Potts and J. C. Ward, Progr. Theoret. Phys. (Kyoto) **13**, 38 (1955).

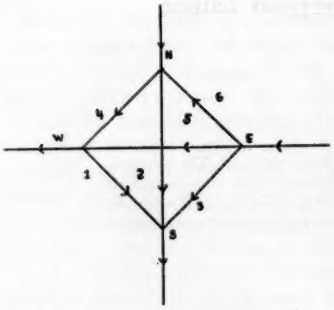

FIG. 1. Terminals at a lattice point.

point to the $k-m$th point. Similarly, a_{k+1} may be associated with the absorption at the kth point of a side drawn from the $k+1$th point, and b_{k+m} with the absorption at the kth point of a side drawn from the $k+m$th point. These matrices are required to satisfy the anticommutation relations

$$\{a_k, a_l^*\}=\{b_k, b_l^*\}=\delta_{kl}$$
$$\{a_k, a_l\}=\{b_k, b_l\}=0$$
$$\{a_k, b_l\}=\{a_k, b_l^*\}=0, \tag{4}$$

where $\{a, b\}\equiv ab+ba$. The reader familiar with the quantum theory of fields[5] will notice that these are similar to the relations satisfied by fermion emission and absorption matrices, as one would expect from the fact that not more than one side of a polygon may be drawn between any pair of neighboring lattice points. The a's and b's require a representation in 2^{2N} dimensions.

The new expression for Z_1 is

$$Z_1=2^{-2N}Tr\{\prod_k[(1+4xyb_k^*a_k^*)(1+b_{k+m}a_{k+1}) -2(xa_k^*+yb_k^*)(a_{k+1}+b_{k+m})]\}. \tag{5}$$

A related expression has been derived by Green and Leipnik[6] in the discussion of a more general type of association problem. The practical equivalence of (5) and (3) can be seen either from the geometrical interpretation of the emission and absorption operators, or algebraically as follows. Every term under the trace in (5) which contains a matrix a_k or b_k without its mate a_k^* or b_k^* will vanish, so only terms which contain correctly paired matrices need be considered. The order of the matrices in (5) has been chosen so that in any term the absorption operators a_{k+1} and b_{k+m} can be moved to the right under the trace, to a position next to their mates a_{k+1}^* and b_{k+m}^*, without changing the sign of the term. Since, e.g.,

$$Tr(Q_1 2a_k a_k^* Q_2)=Tr[Q_1\{a_k, a_k^*\}Q_2]=Tr(Q_1Q_2),$$

a term containing $2a_ka_k^*$ or $2b_kb_k^*$ in (5) is equivalent to a corresponding term containing σ_k^2 in (3). The correspondence between nonvanishing terms is, in fact, complete.

[5] W. Pauli, Revs. Modern Phys. **13**, 203 (1941).
[6] H. S. Green and R. B. Leipnik, Revs. Modern Phys. **32**, 129 (1960).

The next step is to replace the expression following $\prod_k$ in (5) by a product of four factors linear in emission and absorption matrices. To do this, it is necessary to introduce further emission and absorption matrices $c_k^{(i)}$ and $c_k^{(i)*}$ $(i=1, 2, 3, 4, 5, 6)$, with a geometrical interpretation that will soon be explained. The new matrices satisfy

$$\{c_k^{(i)}, c_l^{(j)*}\}=\delta_{kl}\delta_{ij}$$
$$\{c_k^{(i)}, c_l^{(j)}\}=0, \tag{6}$$

and, in addition, anticommute with all the a's and b's already defined. Together with a's and b's they require a 2^{8N}-dimensional representation.

In its new form, (5) is written

$$Z_1=2^{-6N}Tr\{\prod_k[yb_k^*+c_k^{(1)}+c_k^{(2)}+c_k^{(3)}] \cdot[xa_k^*+c_k^{(1)*}+c_k^{(4)}+c_k^{(5)}][b_{k+m}+c_k^{(2)*}-c_k^{(4)*}+c_k^{(6)}] \cdot[a_{k+1}-c_k^{(3)*}+c_k^{(5)*}+c_k^{(6)*}]\}. \tag{7}$$

This is easily reduced to (5) by discarding terms in which a factor $c_k^{(i)}$ appears without its mate $c_k^{(i)*}$, moving $c_k^{(i)}$ with the help of the commutation rules next to its mate $c_k^{(i)*}$, and using

$$Tr[Q_1c_k^{(i)}c_k^{(i)*}Q_2]=\tfrac{1}{2}Tr[Q_1Q_2].$$

(It should be remembered that, because of the change in the dimensions of the matrix representation, a factor 2^{-8N}, rather than 2^{-2N}, should multiply the transformed trace).

We now supply the interpretation of the $c_k^{(i)}$ and $c_k^{(i)*}$. Each lattice point is pictured (see Fig. 1) as a group of four terminals, called the S-, W-, N-, and E-terminals. "Southbound" and "westbound" sides of polygons are emitted from the S- and W- terminals, respectively, and absorbed by the N- and E-terminals of the neighboring lattice point.

Different terminals of the same lattice point can also be connected by lines "emitted" from one terminal and "absorbed" by another terminal. The emission matrices $c^{(1)*}$, $c^{(2)*}$, and $c^{(3)*}$, correspond to lines drawn to S from W, N, and E, respectively; $c^{(4)*}$ and $c^{(5)*}$ correspond to lines drawn to W from N and E, respectively, and $c^{(6)*}$ corresponds to the line drawn from E to N. For every nonvanishing term of (7), there will be just one side or line emitted or absorbed by each terminal. At a lattice point through which no polygon passes, the terminals can be connected in pairs in three different ways. At a lattice point through which a polygon passes only once, the pair of terminals playing no part in the emission or absorption of sides are joined together.

An expression of type (7), i.e., the trace of a product of factors linear in a set of emission and absorption matrices, can be evaluated as what is called a Pfaffian. (This technique has been applied to quantized field theory by Caianiello.[7]) A Pfaffian is a triangular array of numbers such as one has above the main diagonal in an antisymmetric determinant. It is evaluated by expansion with respect to minors in the same way as a deter-

[7] E. R. Caianiello, Nuovo cimento **10**, 1634 (1953).

minant, except that the minor of any element P_{rc} (where $c>r$) of a Pfaffian is obtained by striking out the rth row and column and the cth row and column, instead of merely the rth row and cth column. Thus, in the expansion, a particular suffix appears only once in each term. A Pfaffian has the important property that its square is the corresponding antisymmetric determinant,[8] i.e., $\setminus P|^2=|D|$, where $D_{rc}=-D_{rc}=P_{rc}$ for $c>r$ and $D_{rr}=0$.

The Pfaffian obtained from (7) has its rows and columns numbered according to the order of the $4N$ factors under the trace. If the rth factor contains a particular absorption operator, and the cth factor contains the corresponding emission operator multiplied by the coefficient P_{rc}, the number P_{rc} will be entered in the rth row and cth column of the Pfaffian; otherwise, the entry 0 (zero) will be made. Setting $r=(k, A)$ and $c=(l, B)$, where A and B take the four values S, W, N, and E, the nonvanishing elements $P_{kA,lB}$ of $\setminus P|$ are:

$$P_{kS,kB}=1,\ 1,\ -1 \text{ for } B=W, N, E \text{ respectively},$$
$$P_{kW,kB}=-1,\ 1 \text{ for } B=N, E \text{ respectively},$$
$$P_{kN,kE}=1,$$
$$P_{kE,k+1W}=xP_{kN,k+mS}=y. \tag{8}$$

It is asserted that $Z_1=\setminus P|$. The evaluation of the Pfaffian does, as one can verify directly, yield the same terms as the evaluation of the trace in (7).

The final step makes use of the theorem mentioned above, that the square of a Pfaffian is the corresponding antisymmetric determinant, so that

$$Z_1^2=|D| \tag{9}$$

where, explicitly,

$$|D|=$$

	1			2				$m+1$	
	0 1 1	−1		0 0 0	0		0 0 0	0	
	−1 0	−1 1		0 0 0	0	Zeros	0 0 0	0	
	−1 1	0 1		0 0 0	0		y 0 0	0	
	1 −1	−1 1		0 x 0	0		0 0 0	0	
	0 0	0 0		0 1	1 −1				
	0 0	0 −x		−1 0	−1 1				
	0 0	0 0		−1 1	0 1	Zeros	Zeros		
	0 0	0 0		1 −1	−1 0	0x			

. (10)

[8] R. F. Scott and G. B. Mathews, *Theory of Determinants* (Cambridge University Press, New York, 1904), p. 93.

This determinant is not only antisymmetric, but (almost) cyclic with respect to the 4×4 blocks which it contains. Exceptionally, the elements $D_{1W,NE}$, $D_{kS,N-m+kN}$ $(1\leqslant k\leqslant m)$ spoil the cyclic property by having the wrong sign; but these can be altered without changing the asymptotic value of the partition function, as they represent only edge effects. (When m and $n=N/m$ are odd, the alteration changes the sign of x and y in the exact partition function; cf., Potts and Ward.[4])

EVALUATION OF THE DETERMINANT

To evaluate the cyclic determinant $|D|$, let

$$D_{kA,kB}=U_{AB},$$
$$D_{kA,k+1B}=X_{AB},$$

and

$$D_{kA,k+mB}=Y_{AB}. \tag{11}$$

Since the determinant $|D|$ is the product of the eigenvalues λ of the corresponding matrix D, it can be evaluated in principle by solving the eigenvalue equation $Du=\lambda u$, where u is a $4N$-component vector, i.e.,

$$Uu_k+Xu_{k+1}+Yu_{k+m}-X^*u_{k-1}-Y^*u_{k-m}=\lambda u_k, \tag{12}$$

where the u_k's are four-component vectors. This system of equations can be satisfied by

$$u_k=\exp(2\pi ipk/N)u^{(p)}, \tag{13}$$

where p is any integer from 1 to N. For a particular value of p, this substitution reduces (12) to

$$(U+X\alpha_p+Y\beta_p-X^*\alpha_p{}^*-Y^*\beta_p{}^*)u^{(p)}=\lambda u^{(p)},$$
$$\alpha_p=\exp(2\pi ip/N),\quad \beta_p=\exp(2\pi imp/N), \tag{14}$$

which determines the four values of λ corresponding to the chosen value of p. The product of these four eigenvalues is the determinant $|U+X\alpha_p+Y\beta_p-X^*\alpha_p{}^*-Y^*\beta_p{}^*|$, so the value of $|D|$ is

$$Z_1^2=\prod_p |U+X\alpha_p+Y\beta_p-X^*\alpha_p{}^*-Y^*\beta_p{}^*|$$
$$=\prod_p[(1+x^2)(1+y^2)+2y(1-x^2)\cos(2\pi p/N)$$
$$+2x(1-y^2)\cos(2\pi mp/N)]. \tag{15}$$

Using $N=mn$, one finds for large values of m and n, if

$$p=p_1n+p_2(1\leqslant p_2\leqslant n)$$

and

$$\theta_2=2\pi p_2/n,$$
$$\theta_1=2\pi p_1/m+n\theta_2,$$

$$2(2\pi)^2\log Z_1=N\int_0^{2\pi}\int_0^{2\pi}\log[(1+x^2)(1+y^2)$$
$$+2y(1-x^2)\cos\theta_2+2x(1-y^2)\cos\theta_1]d\theta_1d\theta_2. \tag{16}$$

This is in agreement with the result obtained by other methods. On evaluation it is an even function of x and

y, so that the alteration of (10) to completely cyclic form has had no effect.

The determinantal solution can be given a combinatorial interpretation, similar to that which suggested the Kac-Ward solution. Regarding every lattice point as a set of four terminals, as described in the previous section, the determinant counts oriented polygons connecting opposite terminals of neighboring lattice points and pairs of terminals of the same lattice point. No side or line may be described in the same direction more than once. The Pfaffian counts unoriented polygons on the lattice in a similar way, for it is easy to see that every different way of connecting pairs of terminals corresponds to a particular polygonal configuration, and the correspondence is one to one, excepting the three different ways of connecting the terminals of each point through which no polygon passes.

We finally indicate the connection between our determinantal solution and that obtained by Kac and Ward. Let U^{-1} be the reciprocal of the matrix U; explicitly,

$$U^{-1}=\begin{vmatrix} 0 & -1 & 1 & 1 \\ 1 & 0 & 1 & 1 \\ -1 & -1 & 0 & -1 \\ -1 & -1 & 1 & 0 \end{vmatrix}. \tag{17}$$

The determinant $|U|$, like the determinant $|U^{-1}|$, has the value $+1$; therefore the determinant of the $4N$-dimensional matrix E, defined by

$$E_{kA,\,lB}=\delta_{kl}U_{AB}^{-1} \tag{18}$$

has a determinant with the value $+1$.
Hence

$$Z_1^2=|D|=|DE|, \tag{19}$$

where DE represents the matrix product of D and E. The matrix DE has 4×4-unit matrices in the diagonal blocks, and row matrices off the diagonal, like the matrix of the Kac-Ward determinant in its simplest form (obtainable by shuffling rows and columns). The Kac-Ward determinant contains a fourth root of -1 (denoted by α) or its reciprocal as a factor of many of its off-diagonal elements, but these complex factors can be removed by multiplying corresponding rows and columns by α and α^{-1}. When this is done, the matrix of the Kac-Ward determinant is precisely what we have called DE.

The above is to our knowledge the only direct and mathematically complete derivation of the Kac-Ward determinant, and seems to be the easiest way of putting the combinatorial solution on a sound mathematical basis.

Temperature Dependence of the Rates of Addition of Oxygen Atoms to Olefins*

R. J. CVETANOVIĆ

Division of Applied Chemistry, National Research Council, Ottawa, Canada

(Received May 2, 1960)

Relative rates of addition of oxygen atoms to several representative olefins have been measured at 25° and 125°C, and the ratios of the pre-exponential factors and differences in activation energies have been calculated from the mean values of the relative rate constants at the two temperatures. The results obtained show that the differences in reactivities are primarily due to differences in the activation energies while the pre-exponential factors remain approximately constant.

INTRODUCTION

THE major features of the mechanism of addition of oxygen atoms to olefins have been recently established[1,2] and the relative rates for a number of these reactions in the vapor phase have been measured at room temperature.[3] Some regularities and correlations of the logarithms of rate constants with physical properties of the olefins[3] and with certain theoretically derived quantities[4] were found. Linear "free energy" plots ($\log k - \log k$ plots) with several electrophilic reagents reacting with olefins in solution were also obtained.[3] Such correlations have demonstrated the electrophilic character of oxygen atoms in their reactions with olefins. They also may contribute to the understanding of the factors which affect the rates of chemical reactions of this type. For meaningful interpretations, however, it is also necessary to know whether the trend in the reactivity is predominantly due to variations of activation energies alone, or of entropies of activation alone, or of these two quantities together (as, for example, when a compensating effect is observed). The present work has been carried out in an attempt to obtain experimental information which would help to clarify this point. In addition, knowledge of the temperature dependence of the rates of oxygen atom reactions represents part of the basic information which is being accumulated in this laboratory on the reactions of oxygen atoms with organic compounds.

For very fast reactions such as addition of oxygen atoms to olefins determination of temperature coefficients of rate constants requires considerable experimental accuracy and a fairly large temperature interval. In the course of the previous work[2,3] it was discovered that ethylene was a product from the reaction of oxygen atoms with cyclopentene and it was formed at best only in very small amounts from the other olefins studied. Determination of the relative rate constants can, therefore, be based on a competition for oxygen atoms between cyclopentene and another olefin added in various amounts and the consequent variation in the amount of ethylene formed. As a result of considerable accuracy and convenience with which ethylene can be determined analytically, this technique has proved very valuable and has been employed in the present work for all the reactions reported except for the case of ethylene, for which a different method had to be used.

Oxygen atoms have been generated, as in most of the previous work, by mercury photosensitized decomposition of nitrous oxide. Nitrogen produced served as a measure of the number of oxygen atoms generated in the course of the reaction.

EXPERIMENTAL

The improvement in the accuracy of determination of relative rate constants of oxygen atom reactions necessary in order to obtain meaningful temperature coefficients was achieved by the use of the cyclopentene technique, except in the case of ethylene, and by additional precautions in the handling of the reactants and the products. The reactant olefins were measured manometrically on a constant volume burette and were frozen over into the circulating reaction system (415 ml) without coming in contact anywhere with stopcock grease. For this reason mercury cutoffs were used instead of stopcocks in the relevant part of the apparatus. Nitrous oxide was measured manometrically on a volume of 1000 ml and then was transferred into the reaction vessel. An all-glass vertical plunger type circulating pump was used to mix the reactants before the runs and for their circulation during the runs. A cylindrical quartz reaction cell 5 cm in diameter and 10 cm long was irradiated by two low-pressure mercury lamps, one at each end of the cell.

The analysis was restricted to the noncondensable gases and the C_2 hydrocarbon fraction. Of particular interest were the amounts of ethylene and nitrogen formed, and in the case of the ethylene reaction, the amounts of nitrogen and carbon monoxide. A Le Roy still[5] followed by a "pumpout" trap was used to separate the noncondensable and the C_2 fractions and

* Contribution No. 5933 from the National Research Council, Ottawa, Canada.

[1] R. J. Cvetanović, J. Chem. Phys. **25**, 376 (1956).
[2] R. J. Cvetanović, Can. J. Chem. **36**, 623 (1958).
[3] R. J. Cvetanović, J. Chem. Phys. **30**, 19 (1959).
[4] S. Sato and R. J. Cvetanović, J. Am. Chem. Soc. **81**, 3223 (1959).
[5] D. J. LeRoy, Can. J. Chem. **B28**, 492 (1950).

TABLE I. Formation of ethylene in the reaction of oxygen atoms with cyclopentene.

Run	Temp. °C	Cyclopentene mm	N_2O mm	Irradiation min	ΔN_2 mm	$\frac{CO}{N_2}$	$\frac{C_2H_4}{N_2}$
146	27.1	7.14	492.0	60	2.162	0.024	0.270
148	25.7	6.61	492.8	60	2.073	0.023	0.270
149	26.2	6.11	496.0	60	2.062	0.022	0.269
Mean	26.3						0.270
17	122.8	8.84	500.3	60	2.034	0.028	0.273
20	121.6	9.69	506.4	60	2.025	0.029	0.272
26	122.6	9.99	502.0	60	2.017	0.028	0.277
136	122.5	7.67	495.0	60	2.062	0.032	0.277
139	119.2	6.73	493.5	60	2.052	0.032	0.274
Mean	121.7						0.274

their amounts were measured manometrically on a constant volume burette. From the noncondensables CO and any H_2 were removed by combustion in a copper oxide tube and the small amount of CH_4 in N_2 was determined mass spectrometrically. Carbon monoxide was estimated from the amount of carbon dioxide formed in the copper oxide tube and recovered at −78°. The C_2 fraction contained besides C_2H_4 always small amounts of N_2O, sometimes C_2H_6 and occasionally traces of CH_4. The ratios of these compounds were determined by mass spectrometer.

The reactants were of the best available grade and were degassed and bulb to bulb distilled *in vacuo* before use. In some instances, for example with cyclopentene, there was a tendency for some formation of peroxides even on relatively short exposure of the liquid to air. These were removed by passage through an activated alumina column followed by rapid introduction into the vacuum apparatus and degassing. In all experiments large excess of nitrous oxide and high total pressures were employed. This ensured no interference from chemical quenching reactions by the reactant olefins.

RESULTS AND DISCUSSION

For observation of temperature dependencies of relative rate constants of fast reactions most favorable are pairs of compounds which show relatively large differences in reactivities. Cyclopentene, which has been used in all but one case in this work as the experimental reference compound, fortunately lies approximately in the middle of the range of reactivities of olefins with oxygen atoms. The compounds selected for the present study from this point of view have been tetramethyl ethylene, trimethyl ethylene, butene-1, and ethylene, the first of which is the fastest and the last the slowest of the olefins studied so far. In addition determinations of temperature dependencies have been made also for isobutene, cyclohexene, and in a separate study[6] for 1,3-butadiene. The reactivities of these last three compounds, however, are very close to that of cyclopentene and the temperature coefficients found are, as expected, very small and therefore quantitatively less reliable.

Relative rates have been measured at two temperatures, at approximately 25 and 125°C. From the mean values at the two temperatures the ratios of the pre-exponential factors (A_1/A_2) and the differences in the activation energies (E_1-E_2) were calculated from the Arrhenius equation.[7]

The equations for evaluation of relative rate constants and the appropriate experimental conditions have been discussed in some detail previously.[3] For the cyclopentene technique and the experimental conditions employed in the present work, the following expression can be used[8]

$$k_1/k_2 = \log\{1-[\Delta N_2/(a_1)_i] + [\Delta P_2/\alpha_2(a_1)_i]\}/\log\{1-[\Delta P_2/\alpha_2(a_2)_i]\} \quad (1)$$

where subscript 2 refers to cyclopentene, $(a_1)_i$ and $(a_2)_i$ are the initial amounts of the competing olefin and cyclopentene, respectively, introduced into the reaction vessel, ΔN_2 is the amount (in the same units) of N_2 produced, ΔP_2 is the amount of C_2H_4 produced, and α_2 is the ratio C_2H_4/N_2 in the reaction of oxygen atoms with cyclopentene alone. The values of α_2 at the two temperatures of interest have been obtained from the experiments summarized in Table I. Determinations of the rate constants relative to that of cyclopentene are summarized in Table II for butene-1, isobutene, cyclohexene, trimethyl ethylene, and tetramethyl ethylene, and the mean deviations have been indicated.

In the case of butene-1, isobutene, and trimethyl ethylene very small amounts of ethylene were formed at the higher temperature, and with trimethyl ethylene at room temperature as well. The total values of ethylene in the competing reactions, (ΔC_2H_4) total,

[6] R. J. Cvetanović and L. C. Doyle, Can. J. Chem. (to be published).

[7] In dealing with relative rate constants the Arrhenius equation stands also for the collision theory and the absolute reaction theory rate expressions, since *the ratios* of the pre-exponential factors are temperature-independent in these cases as well.

[8] Equation (5) of footnote 3.

TABLE II. Determination of relative rate constants at two temperatures.

(The amounts of the reactants and of the nitrogen produced are given in mm in 415 ml at 25°C. The amounts of the other products are given relative to the nitrogen produced.)[a]

Run	Temp. °C	$\frac{(a_1)i}{(a_2)i}$	$(a_1)i$ mm	$(a_2)i$ mm	N_2O mm	Irradiation min	ΔN_2 mm	$\frac{CO}{N_2}$	$\frac{CH_4}{N_2}$	$\frac{C_2H_6}{N_2}$	$\frac{C_2H_4}{N_2}$	$\frac{k_1}{k_2}$
					I. a_1=butene-1, a_2=cyclopentene (P_2=ethylene)							
40	24.7	4.48	43.26	9.66	505.2	120	3.588	0.021	...	0.003	0.143	0.182
37	24.8	4.12	45.34	11.01	505.9	60	1.846	0.019	...	0.002	0.144	0.203
38	25.8	3.82	34.82	9.11	505.4	120	3.901	0.021	...	0.003	0.148	0.194
34	27.0	3.15	30.11	9.55	502.5	60	1.926	0.019	...	0.001	0.166	0.190
39	25.4	2.73	26.86	9.84	504.0	120	3.886	0.021	...	0.003	0.170	0.194
36	25.2	2.18	23.59	10.80	503.2	60	2.012	0.019	...	0.001	0.189	0.185
Mean	25.5											0.191±0.006
133	(124.1)	∞	27.64	...	492.0	60	1.944	0.062	...	0.012	0.007	...
126	125.1	4.19	42.66	10.18	501.1	60	1.810	0.057	...	0.009	0.132	0.265
130	126.9	3.70	29.38	7.93	493.7	60	1.913	0.053	...	0.005	0.137	0.271
131	125.6	3.32	23.63	7.11	496.7	60	1.962	0.050	...	0.004	0.146	0.264
128	123.9	3.02	39.36	13.04	492.8	60	1.868	0.052	...	0.010	0.157	0.250
132	125.2	2.97	23.37	7.88	492.5	60	1.961	0.048	...	0.005	0.153	0.264
129	125.0	2.65	24.58	9.29	493.5	60	1.942	0.049	...	0.006	0.154	0.296
Mean	125.3											0.268±0.010
					II. a_1=isobutene, a_2=cyclopentene (P_2=ethylene)							
52	26.2	3.15	26.71	8.49	506.2	60	2.034	0.017	0.001	0.003	0.0748	0.826
50	25.8	3.13	21.09	6.74	499.6	60	2.159	0.018	0.001	0.002	0.0667	0.862
53	26.2	2.67	24.04	8.99	504.7	60	2.074	0.017	0.001	0.003	0.0825	0.849
49	25.5	1.86	14.14	7.61	502.5	60	2.179	0.017	0.001	0.002	0.103	0.864
51	25.0	1.09	10.84	9.93	502.3	60	2.189	0.012	0.001	0.001	0.141	0.825
48	25.3	0.88	9.08	10.34	498.6	60	2.212	0.020	0.001	0.001	0.151	0.803
Mean	25.7											0.838±0.020
59	(128.6)	∞	30.46	...	499.6	60	1.914	0.007	0.010	0.002	0.00057	...
56	129.6	3.53	29.70	8.41	505.4	60	1.848	0.023	0.008	0.001	0.0729	0.785
58	129.4	3.26	24.89	7.64	503.7	60	1.833	0.022	0.007	0.001	0.0759	0.801
55	129.6	2.22	19.21	8.64	504.5	60	2.224	0.024	0.007	0.001	0.100	0.785
57	128.7	1.64	13.71	8.35	500.8	60	1.962	0.025	0.006	0.001	0.117	0.812
54	129.4	1.20	10.13	8.46	499.8	60	2.023	0.028	0.005	0.001	0.141	0.779
Mean	129.3											0.792±0.011
					III. a_1=cyclohexene, a_2=cyclopentene (P_2=ethylene)							
98	(24.2)	∞	4.27	...	496.4	60	0.791	0.025	...	...	...	...
100	26.0	1.01	5.98	5.93	491.8	60	0.750	n.d.	...	...	0.142	0.890
101	25.3	0.65	3.46	5.33	493.7	60	0.767	0.016	...	...	0.166	0.958
103	25.6	0.64	3.81	5.97	495.0	60	0.757	0.023	...	...	0.167	0.961
99	24.6	0.53	3.49	6.60	493.0	60	0.760	0.025	...	...	0.182	0.912
102	26.4	0.41	2.64	6.48	494.2	60	0.755	0.027	...	...	0.202	0.814
Mean	25.6											0.907±0.044
108	(125.0)	∞	4.27	...	494.7	60	0.548	0.029	...	...	...	...
107	123.0	0.68	4.20	6.19	500.6	60	0.546	0.041	...	...	0.163	0.838
104	126.5	0.64	4.26	6.69	497.2	60	0.572	0.042	...	...	0.153	0.836
106	127.0	0.63	4.30	6.87	497.7	60	0.525	0.029	...	...	0.162	0.905
105	124.5	0.60	3.78	6.31	499.6	60	0.575	0.038	...	...	0.170	1.028
Mean	125.3											0.902±0.064

TABLE II.—*Continued.*

Run	Temp. °C	$\frac{(a_1)i}{(a_2)i}$	$(a_1)i$ mm	$(a_2)i$ mm	N_2O mm	Irradiation min	ΔN_2 mm	$\frac{CO}{N_2}$	$\frac{CH_4}{N_2}$	$\frac{C_2H_6}{N_2}$	$\frac{C_2H_4}{N_2}$	$\frac{k_1}{k_2}$
				IV. a_1=trimethyl ethylene, a_2=cyclopentene (P_2=ethylene)								
147	(26.2)	∞	7.35	...	492.3	60	2.092	0.019	0.008	0.120	0.0056	...
144	25.9	0.82	5.69	6.93	491.0	60	2.073	0.015	0.006	0.067	0.092	2.74
142	26.2	0.60	4.60	7.73	496.7	60	2.075	0.017	0.006	0.059	0.114	2.64
145	25.3	0.54	4.37	8.14	497.2	60	2.074	0.019	0.006	0.055	0.124	2.53
143	27.3	0.51	4.07	8.05	493.5	60	2.068	0.017	0.006	0.040	0.123	2.73
Mean	26.2											2.66±0.07
134	(122.5)	∞	31.51	...	494.5	60	1.879	0.001	0.066	0.066	0.0045	...
151	119.6	0.67	6.05	9.03	492.5	60	1.841	0.024	0.052	0.027	0.113	2.34
150	118.5	0.61	4.84	7.88	496.2	60	1.884	0.024	0.040	0.032	0.124	2.16
141	121.4	0.57	4.57	7.99	482.7	60	1.949	0.027	0.039	0.030	0.133	2.04
138	120.6	0.57	4.07	7.14	496.0	60	2.047	0.024	0.033	0.024	0.128	2.26
152	119.2	0.45	3.33	7.46	492.5	60	1.878	0.026	0.035	0.024	0.148	2.14
Mean	119.9											2.19±0.09
				V. a_1=tetramethyl ethylene, a_2=cyclopentene, (P_2=ethylene)								
158	(26.9)	∞	8.91	...	492.3	60	1.900	0.012	0.017	0.151	...	...
161	25.6	0.74	6.34	8.53	490.6	60	1.839	0.014	0.013	0.103	0.0808	3.40
159	27.2	0.55	4.78	8.67	490.1	60	1.890	0.014	0.011	0.089	0.0993	3.44
160	27.2	0.39	3.19	8.11	488.6	60	1.910	0.015	0.009	0.077	0.125	3.38
Mean	26.7											3.41±0.02
153	(118.0)	∞	9.12	...	490.6	60	1.870	0.014	0.055	0.134	...	...
156	120.2	0.69	5.96	8.70	496.0	60	1.832	0.019	0.079	0.054	0.0975	2.82
157	119.6	0.53	4.28	8.14	494.2	60	1.740	0.020	0.062	0.050	0.125	2.44
154	120.0	0.31	2.71	8.85	501.1	60	1.848	0.024	0.048	0.029	0.158	2.65
155	119.6	0.22	1.71	7.85	492.5	60	1.834	0.025	0.036	0.024	0.179	2.83
Mean	119.9											2.69±0.14
				VI. a_1=cyclohexene, a_2=ethylene, (P_2=carbon monoxide)								
98	(24.2)	∞	4.27	...	496.4	60	0.791	0.025	...	...	...	...
116	24.6	0.075	4.57	60.7	494.7	30	1.008	0.149	0.033	n.d.	n.d.	27.38
117	25.0	0.050	3.81	75.7	496.4	30	0.954	0.184	0.039	n.d.	n.d.	26.94
118	25.5	0.044	4.89	112.1	494.7	30	0.836	0.197	0.045	n.d.	n.d.	26.21
115	24.0	0.036	4.13	116.2	497.4	30	0.852	0.215	0.049	n.d.	n.d.	26.58
Mean	24.8											26.78±0.38
108	(125.0)	∞	6.20	...	494.7	60	0.548	0.029	...	...	...	...
113	127.0	0.121	3.63	29.9	494.2	30	1.031	0.209	0.034	n.d.	n.d.	11.57
110	128.0	0.060	3.60	60.0	494.7	30	0.957	0.293	0.047	n.d.	n.d.	10.97
111	126.5	0.055	3.28	59.4	500.1	30	0.977	0.303	0.043	n.d.	n.d.	10.80
112	127.4	0.036	4.28	118.6	501.6	30	0.823	0.369	0.036	n.d.	n.d.	11.30
Mean	127.2											11.16±0.28

[a] n.d.=not determined.

were corrected in these cases for the ethylene produced from these compounds. The corrected values of ethylene, (ΔC_2H_4) corr., were calculated from the expression.[9]

$$(\Delta C_2H_4)\text{ corr.}=[(\Delta C_2H_4)\text{ total}-\beta\Delta N_2]/(1-\beta/\alpha_2) \quad (2)$$

where β is the C_2H_4/N_2 ratio in the absence of cyclopentene. In all cases the corrections were quite small.

[9] Rearranged Eq. (2) of footnote 3.

In studying the temperature dependence of the ethylene reaction the cyclopentene technique obviously cannot be employed. In this case the determination of the relative rate constants was based on carbon monoxide production in the reaction of oxygen atoms with ethylene, as was done in one instance before.[3] Cyclohexene was taken arbitrarily as the competing olefin. In this case the amount of ethylene taken was always relatively quite large and its concentration remained essentially constant during the reaction. Equation (1)

TABLE III. Summary of the mean values obtained for the relative rate constants, the ratios of the pre-exponential factors, and the differences in activation energies. (The subscript *CP* refers to cyclopentene, and *TME* to tetramethyl ethylene.)

Olefin	Relative rate constants[a] at 25° This work	Previous work	A/A_{CP}	$E\text{-}E_{CP}$ cal/mole	$E\text{-}E_{TME}$ kcal/mole
Ethylene	0.040	0.038[b]	1.01	2008	2.60
1-Butene	0.23	0.24[b]	0.74	803	1.40
1,3-Butadiene	...	0.97[c]	1.14	205	0.80
Cyclopentene	1.19	1.20[b]	1	0	0.60
Cyclohexene	1.08	...	0.89	−13	0.58
Isobutene	1	1	0.67	−130	0.47
Trimethyl ethylene	3.17	...	1.18	−485	0.11
Tetramethyl ethylene	4.07	4.18[b]	1.25	−596	0

[a] Isobutene taken as unity.
[b] Footnote 3.
[c] Footnote 5.

therefore reduced to

$$k_1/k_2 = -\frac{(a_2)_i}{\Delta P_2/\alpha_2} 2.303 \log_{10}\{1-[\Delta N_2/(a_1)_i] + [\Delta P_2/\alpha_2(a_1)_i]\} \quad (3)$$

where now subscript 1 refers to cyclohexene and subscript 2 to ethylene, ΔP_2 is the amount of carbon monoxide produced from ethylene (i.e., total carbon monoxide corrected for the small amount of carbon monoxide produced from cyclohexene), and α_2 is the ratio of CO to N_2 from ethylene reacting with oxygen atoms alone under comparable conditions. The corrected amount of CO is readily calculated from the following expression, analogous to Eq. (2)

$$(\Delta CO)\ \text{corr.} = [(\Delta CO)\ \text{total} - \beta \Delta N_2]/(1-\beta/\alpha_2), \quad (4)$$

where now β represents the ratio CO/N_2 from the reaction of oxygen atoms with cyclohexene alone. Since β is much smaller than α_2, the correction is relatively small. The values of α_2 have been determined separately under comparable conditions to the competing experiments but in the absence of cyclohexene. At 25° α_2 was found to be 0.385±0.007, and at 125° there was a slight trend in the values of α_2 from about 0.45 to 0.50, increasing with increasing partial pressure of ethylene. At this temperature the values of α_2 were determined graphically from a plot of α_2 as a function of ethylene pressure. The details of the competing experiments and the relative rate constants obtained are given at the end of Table II (appreciable amounts of hydrogen were formed in these reactions, but are not shown in Table II).

The mean values obtained for the relative rate constants at room temperature, the ratios of the pre-exponential factors and the differences in activation energies are summarized in Table III. The relative rate constants at 25°C are compared with the corresponding values obtained previously[3] and a good agreement is shown. It is believed that the previously given[3] margin of uncertainty of 10 to 15% in the values of the relative rate constants is now narrowed down to only a few percent.

The ratios of the pre-exponential factors in Table III are very close to unity and the different reactivities exhibited by various olefins are evidently primarily due to differences in the activation energies. The likely experimental uncertainty in the ratios of the pre-exponential factors given in Table III is probably comparable in magnitude to the variations in the values and, thus, small changes in the pre-exponential factors in this reaction series would not be inconsistent with the present results. In view of some experimental uncertainty in the relative rates, it is also difficult to say to what extent the small differences in activation energies between the olefins of similar reactivity, such as 1,3-butadiene, cyclopentene cyclohexene, and isobutene, as indicated in Table III, are real. In the last column of Table III the differences in activation energies are given relative to tetramethyl ethylene, the activation energy for which has been taken as zero. These values, therefore, represent the lower limits of the activation energies for oxygen atom reactions with the olefins. The activation energies show the expected trends with olefin structure which is not surprising in view of the approximate constancy of the pre-exponential factors and the previously observed correlations.[3,4]

The activation energy of the reaction of oxygen atoms with tetramethyl ethylene is probably very small. This is suggested by the likely absolute value of the rate constant of this reaction[3] which differs very little from the collision frequency. Also, the trend in the activation energies in Table III is such that, in order to maintain a significant difference in the activation energies between trimethyl ethylene and tetramethyl ethylene, as would be expected on structural grounds, the activation energy of the latter should not be greater than 0.1 to 0.3 kcal/mole. The values in the last column of Table III would then have to be increased by this amount to get the activation energies of the individual reactions. The activation energy of 2.6 to 2.9 kcal/mole for the ethylene reaction would

agree well with the previous tentative estimate[10] of an upper limit of 3 kcal/mole for this quantity.

[10] R. J. Cvetanović, J. Chem. Phys. **23**, 1375 (1955).

ACKNOWLEDGMENTS

The author is indebted to L. C. Doyle for valuable assistance in the performance of the experiments and to Dr. A. W. Tickner for mass spectrometric analyses.

THE JOURNAL OF CHEMICAL PHYSICS VOLUME 33, NUMBER 4 OCTOBER, 1960

Growth Poisoning of Lithium Fluoride from Aqueous Solutions

GERALD W. SEARS*

General Electric Research Laboratory, Schenectady, New York

(Received March 28, 1960)

The presence of a few ppm of step poisons strongly alters both crystal growth and dissolution rates. It was known that a few ppm ferric fluoride was a poison for the dissolution of lithium fluoride. In the present report it is shown that ferric fluoride is also a growth poison for lithium fluoride from aqueous solution. Ferric fluoride has the properties characterizing a step poison for the lithium fluoride-water system.

INTRODUCTION

CRYSTALS grow by the spreading of individual layers across the advancing face. Each incomplete layer is bounded by the peripheral step. It is only at such steps that molecule from a parent fluid phase are incorporated into the crystal lattice at very small supersaturations. It can be more generally stated that equilibrium is only attainable between a crystal and the surrounding fluid phase by the action of growth steps; equilibrium is unattainable between a perfect crystal face and its surrounding fluid phase.

When an individual layer spreads to the edge of a crystal face, the growth step bounding the incompleted layer is destroyed. For the continued advance of a face, new layers and new growth steps must be continually created. Gibbs[1] originally recognized that new layers could only form on a perfect surface by two-dimensional nucleation. Since nucleation can only proceed at an appreciable rate at substantial supersaturations, the observation[2] of crystal growth at small supersaturations could not be accounted for by a nucleation mechanism. A decade ago, Frank[3] pointed out that the intersection of a screw dislocation with a crystal surface provided a perpetual source of growth steps at very low supersaturations, thus accounting for the growth of real crystals in this region of supersaturation.

From this model Burton, Cabrera, and Frank[4] made a detailed analysis of crystal gowth from the vapor phase. They discussed the structure, configuration, and motion of the growth steps. All of their analyses of growth kinetics were based on the assumption of local equilibrium between the crystal and the parent phase at the growth step. This is equivalent to the assumption that the over-all kinetics of the growth process is never limited by the rate of transfer of molecules into the advancing growth step.

Recently, growth poisons have been characterized[5,6] that absorb at the growth step and hinder the motion of the step in either growth or dissolution. The over-all kinetics of crystal growth in the presence of such poisons is limited by the rate of transfer of molecules into the growth step from the parent phase. The adsorption of very minute amounts of a step poison on the crystal surface can control the growth kinetics of the surface. If the interstep spacing on the growth face were 100 atomic distances, less than 0.01 monolayer of poison would reduce the growth rate by several orders of magnitude.

It has long been known that specific soluble impurities[7] alter the normal crystal growth behavior. With few exceptions these previously reported poisons[8] differ in at least two characteristics from step poisons mentioned in the preceding paragraph. They act as growth poisons and not as dissolution poisons; the necessary concentration in the growth solution is about two orders of magnitude greater than required for step poisons.

It has been reported previously that the rate of dissolution of lithium fluoride[9] in water is markedly decreased by a ferric fluoride ocncentration as small as

* Present address: Research Division, Stromberg-Carlson Company, Rochester 3, New York.

[1] J. W. Gibbs, *Collected Works* (Longmans, Green and Company, London, 1928, p. 325.

[2] M. Volmer and W. Schultze, Z. physik. Chem. (Leipzig) **A156**, 1 (1931).

[3] F. C. Frank, Discussions Faraday Soc. **5**, 48,67 (1949).

[4] W. K. Burton, N. Cabrera, and F. C. Frank, Phil. Trans. Roy. Soc. London **A243**, 299 (1951).

[5] G. W. Sears, J. Chem. Phys. **29**, 979 (1958).

[6] G. W. Sears, J. Chem. Phys. **29**, 1045 (1958).

[7] H. E. Buckley, *Crystal Growth* (John Wiley & Sons, Inc., New York, 1951), pp. 330-385.

[8] W. G. France, Colloid Symposium Monograph **7**, 59 (1930).

[9] J. J. Gilman, W. G. Johnston, and G. W. Sears, J. Appl. Phys. **29**, 747 (1958).

10^{-5} molal. In the present paper it is shown that the growth of lithium fluoride from aqueous solution is inhibited by like concentrations of ferric fluoride. In addition, details of the growth in the presence of a step poison agree closely with the predicted growth behavior.

EXPERIMENTAL

Supersaturated solutions of lithium fluoride were made up from stock solutions containing 0.100 g/ml of potassium fluoride and lithium chloride, respectively. The lithium chloride was Matheson, Coleman, and Bell reagent grade. The potassium fluoride was Mallinckrodt analytical reagent grade. The significant impurity with respect to the present experiments was 20 ppm of iron by weight. The solutions were made up following standard procedures of volumetric analysis.

Solutions of desired concentrations were made up from calculated amounts of lithium chloride solution, potassium fluoride solution, distilled water, and saturated ferric fluoride solution. The growth solution was made up by measuring calculated volumes of the first three components from burettes. The ferric fluoride solution was then added by medicine dropper to give the desired poison concentration. The concentration of lithium fluoride in the growth solution was changed by 1% or less upon addition of the poison solution. The total iron introduced into solution from the starting solute was at most 0.06 ppm.

Cleaved samples of Harshaw melt-grown lithium fluoride crystal served as seed crystals upon which the growth process was observed. The seed crystals were pre-etched with acid etch[10] according to procedure described by Gilman and Johnston.

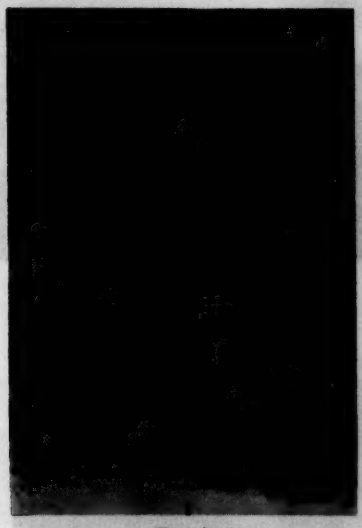

FIG. 1.

[10] J. J. Gilman and W. G. Johnston, J. Appl. Phys. 27, 1018 (1956).

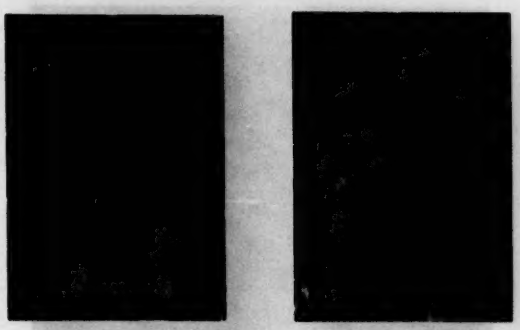

(a) FIG. 2. (b)

After a crystal was removed from the growth solution it was rinsed in turn in two washes of ethyl alcohol and a wash of ethyl ether. The crystal was then dried in a gentle stream of air.

The solubility at 25°C is 1.33 g/liter, as determined by Payne[11] and Meyer and Dunkel.[12] The temperature coefficient[12] of solubility in this range is negligible.

RESULTS

(A) An acid-etched lithium fluoride crystal was placed in a solution containing 3.24 g/liters of lithium fluoride and 2×10^{-5} molal in ferric fluoride. Growth occurred for a 16-hr period. At various sites on the surface an irregular columnar growth occurred upward from the surface. Randomly from the columns, arms branched in the (100) directions parallel to the (100) surface. Most of the arms tapered as they grew and in many instances the tapered arms terminated in whiskers of quite constant width. A typical view of such a field is shown at 100× in Fig. 1. Figure 2(A), (B) show at 75× the same fields of view at 85μ, and 196μ from the surface of the seed crystal. From such observations it is apparent that the whiskers grown at the top of a columnar structure have a much more constant cross section than those grown near the crystal surface. Since the excess solute was depleted in the course of the growth process, the high-level whiskers grew at a lower supersaturation than whiskers near the crystal surface. This was apparent from observations after different growth periods. In Fig. 3 the surface of a tapered side arm is shown at 250×. This group has grown near the crystal surface and at a higher supersaturation than the arms shown in Fig. 4 at 250× which were far above the seed crystal surface. In Fig. 5 a high arm (growth at relatively low supersaturation) is shown at 750×. The axis of the wedge is a (100) direction and it is noted that the ridges and valleys structure characterizing the growth lies in nearly a (100) direction.

(B) An acid-etched crystal of lithium fluoride was immersed in a solution of 3.24 g/liter of LiF and 4×10^{-5} molal in ferric fluoride for 16 hr. Very tiny crystal-

[11] J. H. Payne, J. Am. Chem. Soc. 56, 947 (1937).
[12] K. H. Meyer and M. Dunkel, Z. Physik Chem., 556 (1931).

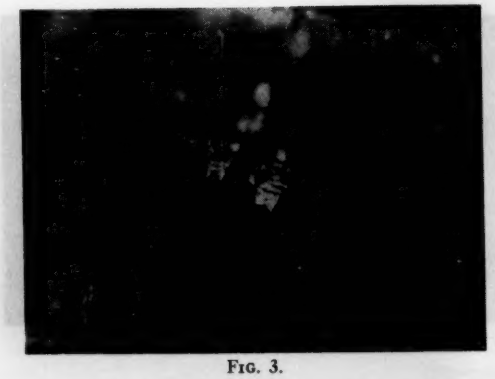

FIG. 3.

FIG. 4.

FIG. 5.

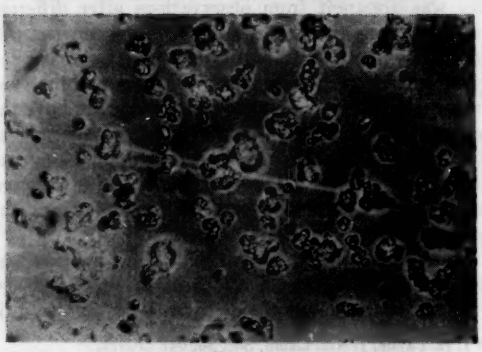

FIG. 6.

FIG. 7.

FIG. 8.

FIG. 9.

FIG. 10.

FIG. 11.

lites had deposited over the entire surface. A typical field of view is shown at 750× in Fig. 6. Most of the individual crystallites are at or below the limit of resolution. A similar deposition of crystallites was deposited from a solution containing 2×10^{-5} molal ferric fluoride. The crystallites were large enough to be resolved in that instance.

The columnar growth was much less than in the preceding experiment. The growth was limited to a small distance from the seed crystal surface. A typical field of view is shown at 100× in Fig. 7. A minor amount of whiskers has grown and they have length/width ratios of about 10. Figure 8 shows the growth of tapered arms at 250×. It is seen that the arms are much less regular in form than those grown at 2×10^{-5} molal in ferric fluoride. In Fig. 9 the surface of an arm is shown at 750×. The roughness of the surface is pronounced as compared to Fig. 5.

The extent of roughening in the presence of 4×10^{-5} molal is shown in Fig. 10. The surface of a small cube is shown at 750×. In Fig. 11 a heavily overgrown whisker is shown at 750×.

The individual crystallites have nucleated on the whisker surface. There is no spreading of growth layers from the sites of the crystallites as would occur in the absence of a poisoning. Step motion is essentially completely absent.

(C) A solution was made up containing 3.0 g/liter of LiF and having an estimated molality no greater than 6×10^{-7} in FeF_3 from the solute impurity. An acid-etched crystal was grown for 2 hr. A typical field of growth is shown at 37.5 in Fig. 12. It can be seen that the cleavage steps have advanced and that a plate structure has grown up from the crystal. The plates are almost all parallel to the seed crystal face and predominantly have their edges parallel to {100} directions of the parent crystal (Fig. 13). However, it can be seen that the plates are sometimes rotated about the {100} axis normal to the seed crystal.

FIG. 13.

In Fig. 14 a less common structure growing in the {100} direction of the parent crystal is shown at 50×. Such oriented structures are also seen in growth from poisoned solutions. The diameter of the columnar elements is much larger in the absence of poison. A platelet surface is shown in Fig. 15 at 750×.

(D) A solution was prepared containing 3.24 g/liters of LiF and 4×10^{-5} molal in ferric fluoride. A crystal of lithium fluoride and a crystal of magnesium oxide were placed side by side in the growth solution for 16 hr.

Almost no growth had occurred on the lithium fluoride crystal. The magnesium oxide crystal was covered with a mass of intergrown and interlaced lithium fluoride whiskers. The whiskers are parallel to the {100} cleavage plane of the MgO crystal and predominantly lie in [100] directions. A typical field of view is shown at 100× in Fig. 16. Imbedded in the mat of whiskers are many blobs of a reddish precipitate of a hydrated iron oxide.

(E) A growth solution containing 3.24 g/liter of LiF and 10^{-5} molal in FeF_3 was made up and allowed to

FIG. 12.

FIG. 14.

FIG. 15.

stand 4 hr. A precipitate formed and lowered the supersaturation of the solution. The supernatant liquid was decanted and an acid-etched crystal was immersed in the solution.

The solution was left open to the atmosphere so that evaporation of solvent could slowly proceed. After 7 days only about a quarter of the solvent remained. The crystal was removed and washed in the usual way.

Whiskers as long as 1 cm were observed. Periodic twists were observed microscopically[13] and were ascribed to the Eshelby twist associated with the axial screw dislocation active in the growth process.

DISCUSSION

(A) Over-all Growth Rate

The poisoning action of ferric fluoride on the net growth rate of lithium fluoride is clearly established by a comparison of experiments (A) and (C). The amount of crystal grown from a solution having an initial concentration of 3.00 g/liter of LiF and 6×10^{-7} molal in ferric fluoride was greater in 2 hr than the amount grown in 16 hr from a solution having an initial concentration of 3.24 g/liter of LiF and 2×10^{-5} molal in ferric fluoride.

The effectiveness of ferric fluoride as a growth poison was even more strikingly demonstrated in experiment (D). Crystals of lithium fluoride and magnesium oxide were placed side by side in a supersaturated solution of lithium fluoride and 4×10^{-5} molal in ferric fluoride. Lithium fluoride crystal formed a thick interlaced mat as seen in Fig. 16 over the surface of the magnesium oxide crystal and grew hardly at all on the lithium fluoride seed crystal.

The magnesium oxide reacted with solvent and ferric fluoride to form an insoluble hydrated ferric oxide. The poison concentration was reduced in the neighborhood of the magnesium oxide crystal so that growth of lithium fluoride was there uninhibited. Any lithium fluoride crystals that started growing away from the magnesium oxide surface essentially stopped as the ferric fluoride concentration in the diffusion field approached the bulk value. Both magnesium oxide and lithium fluoride have sodium chloride structures with lattice constants of 4.20 A and 4.03 A, respectively. In Fig. 16 the lithium fluoride whiskers are parallel to [100] directions in the MgO seed crystal.

[13] G. W. Sears, J. Chem. Phys. **31**, 53 (1959).

(B) Effect of Poison on Two-Dimensional Nucleation Rate

It has been recognized[5] that a step poison must reduce the specific step free energy and the free energy of two-dimensional nucleation at a fixed supersaturation in the parent phase. Blisnakow[14,15] has discussed the influence of adsorption on equilibrium form and free energy of nucleation of crystals. Stranski[16,17] and Kleber[18,19] have considered the effect of adsorption on crystal morphology.

The decreased barrier to two-dimensional nucleation in the presence of a step poison was first demonstrated in the growth of near perfect platelets of potassium chloride from aqueous solution. Thickening of perfect surfaces occurred by two-dimensional nucleation in the presence of 10^{-5} molal $PbCl_2$ at supersaturations that were insufficient to cause two-dimensional nucleation in the absence of lead chloride.

Figure 9 shows the surface of a lithium fluoride crystal at 750× which has grown in the presence of 4×10^{-5} molal ferric fluoride. Two-dimensional nucleation has dominated the growth. In Fig. 16 a crystal surface grown in the presence of 6×10^{-7} molal ferric fluoride is shown at 500×. In this case individual layers have spread over the entire surface. The roughness shown in Fig. 16 occurs because the step bounding a

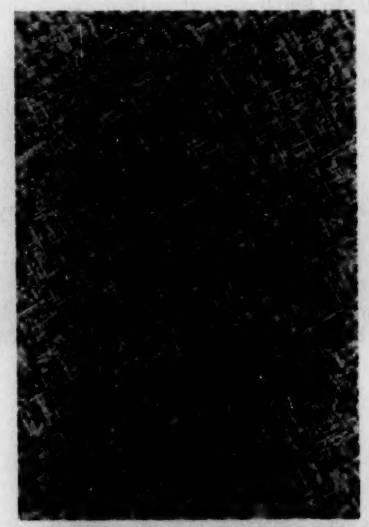

FIG. 16.

[14] G. Blisnakow, Compt. rend. acad. bulgare sci. **6**, 13 (1953).
[15] G. Blisnakow and E. Kirkowa, Z. physik Chem. (Leipzig) **B206**, 271 (1957).
[16] I. N. Stranski, Bull. soc. franç. minéral. et crist. **79**, 359 (1956).
[17] O. Kracke and I. N. Stranski, Z. Elektrochem. **60**, 816 (1956).
[18] W. Kleber, Z. physik Chem. (Leipzig) **B206**, 327 (1957).
[19] W. Kleber, Z. Kristallografixa **109**, 115 (1959).

two-dimensional patch can spread only very slowly after reached a critical radius. Thus the structure is characteristic of a low rate of step motion and a high rate of nucleation.

(C) Poisoning of Step Motion

The poisoning of step motion is most readily shown by observation of whiskers of lithium fluoride. In Fig. 10 one of the rare whiskers which grew to an appreciable length in the presence of 4×10^{-5} molal ferric fluoride is shown. Crystallites have nucleated on the whisker, but the new layers have not spread over the whisker surface to thicken it uniformly as would occur in the absence of a poison. This behavior is the reverse of the usual case in which nucleation is more difficult than spreading.

Whiskers grown in the presence of 2×10^{-5} molal ferric fluoride further show that the poisoning of step motion is not so severe at the lesser poison concentration. Whiskers grown close to the surface (i.e., at an early stage of growth and at a relatively high supersaturation) are overgrown with crystallites to an appreciable extent. However, spreading of layers along the whiskers has occurred, and the local thickening is frequently imaged by closely spaced interference color bands. Whiskers grown high above the surface (i.e., at relatively low supersaturations) are not overgrown. They show lengths up to 1–2 mm of quite uniform thickness as judged by their interference colors.

Final evidence of the very effective step poisoning at 4×10^{-5} molal FeF_3 is furnished by the formation of two-dimensional nuclei right at growth steps. If poisoning of step motion were absent or slight, the solution in the immediate vicinity of a step would be at or near equilibrium respectively with the growing phase. Even in the presence of a poison, two-dimensional nucleation could not occur at low supersaturations. In Experimental (E), whiskers of uniform cross section with no overgrowth grew at low supersaturations in the presence of 4×10^{-5} molal FeF_3.

(D) Effect of Poison on Whisker Growth

The role of poison in the growth of whiskers from a dislocation in a massive crystal is clearly established by a comparison of experiments (A) and (C). No whiskers grow in the absence of poison (i.e., 6×10^{-7} molal FeF_3). Whiskers grow most profusely at the initial supersaturations used in the presence of 2×10^{-5} molal ferric fluoride. This behavior is expected[6] since the rate of rotation of a step at the core of a dislocation is increased by the presence of a step poison, whereas the rate of step motion from the dislocation site is inhibited by a dislocation. A sharp pyramid tapers up from a dislocation and terminates in a whisker of uniform cross section. Figure 1 shows fully developed whiskers as well as all stages on the way to whisker formation.

TABLE I.

	A	B
C_0	7.4×10^{-17}	1.2×10^{-16}
C_0	1.5×10^{-12}	1.2×10^{-11}
C_2	4.7×10^{-8}	1.9×10^{-8}
C_3	7.4×10^{-7}	1.5×10^{-6}
C_4	7.4×10^{-6}	7.6×10^{-6}
C_5	1.7×10^{-6}	7.6×10^{-7}
C_6	1.7×10^{-6}	3.8×10^{-8}

In the presence of 10^{-5} molal FeF_3 relatively few whiskers form in agreement with the observation that poisoning is much less severe than at 2×10^{-5} molal FeF_3.

In the presence of 4×10^{-5} molal FeF_3 almost no whiskers more than 20μ in length formed, since two-dimensional nucleation dominated the growth at the LiF concentration of 3.24 g/liter. In Experimental (E), whisker growth was prolific in the presence of 4×10^{-5} molal FeF_3, since the supersaturation was insufficient to cause an appreciable rate of two-dimensional nucleation.

(E) Active Solute Species

The stability constants are known[20] for the various ferric fluoride complexes $FeF_n(H_2O)_{6-n}^{3-n}$, where the superscript indicates the charge and the subscript indicates the composition. The stability constants, pK_n's, are 5.3, 4.5, 3.2, 2.0, and 0.36 for $n=1, 2, 3, 4, 5$, respectively, where

$$K_n=\frac{[FeF_n^{3-n}]}{[FeF_{n-1}^{2-n}][F^-]},$$

where the coordinated water is ignored. The total stability constant, $pK_n{}'$, is given by

$$pK_n{}'=\sum_1^n pK_i.$$

The value $K_6{}'$ is given as $\sim5\times10^{-16}$ by Latimer.[21]

Solving the equilibria relations for the simultaneous reactions

$$Fe^{+++}+jF^-\rightleftharpoons FeF_j^{3-j} \qquad j=1, 2, 3, 4, 5, 6$$

yields the concentrations of all species. If c_j is the molal concentration of the complex containing j fluorine atoms, the solution for two total concentrations of fluoride and ferric ions are tabulated in Table I. Column A gives ionic concentration for $[F^-]=10^{-1}$ molal and total $[Fe^{+++}]=10^{-5}$ molal. This corresponds to the physical conditions at the start of an experiment. Column B gives complex ion concentrations for $[F^-]=5\times10^{-2}$ molal and total ferric concentration of 10^{-5}

[20] P. J. Bjerrum, G. Schwarzenbach, and L. G. Sillen, *Stability Constants Part II, Inorganic Ligands*, (The Chemical Society, London, 1958), p. 90.

[21] W. Latimer, *Oxidation Potentials* (Prentice-Hall, Inc., Englewood Cliffs, New Jersey, 1952), 2nd ed., p. 226.

molal. This corresponds to conditions when precipitation is nearly complete. It eliminates Fe^{+++} and FeF^{++} as possible poison species and indicates FeF_3, FeF_4^-, and $FeF_5^{=}$ are the most likely species responsible for poisoning.

CONCLUSIONS

It has been shown that a ferric fluoride complex ion is a step poison for the growth of lithium fluoride. The growth behavior has been found to correspond qualitatively to the expected behavior. Step poisons increase rate of two-dimensional nucleation at fixed supersaturations, but markedly decrease the rate of step motion or of spreading of the newly formed layers.

ACKNOWLEDGMENT

The research reported in this paper has been sponsored by the Electronics Research Directorate of the Air Force Cambridge Research Center and the Air Force Research and Development Command.

THE JOURNAL OF CHEMICAL PHYSICS VOLUME 33, NUMBER 4 OCTOBER, 1960

Line Shapes of Electron Paramagnetic Resonance Signals Produced by Powders, Glasses, and Viscous Liquids*

FRITZ KURT KNEUBÜHL

Department of Chemistry, Johns Hopkins University, Baltimore, Maryland

(Received April 22, 1960)

The line shapes arising from randomly oriented particles in a fixed position have been calculated. It has been found that it is possible to determine the three principal g factors with relatively high accuracy and without investigating single crystals. Measurements on powders of $CuCl_2 \cdot 2H_2O$ and $CuSO_4 \cdot 5H_2O$ are used as examples. In addition, the influence of Brownian rotation in viscous liquids on line shapes has been studied. Equations have been derived for the case of high viscosities, supplementing the well-known ones given by McConnell [J. Chem. Phys. **25**, 709 (1956)]. To a first approximation, the effect of decreasing viscosity can be described by an over-all diminishing line width and an unchanged line shape function. The hyperfine splittings are neglected, but can be taken into account.

INTRODUCTION

In recent papers, Sands,[1] O'Reilly,[2] and Roberts[3] determined experimentally $g_{\parallel}$ and $g_{\perp}$ of unpaired electron spins in fields with axial symmetry of different samples by the consideration of the epr-line shapes produced by the paramagnetic substances dissolved in glasses and highly viscous liquids. Searl, Smith, and Wyard[4] have carried out a calculation of line shapes for epr-signals caused by two different principal g values including other broadening effects. No treatment of line shapes produced by paramagnetic materials with three different principal g factors has been published. Therefore, the explanation of the absorption lines of powders of $Cu(NH_3)_4SO_4 \cdot H_2O$ and $Cu(NH_3)_4(NO_3)_2$ measured by Carlson and Spence[5] has encountered some difficulties.

One purpose of this paper is to present the results of a study of the feasibility of determining the principal g values from an examination of the epr-line shapes of powders, solutions in glasses, or highly viscous liquids. Such measurements can provide welcome preliminary information for determining the magnetic axes and g factors of single crystals described by Schonland.[6] In addition, there is some evidence of a difference of the g tensors of a special group of molecules[3] measured in single crystals or in solutions.

The second part of this paper deals with the influence on line shapes of Brownian rotation of the paramagnetic particles with anisotropic g factor in viscous liquids.

THEORY

The following assumptions will be made:

(a) Only systems with $S=\frac{1}{2}$ will be considered.

(b) The paramagnetic molecules are randomly oriented.

(c) Hyperfine splitting is neglected.

(d) Broadening of the absorption lines due only to the anisotropic g factor is taken into account.

(e) The Brownian motion of the paramagnetic particles in viscous liquids is independent of the magnetic interactions between these particles and their neighbors or the external field. This behavior differs

* This investigation was supported in part by a research grant from the division of General Medical Sciences, Public Health Service, National Institutes of Health.

[1] R. H. Sands, Phys. Rev. **99**, 1222 (1955).

[2] D. E. O'Reilly, J. Chem. Phys. **29**, 1188 (1958).

[3] E. M. Roberts, J. Am. Chem. Soc. (to be published).

[4] J. W. Searl, R. C. Smith, and S. J. Wyard, Proc. Phys. Soc. (London) **74**, 491 (1959).

[5] E. H. Carlson and R. D. Spence, J. Chem. Phys. **24**, 471 (1956).

[6] D. S. Schonland, Proc. Phys. Soc. (London) **73**, 788 (1959).

from Brownian rotation influenced by electric dipole-dipole interaction treated by Debye.[7]

Line Shapes Due to Fixed Orientations

First, we calculate line shapes due to particles randomly oriented. Restrictions (a) and (c) lead to the following Hamiltonian:

$$\mathcal{H}=\beta\sum_k H_k' g_k' S_k'$$

for a molecule fixed coordinate system

$$=\beta\sum_k\sum_l H_k G_{kl} S_l$$

for a space fixed coordinate system (1)

where H_k, H_k' are the components of the magnetic field; S_k', S_l the components of the Pauli spin operator; G_{kl} the time dependent g tensor and g_k the principal g values. Taking $H_k=(0, 0, H_z)$ and introducing $g=\hbar\omega/\beta H_z$, we find

$$g^2=g_1^2\sin^2\beta\sin^2\gamma+g_2^2\sin^2\beta\cos^2\gamma+g_3^2\cos^2\beta$$

or

$$g^2=g_1^2+(g_3^2-g_1^2)\cos^2\beta \qquad \text{for} \qquad g_1^2=g_2^2. \quad (2)$$

α, β, γ are the Eulerian angles as defined by Margenau and Murphy.[8]

The normalized shape functions $S(H_z)$ or $S(g^2)$ are determined by the probability of the molecules to absorb in the region H_z to H_z+dH_z or g^2 to $g^2+d(g^2)$. Therefore we can write

$$S(H_z)=\Omega^{-1}\cdot(dH_z)^{-1}\int_{H_z}^{H_z+dH_z} d\Omega,$$

$$\int_0^\infty S(H_z)dH_z=1, \quad (3)$$

$$S(g^2)=S(H_z)\cdot 2H_z^3\cdot\omega^{-2}\beta^2\hbar^{-2}. \quad (3a)$$

Ω is the phase space. Assumption (b) leads to $d\Omega=\sin\beta d\beta d\gamma=-dzd\gamma$, $\Omega=4\pi$, where $z=\cos\beta$.

For $g_1=g_2$, the normalized line shapes can be calculated in a straightforward manner with the aid of Eqs. (2) and (3). They have been evaluated previously by Sands.[1]

$$S(H_z)=H_\perp^2H_{||}(H_\perp^2-H_{||}^2)^{-\frac{1}{2}}H_z^{-2}(H_\perp^2-H_z^2)^{-\frac{1}{2}}. \quad (4)$$

For three different principal g values, we have to consider in more detail the behavior of g^2 in the phase space. The symmetry of Eq. (2) allows us to reduce the space to an area of $\Omega=\pi/2$. Figure 1 shows the variation of g^2 within this region. For the calculation

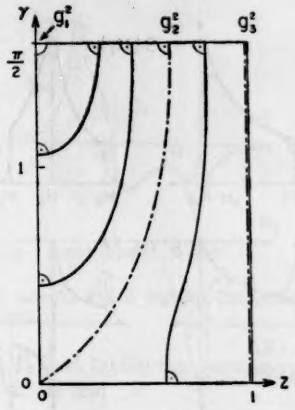

FIG. 1. g^2 as a function of z and γ. g_1, g_2, g_3 are principal g values.

of $S(g^2)$ the following formula is applied:

$$\Omega^{-1}(da)^{-1}\int_a^{a+da} d\Omega(a)=\Omega^{-1}\int_{\Omega'}(d\Omega/|\operatorname{grad}_\Omega a|), \quad (5)$$

where a is a function of n dimensions and $d\Omega$ the corresponding volume element. Ω' is Ω reduced by the condition: $a=$constant. If $d\Omega=dxdy$, this equation becomes

$$(da)^{-1}\int_a^{a+da} dxdy=\int_s(ds/|\operatorname{grad}a|)$$

$$=\int_{a=\text{const}}[dx/a_y(x,a)], \quad (6)$$

where $a_y=\partial a/\partial y$. These expressions can be used to determine shape functions due to Hamiltonians more complicated than (1), e.g., with hyperfine interactions.

The application of (6) leads to the normalized shape functions for $g_3>g_2>g_1$:

for $H_z\leqq H_2$:

$$S(H_z)=2/\pi\frac{H_1H_2H_3H_z^{-2}}{(H_1^2-H_z^2)^{\frac{1}{2}}(H_2^2-H_3^2)^{\frac{1}{2}}}K(k)$$

with

$$k^2=\frac{(H_1^2-H_2^2)(H_z^2-H_3^2)}{(H_1^2-H_z^2)(H_2^2-H_3^2)}$$

for $H_z\geqq H_2$:

$$S(H_z)=2/\pi\frac{H_1H_2H_3H_z^{-2}}{(H_1^2-H_2^2)^{\frac{1}{2}}(H_z^2-H_3^2)^{\frac{1}{2}}}K(1/k). \quad (7)$$

$K(k)$ is the complete elliptic integral of the first kind, see Jahnke and Emde.[9]

$$K(k)=\int_0^{\pi/2} db/(1-k^2\sin^2 b)^{\frac{1}{2}},$$

$$K(0)=\pi/2, \qquad K(1)=\infty. \quad (8)$$

[7] P. Debye, *Polar Molecules* (The Chem. Catalog Company, New York, 1929).

[8] H. Margenau and G. M. Murphy, *The Mathematics of Physics and Chemistry* (Van Nostrand Company, New York, 1956), 2nd ed.

[9] E. Jahnke and F. Emde, *Tables of Functions* (Dover Publications, New York, 1945), 4th ed.

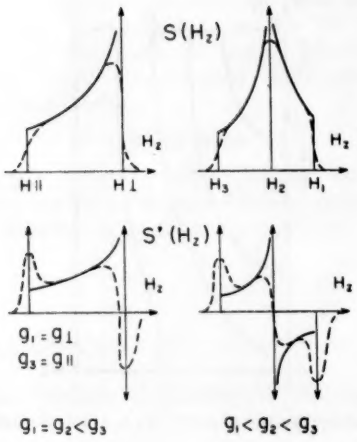

FIG. 2. The shape functions $S(H_z)$ and their derivatives.

Expressions similar to (7) have been found by Bloembergen and Rowland[10] for nmr-line shapes due to anisotropic Knight shift in metals and due to nuclear quadrupole coupling by Cohen and Reif.[11]

What are the line shapes expected? Figure 2 shows the $S(H_z)$ according to (4) and (7). The continuous lines represent the ideal curves; the broken ones are an approach to the real shapes. This figure indicates: (A) We are able to distinguish between signals due to two and three different principal g values g_k. The derivative of the shape corresponding to two g's has five points of inflection; the other one has seven. (B) We can determine or estimate all g factors in both cases. $g_{\|}$, $g_{\perp}$, g_1, and g_3 correspond to maxima, g_2 to a zero point of the derivatives.

With assumption (c), these statements are true in a first approximation. To estimate the errors introduced by Gaussian broadening, we can proceed as follows. For H_z near H_1, H_3, $H_{\|}$, we superimpose a Gaussian shape with the line width $2H_0$ upon a linear approximation of our ideal curve. H_0 can vary with H_z, but special values of H_0 can be found as indicated in Fig. 2 in experimental curves. The superposition of the two shapes is calculated by taking the convolution[8] (Faltung) of the shape functions. The effect of additional Gaussian broadening is in a first approximation a shift of the maxima corresponding to g_1, g_3 and $g_{\|}$ of the derivatives. As an example, we write the equation for the position of the maximum near $H_{\|}$.

$$H_{z,\max}=H_{\|}+H_0^2\{[H_{\|}/(H_{\perp}^2-H_{\|}^2)]-(2/H_{\|})\}. \quad (9)$$

This is a second-order effect. Similar expressions are valid for the shifts near H_1 and H_3. But for the cases corresponding to H_2 and $H_{\perp}$, such equations are difficult to find. Graphical methods or exact calculations, including all broadening effects from the beginning,[4] are necessary to determine the theoretical error of the H_2 or $H_{\perp}$ determination.

[10] N. Bloembergen and T. J. Rowland, Acta Met. **1**, 731 (1953).
[11] M. Cohen and F. Reif, in *Solid State Physics* (Academic Press, Inc., New York, 1957), Suppl. to Vol. 5.

The Effect of Brownian Rotation

For epr measurements dealing with viscous solutions, we must consider the effects of Brownian rotation on the line shapes. We use two probability densities to describe this movement, P_0 and P_τ. They are functions of the orientations determined by the Eulerian angles α, $z=\cos\beta$, γ of the molecules containing unpaired spins. $P_0(\alpha, z, \gamma)$ is the probability density to find such a molecule with an orientation in the interval between α, z, γ and $\alpha+d\alpha, z+dz, \gamma+d\gamma$ at a certain time t_0. P_0 is independent of the time t_0 and with assumption (e), we can easily prove

$$P_0(\alpha, z, \gamma)=1/4\pi. \quad (10)$$

P_τ is the probability density of finding a molecule in the interval at α, z, γ at time $t_0\pm\tau$, if it was or will be in the interval α_0, z_0, γ_0 at time t_0. P_τ is independent of t_0, and it represents a solution of the equation

$$\partial P_\tau/\partial\,|\,\tau\,| = D\Delta_{(\alpha,z,\gamma)}P_\tau. \quad (11)$$

The initial condition for time t_0 or $\tau=0$ is

$$P_\tau(\alpha_0, z_0, \gamma_0, |\,\tau\,|, \alpha, z, \gamma)_{\tau=0}=\delta(\alpha-\alpha_0, z-z_0, \gamma-\gamma_0). \quad (12)$$

Equation (18) follows from assumption (e) and it is related to the laws ruling heat transfer and diffusion. Debye[7] calculated D for spherical particles of volume V in a liquid with a viscosity η at temperature T:

$$D=kT/6V\eta, \qquad \tau_c=1/6D=V\eta/kT. \quad (13)$$

In epr and nmr literature D is usually replaced by τ_c. Because we will deal with averages of functions of z and γ only, we take the following solution of (11) and (12) as P_τ:

$$P_\tau(z_0, \gamma_0, |\,\tau\,|, z, \gamma)=\sum_n \exp\{-[n(n+1)|\,\tau\,|]/6\tau_c\} \times\sum_m Y^*{}_n{}^m(z_0, \gamma_0)\,Y_n{}^m(z, \gamma). \quad (14)$$

$Y_n{}^m$ are normalized spherical functions. Averaging any function of the form

$$f(z, \gamma)=\sum_m a_m Y_n{}^m(z, \gamma)$$

by the aid of P_τ we find

$$\iint f(z, \gamma)\,P_\tau dz d\gamma=\exp\{-[n(n+1)\tau]/6\tau_c\}\cdot f(z_0, \gamma_0). \quad (15)$$

The effect of Brownian rotation on the absorption curves can be described by a contribution to the spin-

lattice relaxation and one to the spin-spin interaction. The former decreases with growing viscosity; the latter increases and causes an asymmetric line shape.

McConnell[12] has given a first approximation for these two effects in slightly viscous liquids, using the relaxation times T_1 and T_2'. Assuming $g_1=g_2$, he found a good formula for the broadening due to spin-lattice relaxation, but his expression for the spin-spin interaction neglects the asymmetry of the line shapes. Therefore, an approximation of the spin-spin effect for high viscosities is needed.

The square of the Hamiltonian (1) as function of time t can be written

$$\mathfrak{IC}^2(t)=\tfrac{1}{4}(\beta H_z)^2 g^2(t)\,U=\tfrac{1}{4}\hbar^2\omega^2(t)\,U. \qquad (16)$$

U is the two-dimensional unity matrix. Assuming a high viscosity and $|g_1-g_3|\ll g_1$, we neglect the spin-lattice contribution and calculate averages of $\omega^2(t)$ or $g^2(t)$ as follows: We consider the paramagnetic particles with an orientation in the region α_0, z_0, γ_0 at about time t_0. Some of their unpaired spins undergo transitions; we call the group of these spins $E(\alpha_0, z_0, \gamma_0)$. Because of our assumptions, the number of particles in such a group is independent of α_0, z_0, γ_0 and t_0. The uncertainty of t_0 is determined by Heisenberg's principle: $\Delta t\approx 1/\omega$. To calculate the shape functions due to Brownian rotation, we replace g^2 of (2) by the averages of g^2 over all particles of a group E and over the time interval $t_0\pm\Delta t$. We introduce the spin-spin relaxation, taking[13] only the interval $|\nu|\leqq 1/\pi T_2'$ of the Fourier spectrum. The relaxation time T_2' is much larger than Δt, because $|g_1-g_3|\ll g_1$. g^2 of (2) is a linear combination of Y_0^0 and Y_2^m. Therefore, we have to consider only Y_2^m. Averaging Y_2^m over E leads to

$$\langle Y_2^m\rangle_{Av}^E=\iint P_\tau Y_2^m\,dz\,d\gamma=Y_2^m(z_0,\gamma_0)\exp[-|\tau|/\tau_c]$$

$$=\int_{-\infty}^{+\infty} a(z_0,\gamma_0,\nu)\exp(i2\pi\nu\tau)\,d\nu. \qquad (17)$$

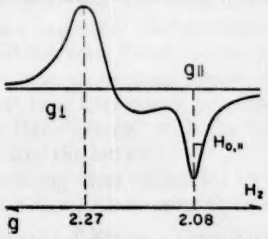

FIG. 3. Derivative presentation of the electron paramagnetic resonance spectrum of polycrystalline $CuSO_4\cdot 5H_2O$ with two principal g values. Measured at room temperature at a frequency of about 9.2 kMc/sec with a Varian 100 kc spectrometer, model V-4500.

[12] H. M. McConnell, J. Chem. Phys. **25**, 709 (1956).

[13] N. Bloembergen, E. M. Purcell, and R. V. Pound, Phys. Rev. **73**, 679 (1948).

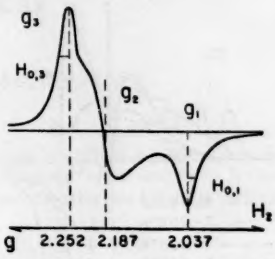

FIG. 4. The same as Fig. 3, but for $CuCl_2\cdot 2H_2O$ with three different g factors.

Introducing T_2' and taking the average over the time interval $t_0\pm\Delta t$, we find

$$\langle Y_2^m\rangle_{Av}=\tfrac{1}{2}\Delta t^{-1}\int_{-\Delta t}^{+\Delta t}d\tau\int_{-1/\pi T_2'}^{+1/\pi T_2'} a(z_0,\gamma_0,\nu)\exp(2\pi i\nu\tau)\,d\tau$$

$$\langle Y_2^m\rangle_{Av}=Y_2^m(z_0,\gamma_0)\,(2/\pi)\,\tan^{-1}(\tau_c/T_2'). \qquad (18)$$

Using this result, we can determine $\langle g^2\rangle_{Av}$.

$$\langle g^2\rangle_{Av}=\sin^2\beta_0\sin^2\gamma_0[s+(g_1^2-s)\,(2/\pi)\,\tan^{-1}(\tau_c/T_2')]$$
$$+\sin^2\beta_0\cos^2\gamma_0[s+(g_2^2-s)\,(2/\pi)\,\tan^{-1}(\tau_c/T_2')]$$
$$+\cos^2\beta_0[s+(g_3^2-s)\,(2/\pi)\,\tan^{-1}(\tau_c/T_2')]$$
$$s=(g_1^2+g_2^2+g_3^2)/3. \qquad (19)$$

Concerning the angular dependence, this equation is similar to (2). Only the g_k's of (2) must be replaced by $s+2/\pi\cdot(g_k^2-s)\cdot\tan^{-1}\tau_c/T_2'$. Therefore, the shape functions $S(g^2)$ and $S(\langle g^2\rangle_{Av})$ are equal. With the assumption $|g_1-g_3|\ll g_1$, we can use the transformation (3a) to determine the first approximation of $S(\langle H_z\rangle_{Av})$. The difference between s and g_0^2, where $g_0=\frac{1}{3}(g_1+g_2+g_3)$, is very small. Therefore the Brownian rotation reduces the over-all width of the absorption line, but it does not affect its shape as long as T_2'/τ_c is small. The points corresponding to $g_{\|}$, $g_\perp$ or g_1, g_2, g_3 move with increasing T_2'/τ_c towards g_0.

EXPERIMENTS

Fixed Orientations

In order to demonstrate the line shapes arising from arbitrarily oriented molecules, the first derivatives of the absorptions due to crystalline powders of $CuSO_4\cdot 5H_2O$ and $CuCl_2\cdot 2H_2O$ have been measured at room temperature and a frequency of about 9.2 kMc/sec. In spite of exchange effects,[14] these powders show the expected curves, as is evident from Figs. 3 and 4.

The principal g values of these salts have been determined by single crystal measurements[14] as $CuSO_4\cdot 5H_2O$: $g_\perp=2.27$, $g_{\|}=2.08$; $CuCl_2\cdot 2H_2O$: $g_1=2.037$, $g_2=2.187$, $g_3=2.252$. To calculate the positions of the peaks of our derivatives, we determine first the half-

[14] K. D. Bowers and J. Owen, Repts. Progr. in Phys. **18**, 304-373 (1955).

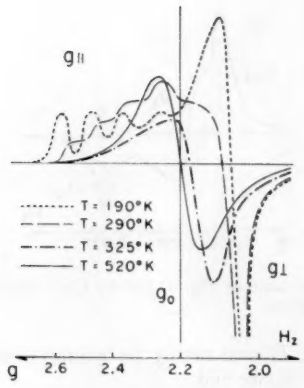

FIG. 5. Derivative presentation of the electron paramagnetic resonance absorption of a solution of $CuSO_4 \cdot xH_2O$ ($x=0-5$), in glycerol at different temperatures. The microwave frequency is about 9.2 kMc/sec. The intensity scale is different for each curve.

line widths H_0 from the experimental curves. We find $H_{0,\|}/H_{\|}=6.6\cdot10^{-3}$, $H_{01}/H_1=7.0\cdot10^{-3}$; $H_{03}/H_3=7.8\cdot10^{-3}$. Using Eq. (9) and related ones, we evaluate theoretical errors of the g determination; $\delta g_{\|}/g_{\|}=0.36\cdot10^{-3}$, $\delta g_1/g_1=0.43\cdot10^{-3}$, $\delta g_3/g_3=1.1\cdot10^{-3}$.

These estimated errors or corrections are comparable with those of single crystal work, $2\cdot10^{-3}$. Our results are plotted in Figs. 3 and 4. There is a good agreement with our theory. The position of the peak corresponding to $g_\perp$ seems to undergo a shift of the same order of magnitude as those just mentioned, whereas the zero point belonging to g_2 moves more.

Effect of Brownian Rotation

To demonstrate the change of the line shapes caused by Brownian rotation, we measured the epr absorption of a solution of $CuSO_4 \cdot xH_2O$ ($x=0-5$) in glycerol at temperatures from -140°C to 250°C. The absorption patterns do not depend on the initial water content (x) of the sulfate. The influence of the concentration of the solute on the shapes can be neglected for our considerations. The viscosity of glycerol is a complex function of the amount of impurities and solutes and varies considerably with temperature. Lutze and Bösnecker[15] have recently investigated the system $CuSO_4$-glycerol by epr. They have related the spectra from 90°K to room temperature to two different paramagnetic centers.

For our measurements, we have varied the temperature in steps of about 5°C and have found a continuous change with increasing temperature of the entire line shape toward a Gaussian or Lorentzian shape. This behavior can be explained by a Hamiltonian slightly different from (1) and a modified Eq. (19). Figure 5 shows four of the measured curves and demonstrates the shift of the peaks toward g_0 predicted by (19).

If we take an anisotropic g factor with axial symmetry and a nuclear-spin coupling with the same properties, we can relate our absorption pattern to a single type of paramagnetic centers. The Hamiltonian is

$$\mathcal{H}=\beta\sum_k\sum_l H_k G_{kl} S_l+\sum_k\sum_l A_{kl} I_k S_l \qquad (20)$$

where A_{kl} and G_{kl} are tensors with the same axis of symmetry. We find from our measurement $g_\perp\approx2.08$, $g_{\|}\approx2.40$, $A_{\|}\approx130$ gauss, $A_\perp$ small, in accordance with the low-temperature results of Lutze and Bösnecker.[15] The assignment of $g_\perp$ and $g_{\|}$ is justified by the ratio of their differences from g_0 and the line shapes. To study the relaxation effects of the system $CuSO_4$-glycerol quantitatively, we need additional information on the influence of impurities on the viscosity as well as detailed knowledge on how the viscosity changes with temperature.

ACKNOWLEDGMENTS

The author is very grateful to the Professor W. S. Koski and Professor T. H. Berlin of The Johns Hopkins University for their advice and support and to Mrs. O. Shaffer for her work on the epr apparatus. Further, my sincere appreciation is expressed to the Schweizerische Stiftung für Stipendien auf dem Gebiete der Chemie and the Ramsay Memorial Fellowships Trust.

[15] E. Lutze and D. Bösnecker, Z. Naturforsch. **14a**, 755–58 (1959).

Structure in Ionic Solutions. IV

GEORGE W. BRADY

Bell Telephone Laboratories, Incorporated, Murray Hill, New Jersey

(Received May 12, 1960)

X-ray measurements in $ErCl_3$ and ErI_3 solutions indicate that there is a firmly held octahedral arrangement of H_2O molecules around the Er^{3+} ion. In addition, there are present $Er^{3+}-Cl_3^-$ and $Er^{3+}-I_3^-$ ion-pair complexes. Finally there is a large amount of order introduced into the structure by the presence of the ions, with evidence for an "icelike" quasi-lattice.

INTRODUCTION

As described in previous papers[1-3] x-ray scattering techniques have been used to measure some properties of ionic solutions. So far we have dealt with hydration numbers, ion pairing or complex ion formation, and effects (on the solvent) of the dissolved species. In this communication we turn our attention to the problem of interactions beyond the first hydration layer.

It was observed by Freed, Weissman, and Jacobsen[4,5] that the spectra of Eu^{3+} salts in solution had unusual properties. Briefly, the spectra consisted of groups of lines in the visible region which arose from transition in the $4f$ shell. This work and subsequent investigation by Sayre, Miller, and Freed[6] established that there were five lines in the blue region, three in the green, and one in the yellow, corresponding, respectively, to transitions from the $^1F_0$ ground state to upper states with $J=2$, 1 and 0, respectively; the degeneracy had been completely removed by the electric field of the environment around the ion. From their experiments they deduced that the symmetry in aqueous solution was D_{2h} and in alcohol solution C_{2v}.

But, in addition to this spectrum, Freed[7,8] noted that the groups of lines were accompanied by faint repetitions of their patterns on the long and short wavelength side, the intervals between the main group and its repetition being consistent with a lattice vibration of the surrounding medium coupling to the electronic vibrations of the ion. From the magnitude of the frequencies and other characteristics of the spectrum in mixed solvents, Freed concluded that around the ion there was an oriented region of considerable extent. Miller[9] in a later paper postulated an ice III structure for this "iceberg" with the Eu^{3+} ion fitting interstitially into the lattice.

These interesting observations led us to do a study of $ErCl_3$ and ErI_3 solutions using the x-ray technique, with a particular view to determining the extent and orientation of the ionic environment. Er^{3+} was chosen instead of Eu^{3+} because of its smaller size which offered the advantage that possible Er^{3+}—H_2O peaks (~2.3 A) would be freer of interference from solvent peaks (~2.9 A). It was assumed that the field symmetry was the same for Er^{3+} as for Eu^{3+}.

EXPERIMENTAL

$ErCl_3$ was prepared by dissolving Er_2O_3 in HCl, evaporating and crystallizing out the chloride. ErI_3 was prepared for us by Michigan Chemical Corporation. This compound is unstable and its solutions gradually decompose to give a white precipitate. It was therefore analyzed immediately after the x-ray scattering pattern was taken. This latter took about 8 hours to obtain and the solution was still clear after this period.

The concentrations were as follows:

Solution I	$ErCl_3$	$Er_{0.016}Cl_{0.048}(H_2O)_{0.936}$
Solution II	$ErCl_3$	$Er_{0.024}Cl_{0.0705}(H_2O)_{0.905}$
Solution III	$ErCl_3$	$Er_{0.045}Cl_{0.135}(H_2O)_{0.820}$
Solution IV	ErI_3	$Er_{0.022}I_{0.0609}(H_2O)_{0.917}$

The measured intensity was processed as previously described[1,2] and the Fourier integrals evaluated on the IBM 704 computer.

RESULTS AND DISCUSSION

The radial distribution curves are shown in Fig. 1. In qualitative features there are both striking similarities in all the curves and at the same time marked differences. We shall briefly discuss these features.

In both $ErCl_3$ and ErI_3, the curves show three sharp peaks whose maxima occur at 2.3, 3.05, and 3.6 A. Following this there is a region between 4 and 5 A where peaks are present, and whose detailed form varies with solute concentration. At the highest $ErCl_3$ concentration, curve III, this peak has a single maximum and an asymmetric shape. At the lower concentrations I and II, there are indications of two maxima. In curve IV ($ErCl_3$) the two maxima are well defined. Finally there is a peak at 6.9 A in all the curves.

[1] G. W. Brady and J. T. Krause, J. Chem. Phys. **27**, 304 (1957).
[2] G. W. Brady, J. Chem. Phys. **28**, 464 (1958).
[3] G. W. Brady, J. Chem. Phys. **29**, 1371 (1958).
[4] S. Freed and H. F. Jacobson, J. Chem. Phys. **6**, 254 (1938).
[5] S. Freed and S. I. Weissmann, J. Chem. Phys. **6**, 297 (1938).
[6] E. V. Sayre, D. C. Miller, and S. Freed, J. Chem. Phys. **26**, 109 (1957).
[7] S. Freed, Revs. Modern Phys. **14**, 105 (1942).
[8] H. S. Frank and M. W. Evans, J. Chem. Phys. **13**, 507 (1945).
[9] D. G. Miller, J. Am. Chem. Soc. **80**, 3576 (1958).

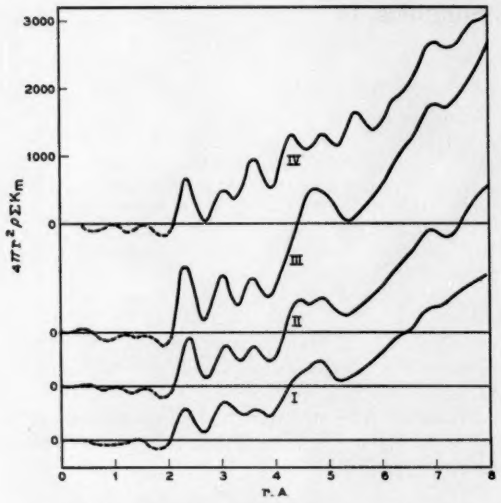

FIG. 1. Radial distribution curves for $ErCl_3$ and ErI_3. Curves I, II, and III, $ErCl_3$; Curve IV, ErI_3.

In addition to these common features curve IV possesses an extra peak at 5.4 A.

The remarkable similarity of the curves leads inevitably to the conclusion that we are dealing with a system in which a large part is held in a configuration that is stable and in the main independent of concentration. This observation is in qualitative agreement with the equivalent insensitivity of the spectra to concentration changes. It will be seen that the evaluation of the peak areas will give quantitative support to this observation.

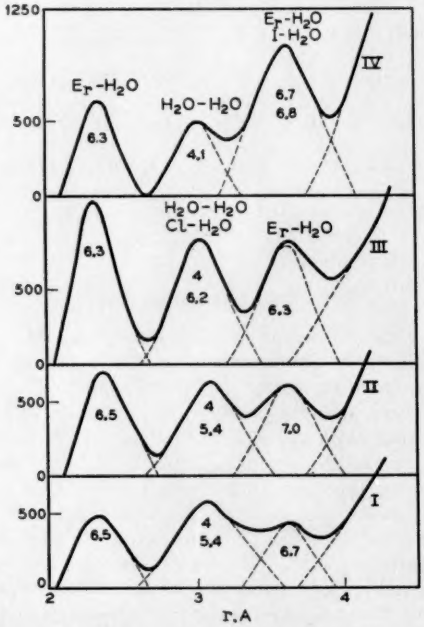

FIG. 2. Part of the radial distribution curves of Fig. 1 showing resolution of peaks out to 4 A.

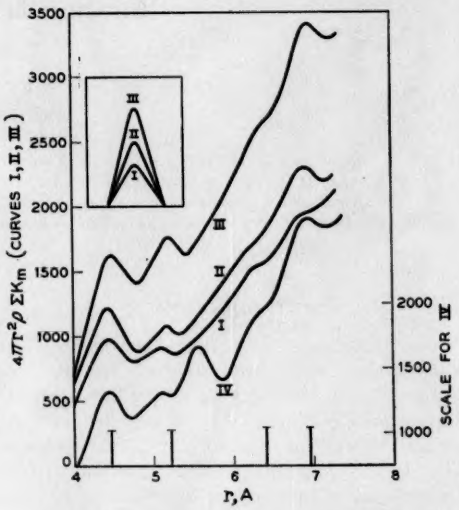

FIG. 3. Part of the radial distribution curves of Fig. 1 showing outer peaks. The vertical lines along the abscissa are the positions of ice peaks.

To facilitate discussion we divide the curves in Fig. 1 into two parts; the first, which covers the range of the first three peaks in the distribution function is shown in Fig. 2. The remainder, showing longer range order is shown in Fig. 3. But before leaving Fig. 1 we can attempt to identify the interaction which results in the large peak at 4.6 A. From the large area it is safe to conclude that Er^{3+}, because of its high atomic number, is a contributor to the peak. Most significant, however, is the fact that the peak moves out a distance ~0.7 A when the Cl^- is substituted by the I^-, indicating that the anion is also involved in the interaction. Thus the first fact established is that there is ion-pairing present to a large degree in the solutions and presently when we establish a model this factor will figure prominently in the discussion.

TABLE I. Nearest and next-nearest neighbor numbers.

n_1, Er—H_2O;

n_2, CL—H_2O;

n_3, Er—2nd H_2O.

Solution	n_1	n_2	n_3
I	6.5	5.4	6.7
II	6.5	5.4	7.0
III	6.3	5.9	6.3
IV	6.3		6.7[a]

[a] Determined by averaging.

We proceed next to a consideration of Fig. 2. Since 2.3 A is the sum of the radii of Er^{3+} and H_2O, we can immediately identify the first peak as resulting from an Er^{3+}—H_2O interaction. The area of the peak will be given by

$$C(2\times K_{Er^{3+}}\times K_O\times n_1),$$

where C is the mole fraction of Er^{3+}, $K_{Er^{3+}}$ and K_O are the effective electron numbers assigned to the respective species, and n_1 is the coordination number of the H_2O molecules around the Er^{3+}. The values of n_1 determined in this way are given in the second column of Table I. It is seen that within experimental error the number is six, indicating that the nearest neighbor configuration around the cation is octahedral. While it is not safe to attach quantitative significance to the peak widths in radial distribution curves, because these are determined to a large extent by experimental conditions and arithmetical details, it is safe to say that the relative sharpness of the peaks compares favorably under the same experimental and arithmetical conditions with that of $FeCl_3$ where one is dealing with actual complex ions. Thus the first hydration sheath is very firmly held to the ion.

We return now to the previous observation that ion-pairing is present. By analogy with Eu^{3+} we can take the field symmetry[4] around Er^{3+} as D_{2h}, which is not consistent with the O_h symmetry of the octahedral H_2O cage. However, when two Cl^- or I^- ions are placed in the center of two edges as shown in Fig. 4, we arrive at a model with the correct symmetry. Even more gratifying, when we construct the model to scale, using as radii for Er^{3+}, Cl^-, I^-, and H_2O the values 0.9, 1.8, 2.2, and 1.4, respectively, the Er^{3+}—Cl^- distance turns out to be 4.6 A, in perfect agreement with the distance to the peak maximum in the radial distribution curve. The analogous Er^{3+}—I^- distance is 5.2 A, slightly less than the peak distance of 5.4 determined from the distribution curve, but this slight difference can easily be accounted for on polarization grounds alone. To the author's knowledge this is the first direct determination of the configuration of an ion-pair complex, and sheds light on the old question as to whether the ion pair touches, or whether the hydration sheath separates the two. In the Er^{3+} solutions at least, the latter appears to be the case. From the spectral data which indicates an insensitivity to concentration we can also conclude that a portion of the peak at ~4.6 A in all the $ErCl_3$ curves will result from this complex. This allows us then to calculate an area which may be applied to the curves as a correction, and thus allow us to determine more accurately other interactions whose peaks occur in this region.

The next two peaks in the distribution curves can be solved by the procedure shown in Fig. 2, where, by extending the left-hand side of the curve at ~4.0 A down to the axis, we get a good resolution of the right-hand side of the peak whose maximum occurs at 3.6 A. The

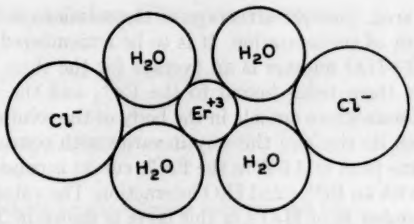

FIG. 4. Planar model of the environment around Er^{3+}. There is an H_2O directly above and below the Er^{3+}.

left side of this peak is then drawn in symmetrically with the right and this then allows resolution of the peak whose maximum lies at ~3–3.1 A. When it comes to determining which interactions give rise to these peaks we must consider from chemical knowledge what spacings to anticipate in these regions. There will certainly be $Cl^-H_2O_3$ and I^-—H_2O interaction distances at 3.2 A and 3.6 A, respectively. We can see this latter peak beautifully displayed in curve IV of Fig. 2, where the peak at 3.6 A (present in all the curves) has more than twice the area of the peak in curve II, although the concentrations are nearly the same. However, the expected Cl^-—H_2O interaction at 3.2 A will be confounded with peaks resulting from H_2O—H_2O distances in both the first hydration layer and in the rest of the solution. From the model in Fig. 4, we can determine that the H_2O—H_2O distance in the first layer is ~3.2 A. In the rest of the solution we anticipate that the distance will be ~2.95 A. Thus the second peak at ~3.05 A (in curves I, II, and III) will be made up of contributions from these three interactions while in curve IV it will include only the H_2O—H_2O interactions. Curve IV can then be used to measure these interactions. The area will be given by

$$0.022\times K_O^2\times n_h+0.917\ K_O^2\times n_s$$

where $K_O=6.6$ is the effective number of electrons of O, n_h is the nearest neighbor number of O's in the first layer and n_s is the corresponding number in the rest of the solution. It can be determined that $n_h=4$ from the octahedral arrangement of the waters in the first layer and we can then directly determine that $n_s=4.1$. Thus the structure of the solvent is tetrahedral, in fact even more so than in pure H_2O where the measured number is 4.6. This result was anticipated qualitatively from the general sharpness of the peaks, and as will be discussed later, is confirmed by the general features of the distribution curves in Fig. 3. With this H_2O—H_2O nearest neighbor number then determined from the ErI_3 curve we can compute the areas resulting from this interaction for the $ErCl_3$ solutions, subtract them from the peak with maxima at 3.05 A and thus determine the Cl^-—H_2O nearest neighbor number, n_2. These figures are given in Table I and shown in Fig. 2. It is seen that there results a fairly constant value for this number indicating, as in the constancy of the first

peak area, that the structure of the solutions is independent of concentration. It is to be remembered that the Cl—H_2O number is an average for the three Cl's, two of them being bound to the Er^{3+}, and the third found somewhere outside in the body of the solution.

From its size and the way it varies with concentration, the peak at 3.6 A in the $ErCl_3$ curves is consistent only with an Er^{3+}—2nd H_2O interaction. The values for the number n_3 of H_2O's in this layer is shown in Table I. The values range from 6.3 to 7.0. The accuracy of the procedure used to separate the peaks could easily account for this variation. Examination of the values in the table shows that in solution I, n_2 is slightly higher than in solutions II and III, and n_3 is slightly lower. This suggests that the apportionment of area between the second and third peak may be in some doubt in solution I, and that no physical significance can be attached to the slight variations in the table.

Finally, we can determine a value, n_4, for the I^-—H_2O interaction by subtracting the average value of n_3 from the area of the third peak in curve IV. This results in a value of 6.8 for n_4, subject to the same conditions as those discussed in the n_2 case, that is that it is a mean value for both kinds of I^-'s, those in the ion-paired configuration, and the free one.

The model shown in Fig. 4 illustrates how the solvents and solute combine to take account of the entry into the solvent of a highly charged species. The orientation of the H_2O in the first layer[1] is such that the two negative charge clouds of the molecule point toward the central Er^{+3}, thus constraining the two O—H bonds to point outward. Free rotation of the H_2O's around their dipolar axis is allowed, and thus when the Cl^- ions occupy their positions in the octahedral edge (Fig. 4) the H_2O's in the plane containing the Cl^-'s will have one of their O—H bonds oriented toward the anion. The result of this will be that only one OH bond will be available for bond formation with the second hydration layer. The two other H_2O's in the octahedron will not be affected in this way, and both O—H bonds will point outward. In sum there will thus be eight free bonds to be saturated by the molecules in the second layer. It is of interest that the measured number of H_2O's in the second layer is ~7. Within the accuracy of the extrapolation procedure used to resolve the peak, this is in close agreement with the number of free bonds available.

In Fig. 3 the outer part of the distribution curves is shown. Calculated peaks resulting from the Er^{3+}—Cl^- interaction are shown in the insert. The effect of subtracting these areas from the curves I, II, and III of Fig. 1 results in a development of two peaks in the curves in the region between 4 and 5.5 A. These two peaks are already present in the ErI_3 curve IV. Further inspection shows a pronounced shoulder at ~6.4 A and a well-defined peak at ~6.9 A. The peaks become less pronounced as one goes to less concentrated solutions.

For comparison the spacings for ice are shown as vertical lines along the abscissa, and it can be seen that the peaks in the distribution curves occur precisely at these distances in the three $ErCl_3$ solutions and in the ErI_3 solution. These peaks are not present in the distribution curve for pure water.[10] Thus direct evidence for a high degree of icelikeness in these solutions is supplied. This observation is in accord with the concept of structural temperature introduced by Bernal and Fowler.[11] The strong local potential fields of the ions remove much of the internal motion of the solvent and constrain it to assume a configuration appropriate to another structural temperature. In some solutions the structural temperature is raised because the solvent structure is too badly disrupted by having to incorporate ions of large size and low field. In the present case, the overwhelming effect is an ordering one and the temperature is lowered. We could speculate also that the highly oriented region around the ion could act as a nucleus for the formation of pseudocrystals of ice, and ascribe a two-phase structure to the system, with actual crystallities present in the solution, but the x-ray results do not allow us to make this claim unambiguously because the resolution is not good enough to do a more detailed analysis in this region. For the same reason it is not possible to measure a structural temperature because of interference from the many other interactions present which have the effect of producing a large background in the distribution curves in the region of the ice peaks.

To conclude, these findings are in excellent agreement with Freed's spectral measurements. The displacement of lines on each side of the electronic spectrum of the Eu^{3+} ion in his experiments was indeed due, as he observed, to interaction with the pseudocrystalline lattice of the solvent environment, which is of a highly ordered nature.

ACKNOWLEDGMENTS

The programing of the Fourier transformation was done by W. J. Romanow; M. Tanenbaum and K. Knox contributed valuable discussion. Their assistance is gratefully acknowledged.

[10] J. Morgan and B. E. Warren, J. Chem. Phys. **6**, 666 (1936).
[11] J. D. Bernal and R. H. Fowler, J. Chem. Phys. **1**, 515 (1933).

Partition Function Ratios for Molecules Containing Nitrogen Isotopes*

G. M. BEGUN,
Chemistry Division, Oak Ridge National Laboratory, Oak Ridge, Tennessee
AND
W. H. FLETCHER,
Chemistry Department, University of Tennessee, Knoxville, Tennessee

(Received May 13, 1960)

Nitrogen isotopic partition function ratios have been calculated for the following molecules and ions: N_2, N_2O, NO, NOCl, NO_2, NO_2^-, NO_3^-, and N_2O_4. All available isotopic and anharmonic data have been used, and values of Q^{15}/Q^{14} are tabulated for temperatures at intervals from 100°K to 600°K. Isotopic equilibrium constants calculated from the partition function ratios are compared with those that have been observed experimentally.

INTRODUCTION

UREY and Rittenberg[1] first calculated isotopic exchange equilibrium constants from spectral data, and Urey[2] has presented extensive calculations for various molecules. These calculations are made from the fundamental vibrational frequencies of the molecules involved, the shift of these frequencies with isotopic substitution, and the anharmonic constants of the molecule. Very little data on isotopic frequency shifts were available when the original calculations were made, and most of the isotopic frequencies were estimated from the normal vibration frequencies. For simple diatomic molecules, the isotopic shifts may be calculated with a high degree of accuracy, but as the molecule becomes more complex this procedure becomes less exact. Recently a considerable amount of isotopic data involving molecules containing N^{15} has become available in this laboratory and elsewhere, and new partition function ratios have been calculated which are believed to be more exact. Although the deviations from the earlier values are often not large, the effects become appreciable in the calculation of isotopic equilibrium constants where one partition function ratio is divided by another to obtain a factor which is very close to 1.

THEORY

The formula given by Urey[2] and Bigeleisen and Mayer[3] for the partition function ratio of two isotopic molecules is

$$Q_2\sigma_2/Q_1\sigma_1=\prod_i \frac{u_{2i}\exp(-u_{2i}/2)[1-\exp(-u_{1i})]}{u_{1i}\exp(-u_{1i}/2)[1-\exp(-u_{2i})]}. \quad (1)$$

The equilibrium constant for the exchange reaction between the compound or species under consideration and the separated atoms is Q_2/Q_1 where 1 and 2 refer to the different isotopic species, σ_1 and σ_2 are the symmetry numbers, $u_i=hc\omega_i/kT$, and ω_i is the ith normal vibrational frequency. This expression is rigorously correct at ordinary temperatures for a rigid-rotator harmonic-oscillator. Since the real systems always involve some anharmonicity which precludes an exact treatment of most molecules, the following procedure (which yields as accurate a result as can be obtained) was used. Zero- order frequencies, where known, were used to evaluate the factor u_{2i}/u_{1i}. This choice was made because this quotient was introduced into the formula by use of the Teller-Redlich product rule which holds rigorously[4] for zero-order frequencies. The factor $\prod_i \exp(-u_{2i}/2)/\exp(-u_{1i}/2)$ involving the actual zero point energy difference was evaluated accurately from anharmonic data where such data were available. In the factors $[1-\exp(-u_i)]$, the observed vibrational frequencies were used in the calculation. For isotopic molecules, observed isotopic data have been used except in the case of N_2^{15} and $N^{14}N^{15}$ where calculated values are quite accurate.

The use of the data in this fashion yields a result which is rigorously correct for ideal gaseous molecules at normal temperatures as far as the rotation, translation, and zero-point energy contributions to the partition functions are concerned. The result is not precise as far as the vibrational contribution is concerned. Sample calculations for nitrogen and nitric oxide taking into account higher anharmonic correction terms, the effects of centrifugal distortion and vibration rotation interaction,[4] however, showed that even at 600°K no change in the partition function ratios by such corrections was produced in the fourth decimal place. There exists no rigorously derived expression to take into account the anharmonicity in polyatomic molecules, but it is doubtful that such corrections here would do more than slightly affect the fourth decimal place in the partition function ratio. A small correction in the fourth decimal place was made for nitrogen and nitric oxide at 100 and 200°K because of a very slight departure from classical behavior in the rotational motion. This correction was negligible for the other molecules.

The spectral data used in the calculations are summarized in Tables I and II along with references to the sources. For molecules reported in Table I, anharmonic

* This paper is based on work performed for the U. S. Atomic Energy Commission by Union Carbide Corporation.

[1] H. C. Urey and D. Rittenberg, J. Chem. Phys. **1**, 137 (1933).
[2] H. C. Urey, J. Chem. Soc. **1947**, 562.
[3] J. Bigeleisen and M. G. Mayer, J. Chem. Phys. **15**, 261 (1947).
[4] G. Herzberg, *Molecular Spectra and Molecular Structure* (D. van Nostrand Company, Inc., Princeton, New Jersey, 1950), Vol. I.

TABLE I. Data for molecules for which exact constants were used (cm^{-1}).

Molecule	Zero-order frequency ω_i	Observed frequency ν_i	Zero point energy ϵ_0	Reference
$N^{14}N^{14}$	2359.6	2330.7	1176.2	a
$N^{14}N^{15}$	2320.1	2292.1	1156.5	b
$N^{15}N^{15}$	2279.8	2252.8	1136.5	b
$N^{14}O$	1904.03	1876.11	948.52	c
$N^{15}O$	1869.98	1843.05	931.62	d
$N^{14}N^{14}O$	1300.3 596.5 2276.9	1285.5 588.8 2223.9	2368.18	e
$N^{14}N^{15}O$	1295.6 582.8 (2) 2228.6	1281.0 575.6 (2) 2177.6	2328.59	e
$N^{15}N^{14}O$	1285.1 593.2 (2) 2254.5	1220.6 585.6 (2) 2202.5	2346.38	e
$N^{15}N^{15}O$	1280.3 578.9 (2) 2206.3	1266.1 571.9 (2) 2156.2	2306.19	e
$N^{14}OCl$	1842.6 626.8 340.8	1800.0 595.5 332.4	1393.83	f
$N^{15}OCl$	1810.1 610.8 339.0	1769 581.5 330.6	1369.05	f
$N^{14}O_2$	1357.8 756.8 1665.5	1318.0 749.8 1617.8	1873.30	g
$N^{15}O_2$	1342.5 747.1 1628.0	1306.0 740.2 1580.3	1842.63	g

[a] See footnote 4.
[b] Calculated.
[c] J. H. Shaw, J. Chem. Phys. **24**, 399 (1956).
[d] W. H. Fletcher and G. M. Begun, J. Chem. Phys. **27**, 579 (1957).
[e] G. M. Begun and W. H. Fletcher, J. Chem. Phys. **28**, 414 (1958).
[f] L. Landau and W. H. Fletcher, J. Mol. Spectroscopy **4**, 276 (1960).
[g] E. T. Arakawa and A. H. Nielsen, J. Mol. Spectroscopy **2**, 413 (1958).

TABLE II. Observed fundamental frequencies (cm^{-1}).

Species	Observed frequency (ν_i) N^{14}	N^{15}	Reference
NO_2^-	1326 808 1232	1305 805 1208	a
NO_3^-	1049.2 830.9 1375.6 (2) 716.8 (2)	1049.2 809.0 1343.7 (2) 714.8 (2)	a
N_2O_4	1380 808 266 150 1712 482 429 672 1748 381 1262 750	1360 797 264 150 1672 478 420 654 1707 380 1251 739	b

[a] G. M. Begun, aqueous measurements made in this laboratory.
[b] G. M. Begun and W. H. Fletcher, J. Mol. Spectroscopy **4**, 388 (1960).

data were available, while only observed frequencies are known for those in Table II. For the latter molecules, the partition function ratios are less accurate. Table III gives the partition function ratios calculated for the various species at selected temperatures. These numbers Q^{15}/Q^{14} are the equilibrium constants for the exchange reaction between the separated atoms and the species in question. To calculate the isotopic separation factor between any two of the species listed, the Q_2/Q_1 values for the two species should be divided. The free atoms thus cancel out. The N^{15} tends to concentrate in the species with the largest Q_2/Q_1 ratio.

DISCUSSION

Calculations of partition function ratios for molecules containing nitrogen have been made previously by

TABLE III. Partition function ratios for molecules containing nitrogen isotopes.

$T°K$	$\frac{N^{15}O_3^-}{N^{14}O_3^-}$	$\left(\frac{N_2^{15}O_4}{N_2^{14}O_4}\right)^{\frac{1}{2}}$	$\frac{N^{15}N^{15}O}{N^{15}N^{14}O}$	$\frac{N^{14}N^{15}O}{N^{14}N^{14}O}$	$\frac{N^{15}N^{15}O}{N^{14}N^{15}O}$	$\frac{N^{15}N^{14}O}{N^{14}N^{14}O}$	$\frac{N^{15}O_2}{N^{14}O_2}$	$\frac{N^{14}N^{15}}{N_2^{14}}$	$\left(\frac{N_2^{15}}{N_2^{14}}\right)^{\frac{1}{2}}$	$\frac{N^{15}O_2^-}{N^{14}O_2^-}$	$\frac{N^{15}OCl}{N^{14}OCl}$	$\frac{N^{15}O}{N^{14}O}$
100	1.7613	1.6850	1.6557	1.6457	1.3323	1.3243	1.4834	1.3043	1.3074	1.3579	1.3605	1.2521
200	1.2764	1.2505	1.2437	1.2413	1.1350	1.1328	1.1900	1.1324	1.1336	1.1427	1.1412	1.1089
273.16	1.1727	1.1580	1.1557	1.1546	1.0884	1.0874	1.1226	1.0905	1.0913	1.0915	1.0910	1.0736
298.16	1.1506	1.1383	1.1372	1.1360	1.0783	1.0772	1.1079	1.0811	1.0818	1.0803	1.0801	1.0656
400	1.0935	1.0873	1.0884	1.0881	1.0510	1.0507	1.0690	1.0553	1.0557	1.0506	1.0514	1.0438
500	1.0638	1.0604	1.0623	1.0628	1.0355	1.0360	1.0479	1.0406	1.0409	1.0348	1.0358	1.0315
600	1.0461	1.0441	1.0462	1.0464	1.0267	1.0269	1.0351	1.0311	1.0313	1.0252	1.0262	1.0237

Urey,[2] Leifer,[5] Bigeleisen and Friedman,[6] McCrea,[7] Spindel,[8] Weston,[9] Weston and Brodasky,[10] and Schaeffer.[11] Detailed examination where comparisons are possible shows that most of the differences in the ratios are in the third and fourth decimal places in the case of the simple (N_2, NO, N_2O) molecules. With the more complex molecules, deviations are somewhat larger because of differences in frequency data. We believe that our selections in the case of NO_2^- and NO_3^- are the closest to the actual conditions of these ions in aqueous solution that can be made at present.

A commonly used formula for the calculation of isotopic partition function ratios is that derived by Bigeleisen and Mayer,[3]

$$(Q_2/Q_1)(\sigma_2/\sigma_1)=1+\sum_i G_i\Delta u_i \qquad (2)$$

where $G_i=\{\frac{1}{2}-(1/u_{2i})+1/[\exp(u_{2i}-1)]\}$ and $\Delta u_i=u_{1i}-u_{2i}$. The subscript 2 denotes the heavy isotope and i is summed over all of the vibrational frequencies. A few examples of differences encountered in using the G function or in using observed frequencies only are given in Table IV. The greatest part of the difference arises in the zero point energy term which cannot be predicted reliably with a harmonic potential function. The G function will suffice for many estimates of isotopic fractionation, but for precise calculations isotopic frequencies and anharmonic data can be quite valuable.

TABLE IV. Partition function ratios at 298.16°K.

	G function with obs. frequencies	Eq. (1) with obs. frequencies only	Eq. (1) with anharmonic data
$\frac{N^{15}O}{N^{14}O}$	1.0618	1.0640	1.0656
$\frac{N^{15}N^{14}O}{N^{14}N^{14}O}$	1.0727	1.0756	1.0773
$\frac{N^{15}O_2^-}{N^{14}O_2^-}$	1.0770	1.0803	
$\frac{N^{15}O_3^-}{N^{14}O_3^-}$	1.1372	1.1506	

[5] E. Leifer, J. Chem. Phys. **8**, 301 (1940).
[6] J. Bigeleisen and L. Friedman, J. Chem. Phys. **18**, 1656 (1950).
[7] J. M. McCrea, J. Chem. Phys. **19**, 48 (1951).
[8] W. Spindel, J. Chem. Phys. **22**, 1271 (1954).
[9] R. E. Weston, J. Chem. Phys. **26**, 1248 (1957).
[10] R. E. Weston, T. F. Brodasky, J. Chem. Phys. **27**, 683 (1957).
[11] R. Schaeffer, Semi-Annual Summary Report in Chemistry, Iowa State College, ISC-976, p. 28 (March 15, 1958).

TABLE V. Observed and calculated separation factors.

Exchange		Temp. °K	Calculated α	Measured α	Reference
$N^{15}O+N^{14}O_3^-$	$\rightleftarrows$	298	1.080	1.073	a
				1.065	b
$N^{15}O_2+N^{14}N^{14}O_4$	$\rightleftarrows$	298	1.027	1.023	c
$N^{15}O+N^{14}O_2$	$\rightleftarrows$	298	1.040	1.028	d
$N^{15}O+N^{14}OCl$	$\rightleftarrows$	223	1.024	1.013	e
		298	1.014	1.005	f

[a] Kauder, Taylor, and Spindel, J. Chem. Phys. **31**, 232 (1959).
[b] L. L. Brown and G. M. Begun, J. Chem. Phys. **30**, 1206 (1959).
[c] G. M. Begun, J. Chem. Phys. **25**, 1279 (1956).
[d] G. M. Begun and C. E. Melton, J. Chem. Phys. **25**, 1292 (1956).
[e] L. B. Yeatts, Jr., J. Chem. Phys. **28**, 1255 (1956).
[f] See footnote 11.

Table V contains the comparable published values for the cases where the separation factor has been reported along with the values calculated from Table III. As can be seen, the agreement is far from good. At the present stage of experimental work, the separation factors for gaseous molecules can be calculated considerably more accurately than they can be measured. For condensed phases and ionic species in solution, the molecules can no longer be regarded as perfect gases and differences between observed and calculated values can be expected to exist. The isotopic fractionation between NO and NO_3^- ion may be such a case as the equilibrium constant has been measured several times by different investigators and good agreement obtained between the different sets of experimental data. The question always arises as to whether the species for which the equilibrium constant is measured are pure or mixed species. Thus the measured separation factor may be due to a combination of several equilibria. It is hoped that with better experimental methods and a better understanding of the chemical systems, closer agreement will be found between experiments and theory in the future.

X-Ray Scattering by a Cell-Model Liquid

L. H. LUND

Missouri School of Mines & Metallurgy, Rolla, Missouri

(Received October 28, 1959)

The x-ray scattering by a cellular model of a liquid is characterized in terms of a cell-center pair distribution function and a function descriptive of the cell model employed. Presented also are cell-center pair distribution functions for liquid argon as calculated by inverting the theoretical formula for the scattered intensity.

INTRODUCTION

OF the many methods that have been used for calculating thermodynamic and equilibrium properties of liquids, the cell model has been one of the most fruitful and amenable to mathematical calculation. As developed by Lennard-Jones and Devonshire,[1] Wheeler[2] and others, the assumption that each molecule moves inside a cage formed by its nearest neighbors and with negligible correlation between its motion and that of its neighbors is certainly an over-simplication. The modification of the cell model by Lennard-Jones and Devonshire to allow the molecule in its cell to move, not freely, but in a spherically symmetric potential due essentially to interaction with nearest neighbors, is a somewhat more realistic picture. After an independent determination of the parameters in the intermolecular interaction, the calculation of the partition function is relatively simple, and reasonably good agreement with experimental values of thermodynamic properties of liquids can be found.

Such a cell model can be used too in the theoretical calculation of the scattering of x rays or neutrons by liquids.[3] However, in such a treatment, it is advantageous to describe the structure of the scattering material by a cell-center pair distribution function rather than by the conventional molecular pair distribution function. In what follows, the calculation is made for the case of x-ray scattering with the molecule characterized by the atomic structure factor. The case of elastic neutron scattering would be the same except for the substitution of the neutron scattering length for the x-ray atomic structure factor.

THEORY

Let the liquid of N identical monatomic molecules be spanned by a virtual lattice of N cells each of volume Δ and consider single-cell occupancy only. Now consider the liquid to be irradiated by a collimated, monochromatic x-ray beam of wavelength λ, and let the directions of the incident and scattered beams be characterized in the usual fashion by unit vectors $\mathbf{S}$ and $\mathbf{S}_0$. Then the coherent part of the electric field scattered in the direction $\mathbf{S}$ for a particular spatial configuration of the molecules is

$$E=f\sum_{i=1}^{N}\exp(i\mathbf{k}\cdot\mathbf{r}_i), \tag{1}$$

where $\mathbf{r}_i$ is a vector from an arbitrary fixed origin to the ith atom, $\mathbf{k}=2\pi/\lambda(\mathbf{S}-\mathbf{S}_0)$ with 2θ the angle between $\mathbf{S}$ and $\mathbf{S}_0$ and the magnitude of $k=4\pi/\lambda\sin\theta$. The atomic structure factor of the molecule is f. The total scattered intensity from this configuration and for fixed $\mathbf{k}$ is

$$I(k)=f^2\sum_i\sum_j\exp(i\mathbf{k}\cdot\mathbf{r}_{ij}), \tag{2}$$

where $\mathbf{r}_{ij}$ is the vector separation of the ith and jth molecules.

Now to effect the averaging of the intensity, still for fixed $\mathbf{k}$, over all spatial configurations, let us denote the position of the jth cell by $\mathbf{R}_j$ and the position of the jth molecule relative to its cell-center by $\mathbf{r}_j$ and write

$$\langle I(\mathbf{k})\rangle=f^2\int_{\Delta_1}\cdots\int_{\Delta_N}P(\mathbf{r}_1,\mathbf{r}_2\cdots\mathbf{r}_N)\sum_{i,j}\times\exp[i\mathbf{k}\cdot(\mathbf{R}_{ij}+\mathbf{r}_i-\mathbf{r}_j)]\prod_k dv_k, \tag{3}$$

where $P(\mathbf{r}_1,\cdots\mathbf{r}_N)$ is the normalized configuration probability density for the molecular assembly and where the integrations are over the configurations accessible to the N molecules in their cells, subject to single-cell occupancy.

Evidently the simplest cell model will be one that ignores correlation effects between the motions of the molecules in their cells. Thus one can begin with

$$P(\mathbf{r}_1,\cdots\mathbf{r}_N)=\prod_{i=1}^{N}p(\mathbf{r}_i),$$

where $p(\mathbf{r}_i)$ is the normalized configuration probability density for a molecule in its cell and a function only of the distance of the molecule from its cell-center. Substitution of this product in Eq. (3) gives first

$$\langle I(\mathbf{k})\rangle=Nf^2\left\{1+\int_{\Delta_1}\int_{\Delta_s}\sum_{s=2}^{\infty}\exp[i\mathbf{k}\cdot(\mathbf{R}_{1s}+\mathbf{r}_1-\mathbf{r}_s)]\times p(\mathbf{r}_1)p(\mathbf{r}_s)dv_1dv_s\right\}, \tag{4}$$

[1] J. E. Lennard-Jones and A. F. Devonshire, Proc. Roy. Soc. (London) **A163**, 53 (1936); **A165**, 1 (1938).

[2] T. S. Wheeler, Indian J. Phys. **8**, 521 (1935); Proc. Indian Acad. Sci. **1**, 165 and 795 (1935); **2**, 1 and 466 (1936); **4**, 291 and 298 (1936).

[3] L. H. Lund, J. Chem. Phys. **21**, 1722 (1953).

where the summation extends from an arbitrary molecule labeled 1 and $\mathbf{R}_{1s}$ is the position vector of the sth molecule relative to the first. Now let us define a function $\rho_c(R)$ as the probability per unit volume of finding a cell-center at R from the first molecule and change $\mathbf{R}_{1s}$ to the continuous variable R to get

$$\langle I(\mathbf{k})\rangle = Nf^2\left[1+[X(k)]^2\int_0^\infty 4\pi R^2[\rho_c(R)-\rho_0]\exp(i\mathbf{k}\cdot\mathbf{R})dR\right],$$

with

$$X(k)=\int_\Delta p(r')\exp(i\mathbf{k}\cdot\mathbf{r}')dv', \qquad (5)$$

just the Fourier transform of $p(r)$ and integrated over the cell volume Δ. Also the usual procedure has been followed in deriving Eq. (5). The upper limit in the integration over R (i.e., the largest linear dimension of the sample) has been replaced by infinity, and ρ_0, the average number of cell centers per unit volume, has been introduced into the integrand with subsequent neglect of the ρ_0 contribution of the added compensating integral.[4] Equation (5) may now be averaged over all $\mathbf{k}$ to give

$$\langle I(k)\rangle = Nf^2\left[1+[X(k)]^2\int_0^\infty 4\pi R^2[\rho_c(R)-\rho_0]\frac{\sin kR}{kR}dR\right]. \qquad (6)$$

Thus the scattered intensity is characterized, not by the usual molecular pair distribution function $\rho(R)$, but by $\rho_c(R)$ a cell-center pair distribution function and the function $X(k)$ obviously dependent on the cell model chosen.

It is important to note that the integrations over the cells in Eq. (3), with or without correlation effects, bear a distinct similarity to the mathematics leading to the temperature-dependent e^M factor as originally introduced by Debye[5] in his theoretical treatment of the effect of thermal molecular motion on the intensity of x rays scattered by a crystal. In the Debye work, the factor, e^M, appears in the expression for the scattered intensity as the mean value of an exponential term containing the random thermal displacements of the molecules. Here, in the uncorrelated case, the function $[X(k)]^2$ appears, too, as the result of an averaging of an exponential term in the expression for the scattered intensity and appears as an averaging of the displacements of the molecules in their cells. Of course, due to the method used to handle the double sum in Eq. (3) and the independent product assumption for $P(r_1,\cdots r_N)$, the averaging for fixed R_{1s} (or R) appears as the product of two independent integrals, one the complex conjugate of the other. In the general case corresponding to correlation in the motion of the molecules such as implied in a normal mode treatment of the displacement of the molecules, one can draw on the Debye result for the average of the exponential term involving $\mathbf{r}_i-\mathbf{r}_j$ in Eq. (3). This will be done later.

Now it is possible to calculate the $[X(k)]^2$ function directly for two simple illustrative cases corresponding to no correlation.

Case 1. A Spherical cell, radius a and uniform probability so that

$$p(r)=[\tfrac{4}{3}\pi a^3]^{-1} \qquad r<a,$$
$$p(r)=0 \qquad r>a,$$

and

$$[X(k)]^2=\{[3/(ak)^3](ak\cos ak-\sin ak)\}^2. \qquad (7)$$

Case 2. An Einstein liquid with the molecule an independent isotropic oscillator of frequency $\nu=kT_E/h$, T_E=Einstein temperature, k=Boltzmann's constant, h=Planck's constant, so that

$$p(r)=\frac{\alpha}{\pi}\left[\frac{1-z}{1+z}\right]^{\frac{1}{2}}e^{-\alpha\left[\frac{1-z}{1+z}\right]r^2},$$

where

$$\alpha=4\pi m\nu/h, \qquad z=\exp(-h\nu/kT),$$

with m the mass of the molecule and T the absolute temperature of the substance, and

$$[X(k)]^2=e^{\frac{-k^2h\coth(h\nu/2kT)}{8\pi^2m\nu}}. \qquad (8)$$

{Here, the k^2 in the exponential is $[4\pi/\lambda]^2\sin^2\theta$, not Boltzmann's constant.[2]}

Case 3. In reality, the molecules are not truly independent, and one might improve the liquid model by assuming the displacement of a molecule in the liquid from its equilibrium site to be a superposition of normal modes approximately as in the case of the corresponding solid. The average of the exponential term for fixed $\mathbf{R}_{ij}$ in Eq. (3) involving $\mathbf{r}_i-\mathbf{r}_j$ has been evaluated by Debye for such a crystal model, and one can thus write at once

$$\langle I(k)\rangle = Nf^2\left[1+e^M\int_0^\infty 4\pi R^2[\rho_c(R)-\rho_0]\frac{\sin kR}{kR}dR\right], \qquad (9)$$

where

$$-M=\frac{12h^2}{mkT_D}\frac{\sin^2\theta}{\lambda^2}\frac{\phi(x)}{x}. \qquad (10)$$

Here h is Planck's constant, m the mass of the molecule, k Boltzmann's constant, T_D is the Debye temperature of the crystal, x is equal to T_D/T, where T is the absolute temperature of the crystal, and $\phi(x)$ is a function of x defined by

$$\phi(x)=\frac{1}{x}\int_0^x\frac{ydy}{e^y-1}.$$

[4] N. S. Gingrich, Revs. Modern Phys. 15, 90 (1943).
[5] P. Debye, Ann. Physik 43, 39 (1914).

Equation (10) is Debye's approximate function[6] (with correction factor of "2" as found by Waller)[7] and valid at all temperatures. It is, of course, strictly applicable to the thermal effect (ignoring zero-point energy) in a crystal containing identical atoms on the lattice corners of a simple translatory cubic lattice. Considering, however, the cellular model of the liquid and the isotropy around any cell in the liquid, the above expression for $-M$ is at least approximately true for the liquid.

Finally, to conclude this section, it is interesting to consider the case where correlation is presumed to be present between cell centers. It will be useful here to consider a "Debye" model in which the vector separation of two atoms is equal to the vector separation of the cell centers about which they oscillate plus a vector Gaussianly distributed about their separation. The average implied in Eq. (3) over $\mathbf{r}_i-\mathbf{r}_j$ for fixed $\mathbf{R}_{ij}$ now gives, after averaging over all vector $\mathbf{k}$

$$I(k) = Nf^2\left[1+\int_0^\infty \exp[-\beta^2(R)]4\pi R^2[\rho_e(R)-\rho_0]\frac{\sin kR}{kR}dR\right], \tag{11}$$

where $\beta^2(R)$ is the average of the square of $\mathbf{r}_i-\mathbf{r}_j$ and has been calculated by Frenkel[8] as

$$\beta^2(R) = \frac{VkT}{N m\pi^2 v^2}\left[k_{\max}-\frac{1}{R}\int_0^{k_{\max}R}\frac{\sin u}{u}du\right], \tag{12}$$

with V the volume, v the velocity of the normal vibrations and $k_{\max}\cong 1/2D$ with D approximately the average spacing between atoms.

APPLICATION

It is clear that in this last expression for the intensity one cannot extricate $\rho_e(R)$ from the integral by the usual Fourier integral inversion procedure, and that now one would have to solve the integral equation for $\rho_e(R)$ by other means. However, for example, from Eq. (6), one has at once by the Fourier inversion theorem

$$\rho_e(R)-\rho_0 = \frac{1}{2\pi^2 R}\int_0^\infty \frac{G(k)k}{[X(k)]^2}\sin kR dk, \tag{13}$$

with

$$G(k) = [I(k)/Nf^2]-1,$$

and one can calculate $\rho_e(R)$ for the uncorrelated model from known experimental scattering data. The presence of $[X(k)]^2$ in the denominator of the integral, however, presages the appearance of a certain phenomenon in the calculations and a few remarks should be made concerning this point. Just as in the Warren and Gingrich[9] procedure which multiplies the intensity curve by $1/f^2$ thereby increasing considerably the resolving power, but also increasing the diffraction effect, one can expect a similar diffraction effect here due to the appearance of $[X(k)]^2$ in the denominator of the integrand of Eq. (13). The difficulty lies, of course, in the fact that one does not truly use infinity as an upper limit in Eq. (13) but must use a k corresponding to the largest scattering angle for which the coherent scattering is discernable. The diffraction effect is due to the sharp "edge" in the intensity function which, in effect, terminates a Fourier series while the terms are yet appreciable. This effect was noted and examined in the case of crystal structure determination, for example, by Bragg and West[10] among others, and an exponential convergence factor was used by Havighurst[11] to hasten the convergence of such terminated Fourier series employed in crystal structure determination. Recently, Thompson and Gingrich[12] in their determination of atomic distribution curves for liquid sulfur, have employed an exponential convergence factor in the integrand of the Fourier inversion integral analogous to Eq. (13).[13] C. Finbak[14] has demonstrated, using liquid mercury at -38°C and liquid tin at 280°C, how several types of systematic errors lead to the appearance of specious peaks in the atomic distribution functions of these liquids. More relevant to the case where absorption errors are less important and incorrect adjustment of the experimental intensity curve less likely, Finbak's second paper shows the subsidiary peaks observed in the distribution curves for a series of liquids to be spurious. Removal of these false peaks shows the distribution curves for the series to be remarkably similar and relatively simple in shape. Some of the error introduced in these distribution functions was shown to have arisen from the fact that an error in a narrow interval of the intensity curve, e.g., an extraordinarily large maximum, introduces a periodic term in the Fourier transform and thus a sequence of small periodic maxima of equal amplitude. The diffraction effect of a cutoff in the intensity also contributed to the error in these distribution curves.

[6] See footnote reference 5 Eq. (56).
[7] I. Waller, Z. Physik **17**, 398 (1923); Dissertation, Uppsala University, Uppsala, Sweden (1925).
[8] J. Frenkel, *Kinetic Theory of Liquids* (Dover Publications, New York, 1955), p. 124. Actually Eq. 12 as given by Frenkel is incorrect and should be divided by $8\pi^3$.
[9] B. E. Warren and N. S. Gingrich, Phys. Rev. **46**, 368 (1934).
[10] W. L. Bragg and J. West, Phil. Mag. **10**, 823 (1930).
[11] R. J. Havighurst, Proc. Natl. Acad. Sci. U. S. **XI**, 489 (1925).
[12] C. W. Thompson and N. S. Gingrich, J. Chem. Phys. **31**, 6 (1959).
[13] This problem of convergence is not restricted to x-ray scattering by liquids and gases. A complete and important reference concerning convergence problems in electron diffraction by gases is that by J. Waser and V. Schomaker, Revs. Modern Phys. **25**, 671 (1953). A discussion of the modification of the experimental intensity function in the case of x-ray scattering by amorphous solids and liquids along with some relevant references may be found on page 680 of this same reference. A summary of convergence problems in Fourier series determination of crystal structure may be found in J. Lipson and W. Cochran, *The Determination of Crystal Structures* (G. Bell and Sons, London, 1953).
[14] C. Finbak, Acta Chem. Scand. **3**, 1279 and 1293 (1949).

A somewhat more mathematical approach due to Sugawara[18] has shown that when the main peaks in the liquid atomic distribution function are diffuse, the error involved in cutting the intensity function in the usual Fourier-inversion for the liquid distribution function to be relatively small. False detail appears when some of the peaks are sharp. Thus the effect would be expected to be small for a monatomic liquid such as argon and perhaps large for a liquid of polyatomic molecules. Nevertheless, all of the foregoing indicates the strong possibility of the introduction of spurious maxima into the calculation of $\rho_e(R)$ from inversion of the experimental scattering data. That the $\rho_e(R)$ may be expected to be more sharply delineated than the usual $\rho(R)$ is considered in the Appendix and the "smoothing" of $\rho_e(R)$ to give $\rho(R)$ is shown in some detail. One, however, can note that a connection between the integral defining $\rho_e(R)$ in Eq. (13) and in integral involving $\rho(R)$ may be succinctly brought out by writing this equation in a form so that the usual Fourier convolution theorem may be employed. Thus

$$4\pi R^2\rho_e(R) = \int_0^\infty Y(k)G(k)\,\exp(-i\mathbf{k}\cdot\mathbf{R})\,dk$$

$$= \int_0^\infty 4\pi l^2\rho(l)\,y(R-l)\,dl, \quad (14)$$

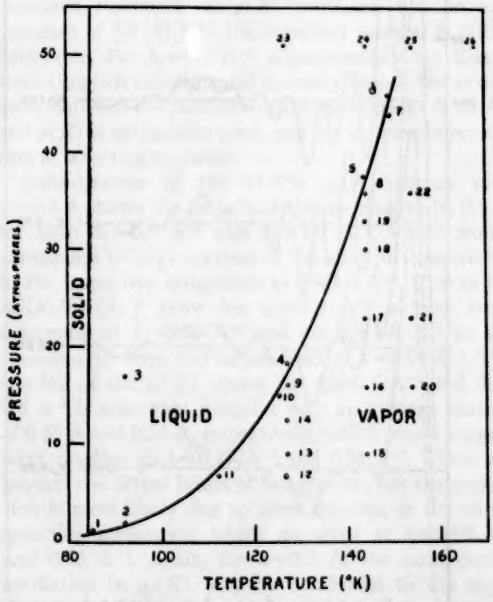

FIG. 1. P–T diagram for argon with data points corresponding to x-ray scattering patterns.

[18] T. Sugawara, Sci. Repts. Research Inst. Tohoku Univ. **A3**, 39 (1951).

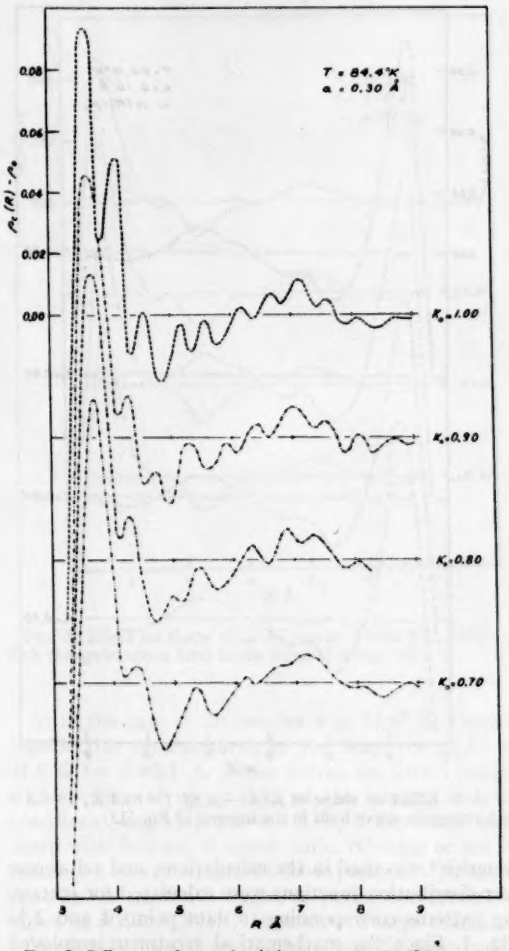

FIG. 2. Effect on shape of $\rho_e(R)-\rho_0$ at $T=84.4°$K $a=0.1$ A with change in upper limit in the integral of Eq. (13).

with $Y(k)=1/[X(k)]^2$, $y(R-l)$ the Fourier transform of $Y(k)$ and $G(k)$ the experimentally known intensity function whose Fourier transform is $4\pi R^2\rho(R)$. It is clear that if $y(R-l)$ is quite sharply peaked at R the smoothing of $4\pi l^2\rho(l)$ in the integral on the right hand side of Eq. (14) is over a small interval and $4\pi R^2\rho_e(R)$ will not differ too much from $4\pi R^2\rho(R)$. Also, if one is willing to accept, for example, diffraction error already present in $\rho(R)$, previously determined by inversion of scattering data, one can readily calculate $\rho_e(R)$ starting from Eq. (14). Clearly, if $[X(k)]^2\equiv 1$, then $\rho_e(R)$ is identical with $\rho(R)$ since then $y(R-l)=\delta(R-l)$.

The uncorrelated model selected for calculation was that corresponding to uniform probability density for a molecule in the cell with $[X(k)]^2$ as given by Eq. (7). The x-ray scattering data of Eisenstein and

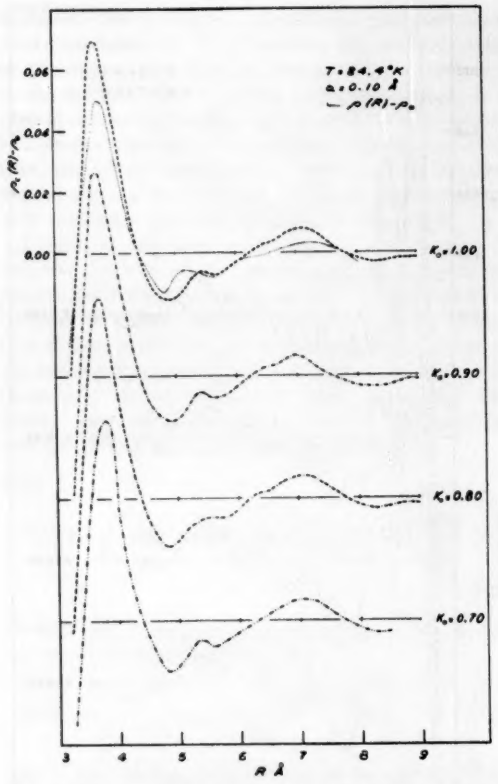

FIG. 3. Effect on shape of $\rho_e(R)-\rho_0$ at $T=84.4°K$, $a=0.3$ A with change in upper limit in the integral of Eq. (13).

Gingrich[16] was used in the calculations, and cell-center pair distribution functions were calculated for scattering patterns corresponding to data points 1 and 2 in Fig. 1. Since the mathematical treatment employed here in the cellular scattering model can be viewed as an artifice to sharpen the conventional atomic or molecular pair distribution function $\rho(R)$, the calculations were set up to examine the effect of the intensity cutoff as well as a variation in cell size on the shape of $\rho_e(R)$. Thus, the upper limit in the Fourier inversion integral was extended and Figs. 2–5 show curves corresponding to upper limits for k from $k_0=0.7$ A^{-1} to 1.0 A^{-1}. Values of a equal to 0.1 A and 0.3 A were used for each temperature and thus Figs. 2–5 show the variation of $\rho_e(R)$ due to this change in cell size. All the calculations were performed at the Missouri School of Mines and Metallurgy computer center on a Royal McBee LPG-computer.

DISCUSSION

It is convenient to consider the curves corresponding to each temperature separately. Evidently the curves for 84.4°K and with $a=0.3$ A show what certainly must be construed as a series of false peaks not indicative of real structure. The periods of the subsidiary maxima for $k_0=0.9$ A^{-1} and $k_0=1.0$ A^{-1} are 0.56 A and 0.49 A, respectively. These are the values to be expected if the corresponding function $kG(k)/[X(k)]^2$ showed a large maximum at $k=0.9$ A^{-1} and $k=1.0$ A^{-1}. Inspection of curves drawn of $kG(k)/[X(k)]^2$ indeed show large peaks at $k=0.88$ A^{-1} and $k=0.96$ A^{-1}. The spacing of the maxima occurring in the curves corresponding to $k_0=0.7$ A^{-1} and $k_0=0.8$ A^{-1} is somewhat irregular, but again is essentially that to be expected, since very large intensity maxima do occur in the corresponding integrands at $k=0.66$ A^{-1} and $k=0.74$ A^{-1}, where again $[X(k)]^2$ has become very small. Thus, it seems safe to assume that the small period oscillation shown in these cell-center distribution functions is due mostly, if not entirely, to the extremely small size of $[X(k)]^2$ at the end of the integration interval. Inspection of the 84.4° K

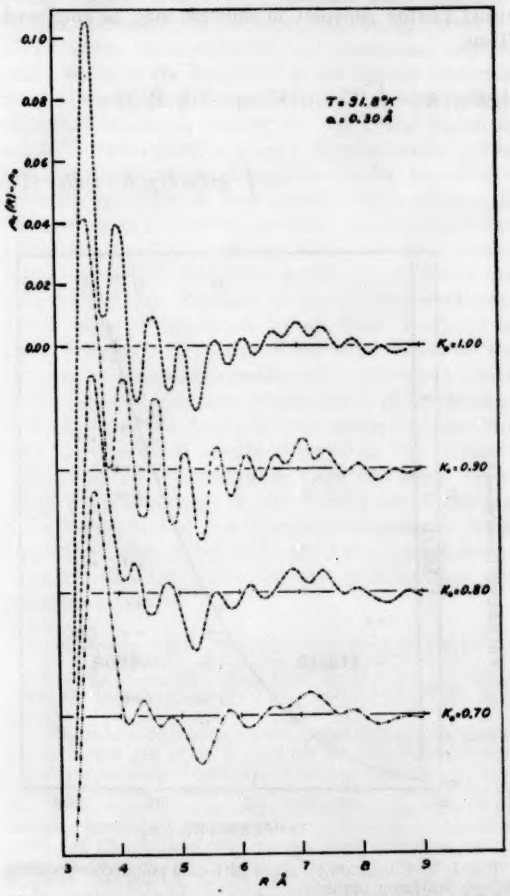

FIG. 4. Effect on shape of $\rho_e(R)-\rho_0$ at $T=91.8°K$, $a=0.1$ A with change in upper limit in the integral of Eq. (13).

[16] A. Eisenstein and N. S. Gingrich, Phys. Rev. **62**, 261 (1942).

curves for $a=0.1$ A shows what appears to be a subsidiary maximum occurring at about 5.5 A in all the curves. Numerous small-period maxima, such as occurred for $a=0.3$ A, seem to be absent. This is reasonable, since now $[X(k)]^2$ does not become as small in the range of integration as occurs in the case for the larger value of a. Inspection of curves of $kG(k)/[X(k)]^2$ show a series of peaks, but here the peaks steadily, and rather quickly, diminish as k increases. Now Sugawara[17] has shown that the positions of the most important diffraction peaks due to an edge or cutoff in the experimental intensity function are symmetrically displaced an amount $\frac{1}{2}k_0$ on either side of the main peak, where k_0 is again the upper integration limit for $\sin\theta/\lambda$. Calculation with this last equation shows that this subsidiary peak is located farther to the right of the first main peak than predicted, and further, its displacement from the first main peak is sensibly constant at about 1.75 A. It seems unlikely that this peak is a diffraction peak belonging to the second main peak. Its persistance when the upper limit of integration is extended makes it plausible to conjecture that it may be due to some error occurring at smaller k in the experimental intensity curve. Shown also with $k_0=1.0$ A^{-1} $\rho_e(R)$ curve is $\rho(R)$ as calculated by Eisenstein and Gingrich.[16] The first main peaks do not quite agree, the $\rho(R)$ first peak being at 3.75 A while the $\rho_e(R)$ first peak is at 3.65 A. The second peak for $\rho_e(R)$ appears at 7.1 A, for $\rho(R)$ at 7.2 A, and the increased resolution in $\rho(R)$ produced by the appearance of $[X(k)]^2$ in the inversion integral is fairly noticeable. For $k_0=0.7$ A^{-1}, approximately the Eisenstein-Gingrich experimental intensity cutoff, the agreement between the positions of the main peaks of $\rho_e(R)$ and $\rho(R)$ is again quite good, and the increase in resolution of structure apparent.

Consideration of the 91.8°K $\rho_e(R)$ curves with $a=0.3$ A shows the periods of the maxima to be 0.5 A for both $k_0=0.9$ A^{-1} and $k_0=1.0$ A^{-1}, which would correspond to large maxima of the kind just considered in the respective integrands at $k=1.0$ A^{-1}. Curves for $kG(k)/[X(k)]^2$ show for $k_0=0.9$ A^{-1} a very large maximum at $k=0.85$ A^{-1} and for $k_0=1.0$ A^{-1} an extraordinarily large and narrow peak at $k=0.97$ A^{-1}. The spacing of the $\rho_e(R)$ curves for $k_0=0.7$ A^{-1} and $k_0=0.8$ A^{-1} is somewhat irregular with an average spacing of 0.65 A and 0.55 A, respectively, which would suggest large maxima at $k=0.77$ A^{-1} and 0.91 A^{-1}. These are beyond the actual limits of integration, but the oscillation is most likely due to large maxima in the corresponding integrands, which do occur at $k=0.68$ A^{-1} and 0.75 A^{-1}. Again, for $a=0.3$ A, the small-period oscillation in $\rho_e(R)$ may be attributed to the rapid decrease of $[X(k)]^2$ in the integrand of the inversion integral resulting in large peaks in the integrand.

[17] See footnote reference 15.

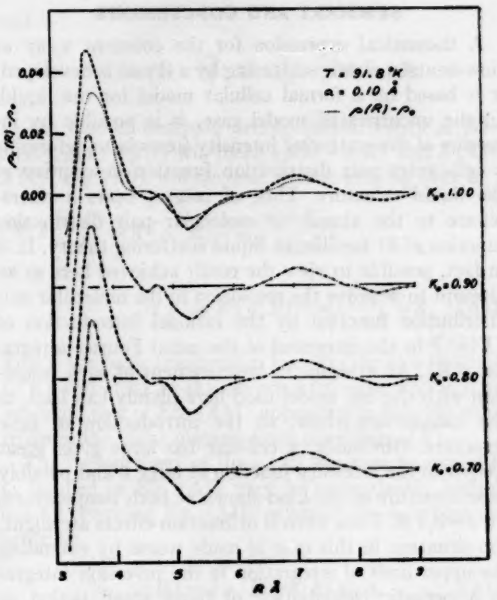

FIG. 5. Effect on shape of $\rho_e(R)-\rho_0$ at $T=91.8$°K, $a=0.3$ A with change in upper limit in the integral of Eq. (13).

As in the case of the smaller a at 84.4° K, there is considerable improvement in the shape of $\rho_e(R)$ at 91.8°K for $a=0.1$ A. These curves are little changed with increase of upper limit of the integral and the persistent peak at about 4.7 A is, if anything, more sharp with increase of upper limit. Whether or not its presence is due to an error in the experimental intensity function at smaller k would be purely conjectural. A curve of $kG(k)/[X(k)]^2$ does show a large maximum at $k=0.44$ A^{-1} which would give a periodic contribution of period 1.1 A to $\rho_e(R)$. Actually, a not too pronounced oscillation of 1.3 A is discernable for the $k_0=0.7$ A^{-1} curve along with what might be a small amplitude ripple of period 1.1 A for the $k_0=0.8$ A^{-1} and $k_0=0.9$ A^{-1} curves. Again comparison of $\rho(R)$ as calculated by Gingrich and Eisenstein with $\rho_e(R)$ for $k_0=1.0$ A^{-1} show both curves showing second main peaks at 7.05 A. The $\rho_e(R)$ first peak distance, just as in the corresponding case at 84.4°K, is somewhat smaller at 3.65 A than the 3.70 A shown by $\rho(R)$. The $\rho_e(R)$ curve for $k_0=0.7$ A^{-1}, essentially the Eisenstein-Gingrich intensity cutoff, shows the same good agreement with $\rho(R)$ with regard to peak positions and again better resolution. It could perhaps be noted that at 91.8°K with $a=0.1$ A, there is not only a maximum at 0.44 A^{-1} in $kG(k)/[X(k)]^2$ but also another maximum almost as large and sharp at $k=0.29$ A^{-1}. Thus, there is the possibility of a super-position of periodic terms giving somewhat irregular ripple in $\rho_e(R)$.

SUMMARY AND CONCLUSIONS

A theoretical expression for the coherent x-ray or slow-neutron elastic scattering by a liquid is developed; it is based on a formal cellular model for the liquid. In the uncorrelated model case, it is possible by inversion of the scattering intensity formula to determine a cell-center pair distribution function descriptive of the liquid structure. This, of course, bears a resemblance to the atomic or molecular pair distribution function $\rho(R)$ familiar in liquid scattering theory. It is in fact, possible to view the result achieved here as an attempt to improve the resolution in the molecular pair distribution function by the rational introduction of $[X(k)]^2$ in the integrand of the usual Fourier integral for $\rho(R)$. An attempt in improvement of such resolution with the cell model used here plainly can lead, as the calculations show, to the introduction of false structure. Obviously, a cell-size too large gives great weight to the intensity function at large k and possibly false structure of the kind shown at both temperatures for $a=0.3$ A. Thus, even if diffraction effects are slight, the situation in this case is made worse by extending the upper limit of integration in the inversion integral as a periodic contribution of fairly small period to $\rho_c(R)$ may be brought about by a large maximum in the integrand at large k.

Diffraction effects, due to an edge or cutoff in intensity, will be augmented by use of $[X(k)]^2$, and, of necessity, the question of the extension of the upper limit of integration becomes important. However, the diffraction effect probably will be no worse using $[X(k)]^2$, and extended upper limit, than with the original limit without $[X(k)]^2$ and the resolution quite possibly improved. This seems to be true for the calculations presented here. Using in the integrand a combination of $[X(k)]^2$ and, say, an exponential convergence factor, in order to suppress the integrand at lagre k, is a possibility not treated here. It appears that a judicious use of such a combination would be fruitful but does not seem to be worthwhile at this time. The other uncorrelated models will also present monotonic decreasing functions of k in the denominator of the integrand of the Fourier inversion integral, and results with these would be generally similar to those presented. Interesting and informative, too, would be the application of the methods here to some cases of slow-neutron elastic scattering, where the scattering extends with considerable certainty to much larger k than in the usual x-ray scattering case. Finally, in any case, it would seem that a fortuitous combination of cell-size, upper limit, and exponential convergence factor, would lead to a worth while increase in resolution of the structure, and without the introduction of specious structure.

ACKNOWLEDGMENTS

The author wishes to thank Professor Ralph Lee, Director of the Missouri School of Mines computer center for making computer time available, and Jon Nance who programed all the calculations.

APPENDIX

The fundamental relationship between the two functions $\rho(R)$ and $\rho_c(R)$ may be derived in another way. Using the same cell picture of the liquid as before, let us call $p(\mathbf{x})$, the probability per unit volume of a vector displacement for a molecule relative to an arbitrary origin. Let $p(\mathbf{x})$ be the Fourier transform of $g(\mathbf{k})$ so that

$$p(\mathbf{x})=\int g(\mathbf{k})\,\exp(i\mathbf{k}\cdot\mathbf{x})\,d\mathbf{k}, \tag{A1}$$

where the integration is over all vector $\mathbf{k}$. Now the probability density of a vector displacement $\mathbf{R}$ between two molecules of the liquid is the volume integral

$$\rho(\mathbf{R})=N^{-1}\int p(\mathbf{x})\,p(\mathbf{x}+\mathbf{R})\,d\mathbf{x}. \tag{A2}$$

Using Eq. (1), this becomes

$$\rho(\mathbf{R})=N^{-1}\int [g(\mathbf{k})]^2\,\exp(i\mathbf{k}\cdot\mathbf{R})\,d\mathbf{k}. \tag{A3}$$

If we choose for $p(\mathbf{x})$ the following,

$$p(\mathbf{x})=\sum_{j=1}^{N} p(\mathbf{r}_j), \tag{A4}$$

where $p(\mathbf{r}_j)$ is zero outside the jth cell,

$$g(\mathbf{k})=\int p(\mathbf{x})\,\exp(-i\mathbf{k}\cdot\mathbf{x})\,d\mathbf{x}$$

$$=\int \sum_j p(\mathbf{r}_j)\,\exp(-i\mathbf{k}\cdot\mathbf{x})\,d\mathbf{x}.$$

Now

$$\mathbf{x}=\mathbf{R}_j+\mathbf{r}_j,$$

so

$$g(\mathbf{k})=\sum_j \int p(\mathbf{r}_j)\,\exp[-i\mathbf{k}\cdot(\mathbf{R}_j+\mathbf{r}_j)]\,d\mathbf{x}$$

$$=\sum_j \exp(-i\mathbf{k}\cdot\mathbf{R}_j)\,X(\mathbf{k}).$$

$$[g(k)]^2=\sum_{j,m} \exp[-i\mathbf{k}\cdot(\mathbf{R}_j-\mathbf{R}_m)]\,[X(\mathbf{k})]^2 \tag{A5}$$

$$[g(k)]^2\cong N\int \rho_c(\mathbf{R})\,[X(\mathbf{k})]^2\,\exp(-i\mathbf{k}\cdot\mathbf{R})\,d\mathbf{R}. \tag{A6}$$

Then

$$\rho(\mathbf{R})=\int\left[\int \rho_c(\mathbf{R}')\,[X(\mathbf{k})]^2\,\exp(-i\mathbf{k}\cdot\mathbf{R}')\,d\mathbf{R}'\right]$$

$$\times\exp(i\mathbf{k}\cdot\mathbf{R})\,d\mathbf{k}. \tag{A7}$$

And the Fourier transform theorem gives

$$[X(\mathbf{k})]^2\int\rho_c(\mathbf{R})\exp(-i\mathbf{k}\cdot\mathbf{R})d\mathbf{R}$$

$$=\int\rho(\mathbf{R})\exp(-i\mathbf{k}\cdot\mathbf{R})d\mathbf{R}. \quad \text{(A8)}$$

This last may be written

$$[X(\mathbf{k})]^2\int[\rho_c(\mathbf{R})-\rho_0]\exp(-i\mathbf{k}\cdot\mathbf{R})d\mathbf{R}$$

$$=\int[\rho(\mathbf{R})-\rho_0]\exp(-i\mathbf{k}\cdot\mathbf{R})d\mathbf{R}, \quad \text{(A9)}$$

where the subtraction of the two dissimilar ρ_0 integrals from both sides of the equation is justified since

$$[X(\mathbf{k})]^2\int\rho_0\exp(-i\mathbf{k}\cdot\mathbf{R})d\mathbf{R}\cong\int\rho_0\exp(-i\mathbf{k}\cdot\mathbf{R})d\mathbf{R}$$

because

$$\int\rho_0\exp(-i\mathbf{k}\cdot\mathbf{R})d\mathbf{R}\cong 0,$$

except at $k=0$, and here $X(0)=1$. Equation (A9) may be inverted to give

$$\rho(\mathbf{R})-\rho_0=(2\pi)^{-1}\int[X(k)]^2\exp(-i\mathbf{k}\cdot\mathbf{R})d\mathbf{k}$$

$$\times\int[\rho_c(\mathbf{R}')-\rho_0]\exp(i\mathbf{k}\cdot\mathbf{R}')d\mathbf{R}'$$

$$=\int[\rho_c(\mathbf{R}')-\rho_0]F(\mathbf{R}'-\mathbf{R})d\mathbf{R}'$$

$$=\int\rho_c(\mathbf{R}+\mathbf{s})-\rho_0]F(\mathbf{s})d\mathbf{s}, \quad \text{with} \quad \mathbf{R}'-\mathbf{R}=\mathbf{s} \quad \text{(A10)}$$

and

$$F(s)=(2\pi)^{-1}\int[X(k)]^2\exp(i\mathbf{k}\cdot\mathbf{s})d\mathbf{k}.$$

In the case of isotropic arrangements, where $\rho_c(\mathbf{R})=\rho_c(R)$, $p(\mathbf{r})=p(r)$ will mean $\rho(\mathbf{R})=\rho(R)$ and $X(\mathbf{k})=X(k)$, Eq. (A9) will become after averaging over $\mathbf{k}$

$$[X(k)]^2\int_0^\infty 4\pi R^2[\rho_c(R)-\rho_0]\frac{\sin kR}{kR}dR$$

$$=\int_0^\infty 4\pi R^2[\rho(R)-\rho_0]\frac{\sin kR}{kR}dR. \quad \text{(A11)}$$

This is the basic relationship between the two functions $\rho_c(R)$ and $\rho(R)$ in the uncorrelated case, and it is the left-hand side of Eq. (A11) appearing in Eq. (6) which replaces the usual integral term involving $\rho(R)$.

The "smoothing" of the $\rho_c(R)$ function to give $\rho(R)$ as implied in Eq. (A7) may be more clearly brought out by rewriting Eq. (A10) without the ρ_0 subtraction artifice.

$$\rho(\mathbf{R})=\int\rho_c(\mathbf{R}+\mathbf{s})F(\mathbf{s})d\mathbf{s}. \quad \text{(A12)}$$

Now letting ϕ be the angle between $\mathbf{R}$ and $\mathbf{s}$ and setting

$$d\mathbf{s}=\int_0^\infty s^2ds\int_0^\pi 2\pi\sin\phi d\phi,$$

we have

$$\rho_c(\mathbf{R}+\mathbf{s})=\rho_c(|\,\mathbf{R}+\mathbf{s}\,|),$$

$$|\,\mathbf{R}+\mathbf{s}\,|=(R^2+s^2+2Rs\cos\phi)^{\frac{1}{2}}$$

and $F(\mathbf{s})=F(s)$. Then

$$\rho(R)=\int_0^\infty 2\pi s^2F(s)ds\int_0^\pi\rho_c[(R^2+s^2+2Rs\cos\phi)^{\frac{1}{2}}]\sin\phi d\phi,$$

Thus, this last equation shows how to calculate $\rho(R)$ from an arbitrary $\rho_c(R)$.

Theory of ESR Linewidths of Free Radicals

DANIEL KIVELSON* †

Department of Chemistry, University of California, Los Angeles 24, California

(Received May 23, 1960)

A theory of ESR linewidths for substances in which the magnetic anisotropy is small and for which the orbital magnetism has been essentially quenched is developed. Nuclear quadrupole moments, zero field splittings, anisotropic Zeeman terms, and intramolecular electron-nuclear dipolar interactions, as well as motional and exchange effects are considered in the strong field case. The theory is developed in a manner that is particularly adaptable to the study of liquids but it is also applied to crystals since the resulting equations, though only applicable for small anisotropies, are particularly simple. The theory provides an extension of previous theories on ESR spectra in liquids. Several applications of the theory are discussed with particular emphasis on V^{4+} chelates. The theory of exchange in liquids, a phenomenon which is complicated by the noncommutivity of the motional and exchange Hamiltonians is considered in special detail. It is shown that this theory can be used to explain Hausser's results—the existence of an optimum viscosity for the observation of hyperfine structure.

I. INTRODUCTION

THE ESR spectra of free radicals are characterized by g values close to 2 and by relatively small anisotropy. Recent experiments on the linewidths of hyperfine components of free radicals in solution have shown a dependence upon the nuclear quantum numbers,[1–3] upon the anisotropy of the g factors,[2,3] and fine structure splitting.[3] There is also a marked dependence upon exchange effects.[4] In this paper the theory of the line widths of free radicals in diamagnetically "diluted" crystals [5–7] and in dilute liquid solutions is developed in considerable detail. Only cases in which the orbital angular momentum has been almost entirely quenched will be considered. The theory is restricted to high (room) temperatures, strong applied fields, small anisotropy, and no relaxation through chemical reactions. Spin-orbit interactions as a mechanism of relaxation will not be dicsussed. It will be assumed that the principal mechanism for nuclear relaxation arises from the interaction of the nucleus with the unpaired electrons. Intermolecular electron-electron and electron-nuclear dipolar interactions have been treated elsewhere[8,9] and will not be discussed here. The effect of fluctuating magnetic fields arising from rotating charges[10] will also be neglected.

In the next two sections, the general theory is developed. The theory is then applied to diamagnetically "diluted" crystals. Although the theory of the ESR spectra of crystals has been thoroughly developed elsewhere, the approximate treatment explicitly given here is useful in situations where the magnetic anisotropy is small. The next sections are devoted to the theory of ESR spectra of those liquids for which the magnetic anisotropy is also small; the theory is developed in considerable detail with consideration given to various competing effects and to nonequivalent interacting groups of nuclei.

In Sec. VII, a theory of exchange effects in liquids is presented; the principal problem in this theory arises from the noncommutivity of the motional and exchange Hamiltonians. In the remaining sections several examples are described.

II. HAMILTONIAN

The Hamiltonian $\mathcal{H}_0$ which describes the interaction of the electron spins of paramagnetic molecules with an applied magnetic field $\mathbf{B}$ is given by the relation

$$\mathcal{H}_0 = -\hbar \sum_k \mathbf{S}_k \cdot \mathcal{G}_k \cdot \mathbf{B} \tag{1}$$

where $\mathbf{S}_k$ is the spin operator for the kth magnetic molecule and $\mathcal{G}_k$ is the gyromagnetic ratio tensor. The nuclear Zeeman terms will be neglected. The intramolecular "dipolar" interactions give rise to the hyperfine terms of the Hamiltonian, $\mathcal{H}_{IS}$

$$\mathcal{H}_{IS} = \hbar \sum_{k\lambda} \mathbf{J}_{k\lambda} \cdot \mathcal{T}_{k\lambda} \cdot \mathbf{S}_k, \tag{2}$$

where $\mathcal{T}_{k\lambda}$ is the hyperfine interaction tensor for the λth group of equivalent nuclei in the kth molecule, and $\mathbf{J}_{k\lambda}$ is the nuclear spin operator for the λth group of equivalent nuclei in the kth molecule.

$$\mathbf{J}_{k\lambda} = \sum_j \mathbf{I}_{k\lambda j}, \tag{3}$$

* Supported in part by a grant from the National Science Foundation and one from the Research Corporation.

† This work was partially completed while the author was a John Simon Guggenheim Fellow at the Centre d'Etudes Nucléaires de Saclay, Gif-sur-Yvette, France.

[1] J. Schreurs, G. E. Blomgren, G. K. Fraenkel, J. Chem. Phys. **32**, 1861 (1960).
[2] H. McConnell, J. Chem. Phys. **25**, 709 (1956).
[3] B. McGarvey, J. Phys. Chem. **60**, 71 (1956); **61**, 1232 (1957).
[4] G. Pake and T. Tuttle, Phys. Rev. Letters **3**, 423 (1959).
[5] V. W. Cohen, C. Kikuchi, and J. Turkevitch, Phys. Rev. **85**, 379 (1952).
[6] S. Weissman (private communication).
[7] C. Hutchison, Jr., and B. W. Mangum, J. Chem. Phys. **29**, 952 (1958).
[8] R. Kubo and K. Tomita, J. Phys. Soc. Japan **9**, 888 (1954).
[9] D. Kivelson, J. Chem. Phys. **27**, 1087 (1957).
[10] M. J. Stephen and G. K. Fraenkel, J. Chem. Phys. **32**, 1440 (1960).

where $\mathbf{I}_{k\lambda j}$ is the nuclear spin operator for the jth nucleus in the λth group of equivalent nuclei within the kth paramagnetic molecule. In molecules where the electronic spin is greater than $\frac{1}{2}$ one must include the effects of electronic spin-spin interactions; these interactions give rise to the fine structure terms $\mathcal{H}_D$,

$$\mathcal{H}_D=\hbar\sum_k \mathbf{S}_k\cdot\mathfrak{D}_k\cdot\mathbf{S}_k. \tag{4}$$

$\mathfrak{D}_k$ is the fine structure tensor for the kth molecule. If there are nuclei with spin greater than $\frac{1}{2}$ one must include quadrupole interaction terms $\mathcal{H}_Q$,

$$\mathcal{H}_Q=\hbar\sum_{k\lambda j}\mathbf{I}_{k\lambda j}\mathfrak{T}_{k\lambda j}\mathbf{I}_{k\lambda j}, \tag{5}$$

where $\mathfrak{T}_{k\lambda j}$ is the quadrupole interaction tensor for the jth nucleus in the λth equivalent group of nuclei in the kth molecule. The exchange terms $\mathcal{H}_e$ are given by the relation

$$\mathcal{H}_e=\tfrac{1}{2}\hbar\sum_i\sum_{j\neq i}A_{ij}\mathbf{S}_i\cdot\mathbf{S}_j, \tag{6}$$

where A_{ij} is the exchange integral connecting the ith and jth molecules. And finally there is a motional Hamiltonian $\mathcal{H}_m$ which will be treated classically.[11] Since A_{ij} is a function of intermolecular distance, it does not commute with $\mathcal{H}_m$.[9]

The gyromagnetic ratio tensor can be written as the sum $\gamma_k\mathbf{1}+\mathbf{\Gamma}_k$, where $\mathbf{1}$ is the unit tensor, γ_k is the scalar gyromagnetic ratio tensor, and $\mathbf{\Gamma}_k$ is the traceless gyromagnetic ratio tensor. The $\gamma_k\mathbf{1}$ term gives rise to the isotropic Zeeman effect, the $\mathbf{\Gamma}_k$ term to the anisotropic one. The hyperfine interaction tensor can be written as the sum $-a_{k\lambda}\mathbf{1}+\mathbf{\Phi}_{k\lambda}$, where $a_{k\lambda}$ is the isotropic hyperfine constant and $\mathbf{\Phi}_{k\lambda}$ is the anisotropic or traceless hyperfine interaction tensor.[12] $\mathfrak{D}_k$ and $\mathfrak{F}_{k\lambda j}$ are traceless tensors.

The various tensors described above can best be evaluated in a molecular coordinate system because the electronic wave functions can be expressed most conveniently in this framework. On the other hand, it is usually preferable to represent the spin operators in a laboratory system, a system that is at least partially determined by the direction of the applied field $\mathbf{B}$. The procedure is, therefore, to evaluate the tensors in a molecular coordinate system (r, s, t) and then to transform the tensors into a laboratory system (x, y, z). It will be assumed that the $\mathfrak{G}_k$ tensor is diagonalized in the molecular framework; the other tensors need not be diagonal in this framework although they often will be. In all the work below the explicit display of the subscript k and the sum over k will be dropped from all but the exchange terms.

It is convenient to define the following quantities:

$$\gamma=(\tfrac{1}{3})(\gamma_r+\gamma_s+\gamma_t) \tag{7}$$

$$\Delta\gamma=\gamma_t-\tfrac{1}{2}(\gamma_r+\gamma_s) \tag{7a}$$

$$\delta\gamma=\tfrac{1}{2}(\gamma_r-\gamma_s). \tag{7b}$$

γ_r, γ_s, and γ_t are components of $\mathfrak{G}$ in the molecule-fixed coordinate system, and γ is the isotropic gyromagnetic ratio discussed above. In this paper the laboratory-fixed coordinate system will be chosen so that $\mathbf{B}$ lies long the z axis; thus $\mathbf{S}$, $\mathbf{J}$, and $\mathbf{I}$ will all be quantized along the direction of the applied field. If $\Delta\gamma$ and $\delta\gamma$ are small compared to γ, and if the applied field is sufficiently strong to make the isotropic Zeeman terms the dominant ones in the Hamiltonian, then the axis of spin rotation lies almost along $\mathbf{B}$.[13] This choice of coordinate system yields a number of off-diagonal terms in the Hamiltonian which can be treated by perturbation theory provided the contributions from the anisotropic terms are small compared to those from the isotropic terms. The choice of the z axis along $\mathbf{B}$ rather than along $\mathfrak{G}\cdot\mathbf{B}+\mathfrak{T}_\lambda\cdot\mathbf{J}_\lambda$ enables one to write the transformations from the molecular to laboratory coordinates in terms of simple functions of orientation angles, functions that have sensible orthogonality properties and can easily be handled when one discusses liquids. Such would not be the case if the usual representation were used.[12]

In the molecular coordinate system the five components of the traceless (anisotropic) hyperfine interaction tensor $\mathbf{\Phi}_\lambda$ are:

$$b_\lambda=\gamma\gamma_\lambda\hbar\left[\left(0\left|\frac{1-3\cos^2\theta_\lambda}{r_\lambda^3}\right|0\right)+S_{b\lambda}\right] \tag{8}$$

$$c_\lambda=-(3/4)\gamma\gamma_\lambda\hbar\left[\left(0\left|\frac{\sin^2\theta_\lambda\exp(-2i\phi_\lambda)}{r_\lambda^3}\right|0\right)+S_{c\lambda}\right] \tag{8a}$$

$$d_\lambda=-(3/2)\gamma\gamma_\lambda\hbar\left[\left(0\left|\frac{\cos\theta_\lambda\sin\theta_\lambda\exp(-i\phi)}{r_\lambda^3}\right|0\right)+S_{d\lambda}\right]. \tag{8b}$$

θ_λ, ϕ_λ, and r_λ are the polar coordinates of any one of the nuclei in the λth group, relative to the unpaired electron, in the molecular framework; γ_λ is the gyromagnetic ratio of any member of the λth group of equivalent nuclei; $(0\,\|\,0)$ indicates the expectation value of the enclosed operator between ground-state orbital electronic wave functions. $S_{b\lambda}$, $S_{c\lambda}$, and $S_{d\lambda}$ are second-order contributions arising from spin-orbit interactions;

[11] N. Bloombergen, E. Purcell, and R. Pound, Phys. Rev. **73**, 679 (1948).

[12] $a_\lambda=\gamma\gamma_\lambda\hbar(\frac{2}{3})\delta(\mathbf{r}_\lambda)+S_{a\lambda}$, where $S_{a\lambda}$ is the contribution from spin-orbit interactions. In organic free radicals $S_{a\lambda}$ is normally small.

[13] If $\delta\gamma=0$, $\mathcal{H}_0$ is usually diagonalized and z then does not lie along B_0. If z' is the z axis in the $\mathcal{H}_0$ representation, then $\mathcal{H}_0=-\gamma' B_0 S_{z'}$ where $\gamma'^2=\gamma_t^2\cos^2\xi+\gamma_r^2\sin^2\xi$. If

$$|\gamma_t-\gamma_r|\ll(\tfrac{1}{3})\,|\gamma_t+2\gamma_r|,\ \gamma'\sim\gamma+(\tfrac{1}{3})\Delta\gamma(3\cos\xi-1)+\cdots.$$

This expansion in $\Delta\gamma$ is equivalent to the perturbation technique used in obtaining Eqs. (12) and (18).

these terms are normally very small in organic free radicals but may be significant in complexes of transition metals. The anisotropy of $\mathfrak{G}$ has been neglected; this restriction is not serious provided $|\Delta\gamma| \ll |\gamma|$. The anisotropy of the nuclear gyromagnetic ratio is negligible.

The tensor $\mathbf{\Phi}_\lambda$ can be transformed into the laboratory system by means of Eulerian rotations. If ζ, ξ, and η are the three Eulerian angles relating the molecular and laboratory systems, and if the notation

$$c_\lambda' = c_\lambda \exp(-2i\eta) \tag{9}$$

$$d_\lambda' = d_\lambda \exp(-i\eta) \tag{9a}$$

is introduced, then the components of $\mathbf{\Phi}_\lambda$, in the laboratory basis, are:

$$\Phi_{zz}^{(\lambda)} = \tfrac{1}{2}b_\lambda(3\cos^2\xi - 1) - \sin^2\xi(2\,\mathrm{Re}c_\lambda') + \sin^2\xi(2\,\mathrm{Im}d_\lambda') \tag{10}$$

$$\Phi_{z+}^{(\lambda)} = [(3/8)ib_\lambda \sin 2\xi + \sin\xi(\mathrm{Im} + i\cos\xi\,\mathrm{Re})(c_\lambda') + (\cos\xi\,\mathrm{Re} + i\cos 2\xi\,\mathrm{Im})(d_\lambda')]\exp -i\zeta \tag{10a}$$

$$\Phi_{++}^{(\lambda)} = [-(3/8)b_\lambda \sin^2\xi + 1/2\{(1+\cos^2\xi)\mathrm{Re} + 2i\cos\xi\,\mathrm{Im}\}(c_\lambda') + \sin\xi\{(-\cos\xi\,\mathrm{Im} + i\,\mathrm{Re})\}(d_\lambda')]\exp -2i\zeta. \tag{10b}$$

All vectors will be expressed in terms of z and $\pm$ components where the latter represent the raising and lowering operators $x \pm iy$. The ansiotropic hyperfine Hamiltonian can be conveniently divided into secular terms $\hbar\Phi_{zz}\mathbf{S}_z\mathbf{J}_z$, pseudosecular terms $\hbar\Phi_{z+}\mathbf{S}_z\mathbf{J}^+$, and nonsecular terms $\hbar(\Phi_{+z}\mathbf{J}_z + \Phi_{++}\mathbf{J}^+ - \tfrac{1}{4}\Phi_{zz}\mathbf{J}^-)\mathbf{S}^+$; of course, the λ's, k's, and the appropriate summations should be included as well as all the terms for which $-$ and $+$ are interchanged.

In liquids where all the Eulerian angles must be averaged over a sphere, the $\mathbf{\Phi}$ tensor vanishes. Since all the other traceless tensors transform in the same way, they, too, will average out in liquids, and only the isotropic terms will remain. The isotropic contributions to hyperfine structure can be divided into secular $\hbar a\mathbf{J}_z\mathbf{S}_z$ and nonsecular $\hbar(1/2)a\mathbf{S}^+\mathbf{J}^-$ components; the isotropic contribution of the Zeeman terms $-\hbar\gamma\mathbf{S}_z\mathbf{B}$ are all secular. The fine structure tensor $\mathfrak{D}$ can be treated in a fashion exactly analogous to that used with the hyperfine structure tensor; D_{tt}, D_{t+}, and D_{++} replace b, d, and c, respectively, while $\mathfrak{D}_{zz}$, $\mathfrak{D}_{z+}$, and $\mathfrak{D}_{++}$ replace $\Phi_{zz}^{(\lambda)}$, $\Phi_{z+}^{(\lambda)}$, and $\Phi_{++}^{(\lambda)}$, respectively.[14] The same is true for the quadrupole interaction tensor $\mathfrak{T}$ for which the components in the molecular system are:

$$q_{tt}^{(\lambda)} = \frac{eQ_0^{(\lambda)}}{6I_\lambda(2I_\lambda - 1)}(0 \mid -1 + 3(\partial^2 V/\partial\ell^2) \mid 0) \tag{11}$$

$$q_{++}^{(\lambda)} = \frac{eQ_0^{(\lambda)}}{6I_\lambda(2I_\lambda - 1)}(3/4)(0 \mid [(\partial/\partial r) - i(\partial/\partial s)]^2 V \mid 0) \tag{11a}$$

$$q_{t+}^{(\lambda)} = \frac{eQ_0^{(\lambda)}}{6I_\lambda(2I_\lambda - 1)} \times (3/2)(0 \mid (\partial/\partial t)[(\partial/\partial r) - i(\partial/\partial s)]V \mid 0), \tag{11b}$$

where $Q_0^{(\lambda)}$ is the electric quadrupole moment of any one of the equivalent nuclei with spin I_λ, and V is the electrostatic potential at the nucleus in question arising from all other nuclei and electrons, provided the contribution from within a small sphere surrounding the nucleus is excluded.[15,16]

The anisotropic Zeeman terms can be treated by substituting $(2/3)\hbar\Delta\gamma$ for b_λ and $(1/2)\hbar\delta\gamma$ for c_λ in Eqs. (10)–(10b). The field $\mathbf{B}$ must also be substituted for the spin operator $\mathbf{J}_\lambda$; this causes the $\mathbf{\Gamma}_{++}$ terms to vanish in the Hamiltonian since $\mathbf{B}$ has only a z component. The secular contribution to the anisotropic Zeeman terms is

$$\mathfrak{IC}_0(\mathrm{anis}) = -\hbar[(1/3)\Delta\gamma(3\cos^2\xi - 1) - \delta\gamma\sin^2\xi\cos 2\eta]\mathbf{S}_z B; \tag{12}$$

the nonsecular contribution has the form $-\hbar\Gamma_{z+}\mathbf{S}^+B$.

The dipolar transitions are induced by an rf field directed along the laboratory x axis. The x component of the dipole moment $\mathbf{P}_x$ is $\hbar\mathbf{S}\cdot\mathfrak{G}\cdot\mathbf{B}'$ where $\mathbf{B}'$ is the magnetic component of the rf field. The isotropic contribution to $\mathbf{P}_x$ is of the form $\hbar(1/2)\gamma\mathbf{S}^+$; the anisotropic contribution has the form $\hbar(\Gamma_{++} + \Gamma_{-+})\mathbf{S}^+ + (\Gamma_{z+} + \Gamma_{z-})\mathbf{S}_z$. There are additional terms where $\mathbf{S}^-$ replaces $\mathbf{S}^+$. The $\mathbf{S}_z$ terms will be neglected.

III. GENERAL THEORY

The procedure followed in this article is based upon the work of Kubo and Tomita[8]; many of the details of the calculations have been discussed previously[9] and will be omitted here. Kubo and Tomita write the Hamiltonian as the sum of three terms, $\mathbf{H}_1 + \mathbf{H}_2 + \mathbf{H}'$, where $\mathbf{H}_1$ represents the zeroth-order terms, $\mathbf{H}_2$ the "modulation" terms, and $\mathbf{H}'$ the perturbing terms[17]

$$[\mathbf{H}_1, \mathbf{H}_2] = [\mathbf{P}_x, \mathbf{H}_2] = 0. \tag{13}$$

[14] $\mathfrak{IC}_D$ in the molecular framework, assuming axial symmetry, is often written as $D[\mathbf{S}_z^2 - (\tfrac{1}{3})S(S+1)] + E(\mathbf{S}_x^2 - \mathbf{S}_y^2)$. In this case $D = \tfrac{3}{2}D_{zz}$ and $E = 2\mathrm{Re}(D_{++})$.

[15] N. Ramsey, *Nuclear Moments* (John Wiley & Sonc, Inc., New York, 1953).

[16] For atoms $b = Q_{zz}p$, $c = Q_{++}p$, and $d = Q_{z+}p$ where $p = -\gamma\gamma_\lambda 6I_\lambda(2I_\lambda - 1)/eQ_0^{(\lambda)}$.

[17] $[\mathbf{P}, \mathbf{H}_2] \neq 0$ when $\mathbf{P}$ is a function of orientation and $\mathbf{H}_2$ represents the motion. However, the results are not affected by this.

At temperatures large compared to the resonance energies the autocorrelation function $G(t)$ can be approximated, to second order, by the relationship[18]:

$$G(t)=(1/2)Q^{-1}\Big\{\langle \mathbf{P}_x^+(t)\mathbf{P}_x^-\rangle$$
$$-\hbar^{-2}\int_0^t\langle[[\mathbf{P}_x^+(t),\mathbf{H}'_\alpha(\tau)],\mathbf{H}'_\alpha(0)\dagger]\mathbf{P}_x^-(t-\tau)\,d\tau$$
$$-\hbar^{-2}\int_0^t\langle \mathbf{P}_x^+(t)\mathbf{H}'_\beta(\tau)\mathbf{H}'_\beta(0)\dagger\mathbf{P}_x^-$$
$$+\mathbf{H}'_\beta(0)\mathbf{H}'(\tau)\dagger\mathbf{P}_x^+(t)\mathbf{P}_x^-\rangle(t-\tau)\,d\tau$$
$$-\hbar^{-2}\int_0^t dt_1\int_0^{t_1}dt_2\langle[[\mathbf{P}_x^+(t),\mathbf{H}_\gamma'(t_1)],\mathbf{H}_\gamma'(t_2)]\mathbf{P}_x^-\rangle\Big\} \tag{14}$$

where

$$Q\approx \mathrm{Tr}\mathbf{1}=\prod_\lambda(2S+1)^N(2I_\lambda+1)^{N+n\lambda} \tag{14a}$$

and n_λ is the number of equivalent nuclei of spin I_λ in any one of the N paramagnetic molecules with spin S. $\dagger$ indicates the Hermitian conjugate of an operator. The time-dependent operators are expressed in a representation that diagonalizes $\mathbf{H}_1+\mathbf{H}_2$. $\mathbf{H}_\alpha'$ represents those terms in $\mathbf{H}'$ that obey the relation:

$$\mathrm{Tr}\{\{[\mathbf{P}_x^+,\mathbf{H}'(t)],\mathbf{H}'(t)\}\mathbf{P}_x^-\}$$
$$=\mathrm{Tr}\{\{[P_x^+,\mathbf{H}'(0)],\mathbf{H}'(0)\}\mathbf{P}_x^-\}. \tag{15}$$

$\mathbf{H}_\beta'$ represents terms in $\mathbf{H}'$ that do not obey this relationship,[19] and $\mathbf{H}_\gamma'$ represents terms in $\mathbf{H}'$ that commute with $\mathbf{H}_2$. The brackets $\langle\ \rangle$ indicate the trace of the enclosed operators summed over all quantum numbers not required to specify the transition frequencies; if the motional and exchange effects are treated classically, the brackets indicate stochastic averages.

In the calculations below it will be assumed that the spectral lines are well separated; that a strong field B is applied so that $\hbar\gamma B$ is by far the largest term in the energy; that the anisotropy of the g factor is small, $|\Delta\gamma|\ll|\gamma|$. In the case of exchange or motional narrowing it will be assumed that $\hbar^{-2}\langle|\mathbf{H}'|^2\rangle\tau_c^2\ll 1$ where τ_c is the correlation time; this guarantees that the line shapes will be approximately Lorentzian near the line peaks.

IV. CRYSTALS: WEAK EXCHANGE

The hyperfine structure of free radicals in crystals can often be seen by diluting the radicals in an isomorphic diamagnetic host. In this article it will be assumed that all paramagnetic sites are identical. The theory of the spectra of paramagnetic crystals has been worked out in great detail,[20,21] and in this article only a simplified first-order treatment applicable to systems with small $\Delta\gamma$ will be presented. The quadrupole and fine structure terms, which enter when I and S, respectively, are greater than 1/2, will be omitted from this discussion; they have been treated extensively elsewhere.[20,21] The quadrupole terms alter the frequencies somewhat while the fine structure terms split the electronic transitions. Since only first-order terms will be retained, the $\mathbf{H}_1$ Hamiltonian in the Kubo and Tomita theory will be composed of the secular and pseudosecular components of $\mathfrak{IC}_0$ and $\mathfrak{IC}_{IS}$. The pseudosecular terms are off-diagonal terms but the corresponding energy levels are separated only by a gap of order a_λ, while for the nonsecular terms this separation is of the order of $\gamma B\gg a_\lambda$. $\mathfrak{IC}_{IS}$ can be rewritten as

$$\mathfrak{IC}_{IS}=-\hbar\sum_\lambda a_\lambda'\mathbf{S}_{z'}\mathbf{J}_{z'} \tag{16}$$

where z' indicates the axis of precession (quantization) of $\mathbf{J}_\lambda$ and

$$a_\lambda'^2=\{(\Phi_{zz}^{(\lambda)}-a_\lambda)^2+4\,|\,\Phi_{z+}^{(\lambda)}\,|^2\}. \tag{17}$$

Note that $\mathbf{S}$ and $\mathbf{J}_\lambda$ are not quantized along the same axis, and that a_λ' is a function of the orientation angles.

The $\mathbf{H}_2$ term of the Kubo and Tomita formulation vanishes in this case and $\mathbf{H}'=\mathfrak{IC}_e$.[22] If a procedure completely analogous to the one described in reference 9 is applied here, the frequency ω of each hyperfine line is given by the following relation[13]:

$$\omega=[\gamma+(1/3)\Delta\gamma(3\cos^2\xi-1)-\delta\gamma\sin^2\xi\cos 2\eta]B$$
$$+\sum_\lambda a_\lambda' M_\lambda-(1/3)S(S+1)K, \tag{18}$$

where M_λ is the quantum number corresponding to the z' component of the spin angular momentum for the λth group of equivalent nuclei in a molecule:

$$K=A^2\sum_{M'\neq M}g_{M'}\Big[\sum_\lambda a_\lambda'(M_\lambda-M_\lambda')\Big]^{-1} \tag{19}$$

$$NA^2=\sum_i\sum_{i\neq j}A_{ij}^2 \tag{20}$$

$$g_M=\prod_\lambda W(n_\lambda,M_\lambda,I_\lambda)/(2I_\lambda+1)^{n_\lambda}. \tag{21}$$

[18] First-order terms all vanish in the calculations described below and so have been omitted from Eq. (14).

[19] These conditions are equivalent to Kubo and Tomita's requirement that $\omega'=-\omega$:, cf footnote reference 8.

[20] S. Weissman, T. Tuttle, and E. de Boer, J. Phys. Chem. **61**, 28 (1957).

[21] B. Bleaney and K. W. H. Stevens, Repts. Progr. in Phys. 108 (1955); A. Abragam, *Resonance Electronique* (Centre d'Etudes Nucléaires de Saclay, France, 1956).

[22] Note that $[\mathbf{H}_2,\mathbf{H}_e]=0$ and $\mathfrak{IC}'$ is thus an $\mathfrak{IC}_\gamma'$ operator, cf. Eq. (14). For one equivalent group

$$G_2(t)=\int_0^t dt_1\int_0^{t_1}dt_2(\tfrac{1}{3})S(S+1)\exp(iam t)$$
$$\times[1+\exp\{ia(m-m')(t_1-t_2)\}$$
$$-\exp\{ia(m'-m)t_1\}-\exp\{ia(m'-m)t_2\}].$$

In liquids $[\mathbf{H}_2,\mathbf{H}_e]\neq 0$ and $G_2(t)$ is modified. See Eqs. (61) and (63).

$W(n_\lambda, M_\lambda, I_\lambda)$ is the degeneracy of an M_λ spin state which is composed of n_λ equivalent nuclei of spin I_λ; for $n=1$, i.e., for one nucleus, $W(1, M, I)=1$ and $g_M=(2I+1)^{-1}$; for $I=1/2$,

$$W(n, M, 1/2)=n!/[(1/2)(n-M)]![(1/2)(n+M)]!. \quad (22)$$

It should be noted that the expression for K is valid only if the relation $\sum_{M'}\sum_\lambda a_{\lambda'}(M_\lambda-M_{\lambda'})=0$ implies that $M_\lambda=M_\lambda'$; if this condition does not apply the degeneracy factor must be altered.

The second moment $\langle\Delta\omega^2\rangle$ of each spectral line is

$$\langle\Delta\omega^2\rangle=(1/3)S(S+1)A^2(1-g_M). \quad (23)$$

The integrated intensity of the line is proportional to $g_M\gamma^2$.

For the special case $n=1$, $\delta\gamma=c_\lambda=d_\lambda=0$[23]:

$$\omega=[\gamma+\Delta\gamma(1/3)(3\cos^2\xi-1)]B+a'M - S(S+1)A^2\sum_{M'\neq M}[3a'(2I+1)(M-M')]^{-1} \quad (24)$$

$$a'^2=[-a+(1/2)b(1-3\cos^2\xi)]^2+9b^2\sin^2\xi\cos^2\xi \quad (25)$$

$$\langle\Delta\omega^2\rangle=S(S+1)A^2 2I/3(2I+1). \quad (26)$$

The integrated intensity $\mathcal{I}$ is given by the equation

$$\mathcal{I}=[NS(S+1)/3(2I+1)]\gamma^2 \times[1+2(\Delta\gamma/\gamma)(\sin^2\xi\sin\zeta-1/3)]. \quad (27)$$

It should be remembered that all these relationships are valid only if $|a'/\gamma B|\ll 1$ and $|\Delta\gamma/\gamma|\ll 1$.

V. CRYSTALS: STRONG EXCHANGE

Strong exchange exists when $A^2\gg a^2$ and extreme exchange exists when $A^2\gg\gamma^2B^2\gg a^2$. By increasing the concentration of radical in the diamagnetic host crystal, the exchange effect can be increased. In the presence of strong exchange the hyperfine and fine structure is obliterated and a single, approximately Lorentzian, line results. Of course, when the concentration of unpaired spins becomes large enough for the exchange effects to be appreciable, one must consider the intermolecular electron-electron dipolar interactions; this has been done elsewhere and the contributions to the linewidth from these dipolar interactions will not be included here.[8,24] The secular Zeeman terms, both isotropic and nonisotropic, constitute the zeroth-order Hamiltonian, $\mathbf{H}_1$. The exchange terms are to be identified with $\mathbf{H}_2$, and the remaining terms can be treated as perturbations $\mathbf{H}'$. The nonsecular Zeeman terms and the quadrupolar terms both commute with $\mathcal{H}_e$ and hence are not affected by the exchange; they affect the frequency in second order and will be neglected here. The frequency of the absorption line is equal to $\omega_0-\Delta$ where Δ is the small nonsecular shift discussed below and

$$\omega_0=[\gamma+(1/3)\Delta\gamma(3\cos^2\xi-1)-\delta\gamma\sin^2\xi\cos 2\eta]B. \quad (28)$$

The effects of $\mathcal{H}_{IS}$ on the spectrum can be calculated by a procedure similar to that of reference 9. The exchange terms are replaced by a classical Gaussian relaxation function,[8,24] $\exp(-\frac{1}{2}\omega_e^2\tau^2)$, where ω_e is the exchange frequency:

$$\omega_e^2=(2/3)S(S+1)A^2. \quad (29)$$

If $2T_2'^{-1}$ is the secular line width and $2T_1'^{-1}$ the nonsecular linewidth, the total linewidth $2T_2^{-1}$ is equal to the sum of the two. If $|\Phi|^2/\omega_e^2\ll 1$, the line shapes are approximately Lorentzian in the frequency range close to the line peak, and[25]

$$T_2'^{-1}(IS)=(\tfrac{1}{2}\pi)^{\frac{1}{2}}\sum n_\lambda I_\lambda(I_\lambda+1) \times[(\Phi_{zz}^{(\lambda)}-a_\lambda)^2+4|\Phi_{z+}^{(\lambda)}|^2]/3\omega_e \quad (30)$$

$$T_1'^{-1}(IS)=(\tfrac{1}{2}\pi)^{\frac{1}{2}}\sum n_\lambda I_\lambda(I_\lambda+1)[(\tfrac{1}{2}\Phi_{zz}^{(\lambda)}+a_\lambda)^2 +2|\Phi_{z+}^{(\lambda)}|^2+4|\Phi_{++}^{(\lambda)}|^2]\exp(-\omega_0^2/2\omega_e^2)/3\omega_e. \quad (31)$$

Note that the results depend upon the angles ξ and η, but not upon ζ. For extreme exchange, the analog to extreme motional narrowing:

$$T_2^{-1}(IS)=(\tfrac{1}{2}\pi)^{\frac{1}{2}}\sum n_\lambda I_\lambda(I_\lambda+1)[(5/4)|\Phi_{zz}^{(\lambda)}|^2 -a_\lambda\Phi_{zz}^{(\lambda)}+2a_\lambda^2+6|\Phi_{z+}^{(\lambda)}|^2+4|\Phi_{++}^{(\lambda)}|^2]/3\omega_e. \quad (32)$$

The contribution to the nonsecular shift Δ arising from $\mathcal{H}_{IS}$ is

$$\Delta(IS)=T_1'^{-1}(IS)\int_0^{\omega_0/\omega_e}\exp(u^2/2)\,du. \quad (33)$$

The special case for which $\delta\gamma=c_\lambda=d_\lambda=0$ and for which the exchange is extreme will be considered.

$$\omega=\gamma+(1/3)\Delta\gamma(3\cos^2\xi-1)-\Delta(IS). \quad (34)$$

$$T_2^{-1}(IS)=(\tfrac{1}{2}\pi)^{\frac{1}{2}}\sum n_\lambda I_\lambda(I_\lambda+1)[(3\cos^2\xi-1) \times(b_\lambda^2/8-b_\lambda a_\lambda/2)+b_\lambda^2+2a_\lambda^2]/3\omega_e. \quad (35)$$

The fine structure terms $\mathcal{H}_D$ are "modulated" by the exchange terms. The various exchange frequencies could be calculated systematically by means of Eq. (87) in reference 8, but since the assumption of a Gaussian relaxation function [8,24] $\exp(-\omega_e^2\tau^2/2)$ is only an approximate procedure, it will be assumed, in analogy with the treatment of motional effects,[11] that one exchange frequency will suffice to characterize the relaxation. It will also be assumed that the exchange frequency is given by Eq. (29). The secular and nonsecular half-linewidths $T_2'^{-1}(D)$ and $T_1'^{-1}(D)$,

[23] If $\Delta\gamma=0=b$, Eqs. (24)–(27) are identical with those given in footnote reference 9.

[24] P. W. Anderson and P. R. Weiss, Revs. Modern Phys. **25**, 269 (1953); P. W. Anderson, J. Phys. Soc. Japan **9**, 316 (1954).

[25] Since $\omega_e^{-2}|\Phi|^2\ll 1$, the pseudosecular terms can be treated by perturbation theory.

respectively, that arise because of the presence of $\mathcal{H}_D$ terms are:

$$T_2'^{-1}(D)=(\tfrac{1}{2}\pi)^{\frac{1}{2}}(4S^2+4S-3)(27/20)\mathfrak{D}_{zz}^2/3\omega_e; \quad (36)$$

$$T_1'^{-1}(D)=(\tfrac{1}{2}\pi)^{\frac{1}{2}}(4S^2+4S-3)6[|\mathfrak{D}_{z+}|^2\exp(-\omega_0^2/2\omega_e^2)$$
$$+(2/5)|\mathfrak{D}_{++}|^2\exp(-2\omega_0^2/\omega_e^2)]/3\omega_e. \quad (37)$$

For the special but important case that $D_{z+}=D_{++}=0$ and the exchange frequency is very large, $\omega_e\gg\omega_0$,

$$T_2^{-1}(D)=(\tfrac{1}{2}\pi)^{\frac{1}{2}}(4S^2+4S-3)(27/40)$$
$$\times(1-\cos^2\xi)D_{zz}^2/3\omega_e. \quad (38)$$

It should be noted that the fine structure effect vanishes for $S=\frac{1}{2}$.

The contribution to the nonsecular shift $\Delta(D)$ arising from the $\mathcal{H}_D$ terms is

$$\Delta(D)=(\tfrac{1}{2}\pi)^{\frac{1}{2}}(4S^2+4S-3)6\Big[|\mathfrak{D}_{z+}|^2$$
$$\exp(-\omega_0^2/2\omega_e^2)\int_0^{\omega_0/\omega_e}\exp(\tfrac{1}{2}u^2)du+(2/5)|\mathfrak{D}_{++}|^2$$
$$\times\exp(-2\omega_0^2/\omega_e^2)\int_0^{2\omega_0/\omega_e}\exp(\tfrac{1}{2}u^2)du\Big]/3\omega_e. \quad (39)$$

VI. LIQUIDS: WEAK EXCHANGE

In low viscosity liquids the motion of the molecules averages out all the anisotropic contributions to the frequency but if the exchange effects are small the isotropic hyperfine contributions remain. The anisotropic interactions are "modulated" by the motion and although they do not contribute much to the frequency they do give rise to line-broadening.[8,9] The nonsecular part of the isotropic hyperfine terms will be neglected; if strong magnetic fields are applied these terms merely affect the frequency in second order. The zeroth order Hamiltonian $\mathbf{H}_1$ is composed of the isotropic secular terms arising from the Zeeman and hyperfine Hamiltonians. All the anisotropic terms are treated as perturbations $\mathbf{H}'$. The motional Hamiltonian $\mathcal{H}_m$ is treated classically by means of a relaxation function $\exp(-|\tau|/\tau_e)$, and a single correlation time τ_e is assumed.[8,11]

The frequency ω is equal to $\omega_0-\Delta$ where Δ is the nonsecular shift discussed later:

$$\omega_0=\gamma B+\sum a_\lambda M_\lambda-(1/3)S(S+1)K'. \quad (40)$$

K' is the same as the K defined in Eq. (19) except that $a'=a$ in the present case. The integrated intensity of each line is given by $\mathcal{I}$ where

$$\mathcal{I}=(1/3)NS(S+1)\gamma^2 g_M \quad (41)$$

and g_M is the degeneracy factor discussed in Sec. IV.

The anisotropic terms can be divided into three groups: the Zeeman and hyperfine contribution, the fine structure components, and the quadrupole interactions. In the second-order theory used to determine linewidths these anisotropic terms enter quadratically into the results and, furthermore, there are no cross terms between members of the three different groups. This enables one to treat each group of terms individually. Attention will first be turned to the Zeeman-hyperfine interactions. The secular and nonsecular linewidths, respectively, arising from these interactions are[26]:

$$T_2'^{-1}(IS)=\tau_c[(4/15)(\Delta\gamma^2B^2/3+\delta\gamma^2B^2)$$
$$+\sum_\lambda\{(3/20)(2S^2+2S+1)\sigma_{\lambda\lambda}^2[\langle J_\lambda(J_\lambda+1)\rangle_M-M_\lambda^2]$$
$$+(\sum_{\lambda'}\sigma_{\lambda\lambda'}^2M_\lambda M_{\lambda'})$$
$$-(4/15)(\Delta\gamma b_\lambda BM_\lambda+2\delta\gamma B[c_\lambda+c_\lambda^*]M_\lambda)\}] \quad (42)$$

and

$$T_1'^{-1}(IS)=(\tau_c/[1+\omega_0^2\tau_c^2])[\Delta\gamma^2B^2/15+\delta\gamma^2B^2/5$$
$$+(1/5)\sum_\lambda\{(7/8)(8S^2+8S-1)\sigma_{\lambda\lambda}^2$$
$$\times[\langle J_\lambda(J_\lambda+1)\rangle_M-M_\lambda^2]+(\sum_{\lambda'}(15/4)\sigma_{\lambda\lambda'}^2M_\lambda M_{\lambda'})$$
$$-(\Delta\gamma b_\lambda BM_\lambda+2\delta\gamma B[c_\lambda+c_\lambda^*]M_\lambda\}]. \quad (43)$$

In these equations

$$\sigma_{\lambda\lambda'}^2=(1/5)(b_\lambda b_{\lambda'}+[c_\lambda^*c_{\lambda'}+c_\lambda c_{\lambda'}^*+d_\lambda d_{\lambda'}^*+d_\lambda^*d_{\lambda'}]8/3) \quad (44)$$

and $\langle J_\lambda(J_\lambda+1)\rangle_M$ is the average value of $J_\lambda(J_\lambda+1)$ for a given value of M_λ:

$$\langle J_\lambda(J_\lambda+1)\rangle_M=\sum J_\lambda'(J_\lambda'+1)[W(n_\lambda,J_\lambda',I_\lambda)$$
$$-W(n_\lambda,J_\lambda'+1,I_\lambda)]/W(n_\lambda,M_\lambda,I_\lambda). \quad (45)$$

The summation extends from $J_\lambda'=M_\lambda$ to $J_\lambda'=n_\lambda I_\lambda$. For $I=\frac{1}{2}$ and only one group of equivalent nuclei

$$\langle J_\lambda(J_\lambda+1)\rangle_M=\tfrac{1}{2}n+M^2 \quad (46)$$

where n is the number of nuclei in the group. If there is only one nucleus of spin I, $\langle J(J+1)\rangle_M=I(I+1)$. For $n=2$, $I=1$, (cf. DPPH), $\langle J(J+1)\rangle_M$ is 6, 4, and 8/3 for M equals 2, 1, and 0, respectively.

In deriving Eqs. (42) and (43) it has been assumed that $\tau_c^2a^2\ll1$ and $a^2\ll\gamma^2B^2$. Furthermore, since $\tau_c^2a^2\ll1$ and $\sigma^2\ll\gamma^2B^2$, the pseudosecular terms in $\mathcal{H}_{IS}$ have been combined with the nonsecular ones. The condition $\tau_c^2\sigma^2\ll1$ also assures that the line shape will be approximately Lorentzian in the region around the peak.[8] These rather complicated formulas can be better understood in a number of special situations. For most free radicals $S=\frac{1}{2}$, and in many cases there is only one group of equivalent interacting nuclei. Under

[26] The pseudosecular terms are $\mathbf{H}_S'$ terms. See Eq. (14).

TABLE I. $T_2'^{-1}(IS)$ in units of $\tau_e\sigma^2/8$ and $T_1'^{-1}(IS)$ in units of $\tau_e\sigma^2/8(1+\omega_0^2\tau_e^2)$ in the case of motional narrowing, weak exchange, negligible g-factor anisotropy, and only one group of equivalent interacting nuclei. The values of $T_1'^{-1}(IS)$ are in parentheses.

		M					
n	I	3	2	3/2	1	1/2	0
1	1/2					3.5(5)	
1	1				11(13)		6(14)
2	1/2				11(13)		3(7)
1	3/2			22.5(24)		12.5(26)	
3	1/2			22.5(24)		7.25(13.75)	
1	2		38(38)		23(41)		18(42)
2	1		38(38)		17(27)		8(18.7)
4	1/2		38(38)		14(20)		6(14)
6	1/2	81(75)	41(55)		17(27)		9(12)

these conditions,

$$T_2'^{-1}(IS)=\tau_e\{[3J(J+1)\rangle_M+5M^2]\sigma^2/8 +(4/15)[(\Delta\gamma)^2/3+(\delta\gamma)^2]B^2 -(4/15)[b\Delta\gamma+2(c+c^*)\delta\gamma]BM\} \quad (47)$$

$$T_1'^{-1}(IS)=[\tau_e/(1+\omega_0^2\tau_e^2)]\{[7\langle J(J+1)\rangle_M-M^2]\sigma^2/8 +[(\Delta\gamma)^2/3+(\delta\gamma)^2]B^2/5 -[b\Delta\gamma/5+2(c+c^*)\delta\gamma/5]MB\}. \quad (48)$$

If the anisotropy of the $\mathfrak{G}$ tensor can be neglected, $\Delta\gamma\approx\delta\gamma\approx 0$, it is readily seen from Eqs. (47) and (48) that the linewidths have a symmetrical dependence upon the nuclear quantum numbers M, i.e., the linewidth is a function of M^2. Table I gives values of $T_2'^{-1}(IS)$ and $T_1'^{-1}(IS)$, in the case that $\Delta\gamma$ and $\delta\gamma$ vanish, in units of $\tau_e\sigma^2/8$ and $\tau_e\sigma^2/8(1+\omega_0^2\tau_e^2)$, respectively. If the anisotropy of the hyperfine interaction terms are negligible, it can be seen from Eqs. (47) and (48) that the linewidths do not depend upon the nuclear quantum number M. If the anisotropy of both tensors is appreciable, then the linewidth has an unsymmetrical dependence upon M, i.e., a linear as well as a quadratic one. The most common situation is the one for which $\delta\gamma=c=d=0$; then $\sigma^2=b^2/5$. The formulas easily obtained under these conditions from Eqs. (47) and (48) represent an extension of the theory of McConnell for paramagnetic ions,[2] and a correction to Eq. (101) of reference 9.

The nonsecular shift arising from these dipolar terms is $\Delta(IS)$,

$$\Delta(IS)=\tau_e\omega_0 T_1'^{-1}(IS). \quad (49)$$

It should again be noted that terms of the order $(\Delta\gamma/\gamma)$ smaller than those appearing in the above theory have been omitted. For organic free radicals the usual situation is $|\Delta\gamma/\gamma|<0.005$; thus the omitted terms are insignificant. For Cu^{++} ions $|\Delta\gamma/\gamma|\approx 0.1$ and the theory is only an approximate one.

The other factors contributing to the linewidth must also be considered. The slight broadening due to weak exchange has been discussed in Sec. IV. The secular quadrupolar terms commute with both $\mathbf{H}_1$ and $\mathbf{P}_z$ and so do not contribute to the linewidth. The nonsecular terms contribute the following[27]:

$$T_1'^{-1}(Q)=\tau_e(3/4)\sum_\lambda \rho_\lambda^2[n_\lambda 2I_\lambda^2(I_\lambda+1)^2-n_\lambda 3I_\lambda(I_\lambda+1) +\sum_m{}^*\sum_j(5m_{\lambda j}^2-2m_{\lambda j}^4)/\prod_{\lambda'}W(n_{\lambda'},M_{\lambda'},I_{\lambda'})] \quad (50)$$

where

$$\rho_\lambda^2=(1/5)[|q_{11}^{(\lambda)}|^2+(16/3)(|q_{+-}^{(\lambda)}|^2+|q_{++}^{(\lambda)}|^2)]. \quad (51)$$

$\sum^*{}_m$ represents the sum over all values of each $m_{\lambda j}$, the quantum number corresponding to the z component of the nuclear spin operator of the jth nucleus in the λth equivalent group, subject to the condition that $\sum_j m_{\lambda j}=M_\lambda$. Remember that J_λ and M_λ are quantum numbers for an equivalent group of nuclei while I_λ is the quantum number for any one of the n_λ nuclei in the group.[28] The assumption has been made that $\rho^2\tau_e^2\ll 1$.

The fine structure terms $\mathfrak{IC}_D$ obey the conditions of Eq. (15).

$$T_2^{-1}(D)=\tau_e(3/10)\mu^2(4S^2+4S-3) [(3/2)+(5/2)/(1+\omega_0^2\tau_e^2)+1/(1+4\omega_0^2\tau_e^2)] \quad (52)$$

where

$$\mu^2=(1/5)[|D_{11}|^2+(16/3)(|D_{+-}|^2+|D_{1+}|^2). \quad (53)$$

The assumption that $\mu^2\tau_e^2\ll 1$, which is used in deriving Eq. (52), is often not valid.[29,30] This represents a generalization of the theory of McGarvey.[3]

The results obtained above can be combined into the relation

$$T_2^{-1}(M)=\alpha+\beta M+\epsilon M^2+\kappa M^4 \quad (54)$$

where α, β, ϵ and κ are parameters that are independent of the nuclear quantum numbers M.[31] The following

[27] $\tau_e^2\omega_0^2\ll 1$.
[28] $\Delta(Q)=T_1'(Q)\tau_e\omega_0$.
[29] $\Delta(D)=(3/10)\tau_e^2\mu^2(4S^2+4S-3)\omega_0[(5/2)(1+\omega_0^2\tau_e^2)^{-1}+(1+4\omega_0^2\tau_e^2)^{-1}]$.
[30] S. Weissman, J. Chem. Phys. **29**, 1189 (1958).
[31] Note the absence of M^3 terms. Even for relatively large values of a, as for vanadyl ions, this form is correct.

assumptions have been made in obtaining these results:

$$T_2^{-1}\tau_c \ll 1 \tag{55}$$

$$a^2 \ll \gamma^2 B^2 \tag{55a}$$

$$T_2^{-1} \ll |\gamma B| \tag{55b}$$

$$(\Delta\gamma/\gamma)^2 \ll 1. \tag{55c}$$

Equation (54) is valid even if relaxations through spin-orbit interactions are included; these modes of relaxation merely alter the value of α provided they can be characterized by an exponential decay. If $T_2^{-1}(M)$ is subtracted from $T_2^{-1}(-M)$, one obtains the interesting quantity $\Delta T_2^{-1}(M)$;

$$\Delta T_2^{-1}(M) = -2\beta M. \tag{56}$$

If the condition given in Eq. (55) applies, the line shape is nearly Lorentzian. If the opposite condition holds, $\gamma^2 B^2 \tau_c^2 \gg 1$, [cf. Eq. (55b)] and the $T_1'^{-1}$ contribution to the line width becomes negligible.

VII. EXCHANGE: ISOTROPIC HYPERFINE INTERACTIONS

The problem of exchange effects in liquids is complicated by the noncommutivity of the exchange and the motional terms. Some of the effects of this noncommutivity were discussed in a previous article.[9] Recently Hausser's anomalous dependence of line widths upon viscosity were ingeniously explained by Tuttle and Pake in terms of exchange effects.[32,4] It, therefore, seems desirable to develop the theory of exchange effects in liquids in somewhat more detail. In this section the discussion will be limited to the interaction between the exchange forces and the isotropic hyperfine interactions.

In dilute solutions the average distance between paramagnetic molecules is great, and the exchange term A is very small at this distance since the exchange integral drops off very rapidly with increasing distance. However, in liquids of low viscosity, the paramagnetic molecules are in motion and spend some time in close proximity to each other. It will be assumed that the exchange integral has the large value A_0 when two paramagnetic molecules are next to each other and that it vanishes when the two molecules are separated. It will also be assumed that the characteristic time that two molecules are adjacent is τ_1 and that τ_2 is the characteristic time between "collisions" of paramagnetic molecules. For dilute ideal solutions $\tau_2 \gg \tau_1$.

By means of the theory of Brownian motion,[33] one can write down approximate expressions for τ_1 and τ_2, assuming ideal solutions. If η is the viscosity of the solvent, M the molar concentration, and λ the interaction radius,

$$\tau_1 = \pi\eta\lambda^3/kT \tag{57}$$

$$\tau_2 = 750\eta/RTM. \tag{57a}$$

λ is also approximately the length of molecular "jumps" in the liquid and it is taken to be about equal to the molecular "equivalent spherical radius."

The theory of magnetic relaxation[8,11,34] involves the *rms* averaging of a stochastic process. Thus if A is the process

$$\langle A(t)A(t+\tau)\rangle = (1/2T)\int_{-T}^{T} |A(t)|^2 dt f(\tau). \tag{58}$$

$f(\tau)$ is a relaxation function. T should be chosen to be very large for the theory to apply; the error in linewidth introduced by the use of finite values of T is of the order of $1/T$. Therefore, T should be chosen such that $T \gg T_2$. On the other hand, the average should not be taken over a time that is longer than the lifetime of the states involved; this lifetime will be of the order of T_1 which is often of the order of T_2. Thus the choice of $T \approx T_2$ seems to be a reasonable one. In the case of simple motional narrowing in low viscosity liquids $\tau_2 \gg \tau_1$, and the averages over a time $T = T_2$ or over $T \to \infty$ are identical. However, if $\tau_1 \gg T_2$, the average must be taken over a time $T \approx T_2$ and it should be remembered that an error of order $1/T_2$ will appear in the expression for the linewidth.

Consider first the situation in which exchange broadening takes place; this occurs if the effective exchange is relatively weak and the linewidths $T_2^{-1}(e)_M$ of the individual hyperfine lines is less than their separation a. The exchange terms are treated as perturbations H′ which are modulated by the motional terms. The correlation time of the motion is τ_1, the time of contact. Aside from normalization terms, the autocorrelation function $G(t)$, for the secular contributions, is

$$G(t) \approx 1 - \int_0^t (t-\tau)\langle A'^2\rangle \exp(-\tau/\tau_1) d\tau \tag{59}$$

where the effective exchange integral A' is

$$A'^2 = (1/3)S(S+1)A^2. \tag{60}$$

[Cf. Eq. (29).] If $A'\tau_1 \gg 1$, the motion is relatively slow, that is, the time of contact τ_1 is sufficiently large to allow exchange to take place on each collision since A' is the exchange frequency. Equation (59) requires that A'^2 be time averaged and according to the discussion below Eq. (58) the average should be taken over a time $T_2(e)$, approximately equal to the lifetime of a spin state. Thus,

$$\langle A'^2\rangle = [(T_2 - \tau_2)/T_2](1/3)S(S+1)A_0^2, \tag{61}$$

[32] K. Hausser, Ampere Conference, London, 1959; Z. Naturforschg. **14a**, 425 (1959).

[33] J. Frenkel, *Kinetic Theory of Liquids* (Dover Publications, New York); S. Chandrasekhar, Revs. Modern Phys. **15**, 1 (1943).

[34] M. C. Wang and G. E. Uhlenbeck, Revs. Modern Phys. (1945).

where $T_2-\tau_2$ is a measure of the average lifetime of a state after a collision. The upper limit in Eq. (59) can be replaced by T_2 where $T_2\gg\tau_1$

$$G(t)\approx 1-|t|\langle A'^2\rangle\tau_1\approx\exp(-|t|\langle A'^2\rangle\tau_1). \quad (62)$$

The spectral density is the Fourier transform of $G(t)$; thus the line width $T_2^{-1}(e)$ is given by the relation

$$T_2^{-1}(e)_M=f_e=1/\tau_2, \quad (63)$$

where f_e is the effective exchange parameter. This equation holds provided $\tau_1/\tau_2\ll 1$ and $\alpha\gg 1$ where

$$\alpha^2=(1/3)S(S+1)A_0^2\tau_1^2. \quad (64)$$

Equation (63) is essentially the formula given by Pake and Tuttle[4] provided their collision factor p is equal to unity. According to Eq. (63) the line width increases with increasing concentration and decreasing viscosity.

If the exchange is weak and the interaction parameter $\alpha\ll 1$, the situation is quite different. In this case the relative phases of two precessing spins are shifted only slightly upon each encounter; it, therefore, requires many encounters to destroy the correlation between two spins. In this case

$$\langle A'^2\rangle=(1/3)S(S+1)A_0^2\tau_1/\tau_2 \quad (65)$$

provided $T_2\gg\tau_2>\tau_1$. $G(t)$ is again given by Eq. (62) and

$$T_2^{-1}(e)_M=f_e=\alpha^2/\tau_2. \quad (66)$$

This can be cast into the form of the equation given by Pake and Tuttle provided their collision factor $p=\alpha^2$. Note that α^2 depends quadratically on the viscosity η; hence, the linewidth in Eq. (66) is proportional to η while in Eq. (63) it is inversely proportional to η. These formulas give the secular linewidth of each of the broadened hyperfine lines.

Now consider the situation in which exchange narrowing takes place; this occurs if the exchange is strong and the effective exchange frequency f_e is greater than the hyperfine frequency a. The hyperfine lines coalesce into a single narrowed line of width T_2^{-1}. The hyperfine line terms are treated as perturbations $\mathbf{H}'$, the exchange terms as a modulation effect $\mathbf{H}_2$, and the motional terms modulate the exchange. A general derivation of $G(t)$ for such a situation is given in the Appendix. Let

$$a'^2=\sum a_\lambda^2 n_\lambda I_\lambda(I_\lambda+1)/3, \quad (67)$$

[cf. Eq. (30)]. By means of Eq. (A–9) in the Appendix, one can obtain, neglecting multiplicative factors, the following autocorrelation function for the secular terms

$$G(t)=\exp\left[-a'^2\int_0^t \exp(-|\tau|f_e)(t-\tau)d\tau\right]. \quad (68)$$

In deriving this relation $\langle A'^2\rangle$ is obtained by averaging A'^2 over the time interval $1/f_e$, the lifetime of the individual spin state. f_e is given by Eqs. (63) and (66). The upper limit of integration in Eq. (68) can be replaced by T_2, the inverse half-width, and since $T_2 f_e\ll 1$,

$$G(t)=\exp(-|t|a'^2/f_e). \quad (68a)$$

If $\alpha\gg 1$,

$$T_2^{-1}(IS)_i=a'^2\tau_2, \quad (69)$$

and if $\alpha\ll 1$,

$$T_2^{-1}(IS)_i=a'^2\tau_2/\alpha^2. \quad (70)$$

The condition $T_2 f_e\ll 1$ can be shown to hold if one remembers that, for exchange narrowing to hold, $a'T_2>1$. Equations (69) and (70) can also be related to the formulas given by Pake and Tuttle provided $p=1$ in Eq. (69) and $p=\alpha^2$ in Eq. (70). The linewidth is proportional to the viscosity in Eq. (72) and inversely proportional to the viscosity in Eq. (70).

If the nonsecular terms are to be considered, it is readily seen that for strong exchange, (exchange narrowing)

$$T_2^{-1}(IS)_i=[1+f_e^2/(f_e^2+\omega_0^2)]a'^2/f_e. \quad (71)$$

Cf. Eqs. (68a), (69), and (70); also Eq. (A–9) in the Appendix. For $f_e^2\gg\omega_0^2$, the case of extreme exchange,

$$T_2^{-1}(IS)_i=2a'^2/f_e \quad (71a)$$

which is twice the secular result [cf. Eq. (68a)]. This is the 6/3 effect obtained previously by the author[9] and independently by Pake.[35] It is to be contrasted with the more usual 10/3 effect. For weak exchange (exchange broadening) the linewidth for each hyperfine line, including the nonsecular terms is

$$T_2^{-1}(e)_M=f_e\{1+\sum_{M'} g_{M'}/[1+a^2(M-M')^2\tau_1^2]\}, \quad (72)$$

where $g_{M'}$ is the weighting factor defined in Eq. (21). For short τ_1, $a^2\tau_1^2\ll 1$,

$$T_2^{-1}(e)_M=2f_e. \quad (72a)$$

This again is a 6/3 effect. Note that in the derivation of Eq. (72) the perturbation operator $\mathbf{H}'$ is the exchange operator and it is of the form $\mathbf{H}_a'$; cf. Eqs. (14) and (15). On the other hand in the derivation of Eqs. (18) through (23), the exchange operator is of the form $\mathbf{H}_\gamma'$ since the motional effects are excluded.

The intermediate coupling case $\alpha\approx 1$ is more difficult to treat since it is then not a simple matter to average A^2. Equations (71) through (72a) are, however, quite general. The formula for f_e in the cases $\alpha\ll 1$ and $\alpha\gg 1$ connect continuously at $\alpha=1$. In lieu of an exact treatment it can, therefore, be assumed that Eq. (66) for f_e holds in the region $\alpha\leq 1$ and Eq. (63) in the region $\alpha\approx 1$; this is at least qualitatively correct. According to this picture f_e has a maximum at $\alpha=1$, the point at which τ_2 is minimized subject to the condition that τ_1 be long enough to permit effective exchange with each collision. At very low viscosity, $\alpha\ll 1$, the hyperfine

[35] G. E. Pake, Bull. Am. Phys. Soc. **5**, 252 (1960).

lines are observed, f_e is given by Eq. (66), and the widths by Eq. (72). As the viscosity increases the linewidths increase and, provided $A_0 \gg a$, the lines finally coalesce into a broad single line of width a'. At higher viscosity the single line narrows if the condition $\alpha \ll 1$ still holds, f_e is still given by Eq. (66) and the linewidth by Eq. (71). As the viscosity increases still further, the single line narrows more and when $\alpha \gg 1$, the width of the single line is given by Eq. (71), but f_e is determined by Eq. (63). With increasing viscosity, the linewidth increases and finally the hyperfine lines reappear. At this point the linewidth of each of the hyperfine components is given by Eq. (72), and f_e by Eq. (63). As the viscosity increases the lines, therefore, become sharper. For still higher viscosities the exchange effect becomes negligible but the dipolar interactions may no longer be motionally narrowed and, hence, broadening would be expected. These results are, at least qualitatively, in agreement with the data of Hausser and of Pake and Tuttle. At very high temperatures, low viscosities, spin-orbit interactions may contribute to the linewidths.

If the solutions are nonideal there may be no simple relationship between τ_1 and τ_2. Furthermore, the model of very short-range exchange forces may not always be valid and there may also be complicated interactions between the unpaired electron and the solvent. Another difficulty arises because of the expressions obtained for τ_1 and τ_2; Eqs. (57) and (57a) are subject to criticism, in particular, the free radical may be solvated and it may require more energy to penetrate the solvation layer than to make an ordinary jump in the liquid.

For very large τ_2, $\tau_2 \rightarrow \infty$, the expression in Eq. (72) reduces to the appropriate result for solids, $T_2^{-1}(e)_M \rightarrow 0$, provided the concentration is very low $\tau_1/\tau_2 \ll 1$. If the concentration is low in solids, exchange narrowing or broadening does not take place; most of the molecules are too far away from their nearest paramagnetic neighbors to be affected by exchange. The few that are close enough are in interaction with only one paramagnetic neighbor and so merely form a singlet-triplet combination. At higher concentrations the average distance between paramagnetic molecules becomes small and one must consider all the free radicals in a solid in interaction with each other; this gives rise to exchange modulation. See Secs. IV and V. It is also clear that the above theory for liquids holds if only pair exchange interactions are important; this condition holds if the solution is sufficiently dilute to reduce the probability of a three-particle free radical "collision" to a negligible value. The probability of a three-particle free radical "collision" is roughly $Z'X$ less than that of a two-particle free radical "collision" where Z' is the number of nearest or "interacting" neighbors and X is the mole fraction; therefore, the theory described above is probably quite good for mole fractions $X < 0.01$.

The theory of exchange in liquids becomes very complicated as X increases over 0.01; however, if the concentration is high enough so that all the paramagnetic molecules are connected through exchange interactions, then the exchange problem in liquids becomes similar to that of exchange in solids, cf. Secs. IV and V. Of course, in liquids it is assumed that all the anisotropic terms are averaged out by "motional narrowing." For strong exchange, (exchange narrowing), a single line of width $T_2^{-1}(e)$ should be observed

$$T_2^{-1}(e) = (\pi/2)^{\frac{1}{2}} a'^2 [1+\exp(-\omega_0^2/2\langle A'^2\rangle)]/\langle A'^2\rangle^{\frac{1}{2}}, \tag{73}$$

where $\langle A'^2\rangle$ is an average taken over the distribution of free radicals. A', of course, still decreases rapidly as the intermolecular distance increases. [Cf. Eqs. (30) and (31)]. Under the same conditions of high concentration, in the presence of weak exchange (exchange broadening) the second moments of the hyperfine lines are given by Eq. (23) except that A^2 is replaced by $\langle A^2\rangle$.

The effect of exchange on anisotropic hyperfine interactions is difficult to treat except in the high concentration limit (cf. the Appendix); this is done in the next section.

VIII. LIQUIDS: STRONG EXCHANGE AT HIGH CONCENTRATIONS

The problem of paramagnetic liquids in which exchange effects are strong is similar to the strong exchange problem in crystals except that in liquids the anisotropic terms must be averaged over all orientations and modulated by both motional and exchange effects. The hyperfine structure vanishes in concentrated solutions, $X \approx 1$. The zeroth-order Hamiltonian $\mathbf{H}_1$ is composed of the isotropic secular terms arising from the Zeeman Hamiltonian. The motional and exchange terms are identified with $\mathbf{H}_2$ while the isotropic hyperfine and all the anisotropic terms are averaged over all orientations and treated as perturbations $\mathbf{H}'$. The linewidth arising from the isotropic hyperfine terms was discussed in the preceding section. The linewidth arising from the anisotropic hyperfine and Zeeman terms is given by the relations

$$T_2'^{-1}(IS)_a = (4/15)[(\Delta\gamma)^2/3+(\delta\gamma)^2]B_0^2\tau_c + (5/6)\sum_\lambda \sigma_{\lambda\lambda}^2 n_\lambda I_\lambda(I_\lambda+1)E_0 \tag{74}$$

$$T_1'^{-1}(IS)_a = (1/5)[(\Delta\gamma)^2/3+(\delta\gamma)^2]B_0^2\tau_c/(1+\omega_0^2\tau_e^2) + (5/6)\sum_\lambda \sigma_{\lambda\lambda}^2 n_\lambda I_\lambda(I_\lambda+1)E_1 \tag{74a}$$

$$\omega_0 = \gamma B_0. \tag{74b}$$

ω_e is defined in Eq. (29). If $\omega_e\tau_c \gg 1$,

$$E_k = [(\pi/2)^{\frac{1}{2}}/\omega_e]\exp(-k^2\omega_0^2/2\omega_e^2) \tag{75}$$

while if $\omega_e\tau_e \ll 1$

$$E_k = \tau_e/(1+k^2\omega_0^2\tau_e^2). \tag{75a}$$

The resonance frequency is $\omega_0 - \Delta$ where $\Delta(IS)$ is given by Eq. (33). If $\omega_e\tau_e \sim 1$ the problem is rather more complicated.[9] See the Appendix.

The $\mathcal{H}_D$ terms can be treated as in the "crystal strong exchange" case except that averages over all orientations must be taken, and thermal relaxation must be included. Then

$$T_2^{-1}(D) = \mu^2(4S^2+4S-3)(3/10)(\tfrac{3}{2}E_0+\tfrac{5}{2}E_1+E_2). \tag{75b}$$

IX. EXAMPLE: EXCHANGE EFFECTS IN DPPH

Pake and Tuttle[4] studied a 0.14M diphenyl picryl hydrazil (DPPH)-toluene solution at 28°C and at −41°C. They estimate, from studies on the solid, that 4×10^{10} sec$^{-1} \leq A_0 \leq 10^{11}$ sec^{-1}. The effective hyperfine constant a' [cf. Eq. (67)] is about 2.4×10^8 sec^{-1}. At 28°C they observed a single narrowed line with a half-width of 6.4×10^7 sec^{-1}; at −41°C they observed a barely resolvable fine structure. At −41°C, $\eta \approx 0.017$ poise and τ_2, according to Eq. (57a), is approximately 4.5×10^{-9} sec; at 28°C $\eta \approx 0.0053$ poise and τ_2 is approximately 1.2×10^{-9} sec. At −41°C Eq. (72a) applies while at 28°C Eq. (71) is valid. Since f_e can be written as p/τ_2, it is, therefore, possible to solve for p: $p=0.27$ at −41°C and $p=1.3$ at 28°C.

According to the above theory, for $\alpha \ll 1$, $p=\alpha^2$ and varies as $(\eta/T)^2$; for $\alpha \gg 1$, $p=1$. It is not possible for $p(-41°) \ll p(28°)$; however, a large error is not surprising in view of the many assumptions in the theory. It may be that an activation process is required to penetrate the layer of solvent surrounding the free radical; this should account for a decrease of $p(-41°)$ over $p(28)°$.

The hyperfine structure of DPPH is just barely resolvable at 28°C in 0.015 M benzene solution and in a 0.007 M acetone solution. An analysis similar to that described in the preceding paragraph yields $p=0.65$ ($\alpha \approx 0.8$) and $p=0.8$ ($\alpha \approx 0.9$) for benzene and acetone solutions, respectively: $\eta(\text{benzene}) \approx 0.58\ cp$, $\eta(\text{acetone}) \approx 0.3$ cp. Again one would expect $\alpha(\text{acetone}) < \alpha(\text{benzene})$ or else to have both α's be unity.

Perhaps the difficulties in the theory lie in the use of the Stokes-Einstein equation, perhaps in the non-ideality of the diffusion process, or perhaps the free radical-solvent interactions affect the exchange appreciably. In any case the agreement between theory and experiment, as indicated by Pake and Tuttle, is quite good considering the number of approximations implicit in the theory.

X. EXAMPLE: EXCHANGE EFFECTS IN BPA

Hausser carried out linewidth measurements with 0.001M α-γ-bisdiphenyl β-phenyl allyl (BPA) in hexane, ethanol and in dimethyl sulfoxide; $a' \approx 0.5\times10^8$ sec^{-1} for BPA, considerably less than for DPPH.

In hexane the BPA hyperfine structure is just barely resolvable at approximately 0°C, ($\eta \approx 0.0039$). In ethanol the BPA hyperfine structure is just barely resolvable at approximately −40°C ($\eta \approx 0.027$). Hausser has already commented on the anomalous fact that at room temperature BPA gives rise to a sharp hyperfine spectrum in dimethyl-sulfoxide ($\eta \approx 1.1$). An analysis similar to that given in the last section yields $p(\text{hex}) \approx 2$, $p(\text{etOH}) \approx 20$, $p(\text{DMS}) \ll 7$, at 0°C, −40°C, and 25°C, respectively. The ethanol value, and not the dimethyl sulfoxide one, seems furthest out of line. If λ, the interaction radius is greater than the "equivalent spherical radius," τ_2 and hence the values of p would be smaller than those obtained previously.

For the present one can only attribute the discrepancies between theory and experiment to specific solvent effects. It should be noted that both for hexane and for ethanol solutions of BPA, the two studied in detail, the hyperfine structure improves at higher η. At very low temperatures, very high η, the lines start to broaden again, presumably due to dipolar interactions.

XI. EXAMPLE: $ON(SO_3)_2^-$

Peroxylamine disulfonate is a free radical ($S=1/2$) that has been studied in crystals diluted with diamagnetic material[20] and also in liquid solution.[36–39] The nitrogen nucleus ($I=1$) is the only interacting nucleus and there are thus three hyperfine components; the isotropic hyperfine interaction constant a is 2.2×10^8 sec^{-1} and c, d, $\Delta\gamma$, and $\delta\gamma$ can be neglected. Weissman *et al.*[20] found that b, which is given by the relation

$$b = \tfrac{4}{3}\gamma\gamma_N\hbar\langle 0 \mid r^{-3} \mid 0\rangle \tag{76}$$

is about 2.5×10^8 sec^{-1}. In dilute liquid solutions exchange effects are negligible. The line breadth arising from intramolecular dipolar effects is[40]

$$2T_2^{-1} = 3.2\times10^{15}\tau_c\{[6+5M^2] + [14-M^2][1+3.7\times10^{21}\tau_c^2]^{-1}\} + \tfrac{3}{8}\tau_c Q_{zz}^2[2+3\mid M\mid]. \tag{76a}$$

Equation (76a) predicts that the $M=\pm1$ lines are much broader than the $M=0$ line; experimentally all three lines have the same width ($\sim 6\times10^6$ sec^{-1}). From this and other information Landesman[38] has concluded that τ_c must be small; i.e., $\tau_c < 5\times10^{-12}$ sec. Hence none of the relaxation mechanisms described

[36] J. P. Lloyd and G. E. Pake, Phys. Rev. **94**, 579 (1954).
[37] S. Weissman and D. Banfill, J. Am. Chem. Soc. **75**, 2534 (1953); Pake, Townsend, and Weissman, Phys. Rev. **85**, 682 (1952); **89**, 606 (1953).
[38] A. Landesman, J. Phys. radium, **20**, 937 (1959).
[39] Eric Chow (private communication).
[40] It has been assumed that $(1/4)a^2\tau_c^2 \ll 1$.

above would appear to be significant in $ON(SO_3)_2^{=}$.[41] BPP[11] give the relation

$$\tau_c = 4\pi\eta R^3/3kT \qquad (76b)$$

for τ_c where η is the viscosity of the medium and R the effective tumbling radius of the molecule, assumed to be a sphere moving according to Stokes' law. For H_2O, $\eta = 10$ mp at 300°K. For $R = 4$ A, a conservative lower limit for $ON(SO_3)_2^{=}$, $\tau_c = 7\times10^{-11}$ sec. This is considerably greater than the measured upper limit for τ_c. Since the radical ion probably is associated with several H_2O molecules the value of R and hence of τ_c should be larger, not smaller, than the one calculated. It is possible that the value of b is greatly reduced in liquids, perhaps because of the presence of some internal motion such as a rotation of the O—N bond. This would account for the observed inefficiency of electronic-nuclear relaxation without requiring that $\tau_c < 5\times10^{-12}$ sec.

XII. EXAMPLE: TRIPLET STATES

Hutchison and Mangum[7] have measured the triplet state ESR spectrum of naphthalene diluted in a durene crystal. $D_{zz} = -3\times10^9$ cps; $D_{++} = D_{--} = -0.21\times10^9$ cps; $g = 2.0133$. It can readily be seen from Eq. (52) that in liquid solution, even with $\tau_c \approx 10^{-11}$ sec, a small value for a large molecule like naphthalene, T_2^{-1} would be greater than 200 gauss. It would thus not be a simple matter to see the naphthalene spectrum in solution. Weissman[30] has discussed this problem.

McGarvey[3] has applied a similar, but more approximate theory to various metal complexes. The experimental data do not warrant a more detailed analysis at this time.

XIII. VANADYL COMPLEXES

The ESR spectrum of vanadyl etioporphyrin in low viscosity solutions consists of eight nearly equally spaced hyperfine lines of unequal widths.[42] The hyperfine lines arise from the isotropic intramolecular dipolar interactions between the electron ($S = 1/2$) and the vanadyl ion ($I = 7/2$). The magnetic constants were determined by O'Reilly by studying the ESR spectrum in highly viscous solutions.[42,43] He obtained: $g = 1.974$, $a = 2.62\times10^8$ cps, $\Delta g = -0.039\pm0.01$, $b = 2.13\times10^8$ cps, and $\delta\gamma = c = d = 0$. Q_{zz} is not known. The ESR linewidths of vanadyl etioporphyrin in benzene solution are given in Table II.[44] These data have been used in a least squares calculation to obtain values for the parameters in Eq. (54):

Table II. Data for vanadyl etioporphyrin.[44]

M	T_2^{-1} (grams)
−7/2	26.9
−5/2	20.8
−3/2	17.9
−1/2	17.3
1/2	18.7
3/2	21.6
5/2	24.4
7/2	30.5

$$\alpha = 17.6 \text{ gauss}$$

$$\beta = 0.66 \text{ gauss}$$

$$\epsilon = 0.88 \text{ gauss}. \qquad (77)$$

κ, and hence the quadrupole contribution to the linewidth, is assumed to be negligible. The data are not accurate enough to provide an accurate check of Eqs. (47) and (48), or even of Eq. (56). α, β, and ϵ can also be calculated in units of τ_c by means of Eqs. (47) and (48) and the magnetic parameters obtained by O'Reilly. Other relaxations mechanisms such as spin-orbit interactions would contribute to α but probably not to β and ϵ; therefore, α will be written as $\alpha' + \alpha''$ where α'' is the contribution from unspecified sources. Then, in (gauss$\times10^{10}$), $\alpha' = 12.1\tau_c$, $\beta = 2.3\tau_c$, $\epsilon = 1.2\tau_c$, if $\omega_0^2\tau_c^2 \gg 1$; and $\alpha' = 33.7\tau_c$, $\beta = 4.1\tau_c$, $\epsilon = 0.9\tau_c$ if $\omega_0^2\tau_c^2 \ll 1$. These values and those given in Eq. (77) are not compatible; however, if one allows for errors of up to 100%, it is seen by a comparison of the experimental and calculated values of ϵ and β that τ_c must lie between 2.5×10^{-11} sec and 8×10^{-10} sec. If $\tau_c > 5\times10^{-11}$ sec, the $T_1'^{-1}$ contribution to the linewidth is negligible and[45,46]

$$\alpha = \alpha'' + \tau_c\left[\tfrac{4}{15}(\Delta\gamma B_0)^2 + \tfrac{3}{16}I(I+1)b^2\right] \qquad (78)$$

$$\beta = -\tau_c\left[\tfrac{4}{15}(b\Delta\gamma B_0) + \{\tfrac{8}{45}\Delta\gamma B_0 a/\gamma\}\right] \qquad (78a)$$

$$\epsilon = \tau_c\left[\tfrac{1}{8}b^2 + \{\tfrac{4}{15}(\Delta\gamma a/\gamma)^2 + \tfrac{4}{15}ba\Delta\gamma/\gamma\}\right]. \qquad (78b)$$

If these equations are used in conjunction with the data in Eq. (77), one obtains the results $\alpha'' = 8.5$ gauss and $\Delta\gamma B_0/b = 0.35$. O'Reilly's parameters yield 0.89 for the ratio $\Delta\gamma B_0/b$. If $\tau_c = 6\times10^{-11}$ sec in benzene ($\eta = 0.006p$), the conditions of Eqs. (55) apply and R, the effective molecular radius of the complex is 4.65 A, a not unreasonable result [cf. Eq. (76b)].

The experimental data could not be fitted exactly with Lorentzian shaped curves; in fact, the "apparent"

[41] Perhaps spin-orbit interactions are effective in relaxing the spins. This effect might also help to explain Hausser's results (cf. footnote 32).

[42] D. E. O'Reilly, J. Chem. Phys. **29**, 1188 (1958).

[43] The nuclear-electronic interaction is often written as $A_1\mathbf{I}S_z + B(\mathbf{I}_x\mathbf{S}_x + \mathbf{I}_y\mathbf{S}_y)$; then in the present notation $a = -3^{-1}(A+2B)$ and $3b = 2(A-B)$.

[44] T_2 has been determined from O'Reilly's spectrum, footnote 42. Lorentzian lines of equal intensity have been assumed, and corrections for overlap have been made.

[45] $B_0 = \omega_0/\gamma$ and $B = (\omega_0 - aM)/\gamma$.

[46] In Eq. (78) the terms in braces { } are small and will be neglected.

[47] G. Pake and R. Rogers J. Chem. Phys. **33**, 1107 (1960).

intensity, peak height times line width squared, is not the same for all the lines. It is not surprising, therefore, that Eqs. (54) and (56) do not fit the data exactly. Rogers and Pake[47] report that these formulas, as well as the Lorentzian fit with constant intensity, seem to apply acceptably in the concentration range near 0.05 M. The differences in the ratio $\Delta\gamma B_0/b$ obtained by O'Reilly and by the method above may be due to the difficulties mentioned or they may be real differences arising from the dependence of $\Delta\gamma$ and b upon the solvent. Further work at lower concentrations, where exchange and intermolecular dipolar interactions are not important, should be carried out.

The second-order shifts in frequency can easily be included in the theory but they have very little effect upon the linewidths.

The theory may not hold too well for Cu complexes since the ratio $|\Delta g/g| \approx 0.1$ for Cu acetylacetone.[3,48] Experiments on Cu complexes are currently being carried out.

ACKNOWLEDGMENTS

The author takes great pleasure in thanking Dr. M. G. Kivelson, Professor G. Fraenkel, Professor R. L. Scott, and Professor A. Abragam for many interesting discussions on various topics included in this article. He is grateful for the fellowship awarded by the John Simon Guggenheim Foundation which enabled him to devote himself to part of this work, and he wishes to thank Professor Abragam for welcoming him to his laboratory at the Centre d'Etudes Nucléaires de Saclay.

APPENDIX

By means of the procedure described by Kubo and Tomita, the autocorrelation function $G(t)$ can be obtained for the isotropic hyperfine interaction $\mathbf{H}'$ modulated by the exchange $\mathbf{H}_e$ which in turn is modulated by the motion $\mathbf{H}_m$.

$$G(t)=\tfrac{1}{2}\gamma^2\exp(i\omega_0 t)Q^{-1}\Big\{\mathbf{S}^+\mathbf{S}^- + it\langle[\mathbf{S}^+,\mathbf{H}']\mathbf{S}^-\rangle - \int_0^t (t-\tau)\,d\tau\langle[[\mathbf{S}^+,\mathbf{H}'],\mathbf{H}'(\tau)]\mathbf{S}^-\rangle\Big\}. \quad \text{(A-1)}$$

The time dependence of $\mathbf{H}'$ is taken relative to the basis $\mathbf{H}_0+\mathbf{H}_m+\mathbf{H}_e$.

$$[\mathbf{H}_0,\mathbf{H}_m]=[\mathbf{H}_0,\mathbf{H}_e]=[\mathbf{H}',\mathbf{H}_m]=0 \quad \text{(A-2)}$$

but $[\mathbf{H}_m,\mathbf{H}_e]\neq 0$. The exponentials $\exp[i(\mathbf{H}_0+\mathbf{H}_m+\mathbf{H}_e)t/\hbar]$ that enter into $\mathbf{H}'(\tau)$ can be expanded in powers of $\mathbf{H}_e$. The second-order term $G_2(t)$ in Eq. (A-1) can be written, after suitable rearrangement, as

$$G_2(t)=-\tfrac{1}{2}\gamma^2\exp(i\omega_0 t)Q^{-1}\times\int_0^t (t-\tau)\,d\tau\exp(-i\omega_{mn}\tau)\Big\langle[[\mathbf{S}^+,\mathbf{H}_{mn}'],\Big\{\mathbf{H}_{nm}'-\int_0^\tau d\tau'(\tau-\tau')[[\mathbf{H}_{nm}',\mathbf{H}_e(\tau)],\mathbf{H}_e]\Big\}]\mathbf{S}^-\Big\rangle. \quad \text{(A-3)}$$

$\mathbf{H}_{mn}'$ is equal to $(m\,|\,\mathbf{H}'\,|\,n)$ and $\hbar\omega_{mn}=(m\,|\,\mathbf{H}_0\,|\,m)-(n\,|\,\mathbf{H}_0\,|\,n)$; $\mathbf{H}_e(\tau)$ is given by the relation

$$\mathbf{H}_e(\tau)=\exp(i\mathbf{H}_m\tau/\hbar)\mathbf{H}_e\exp(-i\mathbf{H}_m\tau/\hbar). \quad \text{(A-4)}$$

The motion is approximated by the usual form of the relaxation function

$$\langle\mathbf{H}_e(\tau)\mathbf{H}_e(0)\rangle=\langle\,|\,\mathbf{H}_e(0)\,|^2\rangle\exp(-\,|\,\tau\,|\,/\tau_1). \quad \text{(A-5)}$$

If $T_2/\tau_1\gg 1$

$$G_2(t)=-\tfrac{1}{2}\gamma^2\exp(i\omega_0 t)Q^{-1}\int_0^t (t-\tau)\,d\tau\exp(-i\omega_{mn}\tau)\times\langle[[\mathbf{S}^+,\mathbf{H}_{mn}'],\{\mathbf{H}_{nm}'-\,|\,\tau\,|\,\tau_1[[\mathbf{H}_{nm}',\mathbf{H}_e],\mathbf{H}_e]\}]\mathbf{S}^-\rangle \quad \text{(A-6)}$$

while if $T_2/\tau_1\ll 1$

$$G_2(t)=-\tfrac{1}{2}\gamma^2\exp(i\omega_0 t)Q^{-1}\int_0^t (t-\tau)\,d\tau\exp(-i\omega_{mn}\tau)\times\langle[[\mathbf{S}^+,\mathbf{H}_{mn}'],\{\mathbf{H}_{nm}'-\tfrac{1}{2}\tau^2[[\mathbf{H}_{nm}',\mathbf{H}_e],\mathbf{H}_e]\}]\mathbf{S}^-\rangle. \quad \text{(A-7)}$$

Equation (A-7) is the expression given by Kubo and Tomita for $G_2(t)$ in the presence of exchange but the absence of motion. They further assume that the exchange relaxation function can be written as a Gaussian and Eq. (A-7) can be re-expressed as

$$G_2(t)=-\tfrac{1}{2}\gamma^2\exp(i\omega_0 t)Q^{-1}\int_0^t (t-\tau)\,d\tau\times\exp(-i\omega_{mn}\tau)\langle[[\mathbf{S}^+,\mathbf{H}_{mn}'],\mathbf{H}_{mn}']\mathbf{S}^-\rangle\exp(-\tfrac{1}{2}\omega_e^2\tau^2). \quad \text{(A-8)}$$

Equation (A-6) can be handled analogously; it gives rise to the relationship

$$G_2(t)=-\tfrac{1}{2}\gamma^2\exp(i\omega_0 t)Q^{-1}\int_0^t (t-\tau)\,d\tau\times\exp(-i\omega_{mn}\tau)\langle[[\mathbf{S}^+,\mathbf{H}_{mn}'],\mathbf{H}_{nm}']\mathbf{S}^-\rangle\times\exp(-\,|\,\tau\,|\,\tau_1\omega_e^2). \quad \text{(A-9)}$$

Equations (A-8) and (A-9) give rise to the line widths determined in Eqs. (73) and (68), respectively.

If $\mathbf{H}'$ represents anisotropic interactions, $[\mathbf{H}',\mathbf{H}_m]\neq 0$ and the problem is more difficult to handle.

[48] A. H. Maki and B. R. McGarvey, J. Phys. Chem. **62**, 31 (1958).

Paramagnetic Relaxation in Solutions of VO^{++}†

R. N. ROGERS AND G. E. PAKE

Department of Physics, Stanford University, Stanford, California

(Received May 23, 1960)

The ESR spectrum of vanadyl ion in solutions has the interesting feature that the linewidths of the individual hyperfine components depend on the nuclear spin orientation, m_I. We have determined that the origin of the effect is the mechanism proposed by H. M. McConnell, namely, the existence of a "microcrystal" about the VO^{++} ion which gives rise to anisotropies in the g tensor and hyperfine interaction. By comparing the results of linewidth measurements made at 9.25 kMc and at 24.3 kMc with the results of calculations made by D. Kivelson, we were able to conclude the validity of the microcrystallite model.

I. INTRODUCTION

THE nuclear hyperfine structure of the electron spin resonance of VO^{++} in liquid solutions was first observed by Garif'ianov and Kozyrev[1] and by Pake and Sands.[2] The observed spectrum arises from the flipping of the unpaired electron of the ionic $3d^1$ configuration and has eight fairly well resolved components, corresponding to a nuclear spin of 7/2. The positions of the lines are well understood and are given by an effective spin Hamiltonian of the form

$$\mathcal{H}=-\hbar\mathbf{S}\cdot\mathcal{G}\cdot\mathbf{B}-\hbar\mathbf{I}\cdot\mathbf{A}\cdot\mathbf{S}$$

as will be discussed in Sec. IV. An interesting feature of the spectrum first noted by Pake and Sands is the variation of the line width of the individual lines with the nuclear quantum number m_I. Spectra with the same characteristic variation have also been observed in solutions of organic compounds containing the VO^{++} ion[3] (Fig. 1).

McConnell[4] first proposed a mechanism which could lead to a variation of the electron linewidth with nuclear orientation. It is well known that many ions, especially those of the transition groups, tend to exhibit relatively stable short-range order between the ion and the nearest surrounding solvent neighbors.[5] McConnell's hypothesis was to assume that this short range solvent order produces a "microcrystal" about each ion thus giving rise to anisotropies in the g tensor and in the hyperfine interaction tensor. He assumed axial symmetry, a well-founded assumption from the symmetry properties of VO^{++} ion in aqueous solutions.[6] By treating the random Brownian tumbling of the microcrystallite and in the same manner as Bloembergen, Purcell, and Pound[7] treat the dipole-dipole interaction of nuclei in a liquid, he obtains the following results, showing a dependence on m_I

$$1/T_1' \propto (\Delta g B_0+3bm_I/2)^2\tau_c/(1+\omega_0^2\tau_c^2)$$

$$1/T_2' \propto (\Delta g B_0+3bm_I/2)^2 \tan^{-1}(2\tau_c/T_2'),$$

where

$$\Delta g=(g_{||}-g_\perp)$$

$$b=2/3(A_{||}-A_\perp)$$

B_0=dc magnetic field.

Recently Kivelson,[8,9] using the formalism of Kubo and Tomita,[10] has encompassed McConnell's ideas in extensive calculations concerning electron spin relaxation times. In the present paper, experimental evidence will be given supporting Kivelson's results and thus confirming the McConnell mechanism.

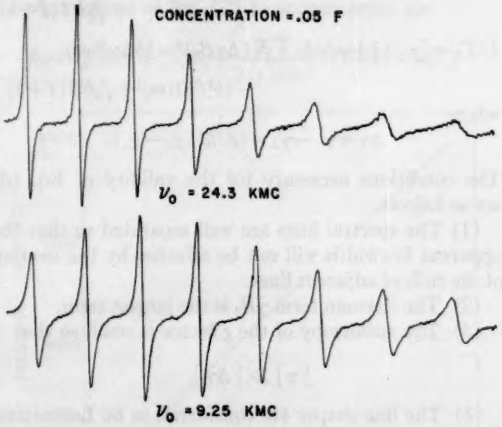

FIG. 1. Electron paramagnetic resonance hyperfine spectra of VO^{++} in aqueous solution. These curves are typical spectra, showing signal-to-noise levels encountered, and also showing the shift of minimum width between 9.25 and 24.3 kMc.

† Supported by the Air Force Office of Scientific Research.

[1] N. S. Garif'ianov and B. M. Kozyrev, Doklady Akad. Nauk S.S.S.R. **98**, 929 (1954).

[2] G. E. Pake and R. H. Sands, Phys. Rev. **98**, 266(A) (1955).

[3] D. E. O'Reilly, J. Chem. Phys. **29**, 1188 (1958); H. M. McConnell, W. W. Porterfield, and R. E. Robertson, J. Chem. Phys. **30**, 442 (1959); W. A. Anderson and L. H. Piette, J. Chem. Phys. **30**, 591 (L) (1959).

[4] H. M. McConnell, J. Chem. Phys. **25**, 709 (1956).

[5] R. A. Robinson and R. H. Stokes, *Electrolyte Solutions* (Butterworth's Scientific Publications, Ltd., London, 1955).

[6] C. K. Jorgensen, Acta Chem. Scand. **11**, 73 (1957).

[7] N. Bloembergen, E. Purcell, and R. Pound, Phys. Rev. **73**, 679 (1948).

[8] D. Kivelson, J. Chem. Phys. **27**, 1087 (1957).

[9] D. Kivelson, J. Chem. Phys. **33**, 1094 (1960), (preceding paper).

[10] R. Kubo and K. Tomita, J. Phys. Soc. Japan **9**, 888 (1954).

II. BRIEF THEORETICAL RESUME

In this section a brief presentation will be made of the pertinent portions of Kivelson's calculations. For details on the application of the general theory of Kubo and Tomita, Kivelson's papers should be consulted.[8,9]

The Hamiltonian for the system is written as the sum of three terms: $\mathcal{H}=\mathbf{H}_1+\mathbf{H}_2+\mathbf{H}'$ where $\mathbf{H}_1$ represents the zeroth-order terms, $\mathbf{H}_2$ the modulation terms, and $\mathbf{H}'$ the perturbations. The required commutation properties are $[\mathbf{H}_1, \mathbf{H}_2]=[\mathbf{M}_x, \mathbf{H}_2]=0$, where $\mathbf{M}_x$ is the x component of the total magnetic moment operator $\mathbf{M}=\sum_i \mathbf{M}_i$. The terms of the Hamiltonian for dilute ionic solutions may be identified as follows:

$$\mathbf{H}_1=\mathcal{H}_0^{(i)}+\mathbf{H}_{IS}^{(ii)},$$

the isotropic Zeeman interaction plus the secular hyperfine interaction;

$$\mathbf{H}_2=\mathcal{H}_m,$$

the modulation term. It is treated classically by means of a correlation function of the form $\exp(-|t|/\tau_c)$ with a single correlation time τ_c.

$$\mathbf{H}'=\mathcal{H}_0^{(a)}+\mathcal{H}_0^{(n)}+\mathcal{H}_{IS}^{(a)},$$

the anisotropic secular and nonsecular terms, and the anisotropic dipolar interaction.

The explicit form of these terms is given in the Appendix.

From footnote reference 9, the relaxation times are found to be

$$1/T_2'=\tau_c\left[\tfrac{4}{45}(\Delta\gamma B_0)^2-\tfrac{4}{15}b\Delta\gamma B_0 m_I+\tfrac{1}{8}b^2m_I^2+\tfrac{3}{40}b^2I(I+1)\right]$$

$$1/T_1'=\left[\tau_c/(1+\omega_0^2\tau_c^2)\right]\left[\tfrac{1}{15}(\Delta\gamma B_0)^2-\tfrac{1}{5}b\Delta\gamma B_0 m_I-(b^2/40)m_I^2+\tfrac{7}{40}b^2I(I+1)\right],$$

where

$$\Delta\gamma=\gamma_{||}-\gamma_\perp=(\beta/\hbar)(g_{||}-g_\perp).$$

The conditions necessary for the validity of Eq. (3) are as follows.

(1) The spectral lines are well separated so that the apparent linewidth will not be affected by the overlap of the tails of adjacent lines.

(2) The Zeeman term γB_0 is the largest term.

(3) The anisotropy of the g factor is small so that

$$|\gamma| \gg |\Delta\gamma|.$$

(4) The line shapes are considered to be Lorentzian implying the relation

$$\tau_c^2\langle|\mathbf{H}'|^2\rangle \ll \hbar^2.$$

(5) The effect of interionic interactions and of spin orbit interactions have been ignored with the understanding that such contributions to the line width may be lumped together in an additive constant as discussed in the following.

III. COMPARISON OF THEORY WITH EXPERIMENT

From Eq. (3) it is seen that the expression for the linewidths may be written as a polynomial in m

$$1/T_2=\pi\sqrt{3}(a_1+a_2m_I+a_3m_I^2),$$

where the constants may be identified as

$$a_1=\tau_c\{7/45(\Delta\gamma B_0)^2+63b^2/16\}+K$$

$$a_2=-\tau_c\{(7/15)b\Delta\gamma B_0\}$$

$$a_3=\tau_c\{b^2/10\}.$$

The constant K is added to take account of contributions from spin-orbit coupling from interionic interactions and in general from all mechanisms not sensitive to the nuclear orientation, m_I.

In order to check the predictions of the microcrystalline model as calculated by Kivelson, the line widths of samples of VO^{++} in aqueous solutions were measured at frequencies of 9250 and 24 300 Mc corresponding to B_0 equal to 3300 and 8670 gauss, respectively. The constant coefficients a_i were then determined from a plot of linewidth versus m_I. In Figs. 2–4 the results of the line width measurements are plotted along with the predicted K-bandwidths as calculated from the coefficients determined from the X-band data. It is seen that there is agreement within the limits of experimental error for the measured solutions of concentration 0.050–0.075 F in VO^{++} ion.

The experimental linewidths were determined by measuring the width of one of the component lines directly and then determining the relative width of the rest of the components from their derivative heights by use of the equality

$$(\text{derivative height})\times(\text{derivative width})^2=\text{constant}$$

for lines of equal intensity. This relation would be anticipated on the basis that the population differences of the different m_I levels should be small corresponding to nuclear Boltzman factors nearly equal to unity. The validity of this assumption was checked from experimental spectra first by performing a double integration by means of a servo integrating machine to check directly the assumed equality of intensities,[11] and second by forming the products hw^2 using widths determined directly by means of a proton resonance gauss-meter. The first method gave a constant answer to the order of 20%, while the second was constant to the order of 10%. Considering the inherent difficulties in both methods the agreement seems quite adequate to justify the indirect method of linewidth measurement.

Furthermore, sources of disagreement of experiment with theory arise through the violation of conditions (1) and (4) of the previous section. It can be seen from Fig. 1 that the line components do in fact overlap;

[11] We wish to thank Professor R. E. Norberg of Washington University for the use of the differential analyzer.

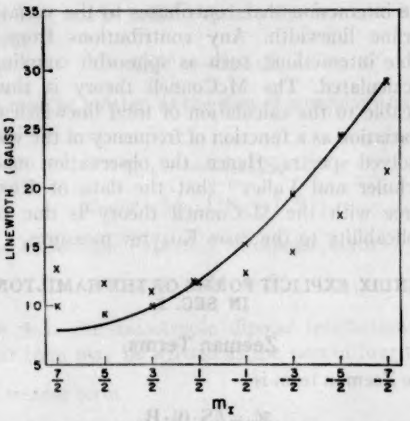

FIG. 2. Plot of linewidth versus m_I. The points marked X and K are the linewidths found at 9.25 kMc and 24.3 kMc, respectively. The solid curve represents the predicted variation of linewidths at 24.3 kMc as given by Eq. (4) and Eq. (5) where the constants a_i have been determined from the 9.25-kMc widths shown. For 0.075 F concentration of VO^{++} the constants (in gauss) determined at 24.3 kMc are(a_1, 13.6; a_2, 2.8; a_3, 0.47. The values predicted from the 9.25-kMc data are: a_1, 13.6; a_2, 3.1; a_3, 0.42.

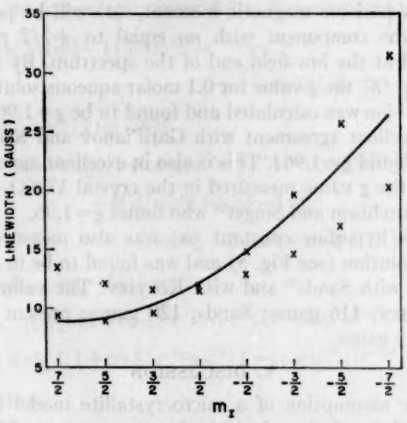

FIG. 4. Plot of linewidth versus m_I. The points marked X and K are the linewidths found at 9.25 kMc and 24.3 kMc, respectively. The solid curve represents the predicted variation of linewidths at 24.3 kMc as given by Eq. (4) and Eq. (5) where the constants a_i have been determined from the 9.25-kMc widths shown. For 0.050 F concentration of VO^{++} the constants (in gauss) determined at 24.3 kMc are: a_1, 13.1; a_2, 3.2; a_3, 0.62. The values predicted from the 9.25-kMc data are: a_1, 13.4; a_2, 2.6; a_3, 0.37.

and it is also found that the lines deviate somewhat from a pure Lorentzian shape. No attempt was made to correct for these factors.

IV. g VALUE AND HYPERFINE CONSTANT

Assuming axial symmetry, the effective spin Hamiltonian may be written as

$$\mathcal{H}=\beta[g_{\|}B_rS_r+g_\perp(B_pS_p+B_qS_q)]+A_{\|}I_rS_r+A_\perp(I_pS_p+I_qS_q)$$

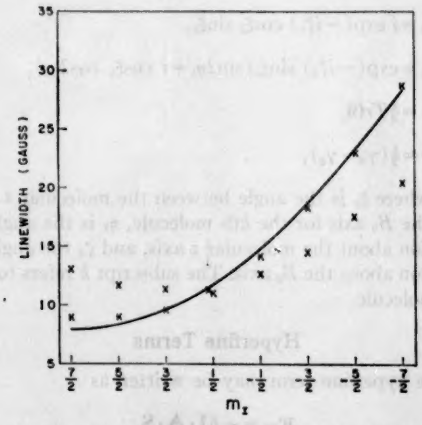

FIG. 3. Plot of linewidth versus m_I. The points marked X and K are the linewidths found at 9.25 kMc and 24.3 kMc, respectively. The solid curve represents the predicted variation of linewidths at 24.3 kMc as given by Eq. (4) and Eq. (5) where the constants a_i have been determined from the 9.25-kMc widths shown. For 0.064 F concentration of VO^{++} the constants (in gauss) determined at 24.3 kMc are: a_1, 12.9; a_2, 2.8; a_3, 0.48. The values predicted from the 9.25-kMc data are: a_1, 13.1; a_2, 2.9; a_3, 0.41.

where p, q, r, refer to the x, y, z coordinates fixed in the microcrystallite. Transforming to the laboratory frame and keeping only the terms independent of time

$$\mathcal{H}=\langle g\rangle\beta\mathbf{B}_0\cdot\mathbf{S}+\langle a\rangle\mathbf{I}\cdot\mathbf{S},$$

where

$$\langle g\rangle=\tfrac{1}{3}(g_{\|}+2g_\perp)$$

$$\langle a\rangle=\tfrac{1}{3}(A_{\|}+2A_\perp).$$

The eigenvalues of Eq. (7) to second order are

$$\hbar\omega=\langle g\rangle\beta B_0+\langle a\rangle m_I+\frac{\langle a\rangle^2}{2\langle g\rangle\beta B_0}[I(I+1)-m_I^2].$$

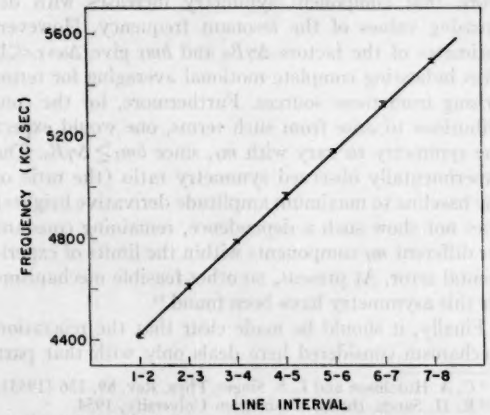

FIG. 5. Variation of the spacing, as measured in proton frequency units, with the successive intervals in the eight line spectrum. Line 1 has $m_I=+7/2$ and line 8 has $m_I=-7/2$; a given line interval, for example that between lines 2 and 3, is designated 2–3. The slope of the line gives a the hyperfine constant.

For a positive magnetic moment, $\langle a \rangle$ will be positive and the component with m_I equal to $+7/2$ will be found at the low-field end of the spectrum. By means of Eq. (8) the g value for 0.1 molar aqueous solution of VO^{++} ion was calculated and found to be $g=1.9624(8)$ in excellent agreement with Garif'ianov and Kozyrev[1] who found $g=1.962$. This is also in excellent agreement with the g value measured in the crystal $VOSO_4 \cdot 2H_2O$ by Hutchison and Singer[12] who found $g=1.96$.

The hyperfine constant $\langle a \rangle$ was also measured for this solution (see Fig. 5) and was found to be in agreement with Sands[13] and with Kozyrev. The values are: Kozyrev, 116 gauss; Sands, 120 gauss; present data, 118(1) gauss.

V. DISCUSSION

The assumption of a microcrystallite model to explain the variation of width of m_I components of VO^{++} has been confirmed. Two further features of the vanadyl spectrum still remain to be explained quantitatively although qualitatively at least one of these is explained by the microcrystalline model. The two features, first reported by Pake and Sands,[2] are: (1) the magnitude of the hyperfine constant varies with the solvent used; (2) the individual component lines are asymmetric with respect to the baseline. The first effect can be qualitatively explained by the change in solvents causing a change in the structure of the microcrystallite thereby perturbing the electronic wave function and hence the hyperfine interaction. The explanation of the second effect is obscure. At first one might consider the effect to be due to the incomplete averaging of the anisotropic g tensor or hyperfine tensor. This view would seem to be supported by the observation of Sands[13] that lower viscosity and higher temperature solutions exhibit a greater component symmetry, and also by observations made in the course of the present work that component symmetry increases with decreasing values of the resonant frequency. However, estimates of the factors $\Delta\gamma B_0$ and bm_I give $\Delta\omega \cdot \tau_c \ll 1$, thus indicating complete motional averaging for terms arising from these sources. Furthermore, for the contributions to arise from such terms, one would expect the symmetry to vary with m_I, since $bm_I \geq \Delta\gamma B_0$. The experimentally observed symmetry ratio (the ratio of the baseline to maximum amplitude derivative heights) does not show such a dependence, remaining constant for different m_I components within the limits of experimental error. At present, no other feasible mechanisms for this asymmetry have been found.[14]

Finally, it should be made clear that the relaxation mechanism considered here deals only with that part of the interaction that contributes to the variation of hyperfine linewidth. Any contributions from other possible interactions, such as spin-orbit coupling, are not calculated. The McConnell theory is thus not applicable to the calculation of total linewidth nor to the variation as a function of frequency of the width of unresolved spectra. Hence, the observation made by Al'tschuler and Valiev[15] that the data of Kozyrev[16] disagree with the McConnell theory is due to the inapplicability to the cases Kozyrev measures.

APPENDIX. EXPLICIT FORMS OF THE HAMILTONIANS IN SEC. 2

Zeeman Terms

The Zeeman term is

$$\mathcal{H}_0 = \hbar \mathbf{S} \cdot \mathfrak{G} \cdot \mathbf{B},$$

where $\mathbf{S} = \sum_k \mathbf{S}_k$, the total electron spin operator; $\mathbf{B}$ is the dc magnetic field; and $\mathfrak{G}$ is the gyromagnetic ratio tensor, which, diagonalized in a molecule-fixed coordinate system, has components $\gamma_p, \gamma_q, \gamma_r$. It may be broken up into the following terms: an isotropic term

$$\mathcal{H}_0^{(i)} = \sum_k \hbar \gamma_k \mathbf{S}_{zk} B_0$$

and anisotropic secular term

$$\mathcal{H}_0^{(a)} = \sum_k \hbar [\tfrac{1}{3} \Delta\gamma_k (3\cos^2\xi_k - 1) - \delta\gamma_k \sin^2\xi_k \cos 2\eta_k] \mathbf{S}_{zk} B_0$$

and an anisotropic nonsecular term

$$\mathcal{H}_0^{(n)} = \sum_k \hbar \tfrac{1}{2} B_0 [\Delta\gamma_k (\mathbf{S}_k^+ R_{1k} + \mathbf{S}_k^- R_{1k}) + \delta\gamma_k (\mathbf{S}_k^+ R_{2k} + \mathbf{S}_k^- R_{2k})],$$

where

$$R_{1k} = i \exp(-i\zeta_k) \cos\xi_k \sin\xi_k,$$

$$R_{2k} = \exp(-i\zeta_k) \sin\xi_k (\sin 2\eta_k + i \cos\xi_k \cos 2\eta_k),$$

$$\gamma = \tfrac{1}{3} Tr \mathfrak{G},$$

$$\delta\gamma = \tfrac{1}{2} (\gamma_p - \gamma_q),$$

and where ξ_k is the angle between the molecular z axis and the B_0 axis for the kth molecule, η_k is the angle of rotation about the molecular z axis, and ζ_k the angle of rotation about the B_0 axis. The subscript k refers to the kth molecule.

Hyperfine Terms

The hyperfine term may be written as

$$\mathcal{H}_{IS} = -\hbar \mathbf{I} \cdot \mathbf{A} \cdot \mathbf{S},$$

where $\mathbf{I} = \sum_k \mathbf{I}_k$ (assuming one paramagnetic nucleus per molecule); and $\mathbf{A}$ is the hyperfine interaction

[12] C. A. Hutchison and L. S. Singer, Phys. Rev. **89**, 256 (1953).
[13] R. H. Sands, thesis, Washington University, 1954.
[14] *Note added in proof.* W. Tank and M. W. P. Strandberg (private communication) have made experimental studies which indicate that the conductivity and dielectric absorption of these solutions provide sufficient mixing of the real and imaginary parts of the resonant magnetic susceptibility to account for the asymmetry of individual lines in our spectra.
[15] S. A. Al'tshuler and K. A. Valiev, Soviet Phys. JETP **4**, 661 (1959).
[16] B. M. Kozyrev, Bull. Acad Sci. U.S.S.R. **21**, 828 (1957).

tensor. This can be broken up into the isotropic hyperfine term

$$\mathcal{H}_{IS}^{(i)} = -\hbar a \mathbf{I}\cdot\mathbf{S},$$

which may be written as the sum of a secular and nonsecular term

$$\mathcal{H}_{IS}^{(is)} = -\hbar a I_z S_z$$

$$\mathcal{H}_{IS}^{(in)} = \hbar \tfrac{1}{2} a (\mathbf{I}^+\mathbf{S}^- + \mathbf{I}^-\mathbf{S}^+)$$

and an anisotropic hyperfine, or dipolar, term

$$\mathcal{H}_{IS}^{(a)} = \hbar \mathbf{I}\cdot\boldsymbol{\Phi}\cdot\mathbf{S},$$

where Φ is the anisotropic dipolar interaction. The dipolar term may be written as the sum of four terms:

(a) a secular term

$$\mathcal{H}_{IS}^{(as)} = \hbar \Phi_{zz} I_z S_z,$$

(b) a "pseudosecular" term

$$\mathcal{H}_{IS}^{(ap)} = \hbar (\Phi_{z+} S_z \mathbf{I}^+ + \Phi_{z-} S_z \mathbf{I}^-),$$

(c) and two nonsecular terms

$$\mathcal{H}_{IS}^{(an)} = \hbar (\Phi_{z+} I_z \mathbf{S}^+ + \Phi_{z-} I_z \mathbf{S}^-) + (\Phi_{++} \mathbf{I}^+\mathbf{S}^+ + \Phi_{--} \mathbf{I}^-\mathbf{S}^-)$$

$$\mathcal{H}_{IS}^{(a+-)} = -\hbar \tfrac{1}{4} \Phi_{zz} (\mathbf{I}^+\mathbf{S}^- + \mathbf{I}^-\mathbf{S}^+),$$

where the symmetric tensor $\boldsymbol{\Phi}$ has the components

$$\Phi_{zz} = \tfrac{1}{2} b (3\cos^2\xi - 1) - \sin^2\xi (c e^{-2i\eta} + c^* e^{2i\eta}) + \sin 2\xi (i d e^{-i\eta} - i d^* e^{i\eta})$$

$$\Phi_{z+} = \Phi_{z-}{}^* = \{ (\tfrac{3}{8}) b i \sin 2\xi + \tfrac{1}{2} i \sin\xi [c(1+\cos\xi) e^{-2i\eta} - c^*(1-\cos\xi) e^{2i\eta}] + \tfrac{1}{2} [d(\cos^2\xi + \cos\xi - 1) e^{i\eta} + d^*(-2\cos^2\xi + \cos\xi + 1)] e^{i\eta} \} e^{-i\zeta}$$

$$\Phi_{++} = \Phi_{--} = \{ -(\tfrac{3}{8}) b \sin^2\xi + \tfrac{1}{4} [c(1+\cos\xi)^2 e^{-2i\eta} + c^*(1-\cos\xi)^2 e^{2i\eta}] + i \tfrac{1}{2} \sin\xi [d(1+\cos\xi) e^{-i\eta} + d^*(1-\cos\xi) e^{i\eta}] \} e^{-2i\zeta},$$

and where

$$b = \gamma\gamma_n \hbar \langle 0 \mid (1 - 3\cos^2\theta)/r^3 \mid 0 \rangle$$

$$c = -\tfrac{1}{4} (3\gamma\gamma_n \hbar) \langle 0 \mid \sin^2\theta e^{-2i\Phi}/r^3 \mid 0 \rangle$$

$$d = -\tfrac{1}{2} (3\gamma\gamma_n \hbar) \langle 0 \mid \cos\theta \sin\theta\, e^{-i\Phi}/r^3 \mid 0 \rangle,$$

θ, ϕ and r are the polar coordinates of the nucleus, relative to the unpaired electron, in the molecular framework; γ_n is the gyromagnetic ratio of the nucleus; $\langle 0 \mid \quad \mid 0 \rangle$ indicates the expectation value of the enclosed operator between orbital electronic wave functions.

Pressure Dependence of Some Infrared and Vacuum Ultraviolet Bands Occurring in Active Nitrogen

ROBERT A. YOUNG*

Boeing Airplane Company, Seattle, Washington

(Received May 25, 1960)

By comparing the infrared (7000 to 11 000 A) and vacuum ultraviolet (1050 to 1350 A) nitrogen afterglow emission to the visible (5300 to 6500 A) afterglow it has been determined that: (1) all these portions of the afterglow spectrum decay identically with time; (2) the predominant emission in the vacuum ultraviolet between 1050 and 1350 A may be attributed to the Lyman-Birge-Hopfield bands from the 6, 5, 4 vibration levels and that the population of these levels is collisionally deactivated by molecular nitrogen with a probability of 1×10^{-2}/collision; and (3) that apparently half the intensity of the first positive infrared bands with $v'<6$ are excited through an intermediate state or complex whose lifetime is no shorter than 10^{-7} sec and which, in the absence of collisions, does not contribute to the emission in the regions between 1050 and 11 000 A that have been monitored.

INTRODUCTION

THERE have been many investigations of the spectral distribution of the 1st positive bands of nitrogen excited in active nitrogen. The most complete of these is that of Bayes and Kistiakowsky[1] which supports the excitation mechanism proposed by Berkowitz *et al.*,[2] for the 1st positive bands. This mechanism which involves the collision induced nonradiative transfer from the weakly bound $^5\Sigma$ state of nitrogen to the $B\,^3\Pi_g$ radiating state, has been enlarged to include the several excited states of molecular nitrogen whose potentials cross that of the $^5\Sigma$ state. The excitation in the afterglow of new infrared bands[3] overlapping some of the first positive bands, the temperature variation of the first positive vibrational distribution,[1] and the selective effects of impurities on this distribution[1] all substantiate this mechanism.

Though evidence exists for a pressure dependence of the vibrational distribution in the 1st positive bands at high pressure in the afterglow,[4] the experimental evidence at lower pressures[1] indicates that the spectral distribution is not pressure-dependent. However, the region below 1 mm Hg has not been investigated in this respect. One of the purposes of the present investigation is to make such observations at very low pressure ($\approx$0.1 mm Hg) particularly in the infrared portion of the spectrum which is most sensitive to experimental conditions.

A second purpose of the present work is to ascertain if the Lyman-Birge-Hopfield (L-B-H) bands which are normally observed in active nitrogen[5] are excited in a manner compatible with the mechanism proposed by Bayes and Kistiakowsky.

EXPERIMENTAL

The formation and containment of active nitrogen have been dealt with in previous papers.[6] The means of investigating its spectral character with high-speed spectrographs and efficient light collection has also been reported.[6,7] It is sufficient for our present purposes to state that either a pulsed high-current arc or a condensed ring discharge produced the active nitrogen which was confined in a 12-liter bulb isolated from the remainder of the vacuum system by magnetically operated glass valves. The interior of the bulb was coated with deliquescent phosphorus pentoxide and the exterior with magnesium oxide. Nitrogen was generated from sodium azide and continuously trapped with liquid nitrogen. Spectroscopically observed contaminants were atomic oxygen and cyanogen. The time dependence of their emissions is markedly different from that of the 1st positive bands of nitrogen.[6]

A silicon solar cell, which is an almost ideal detector for the infrared 1st positive bands, was used for this purpose. It spectral response peaks at about 8000 A, dropping to a negligible value above 11 000 A. The short wavelength response below 7500 A was reduced sufficiently by a Corning colored glass filter. Using a small chip from such a solar cell located at the focus of a 2-in. diam. mirror and measuring its output with a chopper stabilized dc amplifier, the decay of the infrared afterglow was followed over a factor of a thousand while being displayed on a Varian recorder.

The visible first positive bands were measured with a standard photomultiplier having an S11 photocathode response. Such a photocathode is relatively insensitive beyond 6500 A and was limited to wavelengths above 5300 A by a Corning colored glass filter. A high stability power supply (0.01% regulation) provided the dynode

* Now at Stanford Research Institute, Menlo Park, California.

[1] K. D. Bayes and G. B. Kistiakowsky. J. Chem. Phys. **32**, 992 (1960).

[2] J. Berkowitz, W. Chupka, and G. B. Kistiakowsky. J. Chem. Phys. **25**, 457 (1956).

[3] M. Brook, Science Rept. No. 2, contract of the U. S. Air Force Geophysics Directorate with the University of California at Los Angeles (1951); G. B. Kistiakowsky and P. Warneck, J. Chem. Phys. **27**, 1417 (1957); F. LeBlanc, Y. Tanaka, and A. Jursa, J. Chem. Phys. **28**, 979 (1958).

[4] C. R. Stanley, Proc. Roy. Soc. (London) **A241**, 180 (1957).

[5] Y. Tanaka, A. Jursa, and F. LeBlanc, *The Threshold of Space*, edited by M. Zelikoff (Pergamon Press, New York, 1957), p. 89.

[6] R. A. Young and K. C. Clark, J. Chem. Phys. **32**, 604, 607 (1960).

[7] R. A. Young, J. Opt. Soc. Am. **50**, 627 (1960).

voltages through a voltage dropping resistor string. The photomultiplier output was amplified by a chopper stabilized amplifier and applied to a second Varian recorder.

Iodine Geiger counters[8] with lithium fluorite windows and various gas filters[9] were utilized to detect the very weak vacuum ultraviolet radiation. The short wavelength response was limited by the transmission of the windows to above 1050 A and the long wavelength response was limited by the ionization threshold of iodine at 1350 A. These limits were verified by measurements on a vacuum spectrograph. The compounded variation of a weak vacuum ultraviolet source and the iodine Geiger counter *in situ* was less than ±10% over a period of time comparable to that required for the present measurements.

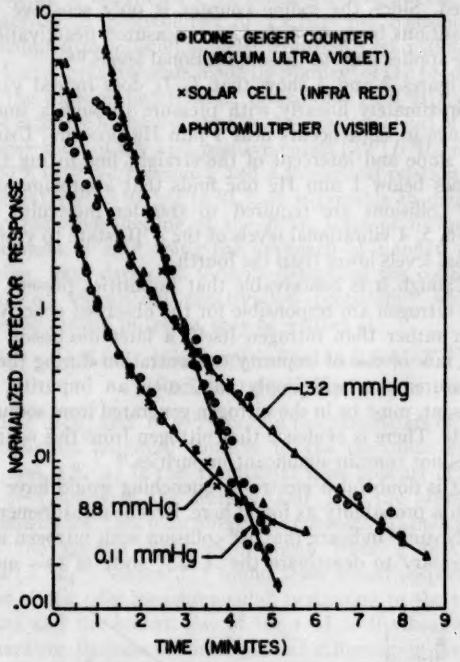

FIG. 1. Representative simultaneous decays of different spectral regions of the nitrogen afterglow: ⊙, 1050–1350 A; ×, 7500–11 000 A; △, 5300–6500 A. At 8.8 mm Hg recombination is the predominant loss while at 0.11 mm Hg diffusion from the observation bulb is most important. The similarity of the vacuum ultraviolet decay with the first positive bands of nitrogen indicate that the major radiation in this region is the Lyman-Birge-Hopfield bands from high-vibration levels ($v'=6, 5, 4$.)

RESULTS

The observed vacuum ultraviolet emission was found to center about 1300 A from the absorption produced by nitrous oxide.[10] Of the species detected by their visible radiation, O, NO, CN, and N_2, only atomic oxygen (the $2p^4\,{}^3P-3s\,{}^3S$ transitions near 1302 A) and molecular nitrogen (the 6–1, 5–0, 4–0 L-B-H bands) have observed emissions near 1300 A.

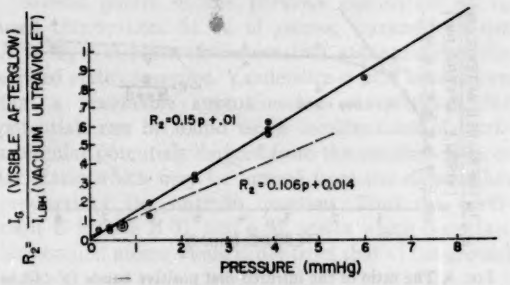

FIG. 2. The ratio of the visible first positive bands ($v'>6$) to the vacuum ultraviolet Lyman-Birge-Hopfield bands from the $v'=6$, 5, 4 vibration levels as a function of pressure indicating vibrational deactivation. The dashed curve with somewhat smaller slope is that derived from the points below 1 mm Hg shown in Fig. 3.

Figure 1 is a plot of the simultaneous decay of all detectors arbitrarily normalized and shown for three representative pressures. At the highest intensity the Geiger counter is seriously overloaded. Note that all bands including those in the vacuum ultraviolet decay together.

Figures 2 and 3 show that, relative to the visible first positive bands, the ultraviolet intensity increases approximately inversely as the pressure.

Figures 4 and 5 indicate an anomalous behavior of the infrared bands. In agreement with Bayes and Kistiakowsky[1] no change is observed above 1 mm Hg, but below 1 mm Hg the infrared bands decrease in intensity relative to the visible bands. Spectrograms taken with a fast spectrograph of the afterglow at 1 mm Hg and at 0.1 mm Hg show that, in fact, the infrared portion of the spectrum ($v'<6$) decreases relative to the visible portion ($v'>6$), and that this

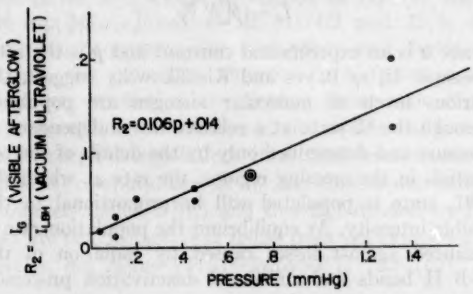

FIG. 3. The ratio of the visible first positive bands ($v'>6$) to the L-B-H bands from $v'=6$, 5, 4 as a function of pressure indicating vibrational deactivation.

[8] R. Brackman, W. Fite, and K. Hagen, Rev. Sci. Instr. **29**, 125 (1958).

[9] T. A. Chubb and H. Friedman, Rev. Sci. Instr. **26**, 493 (1959).

[10] M. Zelikoff, K. Watanabe, and E. Inn, J. Chem. Phys. **21**, 1643 (1953).

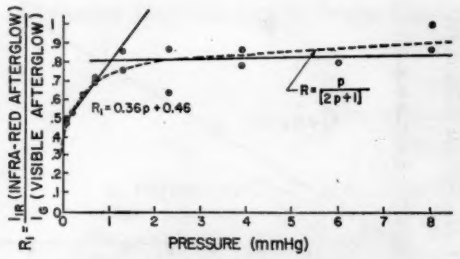

FIG. 4. The ratio of the infrared first positive bands ($v'<6$) to the visible first positive bands ($v'>6$) as a function of pressure. The dashed curve is that of $p/2p+1$ with the addition of a normalizing constant.

reduction is approximately that recorded by the infrared detector.

DISCUSSION

1. Lyman-Birge-Hopfield Bands

From the congruence of the decay curves of the different afterglow detectors in Fig. 1, one may conclude that the observed emission near 1300 A is the 6–1, 5–0, and 4–0 L-B-H bands and that they are excited by the process suggested by Bayes and Kistiakowsky. The L–B–H bands are expected to follow the first positive bands if they are excited through the $^5\Sigma$ state while the atomic oxygen lines, which would most probably be excited by a Chapman reaction involving atomic oxygen and nitrogen,[6] would be expected to decay more rapidly than the first positive bands. Since the L–B–H bands from low v' levels of the $a\ ^1\Pi_g$ state are the only emissions observed from the afterglow in the vacuum ultraviolet,[5] it is not surprising that one should find an extension of this system near 1300 A.

As a first step in analyzing the pressure dependence of the vacuum ultraviolet to the visible afterglow intensity ratio of Figs. 2 and 3, one notes that the visible afterglow intensity I_g has been found[2] to be proportional to the square of the nitrogen atom concentration

$$I_g = ap[N]^2, \tag{1}$$

where a is an experimental constant and p is the total pressure. If, as Bayes and Kistiakowsky suggest, the various levels of molecular nitrogen are populated through the $^5\Sigma$ state at a relative rate independent of pressure and determined only by the details of the potentials in the crossing regions, the rate at which the $a\ ^1\Pi_g$ state is populated will be proportional to the visible intensity. At equilibrium the population rate is balanced against losses caused by radiation of the L–B–H bands and collisional deactivation processes, i.e.,

$$\alpha I_g = [kp + (1/\tau)][N_2(a\ ^1\Pi_g)], \tag{2}$$

where a is a constant independent of pressure, τ is the lifetime of the $a\ ^1\Pi_g$ state, and kp is the collisional deactivation rate constant. However, the L–B–H band intensity I_L is equal to $\tau^{-1}[N_2(a\ ^1\Pi_g)]$ and we find

$$I_g/I_L = C(\tau kp + 1), \tag{3}$$

where C is a constant (α^{-1}) but may be considered to include the sensitivities of the detectors if I_g and I_L are interpreted as their outputs. From the slope and intercept of the straight line resulting from a plot of I_g/I_L vs pressure one can obtain $k\tau$. The radiative lifetime τ has been measured by Lichten[11] as 1.7×10^{-4} sec allowing the collision deactivation rate to be computed. Since the iodine counter is only sensitive to transitions from $v'=6, 5, 4$, the measured deactivation rate applies only to these vibrational levels.[11a]

Figures 2 and 3 show that I_g/I_L does indeed vary approximately linearly with pressure through a small change in slope occurs near 1 mm Hg pressure. Using the slope and intercept of the straight line fitting the points below 1 mm Hg one finds that approximately 400 collisions are required to transfer molecules in $v'=6, 5, 4$ vibrational levels of the $a\ ^1\Pi_g$ state to vibrational levels lower than the fourth.

Though it is conceivable that impurities present in the nitrogen are responsible for the observed deactivation rather than nitrogen itself, a later discussion of the rate of rise of impurity concentration during these measurements will imply that such an impurity, if present, must be in the nitrogen generated from sodium azide. There is evidence that nitrogen from this source does not contain significant impurities.[12]

It is doubtful if electronic quenching would have as high a probability as found here. Recent measurements of Noxon[12] indicate that 10^8 collision with nitrogen are necessary to deactivate the $A\ ^3\Sigma_u^+$ state of this mol-

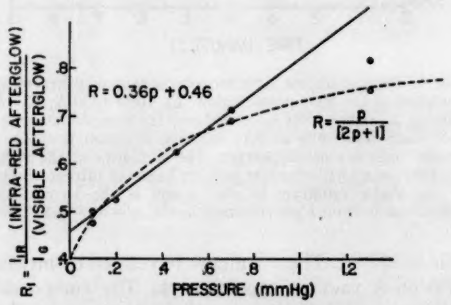

FIG. 5. The ratio of the infrared first positive bands ($v'<6$) to the visible first positive bands ($v'>6$) as a function of pressure showing, on an expanded scale, the decrease of this ratio below 1 mm Hg. The dashed curve is that of $p/2p+1$ with the addition of a normalizing constant.

[11] W. Lichten, J. Chem. Phys. **26**, 306 (1957). (a) Because the radiative lifetime varies as the cube of the frequency and Lichten's measurements refer to the $v'=0$ level of the $a\ ^1\Pi_g$ state, the lifetime appropriate to the higher v' states is 1.1×10^{-4} sec. Variation of the electronic transition moment with internuclear distance has been ignored in this and succeeding calculations.

[12] J. Noxon, "Active nitrogen at high pressure" thesis, Harvard University, Cambridge, Massachusetts, 1957.

ecule. Various atomic mestastable states also require about the same number of collisions to be quenched.[12] Although collision-induced vibrational relaxation of the $v'=1$ levels of both the $A\ ^3\Sigma_u^+$ and $X\ ^1\Sigma_g^+$ states are found to be as improbable as electronic quenching,[12,13] the higher vibrational levels may be more easily deactivated by collision processes because of their smaller vibrational level spacing. The theoretical and experimental results, concerning collision induced vibrational relaxation, have recently been reviewed by McCoubrey and McGrath.[14] Without further evidence to the contrary the roughly measured collision deactivation probability[15] of 1×10^{-2} per collision is attributed to collision induced vibrational relaxation.

Using measurements made by Stanley[4] of the product of the collision deactivation probability $P(B\ ^3\Pi_g)$, and the ratiative lifetime of the $v'=11$ vibrational level of the upper state of the first positive bands $[(P(B\ ^3\Pi_g)\tau_B=1.37\times10^{-10}$ sec/collision], and a theoretical relation for the ratio $P(B\ ^3\Pi_g)/P(a\ ^1\Pi_g)$, it is possible to deduce the radiative lifetime of the $B\ ^3\Pi_g$ state of nitrogen. Schwartz *et al.*,[16] using the approach of Landau and Teller, have derived a formula describing the collision induced vibrational deactivation probability which, for the present purposes, may be written as

$$P(\alpha)=[\Delta E_v(\alpha)/A(\alpha)]\exp[-B(\alpha)(\Delta E_v(\alpha)^2/T)^{\frac{1}{3}}]$$
$$=[\Delta E_v(\alpha)/A(\alpha)]\exp(-3\psi(\alpha), \quad (4)$$

where $A(\alpha)$ and $B(\alpha)$[16a] contain the parameters of the interaction potential suitable to the electronic state α, and $\Delta E_v(\alpha)$ is the vibrational level spacing of the v, $v-1$ levels of the state α, and T is the absolute temperature. One may obtain the constant B applicable to the ground state of nitrogen from a plot of $\ln P(X\ ^1\Sigma_g^+)$ versus $T^{-\frac{1}{3}}$ found from sound dispersion and shock tube measurements[13] pertaining to the $v=1$ level and the known size of the $v=1$ to 0 vibrational quantum. Because of the very small difference in the vibrational level spacing of the $v'=6$, 5, and 4 levels of the $a\ ^1\Pi_g$ state and the $v'=11$ and 10 levels of the $B\ ^3\Pi_g$ state of nitrogen (to which Stanley's work refers), the ratio of deactivation probabilities $P(B\ ^3\Pi_g)/P(a\ ^1\Pi_g)$ is 2.3. The constant $A(\alpha)$ varies slowly with changes of electronic state and is considered constant as has $B(\alpha)$. When combined with the present value for $P(a\ ^1\Pi_g)$ this gives $P(B\ ^3\Pi_g)=2.3\times10^{-2}$/collision which, with Stanley's result for $P(B\ ^3\Pi_g)\tau_B$, leads to $\tau_B=6\times10^{-9}$ sec.

Several points in the previous calculation of τ_B need clarification. It is, of course, incorrect to use $B(X\ ^1\Sigma_g^+)$ in place of the constant appropriate to the excited state concerned. Vanderslice *et al.*,[17] have shown that a reasonable approximation to intermolecular potentials can be found using combinations of intramolecular potentials derived from the possible molecular states which may be formed from the dissociation products of the state in question. Thus the coefficient B for the $B\ ^3\Pi_g$ and $a\ ^1\Pi_g$ states which dissociate into excited atoms would differ from that of the ground state.

Using the measured values of $P(X\ ^1\Sigma_g^+)$ and $P(a\ ^1\Pi_g)$ and Eq. (4), one finds that $B(a\ ^1\Pi_g)\approx\frac{1}{3}B(X\ ^1\Sigma_g^+)$. The $a\ ^1\Pi_g$ state dissociates into two ^2D nitrogen atoms while the $B\ ^3\Pi_g$ state dissociates into one ^4S and one ^2D atom. For want of a better approximation $B(B\ ^3\Pi_g)$ may be taken as intermediate between these extremes, i.e., $B(B\ ^3\Pi_g)\approx\frac{2}{3}B(X\ ^1\Sigma_g^+)$. With these data Eq. (4) gives $P(B\ ^3\Pi_g)/P(a\ ^1\Pi_g)=5.7\times10^{-3}$ or $P(B\ ^3\Pi_g)=3.5\times10^{-6}$/collision and $\tau_B=2.4\times10^{-6}$ sec, while the assumption that $B(B\ ^3\Pi_g)=B(a\ ^1\Pi_g)=\frac{1}{3}B(X\ ^1\Sigma_g^+)$ leads to $\tau_B=1.1\times10^{-8}$ sec. It must be remembered that τ_B refers to the 11th vibrational level: the zero vibrational level would have a lifetime approximately 14 times that of the $n'=11$ level due to the difference in transition energy. Because the $B\ ^3\Pi_g$ and $a\ ^1\Pi_g$ states have the same molecular orbital configuration, their B values are probably closer together than those used in computing $\tau_B=2.4\times10^{-6}$ sec though they are not identical as assumed in computing $\tau_B=1.1\times10^{-8}$ sec. Thus the radative lifetime of the $B\ ^3\Pi_g$ state derived from collision deactivation probabilities of vibrational levels of the $B\ ^3\Pi_g$ and $a\ ^1\Pi_g$ states is consistent with the value of $\approx10^{-6}$ sec computed by Bates[18] when the limitation imposed by the inaccuracies both in form and parameters of Eq. (4) are taken into account.

The anharmonic nature of the high-vibrational levels concerned in the present calculations have not been explicitly considered. Nikitin[19] has shown that a correction factor of γ should be applied to Eq. (4) where $\gamma=\exp[\frac{4}{3}\psi(\alpha)\epsilon]$ and $\epsilon=\Delta E_1(\alpha)/4D$ and D is the dissociation energy. For high-vibrational levels of oxygen this correction amounts to a factor of 10. However, our final results depend either upon direct experimental determinations of the exponential factors or on rough extrapolations from these measurements. Explicit computations of γ are thus unwarranted. However, the $B(B\ ^3\Pi_g)$ and $B(a\ ^1\Pi_g)$ defined by Eq. (4) are not, in fact, that found from the experimental results, but rather $[\psi(\alpha)-\frac{4}{3}\psi(\alpha)\epsilon V]T^{\frac{1}{3}}/\Delta E_v(\alpha)^{\frac{1}{3}}$.

[13] J. S. Lukasik and J. E. Young, J. Chem. Phys. **27**, 1149 (1957).

[14] J. C. McCoubrey and W. D. McGrath, Quart. Revs. **11**, 87 (1957).

[15] The measured deactivation probability for the group of levels $v'=6$, 5, 4 has been divided by three to obtain an approximate value for single quantum steps.

[16] R. Schwartz, Z. Slawsky, and K. Herzfield, J. Chem. Phys. **20**, 1591 (1952). (a) These parameters really depend upon the electronic states of both molecules involved in the deactivating collisions. However, since in all the situations to be discussed one of the molecules is in the ground state, only the excited molecular state is indicated.

[17] J. Vanderslice, E. Mason, and E. Lippincott, J. Chem. Phys. **30**, 129 (1959).

[18] D. R. Bates, Ann. Geophys. **8**, 194 (1952).

[19] E. Nikitin, Proc. Acad. Sci. U.S.S.R., Phys. Chem. Sect. **124**, 161 (1959) (English translation).

Oldenberg and Carlton[20] have experimentally related the radiative lifetime τ_A of the $A\ ^3\Sigma_u^+$ state to the lifetime τ_B of the $B\ ^3\Pi_g$ state (now referring to the $v'=0$) level in all cases in the following manner: $\tau_A = 1.6\times10^{-6}\tau_B$). Our measurements thus restrict τ_A to $0.036<\tau_A<5.0$ sec. The lower limit is approximately that computed by Wilkinson and Mulliken[21] from absorption measurements.

2. Infrared first Positive Bands

There are at least two alternative possible causes for the decrease of the infrared first positive bands relative to the visible bands. If the concentration of an impurity comes into equilibrium with its sources rapidly enough, the impurity partial pressure will remain fixed and its mole fraction will increase as the nitrogen pressure is decreased. At low impurity concentrations the mole fraction would then be approximately inversely proportional to the total pressure, and if the relative infrared reduction is proportional to the mole fraction of impurities, a linear decrease of the relative infrared intensity would occur with decreasing pressure. As Figs. 4 and 5 show, such a linear dependence approximately fits the data. Above 1 mm Hg pressure the mole fraction of impurity would have to be too small to produce a noticeable spectral shift or quenching.

Measurements of the pressure rise in the system as a function of time indicate that the approach to the equilibrium impurity pressure of 5×10^{-3} mm Hg was so slow (2×10^{-3} mm Hg was reached after 11 hours) that the impurity mole fraction would not have become larger than 7×10^{-3}. When the actual impurity pressure rise curve, elapsed time of the observations, and the pressure intervals used are employed to reconstruct the mole fraction versus pressure curve, it is found to be far from linear, rising at an almost exponential rate as the pressure was reduced. The impurity was found to be uncondensable at liquid nitrogen temperature which indicates that it is either molecular nitrogen dissolved in the metaphosphoric acid wall coating or molecular hydrogen derived from the same material.[22] From spectral observation and the behavior of the afterglow decay it is known that negligible amounts of oxygen are present. From the recent measurements of Kistiakowsky and Bayes[1] molecular hydrogen in these concentrations would not be expected to effect the visible spectral distribution. However, if hydrogen was as effective as ammonia (the best quenching agent known) in selectively quenching the infrared bands and if half the total impurity were hydrogen, the observed magnitude of quenching would occur though its pressure dependence would differ from that found. Although the discharge and the reactive nature of active nitrogen may effect the mole fraction vs pressure curve, it is believed that a linear variation would not hold, though some cleanup of the impurity may occur. That the dependence of the infrared reduction on the impurity mole fraction would be of such a complementary nature to the nonlinear variation of mole fraction with pressure as to effect the observed variation of the infrared reduction with pressure is considered improbable. We conclude from these observations, that the reduction in the infrared first positive bands relative to the visible first positive bands is not due to impurity quenching.

Alternatively, the experimental results under discussion may be related to additional excitation process, other than those directly involving the $^5\Sigma$ state. Bayes and Kistiakowsky find evidence that a portion of the infrared bands (designated by them as group 3b) are excited by a process involving two consequentive precursors. On the assumption that a fraction of the infrared 1st positive bands (the 3b group) of intensity I_3 are excited in a collision induced transition from a second precursor $N_2(\alpha)$ at a rate $k(\alpha)p$ and that, in the absence of collisions, this precursor has a lifetime τ_α and does not radiate within the sensitive regions of our detectors and is formed at a rate proportional to the visible first positive bands, we may write the following equations:

$$I_3 = k(\alpha)pN_2(\alpha) \tag{5}$$

$$\mu I_g = [k(\alpha)p + (1/\tau_\alpha)]N_2(\alpha), \tag{6}$$

where μ is a constant. Dividing Eq. (5) by Eq. (6) we find

$$I_3/I_g = C[k(\alpha)\tau_\alpha p/(k(\alpha)\tau_\alpha p+1)]. \tag{7}$$

The dashed curves shown in Figs. 4 and 5, which fit the data quite well, were computed from Eq. (7) with $k(\alpha)\tau_\alpha=2$. If the probability per collision $R(\alpha)$ for inducing the transition from $N_2(\alpha)$ to $N_2(B\ ^3\Pi_g, v'<6)$ is unity and the collision rate for ground state N_2 is appropriate to collisions between $N_2(\alpha)$ and $N_2(X\ ^1\Sigma_g^+)$, the minimum lifetime of $N_2(\alpha)$ is $\tau_\alpha=2\times10^{-7}$ sec.

Bayes and Kistiakowsky have suggested that $N_2(\alpha)$ be identified with $N_2(A\ ^3\Sigma_u^+)$. Our previous computations of τ_A through collisional deactivation of vibrational levels of the $a\ ^1\Pi_g$ and $B\ ^3\Pi_g$ states restricts τ_A and this in turn limits the probability per collision of the electronic state transfer under discussion to $4\times10^{-5} > R(A\ ^3\Sigma_u^+) > 5.5\times10^{-7}$. The lower limit is unrealistic since the actual lifetime of the $A\ ^3\Sigma_u^+$ state is considerably shorter than its radiative lifetime. This is implied by the absence of the Vegard-Kaplan bands in these afterglows.

ACKNOWLEDGMENTS

The experimental work reported here was done in the physics department of the University of Washington through the courtesy of Professor R. Geballe and in the laboratory of Professor K. C. Clark.

[20] O. Oldenberg and N. Carlton (private communication).

[21] P. G. Wilkinson and R. S. Mulliken, J. Chem. Phys. **31**, 674 (1959).

[22] Spectrograms of a Tesla discharge through the gas evolved over a months time showed predominantly nitrogen bands and atomic hydrogen emission.

THE JOURNAL OF CHEMICAL PHYSICS VOLUME 33, NUMBER 4 OCTOBER, 1960

Magnetic Rotation Spectra of Nitric Oxide in the Near Infrared*

GLEN A. MANN AND C. D. HAUSE

Department of Physics and Astronomy, Michigan State University, East Lansing, Michigan

(Received May 2, 1960)

Magnetic rotation spectra of the 3–0 band at 1.8 μ and a portion of the 2–0 band at 2.7 μ of nitric oxide have been observed and recorded. Rotations in excess of 10° in fields of 2400 gauss have been observed in some cases. The P and R branch lines arising from the $^2\Pi_1$ states show negative rotation (counter clockwise when looking against the incident light) while the P and R branches from the $^2\Pi_\frac{1}{2}$ states show positive rotation. The Q branch signals are more complex and both positive and negative rotations are observed. Certain anomalies in the magnetic rotation spectrum of the 3–0 band are noted.

INTRODUCTION

THE magnetic rotation spectrum of a gas is the spectrum of the radiation transmitted through crossed polarizing elements when the magnetized gas is placed between them and arranged such that the light traverses the gas in the direction of the field. For a gas, a magnetic rotation signal or line occurs only if the frequency of the incident radiation is close to an absorption frequency or region of anamalous dispersion of the gas. In addition the absorption frequency must show an appreciable Zeeman effect. Thus the spectrum is essentially an enhanced Faraday effect observed only in the neighborhood of critical absorption frequencies in a longitudinal magnetic field.

The effect was discovered for a monatomic gas by Macaluso and Corbino.[1] For a diatomic gas (Na_2) it was first observed by Wood.[2] Magnetic rotation spectra have been found and investigated for a number of other molecules, including I_2, Br_2, K_2, and Bi_2. Loomis and co-workers[3,4] have used these spectra to extend the vibrational analysis of the spectra of the alkali metals to higher vibrational quantum numbers than was possible from the absorption spectrum. More recently Eberhardt, Cheng, and Renner[5] have obtained magnetic rotation spectra of ICl and IBr and show the application of the phenomena to structure analysis, isotope effects, and the determination of dissociation limits. A theoretical treatment of the Faraday effect in molecules was given by Serber[6] but as we shall see later, this is not directly applicable to the work presented in this paper. Carroll[7] somewhat later extended Serber's work and was able to justify certain anomalies observed in the magnetic rotation spectrum of I_2.

All the magnetic rotation spectra previously observed have been confined to the photographic region (visible and near ultraviolet) and were associated with electronic band systems in which the upper state alone possessed magnetic characteristics or was perturbed by some close-lying state which exhibited magnetic characteristics. In general magnetic rotation lines were observed only for those bands where the heads occurred at low J values. The piling up of the lines at the heads gave more favorable intensities. In addition, lines arising from terms with low J values were sometimes favored because of their relatively large Zeeman splitting. It also appears that it was not possible, at least in the case of the alkali metals, to study in detail an individual magnetic rotation line.

The improvement in infrared techniques in recent years has prompted us to look for magnetic rotation spectra in the near infrared, in the hopes that, if successful, these phenomena might be studied in more detail than was possible heretofore. Nitric oxide was chosen since it is a stable diatomic gas, paramagnetic, and has relatively strong absorption bands in the near infrared. The fundamental (1—0) of nitric oxide is at 5.4 μ, the first overtone (2—0) at 2.7 μ and the second overtone (3—0) at 1.8 μ. The second overtone was particularly suitable in our case since it occurs in a region favorable for our spectrometer, requires only moderate absorption paths for good intensity and is in a region relatively free of water lines. The first overtone was less favorable but still accessible.

The ground state of NO is a $^2\Pi$ with coupling intermediate between Hund's case (a) and case (b) coupling schemes and consists of two narrowly separated substates. Transitions between these two substates do not occur with appreciable intensity so the absorption bands in the near infrared consist of two simple bands with single P, Q, and R branches which are almost superimposed. The ratio of intensities of the two bands is about 3 to 2 with the $^2\Pi_\frac{1}{2}$ substate showing the most intense absorption.

FARADAY EFFECT ASSOCIATED WITH A SINGLE ABSORPTION LINE

General Theory (Qualitative)

Serber[6] has shown that the magnetic rotation near an absorption line depends only on the Zeeman effect, all other effects being negligible in comparison. Following Carroll,[7] this fact may be used to show, in a qualitative

* Supported by a grant from the National Science Foundation.

[1] P. Macaluso and O. M. Corbino, Compt. rend. **127**, 548 (1898).
[2] R. W. Wood, Astrophys. J. **30**, 339 (1909).
[3] F. W. Loomis and R. E. Nusbaum, Phys. Rev. **40**, 380 (1932).
[4] F. W. Loomis and M. J. Arvin, Phys. Rev. **46**, 286 (1934).
[5] W. H. Eberhardt, Wu-chieh Cheng, and H. Renner, J. Mol. pectroscopy **3**, 664 (1959).
[6] R. Serber, Phys. Rev. **41**, 489 (1932).
[7] T. Carroll, Phys. Rev. **52**, 82 (1937).

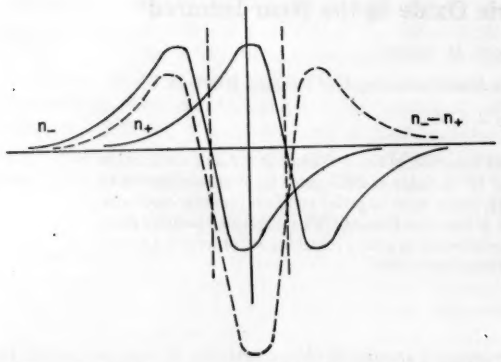

FIG. 1. Dispersion curves and Faraday rotations for light propagated along the magnetic field, for the case of a gas with a single absorption line which shows a normal Zeeman splitting. The solid vertical line shows the position of the center of the field free absorption frequency. The dashed vertical lines show the position of the Zeeman components.

manner, the way in which a single magnetic rotation line arises for an absorption transition showing a normal Zeeman pattern.

Light propagated along the field direction through a magnetized medium exhibits magnetic double refraction. If the incident light is plane polarized, it may be considered as composed of two circular polarized beams, one right circular, the other left. On account of the longitudinal double refraction of the magnetized gas, these two beams are propagated through the medium with different velocities. The equivalent state of polarization at any point in the gas can be found from the phase difference of the two circular polarized beams arising from their unequal velocities and the relative absorption in the magnetized medium. If the absorption for the two components is small, or is equal in magnitude, the result after traversing a distance l in the gas will be a plane polarized beam with its plane of polarization rotated through an angle θ given by

$$\theta=\frac{\pi l}{\lambda}(n^{-}-n^{+}),$$

where n^{-} and n^{+} are the indices of refraction for left and right circular polarized light, respectively. This is shown by the dotted curve in Fig. 1. Since the plane of polarization has been rotated there will be a signal passed by the analyzer and this signal is called a magnetic rotation line. If this qualitative picture is accepted, Fig. 1 also indicates that under low resolution and with weak fields, rotation signals corresponding to the wings of the line only will be observed. (The large absorption at the center will presumably mask the rotation.) On the other hand, with resolved or almost resolved Zeeman patterns a rotation of the opposite sign at the field free frequency may predominate. The sum total of these signals makes up the magnetic rotation spectrum of the gas.

APPARATUS AND METHOD OF MEASUREMENT

The experimental arrangement was simple and straightforward. Plane polarized radiation from the source (300-watt zirconium arc) passed through the absorption cell containing the gas, through an analyzer, and then to the spectrograph. The absorption cell was in the central third of an air core solenoid which provided the longitudinal magnetic field. The arrangement of equipment exterior to the spectrograph is shown in Fig. 2.

The vacuum grating spectrograph was of the Pfund pierced flat type equipped with a cooled (−50°) lead sulfide detector. The spectrograph is designed with a second optical train which includes a Fabry-Perot etalon and photomultiplier detector. Visible radiation from a second source (100-watt concentrated arc) traverses this system and the monochrometer simultaneously with the infrared beam and thus Edser-Butler bands in a higher order of the visible are recorded together with the infrared signal. These bands, which appear at constant frequency intervals, are then used in conjunction with argon emission lines from the source for calibration. In the 1.8-μ region (5500 cm^{-1}) with the grating used in this work and with narrow slits ($w\leq 25$ μ) so that the calibration system can be used the position of absorption peaks can be obtained to ± 0.02 cm^{-1}. A resolution of 0.1 cm^{-1} is attained in this region. Less precise results are obtained at 2.7 μ, where the spectrometer is energy limited.

Type HR polarizers obtained from the Polaroid Corporation were used in the 1.8-μ region and multiple plate silver chloride polarizers set at Brewster's angle

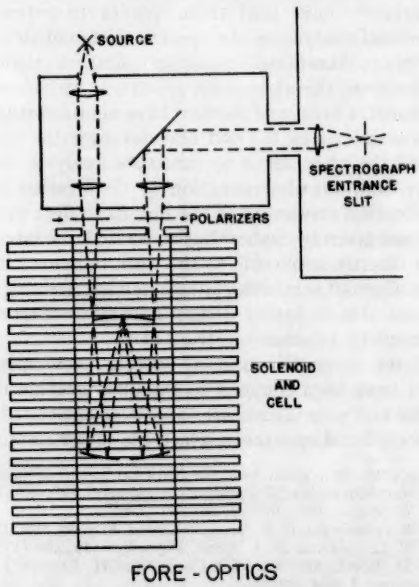

FIG. 2. Arrangement of equipment exterior to the spectrograph to obtain magnetic rotation spectra of a gas.

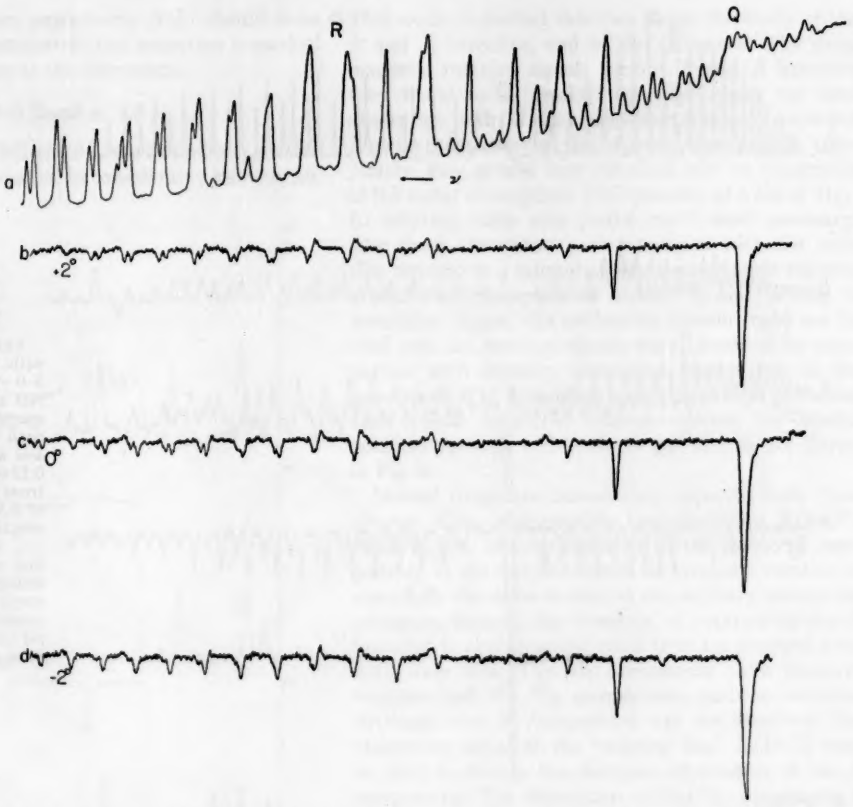

FIG. 3. Absorption and magnetic rotation spectra of the R and Q branches of the 2–0 vibration-rotation band of NO at 2.7 μ. (a) Absorption spectrum obtained with an absorbing path of 1 meter atmosphere. (b), (c), (d) Magnetic rotation spectra with polarizer settings of $+2°, 0°, -2°$, respectively, measured from the crossed position. The effective slit width was 0.28 cm^{-1} in all cases.

in the 2.7-μ region. Since the monochrometer was polarization sensitive, the analyzer was oriented for maximum response. Thereafter the analyzer remained fixed and changes in polarization were made with the polarizer. This insured that the monochrometer would always see radiation in the same state of polarization.

The air core solenoid was constructed of 36 pancake coils each with 90 turns of insulated copper strips $\frac{1}{2}$ inch wide and $\frac{1}{16}$ inch thick. The coils were mounted on an aluminum frame with wood separators. The over-all length of the solenoid was 33 inches. The core diameter was 6.5 inches. The field in the center and within the central third of the solenoid was measured by nuclear magnetic resonance techniques and the variation over the central third found not to exceed 5%. Magnetic rotation spectra were obtained with a field of 2400 gauss.

In order to obtain suitable absorbing paths, a multiple traverse cell of the White type was used. Previous work on NO in the 1.8-μ region indicated the necessity for this. The cell was set for 24 traversals, giving a path length of 8 meters and the pressure of nitric oxide was varied from 1 to 56 cm. of mercury. The cell occupied the central third of the solenoid core.

The magnetic rotation spectra were obtained as a function of the angle between the transmission planes of the polarizer and the analyzer. A rotation of the polarizer in a clockwise direction, as one looks against the incident radiation, was termed a positive rotation, counterclockwise, negative. The zero setting was taken as the crossed position since for this position neither magnetic rotation, positive or negative, would be aided or retarded. The direction and approximate magnitude of the rotation was obtained by noting the setting at which the rotation disappeared. For example, consider a particular frequency which is rotated 10° in the negative direction. Neglecting the absorption that takes place since the polarizers are no longer crossed, a rotation of the polarizer in the positive direction 10° will make the signal disappear. All of the magnetic rotation spectra were obtained in this manner.

RESULTS

A relatively complete magnetic rotation spectrum of the second overtone (3—0) band of NO at 1.8 μ has been obtained, and in addition, the high frequency half of the first overtone (2—0) band at 2.7 μ.

2–0 Band

Only the Q and R branches of this band have been observed in magnetic rotation. This is largely due to

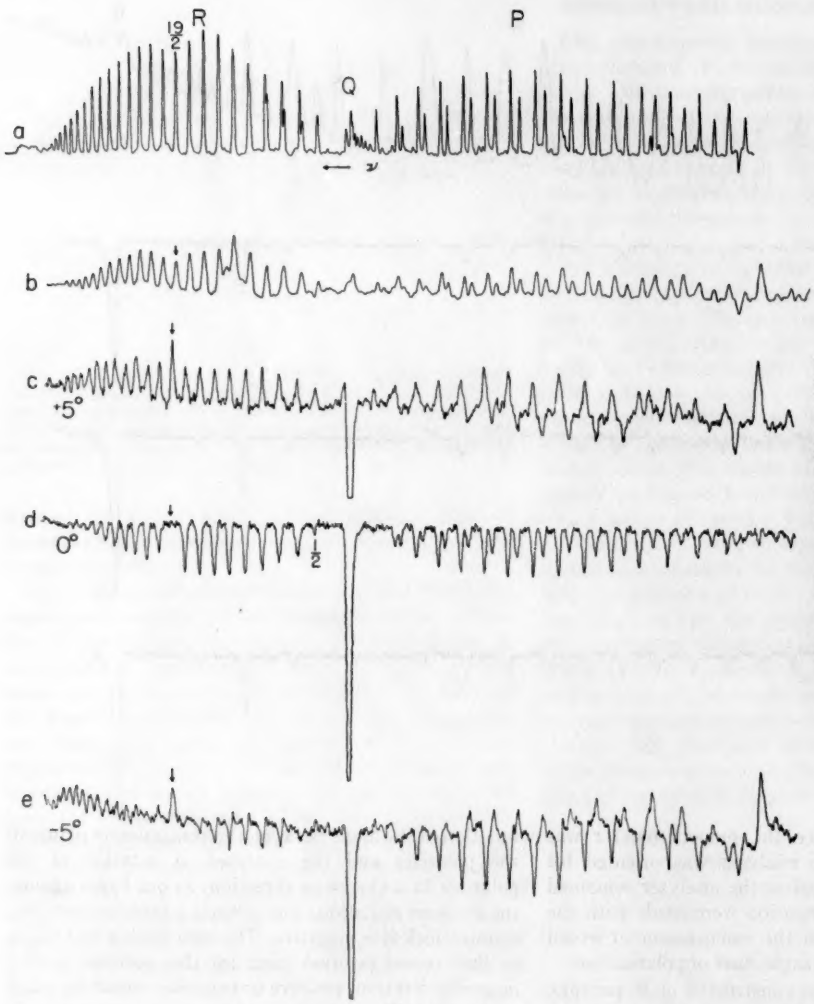

FIG. 4. Absorption and magnetic rotation spectra of the 3–0 vibration-rotation band of NO at 1.8 μ. (a) Absorption spectrum with an absorption path of 4 meter atmospheres and an effective slit width of 0.12 cm^{-1}. (b) Absorption spectrum with an absorption path of 0.5 meter atmosphere and effective slit width of 0.6 cm^{-1}. (c), (d), (e) Magnetic rotation spectrum with polarizer settings of +5°, 0°, −5°, respectively, measured from the crossed position. The gas sample and slit widths were the same as in (b) above.

the progressive decrease in sensitivity of our instrument in this region, the signal being essentially zero immediately after the Q branch. It was, however, possible to observe the R and Q branches with wide slits (200–250 μ equivalent to 0.28 cm^{-1}) and an absorbing path of 1 meter atmosphere. To avoid self-absorption, gas pressures less than 10 cm Hg were required. With the wide slits it was not possible to use the frequency calibration system and obtain measurements of the magnetic rotation frequencies. Consequently these frequencies were identified by comparison with the ordinary absorption spectrum in this region. The absorption spectrum and the magnetic rotation spectrum obtained in this region are shown in Fig. 3. The absorption spectrum, although contaminated with water present in the air path, is sufficient for identification and shows clearly resolved R components. Figure 3(c) shows the magnetic rotation spectrum with the polarizers crossed. The angular notation on these figures indicates the angle between the transmission planes of the polarizers measured from the crossed position. Keeping in mind that deflection upward corresponds to absorption and that deflection downward corresponds to emission, it is apparent from the figures that the R components arising from the $^2\Pi_{\frac{1}{2}}$ states are rotated in the negative direction and those from the $^2\Pi_{\frac{3}{2}}$ states in the positive direction.

The fact that the Q branch signal remains large for the various polarizer settings indicates it is probably complex, having components showing both positive and negative rotation. It is also noted that there is a strong rotation signal for the $R(\frac{5}{2})$ line. If the amount of rotation is dependent upon the magnitude of the Zeeman splitting and the intensity of the absorption

line, neighboring lines, particularly $R(\frac{3}{2})$ should show a strong signal. Unfortunately this transition is masked by a strong water line at this frequency.

3–0 Band at 1.8 μ

The 3—0 band of NO at 1.8 μ was in a more favorable region and could be studied in considerably more detail.

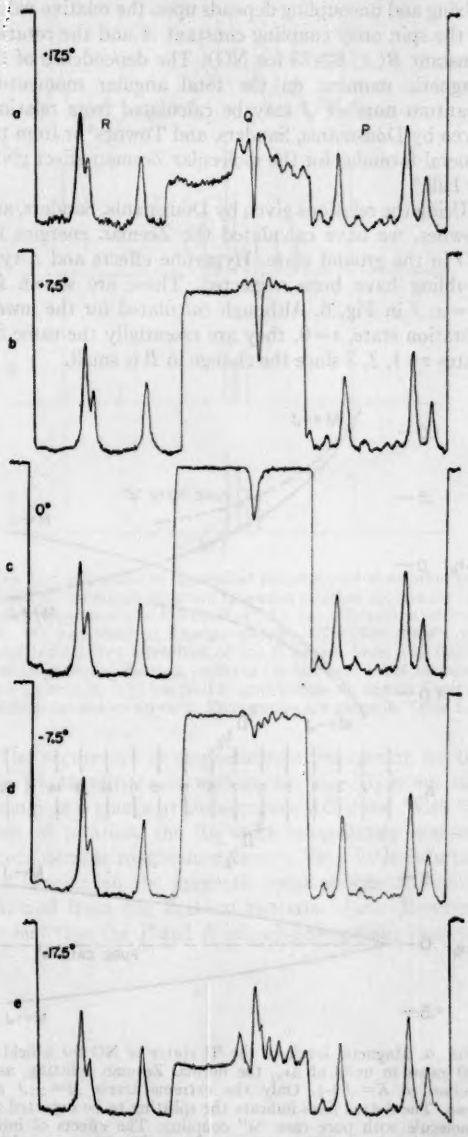

FIG. 5. Magnetic rotation spectrum in the Q branch region of the 3–0 band of NO at 1.8 μ. The central portion of each figure shows the rotation signals for polarizer settings of +17.5, +7.5, 0, −7.5, −17.5°, respectively. P and R branch lines on each side were recorded for calibration purposes. Effective slit width 0.12 cm^{-1}.

This study is divided into two parts: the study of the P and R branches, and of the Q branch. The weak magnetic rotation signals for the P and R branches were found to be greatly dependent upon the total absorption path. If the total absorption path exceeded 2 meter atmospheres the signals disappeared completely. Best results were obtained with an absorption of 0.5 meter atmosphere (NO pressure of 5 cm of Hg). In addition, wide slits (~0.6 cm^{-1}) were necessary. The small absorption path combined with the wide slits resulted in a normal absorption spectrum showing a maximum absorption of about 5% and lacking in resolution. Again, the calibration system could not be used and the rotation signals were identified by comparison with ordinary absorption spectra run at the same speed. The absorption spectrum at high resolution and typical magnetic rotation spectra for several polarizer settings with a single gas sample are shown in Fig. 4.

Several things are immediately apparent from these spectra. First, with possibly two exceptions $R(19/2)$, $R(21/2)$, the relative intensity of the P and R components in the two sub-bands in magnetic rotation is essentially the same as that in the ordinary absorption spectrum. Second, the direction of rotation in the P branches is also apparent since they are resolved even with wide slits. The $^2\Pi_{\frac{1}{2}}$ components show negative rotation and the $^2\Pi_{\frac{3}{2}}$ components positive rotation. Although the R components are not resolved, the absorption signal at the "missing line" $R(19/2)$ may be used to deduce the direction of rotation of the R components. The absorption of the $^2\Pi_{\frac{1}{2}}$ components is greater than that of the $^2\Pi_{\frac{3}{2}}$ components. It follows, therefore, that the polarizer setting which gives the largest absorption signal for the $R(19/2)$ line indicates a direction of rotation in the R component which is similar to that in the P branch component which is weaker in rotation for this same setting. This component is the P branch arising from the $^2\Pi_{\frac{1}{2}}-{}^2\Pi_{\frac{1}{2}}$ transition. Thus in the R branches the $^2\Pi_{\frac{1}{2}}$ components show negative rotation and the $^2\Pi_{\frac{3}{2}}$ components, positive. The weak or near zero signal in rotation for $R(19/2)$ and an observable, although small signal at $R(\frac{1}{2})$ will be commented upon later.

The strong magnetic rotation signal and weak absorption for the Q branch allowed us to make a more detailed study of the rotation in this region. Good signals were obtained with slits of ~27 microns (0.12 cm^{-1}) and absorption paths of 6 meter atmospheres. In addition, the fringe calibration system could be used and the frequencies at which absorption or magnetic rotation occurred, obtained with precision.

Magnetic rotation spectra were obtained of the Q branch region with polarizer settings ranging from +25 to −25 degrees. The procedure was as follows: with the polarizer set at ±25° and zero field, several R branch lines were recorded. The polarizer was then set at the desired position, field turned on, and the Q region re-

TABLE I. Observed and calculated frequencies (cm^{-1}) of the Q branches and the observed magnetic rotation signals for the 3-0 band of NO.

$J+\frac{1}{2}$	$^2\Pi_{\frac{1}{2}}$–$^2\Pi_{\frac{1}{2}}$ Q_1		M.R.S.
	Obs.	Calc.	Obs.
1	5544.10	5544.12	−5544.16[a]
2		5543.97	
$J+\frac{1}{2}$	$^2\Pi_{\frac{3}{2}}$–$^2\Pi_{\frac{1}{2}}$ Q_2		M.R.S.
	Obs.	Calc.	Obs.
2	5543.30	5543.29	−5543.39[a]
			+5543.29
3	5543.04	5543.03	+5542.99
4	5542.66	5542.65	+5542.64
5	5542.13	5542.17	+5542.17
6	5541.57	5541.59	
7	5540.83	5540.89	

[a] Algebraic sign indicates direction of rotation.

corded. The field was reduced to zero, polarizer returned to original setting (±25°) and several P lines recorded. The P and R branch lines with the calibration fringes allowed us to determine the frequency of the absorption or rotation signal with precision. Typical records of this region with several polarizer settings are shown in Fig. 5.

The frequencies at which magnetic rotation signals were observed in the Q branch region together with the observed and calculated frequencies of the Q branch lines are shown in Table I.

Comparison of these frequencies shows that with the exception of the signal at 5543.39 cm^{-1} the magnetic rotation signals occur at the field free absorption frequencies to the precision of our measurements. The signal at 5543.39 cm^{-1} may arise from the wing of the $Q_2(\frac{3}{2})$ absorption line. Consideration of the Zeeman patterns for the Q branches make these statements more plausible.

No quantitative explanation of the above observations can be given at the present time. Serber[6] has shown that the magnetic rotation near an absorption frequency depends directly upon the Zeeman effect. He has carried out the theory for a $^1\Sigma-{}^1\Pi$ transition and obtained an expression for the Verdet constant as a function of the Zeeman splitting and of J. For the simple case which he treated the theory predicts that the R and P branches will be rotated in opposite directions, with the R branch being considerably more intense than the P branch for low J values, and that the intensity of the Q branch lines should fall off very rapidly.

The situation in NO is considerably more complex. The coupling in NO is intermediate between Hund's case (a) and case (b). This intermediate coupling has a pronounced effect upon the molecular magnetic moment and thus upon the Zeeman splitting. In a Hund's case (a) coupling scheme the magnetic moment in the $^2\Pi_{\frac{3}{2}}$ would be large (~2 Bohr magnetons) and close to zero in the $^2\Pi_{\frac{1}{2}}$ state. For the intermediate case an increasing amount of end-over-end nuclear rotation gradually decouples the spin from the nuclear axis. The wave functions become mixed and each pure state acquires an admixture of the other. The extent of this mixing and uncoupling depends upon the relative values of the spin orbit coupling constant A and the rotation constant $B(A/B\cong 73$ for NO). The dependence of the magnetic moment on the total angular momentum quantum number J may be calculated from relations given by Dousmanis, Sanders, and Townes[8] or from the general formulas for the molecular Zeeman effect given by Hill.[9]

Using the relations given by Dousmanis, Sanders, and Townes, we have calculated the Zeeman energies for NO in the ground state. Hyperfine effects and Λ-type doubling have been neglected. These are shown for $M=\pm J$ in Fig. 6. Although calculated for the lowest vibration state, $v=0$, they are essentially the same for states $v=1, 2, 3$ since the change in B is small.

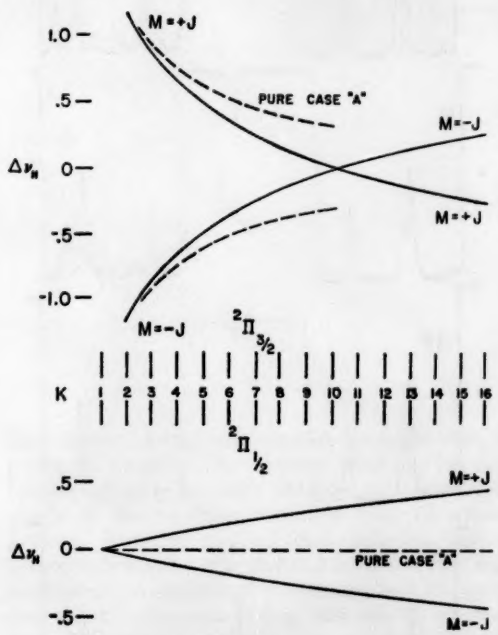

FIG. 6. Magnetic levels of the $^2\Pi$ states of NO for a field of 2500 gauss in units of $\Delta\nu_n$, the normal Zeeman splitting, as a function of $K=J+\frac{1}{2}$. Only the extreme levels $M=\pm J$ are shown. The dotted lines indicate the splitting to be expected for a molecule with pure case "a" coupling. The effects of intermediate coupling on NO are clearly shown. The $^2\Pi_{\frac{1}{2}}$ state quickly obtains a magnetic moment with molecular rotation.

[8] G. C. Dousmanis, T. M. Sanders, Jr., and C. H. Townes, Phys. Rev. **100**, 1735 (1955).
[9] E. L. Hill, Phys. Rev. **34**, 1507 (1929).

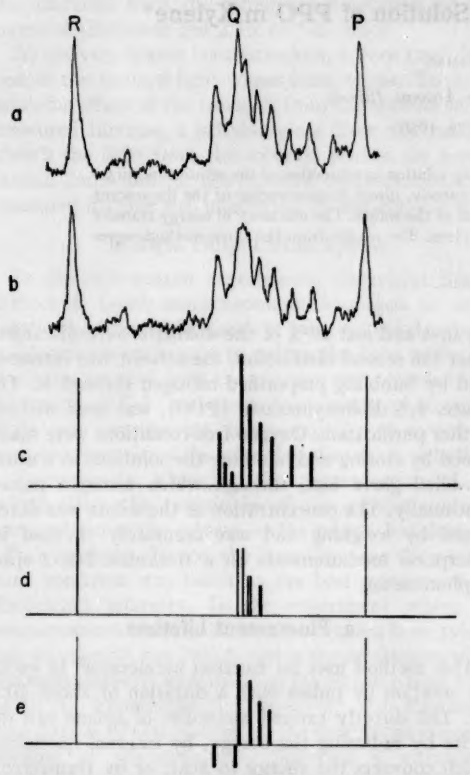

FIG. 7. Comparison of theoretical and observed absorption and Zeeman patterns and observed magnetic rotation spectra for the Q branch region of the 3–0 band of NO. (a) Q branches without field. (b) Longitudinal Zeeman pattern (H=2500 gauss). (c) Calculated relative intensities of the Q branch lines. (d) Calculated longitudinal Zeeman patterns for the first three members of the Q_2 branch. (e) Observed magnetic rotation signals. Positive rotations are drawn upward. Frequencies are given in Table I.

The occurrence of magnetic rotation spectra for the $^2\Pi_{\frac{1}{2}}-{}^2\Pi_{\frac{1}{2}}$ transitions as well as the $^2\Pi_{\frac{3}{2}}-{}^2\Pi_{\frac{1}{2}}$ is not surprising, as a glance at these curves will show. With the onset of rotation, the $^2\Pi_{\frac{1}{2}}$ state immediately acquires a considerable magnetic moment. Very little information bearing on the magnetic rotation spectra can be obtained from the Zeeman patterns alone. However, the fact that the P and R branch lines arising from the $^2\Pi_{\frac{1}{2}}$ states show negative rotation and those from the $^2\Pi_{\frac{3}{2}}$ states show positive rotation may be associated with the fact that in the $^2\Pi_{\frac{1}{2}}$ state the Zeeman splitting is an increasing function of J while in the $^2\Pi_{\frac{3}{2}}$ state the opposite is true.

No adequate explanation of the weak or missing signal at $R(19/2)$ in the 3–0 band can be given at present. The appearance of the Zeeman patterns, and consideration of their relative intensities do not indicate anything unusual in this region. There are, however, small anomalies observed in the ordinary absorption spectrum of the 3–0 band in the neighborhood of $R(19/2)$ and $P(21/2)$. With the exception of this region, the P and R branch magnetic rotation spectra are similar to the ordinary absorption spectra, the amount of rotation being roughly proportional to the relative population of the states involved.

The appearance of a small but definitely real signal for the $R(\frac{1}{2})$ line of the 3–0 band is an indication of the possible use of magnetic rotation work in the infrared to detect small magnetic moments. A calculation of the g factor associated with the $J=\frac{3}{2}$ level of the $^2\Pi_{\frac{1}{2}}$ state gives g=0.0263, yet a signal is obtained in a field of 2400 gauss.

The magnetic rotation signals obtained for the Q branches appear to verify the predictions of the classical case as illustrated in Fig. 1. The longitudinal Zeeman patterns of the Q branch lines are all normal doublets and although not resolved the first two members of the Q_2 branch show considerable broadening at these fields. For comparison purposes the theoretical and observed Zeeman patterns and the magnetic rotation signals for the Q branches are shown in Fig. 7.

A theoretical investigation of these problems and the general problem of the Faraday effect in gases with mixed states is being undertaken. We hope to report on this later. In addition, the experimental work is being extended to include the remainder of the first overtone and the fundamental.

ACKNOWLEDGMENTS

We wish to express our thanks to Professor T. Harvey Edwards for helpful discussions of the experimental aspects of this problem and to Professor Paul M. Parker for enlightening discussions of the theory involved.

Efficiency of Energy Transfer in a Solution of PPO in Xylene*

ISADORE B. BERLMAN

Argonne National Laboratory, Argonne, Illinois

(Received February 25, 1960)

The nonradiative energy transfer of an organic scintillating solution as a function of the solute concentration has been determined by three independent methods: namely, direct measurements of the fluorescent lifetime, the light output of the solvent, and the light output of the solute. The efficiency of energy transfer ranges from 12% at 0.02 *g/l*, to 92% at 2 *g/l* of PPO in xylene. The results from the three methods agree within a few percent.

INTRODUCTION

WHEN a scintillating solution is exposed to either ionizing radiation or short-wavelength ultraviolet radiation, the incident energy is primarily absorbed by the solvent, then partially transferred to the solute, and subsequently emitted in part by the latter as fluorescent radiation. Normally, an increase in solute concentration is accompanied by an increase in the fraction of the absorbed energy which is transferred to the solute. In this report the energy-transfer efficiency of an organic scintillating solution, diphenyloxazole (PPO) in *p*-xylene, has been determined as a function of the solute concentration.

Several reports relating to energy transfer in various organic systems have appeared in the literature.[1-3] Conflicting views have persisted as to whether the energy transfer is radiative or nonradiative.[4,5] The results are difficult to interpret, since most of the studies were made with aerated solutions under conditions in which radiative transfer of energy could take place. In the present work, great care has been taken to minimize the radiative component and to measure only nonradiative transfer; namely, the component that competes with emission by the solvent.

Three different and independent methods have been used. One method is based on the mean lifetime of the fluorescent light following stimulation by a pulsed electron beam, while the other two are based on the light output from the solvent and the solute, respectively, following ultraviolet excitation. The experimental results of each of these methods agree within a few percent.

EXPERIMENTAL TECHNIQUE

One of the more efficient scintillating systems, xylene plus diphenyloxazole, was investigated. The solvent, *p*-xylene, was purified with two distillations in which the first and last 20% of the distillate were discarded. After the second distillation, the solvent was nitrogenated by bubbling prepurified nitrogen through it. The solute, 2,5 diphenyloxazole (PPO), was used without further purification. Oxygen-free conditions were maintained by storing and handling the solutions in a nitrogen-filled glove box, through which nitrogen passed continually. The concentration of the solute was determined by weighing and was accurately checked by absorption measurements on a Beckman DK-2 spectrophotometer.

a. Fluorescent Lifetime

This method uses an electron accelerator[6] to excite the solution by pulses with a duration of about 10^{-10} sec. The directly excited molecules of xylene can deexcite by radiating the energy, by internal quenching which converts the energy to heat, or by transferring some of the energy to the solute molecules. The excited solute molecules can emit, with their own emission spectrum, a portion of the transferred energy.

In this lifetime apparatus a 1P28 photomultiplier and associated electronic equipment detects the emitted light, and an accompanying x–y recorder plots its decay curve. An inherent feature of this equipment is that it responds primarily to the slowest component in the scintillation process and therefore allows the separation of the transfer time from the lifetime of the solute at low solute concentrations.[6,7]

For the lifetime measurements, the solution was contained in special quartz cells with the larger surfaces horizontal and about $\frac{1}{18}$ in. apart. The electron beam impinged on the solution through a $\frac{3}{16}$-in. hole in the center of the top surface. To minimize absorption and re-emission of the fluorescent light, a stainless-steel tube with an inner diameter of $\frac{1}{16}$ in. was inserted through the hole to confine the light, and the thickness of the sample was reduced by only partially filling the cell. Only the solution inside this insert was excited by the electron beam and was involved in the subsequent fluorescent process. To avoid quenching by oxygen, air

* Work performed under the auspices of the U. S. Atomic Energy Commission.

[1] S. G. Cohen and A. Weinreb, Proc. Phys. Soc. (London) **B69**, 593 (1956).

[2] J. B. Birks and A. J. Cameron, Proc. Phys. Soc. (London) **A72**, 52 (1958).

[3] F. H. Brown, M. Furst and H. Kallmann, Discussions Faraday Soc. **27**, 43 (1959).

[4] M. Furst and H. Kallmann, J. Chem. Phys. **31**, 1134 (1959).

[5] J. B. Birks, J. Chem. Phys. **31**, 1135 (1959).

[6] R. K. Swank, H. B. Phillips, W. L. Buck, and L. S. Basile, I.R.E. Trans. on Nuclear Sci. NS-5, 183 (1958).

[7] H. Kallmann, New York Univ. Progr. Rept. N-2560, p. 1 (May 1959).

was excluded from the nitrogenated solution by two layers of aluminum foil 2.5×10^{-4}-in. thick.

At the very lowest concentrations, a very small fraction of the emitted light comes from xylene. To determine the effect of the emission from the solvent on the measured lifetime, a suitable glass filter was used to absorb the light from the solvent. Within the experimental limits and for the reported concentrations, the measured lifetime was unaffected by the use of a filter.

b. Light Output from Xylene

In the light-output experiments, ultraviolet from a Bausch & Lomb monochromator was used to excite solutions contained in standard 1-cm quartz absorption cells with quartz inserts to reduce the light path. The spectrum emitted from the solution was recorded by a Beckman DK-2 ratio-recording spectrophotometer. With this arrangement, it was possible to record the emission from either the solvent or the solute, or both.

Theoretically, changing the concentration of the solute alters the magnitude of the spectral-emission curve of either the solvent or the solute, but does not affect its shape. Hence, the intensity near the peak of each spectrum was taken as the best measure of the fluorescent intensity. In the experiment where the measurements were made on the emission from xylene, this wavelength was 2920 A, and in the experiment where the measurements were made on the emission from PPO, 3820 A. Experimentally, however, the fluorescent spectrum of PPO is modified at the shortest wavelengths because of self-absorption. Selecting a wavelength (3820 A) longer than the absorption edge of PPO and using very thin samples reduces this effect to negligible proportions.

In studying the light output from xylene, the xylene-PPO solutions were excited with 2650-A radiation. The intensity of the emitted light was measured as the solute concentration was increased, the intensities being expressed in terms of that for pure xylene. From the change in the fluorescent intensity of the xylene, it is possible to determine the efficiency of energy transfer, as is explained under "Theory."

In this experiment it was essential to have the smallest possible path length, in order that absorption of the xylene emission by both the solvent and the solute may be minimized. Hence, the solutions, contained in standard 1-cm quartz cells, were reduced to approximately 0.05 mm in thickness by the use of suitable quartz spacers.

From absorption measurements of PPO in cyclohexane, it is known that at a concentration of 1 g/l of PPO in xylene only about 1% of the 2650-A radiation is directly absorbed by the PPO molecules. Hence, at these wavelengths the radiation is almost completely absorbed by xylene. However, at the maximum of the xylene-emission spectrum, namely in the vicinity of 2920A, the absorption coefficient of PPO molecules is larger. At these wavelengths, therefore, a correction must be applied to take account of the absorption of the xylene emission by the PPO molecules. This correction has been made when appropriate.

c. Light Output from PPO

In these experiments the emission from PPO as a result of energy transfer from xylene is measured as a function of the concentration of PPO. The efficiency of energy transfer was determined by the technique of Cohen and Weinreb.[1] The xylene-PPO solution was stimulated successively by 2650-A radiation (to excite both solvent and solute) and 3130-A radiation (to excite the solute only). In each case, PPO was the emitter. Let $E_{2650}{}^{x}$ be the intensity of the emission excited via energy transfer from xylene, and $E_{3130}{}^{x}$ that from direct excitation of PPO. To determine the intensity from PPO excited directly by 2650-A radiation, a solution of PPO in cyclohexane was stimulated successively by 2650-A and 3130-A radiation, and $E_{2650}{}^{c}$ and $E_{3130}{}^{c}$, the respective intensities of PPO emission, were recorded. Since the PPO is excited directly at both wavelengths, the efficiency ϵ for energy transfer is given by

$$\epsilon=(E_{2650}{}^{x}/E_{3130}{}^{x})\cdot(E_{3130}{}^{c}/E_{2650}{}^{c}),$$

where $E_{3130}{}^{c}\neq E_{3130}{}^{x}$ because the solvent affects the quantum yield of PPO. The ratio $E_{3130}{}^{c}/E_{2650}{}^{c}$ essentially calibrates the ultraviolet flux from the monochromator and eliminates the solvent's effect on the quantum yield of the PPO. The only assumptions are that (1) the quantum yield of PPO is the same at both wavelengths, (2) the quantum yield remains constant over the concentration range of the experiment, and (3) $E_{2650}{}^{x}$ is the result of nonradiative transfer. In a separate experiment it was demonstrated that the self-quenching of PPO was negligibly small and that, therefore, assumption (2) was valid. Concerning assumption (3), it is estimated that $E_{2650}{}^{x}$, and therefore ϵ, is at most 5% too large because of radiative transfer at the larger concentrations. This estimate is based on the assumption that the quantum yield of xylene is not more than 20%. No correction has been applied to account for radiative transfer.

THEORY

a. Lifetime Method

The mean lifetime τ_0 of the first electronic excited state of xylene may be expressed as $\tau_0=(p_e+p_q)^{-1}$, where p_e is the probability per second that an excited xylene molecule will emit its excess energy as fluorescent radiation, and p_q is the probability per second for inter- and intra-molecular quenching of the excitation energy. When the solute (PPO) is added to the solvent, the mean lifetime of the excited solvent molecules becomes $\tau_c=(p_e+p_q+p_i)^{-1}$, where p_i is the probability per second for nonradiative transfer which, as written, competes with emission. The quenching probability

TABLE I. Efficiency of energy transfer (%) as a function of the solute concentration.

Conc. PPO (g/ℓ)	Method I (Lifetime)	Method II (Xylene emission)	Method III (PPO emission)
0.02	14±3	12±2	14±2
0.04	26±3	25±2	23±2
0.1	40±3	39±2	41±2
0.2	55±3	59±2	56±2
0.25	59±3	62±2	62±2
0.5	75±3	80±2	77±2
1.0	84±3	88±2	85±2
2.0	90±3		92±2

p_q has the same value in both equations; i.e., as shown below, p_q is constant over the concentration range of these experiments.

By definition, the efficiency ϵ of energy transfer is given by $\epsilon=p_t/(p_e+p_q+p_t)=1-\tau_c/\tau_0$. This expression implies that p_q and p_e are independent of concentration, although this remains to be proved.

b. Measurements of Light Output from Xylene

In this method, the intensity L_0 of the xylene emission is proportional to the xylene quantum yield which is equal to $p_e/(p_e+p_q)$. When the concentration of the solute is increased from 0 to c, the intensity of the xylene emission decreases because of the added probability term p_t in the denominator; i.e., L_c is proportional to $p_e/(p_e+p_q+p_t)$. Hence, the efficiency of energy transfer is $\epsilon=1-L_c/L_0$.

c. Measurements of Light Output from PPO

The intensity D of the PPO emission is proportional to $N\epsilon_c Y$, where N is the number of initially excited xylene molecules, ϵ_c is the efficiency of energy transfer from xylene to PPO at the concentration c, and Y is the quantum yield of PPO. For 100% transfer, the intensity D_0 of the PPO emission is proportional to NY. Therefore, $D/D_0=\epsilon_c$. This expression implicitly assumes that the quantum yield, Y, of PPO is constant over the range of concentrations of this experiment.

DISCUSSION

The results of the three methods of measuring the efficiency of nonradiative energy transfer are shown in Table I. The values obtained from the lifetime measurements are based on a mean lifetime of 20.2×10^{-9} sec for pure xylene. This value of τ_0 was the result of many measurements in which very thin samples were used to minimize absorption effects and in which great care was taken to maintain oxygen-free conditions.

Since the time dispersion in the pulsed beam of the electron accelerator is unknown, it has been neglected in computing τ_c. This correction is small and is not significant for concentrations below 1g/l.

As mentioned before, with pulsed equipment the measured lifetime is unequivocally the mean fluorescent lifetime for the solvent when the concentration of the solute is less than 0.25 g/l, since the lifetime for the solvent is much longer than the mean lifetime of 2.6×10^{-9} sec for the solute (PPO) so that the recorded pulse form is exponential. For concentrations greater than 0.25 g/l, curve-fitting techniques involving the difference of two exponentials, were employed. Sample plots of these curves are shown in Fig. 1.

A significant advantage gained from the use of nitrogenated solutions is that the measured mean lifetime for the solvent is appreciably longer than for the case of an aerated solution, and also is comparatively longer than the mean lifetime of the solute emission. The result is that the curve-fitting techniques, which are laborious and somewhat uncertain, are unnecessary until much larger solute concentrations are involved.

The small uncertainties shown in Table I are the result of many repeated experiments and reflect the author's confidence in the given value of the efficiency of energy transfer.

No correction has been made for the amount of radiative transfer in the PPO emission experiment, because energy transfer to the solute rapidly decreases the magnitude of the xylene emission as the solute concentration is increased. Under the *most* favorable conditions for radiation transfer, and for a quantum yield of 20% for xylene, i.e., for $p_e/(p_e+p_q)=0.2$, it is estimated that ϵ would be about 5% too large.

It is important to show to what extent the assumed constancy of p_q is supported by experimental evidence. Letting $p_q=R+S$, where R is the probability for solvent quenching before the addition of the solute and where S is the additional solvent quenching resulting from the addition of the solute, then $\epsilon=p_t/(p_e+$

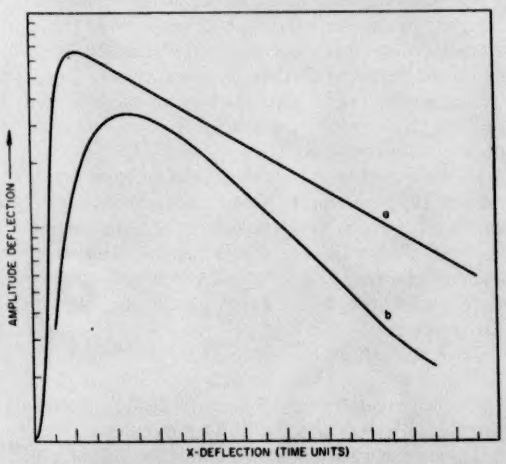

FIG. 1. Curve *a* is a semilog plot of the fluorescent lifetime of pure xylene, and curve *b* is a semilog plot for 1 *g/l* of PPO in xylene. The abscissa for curve *a* has the value of 5.14×10^{-9} sec/time unit, and the abscissa for curve *b* has the value 1.82×10^{-9} sec/time unit.

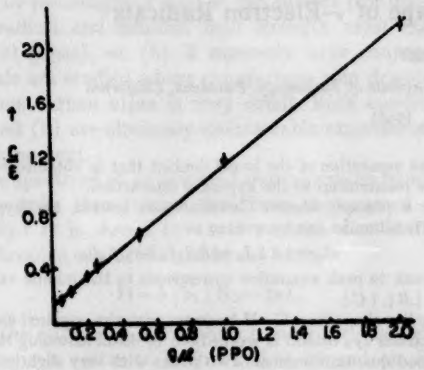

FIG. 2. The ratio of the solute concentration c to the efficiency ϵ of energy transfer, plotted as a function of the solute concentration. The value of ϵ is the one obtained by method III in Table I.

p_t+R+S). If it is assumed that p_t and S vary linearly with concentration,[1,8] i.e., that $p_t=kc$ and $S=fc$, where k and f are constants, then the efficiency of energy transfer is

$$\epsilon=kc/[(k+f)c+q],$$

where $q=R+p_e$. Therefore, $c/\epsilon=Kc+Q$, where $K\equiv(k+f)/k$ and $Q\equiv q/k$. This formula was originally developed by Cohen and Weinreb.[1]

Figure 2 is a plot of c/ϵ vs c, the values of ϵ being those obtained by method III in Table I. Since the points lie on a straight line with a slope of unity, it appears that $K=1$ so $f=0$ and therefore $S=fc=0$; i.e., within the range of concentrations in this experiment $p_e=R$, and the addition of the solute does not affect the quenching of the solvent. This result is consistent with the results of Furst and Kallmann.[4]

As shown in Table I, the energy transfer from the solvent to the solute approaches 100% at large solute concentrations. This result confirms similar results by Brown, *et al.*[3]

CONCLUSIONS

This experiment is characterized by the special precautions taken to insure quantitative as well as qualitative results: very thin samples (0.05 mm) were employed to minimize radiative transfer, the solute concentrations were determined very accurately, and oxygen-free conditions were maintained to enhance the efficiency of energy transfer.

Energy transfer competes with the emission from xylene, and with the quenching of the first excited state of the solvent, as is demonstrated by the decrease in the light output from xylene, and by the shortening of the mean lifetime with increasing solute concentration. These phenomena are consistent with the assumption of nonradiative transfer. Furthermore, the close agreement between the energy-transfer efficiencies obtained by electron excitation and those by ultraviolet suggests that the efficiency of energy transfer is independent of the mode of excitation. This inference agrees with the conclusion of Lipsky and Burton[9] and Brown *et al.*[3] Finally, since the transfer efficiencies obtained from studies of the light outputs from solvent and solute are in substantial agreement, it is reasonable to assume that the excited states of the solvent which give rise to emission are the very ones involved in energy transfer.

ACKNOWLEDGMENT

The author wishes to thank Dr. Arye Weinreb and Warren L. Buck and Robert K. Swank for many helpful discussions, Leonidas D. Marinelli for the encouragement received in pursuing this topic, and Dr. Francis E. Throw for the careful reading of the manuscript.

[4] H. Kallmann and M. Furst, Phys. Rev. 79, 857 (1950).

[9] S. Lipsky and M. Burton, J. Chem. Phys. 31, 1221 (1959).

Polycrystalline Resonance Line Shape of π-Electron Radicals

HIMAN STERNLICHT

Gates and Crellin Laboratories of Chemistry, California Institute of Technology, Pasadena, California*

(Received March 31, 1960)

A general expression in the form of a multiple integral involving a delta function is derived for the polycrystalline spectra of radicals. The expression is exact when the hyperfine structure is due to the interaction of one proton with the unpaired electron. The extension to a system involving the interaction of a number of protons with the unpaired electron is straightforward but was not done here.

Because of the formidable integrations encountered when the complete spin Hamiltonian is used, a simpler case is considered to illustrate the technique developed. It is shown that if one assumes that I_H, the nuclear spin component along the externally applied magnetic field, is a good quantum number, then the peak to peak separation of the broad doublet that is obtained bears a simple relationship to the hyperfine interaction.

For a properly chosen Cartesian axis system, the hyperfine spin Hamiltonian can be written as

$$H_{hf}=hAS_xI_x+hBS_xI_z+hCS_yI_y.$$

The peak to peak separation corresponds to the middle value of $|A|, |B|, |C|$.

The line shape for a C—H fragment with the unpaired electron in a carbon $2p_z$ orbital is worked out in detail assuming that I_H is a good quantum number. Two peaks with very slightly asymmetric shoulders are obtained, the peak to peak separation being 61 Mc.

INTRODUCTION

RECENT EPR work on oriented organic radicals[1–3] has shown that the anisotropic proton hyperfine interactions in π-electron radicals are of the same order of magnitude as the isotropic interactions, corroborating the theoretical calculations of McConnell and Strathdee.[4] Since the anisotropic contributions to the hyperfine splitting are significant, broad resonance lines are obtained when polycrystalline samples are examined.

Previous work on line shapes of polycrystalline resonance spectra have dealt either with the broadening arising from point dipole interactions,[5–7] or from a proton interacting with an electron in an orbital having axial symmetry.[8,9] To the best of the author's knowledge, there is no published work dealing rigorously[10] with the polycrystalline resonance spectra of radicals. It is hoped that this paper will be the basis for a better understanding of their polycrystalline spectra. The subsequent calculations are limited to all radicals (not necessarily π-electron radicals) for which the hyperfine structure is due to the interaction of one proton with the unpaired electron.

* Contribution No. 2564. Supported in part by (a) The National Science Foundation; (b) The U. S. Public Health Service; (c) The Office of Ordnance Research, U. S. Army.

[1] H. M. McConnell, C. Heller, T. Cole, and R. W. Fessenden, J. Am. Chem. Soc. **82**, 766 (1960).

[2] D. K. Ghosh and D. H. Whiffen, Mol. Phys. **2**, 285 (1959).

[3] C. Heller, J. Chem. Phys. (to be published).

[4] H. M. McConnell and J. Strathdee, Mol. Phys. **2**, 129 (1959).

[5] E. R. Andrew, *Nuclear Magnetic Resonance* (Cambridge University Press, New York, 1956), p. 155.

[6] E. R. Andrew and R. Bersohn, J. Chem. Phys. **18**, 159 (1950).

[7] F. S. Waugh, F. B. Humphrey, and D. M. Yost, J. Phys. Chem. **57**, 486 (1953).

[8] H. Zeldes, G. T. Trammell, R. Livingston, and R. W. Holmberg, J. Chem. Phys. **32**, 618 (1960).

[9] S. M. Blinder, J. Chem. Phys. **33**, 748 (1960).

[10] While this article was in press, Dr. R. Lefebvre of the Centre de Mécanique Ondulatoire Appliquée, Paris, informed the author that he has succeeded in calculating the polycrystalline line shape of π^- electron radicals for the most general case by using an electronic computer. His results should appear shortly in print.

SPIN HAMILTONIAN

The spin Hamiltonian for a radical containing one proton can be written[1] as

$$\mathbf{H}=h\nu_e\mathbf{S}_H-h\nu_p\mathbf{I}_H+\mathbf{S}\cdot\mathbf{T}\cdot\mathbf{I}. \quad (1)$$

ν_e and ν_p are the electron and nuclear spin resonance frequencies, respectively, where

$$\nu_e=h^{-1}g_e|\beta|H$$

$$\nu_p=h^{-1}g_n\beta_nH. \quad (2)$$

H is the magnitude of the externally applied field; $|\beta|$ is the absolute value of the electronic Bohr magneton; β_n is the nuclear Bohr magneton; g_e is the electron g factor, and g_n is the nuclear g factor. S_H and I_H are the spin components along $\mathbf{H}$ of the electron and proton, respectively. $\mathbf{T}$ is a symmetric dyadic and includes the combined (electron-spin)-(nuclear-spin) Fermi contact interaction, and the (electron-spin)-(nuclear-spin) dipolar interaction. It is assumed that the (electron-orbit)-(nuclear-spin) and (electron-orbit)-(electron-spin) magnetic interactions are negligible as is generally the case for organic radicals.

$\mathbf{T}$ can be written in diagonal form for a suitably chosen set of cartesian axis x, y, z:

$$\mathbf{T}=hA\mathbf{kk}+hB\mathbf{ii}+hC\mathbf{jj}. \quad (3)$$

$\mathbf{i}$, $\mathbf{j}$, $\mathbf{k}$ are unit vectors in the direction of the positive x, y, z axis, respectively.

For X-band resonance, where H is approximately 3000 gauss, $\nu_e\sim$9500 Mc and $\nu_p\sim$14.5 Mc. It has been shown experimentally for organic π radicals[1–3] that under these conditions ν_p is of the same order of magnitude as $|A|, |B|, |C|$, whereas $\nu_e\gg|A|, |B|, |C|$. (For the case of malonic acid, radical ν_p is approximately $\frac{1}{8}[A^2+B^2+C^2]^{\frac{1}{2}}$.) As a result S_H but not I_H, is a good quantum number, and so-called "forbidden" lines appear in the EPR spectrum. I_H is a good quantum number if (a) the externally applied field is much larger

than the paramagnetic field at the nucleus (for malonic acid radical and external field strength must exceed 200 000 gauss), or (b) if *extremely* large conjugated radicals are studied where the electron spin density at any one carbon atom is very small. Both conditions (a) and (b) are obviously unattainable experimentally at the moment.

The spectrum of an oriented radical arising from the above spin Hamiltonian has been determined previously.[1] It is shown by these authors that the spin Hamiltonian can be written in the form

$$\mathbf{H}=h\,|\,\nu_e\,|\,\mathbf{S}_H-h\nu\mathbf{I}_u. \tag{4}$$

I_u is the nuclear spin component along the axis defined by the unit vector $\mathbf{u}$. Both ν and $\mathbf{u}$ depend on S_H as shown

$$\nu\mathbf{u}=\nu_p\mathbf{u}_H-S_H[\mathbf{k}A\cos\theta+iB\sin\theta\cos\phi+\mathbf{j}C\sin\theta\sin\phi]. \tag{5}$$

$\mathbf{u}_H$ is a unit vector in the direction of the externally applied field $\mathbf{H}'$. $\mathbf{u}$ is defined by the direction of the vector on the right-hand side of the equation, and the frequency ν is the length. Letting $\nu'\mathbf{u}'$ designate the vector when $S_H=\frac{1}{2}$ and $\nu''_u{}''$ the vector when $S_H=-\frac{1}{2}$, the following transition frequencies are obtained:

$$\begin{aligned}\nu_1&=\nu_e+\tfrac{1}{2}(\nu'-\nu'')\\ \nu_2&=\nu_e-\tfrac{1}{2}(\nu'-\nu'')\\ \nu_3&=\nu_e-\tfrac{1}{2}(\nu'+\nu'')\\ \nu_4&=\nu_e+\tfrac{1}{2}(\nu'+\nu'').\end{aligned} \tag{6}$$

ν', ν'' are functions of θ, ϕ.

$$\nu'=[(\nu_p-\tfrac{1}{2}A)^2\cos^2\theta+(\nu_p-\tfrac{1}{2}B)^2\sin^2\theta\cos^2\phi+(\nu_p-\tfrac{1}{2}C)^2\sin^2\theta\sin^2\phi]^{\frac{1}{2}}$$

$$\nu''=[(\nu_p+\tfrac{1}{2}A)^2\cos^2\theta+(\nu_p+\tfrac{1}{2}B)^2\sin^2\theta\cos^2\phi+(\nu_p+\tfrac{1}{2}C)^2\sin^2\theta\sin^2\phi]^{\frac{1}{2}}. \tag{7}$$

Letting $I_i(\theta,\phi)$ $(i=1, 2, 3, 4)$ denote the relative electron transition probabllity for frequency ν_i (induced by an oscillatory field perpendicular to the externally applied field), and $\mathbf{u}'\cdot\mathbf{u}''=\cos\zeta$, then it can be shown[1] that

$$\begin{aligned}I_1(\theta,\phi)=I_2(\theta,\phi)&=\cos^2(\zeta/2)=\tfrac{1}{2}(1+\mathbf{u}'\cdot\mathbf{u}'')\\ I_3(\theta,\phi)=I_4(\theta,\phi)&=\sin^2(\zeta/2)=\tfrac{1}{2}(1-\mathbf{u}'\cdot\mathbf{u}''),\end{aligned} \tag{8}$$

where

$$\mathbf{u}'\cdot\mathbf{u}''=(1/4\nu'\nu'')\{(2\nu_p)^2-[A^2\cos^2\theta+B^2\sin^2\theta\cos^2\phi+C^2\sin^2\theta\sin^2\phi]\}. \tag{9}$$

Summing up, for any orientation the resonance spectrum is a summetrical quartet centered on ν_e. The outer doublet with splitting $|\nu'+\nu''|$ has relative intensity $\sin^2\zeta/2$; the inner doublet with splitting $|\nu'-\nu''|$ has relative intensity $\cos^2\zeta/2$.

For the case where A^2, B^2, $C^2>(2\nu_p)^2$, the outer lines are more intense; when A^2, B^2, $C^2<(2\nu_p)^2$, the inner lines will always be more intense. Experimental work on malonic acid radical[1] has shown that the outer lines are five to 10 times more intense than the inner lines.

POLYCRYSTALLINE LINE SHAPE

So far the discussion has been limited to oriented crystals. How does one extend the discussion to polycrystalline samples?

Initially let us assume that the relative electronic transition probabilities for all four lines are the same and independent of the orientation of the crystal with respect to the external magnetic field. Let us further assume that the polycrystalline spectrum involves no overlap of lines, i.e., $\nu_i(\theta_a,\phi_a)\neq\nu_j(\theta_b,\phi_b)$ $(i\neq j)$.

Under these conditions, the polycrystalline line shape $g_i(\nu)$ corresponding to a transition frequency ν_i is defined by Eq. (10) below. Regarding a polycrystalline sample as a collection of minute crystals each having one radical, Eq. (10) represents a statistical averaging of the random orientations of these minute crystals:

$$g_i(\bar{\nu})\,d\nu\alpha\sum_K\sin\theta_K d\theta_K d\phi_K=\sum_K d\Omega_K.\qquad(\bar{\nu}\leq\nu_i\leq\bar{\nu}+d\nu). \tag{10}$$

In Eq. (10) only those increments of solid angle $d\Omega_K$ are added up such that θ_K, ϕ_K corresponds to a ν_i between $\bar{\nu}_i$ and $\bar{\nu}$ to $d\nu$. The relationship between θ, ϕ, and ν_i is given by Eqs. (6) and (7).

Equation (10) gives equal weight to each increment of solid angle $d\Omega_K$. This is not the correct thing to do since the transition probabilities are not independent of θ and ϕ. On taking into account the transition probability factor, one has

$$g_i(\bar{\nu})\,d\nu\alpha\sum_K I_i(\theta_K,\phi_K)\,d\Omega_K\qquad\bar{\nu}\leq\nu_i\leq\bar{\nu}+d\nu. \tag{11}$$

Equation (11) can be rewritten more conveniently as

$$g_i(\bar{\nu})\,d\nu\alpha\left\{\int_0^{2\pi}d\phi\int_{-1}^{1}\delta[\bar{\nu}-\nu_i(\theta,\phi)]I_i(\theta,\phi)\,d\cos\theta\right\}d\nu_i. \tag{12}$$

$\delta(\bar{\nu}-\nu_i)$ is a delta function. $\delta(\bar{\nu}-\nu_i)d\nu_i$ assures that only those values of θ and ϕ are considered such that their substitution into $\nu_i(\theta,\phi)$ gives ν_i between $\bar{\nu}$ and $\bar{\nu}+d\nu$. Equation (12) can also be written as

$$g_i(\bar{\nu})\alpha\frac{1}{2\pi}\int_{-\infty}^{\infty}\exp\{i\omega[\bar{\nu}-\nu_i(\theta,\phi)]\}d\omega\int_{-1}^{1}I_i(\theta,\phi)\times d\cos\theta\int_0^{2\pi}d\phi. \tag{13}$$

In the event that there is overlap between the

various lines, one has as the complete line shape function

$$g(\bar{\nu})=\frac{N}{2\pi}\sum_{i=1}^{4}\int_{-\infty}^{\infty}\exp\{i\omega[\bar{\nu}-\nu_i(\theta,\phi)]\}d\omega\int_{-1}^{1}I_i(\theta,\phi)\times d\cos\theta\int_0^{2\pi}d\phi. \quad (14)$$

ν_i, I_i are given by Eqs. (6)–(9). N is a normalization factor so that

$$\int g(\bar{\nu})d\bar{\nu}=1.$$

No attempt was made to evaluate Eq. (14) in terms of A, B, C because of the rather formidable form of the integrals. Equation (14) is an expression for the line shape as a function of transition frequency. It is based on the complete spin Hamiltonian with no terms omitted. As an approximation to the spin Hamiltonian Eq. (1), one might be tempted to ignore the nuclear Zeeman term, $h\nu_p\mathbf{I}_H$. This would lead to the prediction of two lines in the spectrum of the oriented crystal. The complete treatment gives four lines; the relative intensity of the inner and outer doublets can be comparable if A^2, B^2, C^2 have about the same value as $(2\nu_p)^2$. For π-electron radicals, the omission of the nuclear Zeeman term *may* not be too serious. The work on malonic acid radical, as stated earlier, has shown that the outer lines are about five to 10 times more intense than the inner lines. For other organic radicals (non-π-electron radicals, or those having most of the unpaired spin on a nitrogen or sulfur atom for example), the outer and inner doublets might have about the same intensity and the approximation would be bad.

One further note, Eq. (14) only involves hyperfine interaction. The actual line shape is altered by relaxation, saturation, and spin exchange effects. The actual observed line shape can be represented more appropriately by

$$g_{\text{actual}}(\nu)=\int h(\nu-\bar{\nu})g(\bar{\nu})d\bar{\nu}, \quad (15)$$

where $h(\nu-\bar{\nu})$ is a function taking into account all factors other than the anisotropic interaction that influence the line shape. (It usually is a normalized Gaussian for crystals).

ILLUSTRATIVE CALCULATION

The following section contains an illustrative calculation based on the foregoing technique for handling line shapes. The assumption was made that I_H is a good quantum number (an experimentally unrealistic assumption for π-electron radicals like malonic acid radical). The more realistic assumption that the nuclear Zeeman term is negligible still leads to serious mathematical difficulties unless one assumes that two terms of the T dyadic are equal ($B=C$, say) whereupon the calculations are still involved and were not carried through. Blinder,[9] has recently considered this latter case.

For a proper choice of the Cartesian axis system, the hyperfine Hamiltonian can be written as

$$\mathbf{H}_{hf}=hA\mathbf{S}_z\mathbf{I}_z+hB\mathbf{S}_x\mathbf{I}_x+hC\mathbf{S}_y\mathbf{I}_y. \quad (16)$$

Since I_H is assumed to be a good quantum number, the substitutions

$$\mathbf{S}_z=\mathbf{S}_H\cos\theta; \quad \mathbf{I}_z=\mathbf{I}_H\cos\theta \quad a=\tfrac{1}{3}(A+B+C)$$

$$\mathbf{S}_x=\mathbf{S}_H\sin\theta\cos\phi; \quad \mathbf{I}_x=\mathbf{I}_H\sin\theta\cos\phi \quad b=\tfrac{1}{6}(B+C-2A) \quad (17)$$

$$\mathbf{S}_y=\mathbf{S}_H\sin\theta\sin\phi, \quad \mathbf{I}_y=\mathbf{I}_H\sin\theta\sin\phi \quad l=\tfrac{1}{2}(C-B)$$

permit Eq. (16) to be written as

$$\mathbf{H}_{hf}=h\nu_{IH}\mathbf{S}_H=h\mathbf{S}_H\mathbf{I}_H[a+b(1-3\cos^2\theta)+l\cos2\phi(\cos^2\theta-1)]. \quad (18)$$

Since I_H does not change during the electronic transition, it is written as a constant. a in Eq. (18) represents the Fermi contact interaction.

The transition frequencies are

$$\nu_1(\theta,\phi)=\nu_e+\nu_{(I_H=\frac{1}{2})}$$

$$\nu_2(\theta,\phi)=\nu_e-\nu_{(I_H=\frac{1}{2})}. \quad (19)$$

Since the transition probability is the same for ν_1 and ν_2, and independent of crystal orientation, the polycrystalline line shape is given by

$$g(\bar{\nu})=\sum_{i=1}^{2}\frac{N}{2\pi}\int_{-\infty}^{\infty}\exp\{i\omega[\bar{\nu}-\nu_i(\theta,\phi)]\}d\omega\int_{-1}^{1}d\cos\theta\int_0^{2\pi}d\phi. \quad (20)$$

One can easily show that if A, B, C have the same sign, $g(\bar{\nu})$ is symmetric about ν_e with no overlap of the doublet occurring. For convenience, A, B, C are assumed to be positive. $g(\bar{\nu})$ becomes

$$g(\bar{\nu})=\frac{N}{2\pi}\int_{-\infty}^{\infty}\exp(i\omega\{\bar{\nu}-I_H[a+b(1-3\cos^2\theta)+l\cos2\phi(\cos^2\theta-1)]\})d\omega\int_{-1}^{1}d\cos\theta\int_0^{2\pi}d\phi. \quad (21)$$

Setting $I_H=\frac{1}{2}$ gives $g(\bar{\nu})$ for positive values of $\bar{\nu}$.

The evaluation of Eq. (21) proceeds as follows:

$$\int_0^{2\pi}\exp\left\{i\left[-\frac{\omega}{2}l(\cos^2\theta-1)\right]\cos2\phi\right\}d\phi=2\pi J_0\left[\frac{\omega}{2}l(\cos^2\theta-1)\right], \quad (22)$$

where J_0 is a bessel function of zero order. Equation

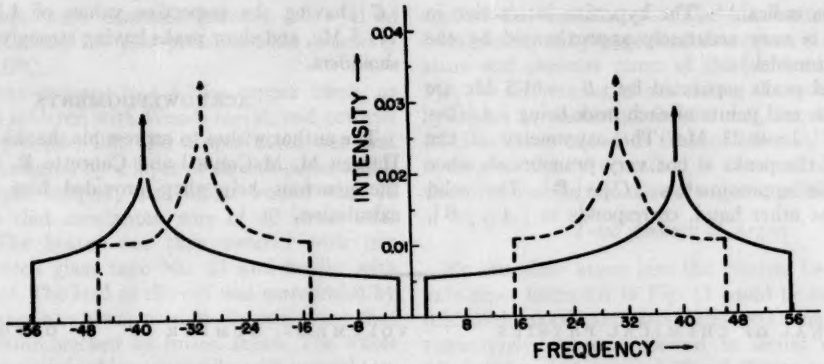

FIG. 1. The dotted curve gives the theoretical polycrystalline line shape as a function of transition frequency in Mc for a π-electron radical in which the odd electron is localized about one carbon atom. It is assumed that (1) I_H, the nuclear spin component along the external field direction, is a good quantum number, and (2) the hyperfine structure arises from the interaction of the unpaired electron spin with a single proton. The origin is taken at ν_e, the electronic Zeeman frequency. The dotted curve is based on the experimental values of A, B, C [Eqs. (16), (17), and (24)], which are -30, -61.5, -92.5 Mc, respectively. The solid curve illustrates how the line shape is modified by an arbitrarily different set of values for A, B, C taken as -5, -78.5, -111.5 Mc, respectively.

(21) now becomes

$$g(\nu)=N\int_{-1}^{1}\left\{\int_{-\infty}^{\infty}\exp(i\omega\{\nu-\tfrac{1}{2}[a+b(1-3\cos^2\theta)]\})\times J_0\left[\frac{\omega l}{2}(\cos^2\theta-1)\right]d\omega\right\}\cos\theta. \quad (23)$$

On letting

$$M\equiv(l/2)(\cos^2\theta-1), \quad p=\nu-\tfrac{1}{2}[a+b(1-3\cos^2\theta)].$$

The expression in brackets evaluates either to zero if $M^2<p^2$ or to $2/(M^2-p^2)^{\frac{1}{2}}$, if $M^2>p^2$.

Equation (21) becomes

$$g(\nu)=4N\int_R\frac{dx}{\{(l^2/4)(x^2-1)^2-[\nu-\tfrac{1}{2}(a+b)+\tfrac{3}{2}bx^2]^2\}^{\frac{1}{2}}}. \quad (24)$$

$x=\cos\theta$. R denotes the range of values of x between 0 and 1 such that $M^2>p^2$. Setting $M^2=p^2$, one obtains

$$x_+=\left[\frac{\nu-1/2(a+b-l)}{1/2(l-3b)}\right]^{\frac{1}{2}}=\left[\frac{\nu-B/2}{A/2-B/2}\right]^{\frac{1}{2}}$$

$$x_-=\left[\frac{1/2(a+b+l)-\nu}{1/2(l+3b)}\right]^{\frac{1}{2}}=\left[\frac{\nu-C/2}{A/2-C/2}\right]^{\frac{1}{2}}. \quad (25)$$

If $A<B<C$ and $A/2\leq\nu<B/2$, R is given by $x_+\leq x\leq x_-$; if $B/2<\nu\leq C/2$, R is defined by $0\leq x\leq x_-$.

The integrand of Eq. (24) becomes infinite at x_+ and x_-. It can be shown, however, that the integral behaves properly except when $\nu=B/2$, $A/2$, $C/2$. When $\nu=A/2$, $x_-=x_+=1$ and the range of integration is zero; when $\nu=C/2$, $x_-=0$ and the range of integration is again zero. (The integrals would have diverged at $\nu=A/2$, $C/2$ if the range of integration were not zero.) $g(A/2)$ and $g(C/2)$ must be obtained by a limiting process. When $\nu=B/2$ the integral diverges. $g(B/2)$ therefore corresponds to the peak and is infinite.

If one assumes $B<C<A$ then the following hold:

$$B/2\leq\nu<C/2, \quad 0\leq x\leq x_+$$
$$C/2<\nu\leq A/2, \quad x_-\leq x\leq x_+. \quad (26)$$

The peak now occurs at $C/2$. $g(B/2)$, $g(A/2)$ must be obtained by a limiting process.

If one assumes $C<A<B$, one has

$$C/2\leq\nu<A/2, \quad 0\leq x\leq x_-$$
$$A/2<\nu\leq B/2, \quad 0\leq x\leq x_+. \quad (27)$$

The peak now occurs at $\nu=A/2$ while $g(C/2)$ and $g(B/2)$ must be obtained by a limiting process.

Other inequalities can be examined. The result is always the same. The maximum peak will always occur at the middle value of $A/2$, $B/2$, $C/2$. A, B, C need not, however, be of the same sign (overlap of the doublet now occurs) and the peak appears at the middle value of $|A|/2$, $|B|/2$, $|C|/2$. If two of the three terms are equal, $B=C$ for example, the maximum value occurs at $|B|/2$ and the line shape is that arising from the interaction of two-point dipoles.[5] If $A=B=C$, there is only the Fermi contact interaction and the spectrum consists of two sharp lines separated by $|A|$.

Figure 1 illustrates the theoretical normalized polycrystalline line shape that would be obtained for a CH fragment if I_H were a good quantum number. (This necessitates an external field strength exceeding 200 000 gauss or an extremely small spin density at the carbon position.) The origin is taken at $\nu=\nu_e$. The dotted curve corresponds to $|A|$, $|B|$, $|C|$ being 30, 61.5, and 92.5 Mc, respectively (A, B, C are negative.[4]) These values are those obtained from the recent experimental work on the oriented

$\dot{C}H(COOH)_2$ radical.[1,4] (The hyperfine interaction in this radical is very accurately approximated by the CH fragment model.)

Two broad peaks separated by $|B|=61.5$ Mc are obtained. The end points of each peak being $|A|/2=15$ Mc; $|C|/2=46.25$ Mc. The asymmetry of the shoulders of the peaks is not very pronounced, since $|B|-|A|$ is approximately $|C|-|B|$. The solid curve, on the other hand, corresponds to $|A|$, $|B|$, $|C|$ having the respective values of 4.7, 78.5, and 111.5 Mc, and show peaks having strongly asymmetric shoulders.

ACKNOWLEDGMENTS

The author wishes to express his thanks to Professor Harden M. McConnell and Concetto R. Giuliano for the generous help they provided him during this calculation.

THE JOURNAL OF CHEMICAL PHYSICS VOLUME 33, NUMBER 4 OCTOBER, 1960

Solubility of Hydrogen and Deuterium in Liquid Argon†

H. VOLK* AND G. D. HALSEY, JR.

Department of Chemistry, University of Washington, Seattle 5, Washington

(Received April 25, 1960)

The solubility of hydrogen and deuterium in liquid argon at pressures from 10 to 100 atm is reported. Solubility isotherms have been measured between 87° and 140°K for hydrogen and between 87° and 120°K for deuterium. The dependence of Henry's constant on temperature, pressure, and concentration, the heats of solution, the partial molar volume of hydrogen in liquid argon, and the second virial coefficients of hydrogen and deuterium in the liquid solution are reported. The increase in the solubility of deuterium over hydrogen is 21.3%, 20.2%, and 18.5%, respectively, at 87, 100, and 120°K. This isotope effect is discussed as a quantum correction to the free volume. Comparison between theory and experiment indicates that the LJD free volume is too large by approximately a factor of five.

INTRODUCTION

IN AN earlier paper,[1] the solubility of helium and neon in liquid argon is reported. The measurements were made at subatmospheric pressures, and so the temperature range was necessarily limited. We have constructed an apparatus for higher temperature measurements, at pressures up to 100 atm. This apparatus allows measurements to be carried up to the critical temperature and at mole fractions of the solute up to 0.15, without the accuracy of the low-pressure method. We have therefore made measurements on the more soluble H_2 and D_2, with the primary purpose of determining the isotope effect.

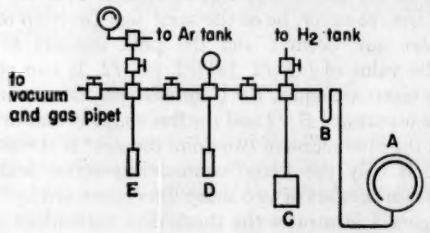

FIG. 1. Apparatus for high-pressure solubility measurements. *A*, pressure gage; *B*, cold trap; *C*, solubility cell; *D*, transfer cell; *E*, pipet bulb.

DETAILS OF APPARATUS AND CALCULATIONS

Apparatus

The apparatus (Fig. 1) was constructed of Autoclave Engineering valves and fittings and was connected on the low-pressure side to a conventional gas transfer apparatus for measuring volumes, purifying argon and pumping out. A 16-in., 1500-psi Heise Bourdon gauge A, calibrated with a dead-weight test gauge, was the pressure measuring element. It was sensitive to pressure changes of 0.02 atm and was calibrated before and after the series of experiments to an accuracy of 0.05 atm. The Bourdon tube and lead were filled with mercury, which was kept out of the rest of the system by the dry ice-acetone trap *B*.

Hydrogen under known pressure was introduced into a stainless steel cell *C* (Fig. 1) of 19.150±0.005 cc volume, and then doses of argon were added from stainless steel pipet bulbs *E* filled at the temperature of liquid oxygen. The cell was mounted so that it could be shaken by twisting and two stainless steel balls were placed in the cell to act as stirrers. The criteria

† This research was supported by the Air Force through the Air Force Office of Scientific Research of the Air Research and Development Command.

* On leave of absence from the University of Vienna. Present address: University of Vienna, I. Chem. Institute, Vienna 9, Austria.

[1] F. E. Karasz and G. D. Halsey, Jr., J. Chem. Phys. **29**, 173 (1958).

for equilibrium were constant pressure after ½ hr stirring, and return to this pressure after warming and cooling 10°C.

The cell was enclosed in a 4.2-kg copper block, to which it was soldered with Woods metal, and covered with a heavy copper lid. The copper block was first electrically insulated by a layer of cigaret paper and a spray of acrylic lacquer, then bifilar wound with 24 gauge nylon clad constantan wire of 40 ohms total resistance. The heater was then covered with two layers of Scotch glass tape No. 27 and finally with aluminum foil. The lead to the cell was surrounded by a similar heater which was used in the rare event that the lead became blocked by frozen argon. The whole assembly was contained in a glass tube with ground top, sealed and fastened to the top plate of the cryostat, and in turn contained in a 6-in. diam Dewar vessel, holding approximately 3 liters of liquid nitrogen (for the runs above 120°K liquid oxygen was used instead of liquid nitrogen). Care was taken that the liquid nitrogen level was always at least 10 cm above the top of the copper block. After cooling the cell assembly to the desired temperature, the glass tube was evacuated to about 0.5 mm Hg. The ac heater current was first transformed to 18 v by a fixed transformer and then regulated manually by means of a variac. Because of the large heat capacity of the copper block it was easy to keep the temperature constant to ±0.05° for the duration of a run.

Temperature

The temperature was measured with a copper-constantan thermocouple, which had been calibrated over the entire temperature range against the vapor pressure of argon[2] (above 100°K) and nitrogen[3,4] (from 86 to 115°K). The calibration was repeated about once a month for one or two temperatures and no measurable change was detected over the whole period of the runs. The temperatures are estimated accurate to ±0.1°.

Concentration

Total Amount of Hydrogen

The total amount of hydrogen or deuterium in the cell was calculated from the equation of state[5,6] and the cell volume. For those temperatures for which the virial coefficients are not reported in the literature, a graphical interpolation was made by plotting the compressibility coefficients F

$$F=(RT+Bp+Cp^2)/RT \qquad (1)$$

against the temperature. The maximum deviations from ideality of hydrogen and deuterium in the temperature and pressure range of this work are less than 5%. For the purpose of calculating the total amount of hydrogen or deuterium in the cell, the lead volume (0.15 cc) was added to the cell volume, because the hydrogen initially contained in the lead is swept into the cell when the first dose of argon is added.

Total Amount of Argon

To introduce argon into the system, two exchangeable pipet bulbs (E in Fig. 1) could be used, holding 0.02039±0.00004 and 0.08132±0.00008 mole of argon, respectively, when immersed in liquid oxygen and filled under a pressure of 50 psi. These volumes were determined by filling the pipet bulbs from a conventional gas buret and determining the sharp pressure rise when the pipets were full. Since the vapor pressure was found to be independent of the amount of argon introduced, this provided at the same time a sensitive check on the purity of our argon. The total volume of the pipets plus deadspace was 2.29 and 3.37 cc, respectively, measured by introducing small amounts of argon from the gasburet and recording the pressure at 25°C.

The pipets were emptied into the system with the help of an intermediate cell (D in Fig. 1) of 2.23±0.01 cc, which was equipped with a manometer. This cell could be immersed in liquid nitrogen. After transferring most of the argon to the system, cell D was cooled with liquid nitrogen and the amount of argon remaining in one of the pipets E (which were at room temperature) was reduced to 0.00003 or 0.00005 mole, respectively. The valve from D to E was then closed, D warmed up to 25±0.1°C, and the valve to the system opened for about five seconds. The pressure in D was then taken to be equal to the pressure reading of the large gauge at the same time. The amount of argon remaining in cell D was calculated from the equation of state.[7]

Amount of Argon in the Cell

The deadspace volume of the system (valves and leads from cell D to cell C and to the mercury filled manometer) was found to be a linear function of pressure, owing to the expansion of the Bourdon tube (2.03 cc at 20 atm and 2.19 cc at 100 atm). A correction was made for the argon remaining in that dead space, this being approximately 0.2–0.8% of the total amount of argon introduced. The number of moles of argon in the cell, calculated as described above, will henceforward be called n_{Ar}'.

Concentration of the Liquid

The concentration of the liquid, expressed in mole fractions x of hydrogen, was calculated from the

[2] A. Michels, T. Wassenaar, and T. Zwietering, Physica **17**, 876 (1951).
[3] A. S. Friedmann and D. White, J. Am. Chem. Soc. **72**, 3931 (1950).
[4] A. S. Friedman, D. White, and H. L. Johnston, J. Am. Chem. Soc. **73**, 5713 (1951).
[5] A. S. Friedmann, thesis, Ohio State University, 1950.
[6] A. Michels, W. de Graaf, T. Wassenaar, J. M. H. Levelt, and P. Louwerse, Physica **25**, 25 (1959).
[7] I. Mason and L. G. F. Dolley, Proc. Roy. Soc. (London) **A103**, 524 (1923).

experimental quantities $n_{Ar}{}^t$, $n_H{}^t$, V^t, and p^t, where $n_{Ar,H}{}^t$ denotes the number of moles of argon or hydrogen in the cell, V^t is the cell volume, and p^t the measured pressure. In order to carry out the calculations the volume of the liquid and gas phase (V^L and V^G) and the number of moles in the respective phases (n^L and n^G) must be obtained. This was done in a step process. An approximate concentration of hydrogen was assumed (after a few points had been made, it could be predicted quite closely from a p versus x diagram) and it was further assumed that all argon was condensed. This led to a first approximation for V^L:

$$V^L=(n_{Ar}{}^tV_{Ar}+xn_{Ar}{}^t\bar{V}_H)[1-\kappa\cdot(p^t-p_{Ar}{}^0)], \qquad (2)$$

where κ is the compressibility coefficient for liquid argon[8] and $p_{Ar}{}^0$ is the vapor pressure of pure argon at the same temperature.[2] V_{Ar} is the molar volume of liquid argon[9] and $\bar{V}_H$ the partial molar volume of hydrogen in argon. Since the earlier measurements of the density of liquid argon, carried out in the Leiden laboratory,[9] have recently been questioned,[10] we redetermined the density at 100°K and 120°K and found values in substantial agreement with Mathias, Onnes, and Crommelin. The partial molar volume of the solute $\bar{V}_H$ ranges from 30 to 42 cc, depending on temperature (Table II). It was measured by successively adding known doses of argon to a small amount of hydrogen in the cell until the latter was filled, as indicated by a sharp pressure rise. The calculated values are somewhat uncertain because of the uncertainty of the compressibility of the solution, which was assumed to be the same as the compressibility of pure liquid argon. For this reason, no attempt was made to measure the change in partial molar volume of hydrogen with concentration or pressure. The reported values are mean values at low concentration (2 to 5 mole %) and pressures under 60 atm.

A first approximation of the quantities of argon in the gas and liquid phase ($n_{Ar}{}^G$ and $n_{Ar}{}^L$) could then be calculated. Raoult's law was assumed to hold for the vapor pressure of argon and correction were made for the increase in vapor pressure with the external pressure (Poynting correction) and for the nonideality of the vapor. The second virial coefficients for argon were calculated from the LJD force constants, since no measurements are reported in the literature below 120°K. Next, $n_{Ar}{}^t$ in Eq. (2) was replaced by $n_{Ar}{}^L$ and the procedure repeated until the change in V^L became less than 0.003 cc.

The amount of hydrogen in the gas phase $n_H{}^G$ was calculated from V^G, the equation of state and (p^t-p^{Ar}), where p^{Ar} denotes the increase in pressure when a small amount of argon, just enough to form a liquid phase, is added to the hydrogen in the cell. At each temperature, p^{Ar} was measured at intervals of 10 atmos of hydrogen pressure. The mole fraction x could then be calculated and compared with the approximate value used in the expression for V^L [Eq. (2)]. If the two quantities differed by more than 1% of their absolute value, the entire procedure was repeated.

The possible error in this calculation is greatest at the highest temperatures (high vapor pressure of argon) and at the beginning of a run (large V^G). However, the latter allows a very sensitive check on our calculations. By variation of the initial hydrogen pressure, almost the same total pressure was repeatedly obtained with widely different amounts of liquid in the cell, but the calculated concentrations never differed more than ±2% of their absolute value.

Fugacity and Henry's Constant

The fugacity of n_1 moles of pure gas 1 in the volume V is given by[11,12]

$$(p_1{}^*)_{pure}=(n_1RT/V)\exp[(2n_1B_{11}/V)+\tfrac{9}{2}(n_1/V)^2C_{111}]. \qquad (3)$$

If n_2 moles of gas 2 are added to the n_1 moles of 1 without any change in volume, the fugacity of 1 in the mixture becomes

$$p_1{}^*=(n_1RT/V)\exp[(2n_1B_{11}/V)+(2n_2B_{12}/V)+\tfrac{9}{2}(n_1/V)^2C_{111}+\text{cross terms in } C]. \qquad (4)$$

If we combine (3) and (4), we obtain

$$p_1{}^*=(p_1{}^*)_{pure}\exp[(2n_2B_{12}/V)+\text{cross terms in } C]. \qquad (5)$$

The fugacity hydrogen would have in the absence of argon in the gas phase $(p^*)_{pure}$ was calculated from

$$(p^*)_{pure}=(p^t-p^{Ar})F^*, \qquad (6)$$

where the fugacity coefficient F^* is given by

$$RT\ln F^*=B_H(p^t-p^{Ar})+\tfrac{1}{2}C_H(p^t-p^{Ar})^2. \qquad (7)$$

The mixed second virial coefficient B_{12} in Eq. (5) was calculated according to the method and with the help of the tables given in Hirschfelder, Curtis, and Bird.[13] Since there is at present no satisfactory method for calculating the mixed third virial coefficients, the cross terms in C, Eq. (5) were neglected. Any error resulting from this would be significant only at the highest temperatures and pressures. In our discussions

[8] J. S. Rowlinson, *Liquids and Liquid Mixtures* (Butterworths Scientific Publications, Ltd., London, 1959), p. 50.

[9] E. Mathias, H. Kamerlingh Onnes, and C. A. Crommelin, Communs. Phys. Lab. Univ. Leyden **A131** (1912).

[10] R. A. H. Pool and L. A. K. Staveley, Nature **180**, 1118 (1957).

[11] E. A. Guggenheim, *Thermodynamics* (Amsterdam, 1957), pp. 221–226.

[12] R. H. Fowler and E. A. Guggenheim, *Statistical Thermodynamics* (Cambridge University Press, New York, 1939), Eqs. (704.1) – (704.14).

[13] J. O. Hirschfelder, C. F. Curtis, and R. B. Bird, *Molecular Theory of Gases and Liquids* (John Wiley & Sons, Inc., New York, 1954), pp. 168–170 and Appendixes IA and IB.

we shall use only the values of the Henry's constant extrapolated to zero fugacity of the solute, which is independent of the mixed third virial coefficients.

From the fugacities, Henry's constant k^* was calculated according to:

$$k^* = p^*/x. \tag{8}$$

EXPERIMENTAL RESULTS

The measured solubility (mole fractions x of the solute), Henry's constant k^*, the fugacity of the solute p^*, and the total pressure p' are given for each temperature in Table I.

The solubility isotherms of hydrogen as a function of the fugacity are shown in Fig. 2.

The experimental values of k^* depend (especially at higher temperatures) very little on pressure and concentration (Fig. 3, drawn line). It will be shown later that this behavior is caused by the opposite sign of $(\partial k^*/\partial p)_{x,T}$ and $(\partial k^*/\partial x)_{p,T}$. This facilitates an accurate extrapolation of k^* to zero fugacity of the solute (dashed line in Fig. 3). The apparent volume for solution per mole of argon was calculated from k^* by

$$V_{app} = RT/k^*. \tag{9}$$

The chemical potential for hydrogen in the liquid phase is

$$\mu_H{}^L = \mu_H{}^* + p\bar{V}_H + RT \ln fx \tag{10}$$

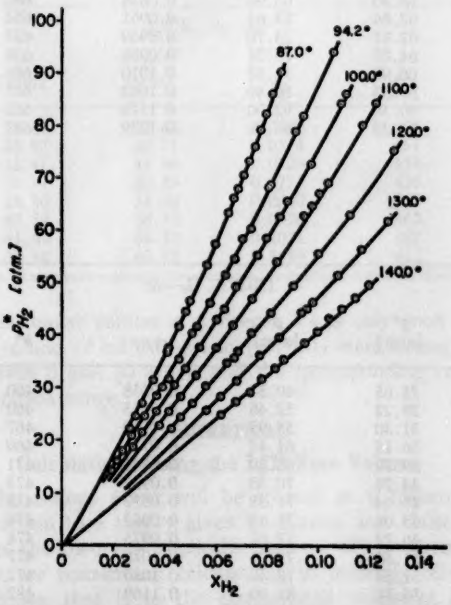

FIG. 2. Solubility isotherms of hydrogen in liquid argon. p^*, fugacity of hydrogen; x, mole fraction of hydrogen.

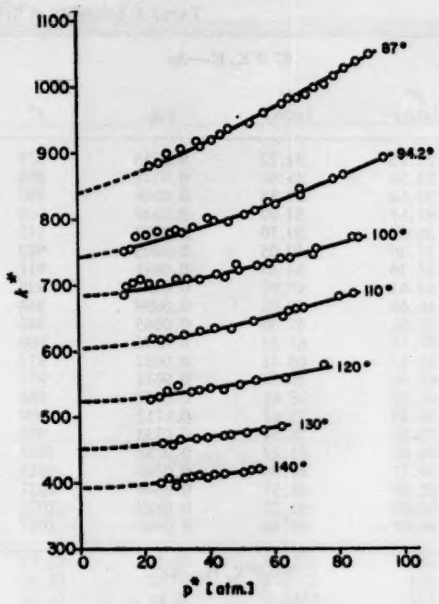

FIG. 3. Dependence of Henry's constant k^* on pressure and temperature for the system hydrogen-argon.

if the compressibility is neglected. We can rewrite Eq. (10)

$$\mu_H{}^L = \mu_H{}^* + p\bar{V}_H + RT \ln x + 2RTBx, \tag{11}$$

where B is defined as the second virial coefficient of hydrogen in the liquid. For the gas we have

$$RT \ln p^* = \mu_H - \mu_H{}^0. \tag{12}$$

If we combine these equations with the definition of k^*, Eq. (8), we find

$$\ln k^* = (\mu_H{}^* - \mu_H{}^0)/RT + p\bar{V}_H/RT + 2Bx. \tag{13}$$

From this we find

$$L^0 = [(\partial \ln k^*)/(\partial 1/RT)] = H_H{}^* - H_H{}^0, \tag{14}$$

which is in physical terms the heat of solution for the transfer of one mole of hydrogen from a dilute ideal gas to the solution.

If we take the derivative with respect to change in pressure

$$(\partial \ln k^*/\partial p)_T = \bar{V}_H/RT + 2B(\partial x/\partial p)_T, \tag{15}$$

the factor $(\partial x/\partial p)_T$ can be evaluated from the data available, so from $(\partial \ln k^*/\partial p)_T$ and a knowledge of $\bar{V}_H$, B can be evaluated. The extrapolated values of k^*, together with the values of V_{app}, $\bar{V}_H$, B, and L^0 are given in Table II. The values of L^0 are the mean between the temperature for which they appear in Table II and the next higher temperature. The values of B are probably not better than $\pm 20\%$, since the

TABLE I. Solubility of hydrogen and deuterium in liquid argon.

87.0°K, H_2—Ar				94.2°K, H_2—Ar			
p^* [atm]	p' [atm]	x_{H_2}	k^*	p^* [atm]	p' [atm]	x_{H_2}	k^*
22.22	24.22	0.0253	878	14.20	16.74	0.0189	751
24.58	26.61	0.0278	884	15.83	18.43	0.0210	754
27.64	29.84	0.0308	897	18.01	20.69	0.0233	773
31.55	33.99	0.0349	904	20.74	23.56	0.0268	774
36.90	39.70	0.0402	917	24.51	27.56	0.0314	780
37.26	40.05	0.0408	913	28.42	31.78	0.0365	779
41.36	44.43	0.0451	917	29.99	33.45	0.0384	781
44.63	47.97	0.0481	928	31.57	34.96	0.0405	780
46.60	50.03	0.0499	934	35.43	39.06	0.0450	787
53.51	57.46	0.0565	947	40.27	44.35	0.0504	799
57.11	61.38	0.0595	960	41.74	45.85	0.0525	795
63.43	68.11	0.0652	973	46.01	50.33	0.0578	796
65.66	70.55	0.0671	978	51.63	56.25	0.0642	804
67.97	73.01	0.0691	983	54.35	59.20	0.0672	809
70.45	75.67	0.0712	989	58.51	63.62	0.0711	823
73.19	78.59	0.0733	998	60.25	65.53	0.0735	820
76.03	81.62	0.0758	1003	68.29	73.90	0.0810	843
79.17	84.96	0.0780	1015	68.46	74.07	0.0820	835
82.58	88.57	0.0804	1027	78.95	85.19	0.0915	862
86.09	92.27	0.0829	1038	81.87	88.19	0.0945	866
90.07	96.46	0.0860	1047	94.26	101.05	0.1056	893

100.0°K, H_2—Ar				110.0°K, H_2—Ar			
p^* [atm]	p' [atm]	x_{H_2}	k^*	p^* [atm]	p' [atm]	x_{H_2}	k^*
13.50	17.46	0.0197	685	22.95	31.34	0.0372	616
14.90	18.91	0.0214	696	25.32	33.89	0.0410	617
16.57	20.65	0.0236	702	28.35	37.03	0.0458	619
18.64	22.85	0.0264	706	32.22	41.10	0.0515	625
21.40	25.77	0.0306	700	37.56	46.60	0.0596	630
25.20	29.71	0.0360	700	37.74	46.78	0.0602	627
30.32	34.96	0.0428	708	41.92	51.29	0.0662	633
30.76	35.30	0.0435	707	47.12	56.77	0.0742	635
33.63	38.31	0.0475	708	53.80	63.96	0.0834	645
37.56	42.32	0.0530	709	62.84	73.63	0.0961	654
42.92	47.84	0.0600	715	62.91	73.70	0.0960	655
45.03	49.99	0.0632	713	64.85	75.74	0.0986	658
49.37	54.61	0.0676	730	66.98	77.88	0.1010	663
49.48	54.71	0.0684	723	69.33	80.40	0.1042	665
55.29	60.76	0.0760	728	80.36	92.00	0.1178	682
58.65	64.24	0.0801	732	84.39	96.30	0.1229	687
62.64	68.35	0.0848	739				
65.25	71.04	0.0878	743				
72.72	78.73	0.0975	746				
73.56	79.48	0.0978	752				
84.52	90.77	0.1095	772				
86.14	92.41	0.1115	773				

120.0°K, H_2—Ar				130.0°K, H_2—Ar			
p^* [atm]	p' [atm]	x_{H_2}	k^*	p^* [atm]	p' [atm]	x_{H_2}	k^*
22.13	36.34	0.0418	529	25.65	49.54	0.0558	460
24.28	38.70	0.0455	533	28.22	52.46	0.0613	460
26.98	41.58	0.0499	541	31.30	55.93	0.0670	467
30.25	45.11	0.0552	548	36.16	61.43	0.0771	469
34.42	49.61	0.0639	539	39.79	65.49	0.0845	471
35.60	50.90	0.0660	539	44.24	70.50	0.0932	475
36.84	52.84	0.0680	542	45.04	71.38	0.0952	473
40.29	55.87	0.0740	544	45.08	71.45	0.0952	474
44.32	60.27	0.0814	544	46.22	72.67	0.0975	474
49.33	65.43	0.0902	549	51.38	78.05	0.1078	477
55.46	72.09	0.1000	555	51.55	78.40	0.1080	477
63.28	80.57	0.1129	560	56.34	83.90	0.1169	482
75.41	94.58	0.1299	580	62.03	90.16	0.1275	486

TABLE I.—*Continued.*

140.0°K, H_2—Ar

p^* [atm]	p' [atm]	x_{H_2}	k^*
24.63	60.49	0.0615	400
27.18	63.11	0.0670	406
28.92	65.80	0.0723	400
31.79	68.86	0.0779	408
32.34	69.47	0.0796	406
33.75	70.76	0.0824	409
34.12	71.45	0.0833	410
35.43	72.88	0.0863	410
38.71	76.69	0.0943	410
39.40	77.50	0.0953	413
40.92	79.21	0.0990	413
43.19	81.86	0.1044	414
43.78	82.54	0.1060	413
50.12	89.82	0.1199	418
52.23	92.13	0.1245	420
54.46	94.65	0.1295	421

87.0°K, D_2—Ar

p^* [atm]	p' [atm]	x_{D_2}	k^*
22.13	24.02	0.0317	698
24.20	26.22	0.0348	695
26.77	28.96	0.0381	703
30.02	32.42	0.0424	708
34.28	36.66	0.0480	714
39.78	42.87	0.0557	714
48.11	51.85	0.0669	719
50.59	54.44	0.0693	730
52.95	57.09	0.0721	734

100.0°K, D_2—Ar

p^* [atm]	p' [atm]	x_{D_2}	k^*
17.31	21.47	0.0298	581
18.85	23.07	0.0322	585
20.63	24.97	0.0353	584
22.80	27.27	0.0388	588
25.55	30.18	0.0432	591
29.07	33.89	0.0489	594
33.70	38.79	0.0564	598
44.13	49.78	0.0734	601
48.23	54.10	0.0782	617
53.24	59.37	0.0860	619
59.60	66.04	0.0970	614
68.04	74.85	0.1088	625
79.84	87.10	0.1236	646
82.22	89.55	0.1270	647

120°K, D_2—Ar

p^* [atm]	p' [atm]	x_{D_2}	k^*
18.42	32.43	0.0409	450
25.92	40.71	0.0574	451
32.47	47.56	0.0720	451
35.17	50.49	0.0771	456
38.50	54.30	0.0840	458
42.59	58.72	0.0920	463
47.69	64.23	0.1021	467
52.84	69.77	0.1119	472

partial molar volume of hydrogen $\bar{V}_H$ is only good to ±4 cc and $(\partial \ln k^*/\partial p)_T$ and $(\partial x/\partial p)_T$ were averaged between 0 and 50 atmos and the corresponding concentration range.

THEORETICAL

Calculations Using the LJD Free Volume

The isotope effect will be treated as a quantum correction to a theory given by Karasz and Halsey.[1] Since the theory is applicable to very dilute systems only, we restrict our calculations to infinitely dilute solutions, that is to the extrapolated values of k^*. The values of the molecular parameters have been taken from the tabulations of Hirschfelder, Curtis, and Bird,[13] using the quantum-mechanical values for H_2 and D_2. The LJD free volume v and w_0 were calcalculated from Eqs. (16) through (19) in footnote reference 1. If we denote the partial molar Gibbs free energy of forming an empty void in the solvent, suitable to contain a molecule of solute, by $\bar{G}_v = H_v - \bar{S}_v \cdot T$, we then find[1]

$$\ln k^* = w_0/kT + \bar{G}_v/kT - \ln(v/kT) \quad (16)$$

$$\bar{G}_v/kT = \ln(v/V_{app}) - w_0/kT \quad (17)$$

$$\bar{S}_v/k = \bar{H}_v/kT - \ln(v/V_{app}) + \delta/kT, \quad (18)$$

TABLE II.

T °K	lim k^* $p^*\to 0$	V_{app} cc/mole	$\bar{V}_H$ cc/mole	B	$L°$[a] cal/mole
H_2—Ar					
87.0	835	8.55	30	−0.87	258
94.2	745	10.37	30	−0.88	271
100.0	685	11.98	31	−0.90	289
110.0	600	15.04	34	−0.80	344
120.0	526	18.72	36	−0.76	442
130.0	456	23.39	39	−0.66	547
140.0	392	30.28	44	−0.52	...
D_2—Ar					
87.0	688	10.38	30	−1.00	250
100.0	570	14.44	31	−0.80	297
120.0	444	22.18	36	−0.65	....

[a] Mean values between the temperature under which they are entered and the next higher temperature.

where $\bar{H}_s$ is the partial molar heat of solution. In the formula for $\bar{S}_v$ a mixprint in footnote reference 1, affecting the last term in the equation, has been corrected.

In order to carry out the quantum corrections, we replace the classical LJD free volume $v(cl)$ by a three-dimensional isotropic harmonic oscillator. The corresponding effective classical frequency ν is then given by[14]

$$\nu=(kT/2\pi m)^{\frac{1}{2}}v(cl)^{-\frac{1}{3}}. \tag{19}$$

In footnote reference 1, the quantum correction was written in terms of the partition functions with the lowest state as zero of energy, and therefore involved a zero-point correction to w_0, before the calculation of the correction. This method though possible in principle was cumbersome enough so that the quantum corrections given in footnote reference 1 are wrong. Here we will calculate an effective frequency from the partition function with the bottom of the potential (w_0) as zero:

$$h\nu'/kT=[1-\exp(-h\nu/kT)]\exp(h\nu/2kT) \tag{20}$$

$$v(qu)=(kT/2\pi m\nu'^2)^{\frac{3}{2}}. \tag{21}$$

No further zero point correction to w_0 is then necessary, since it has been taken care of by $\exp(h\nu/2kT)$ in Eq. (20). The approximation made by changing from the LJD potential to the harmonic oscillator model can perhaps best be seen in Fig. 4 (drawn curve: Lennard-Jones and Devonshire potential, dashed curve: harmonic oscillator).

Next, we have to calculate the small quantity δ in Eq. (18), which will allow for the nonproportionality of $v(qu)$ and T.

$$\delta=d\ln[v(qu)/kT]/d(1/kT). \tag{22}$$

From Eqs. (19) and (21), we find

$$v(qu)/v(cl)=f=(\nu^3/\nu'^3). \tag{23}$$

If $h\nu/kT$ is set equal to x, then with Eq. (20)

$$f=[x\cdot\exp(-x/2)/(1-\exp-x)]^3. \tag{24}$$

It emerges from an examination of tables for the LJD parameter g[15,16] that $v(cl)$ is almost proportional to kT. Therefore

$$d\ln[v(cl)/kT]/d(1/kT)\ll d\ln[v(qu)/kT]/d(1/kT). \tag{25}$$

Hence, from Eqs. (22), (24), and (25), one finally obtains

$$\delta=h\nu(d\ln f/dx)=3h\nu[1/x-\tfrac{1}{2}-1/(e^x-1)]. \tag{26}$$

The calculations were carried out for 87°K, because the substitution of a harmonic oscillator for the LJD potential should be better the higher the density. The results are given in Table III.

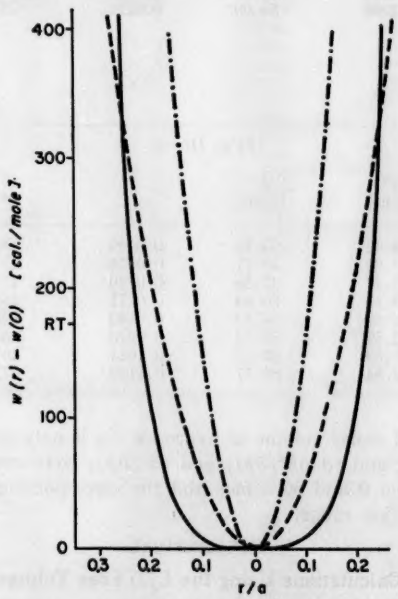

FIG. 4. Comparison between the LJD potential (——) and the harmonic oscillator potential (---). Innermost curve (-·-·-) shows the harmonic oscillator for the free volume calculated from the experimental isotope effect.

[14] Footnote reference 12, Eq. (802.8).

[15] T. L. Hill, J. Phys. Colloid Chem. **51**, 1219 (1947).

[16] I. Prigogine and G. Garikian, J. chim. phys. **45**, 273 (1948).

It should be pointed out there that the quantum corrections when calculated correctly, for Table II of footnote 1 are so small that the classical values given in that table are the correct quantum ones also.

Calculation of Free Volume from the Isotope Effect

We shall assume that, in Eq. (16), the mass of the incorporated atom does not affect the value of the free energy of void formation $\bar{G}_v$ or the depth of the potential w_0, but only the frequency of vibration and thus the effective free volume v. The isotope effect is the result of the different values of $v(qu)$ for the two isotopes. We can then use the ratio of the solubilities of D_2 to H_2 (1.2) to calculate the correct classical free volume, by setting $v(qu)$ $D_2/v(qu)$ $H_2=1.2$, and finding the value of $v(cl)$ in Eqs. (19)–(21) that gives this ratio.

The free volume so estimated, as well as the other quantities calculated from it, are shown in Table IV. This estimate of the free volume, which does not suffer from the limitations of the LJD integration, is a factor of five smaller than the LJD free volume. The corresponding potential is shown in Fig. 4.

TABLE III. Parameters for argon at 87°K, calculated from the LJD free volume.

	H_2 filled holes	D_2 filled holes
$-w_0$	1137 cal/mole	1137 cal/mole
ν	1.836×10^{12}	1.298×10^{12}
ν'	1.915×10^{12}	1.326×10^{12}
v (cl)	1.35 cc/mole	1.35 cc/mole
v (qu)	1.18 cc/mole	1.27 cc/mole
$\bar{S}_v$ (cl)	6.30 e.u.	6.38 e.u.
$\bar{S}_v$ (qu)	6.06 e.u.	6.26 e.u.
$\bar{G}_v$ (qu)	957 cal/mole	936 cal/mole
$-\delta$	43.6 cal/mole	22.0 cal/mole

TABLE IV. Parameters for argon at 87°K, calculated from the isotope effect.

	H_2 filled holes	D_2 filled holes
ν	3.139×10^{12}	2.219×10^{12}
ν'	3.544×10^{12}	2.365×10^{12}
v (cl)	0.2750 cc/mole	0.2750 cc/mole
v (qu)	0.1868 cc/mole	0.2241 cc/mole
$\bar{S}_v$ (qu)	8.8 e.u.	9.2 e.u.
$\bar{G}_v$ (qu)	660 cal/mole	660 cal/mole
$-\delta$	123 cal/mole	63.6 cal/mole

CONCLUSIONS

The rather large entropies for lattice vacancy formation found in footnote reference 1 for the solubility of helium and neon have also been found here for the solubility of H_2 and D_2. By the use of the isotope effect itself, it is possible to avoid the approximations of the LJD theory in estimating these entropies. We realize that other isotope effects, such as the average volume occupied (steric effect) and rotational effects have been neglected, but it is pertinent that recent calculations on the LJD model by Dahler and Hirschfelder[17] also come to the conclusion that the LJD free volume theory is very poor. The theory, when applied to the solution of foreign atoms at zero concentration is free of the logical defects caused by the arbitrary distinction between a wanderer and (identical) cage atoms, but still appears to be very inaccurate indeed.

ACKNOWLEDGMENTS

One of us (H.V.) wishes to thank the University of Vienna for granting leave of absence and the Conference Board of Associated Research Councils, Committee on International Exchange of Persons for travel support.

[17] J. S. Dahler and J. O. Hirschfelder, J. Chem. Phys. **32**, 330 (1960).

Preliminary Analysis of U^{4+} Ion Spectra in Crystals*

ROBERT A. SATTEN AND DONALD YOUNG,
Department of Physics, University of California, Los Angeles, California
AND
DIETER M. GRUEN,
Chemistry Division, Argonne National Laboratory, Argonne, Illinois

(Received January 29, 1960)

An analysis of a number of features of the absorption spectra of U^{4+} ions in crystals is given. Absorption spectra of crystals of the compounds Cs_2UCl_6, and $[N(CH_3)_4]_2$ UCl_6, and to a lesser extent $[N(C_2H_5)_4]_2$ UCl_6 have been studied at room temperature, liquid N_2 and liquid He temperatures. The visible spectrum is essentially entirely vibronic. Pure electronic transitions are absent or very weak in thick crystals in agreement with a model of electric dipole transitions within the $5f^2$ shell at an equilibrium site of inversion symmetry. We believe this to be the first demonstrated case of an essentially purely vibronic spectrum reported for rare earth or actinide salts. The three "ungerade" frequencies of the $UCl_6^{=}$ complex are coupled to the electronic frequencies and are determined by their appearance with the same frequency of superposition in all three salts as well as by being the most intense of the vibronic lines in every group in which they appear. Other lattice modes and internal frequencies of the tetramethylammonium ion are also found to be superimposed. The weak pure electronic transitions are fairly sharp, an indication that there is still considerable shielding in the $5f^n$ electronic states even though this shielding is less than in $4f^n$ states. The independence of superimposed vibration frequencies on $5f^2$ electronic states indicates the fact that the $5f$ states do not contribute much to the binding. The similarity in the spectra of the three salts studied is due to the fact that the nearest-neighbor Cl^- ions are the principal origin of the crystalline field in contrast to the rare earths, wherein this type of similarity is due to the fact that the crystalline field is small and each group of lines represents a multiplet level of the free ion. Evidence is presented that the crystalline field splitting is larger than hitherto believed and is the same order of magnitude as the spin-orbit interaction. Methods of attacking the problem of the experimental classification and calculation of energy levels in the situation in which three major interaction are of comparable size are discussed.

I. INTRODUCTION

IT is by now well recognized that the absorption spectra of crystals containing lanthanide ions involve transitions within the $4f$ shell. Studies of the absorption spectra of crystals containing actinide ions have provided much evidence in the last fifteen years for the belief that these spectra arise from transitions within the $5f$ shell of the ions.[1]

Progress in understanding the complicated spectra of the lanthanide ions has been slow even though this has been an active research field for more than 30 years. At present, only the spectra of the ions Ce^{3+}, Pr^{3+}, Tm^{3+}, and Yb^{3+} with at most two electrons (or holes) in the $4f$ shell are understood in reasonably complete detail. There continue to be contributions to a fuller understanding even of these relatively simple spectra.[2-8]

Our understanding of one and two electron spectra of the actinide ions is still less complete than of the analogous lanthanide spectra.[9-12] In part, this is due to a paucity of data particularly of absorption spectra on single crystals of actinide ion compounds. In addition, there are a number of reasons why one would expect the problem of analyzing actinide ion spectra to be more difficult than the problem of elucidating lanthanide ion spectra. Among these is the fact that the spin-orbit interaction for $5f^n$ electrons is larger than for $4f^n$ electrons resulting in a greater departure from Russell-Saunders coupling of the former compared with the latter. Another complicating factor is the greater spatial extension of the $5f$ compared with the $4f$ wave functions which results in less perfect shielding from the electric field of the crystal and in larger Stark splitting of $5f$ compared with $4f$ electrons. In turn, this has as a consequence a greater degree of mixing of free ion J values.

On the other hand, we hope to show that actinide ion spectra may have "built in" aides to their identification and analysis, which are for the most part lacking in the case of lanthanide ion spectra. These special features will be more fully discussed in subsequent sections of this paper, particularly in the summary.

This paper is the first part of a detailed study of a $5f^2$ configuration and presents the experimental results

* This work was initiated at the Argonne National Laboratory under the auspices of the U. S. Atomic Energy Commission by D.M.G. and R.A.S. during the summer of 1957. Since then, it has been jointly carried forward at UCLA and at Argonne. This work which was presented in part at the American Physical Society Meeting at UCLA in February, 1959, is being submitted by D. Young in partial fulfillment of the requirements for the Ph.D.

[1] G. T. Seaborg and J. J. Katz, *The Actinide Elements* (McGraw-Hill Book Company, Inc., New York, 1954), 1st ed.

[2] G. Dieke and Sarup, J. Chem. Phys. **29**, 741 (1958).

[3] E. V. Sayer, K. M. Sancier, and S. Freed, J. Chem. Phys. **23**, 2060 (1955).

[4] B. Judd, Proc. Roy. Soc. (London) **A241**, 414 (1957).

[5] G. H. Dieke and H. M. Crosswhite, J. Opt. Soc. Am. **46**, 885 (1956).

[6] U. Johnsen, Z. Physik **152**, 454 (1958).

[7] W. A. Runciman and B. G. Wybourne, J. Chem. Phys. **31**, 1149 (1959).

[8] P. P. Feofilov, Optika i Spektroskopia **6**, 150 (1959).

[9] For a general review of rare earth and actinide ion spectra see W. A. Runciman, Repts. Progr. Phys. **21**, 30 (1958); and D. McClure, Solid State Phys. **9**, 399 (1959).

[10] For a general review of the actinides see C. K. Jorgensen, Molecular Phys. **2**, 96 (1959).

[11] J. C. Eisenstein and M. H. L. Pryce, Proc. Roy. Soc. (London) **A238**, 31 (1956).

[12] J. Conway, J. Chem. Phys. **31**, 1002 (1959). Our results differ considerably from Conway's in that we present evidence for a much larger crystalline field. Conway believes his spectra of tetravalent uranium fluorides show no vibronic transitions, whereas our transitions were almost entirely vibronic with an occasional weak, pure electronic transition in sufficiently thick crystals.

together with a number of conclusions that may be reached even in the absence of detailed calculations. The second part of this study will consist of a detailed analysis of the energy levels of the $5f^2$ configuration of the U^{4+} ion in an octahedral crystalline field including spin-orbit and electrostatic interactions.

The compounds chosen for this work were Cs_2UCl_6, $[(CH_3)_4N]_2UCl_6$ (Abbr. TMA), and $[(C_2H_5)_4N]_2UCl_6$ (Abbr. TEA). These substances possess relatively sharp absorption lines, many of which are resolved even at room temperature.

The crystal structures of all three salts are known. In all three compounds the uranium ion is surrounded octahedrally by six chloride ions (U–Cl distance is 2.75 A; reported only in Cs_2UCl_6).[13] The cesium double salt is trigonal ($a=b=7.492$ A, $c=6.038$ A); space group D_{3d}^3. The compound has one molecule per unit cell.[13] The TMA double salt is face-centered cubic space group $O_h^5(a=13.03)$ with four molecules per unit cell.[14] The TEA double salt is orthorhombic; space group $D_{2h}^{23}(a=14.2, b=14.7, c=13.3)$ with four molecules per unit cell.[14] In all three cases the uranium ion is an equilibrium site of inversion symmetry, the site symmetry being D_{3d}, O_h and D_{2h} in the cesium, TMA, and TEA double salts, respectively.

II. EXPERIMENTAL

The salts were prepared by methods previously described.[15,16] The spectra were photographed at room and liquid N_2 temperatures from 3500 to 12 000 A and to 9000 A at liquid He temperature on a Bausch and Lomb large Littrow spectrograph by using a glass prism. For the short-wavelength range a quartz prism was used. Near-infrared tracings to 5000 cm^{-1} were obtained at room temperature on a Spectracord and a Cary model 14 spectrophotometer. In addition, infrared spectra were obtained for all three compounds at room temperature on a Perkin-Elmer model 21 and on a Beckman IR-4 instrument in the NaCl and CsBr regions. The infrared spectrum of the compound $Cs_2UO_2Cl_4$ was also observed for reasons which will be discussed later.

Wavelengths were assigned in the photographic region by linear interpolation between iron lines except in the near-infrared region where Hartmann interpolation was used with sodium, argon, and mercury standards.

III. RESULTS

For Cs_2UCl_6 no absorption bands were found in the region 600 cm^{-1} to 4500 cm^{-1} except at 915 cm^{-1} where there is a sharp band due to uranyl ion. This band arises because of surface oxidation of the Cs_2UCl_6 crystals by air. The band has now been positively identified as due to a UO_2^{++} vibration when it was found to occur as the strongest feature in the infrared spectrum of pure $Cs_2UO_2Cl_4$ grown from an aqueous solution containing UO_2^{++}.

There are two broad bands in the region 600–500 cm^{-1} which occur both in the Cs_2UCl_6 and the TMA salt. These bands peak at 500 and 560 cm^{-1} in the latter and 505 and 565 in the former salt. In addition, absorption bands have been observed in the 300 cm^{-1} region. The validity of the absorption bands in the 300 cm^{-1} region is still in doubt because of the difficulty in making precise measurements on crystals with a prism instrument at these long wavelengths.

The spectra of the three U^{4+} compounds studied are very rich in absorption bands in the 4500 cm^{-1} to 29 000 cm^{-1} region. It is with these bands that the remainder of the discussion will concern itself primarily. Total absorption occurs beyond 28 800 cm^{-1} approximately.

The pure electronic transitions in the photographic region above 8000 cm^{-1} were determined as follows: For thin crystals, and looking at a particular group of bands, one observes a point in the photographed spectrum at which there is no absorption and around which absorption lines are grouped symmetrically at longer and shorter wavelengths. The average position between any pair of such symmetrically situated lines is found to agree within experimental error. The absorption lines on the long wavelength side of this average position disappear at liquid helium temperature. In thick crystals (~4 mm) for many of the observed transitions a very sharp but weak absorption line is seen at this average point. This line does not disappear at liquid helium temperature. Presumably, it is due to a pure electronic transition. The pure electronic level positions determined in this way are given in Table I for both Cs_2UCl_6 and $(TMA)_2UCl_6$ together with the temperature shift of each of the levels.

All together, 18 pure electronic transitions have been observed in the photographic region. The strongest frequencies superimposed on these pure electronic transitions[17] are 94, 113, 257, cm^{-1} in $(TMA)_2UCl_6$ and 94, 114, 260, cm^{-1} in Cs_2UCl_6. It was assumed that the same general features recur in the near-infrared region as well. A clearly discernable example of this is the 5000 cm^{-1} electronic level with two broad main peaks which can be seen on the room temperature Cary model 14 tracings at 2.015 μ. These main bands have a separation of 1.65×10^2 cm^{-1}. One-half of this separation, 83 cm^{-1}, is close to one of the UCl_6^{--} complex vibrations which already had been observed to be strongly coupled to a number of pure electronic transitions in the visible region. Since the Cary spectrophotometer does not

[13] S. Siegel, Acta Cryst. **9**, 827 (1956).
[14] Staritzki and Singer, Acta Cryst. **5**, 536 (1952).
[15] C. Hutchison, G. Candela, J. Chem. Phys. **27**, 707 (1957).
[16] G. Candela, C. A. Hutchison, Jr., and W. B. Lewis, J. Chem. Phys. **30**, 246 (1959).

[17] The tetraethylammonium salt has not yet been as extensively studied and measured as the cesium or tetramethyl ammonium salts. The presence of the same three fundamental frequencies of the UCl_6^{--} have however also been found in TEA salt superimposed on pure electronic transitions. We are grateful to Mr. Slava Pollack for these spectra.

TABLE I.

(a) Cs_2UCl_6

Electronic level (77°K)	Vibronically located	Directly measured (very thick crystals)	Temperature shift (77°K) − (R.T.)	Temperature shift (4°K) − (77°K)
1	5046 cm^{-1} (R.T.)			
2	6282 (R.T.)			
3	7273 (R.T.)			
4	8158 (R.T.)			
5	9232		+38 cm^{-1}	
6	9540		+22	
7	10 065		+46	
8	11 176		−1	+7 cm^{-1}
9	12 125	12 126	+19	+2
10 (a)	12 876			+10
10 (b)	12 983		+46	+8
11	14 788	14 788	−22	−2
12	15 211		+9	+3
13 (a)		15 674	+9	0
13 (b)	15 752		+10	+1
14	16 795	16 796	+61	+11
15		18 828	+28	+1
16	20 482			+7
17	20 760			−2
18	21 814		+27	+5
19	22 203		+28	+3
20	24 721		+68	+11

(b) $(TMA)_2UCl_6$

1				
2				
3				
4				
5	9237 cm^{-1}		+30 cm^{-1}	
6	9612		+21	
7	10 069		+30	
8	11 200		+36	+12 cm^{-1}
9	12 130	12 130 cm^{-1}	+16	+5
10	12 954		+48	+9
11	14 835	14 834	−17	−1
12	15 235	15 234	+12	+4
13 (a)	?			
13 (b)	15 778		+22	+3
14	16 834	16 834	+52	+10
15	18 870		+30	+17
16	20 612			
17	20 753			
18	21 897		+33	+7
19	22 238		+39	+11
20	24 749		+80	+16

possess resolution in the near-infrared region comparable to that of the spectrograph in the photographic region, not all of the near-infrared vibronic transitions are resolved. However, it appears that there are at least four pure electronic levels in the 8325–5000 cm^{-1} region. These are listed in Table I along with those occurring in the photographic region.

The vibrational frequencies found superimposed upon each electronic level for two of the three salts studied are presented in Table II.

A KBr pellet was made with 1% $(TMA)_2UCl_6$ and the spectrum observed in the NaCl region of a Beckman IR-3 spectrograph from 450 to 10 000 cm^{-1}. Table III shows the pellet frequencies along side of some high frequencies which have been found coupled to the electronic levels. The high frequencies are found superimposed only on those electronic levels which have the strongest $UCl_6^{=}$ vibronic transitions. In addition Table III shows some strong infrared absorption frequencies in a single crystal of $(TMA)_2UCl_6$ which are not present in the same region of the Cs_2UCl_6 spectrum and hence must be $(TMA)^+$ ion internal frequencies. Frequencies of the $(CH_3)_4N^+$ ion in solution are also shown for comparison where applicable.

TABLE II. Vibration frequencies found superposed upon electronic levels.[a,b] (cm^{-1}).

(a) Cs_2UCl_6

Electronic level (numbered as in Table I)	
1	
2	
3	
4	
5	44 (39),[a] 94, 113 (108), 253*[b]
6	78
7	89 (82)
8	55, 93 (93), 122, 151, 252
9	63* (55), 81 (82), 96
10 (a)	42 (40), 66, 83 (84), 114 (116), 260
10 (b)	41, 58, 95, (103*), 115, 260
11	42 (40), 58 (55), 69 (68), 113 (113), 125 (125), 260, 272, 298
12	36 (36), 60 (60), 91 (94*), 99, 115 (113), 124, 247, 260, 273, 298
13 (a)	21, 40, 58, 98 (95), 115 (115), 126, 249, 260
13 (b)	60, 96 (95), 114 (116), 132, 260
14	40 (40), 115 (115), 258 (256), 295, 351, 422, 567, 627, 785
15	59 (54), 77, 91 (88), 251, 258*, 292
16	41 (39), 115 (117), 253*, 298
17	115, 248*
18	40 (40), 58 (58), 95 (95), 114 (115), 127, 251, 260
19	58 (59), 79, 92 (94)
20	60, 77, 93 (88*)

(b) $(TMA)_2UCl_6$

Electronic level (numbered as in Table I)	
1	
2	
3	
4	
5	25* (25*), 91 (91), 204, 256
6	27* (27*), 86*, 91
7	21, (26*), 90 (89), 555
8	19, 80, 109, (116), 232, 271, 320, 346
9	18 (17), 36 (34), 73 (72), 93 (95)
10	(23.5*), 32, (72), 90 (92), 110 (111), 254, 269, 309, 333, 561, 952, 1072, 1191, 1293, 1420, 1450, 1487
11	18 (18), 33 (33), 76 (78), 116 (115), 190, 241, 259 (259), 274, 560, 1451, 1726
12	17 (17), 34 (34), 74 (73), 94 (95), 114 (112), 259, 275, 298, 366, 951, 988, 999, 1068, 1171, 1290, 1415, 1451
13 (a)	...
13 (b)	25* (25*), 77, 85, 96 (92*), 112 (112), 182, 202, 258, 331
14	19 (19), 31 (31), 78 (77), 110 (117), 186, 255 (259), 272 (273), 296, 330, 376, 414, 501, 554, 576, 734, 849, 950, 1070, 1179, 1295, 1439, 1488
15	84*, (84*), 259, 930, 1133, 1248, 1721, 1793
16	33, 80, 111, 200, 254, 293, 322, 344
17	34, 80, 96, 114, 242, 547
18	17, (26*), 34, 77, (92*), 114, 125, 242, 255, 268, 304, 337
19	29 (29), 90*, 257*
20	33 (33), 80*, (89), 192, 315

[a] Values in ( ) are determined from difference lines on the long-wavelength side of the pure electronic transition.
[b] Values marked *: This is probably not a true vibration frequency, but an apparent center of two adjacent unresolved lines.

Figures 1 to 4 illustrate the general features of the spectrum. Figure 1 shows selected infrared tracings. Figure 2 is a comparison of $(TMA)_2UCl_6$ and Cs_2UCl_6 spectra in the region of 15 000 cm^{-1}. Note that the pure electronic transitions (locations marked) do not appear. Figure 3 is a comparison of $(TMA)_2UCl_6$ spectra at room, liquid-nitrogen and liquid-helium temperatures. Figure 4 shows the appearance of a weak pure electronic transition in a thick crystal of $(TMA)_2UCl_6$.

A typical energy level diagram for the two salts has been drawn for comparison and appears as Fig. 5. Other energy level diagrams can readily be drawn from the results in Tables I and II.

IV. DISCUSSION

1. General Nature of the Spectra

It has been known for some time that the spectra of Cs_2UCl_6, $(TMA)_2UCl_6$, and $(TEA)_2UCl_6$ are quite

TABLE III. Comparison of vibration frequencies above 900 cm^{-1} found by superposition upon electronic levels with those found directly.

Superimposed frequencies	$(TMA)_2UCl_6$ in KBr pellet infrared frequencies	$(TMA)_2UCl_6$ pure crystal	Silver's[a] $(TMA)^+$ ion in solution infrared frequencies
952, 951, 950	952	950	955
1072, 1068, 1070		1080	
1171, 1179	1170	1175	1173
1293, 1290, 1295	1291	1300	1289
1414, 1420	1414		
1439	1446		
1450, 1451, 1451, 1450	1455		1455
1487, 1488, 1485	1487		
1721, 1726	1733		
1793	1792		

[a] S. Silver, J. Chem. Phys. **8**, 919 (1940).

similar.[18] The present results indicate that the similarities arise in the following ways:

(1) The pure electronic levels are located in very nearly the same positions in these salts. (See Table I). The differences in the positions are usually 5–50 cm^{-1}. Since the crystals differ in composition and crystal structure except for the recurrence of the $UCl_6^{=}$ configuration, it is reasonable to assume that the large crystalline Stark splitting of the U^{4+} ion levels in the crystal is almost entirely due to the influence of the six neighboring chloride ions of the complex; and

(2) the strongest absorption lines in the spectra are due to the three *ungerade* internal vibrational frequencies of the $UCl_6^{=}$ complex at around 94, 114, 258 cm^{-1} which appear superimposed on the pure electronic transitions. These frequencies are essentially the same in all three crystals. (See Table II).

Our results show that if there is a splitting of the electronic levels in going from cubic $(TMA)_2UCl_6$ to trigonal Cs_2UCl_6 it must be quite small (less than 3 cm^{-1}). This fact further strengthens the idea that it is the nearest-neighbor chloride ions which predominantly determine the crystalline field about the uranium ion and that the $UCl_6^{=}$ configuration is very closely octahedral in both compounds. A detailed comparison of the electronic levels of the two salts listed in Table I, however, does show two electronic levels (Nos. 10 and 13) which may seem doubled in Cs_2UCl_6 salt but occur only once in $(TMA)_2UCl_6$. We doubt that this apparent doubling is due to a Stark splitting in the lower symmetry field of the Cs_2UCl_6 salt, as one would expect other levels to be affected in a similar way. Whether or not the $UCl_6^{=}$ vibrational levels are split in Cs_2UCl_6 is a problem currently being studied with a 21-ft. grating instrument. These studies at UCLA which are being carried out at much higher resolution than those described in this paper should also be helpful in deciding whether or not small splittings (too small to be detected with the Bausch and Lomb prism spectrograph) occur in electronic levels.

It has often been remarked that the spectra of actinide compounds resemble those of lanthanide compounds. This is due primarily to the fact that the absorption spectra of both the 5*f* and 4*f* series of elements are characterized by groups of spectral lines, with separations of several hundred wave numbers between groups. It is nevertheless extremely hazardous

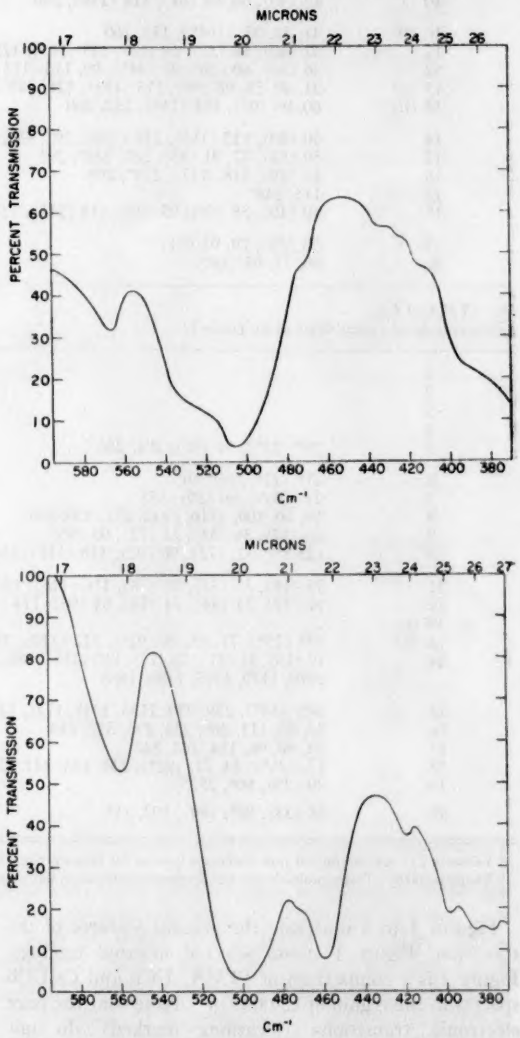

FIG. 1. (a) Absorption bands of Cs_2UCl_6 in the 400–600 cm^{-1} region. (b) Absorption bands of $(TMA)_2UCl_6$ in the 400–600 cm^{-1} region. The 460 cm^{-1} band is most likely due to uranyl impurity as it appears strongly in the $Cs_2UO_2Cl_4$ spectrum. The other weaker bands at 420, 398, 385, 377, 370 cm^{-1} also appear in the latter spectrum.

[18] G. H. Dieke and A. B. F. Duncan, *Spectroscopic Properties of Uranium Compounds* (McGraw-Hill Book Company, Inc., New York, 1949). It should be pointed out that the wavelengths reported in the latter differ considerably from ours.

to make direct comparison between actinide and lanthanide absorption spectra.[19]

In the lanthanides, each group of lines corresponds to a free ion J level, and the lines within a group are due to the crystalline Stark splitting. In the actinides, as in the U^{4+} case for example, it is likely that each group of lines corresponds to a single crystalline Stark level, the lines within a group being due to superimposed vibrational transitions.[20] Conversely, one cannot safely argue in the case of the actinides that a set of electronic levels which happen to be grouped together do in fact arise from the same split J level. The reasons for this situation are twofold. First, in an analysis to be presented in the following, the crystalline potential will be shown to be as much as two orders of magnitude greater in the actinides than in some lanthanides. Second, the spin-orbit interaction parameter in the $5f$ series can be expected to be of the order of $\zeta_{5f}=1600$ cm^{-1} which is about twice as large as in the $4f$ series of elements. This means that some of the crystalline field splittings in the actinides can be of the same order of magnitude as some of the spin-orbit J multiplet splittings. In calculations these two interactions must therefore be diagonalized simultaneously together with the electrostatic interaction between electrons. Second-order perturbation theory, which appears to work quite well in the lanthanides, cannot be used at all in the actinides.

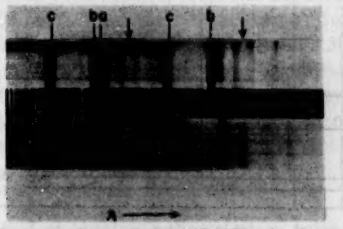

FIG. 2. A comparison of $(TMA)_2UCl_6$ (top) and Cs_2UCl_6 (bottom) spectra at liquid nitrogen temperature in the vicinity of 15 000 cm^{-1} showing vibronic lines associated with electronic levels 11 (left) and 12 (right) of Table I(b). The pure electronic transitions do not appear in these spectra but their virtual positions are marked. The 94, 114, 257 cm^{-1} coupled vibrations of the $UCl_6^{=}$ complex on the short wavelength side of the pure electronic transitions are indicated as a, b, c, respectively. Note that the 94 cm^{-1} vibration is not seen as a vibronic transition coupled to the 14 835 cm^{-1} electronic level. An iron arc comparison spectrum is included.

One can interpolate between two known spectra and obtain a rough tentative value for the ζ_{5f} integral. Racah's value[21] for the $5f^2$ configuration of Th^{2+} is is $\zeta_{5f}=1035$ cm^{-1}, and Goodman's value[22] for the $5f$ electron in NpF_6 is $\zeta_{5f}=2400$ cm^{-1}. If one assumes ζ_{5f} proportional to $(Z_{eff})^4$, then $\zeta_{5f}(U^{4+})=1035\{1+\frac{1}{2}[(2400/1035)^{1/4}-1]\}^4\doteq 1600$ cm^{-1}. This value for ζ_{5f} also assumes that the effective charge for U^{4+} is half-way between Th^{2+} and Np^{6+}, and that the most important reason for the change in ζ is the change in the degree of ionization rather than the change in atomic number.

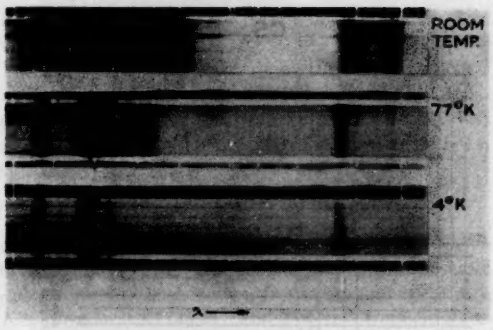

FIG. 3. A comparison of $(TMA)_2UCl_6$ spectra at room, liquid-nitrogen, and liquid-helium temperature in vicinity of 12 500 cm^{-1} showing vibronic lines associated with electronic levels 9 and 10 of Table I(b).

2. Evidence for the Large Size of the Crystalline Field

It is clear from the widely separated electronic energy levels given in Table I that the crystalline Stark splitting in the uranium salts is large compared to the splitting commonly observed in lanthanide salts. Since the separations between excited levels in most regions of the spectrum are of the order of 1000 cm^{-1} or so, one might conclude that the Stark splitting is only about one instead of two orders of magnitude greater in the uranium salts than in lanthanide salts. However, the first excited pure electronic state is about 5000 cm^{-1} above the ground state (see Table I). This is to be compared with 33 cm^{-1} for the first excited state in $PrCl_3$.[2]

Actually there has already been an indication from the work of others that the crystalline field splitting is fairly large. Hutchison and Candela[15] concluded on the basis of magnetic susceptibility measurements that the first (or possibly second) excited Stark level in Cs_2UCl_6 and $(TMA)_2UCl_6$ is 1150 cm^{-1} above the ground state. These workers found the magnetic susceptibility to be constant over the temperature range from room to liquid-helium temperatures. This behavior was ex-

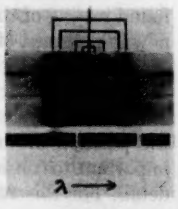

FIG. 4. The absorption spectrum of thick crystal of $(TMA)_2UCl_6$ at liquid-nitrogen temperature showing a weak, sharp pure electronic transition at 12 130 cm^{-1}. The strong absorption "line" on the short wavelength arises from the superposition of the 93 cm^{-1} UCl_6 vibration. Corresponding sum and difference lines are indicated.

[19] Attempts have been made to correlate directly the absorption spectra, for example, of UCl_4 and $PrCl_3$. K. M. Sancier and S. Freed, J. Chem. Phys. **20**, 349 (1952).

[20] This interpretation is in contradiction to that in footnote references 12 and 26.

[21] G. Racah, Physica **16**, 651 (1950).

[22] G. L. Goodman and M. Fred, J. Chem. Phys. **30**, 849 (1959); see also C. Hutchison and B. Weinstock, Tech. Rept. EFINS–59–35 or J. Chem. Phys. **32**, 56 (1960).

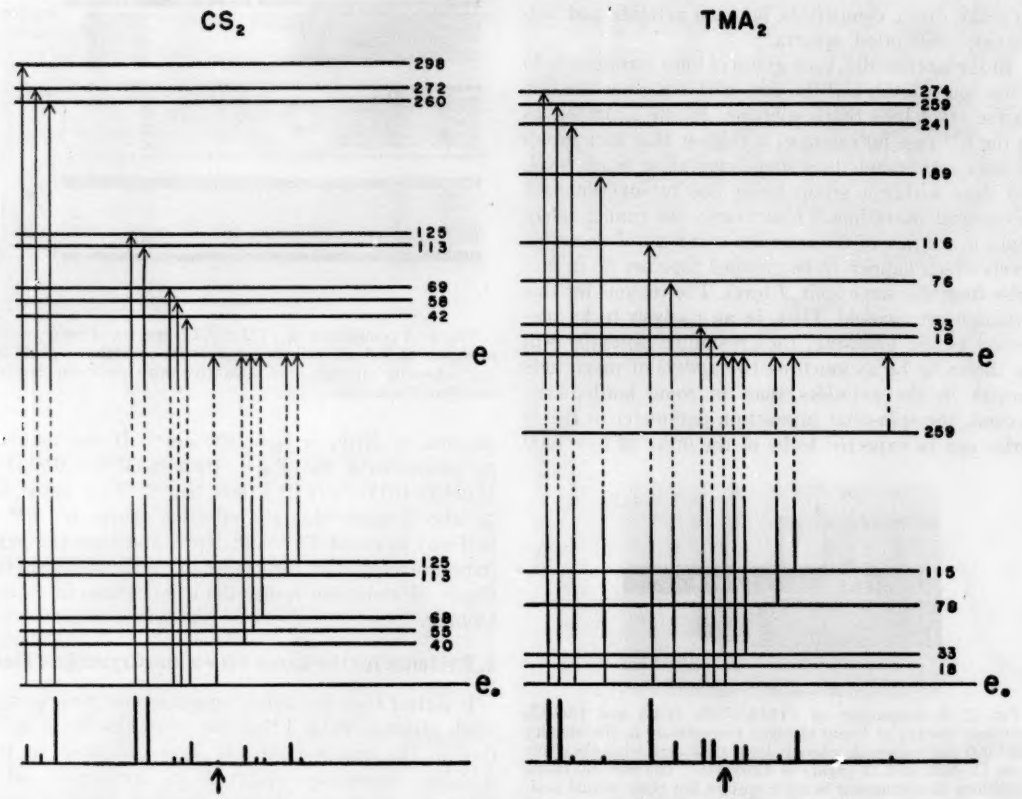

FIG. 5. Empirical level diagrams accounting for the transitions centered about the 14 835 cm^{-1} electronic level in $(TMA)_2UCl_6$ compared with the corresponding ones in Cs_2UCl_6. The corresponding spectral lines appear on the right hand group of the photographed spectrum in Fig. 2. The levels marked e and e_0 are, respectively, excited and ground electronic levels in their lowest vibrational state. Levels above e are vibrational, superimposed upon e. Vibrational levels are also shown superimposed on e_0. The vibrational energy spacings are to scale but there is a huge contraction of scale between e and the highest vibrational level going with e_0.

plained on the basis of a model involving a nondegenerate ($^1\Gamma_1$) ground state and the absence of low-lying degenerate states. Their value of 1150 cm^{-1} for the first excited state was obtained by assuming the magnitude of the susceptibility to be due to the perturbation of the ground $^1\Gamma_1$ by the $^3\Gamma_4$ state in the presence of a magnetic field. The energy E_4 of the $^3\Gamma_4$ level above ground they adjusted to give the experimentally observed value for the susceptibility. Hutchison and Candela calculated the susceptibility using crystalline states determined within the $J=4$ manifold.

However, the large crystalline field required to place the first electronic level at 5000 cm^{-1} produces a profound mixing of the J states. Our detailed calculations, now in progress, of the energies of f^2 states have yielded eigenvectors which can be used to recompute the susceptibility. Such a calculation is discussed in Sec. 6. Since the analysis of the spectrum depends strongly on the position of the first excited electronic level, it is important to consider this question in somewhat greater detail. For this reason, it is planned to make a more thorough study of the entire infrared region in order to be still more certain of not having missed an electronic level. The infrared absorptions which have been observed in the 600–500 cm^{-1} and the 300 cm^{-1} regions are almost certainly connected with vibrational modes of the $UCl_6^{=}$ complex. (The 915 cm^{-1} absorption, it will be recalled is due to UO_2^{++}.)

3. Identification of the Characteristic Frequencies of $UCl_6^{=}$

Only the "ungerade" modes should appear[23a] as vibronic transitions since the equilibrium position of the U^{4+} ion is at a site of inversion asymmetry. During vibration in an odd mode the inversion symmetry is destroyed (except when passing through equilibrium) and electric dipole transitions may occur. Furthermore, since the Cl ions are closest to the U ion it is reasonable to expect the three odd fundamental frequencies of the $UCl_6^{=}$ complex, $^3\Gamma_{5u}$ and $^3\Gamma_{4u}$ (twice), to be the strongest

[23] (a) R. A. Satten, J. Chem. Phys. **29**, 658 (1958); (b) **30**, 590 (1959).

of the vibronic transitions. All three salts have strong superimposed frequencies of about 94, 114, 258 cm^{-1}, and these are identified as Γ_{5u}, Γ_{4u}, Γ_{4u}, respectively, on the basis of the expected order of these odd frequencies using the central force or valence force model.

It is interesting to note that the $^3\Gamma_{5u}$ vibrational frequency appears in the vibronic spectrum although it is forbidden in the infrared.

Once the odd modes frequencies of the $UCl_6^{=}$ complex are known, in principle it should then be possible to determine the even mode ("gerade") frequencies from the appearance in the infrared of combinations of an even plus an odd mode (except $^3\Gamma_{5u}$ plus $^1\Gamma_{1g}$, which is infrared inactive). Since the even modes should have frequencies up to around 300 cm^{-1} it should be possible to account in this way for the transitions in the 600-500 cm^{-1} and 300 cm^{-1} regions which have been observed. In fact, if one interprets the infrared data obtained so far the possible even mode frequencies turn out to be 181, 195, 303 cm^{-1}. Thus the 560 cm^{-1} transition could be a combination of a 257 cm^{-1} ($^3\Gamma_{4u}$) and a 303 cm^{-1} ($^1\Gamma_{1g}$) frequency. These even mode frequencies are extremely tentative because of the uncertainty of the far-infrared data. We do not have a detailed explanation for the 500 cm^{-1} band.

4. Selection Rules

The method of obtaining the selection rules for the vibronic transitions of lanthanide and actinide complexes in crystals has already been presented.[23a] There it was shown that for each vibrational mode of the complex coupled to the electronic motion of the central ion it is necessary to know the transformation properties of the interaction potential energy V_{ev} (which depends on nuclear displacements and central ion electronic coordinates) under transformations of the electronic coordinates. In the Errata[23b] it was stated (without proof) that one did not have to know the detailed modes to determine the desired transformation properties of V_{ev}, but merely the representation to which the mode belongs. Then V_{ev} transforms under electronic coordinate transformations according to the same representation as the mode whose coupling with the electrons is considered. The proof of this convenient theorem is given as an appendix to this paper.

The selection rules as they apply to the octahedral complex in a site of O_h or D_{3d} symmetry are given in an earlier publication.[23b] They are presented here again for convenience for the O_h case.

$^3\Gamma_{4u}$ Modes: $^1\Gamma_1 \leftrightarrow {}^1\Gamma_2$ electronic states

$^3\Gamma_{5u}$ Modes: $^1\Gamma_1 \leftrightarrow {}^1\Gamma_1$ and $^1\Gamma_2 \leftrightarrow {}^1\Gamma_2$ electronic states.

The selection rules are valid under the assumption that V_{ev} produces negligible splitting.

Unfortunately the habit of growth of the Cs_2UCl_6 crystals is such that it is very difficult to obtain crystals suitable for transmitting light perpendicular to the optic axis. Thus the polarization rules for the D_{3d} site have not yet been tested.

The vibronic transition involving the coupled 94 cm^{-1} vibrational frequency is missing in *both* $(TMA)_2UCl_6$ and Cs_2UCl_6 salts for the following electronic levels (as seen from Table II and identified by their TMA frequencies):

14 835; 16 834; 20 612 cm^{-1};

and seen only in the cesium salt at 11 200 cm^{-1}. We conclude that these frequencies represent possible $^1\Gamma_1$ electronic levels. Likewise from the nonappearance of *both* the coupled 114 cm^{-1} and 258 cm^{-1} frequencies as vibronic transitions associated with the following electronic levels:

9615; 10 071; 12 130; 24 749;

in both TMA and Cs salts signifies that the latter frequencies represent possible $^1\Gamma_2$ electronic levels. It should be remarked that the absence of a transition in any particular case is not conclusive evidence of the operation of a selection rule in the usual sense. Thus we do not maintain that all of the above frequencies are now identified. In fact it will be noted that there are four candidates for $^1\Gamma_2$ labels but only three such $^1\Gamma_2$ electronic states.

The experimental results obtained so far tend to confirm the assumption made concerning the wave functions used for deriving the selection rules, namely, that the vibrational eigenfunctions $v(Q)$ are independent of the electronic state. This assumption is verified by the fact that the vibrational frequencies are independent within experimental error of the electronic state upon which they are superimposed. This is in contradistinction to the usual result of applying the Franck-Condon principle in determining molecular vibronic transitions. In the latter case the different electronic states yield different force constants and hence a different set of vibrational frequencies and eigenfunctions for each electronic level. The difference in the two cases is essentially a measure of the extent to which the electronic states affect the binding. The binding in the $UCl_6^{=}$ complex appears to be very insensitive to the 5*f* electronic state.

Since the *pure* electronic transition occurs with very low intensity compared to vibronic transitions in thick crystals (4 mm), the question arises as to whether its appearance is due to a magnetic dipole transition. This question can be investigated by sending polarized light perpendicular to the optic axis in the Cs_2UCl_6 crystal, assuming that the D_{3d} over-all symmetry of the crystal splits the octahedral field levels enough to be observed. If the *pure* electronic transitions for the ray travelling down the optic axis appear in the π spectrum only, then they are magnetic dipole in nature.

In any case it is clear that the very weak appearance of the *pure* electronic transition is proof of the electric dipole nature of the vibronic transitions. No spectra of

lanthanide compounds have as yet been studied in which the ion is at a center of inversion. Consequently, in order to determine the multipolarity of *their* transitions, it is necessary to study the spectra with polarized light, conclusions being definite only for those lines which appear only in the σ or only in the π spectra.

The location of the pure electronic transition may, since it is relatively sharp, make possible a Zeeman effect study. Even if the individual Zeeman lines are not resolvable, some information may be obtainable from the mere broadening or lack of broadening of the pure electronic transition after the magnetic field is turned on. Only $^3\Gamma_4$ and $^3\Gamma_5$ upper electronic states can give rise to such broadening since the $^1\Gamma_1$ and $^1\Gamma_2$ levels cannot split and the $^2\Gamma_3$ levels have no first-order splitting in a magnetic field. The latter follows from the fact that

$$(^2\Gamma_3 \mid \mathbf{L}_z+2\mathbf{S}_z \mid ^2\Gamma_3)=0,$$

since $\mathbf{L}$ and $\mathbf{S}$ transform as $^3\Gamma_4$ and the direct product $^3\Gamma_4\times{}^2\Gamma_3$ does not contain $^2\Gamma_3$.

5. Temperature Shift

Examination of Table I shows that some electronic levels shift toward shorter and some toward longer wave numbers as the temperature is lowered. This can be explained by an increase in the magnitude of the crystalline field parameters as the lattice contracts with decreasing temperature. The ground state energy decreases with decreasing temperature and the excited levels increase or decrease in energy relative to their original position with respect to the ground state at room temperature.

A particular transition decreases in wave number if the excited state is depressed by more than the ground state and vice versa. One expects most transitions to increase in wave number with decreasing temperatures, as is observed. Thus, the temperature shift of each electronic level is a label potentially useful in the identification of the level. The calculated energy states must yield the correct temperature shift for all levels when the appropriate changes in the size of the crystalline field with temperature are employed. See the next section for an example of an attempt to use calculations of temperature shifts to identify an electronic level.

6. Preliminary Attempt to Delimit Crystalline Potential

The matrices in a basis of f^2LSJM eigenfunctions of the Hamiltonian containing electrostatic interaction energy between two f electrons, between an f electron and an octahedral crystalline potential, and the spin-orbit interaction energy have been submitted for publication separately.[24] The octahedral potential used is

$$\begin{aligned}V=&a\sum[(35Z^4-30Z^2r^2+3r^4)+5(x^4-6x^2y^2+y^4)]\\&+b\sum[(231Z^6-315Z^4r^2+105Z^2r^4-5r^6)\\&\quad-21(x^4-6x^2y^2+y^4)(11Z^2-r^2)]\\=&(16/3)\pi^{\frac{1}{2}}a\sum r^4[Y_{4,0}+(5/14)^{\frac{1}{2}}(Y_{4,4}+Y_{4,-4})]\\&+32(\pi/13)^{\frac{1}{2}}b\sum r^6[Y_{6,0}-(7/2)^{\frac{1}{2}}(Y_{6,4}+Y_{6,-4})],\end{aligned}$$

where the summation is over the $5f$ electrons. We shall abbreviate $a\langle r^4\rangle=A$ and $b\langle r^6\rangle=B$.

As the program of identification of levels by the methods indicated in the previous section is still incomplete, it is too early to attempt a fit of the data in order to determine the best values of the parameters. It is of interest, however, to see if it is possible to choose a reasonable set of parameters which will give a first excited level at about 5000 cm^{-1} and have the observed number of electronic levels below 28 000 cm^{-1}.

Eigenvalues and eigenvectors were determined on the "George" high-speed digital computer at the Argonne National Laboratory for a set of values of A ranging from 0 to 10 000 and B ranging from 0 to 6000. In each case we used a set of Slater F_k integrals which were a factor 1.2 times the values given by Racah for the $5f^2$ configuration in Th^{2+}. The value of ζ_{5f} was 1800 in each of these cases.

Certain general features emerged from these trial calculations: (1) $^1\Gamma_1$ is always the lowest eigenvalue and well defines a zero of reference. (2) Values of either A or B (or both) at the large end of their chosen ranges each tend to give too many eigenvalues at too high an energy above the ground $^1\Gamma_1$. Consequently, the number of energy levels remaining in the visible region are far fewer than required by experiment so there are not enough levels to agree with experiment. (3) If one examines the separation of the lowest Γ_3, Γ_4, Γ_5, eigenvalues above ground for values of B varying from zero to 2000 for any value of A, one finds these eigenvalues either first increase to a maximum and then decrease with increasing B or else they simply decrease steadily as all three do for $A>4000$. When $A\leq3000$ all such eigenvalues are in the range below 5000 cm^{-1}, thereby ruling out values of A below 3000 cm^{-1}. In fact, to raise the lowest Γ_3, Γ_4, Γ_5, eigenvalues so that all will be above 5000 cm^{-1} requires A to be of the order of 5000 cm^{-1}. This is due to the fact that these three eigenvalues increase monotonically with A for given B and for $A>4000$ they decrease monotonically with increasing B.

Thus given a set of F_k and ζ parameters at the start, with the additional requirements that the first excited level be near 5000 cm^{-1}, and that there must be at least 21 levels in the region between 5000 cm^{-1} and 28 000 cm^{-1} the choice of values of A and B can be fairly well localized to the vicinity $A=5000$ cm^{-1}, $B=150$ cm^{-1}. The value of A cannot get much larger without displacing the higher eigenvalues to too high energies.

[24] R. A. Satten and J. Margolis, J. Chem. Phys. **32**, 573 (1960).

Even with A as large as 6000 cm^{-1}, B would have to assume a value of about 300 cm^{-1} to bring the first excited state to around 5000 cm^{-1} above ground.

A calculation of the magnetic susceptibility has been made using the parameter values $A=5000$, $B=150$, $\zeta_{5f}=1600$, $F_2=231.6$, $F_4=32.85$, $F_6=3.72$ (F_k ratios hydrogenic). These do not represent final or best values of the parameters but only extremely rough ones, as the calculated levels based on them do not have very good agreement, level for level, with the experimentally found energy levels. No systematic attempt at improvement has been made as yet. However, the susceptibility should not be highly sensitive to the exact value of the parameters, and a rough value of χ is of interest. χ is calculated from the expression

$$\chi=2N\mu_0^2\sum_i[\,|\,(^1\Gamma_1\,|\,L_z+2S_z\,|\,^3\Gamma_4,i)\,|^2/E_i(^3\Gamma_4)].$$

The result is $12.8\times10^{-4}\ N\mu_0^2$ or 3.36×10^{-4} cm^3/mole which is about six times too small—smaller than the experimental value of Hutchison and Candela. However, these calculations do not include the possible temperature independent paramagnetism of the binding electrons of the $UCl_6^{=}$ complex. An experimental determination of this value is now being made by measuring the susceptibility of Cs_2ThCl_6. In summary, it can be stated that the crystalline field cannot be small, (of same order of magnitude as in lanthanide compounds), since this would result in temperature dependent paramagnetism and would also give a spacing of the excited levels much too completely incompatible with experiment. A crystalline field *one* order of magnitude larger than the lanthanides would give energy levels in the region zero to 5000 cm^{-1} contrary to experiment. This leaves one with a crystalline field in which the fourth degree potential is almost two orders of magnitude greater than in the case of the rare earths.

We have considered the possibility that energy levels below 500 cm^{-1} exist with very large values of B which might render the Zeeman splitting of the Γ_4 and Γ_5 states too small to contribute a measurable temperature dependence to the susceptibility, (i.e., a very low effective g value). However, the calculations show that very large values of B increase all but the very lowest energy levels to such a point that again, there are not enough levels in the region between 5000 and 28 000 cm^{-1}.

It is possible that changes in the parameters, particularly the F_k and ζ integrals, will affect the eigenvectors sufficiently to give better agreement with the optical positions, although preliminary trials show that the lowest eigenvalues are not very sensitive to small changes in F_k or ζ integrals.[25]

[25] We should point out the possibility that consideration of the entire f^2 configuration may still not be adequate for any but the lowest states. The fact that there is a (presumably) charge transfer band as low as 29 000 cm^{-1} is an indication that perhaps configuration interaction involving molecular states of the entire $UCl_6^{=}$ complex may be important. A combination of crystalline field and molecular orbital approaches might be desirable.

A glance at the temperature shifts in Table I shows that in going from room to liquid nitrogen temperature in the TMA salt there is only one level in the region 9300 cm^{-1} to 25 000 cm^{-1} which shifts to shorter wave number. If we assume the temperature shifts to be due to changes ΔA and ΔB in the crystalline potential parameters, we can ask the following question: What calculated energy level can have a shift of -17 cm^{-1} while all others in the photographic region have a positive (+) shift when ΔA and ΔB are positive (using the parameters $F_2=231.6$, $F_4=32.85$, $F_6=3.72$, $\zeta_{5f}=1600$, $A=5000$, $B=150$ cm^{-1})? It turns out that there is such a level calculated at 15 078 cm^{-1} and it is a $^1\Gamma_1$ electronic level.

Now the experimentally found level with the -17 cm^{-1} is at 14 835 cm^{-1} and it is one of those levels which we have already singled out as a possible $^1\Gamma_1$ level on the basis of the nonappearance of the coupled 94 cm^{-1} Γ_5 vibration. This consistency seems to make it very likely that the 14 835 cm^{-1} level belongs to $^1\Gamma_1$. The close agreement of the calculated and experimental level is at this stage to be considered somewhat fortuitous, the main emphasis of the argument being on the fact that we have two separate indicators both pointing to the identification $^1\Gamma_1$: selection rules and temperature shifts.

7. Summary and Suggestions for Future Work

The summary of the major conclusions of this paper is given in the abstract. In this section we will not repeat these conclusions but instead summarize, based on our present findings, what we believe to be some features of U^{4+} spectra in crystals which may be useful in the future analysis of actinide spectra. The problem arises from the fact that the three major interactions: electrostatic interaction between $5f$ electrons, spin-orbit, and crystalline field interactions are all large. This is intermediate between the $3d$ group, in which the spin-orbit interaction is small, and the rare earths, in which the crystalline field is small. Thus it seems unlikely that merely adjusting parameters will give a result in which one has much confidence. Rather one must in addition identify (i.e., assign irreducible representations to) the states by experimental means if possible.

The Zeeman effect is usually one of the best aids in analyzing spectra, but it has been reported that the lines in the U^{4+} spectra are too broad[12] for Zeeman studies even at liquid helium temperature. This is true of our spectra also, except possibly the pure electronic transitions. We find these lines to be fairly sharp and isolated although weak. Thus, when it is not possible to dilute a salt, instead of trying to sharpen the lines by going to thinner crystals (which does not work) one should use thicker crystals and look at the pure electronic transitions of ions at inversion symmetry sites.

One can look for the small splittings expected under higher resolution of levels in a cubic field when a given

complex such as $UCl_6^{=}$ is also found in crystals of lower site symmetry at the complex. This can distinguish one-, two-, and threefold degenerate levels.

Vibronic selection rules may be useful in assigning irreducible representations to excited electronic levels if the superimposed modes of vibration are identified as to symmetry type.

The use of actinide ions at centers of inversion makes the distinction between crystalline Stark levels and vibronic levels easier to make experimentally, especially when the crystalline field splitting is as large as in our U^{4+} case. This is one feature of our spectra which is less ambiguous than in the rare earths, where crystalline field splittings and vibronic separations are comparable in energy and often in intensity as well.

The temperature shift of lines is large and convenient to use as an empirical means of deciding in doubtful cases which vibronic lines are superimposed on the same electronic level. The magnitude and sign of this shift may also be of use in checking the validity of theoretical calculations of energy levels.

Finally, there are also certain features of our results which remain puzzling or in contradiction to the work of others:

(1) The matter of the calculated temperature independent magnetic susceptibility value being about six times too small may be an indication that there are missing crystalline field levels in the region of 600 to 5000 cm^{-1} which are too weak to be observed spectroscopically.

(2) The fact that Conway's results for UF_4 in CaF_2 shows a much smaller crystalline field splitting may either indicate that there is a surprising range of crystalline fields, or that he interpreted many vibronic lines as electronic. The difference between our results and his in size of Stark splitting reported, is evident independent of whether or not there are actually levels in the zero to 5000 cm^{-1} range, as a direct comparison of Conway's and our results in the visible region will show. Since the vibronic lines appear as such a strong feature of our spectra, it seems likely that many of his levels may be vibronic.

(3) Jorgensen[26] has interpreted U^{4+} ion spectra in water solution and has assigned bands of about 400 cm^{-1} half-width to be LSJ states of the $5f^2$ configuration. Again, either the ligand field is much reduced in H_2O complexes compared to $UCl_6^{=}$ or else each of his bands are in general to be associated with a single Stark level (except for occasional overlaps) rather than a J level of the free ion.

APPENDIX

Proof that V_{ev} transforms under electronic coordinate transformations according to the same irreducible representation as the vibrational mode of the complex whose coupling with the electrons is being considered.

[26] C. K. Jorgensen, Kgl. Danske Vidensk. Selskabs Mat. fys. Medd. **29**, No. 7 (1954).

Suppose that, when a transformation of coordinates R is made, functions of the central ion electron coordinates are transformed by P_R and functions of the coordinates of the ligand ion positions are transformed by T_R. Since a symmetry operation of the site symmetry group operating on the complex leaves it in physically indistinguishable positions before and after the transformation, we have that

$$P_R T_R V_{ev} = V_{ev} \tag{A1}$$

or

$$P_R V_{ev} = T_R^{-1} V_{ev}. \tag{A2}$$

The latter equation merely says that the effect on V_{ev} is the same, whether we rotate the central ion electron coordinates by R or the surrounding ligand atom coordinates by R^{-1}.

Suppose an arbitrary displacement of the ith atom of the complex ($i=0, \cdots, N$, with central ion having $i=0$) be represented in terms of the normal coordinates Q of the complex at the site:

$$\begin{aligned} \Delta X_i &= \sum_{\alpha,j} S_{ix,j}^{\alpha} Q_j^{\alpha} \\ \Delta Y_i &= \sum_{\alpha,j} S_{iy,j}^{\alpha} Q_j^{\alpha} \\ \Delta Z_i &= \sum_{\alpha,j} S_{iz,j}^{\alpha} Q_j^{\alpha}, \end{aligned} \tag{A3}$$

where the subscript j refers to the jth degenerate normal coordinate belonging to the α irreducible representation.

$$\begin{aligned} V_{ev} = -\sum_{\alpha}\sum_{j}\sum_{i=1}^{N} Q_j^{\alpha} [& S_{ix,j}^{\alpha}(\partial/\partial x) + S_{iy,j}^{\alpha}(\partial/\partial y) \\ & + S_{iz,j}^{\alpha}(\partial/\partial z)] V_i + \sum_{\alpha}\sum_{j} Q_j^{\alpha} \\ \times [& S_{0x,j}^{\alpha}(\partial/\partial x) + S_{0y,j}^{\alpha}(\partial/\partial y) + S_{0z,j}^{\alpha}(\partial/\partial z)] V_c', \end{aligned} \tag{A4}$$

where V_i represents the potential energy between the ith atom of the complex and the electrons of the unfilled shell of the central ion, and V_c is that part of the crystalline potential due to the ligands of the complex. Both terms involving and not involving the central ion motion are of the form

$$V_{ev} = \sum_{\alpha}\sum_{j} f_j^{\alpha} Q_j^{\alpha}, \tag{A5}$$

where the f_j^{α} are defined implicitly by Eqs. (A4) and (A5).

Now we are given that

$$T_R^{-1} Q_j^{\alpha} = \sum_{p} D^{\alpha}(R)_{pj}^{-1} Q_p^{\alpha} \tag{A6}$$

and we assume that we can write

$$P_R f_j^{\alpha} = \sum_{k} A^{\alpha}(R)_{jk} f_k^{\alpha} + \sum B^{\alpha}(R)_{jk} g_k^{\alpha}, \tag{A7}$$

where we need only assume the g_k^{α} are linearly independent of the f_k^{α}. From Eqs. (A2), (A6), and (A7),

it follows that

$$\sum_j\sum_k A_{jk}f_kQ_j+B_{jk}g_kQ_j=\sum_j\sum_k D_{kj}^{-1}f_jQ_k$$
$$=\sum_j\sum_k D_{jk}^{-1}f_kQ_j. \quad \text{(A8)}$$

Hence

$$B_{jk}=0, \quad \text{(A9)}$$

and

$$A_{jk}=D_{jk}^{-1}=D_{kj}^*. \quad \text{(A10)}$$

Thus the knowledge that V_{ee} is of the form of the scalar product (A5) invariant under operations of the symmetry group together with the knowledge that the Q_j^α form a basis for α irreducible representation is enough to determine that the f_σ^α must form a basis for the complex conjugate representation.

Now for the 32 crystallographic point groups, complex conjugate representations are either the same representation or they are two degenerate one-dimensional representations.

ACKNOWLEDGMENT

This research was supported in part by the Atomic Energy Commission and the Office of Ordnance Research.

THE JOURNAL OF CHEMICAL PHYSICS VOLUME 33, NUMBER 4 OCTOBER, 1960

Transport Processes in Liquid Alloys. II. The Electrical Force on an Ion*

PAUL C. MANGELSDORF, JR.†

Institute for the Study of Metals, University of Chicago, Chicago 37, Illinois

(Received March 2, 1960)

The electrolytic migration velocities of impurity ions in liquid metals suggest the existence of strong net electrical forces on these ions, although other mechanisms are possible. On the basis of a detailed model of a liquid metal the early theory of Skaupy is revived and revised. In dilute solution a total electrical force, proportional to the conductivity increment produced by a solute, is exerted on the solute and on nearby solvent when the electric field is applied. The part of the force on the solute ion may be opposed to the part on the solvent. Implications for the resistivity of liquid alloys are discussed, including a possible effect in very dilute solutions when the solute ions are further apart than one mean free path. The effective number of free electrons in pure liquid mercury is provisionally estimated to be 0.3 per atom.

INTRODUCTION

WHEN an electric field is applied to a liquid metal which is slightly contaminated with some impurity, each impurity atom migrates along the direction of the field $\mathbf{E}$ with a drift velocity $\mathbf{v}_i$ given by

$$\mathbf{v}_i=U_i\mathbf{E}. \quad (1)$$

The specific migration velocity U_i, thus defined, is a scalar quantity which depends on both the impurity and the solvent.

The Effective Charge

Because the values of U_i for impurities in liquid metals are about the same as one finds for ionic mobilities in nonconducting liquids, there is a temptation to ascribe the motion to the simple action of the field on one or more free charges on the impurity atom. This is not the correct explanation. While it is probably true that most solutes in liquid metals are ionized, it is also true that the solvent metal is ionized to a similar extent. In the pure metal the solvent ions give no indication of any such forces due to the field, so that there must be something more than just the ionic charges involved.

Baranowski has shown, however, using irreversible thermodynamics, that the phenomenology of the migration is the same as if simple free charges were indeed responsible,[1] so that one can define an effective charge "z_i" by applying the Nernst-Einstein relation which holds for ions in nonconductors

$$U_i="z_i"eD_i/kT, \quad (2)$$

where D_i is the diffusion coefficient of the ion.

This effective charge also appears in the exponential Boltzmann factor which characterizes the no-flow steady-state distribution of the impurity in an electrical potential gradient.

Somewhat earlier, Klemm had also applied irreversible thermodynamics to this problem, treating

* This work was supported in part by the U. S. Office of Naval Research.

† Present address: The Woods Hole Oceanographic Institution, Woods Hole, Massachusetts.

[1] B. Baranowski, Bull. Acad. Pol. Sci. III, 117 (1955); Roczniki Chemii 30, 841 (1956). This author uses the symbol E^* for the product we denote "z" e.

the particular case of isotope separation.[2] He expressed the forces as functions of the fluxes using a set of friction coefficients—a method which Laity has recently advocated as being especially well suited for diffusive processes in fluids.[3] In terms of Klemm's analysis the effective charge can be written

$$"z_i"=z_i-(r_i\langle z\rangle/\langle r\rangle), \tag{3}$$

where z_i is the actual charge on the ion, r_i is the friction coefficient of this ion for the electrons, and $\langle z\rangle$ and $\langle r\rangle$ are the number averages of these quantities for all the ions. When the solvent, which we denote by B, is pure or nearly so, then $\langle z\rangle$ and $\langle r\rangle$ are the solvent properties z_B and r_B, and

$$"z_i"=z_i-(r_iz_B/r_B). \tag{3a}$$

Thus a solvent ion in a pure liquid metal bears no effective charge and feels no net force.

This same analysis also yields an expression for the electrical conductivity. If one ignores the contribution of ionic fluxes to the conductivity, this expression takes the simple form

$$\sigma=e^2\langle z\rangle/\langle r\rangle. \tag{4}$$

The various theories that have been proposed at one time or another to account for the migrations can be classified according to the form which they give to the effective charge. In some cases the electronic friction effects have ostensibly been disregarded or dispensed with, but this can be done only if the metal is to be a superconductor, which would make the question of a field-induced ionic migration entirely academic. In most of these cases some particular implicit assumption about the electronic friction can usually be discerned.

In an early approximate theory of Wagner, for example, every ion was presumed to be migrating in proportion to its charge and self-mobility, but only the net migration of solute ions relative to the solvent was experimentally observable.[4] This theory gives an effective charge of $z_A-z_BD_B^*/D_A^*$, where D_A^* and D_B^* are the self-diffusion coefficients of the solute and solvent, respectively. By comparison with (3a) we see that this theory requires that the drag which an ion exerts on the electrons be proportional to the drag which it exerts on other ions. Such a requirement is most easily justified in terms of some kind of lattice structure through which all of the interactions of the ion with the rest of the medium are carried out. Since Wagner based his theory on much the same assumptions he had used in treating a similar problem in mixed solid salts, this implication of a lattice structure is hardly surprising.

A recent theory by Angus, Verhoeven, and Hucke made the same assumptions but attempted to relate the ionic mobilities to the ionic masses m_A and m_B, and radii R_A and R_B.[5] This theory gives an effective charge of $z_A-z_Bm_AR_A/m_BR_B$.

The theory of Schwarz, for which good agreement with experiment was claimed, carefully avoided an implicit lattice as being inconsistent with the properties of liquids.[6] Instead, the ions competed directly with one another to move to the cathode. This competition appeared as a hydrostatic pressure gradient acting on the volume of the ion. For this model the effective charge is $z_A-z_Bv_A/v_B$. Since a liquid metal is, in fact, electrically neutral, so that no such hydrostatic pressure gradient is produced by the field, it follows that Schwarz's result implicitly requires the electronic friction to be proportional to the ionic volume.

Skaupy's Theory

Oddly enough, the very earliest theory of these migrations, that of Skaupy, clearly and explicitly identified the force on an ion as arising in two ways—from the direct action of the field on the ionic charge and from the electronic friction.[7] These correspond exactly to the two terms in the effective charge. Skaupy also perceived correctly that both of these quantities should be related to the electrical resistance of the metal, and went on to suggest that ions which increase the resistance of a metal should migrate to the anode, while those that decrease the resistance should move to the cathode. This is just the conclusion we would draw from Eq. (4) if we assumed that z_A, z_B, r_A, and r_B were all constants independent of composition. If we take a logarithmic partial derivative of σ with respect to the mole fraction x_A, keeping those things constant we obtain

$$(1/\sigma)(\partial\sigma/\partial x_A)|_{z_A,z_B,r_A,r_B}=("z_A"-"z_B")/\langle z\rangle \tag{5}$$

which is a clear quantitative expression of Skaupy's ideas.

Unfortunately the experimental results show that this relation is not even qualitatively obeyed, presumably because some of the charges or friction coefficients vary strongly with x_A. Wagner, who recognized that Skaupy's electronic friction was an important effect,[8] and who attempted to adapt Skaupy's theory to migrations in solids,[9] also concluded that too many special assumptions were needed to establish such a quantitative connection between the migration and the resistivity.

[2] A. Klemm, Z. Naturforsch. **9a**, 1031 (1954).
[3] R. W. Laity, J. Chem. Phys. **30**, 682 (1959).
[4] C. Wagner, Z. physik. Chem. **B 15**, 347 (1932).
[5] J. Angus, J. Verhoeven, and E. E. Hucke, *Proceedings of the International Symposium on the Physical Chemistry of Process Metallurgy*, AIME, Pittsburgh, 1959 (to be published).
[6] K. E. Schwarz, *Elektrolytische Wanderung in Flüssigen und Festen Metallen* (Johann Ambrosius Barth, Leipzig, 1940; Edwards Brothers, Ann Arbor, Michigan, 1945), p. 81.
[7] F. Skaupy, Verhandl. deut. physik. Ges. **16**, 156 (1914); **18**, 252 (1916).
[8] C. Wagner, Z. Elektrochem. **39**, 554 (1933).
[9] C. Wagner, unpublished.

In the present paper an attempt will be made to justify Skaupy's ideas and give them a correct quantitative expression resting on a minimum of assumptions. In order to do this it will be necessary to look behind the phenomenology and examine the actual forces which are at work causing the migration of the impurity ions.

OTHER MECHANISMS

Self-Transference

Before we proceed too far in seeking out the driving force or forces, which cause electrolytic migration, we might first ask if the migration necessarily implies the existence of a net average force. We are obliged to admit that it does not, even though a net external force could be applied to simulate the migration or to prevent it.

If the ion were driven to migrate by a constant direct external force, the average drift velocity $\mathbf{v}_i$ would be proportional to the force $\mathbf{f}$ and to the ionic mobility μ_i

$$\mathbf{v}_i=\mu_i\mathbf{f}. \tag{6}$$

If we know only that $\mathbf{v}_i$ exists we can only be sure of the average product $\langle\mu_i\mathbf{f}_i\rangle$. In other words, correlations between a fluctuating force and a fluctuating mobility can result in a net average drift velocity even when there is no net average force. According to Huntington such correlations are of primary importance in solids where atoms in transit from one lattice site to another are especially disturbing to the electron stream.[10]

This correlation is exactly the mechanism which Klemm proposed, and which he called "self-transference," to account for the Haeffner effect isotope separations produced in liquid metals by prolonged electrolysis.[2]

It can be shown, using principles which will be developed in the next paper of this series, that the contribution of this self-transference to the migration of any solute should be about the same as the contribution to the migration of a solvent isotope of the same mass as the solute, provided that the mean square fluctuation of electrical force on the solute is the same as the mean square fluctuation of electrical force on a solvent ion. The corresponding contribution to the effective charge of solute A will be given by

$$\text{“}z\text{”}_{\text{self-transference}}=[(m_A-m_B)/m_B)]\kappa_B, \tag{7}$$

where m_A and m_B are the atomic masses of the solute and solvent, respectively, and κ_B is the coefficient tabulated by Lodding for a number of different isotopic migrations.[11] The reported values of κ range from about 0.03 to 0.3.

The effective charges one estimates from (7) are at least an order of magnitude smaller than those actually observed, which range from -3 to $+4$. Moreover, the only correlation with atomic mass thus far observed is in the opposite direction to that predicted by this equation: Angus, Verhoeven, and Hucke point out that in 38 out of the 39 binary and ternary systems for which they could find migration data, the component with the smallest atomic mass concentrates at the cathode—has a positive effective charge.[5] If, as we believe, the only proper mass effect is that given by (7), then this correlation must mean that there is a contrary effect of atomic number which is even more important. In any case it would appear that self-transference is not a major factor in the nonisotopic migrations.

Thermal Diffusion

It was recently shown that some electrolytic migration should be produced by thermal diffusion due to the isothermal heat flux which occurs when a current is passed.[12] For isotope separations this effect was estimated to be less than the self-transference effect, but not negligible. The effective charge contributed by this effect will be

$$\text{“}z\text{”}_{\text{thermal}}=3.45\times10^{-3}\alpha S, \tag{8}$$

where α is the thermal diffusion factor, and S is the absolute thermoelectric power of the metal in microvolts/degree.

If the values of α reported by Winter and Drickamer[13] for a number of binary alloys are representative—they range from 0.1 to 4.1—we can expect the thermal diffusion contribution to "z" to be as large as 0.3 in some cases, but usually only about one-tenth this amount.

Both this effect and self-transference would seem to be generally small and usually negligible compared to the observed migrations. The principal factor in these migrations, then, must indeed be a net average electrical force of the kind described by equation (3).

THE MODEL

A Dynamical Model

We need to examine in some detail what happens to the ions and to the electrons in a liquid metal when an electric field is applied and a current flows. To do this we begin with a model which is entirely classical so far as the ionic behavior is concerned, but which allows the electrons to be treated as a quantum fluid.

We suppose that we can specify exactly the instantaneous positions and momenta of the N ions in the metal. We use the vector coordinate ξ to denote the point in $6N$-dimensional phase space where the system is to be found at a given instant.

If it were not for the electrons we could assign a

[10] H. B. Huntington, private communication.
[11] A. Lodding, Z. Naturforsch. **12a**, 569 (1957).
[12] P. C. Mangelsdorf, Jr., J. Chem. Phys. **32**, 293 (1960).
[13] F. R. Winter and H. G. Drickamer, J. Phys. Chem. **59**, 1229 (1955).

unique trajectory in phase space, passing through the point ξ, which would exactly describe the dynamical condition of the system for as long into the future, or past, as it is undisturbed by changes in the outside forces. Because the electrons make up a quantum-statistical subsystem with its own thermal fluctuations there is, instead of such a single trajectory, a range of trajectories passing through the point ξ. However, we shall assume that this range of trajectories is extremely narrow; that the speed of thermal fluctuations in the electron system is so great, and the forces associated with these fluctuations so small, that they average out before the slowly moving ions can respond.

Similarly we assume for each ξ a well-defined electron density function, $\rho_e(\xi, \mathbf{R})$, describing the spatial distribution of electron density, which is also obtained by averaging out, over many identical systems, the thermal fluctuations in the electron system. A flux density function, $\mathbf{j}_e(\xi, \mathbf{R})$, describing the average local electron current, may also be defined in this way.

In addition to the phase coordinates ξ there are certain macroscopic variables whose influence on the system we might want to know. The external electric field, $\mathbf{E}^0$, will be one of these, of course. We will also include the bulk average electron flux density, $\mathbf{J}_e$ (related to, but not to be confused with, the local flux density, $\mathbf{j}_e$). From a macroscopic experimental point of view it might seem better here to use the total electrical current density, instead of $\mathbf{J}_e$ which only gives the electronic contribution. There is really no difference, however, because ξ is taken as an independent variable and this fully determines the ionic contribution.

One might ask why any current term appears here at all as an independent variable. The experimental effects to be accounted for are zero-frequency effects. At zero frequency the currents are completely determined by the applied dc fields. The answer to this is simply that we need to consider the current dependence separately from the field dependence in order to understand what's going on; we assume that the actual experimental distinction between the two is accessible by appropriate measurements. In any case $\mathbf{J}_e$, like ξ, is an independent variable only in the sense that we can prepare a system with an arbitrary initial value of $\mathbf{J}_e$. From then on the system and the field determine what $\mathbf{J}_e$ and ξ shall be; only the field $\mathbf{E}^0$ continues to be completely independent. If the field remains constant, $\mathbf{J}_e$ quickly settles down to the appropriate steady-state value $\mathbf{J}_e{}^0$.

We are also obliged to leave open the possibility of breaking down $\mathbf{J}_e$ into a number of components $\mathbf{J}_{ek}$, according to the quantum coordinates of the electrons, such as energy level, spin, or k-vector. To make this kind of breakdown we have to commit ourselves to a one-electron approximation in describing the electron fluid, but this commitment seems to be necessary if we are to cope with the properties associated with the presence of more than one kind of current carrier in the electron system.

Having gone this far, we might as well make use of one great advantage of the single-electron picture—the clear distinction between collective electrons and bound electrons. We suppose that it is possible to identify with each ionic nucleus a certain core of electronic charge made up of electrons in separate, localized, low-lying states, such that this core and the nucleus can be treated together as an inseparable, though polarizable, unit. Any momentum which such a bound electron receives from an external source it immediately shares with its nucleus. Collective electrons, on the other hand, can carry momentum from one place to another in various ways. For example, conduction electrons accumulate momentum and carry it an average distance known as a "mean free path" before dumping it.

The Forces

The direction of the phase space trajectory which the system follows is determined by the rates of change of all the ionic positions and momenta—i.e., all the velocities and forces. The velocities are given by the momenta, which are a part of ξ, and by the masses. The forces are determined, at least fundamentally, by purely classical electromagnetic interactions of the nuclear charges: with one another, with the external field, with the electronic charge distribution given by ρ_e, and with the electronic current distribution given by $\mathbf{j}_e$. The interactions between electronic fluctuations, such as produce van der Waals attractions, do not enter into this force scheme except insofar as they help determine ρ_e and $\mathbf{j}_e$.

Even if we know the net force on every ion at every instant, and know how this force is produced, there is still more information we need before we can identify that part of the force which "causes" the electrolytic migration. Because the liquid in which the ions are moving is dense and is grossly stationary, it prevents the ions from accelerating continuously. But if there is no over-all acceleration of an ion, the net force on the ion must average to zero over long times. In other words, the instantaneous net force contains not only the electrical force we are seeking, but also a frictional resistance which exactly balances it in the long run.

In order to separate the net force into these two opposed components compare the actual force on an ion "i," when the field $\mathbf{E}^0$ is applied and the electron current $\mathbf{J}_e$ is flowing, with the force on the same ion in the same system in the same dynamical condition, ξ, but in electrical equilibrium: both $\mathbf{E}^0$ and $\mathbf{J}_e$ equal to zero. The difference between these two forces we will call the instantaneous electrical force on the ion, $\mathbf{f}_i{}^{es}$. Thus

$$\mathbf{f}_i{}^{es} = \mathbf{f}_i(\xi, \mathbf{E}^0, \mathbf{J}_e) - \mathbf{f}_i(\xi, 0, 0). \tag{9}$$

It may not be immediately obvious why it is that we should identify this difference as the electrical force due

to $\mathbf{E}^0$ and $\mathbf{J}_e$, and thus identify the equilibrium force, $\mathbf{f}_i(\xi, 0, 0)$, with the frictional resistance which would presumably also depend on $\mathbf{E}^0$ and $\mathbf{J}_e$. If the electrical force is to have any meaning, we must suppose that it can be equated in some way to a simple mechanical force applied from outside the system. By applying to the ionic nuclei a set of such external forces just equal to the electrical forces, we should be able to reproduce exactly in the equilibrium system the dynamical effects of the given $\mathbf{E}^0$ and $\mathbf{J}_e$. Alternatively, we should be able to apply a set of equal, but opposite, external forces to the nonequilibrium system and exactly cancel out the effects of $\mathbf{E}^0$ and $\mathbf{J}_e$. What we would like to show, then, is that the set of external forces required to force the equilibrium system to follow the nonequilibrium trajectory is exactly equal and opposite to the set of forces needed to force the nonequilibrium system to follow the equilibrium trajectory, and that both sets are given by relations of the form (9).

This would be easy to show if we could be sure that the electronic distribution functions ρ_e and $\mathbf{j}_e$ were not influenced by the external forces applied to the nuclei but were determined solely by ξ, $\mathbf{E}^0$, and $\mathbf{J}_e$. Then, since the forces within the system depend only on ξ, j_e, and ρ_e, as we noted above, the desired result would follow automatically. Unfortunately, however, when we permitted $\mathbf{J}_e$ to enter as an independent variable we admitted, in effect, that the way in which we bring the system to the phase point ξ, and to the field $\mathbf{E}^0$, has some influence on the electron system. We have allowed the electron system to have a memory.

Although this memory interferes in principle, it probably has little influence in practice. In the first place it is short ($\sim 10^{-14}$ sec) compared to the times of molecular excursions ($\sim 10^{-13}$ sec); in the second place the differences which it would have to detect are differences not in ionic positions, nor even ionic velocities, but in ionic accelerations. Thus the memory effect is probably negligible.

Once we have dismissed the memory effect we have only to make it clear how the equilibrium force $\mathbf{f}_i(\xi, 0, 0)$ comes to be identified with the frictional resistance, as Eq. (9) implies. The reason for this, of course, is that this force is *not* a frictional force when taken along its own trajectory with $\mathbf{E}^0$ and $\mathbf{J}_e$ both absent. Only when it is time-averaged "across the grain" along a nonequilibrium trajectory does it emerge as frictional resistance.

Origin of the "Electrical Force"

Even though we have tried to stick to fundamentals, and have considered only the basic electromagnetic forces acting directly on the ionic nucleus, the number of possible ways in which these forces can crop up is enough to make careful bookkeeping necessary. This accounting problem can be simplified in several ways.

We have already agreed to treat the core of bound electrons as an inseparable part of the ion. In terms of force balances this means that the sum of the forces acting on the core electrons of an ion, and arising from outside the ion, must be exactly equal at all times to the force which the core electrons exert on the ionic nucleus—plus, of course, a very small force needed to keep these electrons accelerating along with the nucleus.

With this assumption the ion can be treated as a polarizable unit with a net charge $Z_i e$ where Z_i is some positive integer. The dividing line between ion core electrons and collective electrons, which is what determines Z_i, is entirely arbitrary in one direction: we can always reclassify core electrons as collective electrons in very narrow energy bands.

We can also make things easier by neglecting all magnetic forces except those due to an applied external magnetic field, and to any internal field which it induces. All the electrically induced internal magnetic forces between particles are essentially relativistic effects compared to the electrostatic forces, and are about as significant as other relativistic corrections might be.

Ignoring the magnetic interactions leads to a third simplification which is purely conceptual. By Eq. (9) we are interested only in the *difference* in the forces that can be attributed to $\mathbf{E}^0$ and $\mathbf{J}_e$. Once the internal magnetic effects are put aside this difference must be explained purely electrostatically. Part of it will be due to the direct action of $\mathbf{E}^0$ on the ionic charge, the rest will come from changes in the electronic charge distribution caused by $\mathbf{E}_0$ and $\mathbf{J}_e$. As is often the case with electrostatic problems involving charge distributions, these changes may be simply treated by superposition. In this case the difference in charge distributions can be obtained by the superposition of the nonequilibrium system on the "negative" of the equilibrium system. The ionic charges will cancel out entirely in this process, though the ionic polarizations, like the smile of the Cheshire cat, will remain, in the form of nebulous dipoles.

How the collective electrons, especially the conduction electrons will show up under this superposition is not so clear. We know that electroneutrality will be strictly observed in a metal in any volume of dimensions greater than the electronic screening radius. This must also be true of the superposition of two systems. Any small negative charge clouds of collective electrons that show up in the superposition must be completely compensated by nearby positive charge clouds—the "ghosts" of missing electrons. The further details of the superposed charge distribution need not concern us here. We can go ahead and enumerate the forces on an ion in a quasi-phenomenological way.

Of the possible electrical forces on an ion, those which are linear in $\mathbf{E}^0$ or $\mathbf{J}_e$ are:

a. The force $Z_i e\mathbf{E}^0$ exerted directly by the applied field on the ionic charge.

b. A possible force $\beta_i e\mathbf{E}^0$ due to the polarization of the

collective electrons by the applied field. A perfectly smooth electron distribution could not polarize, a lumpy one might.

c. A necessary force $\delta_i \mathbf{J}_e$ (or $\sum_k \delta_{ik}\mathbf{J}_{ek}$), due to the current polarization of the collective electrons, particularly the conduction electrons. If the electrons are to exert a force by scattering they have to do it by building up charge clouds during the scattering process. Electrons exert a scattering force on an ion by getting out in front of the ion and "pulling" it in the direction of the force. Holes, if one chooses to think of them, must "push" when they scatter.

d. A necessary force $\alpha_i e\mathbf{E}^0$ due to the polarization of all the other ions by the field. This is necessary only in the sense that such polarization is bound to occur. The average effect of this polarization, and hence the value of α_i, will tend to vanish whenever the environment of the ion is roughly spherically symmetrical.

e. A possible force $\gamma_i \mathbf{J}_e$ (or $\sum_k \gamma_{ik}\mathbf{J}_{ek}$) due to the polarization of all the other ions by the current.

These coefficients β_i, δ_i, α_i, and γ_i are all tensor quantities, specific to the ion in the particular situation. By averaging these quantities over long times, or over many ions of the species "s," they can be reduced to the scalar quantities b_s, d_s, a_s, and c_s which are characteristic of the species.

By this reckoning, the total "electrical force" on the ion comes to

$$\mathbf{f}_i^{es} = (Z_i + \beta_i + \alpha_i)e\mathbf{E}^0 + \sum_k (\delta_{ik} + \gamma_{ik})\mathbf{J}_{ek}. \quad (10)$$

From this we get the average force characteristic of the species

$$\mathbf{F}_s^{es} = (Z_s + b_s + a_s)e\mathbf{E}^0 + \sum_k (d_{sk} + c_{sk})\mathbf{J}_{ek}. \quad (11)$$

The total electrical force on all the ions taken together, from which all the ion-ion interactions have disappeared by mutual cancellation, is

$$\mathbf{F}_{\text{All ions}} = \sum_s n_s (Z_s + b_s)e\mathbf{E}^0 + \sum_{s,k} n_s d_{sk}\mathbf{J}_{ek}. \quad (12)$$

The disappearance of the coefficients a_s and c_s from (12) indicates that the force on the average ion due to the polarization of all the other ions is zero, as was suggested when α_i was introduced. We cannot conclude, however, that a_s and c_{sk} should vanish from (11) when more than one species is present.

The Electron System

At this stage we can usefully define the total electrical force exerted on the collective electron system. This will have a part due to the field directly, and another part due to the ions. Because the metal is electrically neutral, the total charge of the electron system on which the field acts has to be $-\sum Z_i e$, just equal and opposite to the total charge of the ions. The force of the ions on the electron system must also be just the opposite of that which the electrons exert on the ions. Thus, altogether, we have for the electrical force on the electrons

$$\mathbf{F}_{\text{Electrons}}^{es} = -\sum_s (Z_s + b_s)e\mathbf{E}^0 - \sum_{sk} n_s d_{sk}\mathbf{J}_{ek} = -\mathbf{F}_{\text{All ions}}^{es}. \quad (13)$$

With a constant field $\mathbf{E}^0$, after the electron current $\mathbf{J}_e$ has settled down to the appropriate steady state value $\mathbf{J}_e^0$, there is no net acceleration of the electrons. The total electrical force on the collective electrons must vanish

$$\sum_s n_s (Z_s + b_s)e\mathbf{E}^0 + \sum_{s,k} n_s d_{sk}\mathbf{J}_{ek}^0 = 0. \quad (14)$$

Since the system we are discussing is a metal, we make no great error if we take the electronic current to be the same as the total current. The contribution of electrolysis, or of self-transference, to the conduction process will be negligible. We then have

$$-e\mathbf{J}_e^0 \cong \mathbf{I}^0 = \sigma\mathbf{E}^0, \quad (15)$$

where σ is the electrical conductivity. This allows us to rewrite Eq. (14) in the form

$$\sigma = e^2 \sum_s n_s (Z_s + b_s) / \sum_{s,k} n_s d_{sk} p_k^0. \quad (16)$$

The quantity p_k^0 introduced here, is the ratio J_{ek}^0/J_e^0—the fraction of the steady state current carried by electrons of the kth description.

If we compare our derivation with one involving a rather more detailed consideration of the electron statistics, which yields[14]

$$\sigma = e^2 N_{\text{eff}}\tau/m, \quad (17)$$

we see that our $\sum n_s(Z_s + b_s)$ corresponds to N_{eff}, the effective number of free electrons, while our $\sum n_s d_{sk} p_k$ corresponds to m/τ, the "frictional coefficient" for the electron motion. The same comparison can be made with the phenomenological derivation of our own (4), but one must be careful not to identify z_s with $(Z_s + b_s)$, with r_s with $\sum_k d_{sk} p_k$. They are not at all the same, except in pure one-component systems in which the conduction electrons are entirely "free."

The term $\sum_s n_s b_s$ which appears in the numerator of (16) represents the forces on the ions due to the polarization of the collective electrons by the field. It mostly allows for the flexibility of distinction between collective electrons and ion core electrons, but it also has to do with screening. If screening clouds are formed around some or all of the ions by the collective electrons, and if these clouds actually "screen" the ions from the external field to any extent, there will be negative contributions to the coefficients b_s on this account and the effective number of free electrons will

[14] N. F. Mott and H. Jones, *The Theory of the Properties of Metals and Alloys* (Oxford University Press, London, 1936; Dover Publications, New York, 1958), p. 263.

be diminished. The "freedom" of free electrons is evidently a freedom from the responsibility to protect ionic charges from the field.

It is customary in solid-state physics nowadays to use an "effective mass," m^*, and the actual total number of collective electrons, N_0, to describe the electronic behavior, instead of m and N_{eff}. For discussing conductivity this is entirely a matter of taste, since the effective ratio $(N/m)_{eff}$ is the same in either description. Because the deviation from "free electron" behavior which is thus expressed is the same, in either case it follows that the difference between m and m^* arises directly from the polarization effects just discussed. This fundamental physical explanation of m^* is not always apparent in band-theory treatments based on Brillouin zone considerations.

The resemblance of Eqs. (10) through (16) to the phenomenological equations can be made quite pronounced if we define the quantities Z_s and R_s

$$Z_s = \mathrm{Z}_s + b_s + a_s$$

$$R_s = \sum_k (d_{sk} + c_{sk})\, p_k. \tag{18}$$

Then, since $\sum_s n_s a_s = \sum_{s,k} n_s c_{sk} p_k = 0$, we can rewrite (16)

$$\sigma = e^2 \langle Z \rangle / \langle R \rangle. \tag{19}$$

Similarly, in the steady state (11) becomes

$$\mathbf{F}_s^{ss} = Z_s e\mathbf{E}^0 + R_s \mathbf{J}_s^0 = \text{"}Z_s\text{"} e\mathbf{E}^0, \tag{20}$$

where "Z_s" is the quantity defined by

$$\text{"}Z_s\text{"} = Z_s - R_s \langle Z \rangle / \langle R \rangle \tag{21}$$

in complete analogy to (3).

Just as before we are almost in a position to reach Skaupy's conclusion as expressed in (5) and are again prevented by the fact that the coefficients Z_s and R_s may vary with composition. But this time around we are able to state explicitly just why and how this variation occurs.

The Influence of Concentration

A part of the dependence on composition is intrinsic and fundamental. Solvent ions right next to a solute ion will be induced chemically to behave somewhat differently than they would in pure solvent. Similarly, solute ions close together will have different properties than when separated by much solvent. As the number of solute ions increases, so will the number of ions of both kinds whose properties have been affected in this way. The averages Z_s and R_s will change. These effects we would like to investigate and understand.

Another part of the concentration dependence at low concentrations, is also microscopic but is only incidental chemically. When the field is applied to the metal all the solvent ions within a mean free path of a solute ion will be subjected to a general "ricochet" effect like innocent bystanders at a shooting fray. They may pick up odd bits of momentum to which they are not chemically entitled, simply because the momentum content of the local atmosphere of conduction electrons has been perturbed by the impurity ion. Again, as the number of solute ions changes, so will the proportion of solvent ions thus exposed to the influence of the solute.

Finally, a third part of the dependence at very low concentrations is wholly incidental and is really macroscopic. Any inhomogeneity in the conductivity of the metal is going to perturb the current and field over relatively long distances. Since our coefficients were only defined phenomenologically in terms of a single $\mathbf{E}^0$, and a single $\mathbf{J}_s$, characteristic of the entire solution, they are altered by such local perturbations of current and field even when the local conductivity is not affected.

The perturbations of this last sort due to a few widely dispersed solute ions should be approximately the same as one would calculate from continuum theory, replacing each solute ion, and some of its environment, with a little sphere of conductivity σ_s, different from that of the pure solvent σ_0.

The conductivity of such a dilute suspension of spheres may easily be shown to be

$$\sigma = \sigma_0(1+2k/1-2k),\ k = f(\sigma_s - \sigma_0)/(\sigma_s + 2\sigma_0), \tag{22}$$

where f is the volume fraction occupied by the spheres. In such very dilute solutions it doesn't make much difference what volume and conductivity we attribute to the spheres so long as they combine to give the right product k. However, there does seem to be a unique volume prescribed by the physics of the situation, and that is the one given approximately by

$$V_s \cong \tfrac{4}{3}\pi\lambda_0^3, \tag{23}$$

where λ_0 is the mean free path of conduction electrons in pure solvent. The direct effect of the solute ion on the local conductivity cannot extend much farther than λ_0; on the other hand the conductivity does not allow itself to be defined in any smaller volume.

To determine the conductivity σ_s to assign to these spheres would require going into rather more detail than would be appropriate here. But we can perform a conceptual experiment in which we pluck these spheres out of the solvent, collect them in a separate vessel, let them coalesce, and then measure the bulk conductivity of the resulting fluid.

The fluid we obtain in this way is just a more concentrated version of the same solution as before—one in which the average distance from one solute ion to the next is less than a mean free path. This solution may be slightly nonrandom since the method of preparation prevents the solute ions from interacting directly with one another; we will be able to allow for this. The solute concentration in this solution will be about

$$x_s = \bar{V}_B/(V_s + \bar{V}_B - \bar{V}_A), \tag{24}$$

where $\bar{V}_A$ and $\bar{V}_B$ are the partial molecular volumes of solute and solvent, respectively.

This concentration is a kind of dividing line. At much lower concentrations (22) is valid, but at much higher concentrations the solution is effectively homogeneous within any volume V_s or greater, so that the average local field and local current are everywhere the same as the bulk averages. Once this happy condition has been attained, the phenomenological coefficients may be regarded as ionic properties, dependent on the composition only because of "chemical" interactions. This is the concentration range which most interests us here. Further details of the very dilute solutions are discussed in the Appendix.

If the mean free path is sufficiently longer than the range of chemical influence of an impurity, then homogeneity in this sense can exist even in solutions consisting almost entirely of solvent ions lying outside the range of chemical influence of any solute ions. Because of the homogeneity, those unaffected solute ions should have the average coefficients Z_B^0 and R_B^0 characteristic of pure solvent, although the ratio between $\mathbf{J}_e^0$ and $\mathbf{E}^0$—i.e., the bulk conductivity—will not be the same as in pure solvent.

Under these circumstances the principal effect on the solvent caused by injecting a new solute ion will be to cause a certain number of the unaltered solvent ions which fall within the solute ion's range of influence—in its chemical shell, so to speak—to take on different values of Z and R. Corresponding to this simple picture, if we define $n_B(Z, R)$ as the number of solvent ions which have been induced by the average solute ion to assume particular values of Z and R, different from Z_B^0 and R_B^0, we can write for Z_B

$$Z_B = (1/x_B)\left[x_B Z_B^0 + x_A \int (Z - Z_B^0) n_B(Z, R)\, dR dZ\right] \tag{25}$$

and a similar expression for R_B.[15]

While the picture which suggested this expression places the solute molecules far apart, as at infinite dilution, the expressions themselves can be rigged by letting $n_B(R, Z)$ vary with x_A so that changes of Z_B and R_B with x_A at higher concentrations will be correctly depicted. This is an important point because our next step involves an extrapolation to infinite dilution to determine what the situation would be there if the momentum transfer by the field and current were as homogeneous as they are at the higher concentrations.

From Eq. (25) we find that at $x_A = 0$

$$Z_B(x_A = 0) = Z_B^0$$

$$(dZ_B/dx_A)\,|_{x_A=0} = \int (Z - Z_B^0) n_{Bx_A=0}\, dR dZ, \tag{26}$$

with similar results for R_B.

If we take a logarithmic derivative of (19) with respect to x_A, and then set $x_A = 0$ we can obtain

$$(1/\sigma_0)(d\sigma/dx_A)\,|_{x_A=0} = (1/Z_B^0)\left("Z_A" + \int "Z" n_{Bx_A=0}\, dR dZ\right), \tag{27}$$

where $"Z" = Z - R(Z_B^0/R_B^0)$. To arrive at this result we have to use $\langle Z\rangle = Z_B^0$ and $\langle R\rangle = R_B^0$ which hold at $x_A = 0$, and also use (26).

Bringing in (20) we finally obtain

$$F_{\text{Total}}^{zz} = F_A^{zz} + \int F^{zz} n_B(x_A = 0)\, dR dZ = Z_B^0 e \mathbf{E}^0 (1/\sigma)(d\lambda/dx_A)\,|_{x_A=0} \tag{28}$$

which represents our completed version of Skaupy's theory.

To interpret this result in a simple way we must avoid the mean free path effect. The function $n_B(R, Z)$ was intended to describe how many solvent ions were *chemically* affected by each solute ion, and to what extent in terms of Z and R. If we were to use the actual limit of $(1/\sigma)(d\sigma/dx_A)$ in (28) we would have to let $n_B(R, Z)$ include solvent ions affected in the other nonchemical ways we have discussed. Instead the proper value of $(1/\sigma)(d\sigma/dx_A)$ to use is the limit which would be reached if the mean free path effect did not set in at low concentrations. This "ideal" limit of the conductivity increment will be determined by the limiting behavior of only the chemical part of $n(R, Z)$. In most cases, of course, the mean free path effect will be so small that the difference between these two limits can be ignored. Apart from this one restriction on the meaning of $(1/\sigma)(d\sigma/dx_A)$ we can make the following general interpretation of (28)

There is, as Skaupy suggested, a force related to the fractional conductivity increment produced by a solute ion. The total force is directly proportional to this increment, to the field strength, and to the average "free" charge of the average solvent ion. If the solute increases the conductivity, this force is directed toward the cathode, otherwise toward the anode, as Skaupy inferred. Unlike the force conceived by Skaupy, however, this is not just a single force acting on the solute ion itself. Instead it includes whatever electrical forces may be exerted on surrounding solvent because of chemical interactions with the solute.

Contrary to a previous statement of our own,[16]

[15] The careful reader will have detected some sleight-of-hand here. Z and R are averages to begin with, by definition. A range of values such as we integrate over can only be achieved by determining these averages for solute-perturbed solvent ions under various specified conditions. In the interests of simplicity we prefer to avoid discussing these conditions; a given distance from the nearest solute ion would be typical.

[16] P. C. Mangelsdorf, Jr., *Proceedings of the International Symposium on the Physical Chemistry of Process Metallurgy*, AIME, Pittsburgh, 1959 (to be published).

this conclusion does not appear to depend on any restrictive assumptions about the nature of the charge carriers so long as the current mechanism is broadly electronic rather than ionic. On the other hand, the result is only exact in infinitely dilute solutions and cannot be expected to be even qualitatively true in solutions concentrated enough for solute-solute interactions to become important.

CONCLUSIONS

The Nature of the Migration

If we now go back to the phenomenology and ask what effective charge will characterize the migration produced by this kind of compound force we see that there is not a simple answer. Certainly that part of the force which acts directly on the solute ion will contribute to the drift velocity an amount proportional to the simple mobility of that solute. The forces exerted on nearby solvent ions will also affect the motion of the solute, but in a way which will depend on the dynamics of the molecular interactions as well as on the distribution of these forces around the central solute. What is the electrical force on ion B at a given distance from ion A? What velocity of ion A is produced when an ion B at the given distance moves under an applied force of this size? In a later paper we will attempt approximate answers to these questions. Meanwhile, we can draw certain broad conclusions from the known data.

Even in dilute alloys there are no obvious correlations between the migration velocities of solutes and the conductivity increments they produce. For example, Pb, Tl, and Bi all enhance the conductivity of Hg quite distinctly,[17] but Pb and Tl do not migrate at all, while Bi migrates as a negative ion—the wrong direction.[18] In all three cases it would appear that the force acting directly on the solute is directed toward the anode, while the forces on the neighboring solvent ions are directed toward the cathode. Since the nearest neighbors alone outnumber the solute about ten to one, it is not difficult for the solvent forces to predominate in the total, as given by the conductivity increment, whereas the direct solute force will be most important in determining the migration velocity. According to this view, the Bi ion would move even more rapidly toward the anode if it were not continually the center and instigator of a local movement of Hg ions toward the cathode. The failure of Pb and Tl to migrate at all would suggest that these ions barely hold their own amidst the local Hg currents they produce.

The Solute Influence on Conductivity

If this description is correct it means that the conductivity increments produced by solutes may depend primarily on the solute-solvent interactions rather than on the solute alone. This is borne out by the correlation shown in Fig. 1, where the fractional conductivity increments of various solutes in Hg are plotted against the corresponding increments in the fractional excess volume as determined by the volume changes on mixing. The conductivity increments for In and Tl were determined from the data of Schulz and Spiegler,[19] for the others from the data of Larsen.[20] In each case the difference ratio $[(\sigma/\sigma_0)-1]/x_0$ was extrapolated to $x_A=0$ to obtain the desired limit. The excess volumes were obtained from the volume data of Kleppa[21] on these systems, taking the molecular volume of the hypothetical super-cooled pure liquid solute as the reference.

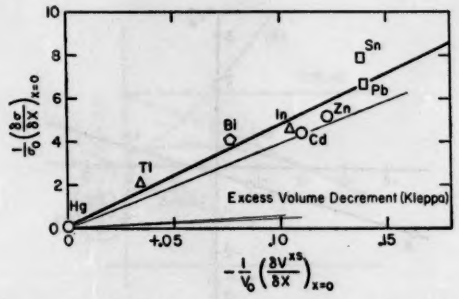

FIG. 1. The correlation between the fractional conductivity increment, $1/\sigma_0(\partial\sigma/\partial x_A)_{x_A=0}$, and the fractional *excess* volume decrement, $-1/v_0(\partial v^{xs}/\partial x_A)_{x_A=0}$, for various solutes in Hg. See text for discussion.

The excess volume, like the other excess thermodynamic properties of solutions, specifically emphasizes the interactions between solute and solvent by discounting the intrinsic properties of the pure components. For this reason the strong correlation found here shows that solute properties are much less important than solute-solvent interactions in determining the conductivity increment.

There is one rather interesting sidelight to this correlation. The slopes of the three faint lines drawn through the origin are the observed ratios of fractional conductivity change to fractional volume change for three simple processes to which pure liquid Hg may be subjected. The two lines of shallow slope represent cooling[22] and compression,[23] respectively. The line of steeper slope which comes much nearer the experimental points corresponds to freezing[24] the Hg. The effect of these solutes in Hg seems to be roughly equivalent to a partial local freezing. Thus the unusual

[17] *International Critical Tables* (1929), Vol. 6, p. 190–191.
[18] K. E. Schwarz, reference 6, p. 57.
[19] L. G. Schulz and P. Spiegler, Trans. AIME **215**, 87 (1959).
[20] A. Larsen, Ann. Physik. **1**, 126 (1900), summarized in work cited in footnote 17.
[21] O. J. Kleppa, unpublished.
[22] *Handbook of Chemistry and Physics* (Chemical Rubber Publishing Company, Cleveland), Sec. IV.
[23] P. W. Bridgman, data reported by A. N. Gerritsen in *Handbuch der Physik*, Vol. XIX (Springer-Verlag, Berlin, 1956), p. 192.
[24] G. Sutra, same source as footnote 23, p. 178.

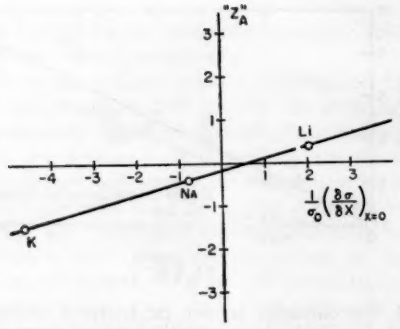

FIG. 2. Relation between the effective charge "z" and the fractional conductivity increment $1/\sigma_0(\partial\sigma/\partial x_A)_{x_A=0}$ for alkali metals in Hg.

general tendency of metallic impurities to *increase* the conductivity of Hg may be simply a reflection of the fact that all these metals have higher melting points than Hg.

The Charge of the Solvent

If there were some way to measure directly the total electrical force on the solute ion and surrounding solvent one could use Eq. (28) and the measured conductivity increment to determine the effective number of free electrons in the pure solvent. This is probably most nearly possible in cases where the solute is firmly bound to surrounding solvent ions so as to be immobilized within a solvation shell. In this situation all of the force exerted on the bound solvent ions will act directly to move the solute, while the forces on the loose solvent ions further away *may* be negligible. The migration velocity would then be directly proportional to the total force and to the mobility of the solute-solvent complex.

This situation is probably most nearly approached in the amalgams of the alkali metals. When these metals are dissolved in mercury a great quantity of heat is generated[25] and there are volume contractions much larger than any shown in Fig. 1.[26] The diffusion coefficients of these metals in Hg are all about the same[27] despite a twenty-fold range in atomic weights, and are less than half the value for the self-diffusion of Hg itself.[28] The stoichiometric compounds $CsHg_{12}$, KHg_{11}, and R_BHg_{11} are reported as stable phases at room temperature.[29]

In Fig. 2 we plot the effective charges of Li, Na, and K in Hg against the fractional conductivity increments they produce in Hg. The effective charges were calculated from the migration velocities reported by Schwarz[18] and the diffusion coefficients at 10° found by von Wogau;[27] the conductivity increments are estimated from the data of Hine.[30] We see that the points do lie on a straight line passing near the origin, but not through it, as the theory suggests. The slope of this line corresponds to 0.3 free electrons per atom in pure Hg.

This estimate is much lower than the value of 2.0 estimated by Schulz[31] from measurements on the optical absorptivity and the reflectance of Hg. We supposed at first that this discrepancy represented a genuine difference between the numbers of electrons contributing to the conductance at optical frequencies and at zero frequency. However, the very recent letter of Kendall and Cusack[32] on the Hall effect in liquid Hg so strongly supports the Schulz value, that we now question the assumptions on which our own estimate is based.

Our weakest link is the assumption that electrical force is exerted only on those Hg ions firmly bound to the solvated alkali ions. If our estimate is wrong it is probably because a major part of the electrical force is acting on unbound Hg ions and is wasted in stirring up the Hg, even in these cases of strong solvation. The fact that our correlation line misses the origin would be some evidence for this.

ACKNOWLEDGMENTS

The author wishes to extend thanks to Professor Morrel H. Cohen for very helpful comments and discussion, and to Professor O. J. Kleppa for his kind permission to use the unpublished volume data shown in Fig. 1.

APPENDIX

The Conductivity of Very Dilute Alloys

We have already noted that the solute concentration x_s within the volumes V_s enclosing all the solute ions is given by (24) as $x_s=\bar{V}_B/(V_s+\bar{V}_B-\bar{V}_A)$. If the apparent size difference $|\bar{V}_B-\bar{V}_A|$ is no more than about one tenth of $\bar{V}_B$, and if V_s is at least ten times greater than $\bar{V}_B$, then we have $x_s=\bar{V}_B/V_s$ to within 1%.

The volume fraction occupied by the spheres is given by

$$f=x_AV_s/[x_A(\bar{V}_A-\bar{V}_B)+\bar{V}_B]. \qquad \text{(A1)}$$

In the dilute range where the continuum model is applicable we have $x_A<x_s$ from which, using our

[25] O. Kubaschewski and J. A. Catterall, *Thermochemical Data of Alloys* (Pergamon Press, London, 1956), pp. 17–22.
[26] R. Suhrmann and E.-O. Winter, Z. Naturforschg. **10a**, 985 (1955).
[27] M. von Wogau, Ann. Physik **23**, 345 (1907); also reported in W. Jost, *Diffusion in Solids, Liquids, Gases* (Academic Press, Inc., New York, 1952), p. 478.
[28] N. H. Nachtrieb and J. Petit, J. Chem. Phys. **24**, 746 (1956).
[29] M. Hansen, *Constitution of Binary Alloys* (McGraw-Hill Book Company, Inc., New York, 1958), 2nd ed., pp. 575–6, 818–20, 834.
[30] T. B. Hine, J. Am. Chem. Soc. **39**, 882 (1917), summarized in work cited in footnote 17.
[31] L. G. Schulz, J. Opt. Soc. Am. **47**, 64 (1957).
[32] P. W. Kendall and N. E. Cusack, Phil. Mag. **5**, 100 (1960).

previous assumptions, we may deduce

$$|(\bar{V}_A-\bar{V}_B)x_A| < |(\bar{V}_A-\bar{V}_B)x_s| \cong |(\bar{V}_A-\bar{V}_B)\bar{V}_B/V_s| \ll \bar{V}_B,$$

so that the approximation $f=x_AV_s/\bar{V}_B=x_A/x_s$ is also good to within 1%.

Now we suppose that at concentrations much greater than x_s the conductivity of the homogeneous solution is given by

$$\sigma=\sigma_0(1+Mx_A+Nx_A^2\cdots) \qquad (A2)$$

This gives a difference ratio of

$$[(\sigma/\sigma_0)-1]/x_A=M+Nx_A\cdots$$

with an apparent value of M at limiting dilution.

We observed that σ_s is the conductivity to be expected of a homogeously conducting solution of composition x_s when the solute ions are not permitted to interact. This interaction can be eliminated from (A2) simply by suppressing the terms in x_A^2 and all higher powers. This gives us $\sigma_s=\sigma_0(1+Mx_s)$ and the relations

$$(\sigma_s-\sigma_0)/(2\sigma_0+\sigma_s)=Mx_s/(3+Mx_s);$$

$$K=Mx_A/(3+Mx_s).$$

From Eq. (22) we now have

$$\frac{(\sigma/\sigma_0)-1}{x_A}=M\left[1-\frac{M(x_s-x_A)}{3+M(x_s-x_A)}\right]. \qquad (A3)$$

The actual limiting slope will be less than the ideal limiting slope, as extrapolated from homogeneously conducting solution, by the fraction $Mx_s/(3+Mx_s)$. If x_s were as large as 0.1, corresponding to a mean free path no greater than an interatomic distance, this deviation could be as large as 15 or 20%. For most liquid metals, however, we would expect λ_0 to be 10 A or larger. Since x_s goes as λ_0^{-3} both x_s and the maximum deviation from the ideal limiting slope should usually be less than 1%. In the cases of the conductivity increments used in Figs. 1 and 2, the errors due to uncertainties in concentration are probably more important than this deviation.

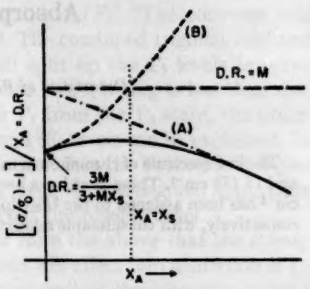

FIG. 3. (Schematic). The effect of solution inhomogeneity at low concentrations on the difference ratio $[(\sigma/\sigma_0)-1]/x_A$. The dotted curve A corresponds to Eq. (30); the dotted curve B corresponds to Eq. (31). The actual behavior will swing from one to the other somewhat as shown by the full curve.

Figure 3 indicates just how this low concentration deviation might be expected to appear in detail if one were to look for it carefully. The estimated "true" curve is drawn so that the deviation from the high concentration asymptote goes, arbitrarily, as e^{-x_A/x_s}.

Absorption Lines of Cr^{3+} in Ruby*

W. Low

Department of Physics, The Hebrew University, Jerusalem, Israel

(Received March 24, 1960)

The line spectrum of chromium in ruby has been investigated. New lines have been found at 14 795, 14 950, and 15 178 cm^{-1}. These lines have been identified as belonging to the $^2F_1$ triplet. Similarly, a line at 21 352 cm^{-1} has been assigned to the $^2F_2$ triplet. It is shown that these levels originate from the ^2G and ^2D levels, respectively, with considerable admixture from the ^2H level.

RECENTLY Sugano and Tanabe[1] made a thorough theoretical study of the absorption bands and lines of Cr^{3+} in ruby. Experimental investigations including Zeeman splittings on the sharp absorption lines have also been reported by Sugano and Tsujikawa.[2] These authors were able to assign the R_1 and R_2 levels at 14 400 cm^{-1} as belonging to the $\bar{E}(^2E)$ and $2\bar{A}(^2E)$ levels.[3])

The $2F_2(t^3)$ level splits into three Kramers doublets, two of which, B_1 and B_2, at about 21 000 cm^{-1}, have been identified and assigned to $2\bar{A}$ and $\bar{E}$ levels, respectively. The third doublet $\bar{E}_b$ should, according to the authors, be on the lower-frequency side, about 150 cm^{-1} from the B_2 line, but has not been observed. Similarly, the three doublets belonging to the $^2F_1$ level have not been found. The authors have predicted the splitting and intensity ratio for these lines. Clearly, the observation and assignment of these lines would be an important check on the theory.

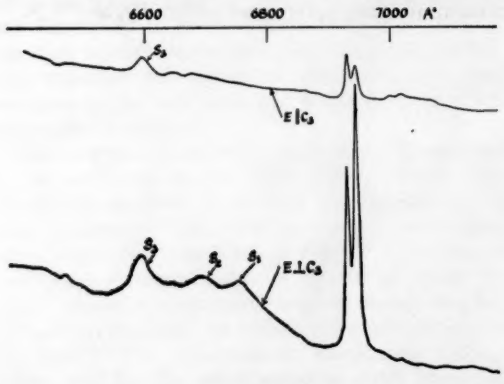

FIG. 1. The absorption spectra of the R and S lines with E parallel or perpendicular to the C_3 axis.

We should like to report here these spectra which have been observed with polarized light ($E \parallel$ or $\perp C_3$). No Zeeman effect studies have been made, because of the relatively large linewidth. Nevertheless, considerations presented below made these assignments fairly certain.

Figure 1 shows the three lines we call S_1, S_2, and S_3 with the electric vector E both perpendicular and parallel to the symmetry axis. The position of these levels for $E \perp C_3$ is given at 14 795, 14 950, and 15 178 cm^{-1}. With $E \parallel C_3$ the S_1 and S_2 levels are very weak and the S_3 level is shifted (by about 20 cm^{-1}) to lower frequency. The intensity ratio $S_3^{\perp}/S_3^{\parallel}$ is about 2:1.

Figure 2 shows the B_1 and B_2 lines under low dispersion and the additional strong line B_3 at 21 352 cm^{-1}. An additional weak and very wide line is observed with $E \parallel C_3$ at 20 760 cm^{-1}. The B_3 line shows an intensity ratio of $B_3^{\parallel}/B_3^{\perp} \sim 1.5:1$. $B_3^{\parallel}$ has approximately the same integrated intensity as $B_1^{\parallel}$.

Sugano and Tanabe suggested that their inability to obtain qualitative agreement of the split components $2\bar{A}$ and $\bar{E}_a$ may in part be caused by the interaction of the $^2F_2$ level with higher excited doublets. This is confirmed by computing the energy levels and eigenvectors for the complete configuration d^3 using the complete matrix (cubic field plus spin-orbit coupling).[4] Such a computation was made for Cr^{3+} in MgO, which is in a cubic field. Since the cubic field and electrostatic parameters are not very different for Al_2O_3, the salient features hold true for this crystal as well. These computations yield the following energy levels and separations:

Assignment			Energy level in cm^{-1}	Separation in cm^{-1}
^2G	^2E	Γ_3	14 845	594
$47\%\,^2H+41\%\,^2G$	$^2F_1$	Γ_6	15 439	398
		Γ_8	15 837	
$49\%\,^2D+32\%\,^2H$	$^2F_2$	Γ_8	21 822	259
		Γ_7	22 081	

The exact positions of the ^2E, ^2F, and $^2F_2$ levels depend on the choice of the electrostatic parameters B, C, α, and λ. No effort is made to give the best fit,

* Supported in part by the Air Research and Development Command, United States Air Force, through its European Office.

[1] S. Sugano and Y. Tanabe, J. Phys. Soc. Japan **13**, 880 (1958).

[2] S. Sugano and I. Tsujikawa, J. Phys. Soc. Japan **13**, 899 (1958). E. O. Deutschbein [Ann. Physik, **14**, 729 (1932)] has also investigated the ruby absorption spectrum, not using polarized light, and found a multiplicity of lines.

[3] The $\bar{E}$ and $2\bar{A}$ levels correspond in the more conventional notation to E_g and E_g levels, respectively. Similarly, the F_1 and F_2 levels are usually written as T_1 and T_2.

[4] G. Schoenfeld, M.Sc. thesis, Jerusalem, 1959.

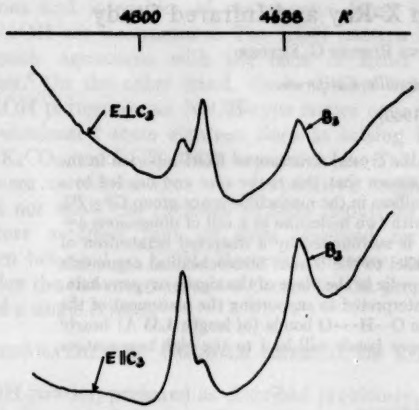

FIG. 2. The absorption spectra of the three B lines with E parallel or perpendicular to the C_3 axis.

because the axial field contribution is not taken into account. The separation of the Γ_6 to Γ_8 levels, however, depends only very slightly on the choice of these parameters B, C, and α.

The following emerges from the above calculations:

(a) There is a considerable admixture from the ^2H level to the ^2G and ^2D levels, even in pure cubic fields.

(b) The F_1 level occurs at about 600 cm^{-1} *higher* frequency than the R lines. This confirms the assignment of the three levels around 15 000 cm^{-1} as the three Kramers doublets belonging to the F_1 level.

(c) Even in the absence of the trigonal field, the Γ_6 and Γ_8 levels are split by about 400 cm^{-1} for the F_1 and 260 cm^{-1} for the F_2 levels. The magnitude of the splittings is consistent with the observed splittings.

(d) The larger line width of the B_i and S_i levels may be explained by the fact that the relative separation of these levels is dependent to the second order on the cubic crystal field parameter through the admixture of the ^2H level.

(e) It is to be noticed that the $\Gamma_6(F_1)$ level is at lower energy than the $\Gamma_8(F_1)$. The converse holds true for the F_2 level. The combined trigonal field and spin-orbit coupling will split up the Γ_8 levels into two doublets. Assuming that this splitting is less than the separation of the Γ_6 or Γ_7 from the Γ_8 state, the order of the observed $^2F_1$ and $^2F_2$ levels can be explained. In particular it is to be noticed that the Γ_7 level is at *higher* frequency than the Γ_8 level. A pure trigonal approximation would have predicted the reverse order.

It is clear from the above that the strong admixture of the ^2H level will effect the calculation of $g_{\|}$ and $g_{\perp}$ for these levels as well as the intensity ratios for the two polarizations. The calculation of these will depend on the detailed evaluation of the complete matrices (cubic field plus trigonal field and spin-orbit coupling) for the d^3 configuration. This is at present being calcaulated by Professor G. Racah.

The polarization shift of about 20 cm^{-1} of the S_3 line may indicate the presence of a level 20 cm^{-1} above the ground state.

The weak and wide line at 20 760 cm^{-1} is possibly caused by an Fe^{3+} impurity which was detected by means of paramagnetic resonance.

The sharp and weak absorption lines on the long wavelength side of the R_1 line are similar to the fluorescence lines observed by Schawlow *et al.*[5] They are presumably caused by Cr—Cr pairs. These lines show also changes in intensity when $E \|$ or $\perp C_3$.

It should also be mentioned that a number of diffuse and sharp lines appear in the ultraviolet in the region between 3350 A→3460 A and around 2900 A, which are presumably transitions to Stark levels of excited doublet states.

ACKNOWLEDGMENT

The author is very grateful to Dr. E. Fischer of the Weizmann Institute of Science for assistance and permission to use the Cary spectrophotometer.

[5] A. L. Schawlow, D. L. Wood, and A. M. Clogston, Phys. Rev. Letters 3, 271 (1959).

Structure of Potassium Hydroxide: An X-Ray and Infrared Study

JAMES A. IBERS, JUNJI KUMAMOTO, AND ROBERT G. SNYDER

Shell Development Company, Emeryville, California

(Received June 15, 1960)

Infrared evidence has been obtained which indicates that the crystal structure of KOH reported in the literature is incorrect. A subsequent x-ray examination has shown that this is the case and has led to a structure compatible with the infrared spectrum. KOH crystallizes in the monoclinic space group $C_s^2-P2_1$ (chosen over $P2_1/m$ on the basis of the infrared evidence), with two molecules in a cell of dimensions $a=3.95$, $b=4.00$, $c=5.73$ A, $\beta=103.6°$. Each potassium atom is surrounded by a distorted octahedron of oxygen atoms. There is an oxygen-oxygen zigzag chain parallel to the b axis. Stereochemical arguments are advanced to suggest that the hydrogen atoms are near to or lie in the plane of the zigzag oxygen chain; infrared data obtained at −180°C for KOH and KOD are interpreted as supporting the placement of the hydrogen atoms in ordered positions along the chain with the O—H···O bonds (of length 3.35 A) nearly or exactly linear. It is argued that breaking of these hydrogen bonds will lead to the high-temperature cubic structure of KOH reported in the literature.

INTRODUCTION

IN the course of an infrared study of crystalline KOH and KOD we observed spectral features which are incompatible with the crystal structure reported in the literature for KOH. A re-examination of the crystal structure of KOH with x-ray diffraction techniques led to a new structure which is compatible with the infrared spectra. In the final stages of the elucidation of the structure, particularly in the location of the hydrogen atoms, the infrared and x-ray results are entirely interdependent. In this first paper we present the x-ray results together with sufficient details of the infrared results to emphasize the interdependence and complementary nature of these two methods of structure analysis. In the following paper[1] we present in greater detail the infrared data and their interpretation.

INFRARED EVIDENCE FOR AN INCORRECT CRYSTAL STRUCTURE OF KOH

At room temperature the O—H stretching mode of a sublimed film of KOH appears as a broad band having maximum absorptivity at 3600 cm^{-1}. As the sample is cooled to −180°C, the band shifts gradually toward lower frequencies and appears as a doublet with maxima at 3556 and 3533 cm^{-1}. Ernst and Schober[2] reported KOH to be isostructural with NaOH[3] with four molecules in a C-centered orthorhombic cell. Infrared selection rules based on the equivalent primitive cell which contains two molecules related by a center of symmetry predict only one O—H stretching band to be active. Indeed, Busing[4] found only one O—H stretching band for NaOH. A possible explanation for the occurrence of two O—H stretching bands for KOH at −180°C is that the symmetry of KOH at −180°C is different from that ascribed to NaOH and KOH at room temperature. The fact that the O—H stretching band changes gradually between room temperature and −180°C suggested that the structure of KOH undergoes no first-order phase transition between these temperatures. On the basis of the infrared evidence, then, we believed that the reported room-temperature structure of KOH was in error and that the structure was different from that of NaOH.

COMPARISON OF X-RAY POWDER PATTERNS OF NaOH, KOH, AND RbOH

Ernst[5] reported that NaOH, KOH, and RbOH are isostructural. In view of the infrared evidence for structural differences between NaOH and KOH it seemed appropriate to obtain x-ray powder patterns of these three hydroxides.

These materials were prepared by reacting vacuum-deposited metal with water and then pumping off the water of hydration. The samples were loaded into soft-glass x-ray capillary tubes (diameter 0.2 to 0.3 mm) without breaking the vacuum, and the tubes were then sealed. The samples are stable over periods of months if the sealing is properly done. No detectable reaction with the glass takes place. All x-ray powder photographs [with the exception of a low-temperature one (see the following)] were taken with CuKα radiation filtered through 0.0005-in. Ni foil on a Philips-type 57.3 mm radius camera.

On the basis of the powder patterns the NaOH structure is different from the KOH or RbOH structure.[6] The NaOH pattern is in good agreement with the data of Ernst[3]; single-crystal data would be required to verify Ernst's structure. On the basis of the

[1] R. G. Snyder, J. Kumamoto, and J. A. Ibers, J. Chem. Phys. **33**, 1171 (1960).
[2] T. Ernst and R. Schober, Nachr. Akad. Wiss. Göttingen, Math.-physik Kl., 49 (1947).
[3] T. Ernst, Nachr. Akad. Wiss. Göttingen, Math.-physik Kl., 76 (1946).
[4] W. R. Busing, J. Chem. Phys. **23**, 933 (1955).
[5] T. Ernst, Angew. Chem. **A60**, 77 (1948).
[6] The structure of LiOH is different from either NaOH or KOH [T. Ernst, Z. phys. Chem. **B20**, 65 (1933)]. No data on the structure of CsOH could be found in the literature. We obtained a powder pattern of CsOH and it is different from that of LiOH, NaOH, or KOH. We plan to obtain single-crystal data in an attempt to elucidate the structure of CsOH.

positions and intensities of the powder lines, KOH and RbOH are isostructural. The KOH pattern is in reasonable agreement with the data of Ernst and Schober.[3] On the other hand, these authors indexed the KOH pattern on an NaOH-type lattice only after they eliminated some eighteen lines as arising from KO_2, K_2CO_3, and $KOH \cdot 2H_2O$ impurities (see Table I). We were convinced that our preparative technique would not allow the presence of such impurities and therefore assumed that all lines observed on the pattern belonged to KOH. However, we were unable to index the pattern, and so we turned to the preparation of a single crystal.

PREPARATION OF A SINGLE CRYSTAL OF KOH

KOH powder, prepared as described previously, was placed in a platinum crucible which was sealed in vacuum within a pyrex tube. The entire system was heated in a furnace to 420°C, the melting point of KOH being 406°C (Khitrov[7]), and was cooled slowly to room temperature. The system was then opened up under a protective layer of high-boiling paraffin oil, and all subsequent operations were carried out with the sample under this medium. The fused KOH was scraped out of the crucible and was examined under polarized light. From the fused mass a small piece, thought to contain a single crystal, was broken off. This piece of KOH was transferred under oil to an oil filled, tapered Pyrex capillary tube. The KOH was pushed down this tube until it jammed against the sides. The tube was then cut off as near to the crystalline mass as possible. Capillary action was sufficient to hold the oil in the tube and hence to protect the crystal from the air, at least for a time long enough for the x-ray photography. The capillary tube containing the crystal was mounted on a glass fiber and placed on an x-ray goniometer.

UNIT CELL AND PROBABLE SPACE GROUP OF KOH

A series of precession photographs was taken of the KOH sample with MoKα radiation.[8] A region of the mass was found that contained only a small number of oriented crystallites. Photographs of this region were readily interpretable in terms of a monoclinic unit cell. The unit cell dimensions enabled a satisfactory indexing of the inner lines of the powder pattern. They were enough in error, however, to preclude an unambiguous assignment of indices to the outer lines. After the crystal structure had been solved, theoretical intensities were compared with the observed ones and the far-out lines (out to d=1.08 A) on the powder pattern were indexed unambiguously. In this manner the entire powder pattern was indexed. A least-squares analysis of the powder pattern led to the final set of unit-cell dimensions

$$a=3.95\pm0.01, \quad b=4.00\pm0.01, \quad c=5.73\pm0.01 \text{ A}, \quad \beta=103.6\pm0.2°.$$

(See Table I for a limited comparison of observed and calculated line positions.) No lines other than those compatible with the above cell dimensions were observed on the powder pattern. This confirms our belief that the KOH was prepared in a manner which would preclude the presence of impurities.[9]

In order to check on a possible phase transition of KOH between room temperature and −180°C, we obtained a low-temperature x-ray powder pattern.[10] Comparison of this pattern (taken at −133°C, the lowest temperature obtainable) with the one taken at 23°C showed only small changes in the positions of the lines. No new lines appeared. The unit cell dimensions at −133°C are (to about 1%)

$$a=3.96, \quad b=3.94, \quad c=5.67 \text{ A}, \quad \beta=105.9°.$$

TABLE I. Data for selected powder lines of KOH.

Index	$\lvert F_{obs} \rvert$ (electrons)	F_{calc}	d_{obs}^{-2} (A^{-2})	d_{calc}^{-2} (A^{-2})
001	6	−6	0.0322	0.0322
100	9	+9	0.0690	0.0680
011	16	−16	0.0947[a]	0.0949
101	19	−18	0.1218[a]	0.1223
11$\bar{1}$	26	+21	0.1414[a]	0.1409
10$\bar{2}$	23	−20	0.1535[a]	0.1529
111	13	−11	0.1855	0.1849
012	16	+14	0.1932[a]	0.1915
11$\bar{2}$	25	+24	0.2163[a]	0.2155
020	39	−32	0.2518[a]	0.2506
20$\bar{1}$	33	+27	0.2619[a]	0.2603
200	18	−19	0.2727	0.2721
021	<2	+4		0.2829
003	13	+12	0.2903[a]	0.2900
10$\bar{3}$	<3	+0		0.2919
112	28	+28	0.3036[a]	0.3036
20$\bar{2}$	9	+10	0.313	0.3129
120	4	−6	0.317	0.3187
21$\bar{1}$	3	−2	0.324	0.3229
12$\bar{1}$	8	−9	0.331	0.3289
210	11	−11	0.3349	0.3347
12$\bar{2}$	14	+15	0.4036	0.4035
211	8	+11	0.4099	0.4110
103	11	+14	0.4244	0.4241
20$\bar{3}$	20	−22	0.4300	0.4299
220	11	+14	0.5228	0.5227

[a] These lines are among those ascribed by Ernst and Schober[3] to impurities in their KOH sample.

[7] V. A. Khitrov, Izvest. Sektora Fiz.-Khim. Anal. Inst. Obshchel Neorg. Khim. Akad. Nauk S.S.S.R. **25**, 236 (1954).

[8] The help of Dr. R. M. Curtis of these laboratories on the precession photography is gratefully acknowledged.

[9] On the basis of the indexed KOH pattern, the RbOH pattern could also be indexed. The unit cell of RbOH is found to have the following dimensions: a=4.13, b=4.23, c=5.96 A, β=106°. These dimensions are reliable to about 1%.

[10] The low-temperature powder photograph was taken in the laboratory of Professor D. H. Templeton at the University of California, Berkeley. We are grateful to him for extending these facilities to us. We thank Dr. I. Olovsson for helping us operate the camera. We are also grateful to Dr. A. Zalkin of the University of California Radiation Laboratory, Livermore, for the loan of the x-ray powder camera.

Some differences in the relative intensities of the lines were observed, and these are probably indicative of changes in the relative positions of potassium and oxygen atoms in the unit cell. However, any such changes are presumably small. The infrared spectrum of KOH changes continuously as the temperature is lowered. By the time −133°C is reached the spectrum is much closer in its appearance to the −180°C spectrum than to the 23°C spectrum. We conclude, therefore, that the structure of KOH is essentially unchanged in going from 23°C to −180°C.

The room-temperature data for KOH lead to a unit cell volume of 87.80 A³ and to a calculated density of 2.12 g/cm³, if two molecules are in the unit cell. Ernst and Schober[2] give an experimental density of 2.05 g/cm³.

The only systematic absences on the precession photographs (*hk*0 and *h*0*l* zones) are 010, 030, and 050. Similarly the only systematic absences on the powder photograph are 010 and 030. The probable space groups are then $C_2^2-P2_1$ or $C_{2h}^2-P2_1/m$. In $P2_1$ the atoms are assigned the positions[11]

$$x, y, z; \bar{x}, \tfrac{1}{2}+y, \bar{z}.$$

In this space group the origin is not fixed along the 2_1 axis, and so we may arbitrarily fix either y for potassium (y_K) or y for oxygen (y_O). We find it convenient to take $y_K=\frac{1}{4}$, because in $P2_1/m$ the positions of the atoms are those given above with $y=\frac{1}{4}$. The x-ray data do not allow us to decide between these two space groups. However, on the basis of the infrared selection rules we conclude that two molecules in $P2_1/m$ would lead to a singlet for the O—H stretching band, while two molecules in $P2_1$ would lead to a doublet, as is observed. Hence, the infrared evidence is consistent with the space group $P2_1$, but not with $P2_1/m$.

SOLUTION OF THE CRYSTAL STRUCTURE

The *hk*0 zone of the precession data is of good quality and exhibits reflections from a single crystal. The *h*0*l* zone exhibits reflections from at least three crystallites which are slightly rotated relative to one another around the *b* (unique) axis. However, owing to differences in their shapes, reflections from the different crystallites can be readily distinguished and the photograph indexed. These two zones were deemed to provide all the data necessary for the solution of such a simple structure problem.

Relative intensities of reflections were estimated visually with an intensity strip. The intensities were reduced to structure amplitudes $|F_{obs}|$ (Table II) from the usual relation

$$I \propto L_p A F_{obs}^2, \qquad (1)$$

where L_p, the Lorentz-polarization correction, was read from the appropriate chart,[12] and where A, the absorption correction, was not applied owing to uncertainties in crystal shape and size. The linear absorption coefficient of KOH for MoKα radiation is only 26 cm^{-1},[13] and so the absorption corrections should not be large.

The x and z parameters of both K and O were readily determined from the two-dimensional Patterson function

$$P(u, w) \propto \sum_{h,l} F^2(h0l)\, \cos 2\pi(hu+lw).$$

The K—K and K—O peaks were well-resolved and with the help of a modified nine-point least-squares technique[14] the following parameters were derived:

$$x_K=0.172, \quad z_K=0.290; \quad x_O=0.32, \quad z_O=0.75.$$

The remaining parameter y_O was determined to be approximately $\frac{1}{4}$ by application of the criteria that cations should be surrounded by anions, anions by cations, and interatomic distances should be close to

TABLE II. Observed and calculated structure amplitudes (in electrons).

Index	F_{obs}	F_{calc}[a]	Index	F_{obs}	F_{calc}[a]	Index	F_{obs}	F_{calc}[a]
100	9	+9	$10\bar{1}$	9	+11	004	16	+15
200	20	−19	$20\bar{1}$	22	+27	$10\bar{4}$	18	+18
300	9	−11	$30\bar{1}$	4	+4	$20\bar{4}$	<3	+1
400	5	−4	$40\bar{1}$	10	−14	$30\bar{4}$	9	−7
			$50\bar{1}$	4	−8	$40\bar{4}$	11	−10
110	36	−35	101	14	−18	$50\bar{4}$	4	−4
210	13	−11	201	20	−20	104	11	−11
310	4	+4	301	9	+5	204	15	−14
410	7	+8	401	15	+15	304	<3	−2
						404	4	+4
020	49	−32	$10\bar{2}$	19	−20			
120	9	−7	$20\bar{2}$	8	+10	005	14	−11
220	14	+14	$30\bar{2}$	13	+11	$10\bar{5}$	8	−6
320	11	+10	$40\bar{2}$	9	+9	$20\bar{5}$	14	+13
420	4	+4	$50\bar{2}$	<3	−1	$30\bar{5}$	14	+14
			102	8	+6	$40\bar{5}$	<3	−3
130	20	+19	202	20	+19	$50\bar{5}$	8	−8
230	9	+9	302	11	+8	105	9	−8
330	3	−3	402	<3	−1	205	<3	+0
430	5	−7				305	10	+10
			003	11	+12			
040	18	+16	$10\bar{3}$	<3	+0	006	6	−4
140	4	+4	$20\bar{3}$	22	−22	$10\bar{6}$	14	−13
240	7	−9	$30\bar{3}$	14	−11	$20\bar{6}$	9	−6
340	9	−8	$40\bar{3}$	9	+9	$30\bar{6}$	<3	+2
440	2	−3	$50\bar{3}$	8	+9	$40\bar{6}$	8	+8
			103	16	+14	106	11	+12
150	7	−11	203	8	+8	206	8	+9
250	3	−6	303	11	−10			
			403	10	−11	007	11	+9
001	3	−6				$10\bar{7}$	9	+8
002	17	−36				$20\bar{7}$	6	−5
						$30\bar{7}$	14	−12
						$40\bar{7}$	<3	−2

[a] Note that the phases are either 0 or 180°, for F was calculated with $y_0=\frac{1}{4}$, in effect for the centrosymmetric space group $P2_1/m$. Hydrogen atom contributions to F_{calc} were neglected.

[11] *International Tables for X-Ray Crystallography* (Kynoch Press, Birmingham, 1953), Vol. I.

[12] J. Waser, Rev. Sci. Instr. **22**, 567 (1951).

[13] *International Tables for the Determination of Crystal Structures* (G. Borntraeger, Berlin, 1935), Vol. II, Sec. XIc.

[14] D. P. Shoemaker, J. Donohue, V. Schomaker, and R. B. Corey, J. Am. Chem. Soc. **72**, 2328 (1950).

those predicted from the usual ionic radii. A comparison of $|F_{obs}|$ with $|F_{calc}|$ from these parameters indicated that the trial structure was satisfactory.

REFINEMENT OF THE STRUCTURE OF KOH

We chose to refine the trial structure by a least-squares procedure, and for this purpose we used the Busing-Levy[15] least-squares program for the IBM 704 computer. We minimized the function

$$\sum_{\text{reflections}} w[\,|F_{obs}|-s|F_{calc}|\,]^2,$$

where s is the scale factor (actually a separate scale factor was used for the $hk0$ and $h0l$ zones), w is the weight of the observed $|F_{obs}|$, and F_{calc} is taken to be

$$F_{calc}(hkl)=\sum_j f_j \exp[-B_j(\lambda^{-1}\sin\theta)^2] \times\exp[2\pi i(hx_j+ky_j+lz_j)]. \quad (2)$$

The scattering factors f used in calculations here are those of Freeman[16] for K and Hoerni and Ibers[17] for O.

The normal equations of the least-square procedure used here have only linear terms in changes in the variables and may be written in the form

$$\sum_i\left[\left(\Delta_i^\circ-\sum_{n=1}^{k}\alpha_n\frac{\partial|F_i^\circ|}{\partial x_n}\right)\cdot\frac{\partial|F_i^\circ|}{\partial x_s}\right]=0 \quad \text{for } s=1,2,\cdots k. \quad (3)$$

Here i refers to the reflection, the superscript $^\circ$ refers to quantities evaluated from the parameters of the previous cycle, $\Delta^\circ=|F_{obs}|-|F_{calc}^\circ|$, $x_n=x_n^\circ+\alpha_n$, where x_n is one of the k variables whose change α_n is being sought. For convenience we have set all w_i equal to unity and have written F_{calc}° for the ith reflection F_i°

The initial refinement was carried out in $P2_1$, with guessed-at B's and with scale factors obtained from a limited number of comparisons of $|F_{obs}|$ with $|F_{calc}|$.[18] It will be recalled that y_O was believed, on the basis of geometrical considerations, to be near to $\frac{1}{4}$. One can readily show that

$$(\partial|F_i|/\partial y_O)_{y_O=1/4}\equiv 0, \quad (4)$$

and here, as is clear from (3), a singularity in the least-squares solution exists. Even if y_O is not $\frac{1}{4}$, but is very near to $\frac{1}{4}$, the least-squares procedure of (3) may not work owing to spurious shifts caused by inherent numerical limitations such as round-off errors. This, in fact, seems to be the case. We attempted at first to refine KOH in $P2_1$, starting with $y_O=0.30$. (This value, rather than 0.25, was chosen in an attempt to circumvent the difficulties mentioned above.) The refinement of y_O and the other parameters proceeded satisfactorily until y_O reached 0.251; on the following cycle the refinement diverged. Such difficulties can be avoided, at least theoretically, if a least-squares procedure is formulated in which higher-order terms are carried. A straightforward extension of the technique used to obtain (3), in which one carries terms sufficient to yield all products $\alpha_r\alpha_s$ in addition to the α_i of (3), leads to the result that

$$\sum_i\left[\left(\Delta_i^\circ-\left\{\sum_{n=1}^{k}\alpha_n\frac{\partial|F_i^\circ|}{\partial x_n}+\tfrac{1}{2}\sum_{p=1}^{k}\sum_{q=1}^{k}\alpha_p\alpha_q\frac{\partial^2|F_i^\circ|}{\partial x_p\partial x_q}\right\}\right)\times\left\{\frac{\partial|F_i^\circ|}{\partial x_s}+\sum_{r=1}^{k}\alpha_r\frac{\partial^2|F_i^\circ|}{\partial x_s\partial x_r}+\tfrac{1}{2}\sum_{u=1}^{k}\sum_{v=1}^{k}\alpha_u\alpha_v\frac{\partial^3|F_i^\circ|}{\partial x_s\partial x_u\partial x_v}\right\}\right]=0 \quad \text{for } s=1,2,\cdots k. \quad (5)$$

Here again we have the k normal equations $s=1, 2, \cdots k$. Note that if we drop all second and higher derivatives, Eq. (5) reduces to Eq. (3). The set of equations (5) suffers from certain disadvantages in a practical sense. First of all, its use obviously entails much computational labor. Second, there is no automatic procedure for finding a solution to the system of nonlinear equations of (5), should a unique solution exist. Instead, one must start out by imposing certain assumptions and approximations. The greatest simplification is achieved by assuming that all cross-terms can be neglected. This is equivalent to the diagonalization procedure which is sometimes imposed on Eq. (3). With this assumption and the fact that at $y_O=\frac{1}{4}$ all first (and remaining third) derivative terms are zero [Eq. (4)], Eq. (5) simplifies to

$$(\delta y_O)^2=2\sum_i\Delta_i^\circ(\partial^2|F_i^\circ|/\partial y_O^2)\Big/\sum_i(\partial^2|F_i^\circ|/\partial y_O^2)^2. \quad (6)$$

Equation (6) was used previously[19] in a slightly differ-

TABLE III. Results of the least-squares refinements of KOH.

Parameter	y_O 0.250	0.255	0.260	0.280	Standard deviation
x_K	0.1746	0.1746	0.1746	0.1749	±0.0016
z_K	0.2885	0.2885	0.2885	0.2885	±0.0014
B_K	0.75	0.75	0.75	0.76	±0.15 A²
x_O	0.3175	0.3175	0.3175	0.3181	±0.0053
z_O	0.7700	0.7700	0.7700	0.7699	±0.0041
B_O	1.24	1.23	1.21	1.07	±0.44 A²
Error of fit	4.070	4.070	4.074	4.116	

[15] We are grateful to W. R. Busing and H. A. Levy not only for supplying us with their 704 program [Busing and Levy, Oak Ridge National Laboratory Rept. 59-4-37 (1959)], but also for helping us solve a machine incompatibility problem which arose in our use of their program.

[16] A. J. Freeman, Acta Cryst. 12, 261 (1959).

[17] J. A. Hoerni and J. A. Ibers, Acta Cryst. 7, 744 (1954).

[18] In this and all subsequent refinements unobserved reflections were assigned zero weight. With the exception of 020 and 002 all observed reflections were given unit weight. The 020 reflection was given zero weight, since interference from another crystallite prevented an accurate measurement of its intensity. The 002 reflection was given zero weight, for its intensity was apparently affected by extinction.

[19] J. A. Ibers, Acta Cryst. 9, 967 (1956).

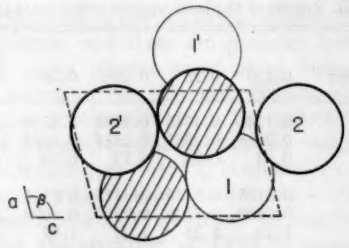

FIG. 1. A projection of the KOH structure onto the ac plane. The cross-hatched circles are K atoms. Heavy circles are at $y=\frac{3}{4}$, light circles at $y=\frac{1}{4}$. The circles are drawn to the scale $r_K=r_O=1.38$ A.

ent form. When Eq. (6) is applied to KOH, we find that $|\delta y_O|=0.007$, i.e., $y_O=0.257$ or 0.243. (Since $|y_K-y_O|$ is the true y variable, these two answers are equivalent.) Such a change in y_O seems quite reasonable. On the other hand this result was obtained by neglecting cross-terms which could be important. The limited accuracy of the data and the labor involved make checks on the cross-terms unappealing. Instead a simpler, though possibly less satisfying, procedure was used for the evaluation of y_O.

A series of refinements were carried out in the formulation of Eq. (3), but with y_O set at the fixed values 0.250, 0.255, 0.260, and 0.280. A given refinement was continued until there was no change in successive cycles. The results are given in Table III. It is clear from these results, first of all, that the other parameters are insensitive to small changes in y_O. If one accepts the error-of-fit function $\{[\sum(w^{\frac{1}{2}}\Delta)^2]/(m-k)\}^{\frac{1}{2}}$ (m=number of observations of nonzero weight, k=the number of variables) as a reasonable criterion by which to judge, then $y_O=0.260$ is possibly worse and $y_O=0.280$ is definitely worse than $y_O=0.250$ as the best solution to the problem. (The error-of-fit function does not approach unity since relative, rather than absolute, weights have been used.) From the results of Table III and from our experience with Eq. (6), it seems reasonable to take y_O as 0.25 with a guessed-at limit of error of 0.01. Then the final parameter values for KOH (space group $P2_1$) are

	K	O
x	0.175±0.002	0.318±0.005
y	1/4	0.25±0.01
z	0.288±0.002	0.770±0.004
B	0.75±0.15 A^2	1.2±0.4 A^2

Values of F_{calc}, based on these parameters for K and O but with the H contributions neglected, are given in Table II. As a final check on the consistency of the powder and precession data we also give in Table I a comparison of F_{calc} with $|F_{obs}|$ values derived from some of the powder line intensities. The intensities of these lines (selected because they were free from overlap) were obtained by numerical integration from microphotometer tracings. These integrated intensities were reduced to the $|F_{obs}|$ values of Table I with the use of the appropriate Lorentz-polarization factor and an absorption correction. The absorption correction was based on an assumed cylindrical KOH sample of radius 0.1 mm and on a calculated linear absorption coefficient of KOH for CuKα radiation of 218 cm^{-1} (International Tables).[13] The absorption correction is a severe one, and any deviation of the sample from the assumed shape or size would markedly affect the results. The agreement exhibited in the table is accordingly very satisfactory.

In order to provide a semiquantitative comparison between observed and calculated structure amplitudes we computed values of the reliability factor, defined as

$$R=\frac{\sum|F_{obs}|-s|F_{calc}|}{\sum|F_{obs}|}. \quad (7)$$

The resultant values are 0.12 for the $hk0$ zone if the 020 reflection is omitted, 0.13 for the $h0l$ zone if unobserved and the 002 reflections are omitted, 0.15 for the $h0l$ zone if only the 002 reflection is omitted, and 0.12 for the powder data. Such values tend to confirm the essential correctness of the proposed structure.

DESCRIPTION OF THE STRUCTURE

The above parameters describe a structure whose main features are depicted in Figs. 1 and 2. In Table IV we give some of the principal interatomic distances. Each K atom is surrounded by a distorted octahedron of O atoms, and these octahedra share edges so that each O atom is surrounded by a distorted octahedron of K atoms. The K and O atoms may be thought of as being in a distorted NaCl arrangement. The O_1—O_2 distances of 3.35 A form a zigzag chain parallel to the b axis in the structure. All other O—O distances are equal to, or are greater than, the unit cell repeat distances (3.95 A).

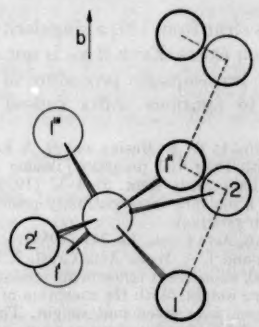

FIG. 2. A view of the oxygen octahedron surrounding the K atom and of the O—O zigzag chain parallel to the b axis. The numbering system is the same as in Fig. 1.

POSITIONS OF THE HYDROGEN ATOMS

It is reasonable to ascribe the short $O_1—O_2$ distance to $O_1—H—O_2$ bonds. The positions of the hydrogen atoms along the zigzag chain cannot be determined from the x-ray data. However, on structural chemical grounds only certain positions for the hydrogen atoms seem likely. In this section we first indicate these likely positions and then show that the infrared evidence favors one of them in particular.

Likely Hydrogen Atom Positions

Owing to the appreciable K—H repulsion which would result, the distribution of K atoms should preclude any large deviations of the H atoms from the plane of the zigzag chain of O atoms. Moreover, the O—O distance of 3.35 A precludes the possibility of a symmetric O—H—O bond, because such bonds, if they occur at all, occur when the O—O distance is quite short (perhaps 2.5 A). With these facts in mind we show in Fig. 3 three likely arrangements of H atoms. In Model (a) we depict a linear O—H···O bond; in Model (b) we make this bond nonlinear; in Model (c) we depict a random arrangement in which the H atoms are allowed to take up with equal probability either of two positions on either side of the O—O bonds. Variations of Models (b) and (c) in which we allow the H atoms to assume positions slightly out of the plane also seem reasonable.

The relation between adjacent chains of O atoms also needs to be considered. The polarities of these adjacent chains might be (a) the same, (b) different, but arranged in an ordered way, or (c) randomized. (The actual arrangement of polarities might be temperature dependent.) The x-ray data, being in essence unaffected by the H atom positions, lend no support to one of these arrangements over the other two. The relative isolation of the chains might favor the randomized arrangement.

It is interesting to note that these likely hydrogen atom positions, derived on the basis of structural chemical reasoning and illustrated in Fig. 3, are consistent with the space group $P2_1$, rather than with $P2_1/m$, in agreement with the infrared evidence. Should the polarities of adjacent chains be randomized and should $y_O \equiv 1/4$, then the effective x-ray space group would be $P2_1/m$, but this subtle distinction is not important for our purposes.

TABLE IV. Principal interatomic distances (in A).

K-O		
K-O		
2′	2.69	±0.03
1′	2.76	
1‴	2.76	
1	2.90	
1″	2.90	
2	3.15	
O-O<3.95 A		
O-O		
1 2	3.35	±0.02[a]
2 1″	3.35	

[a] This limit of error is smaller than that on the K-O distances, for the latter are functions of y_O. The $O_1—O_2—O_{1''}$ angle is 73.4±0.9°.

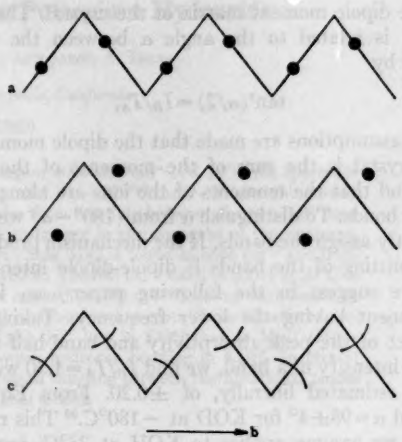

FIG. 3. A sketch of some possible hydrogen atom positions along the zigzag oxygen chain.

Infrared Evidence for a Particular Arrangement

The infrared evidence is not consistent with a disordered arrangement [Model (c), Fig. 3] of hydrogen atoms. If the structure were disordered, then a doubling of the O—H stretching band could be explained only if the environments of the two hydroxyls were different enough to give the stretching frequencies slightly different values. But if this is the case, the spectrum of dilute KOH in KOD should still show both bands, unless the residual OH^- ions had the same environment. In this unlikely case, the position of the residual band should be the same as one of the bands of KOH itself, and for solid solutions containing a larger concentration of KOH both bands should appear separated by the same amount as for pure KOH. Neither of these results is found in an isotopic dilution experiment (described in the following paper[1]) and so a disordered arrangement of hydrogen atoms in KOH is not possible.

Since the hydrogen positions are ordered and there are only two OH^- ions per unit cell, it is possible to estimate the angle between the O—H bonds in the unit cell from the ratio of the intensities of the two components of the stretching band. The two O—H stretching vibrations ω_A and ω_B generate dipole moments which are, respectively, along the b axis of the crystal (OH^- ions vibrating in-phase) and perpendicular to the b axis (OH^- ions vibrating out-of-phase).[1] The intensities I_A and I_B of these vibrations are proportional to μ_A^2 and μ_B^2, where μ_A and μ_B are elements

of the dipole moment matrix of the crystal. The ratio I_B/I_A is related to the angle α between the O—H bonds by

$$\tan^2(\alpha/2) = I_B/I_A, \qquad (8)$$

if the assumptions are made that the dipole moment of the crystal is the sum of the moments of the OH^- ions and that the moments of the ions are along their O—H bonds. To distinguish α from $(180°-\alpha)$ we must correctly assign the bands. If the mechanism producing the splitting of the bands is dipole-dipole interaction (as we suggest in the following paper[1]) ω_A is the component having the lower frequency. Taking the product of the peak absorptivity and band half-width as the intensity of a band, we find $I_B/I_A = 1.30$ with an error, estimated liberally, of ± 0.20. From Eq. (8) we find $\alpha = 98 \pm 4°$ for KOD at $-180°$C.[20] This result, which we assume applies to KOH at 23°C, together with the O—O—O angle of 73.4° (Table IV) suggests that Model (b) (Fig. 3) with an angle of $4 \pm 2°$ between the O—H and O—O bonds is a satisfactory one for the hydrogen atoms in KOH. In view of the assumptions made in this calculation this result is uncertain, but we may conclude that the hydrogen atoms either lie on or very near the O—O axes.

RELATION OF THE ROOM-TEMPERATURE TO THE HIGH-TEMPERATURE KOH STRUCTURE

We have shown that in the room-temperature KOH structure there are linear or nearly linear O_1—H$\cdots O_2$ bonds. It is reasonable to ascribe the distortion of the KOH structure from an NaCl arrangement of the heavy atoms to the formation of hydrogen bonds. If these hydrogen bonds are broken and the directions of the OH dipoles are assumed to be random, then an NaCl arrangement of K and O atoms with a lattice constant of about $b\sqrt{2} = 5.7$ A would be expected. This is precisely the reported high-temperature form of KOH (Teichert and Klemm)[21]: NaCl-type lattice with $a = 5.78$ A (at 300°C). The heat of transition between room-temperature and high-temperature KOH is 1.5 kcal/mole.[22] This value is a reasonable one, for the hydrogen bond in KOH is much weaker than the hydrogen bond in ice, and it takes about 5 to 6 kcal/mole to break the bond in ice. All in all, the relation of the room-temperature to the high-temperature (>248°C) structure of KOH is a very reasonable one.

SUMMARY

The principal steps in the elucidation of the structure of KOH were:

1. Infrared evidence was obtained which indicated that if KOH had two molecules in a primitive unit cell, then these could not, as is the case for NaOH, be related by a center of symmetry. In short, the structures of KOH and NaOH could not be the same.

2. An x-ray examination of KOH led to a new and different structure, compatible with the infrared data, in which there are two molecules in the noncentrosymmetric space group $P2_1$ (chosen in favor of $P2_1/m$ on the basis of the infrared data).

3. The x-ray data provide no information on the hydrogen atom positions, but from a detailed interpretation of the infrared spectra, now possible on the basis of the new crystal structure, the hydrogen atoms in KOH were shown to lie on or very near to the O—O axes.

Thus, KOH provides an illustration of the complementary nature of infrared and x-ray methods of structure analysis.

[20] Scattering of infrared radiation prevented intensity measurements in the O—H stretching region, but did not interfere with such measurements in the O—D stretching region. These measurements were therefore made on KOD rather than on KOH spectra.

[21] W. Teichert and W. Klemm, Z. anorg. u. allgem. Chem. **243**, 138 (1939).

[22] G. von Hevesy, Z. phys. Chem. **73**, 667 (1910).

Vibrational Spectrum of Crystalline Potassium Hydroxide

ROBERT G. SNYDER, JUNJI KUMAMOTO, AND JAMES A. IBERS

Shell Development Company, Emeryville, California

(Received June 15, 1960)

The infrared spectrum of KOH has been obtained in the region 4000–300 cm^{-1}. At 23°C the spectrum shows two broad bands, one at 3600 cm^{-1} and the other at 643 cm^{-1}. At −180°C the O—H stretching band near 3600 cm^{-1} appears as a doublet. Splitting is shown to arise from coupling between the two OH^- ions in the unit cell. Evidence is presented that indicates a small difference in the strengths of the hydrogen bonds in KOH and KOD. The first overtone of the O—H stretching band is found at 6868 cm^{-1} and from this a value of $\omega_e x_e$ of 110±11 cm^{-1} is derived for KOH at −180°C. The 643 cm^{-1} band of KOH at 23°C is identified as a librational fundamental. At −180°C this band appears at 709 cm^{-1} together with bands at 840 and 671 cm^{-1}; these latter two bands are also identified as librational modes. These librational frequencies lead to a considerably higher barrier to rotation of the OH^- ions in KOH than in $Mg(OH)_2$ or $Ca(OH)_2$. This higher barrier is probably the result of the weak hydrogen bonding in KOH. Spectra of KOH—KOD mixtures are interpreted in terms of relatively small coupling between the librational modes of the hydroxyl ions and between the librational and translational modes.

INTRODUCTION

RELATIVELY detailed studies of the vibrational spectra of crystalline alkali metal and alkaline earth hydroxides have been published only on LiOH,[1,2] NaOH,[3] $Mg(OH)_2$,[4,5] and $Ca(OH)_2$.[5,6] The structures of all of these hydroxides are similar in that there are two nonhydrogen bonded hydroxyls, centrosymmetrically related, in a unit cell. The structure of KOH, presented in the preceding paper,[7] though still relatively simple, is fundamentally quite different from the structures of the above hydroxides. In KOH the hydroxyls are noncentrosymmetrically related and they participate in weak hydrogen bonding. We have examined the infrared spectra of KOH and KOD in detail and we report here on the O–H stretching and OH^- ion librational fundamentals. In contrast to the studies referred to above the librational fundamentals in KOH were observed directly.

To our knowledge there exists in the literature no detailed study of the vibrational spectrum of crystalline KOH. Busing[8] obtained the infrared spectrum of KOH, but was handicapped in his interpretation by not knowing the correct crystal structure. Very recently the O–H stretching band was observed in the Raman spectrum of KOH by Krishnamurti.[9] No other bands were observed by him. Also, recently, the near infrared spectrum of crystalline KOH has been reported by Buchanan.[10] However, as we shall show herein, the method of sample preparation used by Buchanan in his infrared study leads to very impure KOH.

EXPERIMENTAL PROCEDURES FOR OBTAINING INFRARED SPECTRA

Thin films of KOH, suitable for obtaining infrared transmission spectra, were prepared directly in a low-temperature infrared cell of the type described by Wagner and Hornig[11] by subliming a film of potassium from a side arm onto a CsBr crystal window and subsequently exposing the sublimed metal to water vapor at a low pressure (<0.1 mm). After the reaction was completed, the film consisted of a hydrate (probably $KOH \cdot H_2O$) which was converted to anhydrous KOH by heating it to 60–100°C while pumping on the cell. The spectrum of the hydrate is quite different from that of anhydrous hydroxide and will be reported on at a later time. Films prepared in the manner described had the troublesome property of scattering radiation at frequencies greater than 2000 cm^{-1}, though there was sufficient transmission for spectra to be recorded at moderate resolution (1–3 cm^{-1}). The disadvantages of scattering films were more than compensated for by the protection afforded the samples from water vapor and CO_2, by the ease of heating and cooling of samples, and by the convenience in exposing the samples to vapors at known pressures. KOH–KOD mixtures were prepared by exposing KOH films to D_2O vapor, followed by conversion of the resultant hydrate to the anhydrous hydroxide.

All the spectra shown in the figures, save Fig. 2, were taken from samples prepared in the above manner. To obtain nonscattering films, several samples were prepared as a "fused sandwich"[12] by melting anhydrous KOH between potassium bromide disks in an inert atmosphere and allowing the materials to cool. The

[1] L. H. Jones, J. Chem. Phys. **22**, 217 (1954).
[2] K. A. Wickersheim, J. Chem. Phys. **31**, 863 (1959).
[3] W. R. Busing, J. Chem. Phys. **23**, 933 (1955).
[4] R. T. Mara and G. B. B. M. Sutherland, J. Opt. Soc. Am. **43**, 1100 (1953).
[5] R. M. Hexter, J. Opt. Soc. Am. **48**, 770 (1958).
[6] W. R. Busing and H. W. Morgan, J. Chem. Phys. **28**, 998 (1958).
[7] J. A. Ibers, J. Kumamoto, and R. G. Snyder, J. Chem. Phys. **33**, 1164 (1960).
[8] W. R. Busing (private communication, 1959).
[9] D. Krishnamurti, Proc. Indian Acad. Sci. **50**, 223 (1959).
[10] R. A. Buchanan, J. Chem. Phys. **31**, 870 (1959).
[11] E. L. Wagner and D. F. Hornig, J. Chem. Phys. **18**, 296 (1950).
[12] K. A. Wickersheim, J. Chem. Phys. **29**, 1197 (1958).

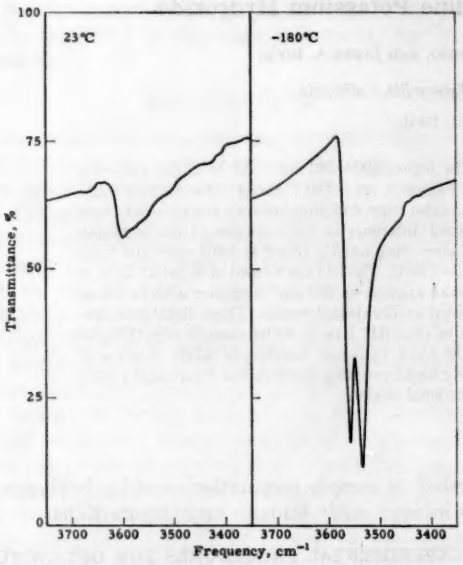

FIG. 1. O—H stretching region of the infrared spectrum of KOH at 23° and −180°C.

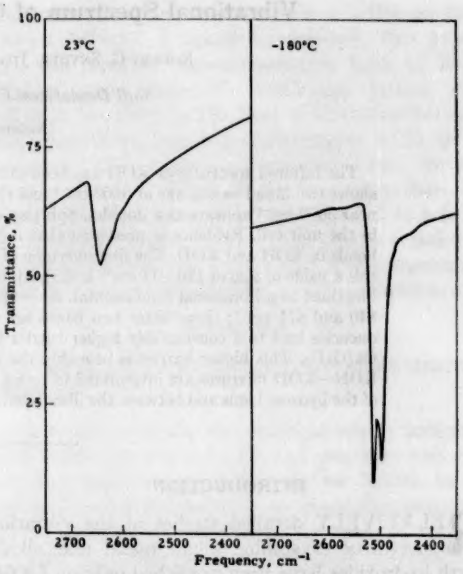

FIG. 3. O—D stretching region of the infrared spectrum of KOD at 23° and −180°C.

resulting sandwich did not scatter much infrared radiation. The spectrum of the KOH sandwich at room temperature showed, in addition to the bands present in the spectrum of the sublimed film, several extra bands in the region 1100–800 cm^{-1} whose intensities were comparable with the KOH bands. The possibility that the extra bands belong to the lowest hydrate of KOH was eliminated by comparison with the hydrate spectrum. Although the O–H stretching regions of the spectra of the sandwich and of the sublimed film were similar at room temperature, at liquid nitrogen temperature there were differences. We conclude that during the heating necessary to form the sandwich considerable chemical reaction takes place. Spectra obtained from our sandwich at room temperature agree with the spectra obtained by Buchanan[10] from a similarly prepared sandwich. Hence Buchanan did not obtain spectra from a pure KOH sample. Because of this contamination problem we abandoned the fused-sandwich method.

Figures 1–4 were drawn from spectra recorded with a Beckman IR-7 spectrophotometer and Figs. 5–7 were drawn from spectra recorded with a Beckman IR-4 spectrophotometer which was equipped with cesium bromide optics. Both instruments were provided with drying columns so that their optical paths could be flushed free of water vapor and carbon dioxide.

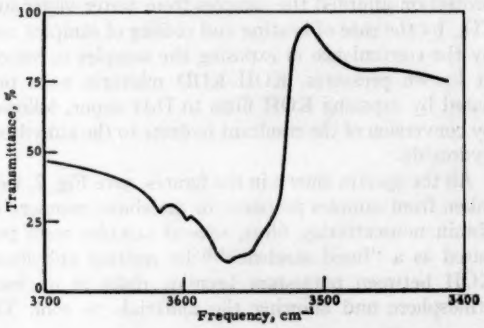

FIG. 2. O—H stretching region of the infrared spectrum of KOH at −180°C. Sample prepared by the "fused-sandwich" method.

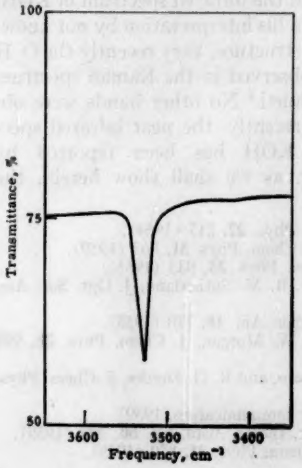

FIG. 4. O—H stretching band for dilute KOH in KOD at −180° C.

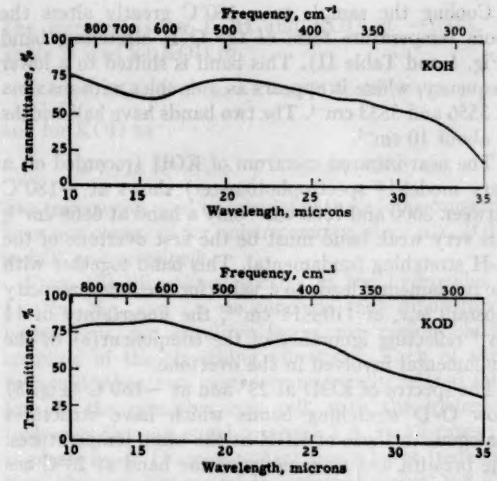

FIG. 5. Infrared spectra of KOH and KOD at 23°C in the region 900–300 cm^{-1}.

STRUCTURE AND VIBRATIONAL SELECTION RULES

As shown in the preceding paper[7] crystalline KOH belongs to the monoclinic system, has two molecules per unit cell, and is in space group $C_2^2-P2_1$. This structure, which is unchanged between 23° and −180°C, has oxygen-oxygen zigzag chains parallel to the twofold axis of the crystal, and one chain traverses each unit cell. Hydrogen atoms are located on or very near the O—O bonds.

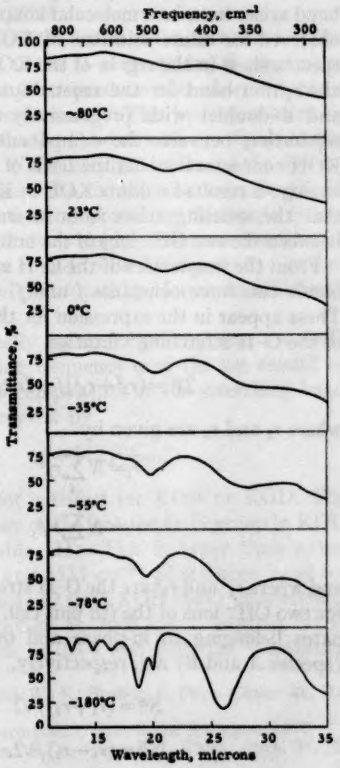

FIG. 6. Temperature dependence of the infrared spectra (900–300 cm^{-1}) of KOD.

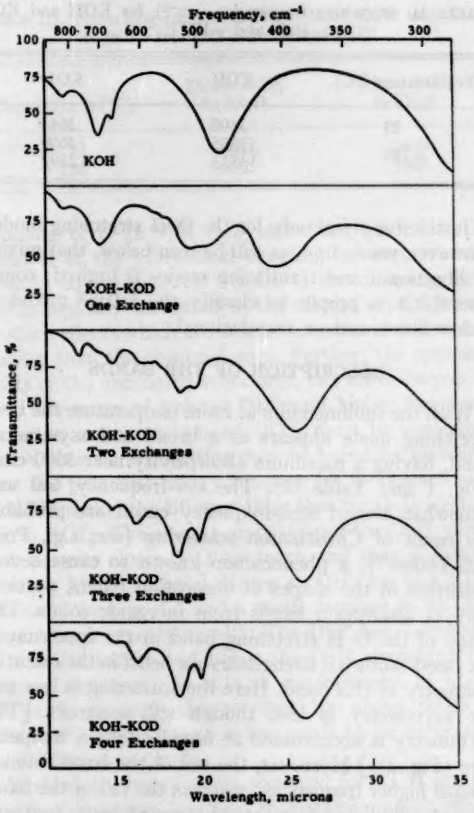

FIG. 7. Infrared spectra in the region 900–300 cm^{-1} of KOH—KOD mixtures at −180°C.

Of the 15 translationally invariant vibrations of the crystal two are O–H stretching modes, four are librational modes of the OH^- ions, and nine are translations of the K^+ and OH^- ions with respect to one another. The classification of these modes into their symmetry species is given in Table I. The low symmetry of the unit cell allows all 15 modes to be active in both the infrared and Raman spectra. The classification of modes as O–H stretching, librational, and translational

TABLE I. Vibrational selection rules for crystalline KOH.

Species[a]	O-H Stretching	Libration	Translation
$A(b)$	1	2	5
$B(ac)$	1	2	4

[a] a, b, and c refer to the crystal axes. b is the unique axis of $C_2^2-P2_1$.

TABLE II. Stretching frequencies (cm^{-1}) for KOH and KOD at 23 and −180°C.

Temperature (°C)	KOH	KOD
23	3600	2643
−180	3556	2609
	3533	2592

is justified *a priori* only for the O–H stretching modes. However, we do find, as will be seen below, that mixing of librational and translation modes is limited; consequently it is proper to classify the lattice modes as either librational or translational.

DESCRIPTION OF THE BANDS

With the sublimed film at room temperature the O–H stretching mode appears as a broad and asymmetric band, having a maximum absorptivity near 3600 cm^{-1} (Fig. 1 and Table II). The low-frequency tail and somewhat abrupt high-frequency cutoff are probably the result of Christiansen scattering (see, e.g., Price and Tetlow[13]), a phenomenon known to cause severe distortion of the shapes of absorption bands, particularly of absorption bands from inorganic solids. The shape of the O–H stretching band in the spectrum of the fused-sandwich strengthens our belief in the essential symmetry of this band. Here the scattering is less and the asymmetry is less, though still apparent. [The asymmetry is accentuated at liquid nitrogen temperature (Fig. 2).] Moreover, the tail of the band extends toward higher frequencies, whereas the tail of the band from the sublimed film extends toward lower frequencies. This behavior is consistent with the fact that the refractive index of KOH is greater than that of a vacuum (KOH in a sublimed film), but less than that of KBr (KOH in a fused sandwich).

The frequency of the band indicates that the oxygen-oxygen distance is greater than about 3.0 A.[14] This is consistent with the x-ray results which give a closest oxygen-oxygen distance of 3.35 A. Further, the frequency of the band is in keeping with the general trend of decreasing frequency with increasing cation size. For comparison, the corresponding frequency for LiOH is 3678 cm^{-1},[1] and for NaOH, 3637 cm^{-1}.[3] We find the half-width (i.e., width at half-height) of the O–H stretching band of LiOH at 23°C to be about 5 cm^{-1} and that of NaOH to be about 8 cm^{-1}. These values are less than the half-width of KOH at 23°C by a factor of at least five.

The frequency (3600 cm^{-1}) of the O–H stretching band of KOH at 23°C is near the Raman line at 3597 cm^{-1} found by Krishnamurti[9] for this substance at room temperature.

Cooling the sample to −180°C greatly alters the room temperature form of the O–H stretching band (Fig. 1 and Table II). This band is shifted to a lower frequency, where it appears as a doublet with maxima at 3556 and 3533 cm^{-1}. The two bands have half-widths of about 10 cm^{-1}.

The near-infrared spectrum of KOH (recorded on a Cary model-14 spectrophotometer) shows at −180°C between 3600 and 7300 cm^{-1} only a band at 6868 cm^{-1}; this very weak band must be the first overtone of the O–H stretching fundamental. This band together with the fundamental leads to a value for the anharmonicity constant $\omega_e x_e$ of 110±11 cm^{-1}, the uncertainty of 11 cm^{-1} reflecting ignorance of the component(s) of the fundamental involved in the overtone.

The spectra of KOD at 23° and at −180°C (Fig. 3) show O–D stretching bands which have structures analogous to those of KOH at the same temperatures. The breadth and asymmetry of the band at 23°C are both somewhat less than those of the same band of KOH. As in KOH, cooling the sample causes narrowing, displacement to a lower frequency, and doubling of the absorption band. O–D stretching frequencies for KOD are given in Table II.

POTENTIAL FUNCTION OF THE O—H STRETCHING VIBRATION

To determine if the splitting of the O–H stretching band arises from intermolecular coupling, this band was observed for dilute solutions of KOH in KOD. These spectra show in the region of the KOH doublet a single absorption band for the most dilute sample (Fig. 4) and a doublet with progressively greater frequency separation between the components with increasing KOH concentration. On the basis of these results (and analogous results for dilute KOD in KOH), we conclude that the splitting arises from intermolecular coupling between the two OH^- ions of the unit cell.

From the frequencies of the O–H and O–D stretching bands two force constants f and f' can be calculated. These appear in the expression for the potential energy of the O–H stretching vibration

$$2V=(r_1^2+r_2^2)f+2r_1r_2f',$$

where r_1 and r_2 are given by

$$r_1=N\sum_i r_1^i$$

$$r_2=N\sum_i r_2^i,$$

and where r_1^i and r_2^i are the O–H stretching coordinates for two OH^- ions of the ith unit cell. Symmetry coordinates belonging to in-phase and out-of-phase modes (species A and B) are, respectively,

$$S^A=(r_1+r_2)/\sqrt{2}$$

$$S^B=(r_1-r_2)/\sqrt{2}.$$

[13] W. C. Price and K. S. Tetlow, J. Chem. Phys. **16**, 1157 (1948).
[14] G. C. Pimentel and C. H. Sederholm, J. Chem. Phys. **24**, 639 (1956).

The frequencies for KOH and KOD at −180°C in Table II lead for KOH to

$$f=7.016\ 10^5\ \text{d/cm}\quad f'=\pm 0.046\ 10^5\ \text{d/cm}.$$

and for KOD to

$$f=7.126\ 10^5\ \text{d/cm}\quad f'=\pm 0.046\ 10^5\ \text{d/cm}.$$

The frequencies used to calculated these force constants were not corrected for anharmonicity, since $\omega_e x_e$ (OD) is still undetermined.

From the vibrational spectra of the hydroxides of Li, Na, Mg, and Ca we conclude that dipole-dipole interactions, not repulsive forces, are responsible for coupling of the stretching vibrations. Each of these hydroxides has two centrosymmetrically related OH^- ions in the primitive unit cell, with the hydrogen-hydrogen distance equal to about 2 A. In all cases the in-phase mode (Raman active) has a lower frequency than the out-of-phase mode (infrared active).[15,16] The lower frequency of the in-phase mode is compatible with a dipole-dipole interaction only, since hydrogen-hydrogen repulsion would lead to a higher frequency for this mode than for the out-of-phase mode. Thus because the OH^- ions are even less favorably disposed for repulsive interactions in KOH than they are in these other hydroxides, it is safe to assume that dipole-dipole interactions are responsible for the splitting of the O–H stretching band in KOH.

We have calculated the value of the derivative of the dipole with respect to the O–H stretching displacement coordinate necessary to produce the observed band splitting in the fundamental. The hydrogen atom is assumed to lie on the O—O bond with the dipole at the hydrogen position. (The calculated value of the derivative is rather insensitive to the angle between the O—H bond and the O—O bond providing this angle is less than about 10°.) Only a single chain was considered. The derivative was found to be 2.0 debye/A, a rather large value equal to that found by Hornig and Hiebert[17] for HCl.

For an isotopically isolated hydroxyl ion the O–H (or O–D) stretching frequency ω of the ion should be related to the two components of the stretching band of the undiluted crystal by

$$\omega^2=\tfrac{1}{2}(\omega_A{}^2+\omega_B{}^2).$$

This relation is not satisfied for KOH or KOD. The stretching frequency of the isolated O–H group in KOD is 3527 cm^{-1} (Table III). This is lower than either component (3556 and 3533 cm^{-1}) of the same band for pure KOH. For dilute KOD in KOH the O–D stretching band frequency occurs at 2608 cm^{-1}, whereas KOD itself has its bands at 2609 and 2592 cm^{-1}. Residual coupling of O–H with O–D stretching modes or the removal of the vibrational coupling between translationally equivalent OH^- (or OD^-) ions in going from the isotopically undiluted to the diluted crystal would produce effects which are at least an order of magnitude smaller than the observed ones. Further, the opposing shifts of the uncoupled vibrations, i.e., lower frequency than the mean of isolated OH^- and higher frequency than the mean for isolated OD^-, must be accounted for. A possible explanation may be found by assuming that the potential energy function for O–H stretching in KOH is slightly different from that for O–D stretching in KOD. The smaller amplitude of the O–D vibration permits closer O–O approach and thus a slightly stronger hydrogen bond. Hence an OH^- ion in a KOD lattice is "squeezed," and a small decrease in its O–H stretching frequency results. The OD^- ion "expands" in a KOH lattice and hence the O–D stretching frequency increases. To give a displacement of about 10 cm^{-1}, r_e need change only by about 0.008 A (Badger[18]); this change is too small to be detectable by diffraction methods.

TABLE III. Stretching frequencies (cm^{-1}) for KOH and KOD in dilute solutions in KOD and KOH.

Temperature (°C)	Dilute KOH in KOD	Dilute KOD in KOH
23	3576	2646
−180	3527	2608

If these frequency shifts observed for KOH are the result of hydrogen bonding, then much smaller effects should be observed for nonhydrogen-bonded hydroxides. We have prepared OH^-–OD^- mixtures of the hydroxides of lithium, magnesium, and calcium and find no anomalous shifts.[19]

Further, we note that some workers have used ω_{OH}/ω_{OD} as a measure of the anharmonicity of the O–H stretching vibration of a hydrogen-bonded OH group in a solid. Our results here for KOH should serve to caution against this procedure which ignores possible differences in the O–H and O–D force constants. Thus if we use for ω_{OH} and ω_{OD} the observed frequencies for KOH and KOD, and assume that[20]

$$\omega_e x_e(\text{OD})=\frac{m_D{}^{-1}+m_O{}^{-1}}{m_H{}^{-1}+m_O{}^{-1}}\omega_e x_e(\text{OH}),$$

we find $\omega_e x_e(\text{OH})=53$ cm^{-1}. This value is about half that found for KOH from the first overtone (110±11 cm^{-1}). If ω_{OH} is taken from KOH and ω_{OD} is taken from dilute KOD in KOH, thus giving each ion a similar environment, $\omega_e x_e$ is found to be 85 cm^{-1}, in much better agreement with that from the first overtone.

[15] B. A. Phillips and W. R. Busing, J. Phys. Chem. **61**, 502 (1957).
[16] S. S. Mitra, dissertation, University of Michigan, 1957.
[17] D. F. Hornig and G. L. Hiebert, J. Chem. Phys. **27**, 752 (1957).
[18] R. M. Badger, J. Chem. Phys. **2**, 128 (1934).
[19] A fuller account of this work will be published in the near future.
[20] J. L. Dunham, Phys. Rev. **41**, 721 (1932).

TABLE IV. Infrared absorption band frequencies of KOH and KOD in the region 900–300 cm^{-1}.

Temp. °C	KOH ω (cm^{-1})	KOD ω (cm^{-1})	$\frac{\omega_{OH}}{\omega_{OD}}$
~80	...	~460 (w, vB)	...
23	643 (w, vB)[a]	472 (w, vB)	1.36
0	...	481 (w, B)	...
	...	352 (w, vB)	...
−35	...	720 (vw, B)	...
	...	573 (vw, B)	...
	...	492 (m, B)	...
	...	356 (m, vB)	...
−55	...	732 (vw, B)	...
	...	580 (vw, B)	...
	...	506 (m, B)	...
	...	362 (m, B)	...
−78	...	741 (w, B)	...
	...	586 (w, B)	...
	...	513 (m, B)	...
	...	368 (s, B)	...
−180		765 (w)	
		670 (w)	
	840 (w)	613 (w)	1.37
	709 (m)	534 (m)	1.33
	671 (w)	501 (w)	1.34
	470 (vs)	385 (vs)	1.22

[a] vs=very strong; s=strong; m=medium; w=weak; vw=very weak; B=broad; vB=very broad.

LATTICE VIBRATIONS

At film thicknesses suitable for studying the O–H stretching region, the infrared spectrum of KOH at 23°C shows in the region below the stretching band and out to 300 cm^{-1} a weak and extremely broad band centered near 643 cm^{-1} (Fig. 5). The only additional feature in the spectrum is an indication of a strong absorption band just beyond 300 cm^{-1}. KOD at 23°C shows a similar spectrum (Fig. 5), with a broad band near 472 cm^{-1} and the tail of a strong band appearing just at the low-frequency end of the spectrum. The ratio of the frequencies of the bands for KOH and KOD is 1.36. This value indicates clearly that the motion is primarily that of the hydrogen atom, and therefore the band must be assigned to a librational mode which has not "mixed" to any extent with translational modes. An assignment of this band to a first or higher overtone of a librational mode or to a binary combination of these modes may be ruled out because of the absence of a band of observable intensity in the region where the fundamental or lower combination would occur. (Remember that the selection rules permit infrared activity for all modes.) Bands belonging to hydrogen modes in the region 500–300 cm^{-1} for KOH (and 450–300 cm^{-1} for KOD) are absent also from the relatively more intense low-temperature spectra. We are then forced to accept the 643 cm^{-1} band of KOH (and the 472 cm^{-1} band of KOD) as fundamental(s) of a librational mode. The frequency of this fundamental for KOH is considerably higher than that for the same motion in either $Ca(OH)_2$ or $Mg(OH)_2$. For these crystals the librational frequency has been estimated both on the basis of neutron diffraction studies[21] and on the basis of the O–H stretching-libration combinations to be about 350 cm^{-1}. In a harmonic oscillator approximation the restoring force for libration is over three times greater for KOH than for $Ca(OH)_2$ or $Mg(OH)_2$. This strongly suggests that in KOH hydrogen bonding makes the principal contribution to the librational force constant. This conclusion is supported by data on other hydroxides that are somewhat more strongly hydrogen bonded than KOH, as judged from their lower O–H stretching frequencies. In these, librational modes occur in the region of 700–1200 cm^{-1}.[22]

The temperature dependence of the bands in this low-frequency region is marked. We have studied the temperature dependence of the bands of both KOH and KOD and find their behavior similar. Since our data for KOD are more complete than they are for KOH we show in Fig. 6 (Table IV) a series of spectra of KOD at temperatures varying from ~80° to −180°C. The band assigned above to a librational mode moves progressively to higher frequencies as the temperature is lowered (460 cm^{-1} at 80°C to 534 cm^{-1} at −180°C), with most of the shift taking place by the time the temperature has been lowered to −78°C. Shifting to higher frequencies as the temperature is lowered is the expected behavior of a librational mode whose force constant must depend entirely on the environment of the ion. At the lowest temperature (−180°C) two weaker bands, 840 and 671 cm^{-1} for KOH and 613 and 501 cm^{-1} for KOD, appear. The ratios of the frequencies of these bands in the spectrum of KOH to those of KOD show that the modes they represent are also librational in character (Table IV). As the temperature is lowered a band near 360 cm^{-1} also appears. There is nothing in the spectrum of the sample at 23°C to suggest the presence of this band, but by the time the temperature has reached −180°C it is by far the most intense in the spectrum. Its isotope frequency ratio is 1.22, indicating that it is not primarily a hydrogen (librational) mode. We assign it, therefore, to a lattice translational mode involving more hydroxide than potassium motion.

Further information on the nature of these low-frequency modes is available from the spectra of KOH–KOD mixtures of varying concentrations. Spectra of such isotopic mixtures at −180°C are shown in Fig. 7. Unfortunately, the concentration of KOD is not known, though it is estimated that at least 50% of the remaining hydrogen atoms were replaced at each exchange with D_2O. The spectrum of the sample after the first exchange is very different from the spectrum of pure KOH. The most notable new feature is the displacement of the very strong band at 470 cm^{-1} for KOH

[21] W. R. Busing and H. A. Levy, J. Chem. Phys. **26**, 563 (1957).
[22] E. Hartert and O. Glemser, Z. Elektrochem. **60**, 746 (1956).

to 411 cm^{-1} for the mixture. In subsequent exchanges the maximum shifts rather gradually to 385 cm^{-1} for the most completely deuterated sample. It is important to note that there is no residual band near 470 cm^{-1} after the final exchange, i.e., the band moves as a whole. This behavior is what is predicted[22] for the translational vibrations of mixed crystals, and this adds weight to the assignment given this band. In contrast the band at 709 cm^{-1}, established as a librational mode, remains relatively stationary in the spectrum upon exchange, while after one exchange there appears near 500 cm^{-1} a new band, which, as seen in successive spectra, is to become the KOD counterpart of the 709 cm^{-1} band of KOH. This behavior strongly suggests that these librational modes involve fairly uncoupled rotational oscillation of hydroxide ions at their lattice sites.

[22] F. Matossi, J. Chem. Phys. **19**, 161 (1951).

In the low-frequency spectrum of dilute KOH in KOD there are two weak bands near the positions of the librational modes of KOH which cannot be accounted for readily as KOD modes; the intensities of these bands decrease with decreasing OH^- ion concentration. We suggest that these bands, which appear at 765 and 670 cm^{-1}, are associated with the two librational modes of an isolated OH^- ion. The nearness of these two frequencies is consistent with a restoring potential for libration which is roughly cylindrical about the O—H bond and which arises primarily from hydrogen bonding. If then the intermolecular force constant coupling the librational modes in undiluted KOH is of the same order of magnitude as that observed for the O–H stretching modes, additional splitting of the order of 100 cm^{-1} will occur. It is reasonable then to assign all three of the bands (840, 709, and 671 cm^{-1}) to librational fundamentals of KOH.

THE JOURNAL OF CHEMICAL PHYSICS VOLUME 33, NUMBER 4 OCTOBER, 1960

Polarized Absorption and Fluorescence Spectra of 2,6-Dimethylnaphthalene at Different Temperatures* †

ADNAN ZMERLI AND HENRI POULET

Laboratoire des Recherches Physiques de la Sorbonne, Paris, Laboratoire Aimé Cotton, Bellevue (Seine et Oise), France, and Department of Physics, Duke University, Durham, North Carolina

(Received May 6, 1960)

2,6-Dimethylnaphthalene melted between two silica disks crystallizes parallel to its cleavage plane σ_{ab}. The polarized absorption spectra obtained at 300°K, 77°K, 20°K, and 4°K show no variation in the relative intensities of the *a* and *b* spectra, suggesting that there is no change of crystal phase between 300°K and 4°K. At 4°K three vibrational progressions were found in the *a* spectrum and only two in the *b* spectrum. The first bands of the strongest *a* and *b* progressions, i.e., the bands at 30 740 cm^{-1} and 30 675 cm^{-1}, respectively, are interpreted as transitions to the exciton levels. The weak progression starting at 30 650 cm^{-1} appears in both polarization directions. The 30 634 cm^{-1} series, which is also weak, is *a* polarized. The origin of these weak bands is discussed. The polarized fluorescence spectra have been obtained at 20°K and interpreted. Possible locations of the *c* exciton transition are mentioned. The comparison of these experimental results and the theoretical predictions leads to the conclusion that the dipolar moment of the first transition of 2,6-dimethylnaphthalene is close to the short axis of the naphthalene ring.

INTRODUCTION

THIS study is a continuation of research formerly done on the absorption and fluorescence spectra in molecular crystals of benzene,[1–3] naphthalene,[2,3] and acenaphthene.[4,5]

In this previous work, in the case of light and heavy naphthalene[2,3] we have reached the two following main conclusions: (1) the strong fluorescence bands located at 31 061 cm^{-1} in the case of the light naphthalene and at 31 180 cm^{-1} in heavy naphthalene, and which appear weakly in absorption, may be interpreted as a vibronic transition $0' \rightarrow 1''$. (2) The exciton splitting is strongly reduced when going from absorption to fluorescence.

Up to now the interpretation of the naphthalene spectra does not seem to have reached unanimous agreement in all cases, and new independent observa-

* Talk given at the twenty-sixth annual meeting of the Southeastern Section of the American Physical Society, at Gatlinburg, Tennessee, in April, 1960.

† This work was supported at Duke University by the Office of Ordnance Research, U. S. Army.

[1] A. Zmerli, H. Poulet, and P. Pesteil, Talk given at Colloque du C. N. R. S. at Bellevue (France) in July, 1957, and Compt. rend. **245**, 517 (1957).

[2] A. Zmerli and H. Poulet, J. chim. phys. **55**, 654 (1958).

[3] A. Zmerli, thesis, Paris (November, 1958), and J. chim. phys. **56**, 387 (1959).

[4] H. Poulet and A. Zmerli, Compt. rend. **248**, 3148 (1959).

[5] H. Poulet and A. Zmerli, Talk given at Spectroscopy International Congress in Bologna (Italy), September, 1959, to be published in *Spectrochimica Acta*.

tions are still needed in order to come to a complete understanding of the spectroscopic behavior of the crystal of this simple molecule. This is why we sought by a study of 2,6-dimethylnaphthalene to acquire new data on naphthalene.

McConnell and McClure[6] studied absorption and fluorescence spectra of 2,6-dimethylnaphthalene in solution of 3-methylpentane at 87°K. These authors attributed the strong bands, observed in absorption at 30 950±20 cm^{-1} and in fluorescence at 30 800±50 cm^{-1}, respectively, to the electronic transitions $0' \leftarrow 0''$ and $0' \rightarrow 0''$. Wolf[7], studying a solution of 2,6-dimethylnaphthalene in ethylalcohol at 87°K, observed an intense absorption band at 30 950 cm^{-1} and an equally strong fluorescence band at 30 875 cm^{-1}. The fluorescence spectrum of the crystal obtained at 87°K and published by Wolf[7] begins with a weak band at 30 510 cm^{-1}.

EXPERIMENTAL

I. Orientation of Samples

(1) Single crystal preparation.

The crystal was formed by slowly freezing the 2,6-dimethylnaphthalene, melted in a tube. This tube terminated in a capillary, in which single crystals were previously formed by immersing it in liquid air. One obtains in this manner a crystalline mass from which one can cut single crystals.

(2) Identification of the crystallographic axes with the principal axes of the index ellipsoid.

The elementary cell is orthorhombic and belongs to the group V^{15}.[8] The parameters are $a=7.54$ A, $b=6.07$ A, and $c=20.20$ A. It contains four molecules forming a a family ($Z=4$): I(0, 0, 0) − II ($\frac{1}{2}$, $\frac{1}{2}$, 0) − III(0, $\frac{1}{2}$, $\frac{1}{2}$), and IV ($\frac{1}{2}$, 0, $\frac{1}{2}$).

Kitajgordsky[8] did not give the correspondence between the axes a, b, c and the principal axes of the index ellipsoid. The 2,6-dimethylnaphthalene possesses a perfect cleavage plane. A rather thin single crystal parallel to this cleavage plane, observed through the polarizing microscope of Descloiseau, shows the classical figure of hyperbolas and allows one to mark the optical axes plane by observation of the isogyres axes eyes, which one can follow by turning the crystal.

In this way we found the cleavage plane is perpendicular to the obtuse bi-sectrix of optical axes. The x-ray diffraction patterns obtained by Dr. P. Herpin (Laboratoire de Mineralogie de la Sorbonne) show that the cleavage plane is the plane σ_{ab} and that the b axis is perpendicular to the plane of the optical axes.

The 2,6-dimethylnaphthalene crystallizes between two fused quartz disks perpendicularly to one optical axes bi-sectrix. The use of two crossed polaroids and a quartz compensator allows one to establish that the highest refraction index of the flake obtained in this way corresponds to the perpendicular to the optical axes plane, therefore, following the b axis; it coincides with the refractive index n_m of the crystal.

To identify the other direction of the flake, we glued on a glass disk a crystal oriented parallel to the cleavage plane σ_{ab} on which we have marked the a axis. We made it sufficiently thin in order to identify easily the directions corresponding to its principal indices with the help of two crossed polaroids and the quartz compensator. We observed that the index n_p corresponds to the a axis.

We can conclude that the melted 2,6-dimethylnapthalene crystallizes between two disks parallel to its cleavage plane σ_{ab}.

The molecules' orientation in the elementary cell lets us anticipate that the index n_g corresponds to the c axis.

We have therefore the following correspondence:

$$a(n_p), \quad b(n_m), \quad c(n_g).$$

II. Apparatus and Description of Experimental Results

All results at 20°K have been achieved at Paris using a medium Hilger quartz spectograph, a Challonge hydrogen arc as absorption excitation source, and a Cotton arc coupled with a chlorine filter as fluorescence excitation source.

The work on the polarized absorption spectra at 300°K, 77°K, and 4°K has been carried out at Duke University using a Hanovia xenon arc as excitation source and a Jarrell-Ash spectrograph (Wadsworth mounting).

It is noteworthy that the a and b spectra obtained at 300°K, 77°K, 20°K, and 4°K show no variation in their relative intensities between 300°K and 4°K. It is therefore concluded that there is no change of crystal phase between 300°K and 4°K.

1. Polarized Absorption Spectrum at 20°K and 4°K

The principal indices of 2,6-dimethylnaphthalene are not known. Because of this, the thickness of the studied flakes could not be obtained by measurements. An estimated thickness was found by interferometry in this way: calling e the thickness of a flake with order p, we have the relation $e \times \text{birefringence} = p \times \lambda$ with $\lambda = 0.550\ \mu$. We have studied the flakes of the orders $p=8$, 2, $\frac{3}{4}$, and $\frac{1}{4}$, but shall limit the description of the spectrum to that of a one-quarter order flake (Figs. 1 and 2).

a. a Spectrum.—The a spectrum consists essentially of wide bands. The width of these bands varies little with the thickness of the flake. The first band begins at 30 600 cm^{-1} and extends to 30 890 cm^{-1} ($\Delta\nu$ = width = 290 cm^{-1}). The microphotometer tracing of the a spectrum at 4°K shows clearly two separate peaks

[6] H. McConnell and D. S. McClure, J. Chem. Phys. **21**, 1296 (1953).
[7] Von H. C. Wolf, Z. Naturforsch. **10a**, 270 (1955).
[8] A. E. Kitajgordsky, Bull. Acad. Sci. U. S. S. R. (Chem. Sec.) **6**, 587 (1946).

located at 30 634±10 cm^{-1} and 30 650±10 cm^{-1}, but the strongest wide peak of this band is located at 30 740±30 cm^{-1} and is followed by two other wide peaks at 30 775±30 cm^{-1} and at 30 810±30 cm^{-1}. This first very broad band is followed by a group of narrow bands situated at 30 992 cm^{-1} (very intense), at 31 038 cm^{-1} (weak), and at 31 087 cm^{-1} (very intense). The second wide band starts at 31 120 cm^{-1} and extends till 31 290 cm^{-1} ($\Delta\nu$=width=170 cm^{-1}). At 4°K a separate peak was clearly distinguished at 31 140 cm^{-1}. The main peaks of this band are at 31 215±15 cm^{-1}, at 31 240±15 cm^{-1}, and at 31 275± 15 cm^{-1}. The third band begins at 31 350 cm^{-1} and extends to 31 560 ($\Delta\nu$=210 cm^{-1}). At 4°K, one can see quite clearly on the microphotometer tracing two peaks at 31 350 cm^{-1} and at 31 366 cm^{-1}, which look like the two peaks at 30 634 cm^{-1} and at 30 650 cm^{-1} observed in the first wide band. The narrow bands at 31 562 cm^{-1} and at 31 578 cm^{-1} show up between the third and the fourth wide ones. On the fourth, we have been able to distinguish the peaks at 31 615±10 cm^{-1}, at 31 655±10 cm^{-1}, and at 31 700±10 cm^{-1}. Two narrow maxima at 31 788 cm^{-1} and 31 809 cm^{-1} show up before the fifth wide band, which begins with a shoulder at 31 840 cm^{-1} and it extends till 32 830 cm^{-1}. From there it becomes very hard to analyze the tracing because of the very strong absorption of the spectrum. Nevertheless we have been able to distinguish some new peaks for which wave numbers are listed in Table I. One plate taken at 20°K with a $\frac{3}{4}$-order flake showed a very weak band on the long wavelength side of the first main band at 31 472 cm^{-1}.

b. b Spectrum.—The first band, the only wide one of this spectrum, begins at 30 640 cm^{-1} and extends to 30 740 cm^{-1} ($\Delta\nu$=100 cm^{-1}). It exhibits a resolution which the naked eye can distinguish on a plate taken at 20°K and which is clearly demonstrated on a microphotometer tracing of 4°K spectrum. Particularly, we have been able to locate in this tracing a weak peak at 30 650 cm^{-1} which coincides with the one mentioned before in the *a* spectrum. The main peak of this band is located at 30 675 cm^{-1}. This first broad band is followed by a great number of narrow bands, the wave numbers of which are listed in Table I. Note that the bands at 31 166 cm^{-1} and 31 390 cm^{-1}, like the main peak at 30 675, are accompanied on the short wavelength side by bands much weaker and may be attributable to crystal vibrations.

The *a* spectrum appears stronger than the *b* spectrum, although one should have observed $I_b > I_a$ from the orientation of the molecules in the elementary cell. Therefore, there is an important effect on the intensities due to second-order perturbation.

2. *Polarized Fluorescence Spectra at 20°K.* (*Figs. 3 and 4*)

The study of the polarized fluorescence spectrum of an oriented crystal shows that this spectrum, which is

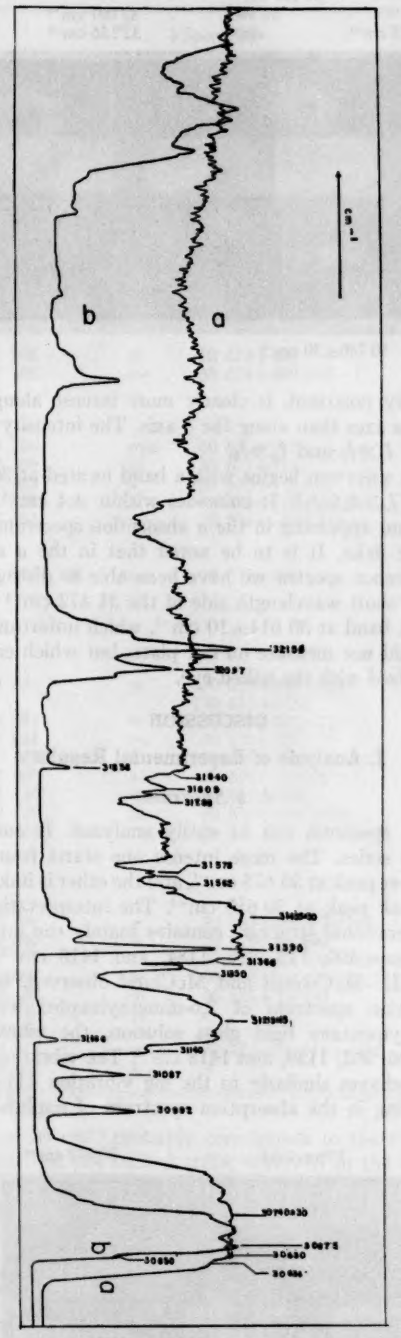

FIG. 1. Microphotometer tracing of a representative plate of the *a* and *b* absorption spectra of 2,6-dimethylnaphthalene crystal at 4°K.

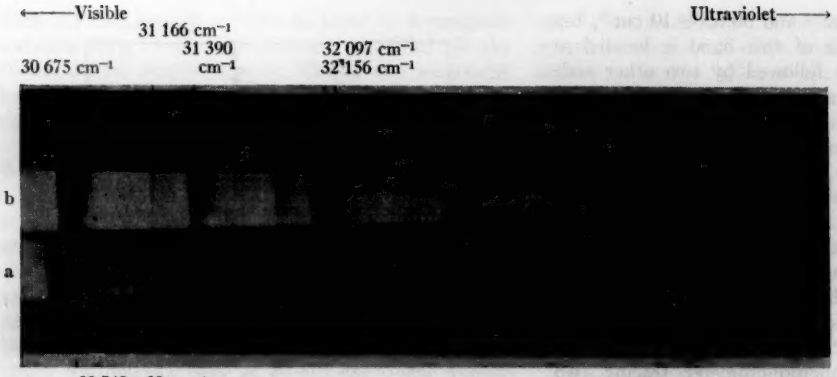

FIG. 2. Polarized absorption spectra of 2,6-dimethylnaphthalene ($\frac{1}{4}$-order flake) at 20°K. In the top the spectrum along the b axis, in the bottom the spectrum along the a axis.

partially polarized, is clearly more intense along the *c* and *a* axes than along the *b* axis. The intensity relation is $I_c \gg I_b$ and $I_a \gg I_b$.

This spectrum begins with a band located at 30 472 cm^{-1} ($I_c > I_a \gg I_b$). It coincides within ±4 cm^{-1} with the band appearing in the *a* absorption spectrum of a $\frac{3}{4}$-order flake. It is to be noted that in the *a* and *c* fluorescence spectra we have been able to distinguish on the short wavelength side of the 31 472 cm^{-1} band a weak band at 30 614±10 cm^{-1}, which unfortunately we could not measure on our plate, but which can be recognized with the naked eye.

DISCUSSION

I. Analysis of Experimental Results

1. b Spectrum

This spectrum can be easily analyzed. It consists of two series. The more intense one starts from the strongest peak at 30 675 cm^{-1}, and the other is linked to the weak peak at 30 650 cm^{-1}. The interpretation of the vibrational structure contains mainly the internal vibrations 490, 715, 926, 1184, and 1418 cm^{-1} (see Table I). McConnell and McClure[6] observed, in the absorption spectrum of 2,6-dimethylnaphthalene in 3-methylpentane rigid glass solution, the vibrations 485, 706, 902, 1189, and 1418 cm^{-1}. The vibration 490 cm^{-1} behaves similarly to the big vibration 433 cm^{-1} appearing in the absorption spectrum of naphthalene crystal. A Fermi resonance exists between 1418 cm^{-1} and 926+490=1416 cm^{-1}. It causes the appearance of two vibrations 1417±64 cm^{-1} which allow explanation of the weak band at 32 031 cm^{-1} (30 675+1353=32 028) and the very strong one at 32 156 cm^{-1} (30 675+1481=32 156 cm^{-1}). The lattice vibrations 35 cm^{-1} and 118 cm^{-1} appear linked to the pure electronic band 30 675 cm^{-1} and to the vibronic bands 31 166, 31 390, and 32 156 cm^{-1}.

2. a Spectrum

This spectrum consists of three series. The very strong one starts from the strongest peak at 30 740± 30 cm^{-1}. The two much weaker ones are connected with the two peaks at 30 634 and 30 650 cm^{-1}. The series starting at 30 650 cm^{-1} is identical with the weak series registered in the *b* spectrum. The vibrational structure of these three series is the same as observed in the *b* spectrum. (See Table I). The lattice vibration 35 cm^{-1} appears superimposed on the pure electronic band 30 740±30 cm^{-1} and the vibronic bands 31 125± 15 cm^{-1} and 31 455±30 cm^{-1} of the strongest series.

3. Fluorescence Spectrum

The fluorescence spectrum is also easily analyzed (see Table II) by starting at 30 472 cm^{-1} and sub-

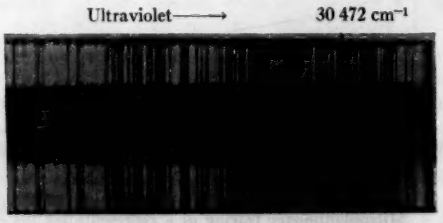

FIG. 3. Polarized fluorescence spectra of 2,6-dimethylnaphthalene at 20°K. In the top the spectrum along the c axis, in the bottom the spectrum along the b axis.

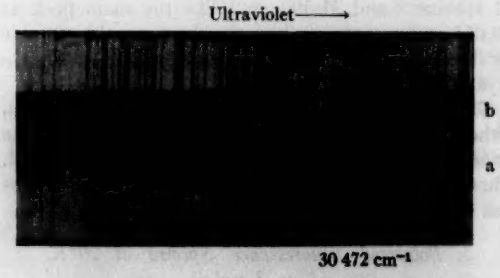

FIG. 4. Polarized fluorescence spectra of 2,6-dimethylnaphthalene at 20°K. In the top the spectrum along the b axis, in the bottom the spectrum along the a axis.

TABLE I. Absorption spectrum of 2,6-dimethylnaphthalene crystal (½-order flake) at 4°K, in both *a* and *b* polarizations.

a Spectrum			*b* Spectrum		
ν cm^{-1}	Int.	Assignment	ν cm^{-1}	Int.	Assignment
30 634±10	m	0″→0′ trapped exciton or imperfection			
30 650±10	m	0″→0′ trapped exciton or imperfection	30 650	w	0″→0′ trapped exciton or imperfection
			30 675	vvs	0″→0′ free exciton band
			30 710	vs	30 675+35
30 740±30	vvs	0″→0′ free exciton band	30 745	m	30 675+2×35
30 775±30	vs	30 740±30+35	30 793	w	30 675+118
30 810±30	s	30 740±30+2×35			
30 992	m	30 740±30+252			
31 038	w	30 740±30+298			
31 087	m	30 740±30+347			
31 140	s	30 650+490			
			31 166	m	30 675+490
31 215±15	vs	30 740±30+490	31 202	vw	30 675+490+35
31 250±15	s	30 740±30+490+35			
31 285±15	s	30 740±30+490+2×35			
31 350	m	30 634+715			
31 366	m	30 650+715	31 366	vvw	30 650+715
			31 390	vs	30 675+715
			31 425	s	30 675+715+35
31 455±30	vvs	30 740±30+715	31 460	w	30 675+715+2×35
			31 502	vw	30 675+715+118
31 562	m	30 634+926			
31 578	m	30 650+926			
			31 610±10	vw	30 675+926
31 655±10	vs	30 740±30+926			
31 700±10	vs	30 740±30+2×490			
31 788	m	30 634+1158			
31 809	m	30 650+1158			
31 840	w	30 634+490+715			
31 856	s	30 650+490+715	31 856	m	{30 650+490+715 {30 675+1184
			31 882	w	30 675+490+715
			32 031	vw	30 675+1353
32 082±10	m	30 650+2×715	32 082±5	m	30 650+2×715
			32 097	s	30 675+2×715
			32 156	vs	30 675+1481
			32 189	m	30 675+1481+35
			32 210	vw	?
32 275	w	30 634+715+926			
32 347	w	30 650+2×490+715			
32 386	w	30 740±30+715+926			
32 464	w	30 740±30+2×490+715			
			32 562	w	30 650+490+2×715
			32 648	w	30 675+4×490
			32 857	s	30 675+3×490+715
			33 095	m	30 675+2×490+2×715
			33 133	m	30 675+5×490
			33 313	m	?
			33 476	vs	?
			33 576	s	30 675+2×715+1481
			33 604	s	?

tracting from it the wave numbers of the vibrations published by Luther and Reichel,[9] or their combinations. One of us (A.Z.) in collaboration with Dr. Monique Harrand (Laboratoire de Recherches Physiques de la Sorbonne) obtained the Raman spectrum of the crystal powder of 2,6-dimethylnaphthalene. The wave numbers of lines observed coincide within 2 or 3 cm^{-1} with those published by Luther and Reichel. In addition we were able to distinguish some lattice vibrations in the same spectrum. The very distinct one at 39 cm^{-1} probably corresponds to the vibration 35 cm^{-1} of the excited state, observed in the *a* and *b* spectra in absorption.

[9] H. Luther and C. Reichel, Z. physik. Chem. (Leipzig) **195**, 103 (1950).

II. Interpretation

For the molecular symmetry C_i there is no restriction on the specific orientation of the transition moment. To the molecular transition $A_g \rightarrow A_u$ there correspond in the crystal (V^{15}) four exciton energy levels: A_u, forbidden by symmetry, and B_{1u} (polarization along the *c* axis), B_{2u} (polarization along the *b* axis), and B_{3u} (polarization along the *a* axis), allowed

TABLE II. Fluorescence spectrum of 2,6-dimethylnaphthalene at 20°K in the c polarization. ($\Delta\nu$ cm^{-1}=ν cm^{-1} observed—ν cm^{-1} calculated).

ν cm^{-1} Observed	Int.	Assignment	ν cm^{-1} Calculated	$\Delta\nu$ cm^{-1}
30 614±10	vvw	0′→0″ free exciton band or 0′→0″ trapped exciton or imperfection		
30 472	vs	0′→1″ 30 680−208 or 0′→0″ free exciton band	30 472	0
30 149	s	30 472−325	30 147	2
29 947	vs	30 472−527	29 945	2
29 720	s	30 472−755	29 717	3
29 631	m v wide	30 472—325—527	29 620	11
29 505	s	30 472−962	29 510	−5
29 417	v wide	30 472−2×527	29 418	−1
29 295	m	30 472−1177	29 295	0
29 187	m	30 472−325−962 or 30 472−527−755	29 185 29 190	2 −3
29 092	vs	30 472−1378	29 094	−2
28 757	m	30 472−755−962	28 755	2
28 564	vs	30 472−527−1378	28 567	−3
28 464	w	30 472−527−1484	28 461	3
28 333	w	30 472−527−2×755	28 335	−2
29 295	m	?		
28 239	m	30 472−2×527−1177	28 241	−2
28 121	m	30 472−2×1177	28 118	3
28 022	m	30 472−1177−1274	28 021	1
27 928	m	30 472−2×1274	27 924	4
27 711	vs	30 472−2×1378	27 716	−5
27 603	s	30 472−1378−1484	27 610	−7
27 167	s	30 472−755−2×1274	27 169	−2
27 077	w	30 472−527−1378−1484	27 083	−6
26 845	m	30 472−325−755−2×1274	26 844	1

by symmetry. In order to get an idea of the order in which the exciton energy levels are placed, we have calculated them, using the ordinary first order perturbation method,[10] for the following limiting cases: (a) the transition moment M directed along the short axis of the naphthalene ring; (b) M directed along the long axis of the naphthalene ring. The perturbating potential has been reduced to dipole-dipole interaction. According to the results of McConnell and McClure,[6] we can estimate the oscillator strength of the electronic transition as f=0.006. (Induced vibrational part of f has not been taken into account.) Therefore M^2= 0.02 A^2. With this value of M^2 we obtain, using hypothesis (a), for the transition energies to the exciton levels in the three polarization directions:

$$\Delta E_a > \Delta E_b > \Delta E_c$$

with

$$\Delta E_a - \Delta E_b = 16 \text{ cm}^{-1}$$

and

$$\Delta E_a - \Delta E_c = 50 \text{ cm}^{-1}$$

and for hypothesis (b):

$$\Delta E_b > \Delta E_c > \Delta E_a$$

with

$$\Delta E_b - \Delta E_a = 260 \text{ cm}^{-1}$$

and

$$\Delta E_b - \Delta E_c = 96 \text{ cm}^{-1}.$$

The multipole-multipole interactions can affect these values notably, but it is almost impossible that they change the order of the levels obtained in the (b) hypothesis. From the analysis of the absorption spectra we can attribute the very strong bands at 30 740±30 and 30 675 cm^{-1}, which are the origin of the strongest series in the a and b spectra, respectively, to the pure electronic transition 0″→0′ of the free exciton. Therefore, we can write ΔE_a=30 740±30 cm^{-1} and ΔE_b= 30 675 cm^{-1}. The comparison of these experimental results with the theoretical predictions leads us to the conclusion that the dipole moment is very close to the short axis of the naphthalene ring for the first transition of 2,6-dimethylnaphthalene. This appears to be in agreement with the orientation of the "spectroscopic moment" due to the methyl substituents for a transition of type L_b in Platt notations.[11]

It remains to locate the exciton transitions ΔE_c. There are several possibilities.

First, the appearance of 30 472 in absorption. (This appearance is perhaps due to the imperfect orientation of our $\frac{3}{4}$-order flake.) Its very strong intensity in the c fluorescence spectrum, and the ease with which we can explain almost all the fluorescence bands would make it possible to consider the 30 472 cm^{-1} band as electronic transition of the crystal polarized along the c axis.

[10] D. P. Craig and P. C. Hobbins, J. Chem. Soc. **1955**, 539.

[11] J. R. Platt, J. Chem. Phys. **19**, 263 (1951).

On the other hand, the appearance of the very weak band 30 614±10 cm^{-1} along the c axis in fluorescence, and the weak absorption band 30 472 cm^{-1} which coincides with the strongest fluorescence band recalls the situation encountered by McClure in the case of the naphthalene[12] with the bands 31 476 cm^{-1} (31 476 cm^{-1} in absorption and 31 463 cm^{-1} in fluorescence) and 31 062 cm^{-1}.

By analogy with naphthalene we may attribute the band 30 614±10 cm^{-1} to the pure electronic transition connected with the exciton energy level E_c. Still following the analogy with naphthalene[2,3] we could attribute the band at 30 472 cm^{-1} to a vibronic transition $1''\leftrightarrow 0'$. Nevertheless, in this case, the vibration quantum should be rather small. The vibration of 208 cm^{-1} would fit very well in order to make the fluorescence start from a level at the middle of the exciton band as in the case of naphthalene.[2,3] This assignment would remain valid for any location of ΔE_c between 30 472 cm^{-1} and 30 675 cm^{-1}. The two previous assumptions on the location of ΔE_c would agree with the theoretical predictions of a dipole moment almost directed along the short axis of the naphthalene ring, and in this case we should have $\Delta E_c < \Delta E_b < \Delta E_a$.

The two weak series appearing in absorption might be analogous to some bands observed in anthracene and phenanthrene by Sidman[13] and McClure[14] who attributed them to trapped excitons. Nevertheless, it could be reasonable to link them to some crystal imperfections in which the molecules could be enclosed. The way of preparing our flakes by pressing the melted substance between two silica disks may create such imperfections.

III. Conclusion

We have presented an analysis of the polarized absorption and fluorescence spectra of 2,6-dimethylnaphthalene. The absorption bands at 30 470±30 cm^{-1} (a spectrum) and 30 675 cm^{-1} (b spectrum) are assigned to the electronic transition to the exciton energy levels E_a and E_b. From our results it is very difficult to locate with certainty the transition ΔE_c. Two possibilities have been mentioned. In spite of this uncertainty it is possible to assign the first transition of 2,6-dimethylnaphthalene to a dipolar moment very close to the naphthalene ring.

ACKNOWLEDGMENTS

The authors acknowledge several stimulating discussions with Professor H. Sponer at Duke University and Professor J. P. Mathieu at "La Sorbonne." They thank very much Dr. P. Herpin for obtaining the x-ray diffraction patterns.

[12] D. S. McClure and O. Schnepp, J. Chem. Phys. **23**, 1575 (1955).

[13] J. W. Sidman, Phys. Rev. **102**, 96 (1956).

[14] D. S. McClure, J. Chem. Phys. **25**, 481 (1956).

Three Remarks on Molecular Orbital Theory of Complex Molecules*

ROBERT G. PARR†

Department of Chemistry, Carnegie Institute of Technology, Pittsburgh, Pennsylvania

(Received March 10, 1960)

Three suggestions are made and discussed concerning the generalized Hückel and related methods for treating the quantum chemistry of complex unsaturated molecules: (1) Justification for the assumptions of zero overlap and zero differential overlap resides in two facts: (a) For many molecules the atomic orbitals in the LCAO molecular orbitals may be replaced by the corresponding orthogonalized atomic orbitals of Löwdin, without effect on the molecular orbitals. (b) Integrals involving charge distributions which are products of orthogonalized atomic orbitals are small. (Observations previously made by several authors.) (2) Molecules isoelectronic with benzene are conveniently handled making use of molecular orbitals appropriate to the full benzene symmetry, for then deviations from benzene symmetry can be classified and treated systematically using symmetry combinations of basic integrals. (Formulas are given.) (3) The two-center coulomb repulsion integrals, previously dealt with by rather arbitrary semiempirical procedures, may be expanded by multipole expansion methods, leaving the independent multipoles of each atomic orbital as its defining theoretical or semiempirical characteristics.

I. INTRODUCTION

RECENT research in the theory of the electronic structure of complex unsaturated molecules[1-9] has produced a fundamentally more satisfactory theory and improved agreement between theory and experiment, but the methods that have been developed have admittedly been in need of further modification and clarification. The comments in the present paper are intended to provide insight into certain theoretical aspects of these methods, to suggest techniques for carrying out calculations with these methods on certain classes of molecules, and to propose for study a new way of looking at certain integrals basic in these methods.

More specifically, in Sec. II the point is made and amplified that when zero overlap and zero differential overlap[3] properties are ascribed to atomic orbitals in the semiempirical LCAO molecular orbital method called the generalized Hückel method,[7] the most satisfactory interpretation is that these atomic orbitals are orbitals that have been orthogonalized by the method of Löwdin[10]; and further, that this assumption produces no error whatsoever in certain important cases. In Sec. III formulas for handling molecules isoelectronic with benzene are displayed in a convenient format. Finally, in Sec. IV the idea is broached of using multipole expansion formulas for two-center electronic repulsion integrals of the simple coulomb type.

II. REMARK CONCERNING THE USE OF ORTHOGONALIZED ATOMIC ORBITALS

Sometime ago Löwdin[10] proposed using in molecular calculations orthogonalized atomic orbitals ($\overline{\text{AO}}$) built from the ordinary atomic orbitals (AO) by a certain orthogonalization process, and he indicated various formal advantages proffered by such functions. Later McWeeny[11] actually employed such orthogonalized orbitals in some calculations by a rigorous valence bond method. While he obtained interesting numerical results and developed various significant theorems, he found that the individual "contributing structures" in the orthogonalized atomic orbital scheme, which he labeled the $\overline{\text{VB}}$ scheme, do not have the same physical significance as the corresponding structures in the usual nonorthogonalized or VB scheme—a rather disappointing circumstance.

It will be shown in the following that the situation is often much more satisfactory when the LCAO molecular orbital scheme is used: Quite arbitrary replacement of AO with $\overline{\text{AO}}$ may not change the physical signficance of a molecular orbital configurational wave function at all.

Hydrogen Molecule

The hydrogen molecule illustrates well what is involved. To obtain an approximate wave function for its ground state by the valence bond method, starting from the usual nonorthogonal atomic orbitals $1s_a$ and $1s_b$, with overlap integral S, one would ordinarily merely linearly mix the two (unnormalized) structures,

$$\Phi_{\text{covalent}}=1s_a(1)1s_b(2)+1s_a(2)1s_b(1),$$

$$\Phi_{\text{ionic}}=1s_a(1)1s_a(2)+1s_b(1)1s_b(2), \qquad (1)$$

* Supported in part by research grants from the National Science Foundation, the Office of Ordnance Research, U. S. Army, and the Petroleum Research Fund of the American Chemical Society.

† Alfred P. Sloan Fellow.

[1] R. Pariser and R. G. Parr, J. Chem. Phys. **21**, 466, 767 (1953).
[2] J. A. Pople, Trans. Faraday Soc. **49**, 1375 (1953).
[3] R. G. Parr, J. Chem. Phys. **20**, 1499 (1952).
[4] R. Pariser, J. Chem. Phys. **21**, 568 (1953).
[5] F. G. Fumi and R. G. Parr, J. Chem. Phys. **21**, 1864 (1953).
[6] R. G. Parr and R. Pariser, J. Chem. Phys. **23**, 711 (1955).
[7] R. G. Parr and F. O. Ellison, Ann. Rev. Phys. Chem. **6**, 171 (1955).
[8] R. Pariser, J. Chem. Phys. **24**, 250 (1956); **25**, 1112 (1956).
[9] P. G. Lykos and R. G. Parr, J. Chem. Phys. **24**, 1166 (1956), **25**, 1301 (1956).
[10] P. O. Löwdin, J. Chem. Phys. **18**, 365 (1950).
[11] R. McWeeny, Proc. Roy. Soc. (London) **A223**, 63, 306 (1954); **A227**, 288 (1955).

to give a covalent-plus-ionic function of the form

$$\Psi = A_c\Phi_{\text{covalent}} + A_i\Phi_{\text{ionic}}. \tag{2}$$

Alternatively, however, one could start from the orthogonal atomic orbitals

$$\lambda_a = [\tfrac{1}{2}(1+S)^{-\frac{1}{2}} + \tfrac{1}{2}(1-S)^{-\frac{1}{2}}](1s_a) + [\tfrac{1}{2}(1+S)^{-\frac{1}{2}} - \tfrac{1}{2}(1-S)^{-\frac{1}{2}}](1s_b),$$

$$\lambda_b = [\tfrac{1}{2}(1+S)^{-\frac{1}{2}} - \tfrac{1}{2}(1-S)^{-\frac{1}{2}}](1s_a) + [\tfrac{1}{2}(1+S)^{-\frac{1}{2}} + (1-S)^{-\frac{1}{2}}](1s_b). \tag{3}$$

One would then mix the two structures

$$\bar{\Phi}_{\text{covalent}} = \lambda_a(1)\lambda_b(2) + \lambda_a(2)\lambda_b(1),$$
$$\bar{\Phi}_{\text{ionic}} = \lambda_a(1)\lambda_a(2) + \lambda_b(1)\lambda_b(2), \tag{4}$$

and obtain

$$\Psi = \bar{A}_c\bar{\Phi}_{\text{covalent}} + \bar{A}_b\bar{\Phi}_{\text{ionic}}. \tag{5}$$

Equations (2) and (5) give the final wave function in the VB and $\overline{\text{VB}}$ procedures, respectively. These are naturally the same. However, and this is the essential point which vitiates the $\overline{\text{VB}}$ procedure,

$$\Phi_{\text{covalent}} \not\equiv \bar{\Phi}_{\text{covalent}}$$

and

$$\Phi_{\text{ionic}} \not\equiv \bar{\Phi}_{\text{ionic}}, \tag{6}$$

which means that any truncation of the covalent-ionic mixing (as, for example, by restriction of the structures to be mixed to the single one covalent in type) will give different results in the VB and $\overline{\text{VB}}$ methods. Indeed, as Slater first showed,[12] the single $\overline{\text{VB}}$ structure Φ_{covalent} is a poor approximation indeed for the ground state of the hydrogen molecules, whereas Φ_{covalent} is the original description of Heitler and London.

The molecular orbital situation is different. In the customary LCAO form of this method, starting from the same atomic orbitals $1s_a$ and $1s_b$ one defines molecular orbitals

$$\phi_1 = [2(1+S)]^{-\frac{1}{2}}(1s_a + 1s_b),$$
$$\phi_2 = [2(1-S)]^{-\frac{1}{2}}(1s_a - 1s_b), \tag{7}$$

builds configurational wave functions,

$$\Phi_1 = \phi_1(1)\phi_1(2), \qquad \Phi_2 = \phi_2(1)\phi_2(2), \tag{8}$$

and mixes these to give the final approximate wave function

$$\Psi = B_1\Phi_1 + B_2\Phi_2. \tag{9}$$

This is the MO method, including configuration interaction. Alternatively, in what may be termed the $\overline{\text{MO}}$ method, one would start from molecular orbitals

$$\bar{\phi}_1 = 2^{-\frac{1}{2}}(\lambda_a + \lambda_b),$$
$$\bar{\phi}_2 = 2^{-\frac{1}{2}}(\lambda_a - \lambda_b), \tag{10}$$

build configurational wave functions

$$\bar{\Phi}_1 = \bar{\phi}_1(1)\bar{\phi}_2(2), \qquad \bar{\Phi}_2 = \bar{\phi}_2(1)\bar{\phi}_2(2), \tag{11}$$

and mix these to give

$$\Psi = \bar{B}_1\bar{\Phi}_1 + \bar{B}_2\bar{\Phi}_2. \tag{12}$$

Again the final result is the same (and the same as in either the VB or $\overline{\text{VB}}$ methods), but this time one has a more detailed identity, namely,

$$\phi_1 \equiv \bar{\phi}_1 \quad \text{and} \quad \phi_2 \equiv \bar{\phi}_2. \tag{13}$$

From this it follows that

$$\Phi_1 \equiv \bar{\Phi}_1 \quad \text{and} \quad \Phi_2 \equiv \bar{\Phi}_2. \tag{14}$$

That is, the MO and $\overline{\text{MO}}$ methods are identical "step by step": they give identical descriptions whether or not configuration interaction is carried to its full limit.

General Case of High Symmetry[13]

In the case of the hydrogen molecule it thus turns out that the coefficients of the $\overline{\text{AO}}$ in the $\overline{\text{MO}}$ are in the same ratios as the coefficients of the AO in the MO. This result is of more practical interest than the simple identity between the MO and the $\overline{\text{MO}}$, for it implies that, for such a case, the LCAO coefficients themselves, as well as later results of calculations, are essentially the same in the MO and $\overline{\text{MO}}$ methods. For purely theoretical work this is not so helpful, because precise orbital forms must be specified before purely theoretical calculations can be carried out, but the advantages are definite for semiempirical schemes, in which integrals are evaluated by more devious means.

The MO and $\overline{\text{MO}}$ methods unfortunately are not always identical in this "complete sense." The simplest case when they are is when the molecular symmetry is high enough to determine the LCAO coefficients uniquely, that is, when each molecular orbital is a symmetry orbital for the problem. (Hydrogen falls in this class of molecules, as do ethylene, cyclobutadiene, and benzene, but not butadiene.)

To lay the argument out precisely, in the usual MO method one sets out to determine the coefficients C_{pj} in the expansions,

$$\phi_j = \sum_p \chi_p C_{pj}, \tag{15}$$

of the molecular orbitals ϕ in terms of overlapping atomic orbitals χ. But alternatively, one can write as well the molecular orbitals in terms of the orthogonalized orbitals λ of Löwdin,[10]

$$\bar{\phi}_j = \sum_q \lambda_q D_{qj}. \tag{16}$$

[12] J. C. Slater, J. Chem. Phys. **19**, 220 (1951).

[13] Compare F. Peradejordi, Compt. rend. **243**, 276 (1956).

Here,

$$\lambda_q=\sum_p \chi_p T_{pq}$$

and

$$C_{pj}=\sum_q T_{pq}D_{qj}, \tag{17}$$

where T_{pq} is the element in the pth row and qth column of the matrix

$$T=(S)^{-\frac{1}{2}}=\begin{pmatrix} 1 & S_{12} & S_{13} & \cdots \\ S_{12} & 1 & S_{23} & \cdots \\ \cdot & \cdot & \cdot & \cdots \end{pmatrix}^{-\frac{1}{2}}, \tag{18}$$

in which

$$S_{p'p}=\int \chi_{p'}{}^*\chi_p dv.$$

The question now is, are the D_{qj} of Eq. (16) the same as the C_{pj} of Eq. (15)?

In general, the answer to this question is no, but in case the C_{pj} are determined by symmetry the D_{qj} are also, and the two sets of coefficients differ at most by constants N_j:

$$\bar{\phi}_j=\sum_p \lambda_p D_{pj}\equiv N_j\sum_p \chi_p D_{pj}=\phi_j. \tag{19}$$

This follows from the fact that the transformation to Löwdin orbitals, Eq. (17), leaves the symmetry properties of the orbitals unchanged.

The outside identity of Eq. (19), $\bar{\phi}_j\equiv\phi_j$ is not so surprising, for any reasonable method for arriving at LCAO molecular orbitals would be expected to give results unaffected by an intermediate linear transformation of the starting orbitals. It is the inside equality that is interesting and important; it shows that in determining the coefficients C_{pj} (up to constants) one can work as well with the λ as with the χ.

What this means becomes clear when one considers the example of the benzene molecule. In the usual rigorous treatment of the pi electrons in this molecule,[14] one starts with molecular orbitals

$$\phi_j=(1/6\sigma_j)^{\frac{1}{2}}\sum_{p=1}^{6}\omega^{jp}\chi_p, \tag{20}$$

where $\omega=\exp(2\pi i/6)$ and the σ_j are normalizing factors; the χ_p are overlapping. One then builds various many-electron wave functions and mixes them variationally to give approximations for the wave functions for the several molecular states.[15] The calculation is very tedious, mainly because of the host of integrals of several kinds which enter the formulas.

One could start from the molecular orbitals expressed more simply in terms of Lowdin orbitals λ derived from the χ by the transformation of Eq. (17). By Eq. (19), one would have

$$\bar{\phi}_j=(1/6)^{\frac{1}{2}}\sum_{p=1}^{6}\omega^{jp}\lambda_p\equiv\phi_j. \tag{21}$$

The many-electron functions consequently are expressible as well in terms of the $\bar{\phi}$ as in terms of the ϕ, and *the various integrals that enter the final formulas may be interpreted as over orthogonalized orbitals λ just as well as over nonorthogonal orbitals χ, with no error.* Overlap integrals may be struck out identically, and integrals involving electron distributions divided between different orthogonal orbitals may be set equal to zero as a reasonable approximation. Explicit calculations verify that this last, which is no more or less than the approximation of zero differential overlap, is a good approximation in this problem.[16]

Equation (21) has already been written down by Löwdin for Bloch orbitals in a crystal[10]; its implications for calculations on benzene have, however, not been pointed out so explicitly before.

Alternant Hydrocarbons and Similar Cases

Consider now a case in which the molecular orbital coefficients C_{pj} are determined not by symmetry alone but by solution of secular equations of the type

$$\sum_p[{}^{\chi}M_{rp}-S_{rp}\mu_j]C_{pj}=0. \tag{22}$$

Here,

$${}^{\chi}M_{rp}=\int \chi_r{}^*\mu\chi_p dv, \tag{23}$$

where μ is an approximate one-electron operator, as, for example, the LCAO SCF operator in Roothaan's method[17]; the μ_j are constants. Solution of these equations provides molecular orbitals ϕ from which many-electron wave functions can be built.

Alternatively, molecular orbitals $\bar{\phi}$ are defined by the coefficients D_{qj} which are solutions of the secular equations of simpler form,

$$\sum_q[{}^{\lambda}M_{sq}-\delta_{sq}\mu_j]D_{qj}=0, \tag{24}$$

where

$${}^{\lambda}M_{sq}=\int \lambda_s{}^*\mu\lambda_q dv, \tag{25}$$

and the δ_{sq} are Kronecker deltas.

The ϕ and the $\bar{\phi}$ are identical, so again the MO and $\overline{\text{MO}}$ methods are identical step by step. This time, however, the coefficient C_{pj} and D_{qj} will in general be different.

Suppose, though, that the matrices ${}^{\chi}M=({}^{\chi}M_{rp})$ and $S=(S_{rp})$ happened to commute. Then ${}^{\lambda}M$ and T

[14] M. Goeppert-Mayer and A. L. Sklar, J. Chem. Phys. **6**, 645 (1938).

[15] R. G. Parr, D. P. Craig, and I. G. Ross, J. Chem. Phys. **18**, 1561 (1950).

[16] R. McWeeny, Proc. Roy. Soc. (London) **A227**, 288 (1955). See also G. G. Hall, Trans. Faraday Soc. **50**, 773 (1954).

[17] C. C. J. Roothaan, Revs. Modern Phys. **23**, 69 (1951).

would commute,

$$\sum_s T_{rs}\,{}^{\lambda}M_{sq}=\sum_s {}^{\lambda}M_{rs}T_{sq}. \tag{26}$$

Therefore, multiplying Eq. (24) by T_{rs}, summing over s, and using Eqs. (26) and (17), one finds

$$\sum_s[{}^{\lambda}M_{rs}-\delta_{rs}\mu_j]C_{sj}=0. \tag{27}$$

That is, the C_{pj} satisfy the same secular equations as do the D_{qj}. Or: For a given j, the set D_{pj} differs from the set C_{pj} by a common constant factor at most, the $\overline{\text{MO}}$ and MO methods are equivalent in the complete sense, no error is incurred if the assumption is made in semiempirical calculations that the atomic orbitals of the problem are orthogonal.

As was first suggested by Löwdin,[10] alternant hydrocarbons are an important large class of molecules for which the assumption that the matrices S and ${}^{\kappa}M$ commute, with μ the LCAO SCF operator, should be very good.[18]

General Case

No matter what the molecule is, the MO and $\overline{\text{MO}}$ methods would be equivalent step by step if the operator μ were taken to be the same in Eqs. (23) and (25), although the C_{pj} and D_{qj} would be different.

Furthermore, the approximation that the matrices S and ${}^{\kappa}M$ commute may often be a good one, with μ the LCAO SCF operator, in which case the D_{qj} and C_{pj} will be nearly the same. (Peradejordi has demonstrated this for butadiene.[13]) It may then prove expeditious to solve Eq. 24 and make up for the minor deficiencies in the molecular orbitals obtained by a later configuration interaction calculation. Or, the operator μ might be slightly modified in order to make S and ${}^{\kappa}M$ commute and the D_{qj} and C_{pj} be the same, again with configuration interaction included later.[19]

Discussion

One may conclude from this discussion that purely theoretical $\overline{\text{MO}}$-type methods have advantages that could be explored further. Probably more important is the inference that semiempirical $\overline{\text{MO}}$-type methods have good justification; the atomic orbitals in the generalized Hückel method, for example, may be thought of as Löwdin orthogonalizations of ordinary atomic orbitals. The approximation of zero differential overlap then is the approximation that charge distributions which are products of orthogonalized atomic orbitals may be ignored. Further numerical calculations, checking this, would be helpful.

Interpretation of the basic integrals in the generalized Hückel method as over orthogonalized atomic orbitals has one consequence that has not yet been mentioned: The orthogonalized analog of each atomic orbital will have a form which varies from one molecule to the next. Because of this, the invariance of the basic integrals from one molecule to another, which has been postulated,[1–6] will require verification and perhaps modification.[20] A careful comparative study of the naphthalene and benzene molecules could shed much light on this question.

On the other hand, there is a final strong argument that can be given in favor of these semiempirical procedures.[21] The form of the "ordinary" atomic orbitals has not been specified anywhere in this discussion—it is a degree of freedom which one should recognize. Thus the precise values for the overlap integrals $S_{p'p}$ can be considered variable. (It has already been pointed out that the integrals ${}^{\kappa}M_{p'p}$ can be adjusted by changes in μ). Or, one can transform back from very good molecular orbitals to an orthogonalized atomic basis; this would make the orthogonalized atomic orbitals identical with what Lennard-Jones and Hall have termed equivalent orbitals.[16]

III. REMARK CONCERNING THE TREATMENT OF BENZENE-LIKE MOLECULES

In an earlier paper[6] equations were given for treating by the generalized Hückel method molecules like ethylene which have two π electrons, and it was demonstrated how setting up such a problem in a certain way gives formulas in which theoretical electronegativity differences appear perspicuously. Here the same sort of procedure will be applied to analogs of the benzene molecule.

A *benzene-like molecule* is defined as a molecule such as benzene, toluene, or pyridine, the properties of which may be well described in terms of the behavior of six π electrons which have available six $2\pi p$ atomic orbitals arranged more or less hexagonally. In toluene a better description requires explicit consideration of two extra π electrons from the CH_3 group (hyperconjugation); in the terminology that has been suggested[6] this would involve "mesomeric effects" of a substituent. The problem treated in the present paper is just the six-electron one—only "inductive effects" of substituents are covered.[22]

Encouraging results for the spectra of several nitrogen heterocyclic analogs of benzene have already been reported.[23] The present more systematic development will deal with all benzene-like molecules; it should provide

[18] See also B. H. Chirgwin, and C. A. Coulson, Proc. Roy. Soc. (London) **A201**, 196 (1950).

[19] For example, Mulliken-type approximations in the LCAO SCF operator probably reduce its commutator with S.

[20] Professor K. Ruedenberg has informed the author that he has developed a theory explicitly dealing with overlap of nearest neighbors. Also see work cited in footnote reference 29.

[21] Compare the introductory remarks in R. McWeeny, Proc. Roy. Soc. (London) **A237**, 355 (1956).

[22] See however Sec. 5 of footnote reference 6.

[23] Work cited in footnote 1, p. 767. R. C. Hirt, F. Halverson, and R. G. Schmitt, J. Chem. Phys. **22**, 1148 (1954); R. McWeeny and T. E. Peacock, Proc. Phys. Soc. (London) **A60**, 41 (1957); J. N. Murrell, Mol. Phys. **1**, 384 (1958).

TABLE I. Character table for the group C_6.[a]

$^6C_6$	Operation[b]					
Representation	E	C_6	C_6^2	C_6^3	C_6^4	C_6^5
Γ_0 or A	1	1	1	1	1	1
Γ_1 or E_{1+}	1	ω	ω^2	-1	ω^4	ω^5
Γ_{-1} or E_{1-}	1	ω^5	ω^4	-1	ω^2	ω
Γ_2 or E_{2+}	1	ω^2	ω^4	1	ω^2	ω^4
Γ_{-2} or E_{2-}	1	ω^4	ω^2	1	ω^4	ω^2
Γ_3 or B	1	-1	1	-1	1	-1

[a] The two degenerate representations of the group C_6 can be treated as made up of two one-dimensional representations each if complex characters are used, as shown: $\omega=\exp(2\pi i/6)$.

[b] Here C_6^n is the symmetry operation: rotate the molecule the angle $60n°$ about its sixfold axis of symmetry.

a useful framework for studying many properties of many such molecules.

Starting Wave Functions

The key to a simple and general treatment of benzene-like molecules is to set up the problem unprejudiced as to the type or location of the perturbation from the parent "standard" molecule benzene. With six π electrons and six $2p\pi$ overlapping atomic orbitals χ_0, χ_1, χ_2, χ_3, χ_4, χ_5 arranged hexagonally, the orthonormal molecular orbitals appropriate for the full benzene symmetry may be written, according to Eq. (21) (changing the numbering of the orbitals for convenience),

$$\phi_j=6^{-\frac{1}{2}}\sum_{p=0}^{5}\omega^{jp}\lambda_p, \qquad j=0,\pm1,\pm2,3, \qquad (28)$$

where $\omega=\exp(2\pi i/6)=\cos(2\pi/6)+i\sin(2\pi/6)$ and the λ_p are the orthonormal Löwdin analogs of the χ_p, expressible in terms of the χ_p by Eq. (17).

The subscript j which labels a molecular orbital indicates the irreducible representation of the group C_6 to which the orbital belongs. The character table for this group is given in Table I; the determination of the ϕ_j from this table and the transformation properties of the χ_p or λ_p follows the usual standard procedure.

Now the molecular orbitals of Eq. (28) will not be quite the best ones for the ground state of the arbitrary benzene-like molecule. For each molecule an LCAO SCF calculation could be performed to improve them,[17] but an alternative method is better. This is to make up for deficiencies in the Eq. (28) orbital description for a given state of a given molecule by linearly mixing in corresponding functions for other states—the configuration interaction procedure. Symmetry present in benzene itself will make many of the configuration interaction matrix elements zero for benzene itself; nonzero values of these elements in a molecule which does not have full benzene symmetry produce the same effects as would alteration of the linear coefficients in the LCAO MO. This method takes advantage of the uniquely simple form of the linear coefficients in the benzene orbitals, and it gives formulas which are quite general.

Of the great many "states" that could be admixed, only the most important will be considered here: the "ground state" coming from assignment of two electrons each to the lowest-energy molecular orbitals ϕ_0, ϕ_1, and ϕ_{-1} and the "singly excited states" coming from promotion of one electron from one of these orbitals to a higher orbital. Every such "one-electron jump" gives rise to one singlet and one triplet state, so that ten starting singlet wave functions and nine starting triplet wave functions are thus defined. In Table II these "set A starting functions are explicitly given in terms of Slater determinants formed from the basic one-electron orbitals of Eq. (28). The notation adopted is that V_{jk} represents the singlet state (or its wave function) arising from excitation of one electron from the orbital ϕ_j to the orbital ϕ_k from the (singlet) ground state N; T_{jk} represents the corresponding triplet.

The assumption now is that the ground-state π-electronic wave function of a benzene-like molecule and the wave functions for its lower π-excited states are expressible in the form

$$\Psi=A_1\Phi_1+A_2\Phi_2+\cdots, \qquad (29)$$

where the Φ are the starting functions of Table II, or suitable combinations of them. This would in fact give for the ground state a function equivalent to the LCAO SCF function, provided the SCF MO differed only infinitesimally from the MO of Eq. (28). (Just such a procedure has been effectively used by Brion and others[24] to generate SCF MO by successive approximations.) To get comparable accuracy for excited states one should include two-electron as well as one-electron jumps,[25] which will not be done here; nevertheless, the results for the lower excited states should be reasonably good.

The problem then is a linear variational one of some magnitude; in the general case determination of the coefficients A in Eq. (29) requires computation of a large number of matrix elements and solution of equations of high order.

The secular equations would be the more easily dealt with the more completely diagonal they were for the special case of full benzene symmetry. If the set A functions were used, the symmetry characteristics,

$$V_{jk} \text{ and } T_{jk} \subset \text{Representation } \Gamma_{k-j} \text{ of } C_6, \qquad (30)$$

[24] H. Brion, R. Lefebvre, and C. M. Moser, J. Chem. Phys. **23**, 1972 (1955). See also J. A. Pople, Proc. Roy. Soc. (London) **A233**, 233 (1955), and J. A. Pople and P. Schofield, idem **A233**, 241 (1955).

[25] The importance of two-electron jumps has been emphasized by J. N. Murrell and K. L. McEwen, J. Chem. Phys. **25**, 1143 (1956).

TABLE II. Starting wave functions for benzene-like molecules: set A.

Configuration[a]	Starting state[b,c]	Starting wave function[d,e]
$0^2 1^2 - 1^2$	$N \equiv V_{00}$	$(0\bar{0}1\bar{1}-1-\bar{1})$
$0^2 1 - 1^2 2$	V_{12} and T_{12}	$2^{-\frac{1}{2}}[(0\bar{0}1\bar{2}-1-\bar{1}) \pm (0\bar{0}2\bar{1}-1-\bar{1})]$
$0^2 1^2 - 1 - 2$	V_{-1-2} and T_{-1-2}	$2^{-\frac{1}{2}}[(0\bar{0}1\bar{1}-1-\bar{2}) \pm (0\bar{0}1\bar{1}-2-\bar{1})]$
$0^2 1 - 1^2 - 2$	V_{1-2} and T_{1-2}	$2^{-\frac{1}{2}}[(0\bar{0}1-\bar{2}-1-\bar{1}) \pm (0\bar{0}-2\bar{1}-1-\bar{1})]$
$0^2 1^2 - 12$	V_{-12} and T_{-12}	$2^{-\frac{1}{2}}[(0\bar{0}1\bar{1}-1\bar{2}) \pm (0\bar{0}1\bar{1}2-\bar{1})]$
$01^2 - 1^2 2$	V_{02} and T_{02}	$2^{-\frac{1}{2}}[(0\bar{2}1\bar{1}-1-\bar{1}) \pm (2\bar{0}1\bar{1}-1-\bar{1})]$
$01^2 - 1^2 - 2$	V_{0-2} and T_{0-2}	$2^{-\frac{1}{2}}[(0-2\bar{1}1-1-\bar{1}) \pm (-2\bar{0}1\bar{1}-1-\bar{1})]$
$0^2 1 - 1^2 3$	V_{13} and T_{13}	$2^{-\frac{1}{2}}[(0\bar{0}1\bar{3}-1-\bar{1}) \pm (0\bar{0}3\bar{1}-1-\bar{1})]$
$0^2 1^2 - 13$	V_{-13} and T_{-13}	$2^{-\frac{1}{2}}[(0\bar{0}1\bar{1}-1\bar{3}) \pm (0\bar{0}1\bar{1}3-\bar{1})]$
$01^2 - 1^2 3$	V_{03} and T_{03}	$2^{-\frac{1}{2}}[(0\bar{3}1\bar{1}-1-\bar{1}) \pm (3\bar{0}1\bar{1}-1-\bar{1})]$

[a] Here $0^2 1^2 - 1^2$, for example, denotes the configuration $\phi_0^2 \phi_1^2 \phi_{-1}^2$.
[b] These starting states do not necessarily correspond to actual molecular states. See text.
[c] V_{jk} and T_{jk} denote singlet and triplet starting states arising from the one-electron excitation $\phi_k \leftarrow \phi_j$ from the ground starting state N.
[d] Here $(0\bar{0}1\bar{1}-1-\bar{1})$, for example, denotes the normalized Slater determinant $(6!)^{-\frac{1}{2}}\Sigma^P(-1)^P[(\phi_0\alpha)^1(\phi_0\beta)^2(\phi_1\alpha)^3(\phi_1\beta)^4(\phi_{-1}\alpha)^5(\phi_{-1}\beta)^6]$.
[e] The upper sign goes with V, the lower sign with T. Only one component of the three degenerate components of each triplet state is listed.

plus the fact that nonzero interaction between two functions for benzene requires that their product have symmetry Γ_0, show that one would have nothing worse than a 3×3 equation for benzene, but one can in fact do much better than this if one replaces the set A functions of Table II with the set B functions of Table III.

The set B functions are, up to constant factors, sums and differences of set A functions which are degenerate because they are complex conjugates of each other. Regardless of the molecular symmetry,

$$V_{jk} = V_{-j-k}^* \quad \text{and} \quad T_{jk} = T_{-j-k}^*, \tag{31}$$

so that replacement of V_{jk} and V_{-j-k} by $V_{jk}^+ = 2^{-\frac{1}{2}}(V_{jk}+V_{-j-k})$ and $V_{jk}^- = i2^{-\frac{1}{2}}(V_{jk}-V_{-j-k})$ gives two real orthonormal functions, and similarly with the triplets. And, as will be shown, in the case of full benzene symmetry, $^+$ and $^-$ functions do not interact. Consequently in the case of full benzene symmetry the only interactions among the set B functions which are not zero are between V_{1-2}^+ and V_{03}, between V_{02}^+ and V_{13}^+, between V_{02}^- and V_{13}^-, and between the corresponding triplets.

The V_{03} and V_{13} states, and the T_{03} and T_{13} states, are accidentally almost degenerate in the benzene case, which suggests that a final transformation of the basic functions would bring the secular equations still closer to a completely diagonal form for the case of full benzene symmetry:

$$\begin{aligned}
V_{02}^{++} &= 2^{-\frac{1}{2}}(V_{02}^+ + V_{13}^+), & T_{02}^{++} &= 2^{-\frac{1}{2}}(T_{02}^+ + T_{13}^+),\\
V_{02}^{+-} &= 2^{-\frac{1}{2}}(V_{02}^+ - V_{13}^+), & T_{02}^{+-} &= 2^{-\frac{1}{2}}(T_{02}^+ - T_{13}^+),\\
V_{02}^{-+} &= 2^{-\frac{1}{2}}(V_{02}^- + V_{13}^-), & T_{02}^{-+} &= 2^{-\frac{1}{2}}(T_{02}^- + T_{13}^-),\\
V_{02}^{--} &= 2^{-\frac{1}{2}}(V_{02}^- - V_{13}^-), & T_{02}^{--} &= 2^{-\frac{1}{2}}(T_{02}^- - T_{13}^-).
\end{aligned} \tag{32}$$

TABLE III. Starting wave functions for benzene-like molecules: set B.[a]

Starting state[b,c]	Starting wave function[c,d,e]
N	N
V_{12}^+ and T_{12}^+	$V_{12}^+ = 2^{-\frac{1}{2}}(V_{-1-2}+V_{12})$ and $T_{12}^+ = 2^{-\frac{1}{2}}(T_{-1-2}+T_{12})$
V_{1-2}^+ and T_{1-2}^+	$V_{1-2}^+ = 2^{-\frac{1}{2}}(V_{1-2}+V_{-12})$ and $T_{1-2}^+ = 2^{-\frac{1}{2}}(T_{1-2}+T_{-12})$
V_{02}^+ and T_{02}^+	$V_{02}^+ = 2^{-\frac{1}{2}}(V_{0-2}+V_{02})$ and $T_{02}^+ = 2^{-\frac{1}{2}}(T_{0-2}+T_{02})$
V_{13}^+ and T_{13}^+	$V_{13}^+ = 2^{-\frac{1}{2}}(V_{-13}+V_{13})$ and $T_{13}^+ = 2^{-\frac{1}{2}}(T_{-13}+T_{13})$
V_{03} and T_{03}	V_{03} and T_{03}
V_{12}^- and T_{12}^-	$V_{12}^- = i2^{-\frac{1}{2}}(V_{-1-2}-V_{12})$ and $T_{12}^- = i2^{-\frac{1}{2}}(T_{-1-2}-T_{12})$
V_{1-2}^- and T_{1-2}^-	$V_{1-2}^- = i2^{-\frac{1}{2}}(V_{1-2}-V_{-12})$ and $T_{1-2}^- = i2^{-\frac{1}{2}}(T_{1-2}-T_{-12})$
V_{02}^- and T_{02}^-	$V_{02}^- = i2^{-\frac{1}{2}}(V_{0-2}-V_{02})$ and $T_{02}^- = i2^{-\frac{1}{2}}(T_{0-2}-T_{02})$
V_{13}^- and T_{13}^-	$V_{13}^- = i2^{-\frac{1}{2}}(V_{-13}-V_{13})$ and $T_{13}^- = i2^{-\frac{1}{2}}(T_{-13}-T_{13})$

[a] The final, set C, starting functions are these set B function modified as indicated in the text, Eq. (32).
[b] See Table II, note b.
[c] The symbols N, V, and T denote both states and wave functions for states.
[d] The wave functions are given in terms of the set A starting functions of Table II.
[e] In D_{6h} symmetry, the symmetries of these starting functions are as follows: $N \subset A_{1g}$; V_{12}^+, $V_{1-2}^- \subset E_{1u}$; V_{1-2}^+, $V_{03} \subset B_{1u}$; $V_{1-2}^- \subset B_{2u}$; V_{02}^+, V_{13}^+, V_{02}^-, $V_{13}^- \subset E_{2g}$; triplets same as corresponding singlets.

TABLE IV. Integrals over molecular orbitals for benzene-like molecules.

Symmetry classification[a]	Core integrals[b,d]	Electronic repulsion integrals[c,d]
Γ_0	$I_{00}=I_0=\epsilon_0$ $I_{1-1}=I_1=\epsilon_1$ $I_{2-2}=I_2=\epsilon_2$ $I_{3-3}=I_3=\epsilon_3$	$L_{00}=J_{ij}=J=\gamma_{ij}$ $L_{1-1}=K_{01}=\delta_{01}$ $L_{2-2}=K_{02}=\delta_{02}$ $L_{3-3}=K_{03}=\delta_{03}$
Γ_1 or Γ_{-1}	I_{10} and $I_{-10}=I_{10}^*$ I_{2-1} and $I_{-21}=I_{2-1}^*$ I_{3-2} and $I_{-32}=I_{3-2}^*$	L_{10} and $L_{-10}=L_{10}^*$ L_{2-1} and $L_{-21}=L_{2-1}$ L_{3-2} and $L_{-32}=L_{3-2}^*$
Γ_2 or Γ_{-2}	I_{11} and $I_{-1-1}=I_{11}^*$ I_{20} and $I_{-20}=I_{20}^*$ I_{3-1} and $I_{-31}=I_{3-1}^*$ I_{4-2} and $I_{-42}=I_{4-2}^*$	L_{11} and $L_{-1-1}=L_{11}^*$ L_{20} and $L_{-20}=L_{20}^*$ L_{3-1} and $L_{-31}=L_{3-1}^*$ L_{4-2} and $L_{-42}=L_{4-2}^*$
Γ_3	I_{21} and $I_{-21}=I_{21}^*$ I_{30} and $I_{-30}=I_{30}^*=I_{30}$ $I_{4-1}=I_{-2-1}$ and $I_{-41}=I_{21}=I_{4-1}^*$	L_{21} and $L_{-2-1}=L_{21}^*$ L_{30} and $L_{-30}=L_{30}^*=L_{30}$ $L_{4-1}=L_{-2-1}$ and $L_{-41}=L_{21}=L_{4-1}^*$

[a] Irreducible representation of group C_6, see Table I.

[b] For definition of I_{jk} see Eq. (35) of text. The contraction $I_j=I_{jj}$ is convenient; the notation $\epsilon_j=I_{jj}$ has also been used by certain authors.

[c] For definition of $L_{\mu\nu}$ see Eqs. (37) and (39) of text. The J, K notation for the first four of these integrals is more standard; the γ, δ notation has also been used by certain authors.

[d] For full benzene symmetry, all integrals vanish except those having symmetry Γ_0, leaving four distinct integrals of each type. In the general case, the number of *independent* integrals of each type is 21; the integrals, I_{-30}, I_{4-1}, I_{-41}, L_{-30}, L_{4-1} and L_{-41}, are redundant but are included for convenience.

These functions together with the other unmodified set B functions of Table III, N, V_{12}^+, V_{12}^-, V_{1-2}^+, V_{1-2}^-, V_{03}, T_{12}^+, T_{12}^-, T_{1-2}^+, T_{1-2}^-, T_{03}, are the final, set C, starting wave functions for the problem.

Secular Equations

The Hamiltonian operator for the π electrons has the form[9]

$$H=\sum_{\mu=1}^{6}H_{\text{core}}(\mu)+\tfrac{1}{2}\sum_{\mu,\nu=1}^{6}{}'\,(e^2/r_{\mu\nu}); \qquad (33)$$

the problem is to determine S-matrix elements,

$$S_{mn}=\int\Phi_m^*\Phi_n dv,$$

and H-matrix elements

$$H_{mn}=(\Phi_m\,||\,\Phi_n)=\int\Phi_m^*H\Phi_n dv, \qquad (34)$$

where the Φ are the set C starting functions of Table III and Eq. (32). The secular equations for the singlet and triplet states then are 10×10 and 9×9 equations of the form $|(H_{mn}-S_{mn}E)|=0$, where E is the total π-electron energy; the corresponding wave functions are of the form of Eq. (29), with $\sum_n A_n(H_{mn}-S_{mn}E)=0$.

The set C functions are orthonormal by construction; hence $S_{mn}=\delta_{mn}$. The H matrix presents more difficulty. Rules for obtaining matrix elements between Slater determinants for an operator of the form of Eq. (33) are available, however,[26] and each set C function is a linear combination of Slater determinants. Such matrix elements always are expressible as linear combinations of two kinds of integrals over the molecular orbitals ϕ_j, integrals arising from the terms H_{core} in Eq. (33) and integrals arising from the terms $e^2/r_{\mu\nu}$.

The first class of integrals are the core integrals,

$$I_{jk}=\int\phi_j(1)H_{\text{core}}(1)\phi_k(1)dv(1). \qquad (35)$$

There are 21 distinct ones of these, since from Eqs. (28) and (35) one has the identities

$$I_{jk}=I_{kj}=I_{-j-k}^*=I_{j,k+6}=I_{j+6,k}. \qquad (36)$$

In Table IV are listed those of these integrals, which are taken here as independent, and their symmetry classifications.

The second class of integrals are the electronic repulsion integrals,

$$(ij\,|\,kl)$$

$$=\iint\phi_i^*(1)\phi_k^*(2)(e^2/r_{12})\phi_j(1)\phi_l(2)dv(1)dv(2). \qquad (37)$$

There are a great many of these. If, however, one assumes *zero differential overlap*,

$$\lambda_p(1)\lambda_q(1)dv(1)=0 \quad \text{for} \quad p\neq q, \qquad (38)$$

one can see that two indices, $\mu=j-i$ and $\nu=l-k$, suffice to define these integrals, so that a more compact notation suffices for them:

$$L_{\mu\nu}=(i,\,i+\mu\,|\,k,\,k+\nu). \qquad (39)$$

Further, one has the identities,

$$L_{\mu\nu}=L_{\nu\mu}=L_{-\mu-\nu}^*=L_{\mu,\nu+6}=L_{\mu+6,\nu}. \qquad (40)$$

[26] For example, E. U. Condon and G. H. Shortley, *Theory of Atomic Spectra* (Cambridge University Press, Cambridge, England, 1935).

Consequently the number independent of these integrals also is 21; in Table IV are listed those here chosen as basic and their symmetries.

In Table V the H matrices for the singlet and triplet states of benzene-like molecules are given in terms of real parts, I_{jk}^{r} and $L_{\mu\nu}^{r}$, and imaginary parts, I_{jk}^{i} and $L_{\mu\nu}^{i}$, of the integrals $I_{jk}=I_{jk}^{r}+iI_{jk}^{i}$ and $L_{\mu\nu}=L_{\mu\nu}^{r}+iL_{\mu\nu}^{i}$ listed in Table IV.

Three sample calculations of H-matrix elements may be given without detailed comment:

$$
\begin{aligned}
(N\,||\,N)&=[(0\bar{0}1\bar{1}-1-\bar{1})\,||\,(0\bar{0}1\bar{1}-1-\bar{1})]\\
&=2I_{00}+2I_{-11}+2I_{1-1}+J_{00}+(4J_{01}-2K_{01})\\
&+(4J_{0-1}-2K_{0-1})+J_{11}+(4J_{1-1}-2K_{1-1})+J_{-1-1}\\
&=2I_0+4I_1+15J-4K_{01}-2K_{02},\\
(N\,||\,V_{12}{}^{+})&=2^{-\frac{1}{2}}[(N\,||\,V_{-1-2})+(N\,||\,V_{12})]\\
&=2^{-\frac{1}{2}}[(N\,||\,V_{12})^{*}+(N\,||\,V_{12})]\\
&=2^{\frac{1}{2}}\,\mathrm{Re}(N\,||\,V_{12})\\
&=\mathrm{Re}\{[(0\bar{0}1\bar{1}-1-\bar{1})\,||\,(0\bar{0}1\bar{2}-1-\bar{1})]\\
&\quad+[(0\bar{0}1\bar{1}-1-\bar{1})\,||\,(0\bar{0}2\bar{1}-1-\bar{1})]\}\\
&=2\,\mathrm{Re}[(0\bar{0}1\bar{1}-1-\bar{1})\,||\,(0\bar{0}1\bar{2}-1-\bar{1})]\\
&=2\,\mathrm{Re}[I_{-12}+2(12\,|\,00)-(10\,|\,02)\\
&\quad+(12\,|\,11)+2(12\,|\,-1-1)-(1-1\,|\,-12)]\\
&=2(I_{2-1}+5L_{10}-L_{2-1}-L_{3-2})^{r},\\
(V_{12}{}^{+}\,||\,V_{12}{}^{-})&=\tfrac{1}{2}i[V_{-1-2}+V_{12})\,||\,(V_{-1-2}-V_{12})]\\
&=-\tfrac{1}{2}i\{[V_{12}\,||\,V_{12})-(V_{12}\,||\,V_{12})^{*}]\\
&\quad+[(V_{-1-2}\,||\,V_{12})-(V_{-1-2}\,||\,V_{12})^{*}]\}\\
&=\mathrm{Im}[(V_{12}\,||\,V_{12})+(V_{-1-2}\,||\,V_{12})]\\
&=\mathrm{Im}(V_{-1-2}\,||\,V_{12})\\
&=\tfrac{1}{2}\,\mathrm{Im}\{[(0\bar{0}1\bar{1}-1-\bar{2})+(0\bar{0}1\bar{1}-2-\bar{1})]\,||\\
&\quad\times[(0\bar{0}1\bar{2}-1-\bar{1})+(0\bar{0}2\bar{1}-1-\bar{1})]\}\\
&=\mathrm{Im}\{[(0\bar{0}1\bar{1}-1-\bar{2})\,||\,(0\bar{0}1\bar{2}-1-\bar{1})]\\
&\quad+[(0\bar{0}1\bar{1}-1-\bar{2})\,||\,(0\bar{0}2\bar{1}-1-\bar{1})]\}\\
&=\mathrm{Im}[(12\,|\,-2-1)-(1-1\,|\,-22)\\
&\quad+(12\,|\,-2-1)]\\
&=(2L_{11}-L_{4-2})^{i}.
\end{aligned}
$$

Here Re and Im refer to real and imaginary parts of the quantities indicated; other notations are explained in Table IV.

Reduction to Integrals over Atomic Orbitals

The matrix elements in Table V are expressible in terms of integrals over orthogonalized atomic orbitals λ_p, through the use of Eq. (28). These integrals again involve either the core Hamiltonian or electron repulsion, and there are again 21 independent ones of each type. These are listed in Table VI.

The matrix elements can be classified by their symmetry, according to the rules

$$
\begin{aligned}
&I_{jk}\subset\text{Representation }\Gamma_{j+k}\text{ of }C_6,\\
&L_{\mu\nu}\subset\text{Representation }\Gamma_{\mu+\nu}\text{ of }C_6.
\end{aligned}
\tag{41}
$$

It, therefore, is expedient to introduce as the entities to be algebraically manipulated in the problem *symmetry combinations* of the basic atomic integrals; these are listed in Table VII.

One then has, in the notation of the tables,

$$
\begin{aligned}
I_{jk}&=A_{j+k}+2B_{j+k}{}^{01}\cos[(j-k)\pi/6]\\
&\quad+2B_{j+k}{}^{02}\cos[(j-k)\pi/3]+B_{j+k}{}^{03}\cos[(j-k)\pi/2]
\end{aligned}
\tag{42}
$$

and

$$
\begin{aligned}
L_{\mu\nu}&=C_{\mu+\nu}{}^{00}+2C_{\mu+\nu}{}^{01}\cos[(\mu-\nu)\pi/6]\\
&\quad+2C_{\mu+\nu}{}^{02}\cos[(\mu-\nu)\pi/3]+C_{\mu+\nu}{}^{03}\cos[(\mu-\nu)\pi/2].
\end{aligned}
\tag{43}
$$

From these two basic formulas one can determine any desired I_{jk} or $L_{\mu\nu}$ for any given values of the integrals in Table VII, and hence determine all secular equation elements in Table V for given values of the integrals.

Simplification: Introduction of Atomic Electronegativities

The quantities A_j, which enter the secular equations through the dependence of the I_{jk} on them, Eq. (42), are symmetry combinations of the α_p; each α_p in turn is a one-electron energy in the field of the molecular core, for an electron in a Löwdin orbital λ_p. An approximate treatment of these terms much simplifies the secular equations.

The first approximation is that in those combinations of the α_p which vanish for full benzene symmetry; the Löwdin orbitals λ can be replaced by the nonorthogonal atomic orbitals χ, that is,

$$
A_j\approx{}^{\chi}A_j=(1/6)\sum_p\omega^{jp}{}^{\chi}\alpha_p,\qquad j\neq 0,
\tag{44}
$$

where

$$
{}^{\chi}\alpha_p=\int\chi_p{}^{*}(1)H_{\mathrm{core}}(1)\chi_p(1)\,dv(1).
\tag{45}
$$

Strictly speaking the α_p contain not only terms ${}^{\chi}\alpha_p$ but also terms ${}^{\chi}\beta_{pq}$, but it is reasonable to suppose that these last cancel in the A_j having $j\neq 0$. (In A_0, which would enter importantly the theoretical expression for the ionization potential, for example, this approximation would not be so good.)

TABLE V. H matrices for singlet and triplet states of benzene-like molecules in terms of integrals over molecular orbitals.

Matrix element[a]	Formula[b,c,d]	Corresponding triplet element[c,e]
$(N \mid\mid N)$	$2I_0+4I_1+15J-4K_{01}-2K_{02}$	—
$(V_{12}^+ \mid\mid V_{12}^+)$	$-I_1+I_2+2K_{01}-K_{03}+[2L_{11}-L_{4-2}]^r$	$-2K_{01}-[2L_{11}]^r$
$(V_{1-2}^+ \mid\mid V_{1-2}^+)$	$-I_1+I_2-K_{02}+3K_{03}$	$-4K_{03}$
$(V_{02}^{++} \mid\mid V_{02}^{++})$	$-\frac{1}{2}(I_0+I_1)+\frac{1}{2}(I_2+I_3)+3K_{02}-K_{03}+\frac{1}{2}[I_{4-2}+I_{11}-2L_{3-1}+7L_{4-2}-L_{11}]^r$	$-4K_{02}-[4L_{4-2}]^r$
$(V_{02}^{+-} \mid\mid V_{02}^{+-})$	$-\frac{1}{2}(I_0+I_1)+\frac{1}{2}(I_2+I_3)+2K_{01}-K_{02}-K_{03}+\frac{1}{2}[I_{4-2}-I_{11}-2L_{3-1}-L_{4-2}+3L_{11}]^r$	same
$(V_{03} \mid\mid V_{03})$	$-I_0+I_3+2K_{01}-2K_{02}+K_{03}$	$-2K_{03}$
$(V_{12}^- \mid\mid V_{12}^-)$	$-I_1+I_2+2K_{01}-K_{03}-[2L_{11}-L_{4-2}]^r$	$-2K_{01}+[2L_{11}]^r$
$(V_{1-2}^- \mid\mid V_{1-2}^-)$	$-I_1+I_2+K_{02}-K_{03}$	same
$(V_{02}^{-+} \mid\mid V_{02}^{-+})$	$-\frac{1}{2}(I_0+I_1)+\frac{1}{2}(I_2+I_3)+3K_{02}-K_{03}-\frac{1}{2}[I_{4-2}-I_{11}-2L_{3-1}+7L_{4-2}-L_{11}]^r$	$-4K_{02}+[4L_{4-2}]^r$
$(V_{02}^{--} \mid\mid V_{02}^{--})$	$-\frac{1}{2}(I_0+I_1)+\frac{1}{2}(I_2+I_3)+2K_{01}-K_{02}-K_{03}-\frac{1}{2}[I_{4-2}-I_{11}-2L_{3-1}-L_{4-2}+3L_{11}]^r$	same
$(N \mid\mid V_{12}^+)$	$2[I_{2-1}+5L_{10}-L_{3-2}-L_{3-2}]^r$	0
$(N \mid\mid V_{1-2}^+)$	$2[I_{21}+5L_{30}-2L_{21}]^r$	0
$(N \mid\mid V_{02}^{++})$	$2^{\frac{1}{2}}[I_{20}+I_{3-1}+10L_{20}-2L_{3-1}-L_{11}-L_{4-2}]^r$	0
$(N \mid\mid V_{02}^{+-})$	$2^{\frac{1}{2}}[I_{20}-I_{3-1}-L_{11}+L_{4-2}]^r$	0
$(N \mid\mid V_{03})$	$2^{\frac{1}{2}}[I_{30}+5L_{40}-2L_{21}]^r$	0
$(N \mid\mid V_{12}^-)$	$2[I_{2-1}+5L_{10}-L_{3-1}-L_{3-2}]^i$	0
$(N \mid\mid V_{1-2}^-)$	$2[I_{21}+5L_{30}-2L_{21}]^i$	0
$(N \mid\mid V_{02}^{-+})$	$2^{\frac{1}{2}}[I_{20}+I_{3-1}+10L_{20}-2L_{3-1}-L_{11}-L_{4-2}]^i$	0
$(N \mid\mid V_{02}^{--})$	$2^{\frac{1}{2}}[I_{20}-I_{3-1}-L_{11}+L_{4-2}]^i$	0
$(V_{12}^+ \mid\mid V_{1-2}^+)$	$[I_{4-2}-I_{11}+L_{11}+2L_{3-1}-L_{4-2}]^r$	$-[4L_{3-1}]^r$
$(V_{12}^+ \mid\mid V_{02}^{++})$	$2^{-\frac{1}{2}}[I_{3-2}-I_{10}-2L_{3-2}+4L_{2-1}-2L_{4-1}+4L_{21}]^r$	$-2^{-\frac{1}{2}}[4L_{3-1}+4L_{21}]^r$
$(V_{12}^+ \mid\mid V_{02}^{+-})$	$-2^{-\frac{1}{2}}[I_{3-2}+I_{10}+10L_{10}-2L_{3-2}-2L_{3-1}]^r$	same
$(V_{12}^+ \mid\mid V_{03})$	$2^{\frac{1}{2}}[2L_{3-1}-L_{11}]^r$	$-2^{-\frac{1}{2}}[2L_{3-1}]^r$
$(V_{12}^+ \mid\mid V_{12}^-)$	$[2L_{11}-L_{4-2}]^i$	$-[2L_{11}]^i$
$(V_{12}^+ \mid\mid V_{1-2}^-)$	$-[I_{4-2}+I_{11}+10L_{20}-2L_{3-1}-L_{4-2}-L_{11}]^i$	same
$(V_{12}^+ \mid\mid V_{02}^{-+})$	$2^{-\frac{1}{2}}[I_{3-2}-I_{10}-2L_{3-2}+4L_{2-1}-2L_{4-1}+4L_{21}]^i$	$-2^{-\frac{1}{2}}[4L_{3-1}+4L_{21}]^i$
$(V_{12}^+ \mid\mid V_{02}^{--})$	$-2^{-\frac{1}{2}}[I_{3-2}+I_{10}+10L_{10}-2L_{3-2}-2L_{3-1}]^i$	same
$(V_{1-2}^+ \mid\mid V_{03}^{++})$	$2^{-\frac{1}{2}}[I_{3-2}-I_{10}+6L_{3-2}-2L_{3-1}]^r$	$-2^{-\frac{1}{2}}[8L_{3-2}]^r$
$(V_{1-2}^+ \mid\mid V_{02}^{+-})$	$-2^{-\frac{1}{2}}[I_{3-2}+I_{10}+10L_{10}-2L_{3-2}-2L_{3-1}]^r$	same
$(V_{1-2}^+ \mid\mid V_{03})$	$2^{\frac{1}{2}}(2K_{03}-K_{01})$	$-2^{-\frac{1}{2}}[2K_{03}]$
$(V_{1-2}^+ \mid\mid V_{12}^-)$	$-[I_{4-2}-I_{11}+L_{11}+2L_{3-1}-L_{4-2}]^i$	$+[4L_{3-1}]^i$
$(V_{1-2}^+ \mid\mid V_{1-2}^-)$	0	same
$(V_{1-2}^+ \mid\mid V_{02}^{-+})$	$-2^{-\frac{1}{2}}[I_{3-2}-I_{10}+6L_{3-2}-2L_{3-1}]^i$	$+2^{-\frac{1}{2}}[8L_{3-2}]^i$
$(V_{1-2}^+ \mid\mid V_{03}^{--})$	$2^{-\frac{1}{2}}[I_{3-2}+I_{10}+10L_{10}-2L_{3-2}-2L_{3-1}]^i$	same

TABLE V.—*Continued.*

Matrix elements[a]	Formula[b,c,d]	Corresponding triplet element[c,e]
$(V_{02}^{++} \mid\mid V_{02}^{+-})$	$-\frac{1}{2}(I_0-I_1-I_2+I_3)+[I_{4-2}+I_{11}+10L_{20}-2L_{2-1}-L_{4-2}-L_{11}]^r$	same
$(V_{02}^{++} \mid\mid V_{00})$	$[I_{2-2}-I_{10}+2L_{0-2}]^r$	$-[4L_{0-2}]^r$
$(V_{02}^{++} \mid\mid V_{12}^{--})$	$-2^{-\frac{1}{2}}[I_{2-2}-I_{10}-2L_{2-2}+4L_{2-1}+2L_{4-1}-4L_{21}]^i$	$+2^{-\frac{1}{2}}[4L_{2-1}-4L_{21}]^i$
$(V_{02}^{++} \mid\mid V_{1-2}^{--})$	$-2^{-\frac{1}{2}}[I_{2-2}+I_{10}+10L_{10}-2L_{2-2}-2L_{2-1}]^i$	same
$(V_{02}^{++} \mid\mid V_{02}^{-+})$	$-\frac{1}{2}[I_{4-2}-I_{11}-2L_{2-1}+7L_{4-2}-L_{11}]^i$	$+[4L_{4-2}]^i$
$(V_{02}^{++} \mid\mid V_{02}^{--})$	$-\frac{1}{2}[I_{4-2}+I_{11}+10L_{20}-2L_{2-1}-L_{4-2}-L_{11}]^i$	same
$(V_{02}^{+-} \mid\mid V_{00})$	$[I_{2-2}+I_{10}+10L_{10}-2L_{2-2}-2L_{2-1}]^r$	same
$(V_{02}^{+-} \mid\mid V_{12}^{--})$	$2^{-\frac{1}{2}}[I_{2-2}+I_{10}+10L_{10}-2L_{2-2}-2L_{2-1}]^i$	same
$(V_{02}^{+-} \mid\mid V_{1-2}^{--})$	$2^{-\frac{1}{2}}[I_{2-2}-I_{10}+2L_{2-1}-2L_{2-2}]^i$	same
$(V_{02}^{+-} \mid\mid V_{02}^{-+})$	$-\frac{1}{2}[I_{4-2}+I_{11}+10L_{20}-2L_{2-1}-L_{4-2}-L_{11}]^i$	same
$(V_{02}^{+-} \mid\mid V_{02}^{--})$	$-\frac{1}{2}[I_{4-2}-I_{11}-2L_{2-1}-L_{4-2}+3L_{11}]^i$	same
$(V_{00} \mid\mid V_{12}^{--})$	$-2^{\frac{1}{2}}[2L_{2-1}-L_{11}]^i$	$+2^{\frac{1}{2}}[2L_{2-1}]^i$
$(V_{00} \mid\mid V_{1-2}^{--})$	0	same
$(V_{00} \mid\mid V_{02}^{-+})$	$-[I_{2-2}-I_{10}+2L_{0-2}]^i$	$+[4L_{0-2}]^i$
$(V_{00} \mid\mid V_{02}^{--})$	$-[I_{2-2}+I_{10}+10L_{10}-2L_{0-2}-2L_{2-1}]^i$	same
$(V_{12}^{--} \mid\mid V_{1-2}^{--})$	$-[I_{4-2}+I_{11}+10L_{20}-2L_{2-1}-L_{1-2}-L_{11}]^r$	same
$(V_{12}^{--} \mid\mid V_{02}^{-+})$	$2^{-\frac{1}{2}}[I_{2-2}-I_{10}-2L_{2-2}+4L_{2-1}+2L_{4-1}-4L_{21}]^r$	$-2^{-\frac{1}{2}}[4L_{2-1}-4L_{21}]^r$
$(V_{12}^{--} \mid\mid V_{02}^{--})$	$-2^{-\frac{1}{2}}[I_{2-2}+I_{10}+10L_{10}-2L_{2-2}-2L_{2-1}]^r$	same
$(V_{1-2}^{--} \mid\mid V_{02}^{-+})$	$-2^{-\frac{1}{2}}[I_{2-2}+I_{10}+10L_{10}-2L_{2-2}-2L_{2-1}]^r$	same
$(V_{1-2}^{--} \mid\mid V_{02}^{--})$	$2^{-\frac{1}{2}}[I_{2-2}-I_{10}+2L_{2-1}-2L_{2-2}]^r$	same
$(V_{02}^{-+} \mid\mid V_{02}^{--})$	$-\frac{1}{2}(I_0-I_1-I_2+I_3)-\frac{1}{2}[I_{4-2}+I_{11}+10L_{20}-2L_{2-1}-L_{4-2}-L_{11}]^r$	same

[a] $(\Phi_m \mid\mid \Phi_N)=\int \Phi_m^* H \Phi_n d\tau$, where the Φ are the real set C functions of Table III and Eq. (32).
[b] For definitions of I_{jk} and $L_{\mu\nu}$, see Eqs. (35), (37), and (39) of text.
[c] For full benzene symmetry, all terms in brackets [ ] vanish. For full benzene symmetry, therefore, the only nonzero off-diagonal matrix elements are

$$(V_{1-2}^{+} \mid V_{00}),\ (V_{02}^{++} \mid\mid V_{02}^{+-}),\ (V_{02}^{-+} \mid\mid V_{02}^{--}),$$

and the corresponding triplet elements.
[d] Except for $(N \mid\mid N)$ itself, diagonal elements are relative to $(N \mid\mid N)$.
[e] All elements relative to the corresponding singlet elements in the previous column, except those which are zero, which are so marked.

Elucidation of the ${}^x\alpha_p$ now follows familiar lines.[1,8,14] Breaking down H_{core}, one finds

$${}^x\alpha_p=-I_p-P_p-\sum_{q\neq p}\gamma_{pq}, \tag{46}$$

where I_p is the ionization potential for a neutral atom p and P_p is the total attraction of the neutral atom p in the molecule for the rest of the molecule; the γ_{pq} strictly are electron repulsion integrals over the χ, but they may be supposed instead to be over the λ (actually, the corresponding terms in α_p involve both the χ and the λ). One also sets[1,4]

$$\gamma_{pp}=I_p-A_p, \tag{47}$$

where A_p is the electron affinity for atom p, and one defines the *effective electronegativity* of atom p in the molecule as[8]

$$y_p=\tfrac{1}{2}(I_p+A_p)+P_p. \tag{48}$$

Then one obtains

$${}^x\alpha_p=-y_p-\tfrac{1}{2}\gamma_{pp}-\sum_{q\neq p}\gamma_{pq}, \tag{49}$$

and finally, for $j\neq 0$,

$$A_j\approx -Y_j-6L_{j0}-\tfrac{1}{2}(\textstyle\sum L_{\mu\nu})_j. \tag{50}$$

Here $(\sum L_{\mu\nu})_j$ is the sum over $\mu-\nu=0,\ \pm 2,\ \pm 4,\ 6$ or $\pm 1,\ \pm 3,\ \pm 5$ of all the $L_{\mu\nu}$ having $\mu+\nu=j$, and the

TABLE VI. Integrals over atomic orbitals for benzene-like molecules.

Core integrals[a,c]	Electronic repulsion integrals[b,c]
α_0	γ_{00}
α_1	γ_{11}
α_2	γ_{22}
α_3	γ_{33}
α_4	γ_{44}
α_5	γ_{55}
β_{01}	γ_{01}
β_{12}	γ_{12}
β_{23}	γ_{23}
β_{34}	γ_{34}
β_{45}	γ_{45}
β_{50}	γ_{50}
β_{02}	γ_{02}
β_{13}	γ_{13}
β_{24}	γ_{24}
β_{35}	γ_{35}
β_{40}	γ_{40}
β_{51}	γ_{51}
β_{03}	γ_{03}
β_{14}	γ_{14}
β_{25}	γ_{25}

[a] $\alpha_p=\int\lambda_p^*(1)H_{\text{core}}(1)\lambda_p(1)d\tau(1)$; $\beta_{pq}=\int\lambda_p^*(1)H_{\text{core}}(1)\lambda_q(1)d\tau(1)$.
[b] $\gamma_{pq}=\int\int\lambda_p^*(1)\lambda_p(1)(e^2/r_{12})\lambda_q^*(2)\lambda_q(2)d\tau(1)d\tau(2)$.
[c] For full benzene symmetry, only four core integrals are distinct, α_0, β_{01}, β_{02}, and β_{03}; and only four electronic repulsion integrals, γ_{00}, γ_{01}, γ_{02}, and γ_{03}.

quantities

$$Y_j=(1/6)\sum_p\omega^{jp}y_p \tag{51}$$

are generalized electronegativity differences—symmetry combinations of effective atomic electronegativities. Specifically, Eq. (50) gives the following approximate equations:

$$\begin{aligned}A_1+5L_{10}-L_{2-1}-L_{3-2}&\approx -Y_1,\\ A_2+5L_{20}-2L_{3-1}-L_{4-2}-L_{11}&\approx -Y_2,\\ A_3+5L_{30}-2L_{21}&\approx -Y_3.\end{aligned} \tag{52}$$

TABLE VII. Symmetry combinations of integrals over atomic orbitals for benzene-like molecules.[a,b]

Core integrals[c,d]	Electronic repulsion integrals[c,d]
$A_j=B_j^{00}=(1/6)\Sigma_p\omega^{jp}\alpha_p$	$C_j^{00}=(1/36)\Sigma_p\omega^{jp}\gamma_{pp}$
$B_j^{01}=(1/6)\Sigma_p\omega^{j(p+1)}\beta_{p,p+1}$	$C_j^{01}=(1/36)\Sigma_p\omega^{j(p+1)}\gamma_{p,p+1}$
$B_j^{02}=(1/6)\Sigma_p\omega^{j(p+1)}\beta_{p,p+2}$	$C_j^{02}=(1/36)\Sigma_p\omega^{j(p+1)}\gamma_{p,p+2}$
$B_j^{03}=(1/6)\Sigma_p\omega^{j(p+1)}\beta_{p,p+3}$	$C_j^{03}=(1/36)\Sigma_p\omega^{j(p+1)}\gamma_{p,p+3}$

[a] Sums over p are from 0 to 5; $\omega=\exp(2\pi i/6)$.
[b] The subscript j indicates the irreducible representation of the group C_6 to which a given symmetry combination belongs.
[c] For full benzene symmetry, all symmetry combinations not having $j=0$ vanish, leaving four distinct core integrals and four distinct electronic repulsion integrals: $A_0=\alpha_0$, $B_0^{01}=\beta_{01}$, $B_0^{02}=\beta_{02}$, and $B_0^{03}=\beta_{03}$; $C_0^{00}=1/6\gamma_{00}$, $C_0^{01}=1/6\gamma_{01}$, $C_0^{02}=1/6\gamma_{01}$ and $C_0^{03}=1/6\gamma_{03}$.
[d] In each case $j=0$, ±1, ±2, 3, with the $j=\pm1$ and $j=3$ integrals redundant for B_j^{03} and C_j^{03}. Thus the number of *independent* integrals of each type in the most general case is 21.

TABLE VIII. Simplified formulas for selected matrix elements.[a]

Matrix element[b]	Formula[b]	Corresponding triplet element[b]
$(N \mid\mid V_{12}^+)$	$-2Y_1^r$	0
$(N \mid\mid V_{1-2}^+)$	$-2Y_3^r$	0
$(N \mid\mid V_{02}^{++})$	$-8^{\frac{1}{2}}Y_2^r$	0
$(N \mid\mid V_{02}^{+-})$	$-2^{\frac{1}{2}}(-2B_2^{01}+L_{11}-L_{4-2})^r$	0
$(N \mid\mid V_{03})$	$-2^{\frac{1}{2}}Y_3^r$	0
$(N \mid\mid V_{12}^-)$	$-2Y_1^i$	0
$(N \mid\mid V_{1-2}^-)$	$-12^{\frac{1}{2}}(-B_2^{01})^i$	0
$(N \mid\mid V_{02}^{-+})$	$-8^{\frac{1}{2}}Y_2^i$	0
$(N \mid\mid V_{02}^{--})$	$-2^{\frac{1}{2}}(-2B_2^{01}+L_{11}-L_{4-2})^i$	0
$(V_{12}^+ \mid\mid V_{1-2}^+)$	$(-4B_2^{01}+L_{11}+2L_{3-1}-L_{4-2})^r$	$-4L_{3-1}^r$
$(V_{12}^+ \mid\mid V_{12}^-)$	$(2L_{11}-L_{4-2})^i$	$-2L_{11}^i$
$(V_{12}^+ \mid\mid V_{1-2}^-)$	$2Y_2^i$	same
$(V_{1-2}^+ \mid\mid V_{12}^-)$	$-(-4B_2^{01}+L_{11}+2L_{3-1}-L_{4-2})^i$	$+4L_{3-1}^i$
$(V_{1-2}^+ \mid\mid V_{1-2}^-)$	0	same
$(V_{12}^- \mid\mid V_{1-2}^-)$	$2Y_2^r$	same

[a] From Table V and Eqs. (42), (52), and (53).
[b] See Table V, notes a, b, and e.

TABLE IX. H matrices for benzene-like molecules possessing a vertical plane of symmetry.[a,b]

Matrix element[c,d]	Formula[e]	Corresponding triplet element[f]
$(N \mid\mid N)$	$2I_0+4I_1+15J-4K_{01}-2K_{02}$	—
$(N \mid\mid V_{12}^+)$	$[-2Y_1]^r$	0
$(N \mid\mid V_{1-2}^+)$	$[-2Y_3]^r$	0
$(N \mid\mid V_{12}^-)$	0	0
$(N \mid\mid V_{1-2}^-)$	0	0
$(V_{12}^+ \mid\mid V_{12}^+)$	$-I_1+I_2+2K_{01}-K_{02}+[2L_{11}-L_{4-2}]^r$	$-2K_{01}-[2L_{11}]^r$
$(V_{12}^+ \mid\mid V_{1-2}^+)$	$[-4B_2^{01}+L_{11}+2L_{3-1}-L_{4-2}]^r$	$[-4L_{3-1}]^r$
$(V_{12}^+ \mid\mid V_{12}^-)$	0	0
$(V_{12}^+ \mid\mid V_{1-2}^-)$	0	0
$(V_{1-2}^+ \mid\mid V_{1-2}^+)$	$-I_1+I_2-K_{02}+3K_{03}$	$-4K_{03}$
$(V_{1-2}^+ \mid\mid V_{12}^-)$	0	0
$(V_{1-2}^+ \mid\mid V_{1-2}^-)$	0	0
$(V_{12}^- \mid\mid V_{12}^-)$	$-I_1+I_2+2K_{01}-K_{02}-[2L_{11}-L_{4-2}]^r$	$-2K_{01}+[2L_{11}]^r$
$(V_{12}^- \mid\mid V_{1-2}^-)$	$[2Y_2]^r$	same
$(V_{1-2}^- \mid\mid V_{1-2}^-)$	$-I_1+I_2+K_{02}-K_{02}$	same

[a] From Tables V and VIII, from which matrix elements involving higher states also may be determined. To obtain matrix elements in terms of integrals over atomic orbitals, use Eqs. (42) and (43).
[b] Plane of symmetry through atoms 0 and 3, or bonds 0—1 and 3—4.
[c] See Table V, note a.
[d] For D_{6h} symmetries, see Table III, note e.
[e] See Table V, notes b to d.
[f] See Table V, note e.

A second approximation, of comparable accuracy, is that the nonneighbor β_{pq} may be neglected in those combinations of the β_{pq} which vanish for full benzene symmetry, that is,

$$B_j^{02} \approx 0 \quad \text{and} \quad B_j^{03} \approx 0 \quad \text{for} \quad j \neq 0. \qquad (53)$$

Equations (52) and (53), together with Eq. (42), lead to considerable simplification in many of the matrix elements in Table V. Modified formulas for some of the most important are displayed in Table VIII.

Secular Equations for Molecules with a Vertical Plane of Symmetry

While the present purpose is not to perform specific calculations, it may be useful to display the formulas for one special case of very frequent occurrence, that in which the molecule retains one or more planes of symmetry in addition to the molecular plane. If such a plane passes through either atoms 0 and 3 (for example, any mono-substituted benzene) or through bonds 0—1 and 3—4 (for example, any ortho di-substituted benzene), all interactions between + and − states vanish, and one gets the simplified secular equation matrix elements listed in Table IX.

For such molecules the secular equations take factored forms, with further simplifications for cases of still greater symmetry. Table IX includes as special cases, among others, the secular equations for *s*-triazine, pyridine, pyrazine, and pyrimidine given in Tables VIII–XI of the second work cited in footnote 1, and the secular equations for borazole.

It will be noted that effects of perturbations are of two kinds, nonvectorial and vectorial, or symmetry-independent and symmetry dependent. A perturbation may affect one or more of the basic integrals of Table VI and hence change the integrals I_0, I_1, I_2, J, K_{01}, K_{02}, K_{03} which enter the formulas of Table IX even for full benzene symmetry. Or, depending on its symmetry, a perturbation may cause one or more of the bracketed quantities in Table IX to become nonzero, the L_{pp} terms and the terms involving electronegativity differences. A spectroscopic shift relative to benzene in general thus is compounded from a part independent of symmetry and a part which depends on symmetry.

For actual numerical calculations, the suggested procedure is first to compute all integrals for benzene itself, and then to compute integral increments for the molecule(s) of interest relative to benzene. When the latter are small, perturbation techniques may suffice for determination of spectroscopic shifts.

Dipole and Transition Moments

To obtain formulas for dipole and transition moments, one may assume that all molecules have the regular hexagonal shape with side R. Assuming further a center of charge of the orbital λ_p at nucleus p and ignoring overlap effects, one then has the basic formula for determining pi-electron moments,

$$\int \phi_j \mathbf{r} \phi_k d\tau = (R/2)[\mathbf{i}(\delta_{j+k,1} + \delta_{j+k,-1}) + \mathbf{j}(\delta_{j+k,1} - \delta_{j+k,-1})i], \qquad (54)$$

where $\mathbf{i}$ and $\mathbf{j}$ are unit vectors from the molecular center toward atom 0 and the 1—2 bond, respectively, and the δ are Kronecker deltas. From this formula follow the matrix elements $(\Phi_m \mid \mathbf{M}_r \mid \Phi_n)$ for the total pi-electron moment

$$\mathbf{M}_r = -e\sum_{\mu=1}^{6} \mathbf{r}_\mu$$

among the set C starting functions of Table III and Eq. (32). Namely,

$$(N \mid \mathbf{M}_r \mid V_{12}^+) = -eR\mathbf{i}, \qquad (N \mid \mathbf{M}_r \mid V_{12}^-) = -eR\mathbf{j},$$
$$\text{all other matrix elements of } \mathbf{M}_r = 0. \qquad (55)$$

These simple results imply that all dipole and transition moments are zero except those involving both the starting function N and one of the functions V_{12}^+ and V_{12}^-.

Consider for example the question of the dipole moment of the ground state. If N is the main component of its wave function, with V_{12}^+, V_{12}^- and other states making small contributions only, the dipole moment will be given by the formula

$$(\mu_r/eR) = -(4/\Delta E)\mathbf{Y}_1. \qquad (56)$$

Here the quantity

$$\mathbf{Y}_1 = Y_1^r\mathbf{i} + Y_1^i\mathbf{j} \qquad (57)$$

is an average of electronegativity vectors for the six atoms, the vector $\mathbf{y}_{p1}$ for atom p being directed from the molecular center toward atom p, as shown by Eq. (51). ΔE is the ${}^1A_{1g} - {}^1E_{1u}$ energy difference for benzene itself (+7.0 ev).[1,8]

Or, consider the moment for the ${}^1A - {}^1L_b$ transition in a benzene-like molecule,[27] the transition which for benzene itself is ${}^1A_{1g} - {}^1B_{2u}$ or $N - V_{1-2}^-$. For benzene itself this transition moment is zero, since V_{1-2}^- does not mix with V_{12}^+ or V_{12}^-, and neither does N. But in a perturbed benzene these mixings may occur. From assuming they are small, the formula for the transition moment is

$$\mathbf{m}({}^1A - {}^1L_b)/eR = (2/\Delta E')\mathbf{Y}_2. \qquad (58)$$

Here $\Delta E'$ is the ${}^1B_{2u} - {}^1E_{1u}$ energy difference in benzene itself (+2.1 ev)[1,8] and the quantity

$$\mathbf{Y}_2 = Y_2^i\mathbf{i} + Y_2^r\mathbf{j} \qquad (59)$$

is an average of electronegativity vectors $\mathbf{y}_{p2}$ on the six atoms, $\mathbf{y}_{p2}$ being perpendicular to the radius vector

[27] J. R. Platt, J. Chem. Phys. **19**, 263 (1951). See also J. A. Petruska, Ph.D. thesis, University of Chicago, 1960.

to atom p, pointing in the clockwise direction if p is odd, in the counterclockwise direction if p is even, as required by Eq. (51).

Similar arguments could be given concerning other transition moments, or dipole moments of excited states.

Such vectorial constructions of transitions moments have been previously discussed at length by Platt.[27] Platt did not obtain explicit formulas from an orbital theory, but rather introduced empirical parameters for substituents which he called *spectroscopic moments*. Equation (58) is explicit; it makes clear the relation between spectroscopic moments and atomic electronegativities.

One simple example of the use of the foregoing equations will suffice to illustrate what may be done with them. For pyridine, a previous calculation gave, essentially through an equation like Eq. (58), an f value for the ${}^1A-{}^1L_b$ transition of 0.046, compared with an experimental 0.041.[28] The parameters used there give $Y_1=0.26$ ev, from which according to Eq. (56) the pi dipole moment for the ground state would be

$$\mu_\pi=4(0.26)(4.8)(1.4)/(7.0)=1.0\text{D}.$$

The experimental moment is more than twice this, but a substantial part of the total moment would be expected to be lone pair and/or sigma electron contributions.

Discussion

Many extensions of this analysis are possible, and there are many applications of it.

Among the properties that have not been considered here are ionization potential, electron affinity, resonance energy, electron densities, and bond orders. Formulas for these can be written out, although there are special problems associated with each of them.[29] It seems important to try to work more properties into a single coherent semiempirical scheme.

Among the further developments or extensions of the mathematical treatment that should be examined are: (1) The systematic cataloging of the various types of perturbations and their effects, using group theory. (2) The systematic simplification of the equations for the case that all perturbations are small. (3) The inclusion of two-electron jumps. (4) The extension to include mesomeric effects.[6] (5) The development of the equations for the LCAO SCF orbitals as obtained from this treatment.[24] (6) The further examination of the effective electronegativities y_p and the changes in them produced by charge transfer.[30]

Especially interesting would be the extension to the arbitrary cyclic polyene (which is essentially trivial).[29] The cross-linking in molecules such as naphthalene can be viewed as a perturbation of corresponding cyclic polyenes. This approach was employed by Moffitt[31]; the present method would provide theoretical formulas for some elements treated by Moffitt as being purely empirical.

The most dubious point about the analysis is not the pi-electron approximation itself, which is quite securely based,[32] but the replacement of atomic orbitals by their orthogonalized counterparts and the subsequent neglect of overlap distributions. There seems to be no simple alternative to this last, however. The most general benzene-like molecule as here treated is a 42-parameter problem; treated without the zero differential overlap assumption it involves many hundreds of parameters.

It may be pointed out that formulas for various simpler theories of benzene-like molecules can be obtained from those given here. If one wished to neglect electron repulsion altogether, for example, one could merely strike out J, K_{01}, K_{02}, K_{03}, and all $L_{\mu\nu}$.

The most notable result of the analysis is the demonstration that the atomic electronegativities of Mulliken, modified as required by the molecular environment, determine in a simple way all charge distributions in benzene-like molecules.

IV. REMARK CONCERNING USE OF MULTIPOLE EXPANSION FORMULAS FOR ELECTRONIC REPULSION INTEGRALS

Following are reasons for considering evaluation of two-center coulomb repulsion integrals in the generalized Hückel method by multipole expansion methods:

(1) Pariser and Parr[1] introduced nonoverlapping uniformly charged sphere approximations for pi orbitals, which gave a formula for two-center coulomb integrals that involves reciprocal square roots of distances. Expanded in inverse powers of the internuclear distance R, this becomes an infinite series in $(1/R)$. Just the first term in this series, (e^2/R), was used by Pople,[2] but he later turned to the Pariser-Parr values.[33] Simpler than the complete Pariser-Parr series and yet more accurate than the simple Pople expansion, the multipole expansion formula involves only odd powers of $(1/R)$ up to the fifth, and the successive terms have simple physical interpretations.

(2) Mulligan[34] and Parr and Taylor[35] observed that multipole expansions formulas of a variety of purely theoretical electronic repulsion integrals over Slater orbitals are surprisingly accurate, even down to nearest neighbor distances, and that such expansions can be

[28] Work cited in footnote reference 1, p. 767.
[29] P. G. Lykos, Ph.D. Thesis, Carnegie Institute of Technology, 1954.
[30] J. M. Parks and R. G. Parr, J. Chem. Phys. **28**, 335 (1958); **32**, 1657 (1960).
[31] W. Moffitt, J. Chem. Phys. **22**, 320 (1954).
[32] P. G. Lykos and R. G. Parr, J. Chem. Phys. **24**, 1166 (1956); **25**, 1301 (1956).
[33] A. Brickstock and J. A. Pople, Trans. Faraday Soc. **50**, 901 (1954).
[34] J. F. Mulligan, J. Chem. Phys. **19**, 347 (1951).
[35] R. G. Parr and G. R. Taylor, J. Chem. Phys. **19**, 497 (1951).

obtained from purely theoretical formulas by merely striking out terms behaving as e^{-R}. As was shown in Sec. II the repulsion integrals in the generalized Hückel method may be regarded as over orthogonalized atomic orbitals. These might be expected to more closely follow multipole expansion formulas than do Slater orbitals, since they more closely obey the necessary condition for a multipole expansion formula to be an exact formula—detailed nonoverlapping of the electronic distributions (zero differential overlap).

(3) Adoption of multipole expansion formulas would allow the characterization of each pi orbital in a problem by specification of a value for its quadrupole moment, from which all two-center repulsion integrals involving it could be computed from simple classical formulas.

Multipole expansion formulas for electronic repulsion integrals between two electrons in two p orbitals on two atoms will be given and discussed later. Calculations testing the validity of such expansions will be performed, and an examination will be made of the effects of the Löwdin orthogonalization process. Finally, advantages and disadvantages of the multipole expansion formulation will be summarized.

Multipole Expansion Formulas for Two-Center Coulomb Repulsion Integrals Involving p Orbitals

An electron in a p orbital χ on an atom defines a distribution of electricity $e\Omega=e\chi^2$ which has a charge (monopole moment) e and quadrupole moments, but no dipole or other moments. This distribution is cylindrically symmetrical about some axis z, as a result of which the nonzero elements of the traceless quadrupole moment tensor can be expressed in terms of a single element,[36]

$$Q_{zz}=e\int(3z^2-r^2)\Omega dv=eq. \tag{60}$$

Indeed, $Q_{zz}=Q_{yy}=-\frac{1}{2}eq$. The quantity q is the *scalar quadrupole moment* of the distribution Ω.

Consider now two p orbitals χ_A and χ_B, centered at points A and B, a distance R apart. Let the corresponding distribution be Ω_A and Ω_B, with scalar quadrupole moments q_A and q_B. Then the coulomb repulsion integral,

$$\gamma_{AB}=\iint\Omega_A(1)\,(e^2/r_{12})\Omega_B(2)dv(1)dv(2), \tag{61}$$

has a multipole expansion in powers of $(1/R)$ provided R is not zero. Namely, if θ_A, ϕ_A and θ_B, ϕ_B are polar coordinates of the axes of χ_A and χ_B with respect to the $A-B$ line of centers, one has the formula,[36]

$$\begin{aligned}\gamma_{AB}\sim e^2\{&R^{-1}+(4R^3)^{-1}[q_A(3\cos^2\theta_B-1)\\&+q_B(3\cos^2\theta_A-1)]\\&+(3q_Aq_B/16R^5)[(1-5\cos^2\theta_A-5\cos^2\theta_B\\&-15\cos^2\theta_A\cos^2\theta_B)+2(\sin\theta_A\sin\theta_B\cos(\phi_A-\phi_B)\\&-4\cos\theta_A\cos\theta_B)^2]\}.\end{aligned} \tag{62}$$

Here the successive terms represent charge-charge, charge-quadrupole, and quadrupole-quadrupole interactions.

The special case of most interest is the one in which χ_A and χ_B are parallel pi-type orbitals, a and b.[37] Here $\theta_A=\theta_B=\frac{1}{2}\pi$, $\phi_A-\phi_B=0$, and Eq. (62) gives

$$\gamma_{ab}\sim e^2\{R^{-1}-[(q_A+q_B)/4R^3]+(9q_Aq_B/16R^5)\}. \tag{63}$$

If χ_A and χ_B are pi-type but mutually perpendicular orbitals, a and b_z,[37] on the other hand, $\theta_A=\theta_B=\frac{1}{2}\pi$ but $\phi_A-\phi_B=\frac{1}{2}\pi$, and Eq. (62) gives

$$\gamma_{ab_z}\sim e^2\{R^{-1}-[(q_A+q_B)/4R^3]+(3q_Aq_B/16R^5)\}. \tag{64}$$

If finally χ_A is a pi-type orbital a and χ_B a sigma-type orbital b_r,[37] $\theta_A=\frac{1}{2}\pi$, $\theta_B=0$, $\phi_A-\phi_B=0$, and Eq. (62) gives

$$\gamma_{ab_r}\sim e^2\{R^{-1}-[(q_A-2q_B)/4R^3]-(3q_Aq_B)/16R^5)\}. \tag{65}$$

For the homonuclear case $q_A=q_B=q$, these formulas reduce to the following:

$$\gamma_{ab}\sim e^2\{R^{-1}-(q/2R^3)+(9q^2/16R^5)\}$$

(homonuclear case), (66)

$$\gamma_{ab_z}\sim e^2\{R^{-1}-(q/2R^3)+(3q^2/16R^5)\}$$

(homonuclear case), (67)

$$\gamma_{ab_r}\sim e^2\{R^{-1}+(q/4R^3)-(3q^2/4R^5)\}$$

(homonuclear case). (68)

All of these formulas would be exact for all R for distributions Ω_A and Ω_B which are point (ideal) charge-quadrupoles, or which are "spherically disconnected" and have the indicated moments[38]; for actual p functions they are asymptotically valid for large R.

Up to this point the radial factors in the p orbitals have not been specified. For $2p$ hydrogen-like orbitals, effective charge Z, one would have

$$q=24a_0^5/Z^3 \quad (2p \text{ orbitals}), \tag{69}$$

[36] J. O. Hirschfelder, C. F. Curtiss, and R. B. Bird, *Molecular Theory of Gases and Liquids* (John Wiley & Sons, Inc., New York, 1954), pp. 26-28, 839-840.

[37] R. G. Parr and B. L. Crawford, Jr., J. Chem. Phys. **16**, 1049 (1948).

[38] Per-Olov Löwdin, Phil. Mag. Suppl. **5**, 1 (1956).

TABLE X. Exact and asymptotic values for coulomb integrals involving $2p$ orbitals.[a]

ρ[b]	6	8	10	14
$Z^{-1}\gamma_{ab}$				
Exact[c]	0.1308	0.1080	0.0906	0.0676
Asymptotic[d]	0.1528	0.1115	0.0912	0.0677
Truncated Asymptotic[e]	0.1111	0.1016	0.0880	0.0671
Orthogonalized[f]	0.1216	0.1045	0.0895	0.0676
$Z^{-1}\gamma_{ab_z}$				
Exact[c]	0.1242	0.1047	0.0890	0.0673
Asymptotic[d]	0.1250	0.1049	0.0891	0.0673
$Z^{-1}\gamma_{ab_x}$				
Exact[c]	0.1422	0.1200	0.1003	0.0727
Asymptotic[d]	0.1389	0.1235	0.1017	0.0728

[a] Values in e^2/a_0 units.
[b] $\rho=ZR/a_0$.
[c] Footnote reference 39.
[d] From Eqs. (70) to (72) of text.
[e] Quadrupole-quadrupole term omitted. See text.
[f] From Eq. (75) of text and numerical values from footnote reference 39.

and in this case Eqs. (66) to (68) give, with $\rho=ZR/a_0$,

$$\gamma_{ab}\sim Z(e^2/a_0)[(1/\rho)-(12/\rho^3)+(324/\rho^5)] \quad \text{(homonuclear case, } 2p \text{ orbitals)}, \quad (70)$$

$$\gamma_{ab_z}\sim Z(e^2/a_0)[(1/\rho)-(12/\rho^3)+(108/\rho^5)] \quad \text{(homonuclear case, } 2p \text{ orbitals)}, \quad (71)$$

$$\gamma_{ab_x}\sim Z(e^2/a_0)[(1/\rho)+(6/\rho^3)-(432/\rho^5)] \quad \text{(homonuclear case, } 2p \text{ orbitals)}. \quad (72)$$

These formulas have been given previously by Mulligan.[34] Corresponding formulas for the heteronuclear case may be obtained by setting $q_A=24a_0^2/Z_A^2$ and $q_B=24a_0^2/Z_B^2$ in Eqs. (63) to (65).

Numerical Values. Effects of Orthogonalization

In Table X are given typical exact values of $Z^{-1}\gamma_{ab}$, $Z^{-1}\gamma_{ab_z}$ and $Z^{-1}\gamma_{ab_x}$, taken from the tables of Kopineck,[39] and approximate values calculated from Eqs. (70) to (72).

As would be expected, the approximate values are very good for large values of R. The remarkable feature is how good they remain for small values of R. For a carbon $2p\pi$ orbital with the Slater Z equal to 3.18, for instance, for R equal to the neighbor C—C distance in benzene, ρ is 8.37, and it can be seen from Table X that the asymptotic formulas are good to a few percent for this ρ value.

Also included in Table X are some integral values calculated from Eq. (70) with the quadrupole-quadrupole term deleted. Truncation produces considerable error for ρ equal to six, but only a few percent error for ρ equal to eight or higher.

Effects of transforming the atomic orbitals to a localized orthogonal set may be examined by explicitly carrying out the Löwdin orthogonalization procedure.[10] The Löwdin orthogonalized analogs of χ_a and χ_b are, by Eq. (3) of Sec. II,

$$\lambda_a=A\chi_a+B\chi_b$$

and

$$\lambda_b=B\chi_a+A\chi_b, \quad (73)$$

where

$$2A=(1+S)^{-\frac{1}{2}}+(1-S)^{-\frac{1}{2}},$$

$$2B=(1+S)^{-\frac{1}{2}}-(1-S)^{-\frac{1}{2}}, \quad (74)$$

and S is the $\chi_a-\chi_b$ overlap. The coulomb repulsion integral between λ_a and λ_b accordingly is given by the formula.

$$^{\lambda}\gamma_{ab}=(A^4+B^4)\gamma_{ab}+2A^2B^2\gamma_{aa}+4AB(A^2+B^2)(aa\,|\,ab)+4A^2B^2(ab\,|\,ab), \quad (75)$$

where $(aa\,|\,ab)$ and $(ab\,|\,ab)$ are hybrid and exchange integrals.[37] All quantities in this formula may be found in the literature[39]; some values are included in Table X.

The orbitals λ_a and λ_b differ from the orbitals χ_a and χ_b by terms that become exponentially small for large R. This means that $^{\lambda}\gamma_{ab}$ has the same asymptotic expansion as γ_{ab}, namely, Eq. (70).[40] The numbers in Table X thus show that the discrepancies between asymptotic and exact values for $^{\lambda}\gamma_{ab}$ in fact are greater than the corresponding discrepancies for γ_{ab}, contrary to the supposition (2) at the beginning of this section. The errors remain small, however, so that one may say that multipole expansions are essentially as good for the coulomb integrals over orthogonalized orbitals as for these integrals over nonorthogonalized orbitals.

Discussion

The foregoing would appear to indicate that multipole expansion formulas might well be systematically studied in the context of the generalized Hückel method. They can reproduce purely theoretical integrals with a precision matching the inherent precision of the method as a whole. They involve a single parameter for each pi orbital, its quadrupole moment, which has a simple physical meaning, and *they accordingly provide a simple means for evaluating pi repulsions in heteropolar systems.*[41] They are independent of the form of the radial factors in the actual orbitals and so have an inherent accuracy which transcends the accuracy limit imposed by a particular orbital form. They are purely classical in nature and so have attraction as possible ingredients in a possible complete unified semi-quantum-mechanical theory of chemistry.

On the other side, use of multipole expansion formulas precludes use of a single formula for integrals γ_{ab}

[39] H. J. Kopineck, Z. Naturforsch. **5a**, 420 (1950).

[40] The moments of the distribution λ_a^2 actually differ from those of the distribution χ_a^2. These differences go to zero as S, however, and are here neglected.

[41] The prescription is provided by Eqs. (63)–(65). It may be noted that to the extent the quadrupole-quadrupole terms may be neglected, a heteropolar integral is an arithmetic mean of the corresponding homopolar integrals. Thus $\gamma_{cn}\approx\frac{1}{2}(\gamma_{cc}+\gamma_{nn})$.

for all distances, including $R=0$, which would have certain advantages. (Spectroscopic intervals depend on differences $\gamma_{aa}-\gamma_{ab}$, not on absolute values of γ_{ab}.[29]) The quadrupole-quadrupole terms tend to get suspiciously big for the small Z values required by attempts[29] to fit empirical γ_{ab} values[8] with purely theoretical integral values.[42]

V. ACKNOWLEDGMENTS

Section III was first written during 1953–1954 while the author was Guggenheim Fellow and Fulbright Scholar at the University of Cambridge. He is grateful for these fellowship awards, and he also would like to record his appreciation to the members of the Theoretical Chemistry Department at Cambridge for their gracious hospitality, most especially Dr. Frank S. Boys.

The author has profited from numerous discussions regarding the material in Secs. II and III with Professor Peter G. Lykos. Dr. Lykos has examined the application of some of these methods to the benzene and naphthalene molecules,[29] and plans to describe his results elsewhere. Discussions about Sec. II with Professor Klaus Ruedenberg and Dr. Rudolph Pariser also have been helpful.

[42] P. G. Lykos and R. G. Parr, J. Chem. Phys. **28**, 361 (1958).

THE JOURNAL OF CHEMICAL PHYSICS VOLUME 33, NUMBER 4 OCTOBER, 1960

Charge Transfer and Fluorescence Quenching

DILIP KUMAN MAJUMDAR AND SADHAN BASU

Department of Chemistry, University College of Science & Technology, Calcutta-9, India

(Received March 14, 1960)

A charge-transfer-interaction mechanism has been proposed for the quenching of fluorescence of a number of polynuclear aromatic hydrocarbons by aromatic solvents, especially methylated benzenes. The quenching efficiency has been found to be in the order benzene<toluene<xylene<mesitylene, which is also the order in which ionization energy of the solvents diminishes.

IT was suggested by Weiss[1] that the quenching of fluorescence of a compound by foreign substances is due to electron-transfer reaction between the fluorescent and the quencher molecule. It was later pointed out by Orgel[2] that the efficiency of various anions in quenching the fluorescence of organic dyestuffs in aqueous solution follows closely the order in which the anions can undergo electron-transfer reaction. Thanks to Mulliken's recent work[3] on the quantum mechanical basis of molecular complexes, we have now a better understanding of the donor and acceptor strength of a number of closely related compounds. This has led us to examine the proposed charge-transfer mechanism for fluorescence quenching more closely.

As a first step, we proceeded to examine the solvent-quenching phenomenon. It has been known for quite some time that the intensity of fluorescence of aromatic hydrocarbons diminishes as we go over from benzene to xylene solution.[4] As we had experimental data on the ionization energy of a series of methylated benzenes, our objects were to measure the fluorescence intensity of a number of polynuclear aromatic hydrocarbons in benzene, toluene, xylene, and mesitylene and to see how well they could be explained in terms of donor-acceptor reaction between the solute and the solvent molecules.

[1] J. Weiss, Trans. Faraday Soc. **34**, 451 (1938); **35**, 48 (1939).
[2] L. Orgel, Quart. Revs. (London), 422, 1954.
[3] R. Mulliken, J. Amer. Chem. Soc. **64**, 811 (1952).
[4] Hirschleff, *Fluorescence & Phosphorescence* (Methuen & Co., Ltd., London) 1938.

EXPERIMENTAL

The fluorescence measurements were made in a right-angle scattering setup described by Kuhn and Stupp.[5] Our intensity meter consisted of a 1P21 photomultiplier tube in conjunction with a dc amplifier, similar to the Photovolt light-scattering instrument. The concentration of the fluorescent hydrocarbon was so adjusted that the light intensity was in the linear part of the phototube response curve, and the phototube output current was taken as directly proportional to light intensity.

The exciting light was isolated from a stabilized AH4 mercury-arc lamp by means of a Corex filter with transmission characteristics that showed a maximum transmission at 365 mμ and dropped to zero at 350 mμ and 375 mμ. The transmission characteristics were measured in a Beckman spectrophotometer, Model DU.

The solvent used were all Merck's chromatographically pure samples, which were degassed and freshly distilled before use. The hydrocarbons were supplied by B.D.H. and L. Light & Company and were

[5] R. Stupp and H. Kuhn, Helv. Chim. Acta., **35**, 2469 (1952).

TABLE I. Intensity of fluorescent emission of polynuclear aromatic hydrocarbons in solutions.

Concentration of hydrocarbon (M/1)	Intensity in arbitrary units $I.E.$ (ev) Benzene 9.24	Toluene 8.81	Xylene 8.56	Mesitylene 8.39
	Anthracene			
2.92×10^{-5}	2.88	2.06	2.02	1.75
2.19	2.27	1.73	1.67	...
1.64	2.09	1.48	1.35	1.03
1.23	1.57	1.29	1.08	...
0.92	1.32	1.00	0.88	0.67
0.69	0.99	0.80	0.74	...
	Coronene			
4.19×10^{-5}	1.00	0.76	0.72	0.55
3.14	0.80	0.58	0.51	0.42
2.36	0.60	0.44	0.39	0.32
1.77	0.46	0.35	0.32	0.24
1.33	0.36	0.26	0.24	0.18
0.99	0.28	0.20	0.18	0.15
	Fluoranthene			
6.06×10^{-5}	...	2.29	2.03	1.93
4.54	2.21	2.08	1.82	...
3.41	2.10	1.89	1.64	1.39
2.56	1.68	1.54	1.47	...
1.92	1.52	1.36	1.21	0.95
1.08	1.00	0.95	0.75	0.66
0.81	0.81	0.76	0.54	...
	Decacyclene			
2.20×10^{-5}	0.83	0.66	0.59	0.53
1.60	0.62	0.52	0.48	0.42
1.20	0.49	0.41	0.37	0.33
0.90	0.39	0.32	0.30	0.26
	Pyrene			
4.91×10^{-4}	0.76	0.56	0.49	0.40
3.68	0.58	0.43	0.37	0.30
2.76	0.45	0.34	0.28	0.22
2.07	0.35	0.28	0.22	0.18
1.55	0.28	0.21	0.17	...
	Triphenylene			
1.83×10^{-5}	...	0.77	0.72	0.60
1.37	0.72	0.59	0.54	0.47
1.03	0.55	0.44	0.40	0.35
0.77	0.43	0.35	0.31	0.28
0.59	0.35	0.26	0.24	0.20

stated to be 99.9% pure. They were further purified by chromatographic adsorption on alumina and by repeated crystallization from aldehyde-free 'Specpure' ethanol. The solutions were prepared by direct weighing and dissolution in appropriate solvent in diffused day light. The irradiating cell was completely filled with solution and then tightly closed, so that during irradiation the solution did not come into contact with atmospheric oxygen. In the range of 350 mμ to 375 mμ all the solvents showed 100% transmission against dust-free water. No appreciable distortion of the absorption spectrum of the hydrocarbons was noticed in the various solvents.

RESULTS

In Table I the intensity of fluorescent light (in arbitrary units) of six different hydrocarbons at different concentrations in four benzenoid solvents are summarized. Within the concentration range used in the present study, the plot of intensity against hydrocarbon concentration was found to be perfectly linear. It may also be observed that for all hydrocarbons and at all concentrations the fluorescence intensity in different solvents appear in the order benzene > toluene > xylene > mesitylene.

DISCUSSION

The fluorescence intensity of a substance may be different in different solvents, owing to the dispersing effect of the solvent alone. Thus, if the intensity in toluene is I_t and that in benzene is I_b, then $I_t/I_b = \mu_t^2/\mu_b^2$ where μ_t and μ_b are the refractive indices of toluene and benzene, respectively. This ratio comes out to be 0.994. It may be observed from the above table that the experimental value of I_t/I_b at all concentrations and in all solvents is much less than this; consequently the observed intensity difference can not be attributed to the dispersing effect of the solvent alone.

As the solvents are transparent to the exciting radiation, and the absorption spectra of the hydrocarbons are not appreciably different in different solvents in the range of 350 mμ to 375 mμ, the difference in fluorescence intensity of a hydrocarbon in different solvents but at the same concentration can not be due to the "inner filter" effect of the solvent or to unequal energy absorption by the solute molecules. However, anthracene has very steep vibrational-band structure in the range of 350 mμ to 375 mμ and a very small change in band position can greatly affect the fraction of the light absorbed in different solvents. It has been observed that in going from a benzene to a toluene solution the optical density at 365 mμ (the maximum-intensity position in the exciting band) for anthracene is actually increased by about 3%; i.e., the fraction of light absorbed is increased. The intensity of fluorescence in toluene should therefore be higher than that of benzene, but the reverse appears to be the case. For other hydrocarbons, the differences in optical density at 365 mμ in different solvents were less than that of anthracene. The unequal energy absorption in different solvents is not, in all probability, the cause for quenching.

Further, as both solute and solvent molecules are nonpolar, the contribution of any dipolar interaction in the radiationless degradation of the excitation energy is practically nil. The resonance interaction between solute and solvent molecule may be the primary cause for quenching. If we assume that this interaction is of

charge transfer type, i.e., donor-acceptor interaction, then the quenching efficiency will depend on either the donor or the acceptor strength of the solvent. It is evident from the Table I that for all hydrocarbons and at all concentrations over which the intensity-against-concentration curve is linear, the intensity appears in the order benzene > toluene > xylene > mesitylene. This happens to be the order in which the donor strength of these hydrocarbons increases, as indicated by their ionization energy. So we may suggest that the quenching effect of the solvent is due to a donor-acceptor reaction between the solute and the solvent molecules in which the solvent molecules act as donor. Further, as the absorption spectrum of the solute is not appreciably affected (indicating no molecular complex formation), we may suggest that this interaction takes place with the excited state of the solute molecule.

It was noticed that in *n*-heptane solution the fluorescence intensity of these hydrocarbons was not affected at all by the addition of methylated benzenes up to a concentration of $4M$. In order to be effective the methylated benzenes must be in constant contact with the solute molecules. This may mean that charge-transfer interaction is of a contact type and does not lead to the formation of any molecular complex. It is to be noticed further that even when the solute molecules are in constant contact with the solvent molecules, the quenching is only partial. This evidently means that not all contact are effective and the molecules must be suitably oriented before any energy degradation can take place on encounter. In fact it has been shown by Mulliken[3] that in the case of π-donors and π-acceptors the molecules must be suitably oriented before any charge transfer can take place.

If we propose the following kinetic scheme for the quenching process:

	rate
$A+h\nu \rightarrow A^*$	1
$A^* \rightarrow A+h\nu'$	k_1
$A^*+S \rightarrow A+S$	k_2

where A stands for hydrocarbon and S for solvent molecules, then it follows that

$$(1/F)-1=k_2/k_1,$$

where F is the fluorescence yield. If we assume that k_2 is determined by charge-transfer-interaction energy, then $\log k_2$, i.e. $\log(1/F-1)$ since k_1 is constant in different solvents, is expected to vary linearly with $I.E.$ of the solvent at constant temperature. Bowen and Williams[4] have reported a value of 0.24 as the fluorescence yield of anthracene in benzene. With this

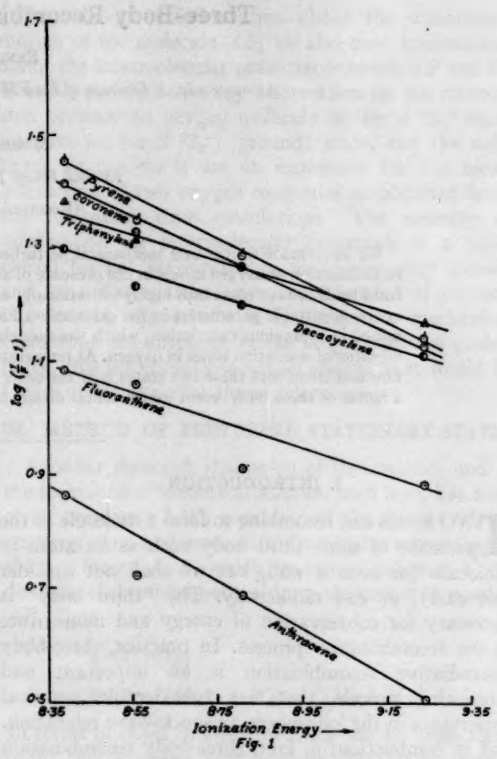

FIG. 1.

as reference, the intensity data in other solvents were converted to yield value for anthracene. It was observed that the plot of $\log(1/F-1)$ against $I.E.$ was fairly linear, as was expected. Similar linear plots were obtained for other hydrocarbons, but in those cases only relative yield values could be measured (Fig. 1).

Now the question is how charge transfer brings about a dissipation of electronic excitation energy by a radiationless process. There may be several routes: (i) interaction may deform the potential-energy curve so much that the electron passes smoothly from the singlet to the triplet level, from which it returns to the ground state by a radiationless process at room temperature; (ii) interaction may enhance the spin-orbit coupling effect; or (iii) interaction may bring about an easy matching of vibronic energy so that the low frequency vibrations in solvent is easily excited. The present investigation, however, can not settle these points.

Our sincere thanks are due to Prof. E. J. Bowen, Oxford, for helpful suggestions and constructive criticisms, to M/S Emission Radio & Varieties, Calcutta, for their kind help in the construction of the instrument, and to Council of Scientific & Industrial Research, India, for a Junior Research Fellowship to one of us (D.K.M.).

[4] E. Bowen and R. Williams, Trans. Faraday Soc., 35, 765 (1939).

THE JOURNAL OF CHEMICAL PHYSICS VOLUME 33, NUMBER 4 OCTOBER, 1960

Three-Body Recombination of Oxygen Atoms*

ERNEST BAUER

Aeronutronic, A Division of Ford Motor Company, Newport Beach, California

AND

MORRIS SALKOFF

Institut Blaise Pascal, Paris, France

(Received May 16, 1960)

We have made a quantum mechanical perturbed stationary state calculation of the rate of three-body recombination of oxygen atoms in the presence of an oxygen molecule as third body. The recombination is considered to take place into highly vibrationally excited states ($v=9, 10$) of the $A\ ^3\Sigma_u^+$ state of O_2. There are no adjustable parameters in the calculation. For the interaction potential we have used the results obtained in a previous calculation, which were obtained by comparison with experimental measurements of vibrational relaxation times in oxygen. At temperatures of the order 300–3000°K, the calculated recombination coefficient into these two states is of the order $1-10\times10^{-33}$ cm^6/sec, and agrees to within better than a factor of three with recent experimental measurements.

I. INTRODUCTION

TWO atoms can recombine to form a molecule in the presence of some third body such as an atom or molecule (or even a wall, but we shall not consider this case), or else radiatively. The "third body" is necessary for conservation of energy and momentum in the recombination process. In practice, three-body nonradiative recombination is an important and interesting process that has considerable practical importance in the ionosphere, in shock-wave relaxation, and in combustion; in fact, three-body recombination is the prototype of an important class of chemical reactions.

It has only recently become possible to measure recombination rates quantitatively for simple systems for which calculations are possible, and what calculations have been made (other than strictly empirical ones) have not been able to explain the large recombination rates, of gas kinetic-order, that have been observed. The purpose of the present calculation was to attempt a relatively thorough and rigorous quantum mechanical calculation to examine whether there was in fact any basic discrepancy; and no such discrepancy appears to exist.

For definiteness, we shall examine the recombination of two oxygen atoms in presence of an oxygen molecule

$$O(^3P)+O(^3P)+O_2(X\ ^3\Sigma_g^-)\rightarrow O_2(A\ ^3\Sigma_u^+)+O_2(X\ ^3\Sigma_g^-), \quad (1)$$

which we shall write as

$$A+B+C\rightarrow AB'+C''. \quad (2)$$

The primes indicate that the molecule AB is in general formed in an internally excited state, and the third body C may also carry away some internal excitation after impact.

It must be stressed that the present calculation is quite schematic; thus the detailed labeling $O_2(A\ ^3\Sigma_u^+)$ should not be taken too seriously. We choose this particular state because its vibrational levels are known right up to the dissociation limit.[1] The purpose of the present calculation is to sketch the general order of magnitude of a typical three-body recombination process, rather than to make a detailed calculation for one specific process.

The most obvious way to understand the large experimental values of three-body recombination coefficients is to suppose that the molecule AB is formed in a highly vibrationally excited state. On theoretical grounds[2,3] we believe that the molecule AB is very likely to be formed in a highly excited vibrational state, because in this way a minimum of energy has to be transferred into kinetic energy of C from the "continuum" vibration of A and B (that is, from their relative kinetic energy of motion); and it is well known that the coupling of translational and vibrational energy is weak, so that energy transfer between these two modes of motion is difficult.[4] It should however be noted that thus far there appears to be no experimental evidence for the existence of such highly vibrationally excited states.[5] The observations would be very difficult, but one should make further attempts

* Part of this work was carried out at the Institute of Mathematical Sciences, New York University, under support of the U. S. Atomic Energy Commission and the U. S. Air Force.

[1] G. Herzberg, Can. J. Phys. **30**, 185 (1952); P. Brix and G. Herzberg, *ibid.* **32**, 110 (1954).

[2] K. F. Herzfeld and V. Griffing, *1959 Wisconsin Meeting on Absolute Reaction Rate Theory*, see also K. F. Herzfeld, *Seventh Symposium on Combustion* (Butterworths Scientific Publications, Ltd., London, 1959), p. 27.

[3] Cf. F. T. Wall, L. A. Hiller, Jr., and J. Mazur, J. Chem. Phys. 255 (1958); F. T. Smith, *ibid.* **31**, 1352 (1959); J. C. Polanyi, *ibid.* **31**, 1338 (1959).

[4] N. F. Mott and H. S. W. Massey, *Theory of Atomic Collisions* (Oxford University Press, New York, 1949), 2nd ed., p. 292.

[5] Cf. J. L. Golden and A. L. Myerson, J. Chem. Phys. **28**, 978 (1958).

to make the measurements, as well as to calculate the rate of degradation of vibrational energy in collisions.

Let us examine the implications of this physical picture somewhat further. From our present overall viewpoint we may discount electronic or vibrational excitation of C during the collision, since the transfer of large amounts of energy into these modes of motion will be difficult except in rather special cases. We are considering our molecule AB to be formed in an electronically excited state. Two oxygen atoms in the ^3P ground electronic state may recombine to form a molecule in any one of four electronic states: $X\,^3\Sigma_g^-$, $a\,^1\Delta_g$, $b\,^1\Sigma_g^+$, or $A\,^3\Sigma_u^+$; we consider recombination into the A state only for convenience, because its vibrational levels are known right up to the continuum.

There remains the problem of rotational motion. Most actual collisions will not be colinear, so that there will be relative angular momentum of AB and C, and the effects of this should certainly be examined. However, it is well known[4] that transfer of energy between translation and rotation is easy for all molecules other than hydrogen, and thus we feel that we can obtain an initial physical understanding of the situation by merely examining a colinear collision, in which rotational motion is disregarded. For definiteness we examine recombination into the two highest vibrational states, $v=9$, 10.

II. MODEL

We consider the colinear collision of two atoms A, B with a third body C. The free atoms A, B are regarded as in the vibrational continuum of some electronic state of the molecule AB, and they fall into a bound, but still highly vibrationally excited, state of AB (still in the same electronic state of the molecule). The balance of the "vibrational" energy of A and B is transferred into kinetic energy of the third body C, measured relative to the center of mass of AB. Thus we make a calculation of the transfer of energy between vibrational and translational degrees of freedom, analogous to earlier calculations of vibrational relaxation times in gases.[6,7]

This is an adequate model within its very obvious physical limitations; in practice we use the quantum mechanical "method of perturbed-stationary-states", which is entirely adequate for vibrational relaxation processes (i.e., the $v=0$ to $v=1$ transition, which is very improbable), but, which is not appropriate for a very probable process like three-body recombination, because the method is essentially a perturbation method. Actually the gravest objection to a perturbation method does not apply in the present application, because we have taken care to be sure that the resulting partial cross sections satisfy the limitations set by conservation of flux (see Sec. VI).

[6] M. Salkoff and E. Bauer, J. Chem. Phys. **29**, 26 (1958); see also Research Rept. CX-31 (1957), Institute of Mathematical Sciences, New York University.

[7] M. Salkoff and E. Bauer, J. Chem. Phys. **30**, 1614 (1959).

In addition to information about the vibrational motion of the molecule AB, we also need information about the intermolecular potential between AB and C. There is not available any information on the interaction between an oxygen molecule in the $A\,^3\Sigma_u^+$ state and one in the $X\,^3\Sigma_g^-$ (ground) state, and the only thing we can do is use an expression for the mean interaction of two oxygen molecules as obtained from the relaxation time calculations.[7] The scarcity of information on intermolecular potentials is a valid reason for not attempting to make any very specific and quantitative calculations of this kind of process, but because the details of the quantum mechanical calculation are obscured by the large transition probability, this uncertainty is not as critical as it would be for processes like vibrational relaxation.

III. METHOD OF PERTURBED STATIONARY STATES

A rather thorough discussion of the method, and of the technique of numerical solution used here, has been given previously.[6] We separate off the motion of the center of mass and work with the relative separation of the two atoms A, B, which we call $\boldsymbol{\rho}$, and with $\mathbf{r}$, the distance of the third body C from the center of mass of AB. Thus

$$\boldsymbol{\rho}=\mathbf{r}_A-\mathbf{r}_B,$$
$$\mathbf{r}=\mathbf{r}_C-(M_A\mathbf{r}_A+M_B\mathbf{r}_B)/(M_A+M_B). \tag{3}$$

In terms of these coordinates there are no cross terms in the kinetic energy, and the wave equation becomes

$$[H_i(\boldsymbol{\rho})+H_e(\mathbf{r})+V'(\boldsymbol{\rho},\mathbf{r})-E]\Psi_j(\boldsymbol{\rho},\mathbf{r})=0, \tag{4}$$

where $j=f$, b ("free" and "bound," respectively), and the "internal" and "external" Hamiltonians H_i and H_e are given by the expressions

$$H_i(\boldsymbol{\rho})=-(\hbar^2/2M_i)\nabla_\rho^2+V_i^0(\boldsymbol{\rho});$$
$$M_i=M_AM_B/(M_A+M_B),$$
$$H_e(\mathbf{r})=-(\hbar^2/2M_e)\nabla_r^2+V_e^0(\mathbf{r});$$
$$M_e=(M_A+M_B)M_C/(M_A+M_B+M_C). \tag{5}$$

We solve the wave equation (4) in terms of the unperturbed Hamiltonian $H_0=H_i(\boldsymbol{\rho})+H_e(\mathbf{r})$, by the method of perturbed stationary states. That is, we evaluate the eigenfunctions $\Psi_j(\boldsymbol{\rho},\mathbf{r})$ of H_0, and calculate the transition matrix elements

$$\langle\Psi_f(\boldsymbol{\rho},\mathbf{r})\mid V'(\boldsymbol{\rho},\mathbf{r})\mid\Psi_b(\boldsymbol{\rho},\mathbf{r})\rangle.$$

The eigenfunctions $\Psi_j(\rho, r)$ are solutions of the following wave equation:

$$(H_0-E)\Psi_j(\boldsymbol{\rho},\mathbf{r})=0;$$
$$\Psi_j(\boldsymbol{\rho},\mathbf{r})=\phi_j(\boldsymbol{\rho})\psi_j(\mathbf{r}),$$
$$\psi_j(\mathbf{r})=\sum_{l=0}^{\infty}(1/r)\chi_l(k_jr)P_l(\cos\theta), \tag{6}$$

TABLE I. Highly vibrationally excited levels of the $A\,^3\Sigma_u^+$ state of O_2.[a]

Vibrational quantum number v	Binding energy $\mid \epsilon_b(v) \mid$ (cm^{-1})	Equilibrium nuclear separation $\rho_0(v)$ (a_0)
10	104	3.96
9	340	3.56
...	...	...
0	5570	2.90

[a] See footnote reference 1.

where $\chi_l(k_f r)$ are solutions of the radial wave equation

$$[d^2/dr^2 - l(l+1)/r^2 - 2M_e V_e^0(r)/\hbar^2 + k_f^2]\chi_l(k_f r) = 0 \quad (7)$$

while the vibrational wave functions $\phi_f(\rho)$ are solutions of an appropriate vibrational wave equation (cf. Sec. IV). In fact the quantitative difficulty of this problem lies in the evaluation of the $\chi_l(k_f r)$; typically one has to go up to $l \sim 100$, and this is best done on a high-speed computer.

In addition to this computational difficulty, there is a complication of a somewhat more fundamental nature that arises from the fact that we go from a "free" to a "bound" state (or vice versa). Thus the cross section for the excitation of a molecule from a discrete (bound) vibrational state b into a continuum (free) state f is given by the following expression:

$$\partial\sigma_{fb}(l;\epsilon_f)/\partial\epsilon_f = \pi(k_f/k_b)(4M_i/\hbar^2)^2 \mid V_{fb}'(l) \mid^2, \quad (8)$$

where ϵ_f is the vibrational energy in the state f, and

$$V_{fb}'(l) = \iint d\rho dr \phi_f(\rho)\chi_l(k_f r) V'(\rho, r)\phi_b(\rho)\chi_l(k_b r). \quad (9)$$

(The ρ-motion is one dimensional for a colinear collision and

$$[\chi_l(k_j r) \underset{r\to\infty}{\longrightarrow} (1/k_j)\sin[k_j r + \delta_{jl} - (lr/2)] \quad \text{for} \quad j = b, f.$$

The reason for defining the dissociation cross section per unit energy range is that the continuum "vibrational" wave function $\phi_f(\rho)$ is normalized per unit energy range (cf. Sec. IV). The actual (partial) cross section for dissociation is simply obtained by integrating the expression (8) as follows:

$$\sigma_{fb}(l;\epsilon_f) = \int_0^{\epsilon_f} d\epsilon_f'[\partial\sigma_{fb}(l;\epsilon_f')/\partial\epsilon_f']. \quad (10)$$

The character of the dissociation or recombination transition, in which we pass from a bound vibrational state having a *discrete* energy $\epsilon_b(<0)$ into a free-vibrational-state-of-energy $\epsilon_f = \hbar^2 p_f^2/2M_i$ so that $\epsilon_f > 0$ and the state f is a *continuum* state, should be examined a little further. The condition of conservation of energy is

$$E = \hbar^2 k_b^2/2M_e - \mid \epsilon_b \mid = \hbar^2 k_f^2/2M_e + \hbar^2 p_f^2/2M_i. \quad (11)$$

In an actual situation we have a definite bound vibrational state b with a fixed and definite value of ϵ_b. The value of ϵ_f is not fixed, but covers some kind of statistical range—typically a Maxwell-Boltzmann distribution corresponding to the gas temperature. The incident "external" momentum k_f also covers an independent statistical range (which will of course also be a Maxwell-Boltzmann distribution for the appropriate temperature in a typical situation). Thus we shall take energy conservation into account as follows. ϵ_b is fixed; ϵ_f and k_f are treated as independent, and Eq. (11) then fixes the value of k_b for a given set of values of ϵ_f and k_f. To obtain a temperature-averaged dissociation cross section or recombination coefficient, we thus have to carry out *separate* and *independent* Boltzmann averages over ϵ_f and k_f.

IV. VIBRATIONAL MOTION

The vibrational levels of the $A\,^3\Sigma_u^+$ state of O_2 are known right up to the dissociation limit[1]; data for the highest excited levels are shown in Table I. One could describe the vibrational motion in terms of a Morse potential, but this leads to a rather complicated expression for the matrix element of $(\rho - \rho_0)$ between the free and bound states. In view of the approximations made in other parts of the analysis, there does not seem to be much point in treating the internal motion in a very refined way. Consequently we approximate the potential function $V_e^0(\rho)$ of the vibrational motion by a square well of depth D, the dissociation energy of the state $A\,^3\Sigma_u^+$ of O_2, and width L; the width L is chosen to meet the matching requirements of the WKB approximation to the wave function $\phi_b(\rho)$.[8]

Define[8]

$$\hbar^2 P^2/2M_i = D + \epsilon_f; \quad \hbar^2 Q^2/2M_i = D - \mid \epsilon_b \mid. \quad (12)$$

Then for a square well of depth D and width L, which is strongly repulsive for $\rho < \rho_1$, the WKB wave functions are

$$\phi_b(\rho) = N_b \cos[Q(\rho - \rho_1) - \pi/4];$$
$$N_b^2 = 2/L + 1/Q \doteq 2/L,$$
$$\phi_f(\rho) = N_f \cos[P(\rho - \rho_1) - \pi/4];$$
$$N_f^2 = 2M_i/\pi\hbar^2 P, \quad (13)$$

where $\phi_f(\rho)$ is thus normalized per unit energy range. For there to exist a bound state b of energy ϵ_b, we must have the quantum condition

$$QL = (v + \tfrac{1}{2})\pi,$$

v = an integer (vibrational quantum number). (14)

If we now take $\rho_1 \doteq \rho_0$, where ρ_0 is the equilibrium nuclear separation of the AB molecule, then the matrix element of $(\rho - \rho_0)$ between the free and bound

[8] E. Bauer, Phys. Rev. **84**, 315 (1951); **85**, 277 (1952).

states is given by the expression

$$(\rho-\rho_0)_{fb}=(N_fN_b/2)\cdot\left[\frac{(-1)^v\sin PL}{(P-Q)^2}-\frac{(-1)^vL\cos PL}{(P-Q)}-\frac{1}{(P-Q)^2}\right] \quad (15)$$

where terms of order $(P+Q)^{-1}$ and $(P+Q)^{-2}$ have been neglected.

V. INTERMOLECULAR POTENTIAL

As in our previous work,[6,7] we neglect the angular dependence of $V(r)$, and use a Morse potential to describe the r dependence of $V_e^0(r)$ and $V'(\rho, r)$. The numerical values used are those obtained in our previous work on oxygen[7]:

$$V_e^0(r)=U_e^0\{\exp[-2a(r-d)]-\exp[-a(r-d)]\},$$
$$U_e^0=1.43\times10^{-3}e^2/a_0;$$
$$a=1.1a_0^{-1}; \quad d=6.63a_0. \quad (16)$$

$$V'(\rho, r)=(\rho-\rho_0)U'a\{\exp[-2a(r-z)]-\exp[-a(r-z)]\}$$
$$U'=0.262\times10^{-3}e^2/a_0; \quad z=7.40a_0. \quad (17)$$

In deriving Eq. (17),[6] we have expanded V' in powers of $(\rho-\rho_0)$, where ρ_0 is the equilibrium internuclear separation of the AB molecule, and discarded all but the first term. This has some justification for the vibrational-relaxation-time problem, since the mean amplitude of oscillation, and the anharmonicity, of the lowest vibrational states $v=0$, 1 is not large. This assumption is certainly not justified in the present case, not more than is neglect of the angular dependence of $V(r)$. However, we certainly do not have sufficient information to justify any additional complication in these directions. Furthermore, the large value of the transition probability will obscure certain detailed features of the intermolecular potential that would produce very significant changes in the vibrational-relaxation problem.

VI. FLUX CONSERVATION

Some of the results obtained by the numerical perturbation method violate the condition of flux conservation. That is, if we write the cross section for dissociation as

$$\sigma_{fb}=\sum_{l=0}^{\infty}(2l+1)\sigma_{fb}(l), \quad (18)$$

then

$$\sigma_{fb}(l)>\pi/k_b^2 \quad \text{for} \quad l<l_{\text{crit}}, \quad (19)$$

and π/k_b^2 is the maximum value permitted for an inelastic scattering cross section by flux conservation.[9]

[9] Cf. N. F. Mott and H. S. W. Massey, *Theory of Atomic Collisions* (Oxford University Press, New York, 1949), 2nd ed., p. 133 ff; J. M. Blatt and V. F. Weisskopf, *Theoretical Nuclear Physics* (John Wiley & Sons, Inc., New York, 1952), Chap. 8.

The fact that the perturbation method gives results that violate flux conservation is due to the relatively small energy transfer between translational and vibrational degrees of freedom, and the consequent strong coupling between these two modes of motion. Similar difficulties involving violation of flux conservation are familiar in problems such as the elastic scattering of a particle by a center of force, where the exact expression for the solution is

$$\sigma(l)=(4\pi/k^2)\sin^2\delta_l,$$

while perturbation theory gives the result

$$\sigma(l)=(4\pi/k^2)\tan^2\delta_l.$$

A simple way to get a result that may be meaningful if the numerical calculations violate flux conservation is to put

$$\sigma_{fb}^{\text{corr}}(l)=\begin{cases}\pi/k_b^2 & \text{for } l<l_{\text{crit}}\\ \sigma_{fb}^{\text{pert}}(l) & \text{for } l>l_{\text{crit}},\end{cases} \quad (20)$$

where l_{crit} is obtained from the numerical (perturbation) cross section $\sigma_{fb}^{\text{pert}}(l)$ by using Eq. (19). This correction has been applied to all the numerical results quoted here, and is implicit in all equations used in their derivation.

VII. THREE-BODY RECOMBINATION COEFFICIENT

When two atoms A, B combine from the "free" state f of the molecule AB into the bound state b, in the presence of a third body C (to conserve energy and momentum), the number of recombinations per unit volume and unit time is

$$dn_{\text{rec}}/dt=C_{bf}n_An_Bn_C, \quad (21)$$

where n_A, n_B, n_C are the numbers of A, B, C atoms per unit volume; C_{bf} is the three-body recombination coefficient.

Three-body recombination is the inverse process to dissociation of the molecule AB by collision with C, and thus the three-body recombination coefficient C_{bf} is related to the dissociation cross section σ_{fb} by the principle of detailed balance. In particular, for the inverse to process (2), the number of dissociations per unit volume and unit time is given by

$$dn_{\text{diss}}/dt=\sigma_{fb}(\hbar k_b/M_e)n_{AB'}n_{C''}. \quad (22)$$

In a state of statistical equilibrium,

$$dn_{\text{diss}}/dt=dn_{\text{rec}}/dt, \quad (23)$$

so that

$$C_{bf}=(n_{AB'}n_{C''}/n_An_Bn_C)(\hbar k_b/M_e)\sigma_{fb}. \quad (24)$$

Now, from equilibrium considerations[10] one can obtain

[10] Cf. H. E. Moses and T.-Y. Wu, Phys. Rev. **83**, 109 (1951), Appendices 1, 5.

TABLE II. Numerical results for the capture cross section $\sigma_{fb}(\epsilon_f)$.[a]

Vibrational state $v=10$				Vibrational state $v=9$			
k_b	p_f	l_{crit}	$\sigma_{fb}(\epsilon_f)$	k_b	p_f	l_{crit}	$\sigma_{fb}(\epsilon_f)$
15	1	...	26	20	1	...	2.4
	2	40	81		2	...	8.1
	3	60	93		3	...	12.4
	4	⏐	99		4	...	15.2
	5	↓	105				
20	1	...	53	25	1	...	7.6
	2	80	111		2	...	27
	3	(>100)	121		3	40	42
	4	⏐	124		4	60	51
	5	⏐	127				
	6	↓	132				
25	1	60	72	30	1	...	15.5
	2	120	112		2	80	46
	3	(>140)	135		3	100	52
	4	⏐	137		4	100	54
	5	↓	139		5	(>120)	56
30	1	100	73	35	1	...	32
	2	140	89		2	120	68
	3	(>160)	93		3	150	80
	4	⏐	94		4	150	81
	5	↓	95		5	150	82
40	1	180	84	40	1	120	52
	3	210	108		3	180	86
	5	210	117		5	⏐	93
	7	(>240)	118		7	↓	96
	9	↓	121				
				50	1	180	68
					3	240	100
					5	(>270)	117
					7	↓	119

[a] (i) The units of k_b, p_f are a_0^{-1}; $\sigma_{fb}(\epsilon_f)$ is measured in a_0^2. (ii) For the definition of l_{crit}, see Eq. (19); $\sigma_{fb}(\epsilon_f)$ is obtained from Eq. (20) when flux conservation is violated, so that there exists a value of l_{crit}. (iii) A numerical value of l_{crit} in parentheses, such as (>100), means that flux conservation was violated up to the highest value of l (in this case 100) for which calculations were made. Effective values of $\sigma_{fb}(\epsilon_f)$ could however be inferred from other results. (iv) The calculations have been made for given p_f and k_b, with k_f fixed by energy conservation [Eq. (11)], rather than for given p_f, k_f, as is suggested in the text. This does not affect the final results.

the result[11]

$$(n_{AB}n_{C''}/n_An_Bn_C)=\Gamma_{bf}=[G_{AB}/G_AG_B(1+\delta_{AB})]\times(4\pi^2\rho_0^2k_b/p_fk_f), \quad (25)$$

where G_A, G_B, G_{AB} are electronic statistical weights of A, B, AB, and $\delta_{AB}=1$ if A and B are identical species, and zero otherwise. For our process(1) $\delta_{AB}=1$ and $G_{AB}=3G_AG_B$, so that

$$\Gamma_{bf}=6\pi^2(\rho_0^2k_b/p_fk_f). \quad (26)$$

We are interested in the temperature-averaged three-body recombination coefficient. From the discussion following Eq. (11) we see that before the temperature averaging, C_{bf} depends on any two of (k_b, k_f, ϵ_f) because of the condition (11) of energy conservation linking these three quantities. For definiteness, let us treat k_f and ϵ_f as independent variables. Under normal conditions, k_f and ϵ_f are separately and independently distributed in Maxwellian fashion characterized by a temperature T. Then, integrating first over ϵ_f, we get

$$C_{bf}(k_f, \epsilon_{f,avT})=\int d\epsilon_f\Gamma_{bf}(\hbar k_b/M_e)\sigma_{fb}(k_f, \epsilon_f)A\epsilon_f^{\frac{1}{2}}\exp-\epsilon_f/kT$$

$$A=2\pi/(\pi kT)^{\frac{1}{2}}, \quad (27)$$

and carrying out the second Maxwell-Boltzmann average, we get

$$C_{bf}(T)=A^*\int k_f^2dk_f\ \exp(-\hbar^2k_f^2/2M_ekT)C_{bf}(k_f, \epsilon_{f,avT})$$

$$A^*=4\pi(\hbar^2/2\pi M_ekT)^{\frac{1}{2}}. \quad (28)$$

The integrations extend over $0<\epsilon_f<\infty$, $0<k_f<\infty$; σ_{fb} just vanishes for those values of (k_f, ϵ_f) that do not satisfy energy conservation.[12]

VIII. RESULTS AND DISCUSSION

The results of the Univac calculation (as corrected by the technique of Sec. VI) are given in Table II. They are compared in Fig. 1 with the latest experimental results.[13,14] We see that the experimental and theoretical results agree to within a factor of 3, which is a very considerable improvement over any previous detailed quantum mechanical calculations.[2,8] One thing that is demonstrated quite clearly by the calculations is that recombination will lead to molecules in highly vibrational excited states. This has been predicted by theorists for quite a long time,[3,8] but thus

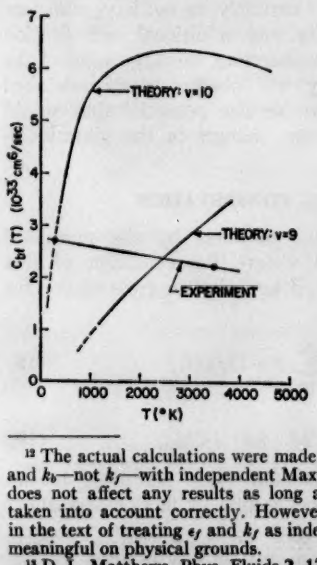

FIG. 1. Three-body recombination coefficient for oxygen, C_{bf}, as a function of temperature.

[11] E. Bauer and M. Salkoff, Research Rept. CX-47 (1960), Institute of Mathematical Sciences, New York University.

[12] The actual calculations were made by averaging over ϵ_f and and k_b—not k_f—with independent Maxwellian distributions. This does not affect any results as long as energy conservation is taken into account correctly. However, the procedure outlined in the text of treating ϵ_f and k_f as independent certainly is more meaningful on physical grounds.

[13] D. L. Matthews, Phys. Fluids **2**, 170 (1959).

[14] R. R. Reeves, G. Manella, and P. Harteck, J. Chem. Phys. **32**, 632 (1960).

far there is not much definite experimental evidence for it.[5]

To be more specific, it has always been hard on strictly theoretical grounds to understand the large experimental values of recombination rates: the fact that the present calculations—which take due account of the upper bounds on cross sections imposed by flux conservation—still exceed the experimental values is thus an error in the right direction. This may be corrected by a more appropriate choice of intermolecular potential, perhaps, or by detailed considerations that might indicate that a certain fraction of $O(^3P)$ atoms will recombine into some state such as $O_2(X\,^3\Sigma_g^-)$, which might possibly have its highest-bound vibrational state bound significantly more strongly than the state $v=10$ of $O_2(A\,^3\Sigma_u^+)$, leading to a smaller effective recombination coefficient. Of course, it must be stressed that the experimental data are subject to some errors, while the theoretical results certainly cannot be relied upon to within better than a factor of 2–3, on account of uncertainties arising from such considerations as the intermolecular potentials or the bound vibrational states. A further source of error in the present calculation is the neglect of molecular rotation: clearly the majority of collisions will be far from colinear, and this is bound to change the final result.

One major criticism that can be made of calculations like the present one is that it is clearly unreasonable to apply perturbation theory—which is satisfactory for processes having small transition probabilities—to problems like the present one, which has a very large transition probability. However, we have used the numerical calculations essentially just to get values of l_{crit}, that is to estimate the limits (in l) beyond which the transition probability is small. Thus, while there are undoubtedly errors in the scheme, they will probably be relatively small.

A different criticism is that the present method is rather wasteful, in that a large amount of numerical data has to be taken to obtain a relatively small amount of useful information. However, a calculation like the present one can give us definite information of the absolute magnitude of transitions probabilities, and on how the recombination coefficient changes with the binding energy $|\epsilon_b|$. It is not clear how one could get such information otherwise. A number of classical calculations of three-body recombination have been made recently, using various kinds of semiempirical assumptions.[15] These calculations are extremely valuable in supplementing calculations like the present one by exploring the statistical factors that are very important in this kind of problem. Clearly the results of our calculation can be used to get a better physical insight on which such statistical models can be based: a very simple model is discussed in the Appendix.

[15] J. C. Keck, J. Chem. Phys. **29**, 410 (1958); **32**, 1035 (1960). D. L. Bunker, *ibid.* **32**, 1001 (1960).

To sum up, it was clear from the outset that a quantum mechanical calculation of a problem as complicated as three-body recombination could hardly aim to obtain detailed quantitative results, because of all the various complications that arise when one really tries to take all relevant physical effects into account; and to make an estimate of these—even if one were willing to undertake the labor—would call for detailed experimental information that is simply not available. The present calculation is thus a schematic one using a greatly oversimplified model. However, within its very obvious limitations the present calculation does indicate that the orders of magnitude of experimental recombination coefficients can be understood if one supposes the molecules resulting from recombination to be formed in highly vibrationally excited states. In fact, it might be possible from the temperature variation of the recombination coefficient to get some information on the binding energy of the vibrational states involved.

ACKNOWLEDGMENT

We should like to thank Dr. James C. Keck of Avco-Everett Research Laboratory, Dr. Kazuo Takayanagi of Saitama University, and Dr. Ta-You Wu of the National Research Council of Canada, for their interest and help at various stages of this work.

APPENDIX: A SIMPLE MODEL FOR THE RECOMBINATION COEFFICIENT

In a situation like the present, where perturbation theory fails because the predicted cross section is so large that it violates flux conservation, we can try to get a rough analytical estimate of l_{crit} of Eq. (19), and then use Eq. (20) or some suitable modification of it to give a value of σ_{fb}, and hence of C_{bf}.

Evidently if the intermolecular potential has a mean range R, this gives a characteristic angular momentum l_{crit} from the standard "impact parameter" condition

$$\hbar l_{\text{crit}} = \hbar k_b R. \tag{A1}$$

If we make use of the fact that $k_b \doteq k_f$, and replace Eq. (20) by the form

$$\sigma_{fb}(l) = \begin{cases} \pi/k_b^2 & \text{for } l < l_{\text{crit}} \\ 0 & \text{for } l > l_{\text{crit}} \end{cases}, \tag{A2}$$

then we get the result

$$\sigma_{fb}(\epsilon_f, k_f) = \sum_{l=0}^{l_{\text{crit}}} (2+1)(\pi/k_b^2) = \pi R^2. \tag{A3}$$

Substituting this expression in Eqs. (27) and (28), we get the expression

$$C_{bf}(v; T) \doteq 24\pi^2 \rho_0(v)^2 R^2 \hbar/(M_i M_e)^{\frac{1}{2}}. \tag{A4}$$

We see that the result (A4) depends on temperature T only insofar as the effective range R of the intermolecular potential depends on temperature, and on the vi-

brational state v only insofar as the equilibrium nuclear separation $\rho_0=\rho_0(v)$. However, this admittedly very rough approximation indicates that C_{bf} increases with increasing v (cf. Table I), and possibly decreases very slightly with increasing T. To get a simple numerical estimate, let us put $R=7a_0\doteq d$ of Eq. (16); then inserting $\rho_0(v)$ from Table I, we get

$$C_{bf}^{\text{app}}(v=9)=6\times10^{-33}\text{ cm}^6/\text{sec}$$
$$C_{bf}^{\text{app}}(v=10)=8\times10^{-33}\text{ cm}^6/\text{sec}. \quad \text{(A5)}$$

A number of approximate estimates of three-body recombination coefficients have been made by different people. The simplest sort of considerations, obtained virtually from dimensional analysis, give[10]

$$C_{\text{rec}}\sim fR^5\bar{v} \quad \text{(A6)}$$

where $\bar{v}=(8kT/\pi M)^{\frac{1}{2}}$ is the mean molecular speed, $M=$reduced mass, and f some kind of probability factor. Putting $f=1$, $R=7a_0$, $\bar{v}=10^5$ cm/sec, we get $C_{\text{rec}}\sim5\times10^{-33}$ cm^6/sec.

THE JOURNAL OF CHEMICAL PHYSICS VOLUME 33, NUMBER 4 OCTOBER, 1960

Axial Crystal Fields in the Ionic Model

T. S. PIPER AND R. L. CARLIN*

William Albert Noyes Laboratory of Chemistry, University of Illinois, Urbana, Illinois

(Received June 20, 1960)

Expressions for the axial components of crystal fields of tetragonal, trigonal, and cylindrical symmetry are developed in terms of the parameters *Ds* and *Dt*. These parameters are calculated in the ionic model using Hartree-Fock 3d radial wave functions. The calculated parameters are compared to experimental values obtained from the spectra of V(III) in Al_2O_3 and Co(II) in CoO. Tentative assignments of the bands in the spectrum of $(C_5H_5)_2Ni$ are made.

THE bands in the optical spectra of the first transition series metal ions which are octahedrally coordinated may be described with fair accuracy in terms of a single crystal field parameter, *Dq*, in addition to the parameters of the electron-electron repulsions.[1] The parameter *Dq* is most conservatively viewed as a quantity to be determined experimentally; however, it has been found possible to estimate *Dq* in the ionic model, i.e., the model in which the ligands are replaced by point charges or dipoles.[2,3]

We will examine here the parameters which may be used to describe the 3*d* orbital energy levels in fields which are predominantly octahedral but which also possess components with axial symmetry. In such systems three parameters are required. A further test of the ionic model is then offered since the model predicts the ratios of some of these parameters and these ratios are altered by covalency.[4] The oxides and fluorides are the most ionic compounds of the transition metal ions; in these compounds the metal ion is often surrounded by a slightly distorted octahedron of anions. Accordingly we have developed convenient expressions for the parameters describing the field of an octahedron of point charges distorted along a trigonal or tetragonal axis.

There is no commonly accepted notation for the axial field parameters. Following and extending the notation of Moffitt and Ballhausen[5] we propose that, irrespective of the symmetry of the particular field, the two parameters associated with the axial potential terms be labeled *Ds* and *Dt*.

CALCULATIONS OF THE PARAMETERS IN THE IONIC MODEL

The electrostatic potential experienced by a single 3*d* electron in the crystal field is expanded:

$$V_{CF}=\sum_{l,m}A_l^m Y_l^m(r_<^l/r_>^{l+1}).$$

The A_l^m are constants, the $Y_l^m(\theta,\phi)$ are spherical harmonics, and $r_<(r_>)$ is the lesser (greater) of the two distances, r, the distance of the electron from the metal ion nucleus, and R, the metal ion-ligand distance. In an octahedral field the term of this expansion with $l=4$ gives rise to the familiar splitting of the 3*d* orbitals into the sublevels T_2 and E separated by 10 *Dq*. In the field of 6-point charges of magnitude Z

$$Dq=\tfrac{1}{6}Z\langle r_<^4/r_>^5\rangle.$$

A. The Trigonal Field

A trigonal field may be obtained by compression or elongation of an octahedron of point charges along a

* Present address: Department of Chemistry, Brown University, Providence, Rhode Island.

[1] See for example the chapter written by D. S. McClure, *Solid State Physics*, edited by F. Seitz and D. Turnbull (Academic Press, Inc., New York, 1959), Vol. 9.

[2] R. L. Belford and M. Karplus, J. Chem. Phys. **31**, 394 (1959).

[3] R. E. Watson, Phys. Rev. **117**, 742 (1960).

[4] H. S. Jarrett, J. Chem. Phys. **31**, 1579 (1959).

[5] W. Moffitt and C. J. Ballhausen, Ann. Rev. Phys. Chem. **7**, 107 (1956).

threefold axis (labeled z) without change in the metal ion-ligand distance. The resulting field has D_{3d} symmetry and may be characterized by two geometrical parameters: the distance R, and the azimuthal angle, a. The potential terms and associated parameters are

$$A_4^3[-Y_4^0+i(\tfrac{10}{7})^{\frac{1}{2}}(Y_4^3+Y_4^{-3})](r_<^4/r_>^5)\sim Dq$$

$$A_2^0Y_2^0(r_<^2/r_>^3)\sim Ds$$

$$A_4^0Y_4^0(r_<^4/r_>^5)\sim Dt.$$

The appropriate linear combinations of $3d$ orbitals which form both octahedral and trigonal bases are

$$e_\pm=3^{-\frac{1}{2}}(\mp\sqrt{2}d_{\pm1}\pm id_{\mp2})$$

$$t_\pm=3^{-\frac{1}{2}}(\mp d_{\pm1}\mp i\sqrt{2}d_{\mp2})$$

$$t_0=d_0.$$

The first-order perturbation matrix of the potential is

$$\begin{array}{c} \\ e_\pm \\ t_\pm \\ t_0 \end{array}\begin{array}{c} \begin{array}{ccc} e_\pm & t_\pm & t_0 \end{array} \\ \begin{vmatrix} 6Dq-7Dt & -\sqrt{2}Ds-5\sqrt{2}Dt & 0 \\ -\sqrt{2}Ds-5\sqrt{2}Dt & -4Dq+Ds-2Dt & 0 \\ 0 & 0 & -4Dq-2Ds+18Dt \end{vmatrix} \end{array}.$$

In the ionic model the parameters are

$$Dq=-\tfrac{9}{5}\tfrac{5}{6}(\tfrac{3}{3}\cos^4a-10\cos^2a+1)Z\langle r_<^4/r_>^5\rangle$$

$$Ds=-\tfrac{3}{7}(3\cos^2a-1)Z\langle r_<^2/r_>^3\rangle$$

$$Dt=\tfrac{1}{1}\tfrac{1}{2}[\tfrac{3}{2}(\tfrac{3}{3}\cos^4a-10\cos^2a+1)+\tfrac{1}{9}\tfrac{4}{9}]Z\langle r_<^4/r_>^5\rangle.$$

The parameters Ds and Dt as defined are positive for axial compression, i.e., increase of the angle a. The parameter Dq will be seen to depend upon the angle, a.

B. The Tetragonal Field

A point charge representation of a tetragonal field may be obtained by compression or elongation of an octahedron of point charges along a four-fold axis labeled z. This case has been previously investigated by several authors[6,7] who give the matrix elements in units of the radial integrals. Several authors[8–10] have proposed expansion terms and the associated parameters without however giving the expressions in terms of the ionic model. The energies of the levels and parameters are given below.

$$E(z^2)=6Dq-2Ds-6Dt$$

$$E(x^2-y^2)=6Dq+2Ds-Dt$$

$$E(xy)=-4Dq+2Ds-Dt$$

$$E(xz,yz)=-4Dq-Ds+4Dt$$

$$Dq=(1/6)Z\langle r_<^4/r_>^5\rangle_{xy}$$

$$Ds=(2/7)Z[\langle r_<^2/r_>^3\rangle_{xy}-\langle r_<^2/r_>^3\rangle_z]$$

$$Dt=(2/21)Z[\langle r_<^4/r_>^5\rangle_{xy}-\langle r_<^4/r_>^5\rangle_z].$$

The parameters Ds and Dt as defined above are positive for axial elongation.[11]

C. The Cylindrical Field

One possible ionic model[12] for the di-π-cyclopentadienyl compounds is a pair of rings parallel to each other each bearing a negative charge at a distance R from the metal ion and at an azimuthal angle, a. This is a purely axial field. The results of the calculations are given below.

$$E(d_0)=2Ds-6Dt$$

$$E(d_{\pm1})=Ds+4Dt$$

$$E(d_{\pm2})=-2Ds-Dt$$

$$Ds=\tfrac{1}{7}(3\cos^2a-1)\langle r_<^2/r_>^3\rangle$$

$$Dt=-\tfrac{1}{2}\tfrac{1}{8}(\tfrac{3}{3}\cos^4a-10\cos^2a+1)\langle r_<^4/r_>^5\rangle.$$

APPLICATIONS OF THE PARAMETERS

A. Trivalent Ions in Al_2O_3

The spectra of V(III)[13] and Cr(III)[14,15] in the α-Al_2O_3 (corundum) structure have been obtained

[6] C. J. Ballhausen, Kgl. Danske Videnskab. Selskab, Mat.-fys. Medd. **29**, No. 4 (1954).

[7] R. L. Belford, M. Calvin, and G. Belford, J. Chem. Phys. **26**, 1165 (1957).

[8] A. Abragam and M. H. L. Pryce, Proc. Roy. Soc. (London) **A206**, 173 (1951).

[9] T. Moriya, K. Motizuki, J. Kanamori, and T. Nagamiya, J. Phys. Soc. Japan **11**, 211 (1956).

[10] Footnote reference 5, p. 123.

[11] It is also possible to define a Dq' as the weighted average $\frac{2}{3}Dq(R_{xy})+\frac{1}{3}Dq(R_z)$. Then the coefficients of Dt' in the above energy expressions become -3, $+3$, -4, and $+2$ while the numerical factor in the expression for Dt' becomes 5/63. This definition is much less convenient because the potential term corresponding to Dt' no longer has axial symmetry.

[12] F. A. Matsen, J. Am. Chem. Soc. **81**, 2023 (1959). In this note the term with $l=4$ was omitted.

[13] M. H. L. Pryce and W. A. Runciman, Disc. Faraday Soc. **26**, 34 (1958).

[14] S. Sugano and Y. Tanabe, J. Phys. Soc. Japan **13**, 880 (1958).

[15] S. Sugano and I. Tsujikawa, J. Phys. Soc. Japan **13**, 899 (1958).

TABLE I. Radial expectation values calculated with Hartree-Fock wave functions.

Ion	R	$\langle r_<^2/r_>^3\rangle$	$\langle r_<^4/r_>^5\rangle$
	a.u.	a.u.	a.u.
V(III)	3.76	0.03086	0.00713
	3.50	0.03814	0.01006
	2.76	0.07572	0.02906
	2.50	0.09907	0.04298
Co(II)	4.00	0.01948	0.003531
	3.9533	0.02018	0.003736
	3.05	0.04350	0.012693
	3.0033	0.04551	0.013596

and interpreted. The trigonal field parameters were assumed[14] to take the form

$$\begin{array}{c} e_\pm \\ t_\pm \\ t_0 \end{array}\begin{pmatrix} 0 & K' & 0 \\ K' & K & 0 \\ 0 & 0 & -2K \end{pmatrix}.$$

It was furthermore assumed that K' could be neglected. Calculations based on the experimental data indicated that for Cr(III), $K=-350$ cm^{-1} and for V(III)[13], $K=-400$ cm^{-1}. Note that $K=Ds-9Dt$. This representation of the trigonal field differs from ours by a similarity transformation and hence the basis functions of the matrix in K and K' are not accurate octahedral basis functions. The values of K and Dq determined from the experimental frequencies in this manner will be accurate only if Dt is negligible compared to Ds and if Ds is small compared to Dq.

We will now calculate numerical values of the parameters in the ionic model. The corundum lattice[16] is rhombohedral and the site symmetry at the metal ions is C_3. The metal ions are in equivalent positions. The octahedron of oxide ions about each aluminum ion is badly distorted; the coordinates of the two sets of three oxide ions are $R_1=1.99$ A, $a_1=46.4°$ and $R_2=1.845$ A, $a_2=64.3°$. These values may be compared to the octahedral angle of 54.7°. We will assume that the impurity ions do not appreciably distort the lattice, at least as far as the angular coordinates of the oxide ions are concerned. This seems reasonable in view of the similarity of the rhombohedral angle of α-Al_2O_3 (55°17′) to that of α-Cr_2O_3 (55°6′).

The radial expectation values in Table I were calculated using the point charge model and the Hartree-Fock radial functions calculated by Watson.[17] The calculated field parameters and experimental results for V(III) are compared in Table II. In case I the observed distances $R_1=3.76$ a.u. and $R_2=3.50$ a.u. were used. Since the calculated parameters in case I are much too small, the ligand distances were reduced to fit $E(e_\pm)-E(t_\pm)$; then $R_1=2.76$ a.u. and $R_2=2.50$ a.u. (Case II). The necessity for reduction of the ligand distances has been explained as an allowance for polarization and for the fact that the ligand charge is not a point charge.[2]

Once the larger splitting is fitted it can be seen that the sign of the trigonal splitting is correctly predicted. Since the potential of the three ions at the shorter of the two distances predominates, the sign of K is that for a trigonal compression. The magnitude of the trigonal splitting is only approximately fitted. However the observed values are in doubt because of the neglect of K'. It can be seen that the neglect of K' leads to an underestimation of K.

B. Tetragonal Cobaltous Oxide

Cobaltous oxide is the only oxide for which tetragonal splittings have been reported.[18] At room temperature the crystal is cubic but at 78°K it is tetragonal with axial compression[19]: $R_{sy}=2.123$ A and $R_s=2.099$ A. Pratt and Coelho analyzed the spectra at 78°K in terms of the parameters of Abragam and Pryce.[20] With neglect of spin-orbit coupling they found $Dq=942$ cm^{-1}, $H=410$ cm^{-1}, and $I=428$ cm^{-1} from which $Ds=-117$ cm^{-1} and $Dt=-33$ cm^{-1}.

Using the radial expectation values calculated for the observed distances (the first pair of distances under cobalt in Table I), the field parameters are $Dq=258$ cm^{-1}, $Ds=-88$ cm^{-1}, and $Dt=-9$ cm^{-1}. Since the calculated Dq is much too small we have calculated the parameters with a 25% reduction in the ligand distances and find $Dq=948$ cm^{-1}, $Ds=-252$ cm^{-1}, and $Dt=-38$ cm^{-1}.

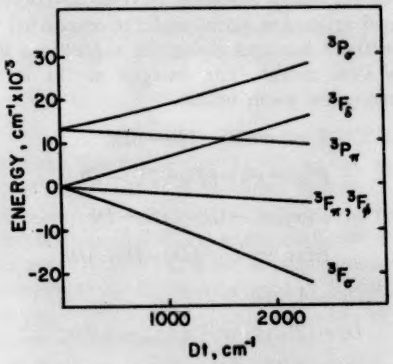

FIG. 1. Splittings of the triplet terms of $3d^8$ in an axial field with $4Ds=5Dt$.

[16] L. Pauling, Z. Krist. **69**, 415 (1928).

[17] R. E. Watson, *Iron Series Hartree-Fock Calculations*, Tech. Rept. No. 12, Solid-State and Molecular Theory Group, Massachusetts Institute of Technology, June 15, 1959 (unpublished). See also R. E. Watson, Phys. Rev. **118**, 1036 (1960).

[18] G. W. Pratt, Jr., and R. Coelho, Phys. Rev. **116**, 281 (1959).

[19] N. C. Tombs and H. P. Rooksby, Nature **165**, 442 (1950).

[20] See footnote reference 8. The axial parameters associated with the potential terms in Cartesian coordinates are multiplied by $-2/7$ and $-8/105$ to obtain Ds and Dt as defined here. There is some question as to how the analysis was carried out in that the potential term for the parameter I does not have axial symmetry (cf. footnote reference 9).

TABLE II. Comparison of calculated and observed crystal field parameters for V(III) in Al_2O_3.

	Dq cm^{-1}	Dt cm^{-1}	Ds cm^{-1}	K cm^{-1}	$E(t_0)-E(t_\pm)$ cm^{-1}	$E(e_\pm)-E(t_\pm)$ cm^{-1}
Calc case I	446	41	330	−35	38[a]	4 207[a]
Calc case II	1 846	175	1 036	−539	822	17 410
Obs V(III)	1 750	...	...	−400	1 200	17 900
Obs Cr(III)	...	...	...	−350	1 050	18 000

[a] With interchange of b and $t_\pm$; i.e., b is at lower energy.

C. Di-π-cyclopentadienyl Nickel

Very little is known of the excited states of the sandwich compounds. As an illustration of the use of the parameters we will make some tentative assignments of the observed bands in the spectrum of $(C_5H_5)_2Ni$. We will make the assumption that the electrons are in pure $3d$ orbitals. Furthermore we assume with Robertson and McConnell[21] that the $d_{\pm 2}$ and d_0 orbitals are nearly degenerate, i.e., $4Ds \approx 5Dt$. With these assumptions the ground state is the $^3F_\sigma$ component of the term ^3F. The relevant matrix elements were calculated starting with the free-ion wave functions. The diagonal matrix elements are $Ds-3Dt(^3F_\phi)$, $7Dt(^3F_\delta)$, $-\frac{2}{5}Ds-Dt(^3F_\pi)$, $-\frac{4}{5}Ds-6Dt(^3F_\sigma)$, $-(7/5)Ds(^3P_\pi)$ and $(14/5)Ds(^3P_\sigma)$. The off-diagonal element for the π orbitals is $\frac{1}{2}6^{\frac{1}{2}}(-4Ds+5Dt)$ and that for the σ orbitals is $\frac{1}{7}(-3Ds-5Dt)$. This treatment neglects off diagonal elements which would appear in the lower symmetry D_{3d} to which the molecule actually belongs. The calculated energy level diagram is shown in Fig. 1.

We have measured the spectrum of $(C_5H_5)_2Ni$ in cyclohexane solution. There is a broad band at 14 500 cm^{-1} ($\epsilon=64$) and another at 32 700 cm^{-1}($\epsilon=1\,200$) with shoulders at 29 000 cm^{-1} and 36 000 cm^{-1}. A tentative assignment of these bands may be made from the diagram with $Dt \approx 1800$ cm^{-1}. The low energy band is assigned to $^3F_\sigma \rightarrow {}^3F_\pi$ and $^3F_\phi$ and the higher energy band to $^3F_\sigma \rightarrow {}^3P_\pi$ and $^3F_\delta$.

CONCLUSION

The octahedral field parameter, Dq, has been found to be underestimated by a factor of three to four by the simple ionic model in which the ligands are replaced by point charges at the observed ligand distances and in which Hartree-Fock wave functions of the free metal ion are used. This is not surprising in view of the crudity of a model which neglects the finite extension of the ligand electron density and exchange with the metal ion electron density. Only a small improvement could be obtained by allowing the t_{2g} and e_g electrons to have different radial functions as determined by a self-consistent field calculation.[22] It is possible to fit the octahedral splitting by decreasing the ligand distance by about 25%. Another possibility is to add a point dipole to allow for polarization. However, these modifications remain arbitrary unless other experimental data are simultaneously fitted.

Our calculations indicate that approximate values of the axial field parameters are obtained by decreasing the ligand distance and hence this modification of the ionic model does promise to be of aid in estimating parameters. Unfortunately a more detailed comparison with experimental results is not possible at present since none of the spectra have been completely analyzed. In particular it will be interesting to determine whether the angular portions of the parameters are accurately predicted by this treatment.

ACKNOWLEDGMENTS

We thank the National Science Foundation for a grant and a fellowship (RLC). We wish to thank Professor Martin Karplus for helpful discussions and Dr. Robert P. Hurst for his kind assistance in the numerical calculations.

[21] R. E. Robertson and H. M. McConnell, J. Phys. Chem. 64, 70 (1960).

[22] See footnote references 2 and 3. It should be noted that the calculated values of Dq in footnote reference 3 are too large by a factor of about 2.2 due to an error in the numerical coefficient of Eq. (6).

Inter- and Intra-Atomic Correlation Energies and Theory of Core-Polarization

OKTAY SINANOĞLU*

Department of Chemistry and Lawrence Radiation Laboratory, University of California, Berkeley 4, California

(Received March 18, 1960)

Atomic and molecular energies depend strongly on the correlation in the motions of electrons. Their complexity necessitates the treatment of a chemical system in terms of small groups of electrons and their interactions, but this must be done in a way consistent with the exclusion principle. To this end, a nondegenerate many-electron system is treated here by a generalized second-order perturbation method based on the classification of all the Slater determinants formed from a complete one-electron basis set. The correlation energy of the system is broken down into the energies of pairs of electrons including exchange. Also some nonpairwise additive terms arise which represent the effect of the other electrons on the energy of a correlating pair because of the Pauli exclusion principle. All energy components are written in approximate but closed forms involving only the initially occupied H.F. orbitals. Then each term acquires a simple physical interpretation and becomes adoptable for semiempirical usage. The treatment is applied in detail to two particular problems: (a) The correlation energy between an outer electron in any excited state and the core electrons, e.g., in the Li atom, is represented by a potential acting on the outer one. This potential can be regarded as the mean square fluctuation of the Hartree-Fock potential of the core, and applies even when the outer electron penetrates into the core. The magnitudes of some of the correlation effects are calculated for Li. (b) Starting from a complete one-electron basis set of SCF MO's, the energy of a molecule is separated into those of groups of electrons and of *intra*-molecular dispersion forces acting between the groups. The assumptions that are usually made in discussing dispersion forces at such short distances are then removed and generally applicable formulas are given. Some three or more electron-correlation effects and limitations in the use of "many electron group functions" for overlapping systems are also discussed.

I. INTRODUCTION

THE total energy of a many-electron system is well approximated by independent particle theories, in particular by the Hartree-Fock (H.F.) method.[1,2] But the remaining error, which results from the tendency of the electrons to avoid one another, is usually of the order of chemically interesting quantities. This error i.e., the difference between the completely self-consistent field (SCF) H.F. solution to the energy and the exact solution of the many-electron nonrelativistic Hamiltonian, will be taken here as the precise definition[2] of "correlation energy" unless otherwise indicated. Considerable effort has been devoted to obtaining the correlation energies of atoms and molecules by variational techniques, especially by the method of configuration-interaction.[2] In spite of slow convergence, computers now allow some progress by these techniques for simpler systems, e.g., molecules from the first row of the periodic table. But, generally, it is necessary to have schemes that lend themselves to simple physical interpretation and generalization. It is also important in view of the complexity of most molecules and atoms that such schemes should be usable in a semiempirical but still well-defined way.

There exists a special class of problems where it has been possible to treat the correlation effects very simply. These involve the correlation energies between nonoverlapping charge distributions; or more precisely, in these cases different electron groups are assumed to be localized in totally isolated regions of space, each group with its own complete set of eigenfunctions. The best example is the familiar London dispersion attraction[3,4] between two atoms in their ground states.[5] This energy, which has the very useful property of being pairwise-additive for a system of atoms, also has a very simple physical interpretation. It arises from the mean square fluctuations of the instantaneous atomic dipoles.

A different case concerning correlation energy between separable groups arises in the theory of atomic spectra. In alkalilike configurations optical transitions occur by the excitation of a "series," i.e., valence, electron, outside an inner "core" giving a hydrogenlike spectrum. The H.F. SCF method for such an atom, takes the average effect of the outer orbital on the core into account, but the correlation between the instantaneous position of the series electron and the core electrons is left out. This correlation effect has come to be known under the name of "core polarization."[1] The simplification in this case arises when the series electron is in a highly excited "nonpenetrating" orbit, i.e., when the core and the valence electron can be separated. Then it is possible to represent the correlation energy between the core electrons and the series electron by an additional effective potential which is determined only by the core and acts on the outer electron in any one of its higher orbits. A classical argument indicates that at large separations this potential is given by $-\frac{1}{2}\alpha r^{-4}$ where α is the polarizability of the ion core and r is the distance of the series electron from the nucleus. Several quantum mechanical derivations have

* University of California Lawrence Radiation Laboratory Postdoctoral Fellow 1959–60. Present address: Sterling Chemistry Laboratory, Yale University, New Haven, Connecticut.

[1] For reviews see D. R. Hartree, *Calculation of Atomic Structures* (John Wiley and Sons, Inc., New York, 1957).

[2] P. O. Löwdin, Advances in Chem. Phys. **2**, 207 (1959).

[3] F. London, Z. Physik. Chem. **B11**, 222 (1930).

[4] H. Margenau, Revs. Modern Phys. **11**, 1 (1939).

[5] In this case, the definition given for correlation energy is somewhat altered; it still applies, however, if the electrons of one system are considered to move in the self-consistent field of the other.

been given for this asymptotic potential. The "adiabatic approximation"[6] method distinguishes a tightly bound core electron from an outer one in any orbital with high quantum numbers, e.g., in the excited states of He, and replaces the exact two-electron wave functions by

$$\psi_k(\mathbf{r}_1, \mathbf{r}_2) = u_c(\mathbf{r}_1; \mathbf{r}_2)\, u_v^k(\mathbf{r}_2), \qquad (1)$$

where $\mathbf{r}_1$ and $\mathbf{r}_2$ refer to the coordinates of the inner and outer electrons, respectively; $u_v^k(\mathbf{r}_2)$'s are the various states of the outer electron; $u_c(\mathbf{r}_1; \mathbf{r}_2)$ describes the core electron and depends only parametrically on $\mathbf{r}_2$. This approximation is very similar to the Born-Oppenheimer separation of nuclear and electronic motions in molecules. Since the outer electron is much less tightly bound than the inner one, it can be considered, in view of the virial theorem, to move slowly compared to the latter. Then the energy of the core can be determined for various fixed values of $\mathbf{r}_2$, thus depending on $\mathbf{r}_2$ parametrically; and it, in turn, acts as a potential energy for the motion of the outer electron. Bethe[7] has treated the highly excited states of He by this approach, considering the stationary charge of r_2 as a perturbation on the free "core" function, $u_c^0(r_1)$. This discussion should emphasize that the name "core polarization" refers to the polarization of the core by the outer electron at its instantaneous position. This *is* the entire correlation effect and should not be confused with the polarization of the core only by the smeared-out over-all charge distribution of the outer *orbital*. The latter which we shall call the "orbital average polarization" is a much smaller effect and in fact vanishes if completely SCF H.F. orbitals are used (see Sec. II).

Mayer and Mayer[8] and Van Vleck and Whitelaw[9] have treated the core-polarization energy by conventional second-order perturbation theory with hydrogen-like orbitals for the outer electron and by assuming the valence electron and the core to be essentially independent systems. This treatment shows that the analogy between core polarization and the interatomic London forces mentioned previously, is perfect. We may even be tempted to refer to the attraction arising between the outer electron and the core in the former case, as a Van der Waals force.

The particular advantage of both London forces and the use of a correlation potential, is that they both relate the interactions in the composite system to the properties of the component parts. This advantage has induced attempts at using both theories under more general conditions.

Pitzer[10] has reviewed the use of London forces not only at the usual large separations, but even within the same molecule, e.g., to estimate the correlation energies between the lonepair electrons in the halogen series, F_2 to I_2, and to account for the isomerization energies of the hydrocarbons. Similarly, Douglass[11] has assumed the feasibility of using a core-polarization potential even inside the core and has determined such a potential semiempirically by comparing the observed and H.F. energy values for the first few series levels in alkaline ions. Various other empirical attempts at obtaining such a potential for cases where the outer electron penetrates well into the core are summarized by Hartree.[1,12] If it were possible to write a correlation potential which could act over the whole range of an outer orbital coordinate another interesting application would be justified: In molecules where the inner cores may be assumed to be quite unchanged by the binding, the correlation energy between the cores and the valence electrons could be obtained simply by taking the expectation value of the core polarization potentials (obtained perhaps partly from atomic spectra) over the outer molecular orbitals. Callaway[13] did this for Li, Na, and K atoms[14] in their ground states and for their metals, but he used Bethe's[7] method and neglected the penetration effects. This type of application of the core polarization idea is of course also implied in the "II-electron" approximation[15] used for organic molecules.

Both the use of London forces *within* a single molecule and the representation of inner-outer electron, or sigma-pi correlation effects by effective potentials when there is penetration, are open to question. Some of the difficulties involved in the case of intra-molecular London forces have already been mentioned by Coulson.[16] On the other hand, the need for the clarification of the form or the feasibility of a correlation potential for penetrating orbitals has been emphasized by Hartree.[1,12] In both cases, multipole expansions are often used at short distances and, sometimes, only the dipole terms are retained. But this is a defect whose elimination is relatively straightforward (see Secs. II and VI). All the other difficulties have to do with the exclusion principle and the validity of separating electrons into distinguishable (either by strong localization around different centers or by large differences in energy) groups.

The preceding discussion indicates that important simplifications have been possible in dealing with correlation effects whenever a system of electrons could

[6] I am indebted to Professor W. T. Simpson for a stimulating discussion on this approach.

[7] (a) H. A. Bethe, *Handbuch der Physik* (Edwards Brothers, Inc., Ann Arbor, Michigan, 1943), Vol. 24/1, p. 339; see also Bethe and E. E. Salpeter, *Encyclopedia of Physics* (Springer-Verlag, Berlin, Germany, 1957), Vol. 35, p. 223 ff; (b) G. Ludwig, Helv. Physica Acta **7**, 273 (1934).

[8] J. E. and M. G. Mayer, Phys. Rev. **43**, 605 (1933).

[9] J. H. Van Vleck and N. G. Whitelaw, Phys. Rev. **44**, 551 (1933).

[10] K. S. Pitzer, Advances in Chem. Phys. **2**, 59 (1959).

[11] A. S. Douglas, Proc. Cambridge Phil. Soc. **52**, 687 (1956).

[12] D. R. Hartree, Repts. Progr. Phys. Kyoto **11**, 113 (1946).

[13] J. Callaway, Phys. Rev. **106**, 868 (1957).

[14] The adiabatic method has also been applied to alkali by G. Veselov and I. B. Bersuker, Vestnik Leningrad Univ. Ser. Fiz. i Khim. No. 16, 55 (1957).

[15] R. Pariser and R. G. Parr, J. Chem. Phys. **21**, 466 (1953).

[16] C. A. Coulson, *Symposium on Hydrogen Bonding, Ljubljana, 1957* (Pergamon Press, New York, 1959), p. 349.

be divided up into groups in a clear-cut way, but that as soon as this condition is relaxed difficulties are encountered. Now if similar simplified treatments of correlation effects are to be possible in the general case of a system of many electrons all spread out in nearly the same region of space, the following question, which is fundamental to all quantum chemistry, must be answered:

Given an atom or molecule with some N electrons, can we consider this system in a nonarbitrary way as made up of certain groups of electrons in spite of the fact that all these electrons are indistinguishable from one another? The presence of a periodic table of the elements and chemistry suggest that the answer should be yes, not only in single particle theories, but also after the inclusion of correlation energies. Clearly if this is to be done in a nonarbitrary way: (1) All effects of the Pauli exclusion principle must be included, (2) If we start with a method based on the expansion of a many electron function in terms of single particle functions, then all electrons must use the *same* complete basis set of one-electron orbitals. Previous separations of an electronic system into simpler systems do not satisfy the second condition and therefore neither the first. In these treatments, either a one-electron basis set is divided into two mutually exclusive subsets as in connection with the sigma-pi problem,[17] or else, antisymmetrized products of many-electron group functions satisfying generalized orthogonality conditions are used.[18] These conditions, which we shall refer to again in Sec. VI, are too restrictive and they imply the subdivision of the basis set, too.

The general problem of formulating a scheme such that the correlation energy of a system with a large number of electrons can be obtained in terms of its simpler components, can now be broken down into two phases: (a) The separation of the total correlation energy into that of small groups of electrons. (b) The evaluation of the interactions within or between these small groups. The extensions of London-force or core-polarization type treatments to systems with no strongly localized groups now become special cases of (b).

With the objectives (a) and (b) in view, we shall now present a generalized second-order perturbation theory of a many-electron system whose zero-order wave function is a single Slater determinant of Hartree-Fock orbitals. The perturbation method will be based on the use of all "ordered configurations,"[2] i.e., all unique Slater determinants that can be formed from a complete one electron basis set. By a systematic classification of all the virtual transitions represented by the ordered configurations, the correlation energy of the system will be broken down into the energies of pairs of electrons including exchange. Some non-pairwise additive terms will also arise. These represent the tendency of a correlating pair of electrons to avoid the other electrons of the system, because of the Pauli exclusion principle. These extra terms will be defined here as the "exclusion" terms and in future work they may turn out to be the most important three or more particle effects. The use of Hartree-Fock energy as a starting point is convenient, but is not a requirement. The approach presented here also provides a link with the recent "many-body" methods developed in different fields of physics.[19] Definition of "mean excitation energies" for each pair of electrons will allow the estimation of both the pair energies and the exclusion effects, using only the initially occupied spin-orbitals. This procedure, although semiquantitative, is useful for giving many simple physical interpretations, e.g., as in London forces. For instance, in Sec. II, a core-polarization potential which is applicable even near the nucleus will be derived and shown to be the mean-square fluctuation of the Hartree-Fock potential acting on an electron. A large portion of this article will be devoted to the core polarization problem, not only because it is of interest in itself, but also because a system with a "series" electron is more general than a system of closed shells, and the excited states, as well as the ground state of the former, can also be treated. Detailed derivations will be given, for convenience, with specific reference to the lithium atom, although generalization to any other appropriate atom or molecule is straightforward. Section III discusses the "exclusion" effect of an outer orbital, e.g., in Li, on the correlation energy of the core (Li^+) itself. In Sec. IV, numerical magnitudes of some of these effects will be calculated for Li and the penetration parts of the core-polarization potential will be examined. In Sec. V, molecules are discussed, in general, and both the use of intramolecular London-type energies and of "core polarization" justified eliminating the usual approximations mentioned previously by starting from a complete one-electron basis set of molecular orbitals, SCF MO's. In the last section, some higher-order correlation effects are mentioned; a "dispersion" energy formula including such effects, but for use only with asymptotic intermolecular forces, is derived, and the use of many-electron group functions[18] is discussed.

II. SEPARATION OF VARIOUS CORRELATION EFFECTS AND THEORY OF CORE POLARIZATION

The basic theorem[2] of the method of "superposition of configurations" is that if $\{u_k(\mathbf{x})\}$ form a complete orthonormal basis set for the space of a single electron ($\mathbf{x}$ including both spatial and spin coordinates), than any antisymmetric N electron function can be ex-

[17] P. G. Lykos and R. G. Parr, J. Chem. Phys. **24**, 1166 (1956).
[18] R. McWeeny, Proc. Roy. Soc. (London) **A253**, 242 (1959).

[19] For a brief introduction, see D. ter Haar, *Introduction to the Physics of Many-Body Systems* (Interscience Publishers, Inc., New York, 1958).

panded as

$$\psi(\mathbf{x}_1, \mathbf{x}_2, \cdots \mathbf{x}_N) = \sum_K^{\infty} C_K \psi_K(\mathbf{x}_1, \mathbf{x}_2, \cdots \mathbf{x}_N), \quad (2)$$

where ψ_K represents the normalized Slater determinants

$$\psi_K(\mathbf{x}_1, \mathbf{x}_2, \cdots \mathbf{x}_N) = (N!)^{-\frac{1}{2}} \det\{u_{k_1}, u_{k_2}, \cdots u_{k_N}\}, \quad (3)$$

and K runs over every unique selection of the one-electron indices $k_1 < k_2 < \cdots < k_N$, i.e., all "ordered configurations."[2] The ψ_K now form a complete orthonormal basis set for the space of N electrons. In this representation, the energy eigenvalues are the solutions of the secular equation

$$|\mathbf{H} - E\mathbf{I}| = 0, \quad (4)$$

with $\mathbf{H} = \{\langle \psi_K | H | \psi_L \rangle\} \equiv \{\langle K, HL \rangle\}$ and $\mathbf{I}$ the unit matrix. If any one of the nondegenerate ψ_K in Eq. (2), say, ψ_a, is chosen as the first approximation to ψ, then E can be written[2] rigorously as the solution of

$$E = H_{aa} + \mathbf{H}_{ab}(E\mathbf{I}_{bb} - \mathbf{H}_{bb})^{-1}\mathbf{H}_{ba}, \quad (5)$$

where the matrix $\mathbf{H}$ has been partitioned into four submatrices. A great variety of perturbation methods can be derived[2,20] from Eq. (5) by making various approximations in the exact remainder after taking H_{aa} as the "unperturbed" energy. Thus, if the off-diagonal elements of $\mathbf{H}_{bb}$ are neglected and E replaced by H_{aa}, a Schrödinger-type generalized perturbation equation is obtained. This equation, first given by Epstein,[21] is

$$E_\mu \cong H_{MM} - \sum_{K \neq M}^{\infty} [H_{MK}H_{KM}/(H_{KK} - H_{MM})]$$
$$= H_{MM} + E_M^{(2)}. \quad (6)$$

Here, among all the diagonal elements of $\mathbf{H}$, H_{MM} is assumed to be the closest to the exact eigenvalue E_μ. In the summation, K covers the entire orthonormal many-electron basis set, as in Eq. (2), except ψ_M. Because of the orthonormality of $\{u_k\}$ the only H_{MK} that contribute to Eq. (6) are those in which K differs from M [Eq. (3)] by only one or two spin-orbitals. These will be referred to as single and double virtual excitations from M. Further, if $\{u_k\}$ are chosen as Hartree-Fock functions, then the contribution of single virtual excitations vanishes. This use of Eq. (6) was proposed by Brillouin[22a] and Møller and Plesset[22b] for nondegenerate ψ_M.[22c] Extension to degenerate states has been discussed by Nesbet.[23] In this article we shall deal only with systems whose zero-order wave function can be taken as a single Slater determinant and use a more general basis set, $\{u_k\}$.

Consider first an N electron system of closed shells. For these, the first N spin-orbitals will be the occupied H.F. SCF orbitals of the system. The rest of the basis set $\{u_k\}$ $(k > N)$ may be assumed to be completed, e.g., as described by Löwdin,[22a] by taking independent functions and using the Schmidt orthogonalization process. As we shall see, in the following, the specification of $\{u_k\}$ for $k > N$ will be unnecessary. Now, consider the more general case of a system of closed shells plus an outer electron, e.g., an alkali atom. The treatment of this case will include the treatment of closed shells only, and, in addition, will allow a theory of core polarization for the outer electron in its various states. We shall return to a discussion of all closed shells in the section on molecules (Sec. V). For the more general case, if a polarization potential independent of the state of the outer electron is to be obtained, the initially occupied core orbitals must be chosen so as to be independent of the outer orbitals. The following modified basis set $\{u_k\}$ is the most suitable one for the core-polarization problem: Let the system contain N core electrons and the $(N+1)st$ outer electron, and let us suppose that we are interested in, say, n actual states of the outer electron including the lowest one corresponding to the ground state of the atom. Then the first N spin-orbitals $u_1, u_2, \cdots, u_N$ are to be obtained from a complete H.F. SCF solution of only the closed shell part of the system after stripping the $(N+1)$st outer electron. The next n orbitals $u_{(N+1)}, u_{(N+2)}, \cdots, u_{N+n}$ will be taken as the solutions of the H.F. equation for an electron in the field of the already determined *fixed* core orbitals. The rest of the basis set may be completed again, e.g., by a Schmidt orthogonalization process. The complete basis set of spin orbitals thus obtained will now be denoted by $\{u_k(\mathbf{x})\} = \{k\} = 1, 2, 3, \cdots$, all odd integers designating the spin-orbitals with spin α, and all even integers those with spin β. For concreteness and convenience, we now continue the treatment on the simplest case, the Li atom, although extension to larger systems is straightforward. For any state $[1/(3!)^{\frac{1}{2}}]$ det $(1s_\alpha 1s_\beta u_{k\alpha})$ or det′ $(12k)$ [det′ denoting the normalized determinant] of Li, the first few spin orbitals by our choice satisfy the equations

$$h_1^0 1s(\mathbf{r}_1) + \left(\int |1s(\mathbf{r}_2)|^2 r_{12}^{-1} d\tau_2\right) 1s(\mathbf{r}_1) = \epsilon_{1s} 1s(\mathbf{r}_1), \quad (7)$$

where

$$h_1^0 \equiv -\tfrac{1}{2}\nabla_1^2 - (Z/r_1) \quad (8)$$

and

$$h_{\text{core}}^{\text{eff}} u_k \equiv h_1^0 u_k(\mathbf{r}_1) + 2\left(\int |1s(\mathbf{r}_2)|^2 r_{12}^{-1} d\tau_2\right) u_k(\mathbf{r}_1)$$
$$- \left(\int 1s^*(\mathbf{r}_2) u_k(\mathbf{r}_2) r_{12}^{-1} d\tau_2\right) 1s(\mathbf{r}_1) = \epsilon_k u_k(\mathbf{r}_1)$$

for $u_{k\alpha} \equiv k \geq 3$. The second-order correlation energy is given by Eq. (6) in conjunction with Eq. (2) and the

[20] See also; W. B. Riesenfeld and K. M. Watson, Phys. Rev. **104**, 492 (1956).

[21] P. S. Epstein, Phys. Rev. **28**, 695 (1926); see also; L. C. Pauling and E. B. Wilson, *Introduction to Quantum Mechanics*, (McGraw-Hill Book Company, Inc., New York, 1935), p. 191.

[22] (a) L. Brillouin, Actualites sci. et ind., **No. 159 (1934)**; **No. 71 (1933)**; (b) C. Møller and M. S. Plesset, Phys. Rev. **46**, 618 (1934); (c) see, also, footnote reference 2, p. 283.

[23] R. K. Nesbet, Proc. Roy. Soc. (London) **A230**, 312 (1955).

one-electron basis set just defined. To separate this energy into parts, all the ordered configurations (with any orthonormal $\{u_k\}$) that would give matrix elements in Eq. (6) can be classified according to which one or two spin-orbitals of the initial state det′(12k) have been virtually excited to give the particular configuration. Consider first the ground state det′(123), i.e., $(1/\sqrt{6})$ det $(1s_\alpha 1s_\beta 2s_\alpha)$. From this state, keeping in mind that the indices k_1, k_2, k_3 which make up K in Eq. (2) must satisfy the condition $k_3>k_2>k_1(k_1=1$ to $\infty)$, the following types of virtual excitations are possible:

Single excitations:

$$\begin{aligned} 1,2,3&\rightarrow 1,2,l && l>3\\ &\rightarrow 1,k,3 && k>3\\ &\rightarrow m,2,3 && m>3 \end{aligned} \tag{9}$$

Double excitations:

$$\begin{aligned} 1,2,3&\rightarrow 1,k,l && l>k>3\\ &\rightarrow m,2,l && l>m>3\\ &\rightarrow m,k,3 && k>m>3. \end{aligned} \tag{10}$$

All higher excitations $l>k>m>3$ give $H_{OK}=0$. We have labeled the indices differently depending upon which initial orbitals remain unchanged. The first thing to notice is that with our choice of the orbitals all H_{OK} for the single virtual excitations of the *outer* electron[24] vanish by the *generalized* [22c] *Brillouin theorem*,[25] i.e.,

$$\begin{aligned} H_{OK}&=\langle \det'(123), H\ \det'(12l)\rangle=\langle l, h_{\text{core}}^{\text{eff}}3\rangle\\ &=\epsilon_3\langle l,3\rangle=0; \qquad (l\neq 3). \end{aligned} \tag{11}$$

On the other hand, single excitations from the core and double excitations lead to

$$\begin{aligned} \langle \det'(123), H\ \det'(1k3)\rangle&=\langle \det'(23), g_{12}\ \det'(k3)\rangle\\ \langle \det'(123), H\ \det'(m23)\rangle&=\langle \det'(13), g_{12}\ \det'(m3)\rangle \end{aligned} \tag{12}$$

where Eq. (7) has been used; and,

$$\langle \det'(123), H\ \det'(1kl)\rangle=\langle \det'(23), g_{12}\ \det'(kl)\rangle \tag{13}$$

and, similarly, for the rest of Eqs. (10). Here $g_{12}=r_{12}^{-1}$ and det′ denotes $(1/\sqrt{6})$ det on the left and $(1/\sqrt{2})$ det on the right of Eqs. (12) and (13). Notice that Eqs. (12) do not yield zero, because the core orbitals 1 and 2 have been chosen as the H.F. SCF solutions of Li^+ rather than of Li. This point will be discussed in detail after stating Eq. (17c).

Equations (9) through (13) allow the separation of the second-order energy in Eq. (6) into correlation energies of pairs of electrons. Of course it is a general result that, whenever, orthonormal functions are used and overlap, and exchange effects are neglected, second-order energies come out "pairwise additive"[4] as in intermolecular "dispersion" forces. Three-body and higher correlations appear in higher orders of perturbation. However, we shall see shortly that, here, the Pauli exclusion principle has already introduced some many-body correlations into the second-order. The first-order energy in Eq. (6) can be written as the energy of the ion core in the field of the bare nucleus and the energy of the outer electron in the SCF field of the ion core. For the ground state

$$\begin{aligned} H_{00}&=\langle \det'(123), (\sum_{i=1}^{3}h_i^0+\sum_{i>j}^{3}g_{ij})\ \det'(123)\rangle\\ &=\epsilon_{\text{core}}{}^0(12)+\langle 3, h_{\text{core}}{}^{\text{eff}}3\rangle, \end{aligned} \tag{14}$$

where

$$\epsilon_{\text{core}}{}^0(12)=2\langle 1s, h_1{}^0 1s\rangle+\langle 1s1s, g_{12}1s1s\rangle.$$

With the systematic classification of the virtual transitions given by Eqs. (9) and (10), $E_0^{(2)}$ in Eq. (6) can be broken down into the following terms, depending upon which initial orbitals are involved:

$$E_0^{(2)}(123)=E_0^{(2)}(12)+E_0^{(2)}(23)+E_0^{(2)}(13). \tag{15}$$

Again numbers in parentheses label the orbitals, and not the electrons; and,

$$-E_0^{(2)}(12)=\sum_{k>m>3}\frac{\langle \det'(12), g_{12}\ \det'(mk)\rangle^2}{\Delta(1,2,3\rightarrow m,k,3)} \tag{16a}$$

$$\begin{aligned} -E_0^{(2)}(23)&=\sum_{k>3}\frac{\langle \det'(23), g_{12}\ \det'(k3)\rangle^2}{\Delta(1,2,3\rightarrow 1,k,3)}\\ &+\sum_{l>k>3}\frac{\langle \det'(23), g_{12}\ \det'(kl)\rangle^2}{\Delta(1,2,3\rightarrow 1,k,l)} \end{aligned} \tag{17a}$$

$$\begin{aligned} -E_0^{(2)}(13)&=\sum_{m>3}\frac{\langle \det'(13), g_{12}\ \det'(m3)\rangle^2}{\Delta(1,2,3\rightarrow m,2,3)}\\ &+\sum_{l>m>3}\frac{\langle \det'(13), g_{12}\ \det'(ml)\rangle^2}{\Delta(1,2,3\rightarrow m,2,l)}. \end{aligned} \tag{18a}$$

The Δ's in the denominators represent the energies of the respective virtual transitions and are given from Eq. (6) by

$$\begin{aligned} \Delta(1,2,3\rightarrow m,k,l)&\equiv\langle \det'(mkl), H\ \det'(mkl)\rangle\\ &-\langle \det'(123), H\ \det'(123)\rangle. \end{aligned} \tag{19}$$

[24] Because of complete antisymmetry, we cannot refer to a definite electron. What we mean by "outer" electron is *any* one of the electrons occupying the particular *orbital* 3.

[25] Notice that with this generalization,[22] only the initially occupied orbital 3 must be an eigenfunction of $h_{\text{core}}{}^{\text{eff}}$ to make Eq. (11) vanish. There is no such condition for l.

In particular, when m is odd and k is even,

$$\Delta(1,2,3\rightarrow m,k,3)=\Delta h^0(1\rightarrow m)+\Delta h^0(2\rightarrow k)+(J_{mk}-J_{12})+(J_{k3}-J_{23})+(J-K)_{m3}-(J-K)_{13}, \quad (16b)$$

$$\Delta(1,2,3)\rightarrow 1,k,3)=\Delta h^0(2\rightarrow k)+(J_{k1}-J_{21})+(J_{k3}-J_{23}), \quad (17b)$$

$$\Delta(1,2,3\rightarrow 1,k,l)=\Delta h^0(2\rightarrow k)+\Delta h^0(3\rightarrow l)+(J_{k1}-J_{21})+(J_{kl}-J_{23})+(J-K)_{l1}-(J-K)_{31}, \quad (17c)$$

and, similarly, for Eq. (18a). J's and K's are the usual coulomb and exchange integrals,

$$J_{rs}=\langle rs, g_{12}rs\rangle; \qquad K_{rs}=\langle rs, g_{12}sr\rangle$$

and $\Delta h^0(r\rightarrow s)=\langle s,\ h^0 s\rangle-\langle r,\ h^0 r\rangle$. The numerical evaluation of $E^{(2)}$ for any one case is a lengthy procedure because large contributions to such sums are to be expected[2] from the continuum (or from what would take the place of the continuum) part of the basis set $\{k\}$. Our objective here, instead, is to investigate, semiquantitatively, various physical aspects of Eqs. (16a)–(18a) and their variation with respect to the different *actual* excited states of the "series" electron. (See, however, Sec. IV.)

The first part, Eq. (16a), corresponds to the correlation energy of the ion-core $(1s_\alpha 1s_\beta)$ as it exists in the neutral atom. The effect of the "outer" electron by means of the exclusion principle, on this core energy will be taken up later in Sec. III. Equations (17a) and (18a) give the correlation energy between an electron occupying 3, i.e., $2s_\alpha$ and those in 1 (i.e., $1s_\alpha$) and 2 (i.e., $1s_\beta$), respectively. The first terms on the right hand sides of Eqs. (17a) and (18a) represent the inner electrons in orbitals 1 and 2 making virtual transitions in the average field of the orbital 3. These are the "orbital average polarization" terms as we referred to them in the Introduction. Notice that they arose only because 1 and 2 were chosen as the SCF orbitals of Li^+ without introducing the H.F. field of $2s$ into Eq. (7). [See also Eq. (12).] Actually "orbital average polarization" is a very small effect and, therefore, in Hartree-Fock calculations on alkalilike configurations the same core orbitals are often used[1,26] for the free ion and the atom as we have done for Li^+ and Li. On the other hand, the real correlation energy that remains after a completely SCF calculation has been made, is given by the second terms of Eqs. (17a) and (18a). These terms are due to one core electron at a time making virtual transitions *simultaneously* with the outer electron. Such double excitation effects are sometimes referred to as "dispersion" energy in analogy to London forces.[18] Here we have referred to the totality of Eqs. (17a) and (18a), including "dispersion," by "core-polarization" energy (see Introduction). Unfortunately, the possibility of confusion exists, because sometimes the "orbital average polarization" is simply referred to as "polarization."[18,23] Such "orbital average polarization" effects, which also arise in going from various "restricted" types of H.F. calculation to "unrestricted" types, have been discussed[23] for Li. As it has been shown,[27] however, these are much smaller effects than the correlation energy (in fact, about 10^{-3} of it), i.e., than the "core-polarization" energy given by Eqs. (17a) and (18a). Although a small effect, here, we have included the "orbital average polarization" energy in the total "core-polarization" for completeness and convenience.

The sums in Eqs. (16a) to (18a) can be put into approximate but closed forms which are physically interesting by taking out the energy denominators as "mean excitation energies" in each case. This type of approximation has been made in many different contexts since Unsöld[28] and is used, for instance, in London forces.[3,10] In the first parts of Eqs. (17a) and (18a), Δ's consist of excitations of a single core electron at a time, and we write

$$\langle\Delta(1,2,3\rightarrow 1,k,3)\rangle_{Av}^{k}\approx\langle\Delta(1,2,3\rightarrow m,2,3)\rangle_{Av}^{m}=\bar{\delta}_c, \quad (20)$$

where $\langle\ \rangle_{Av}$ denote averages. The second, i.e., "dispersion" parts, of Eqs. (17a) and (18a) involve a similar single core excitation, but, in addition, virtual transitions of the outer electron in the field of the already excited core. [See Eq. (17c).] Thus to define a "mean excitation energy" for the outer electron, an averaging over both k and l in Eq. (17c) is necessary, i.e.,

$$\langle\Delta(1,2,3\rightarrow 1,k,l)\rangle_{Av}^{k,l}\approx\langle\Delta h^0(2\rightarrow k)+(J_{k1}-J_{21})\rangle_{Av}^{k}+\langle\Delta h^0(3\rightarrow l)+(J-K)_{l1}-(J-K)_{31}+(J_{kl}-J_{23})\rangle_{Av}^{k,l}$$

and

$$\langle\Delta(1,2,3\rightarrow 1,k,l)\rangle_{Av}^{k,l}\approx\langle\Delta(1,2,3\rightarrow m,2,l)\rangle_{Av}^{m,l}\equiv\bar{\delta}_C+\bar{\delta}_V^*(3) \quad (21)$$

where $\bar{\delta}_V^*(3)$ refers to the "mean excitation energy" of the valence, i.e., the "series" electron initially occupying orbital 3. For our purposes only very rough ideas of the magnitudes of δ's are necessary. The best use of δ's would be as semiempirical parameters. If the part of the basis set $\{u_k\}$ corresponding to the continuum[2] had not made a large contribution to the second order energy sums, δ's would have been of the order of ionization potentials, I. But actually more than half the second order energy, e.g., in He, comes from the continuum. Thus in general δ's will be several times the ionization potentials. The use of ionization potentials is

[18] See for example: D. R. Hartree and W. Hartree, Proc. Cambridge Phil. Soc. **34**, 550 (1938).

[27] R. E. Watson and R. K. Nesbet, Mass. Inst. Technol. Quart. Progr. Rept., October 15, 1959, p. 35.

[28] A. Unsöld, Z. Physik. **43**, 563 (1927).

permissible, however, only where lower limits to energy terms are desired. Thus we write $\bar{\delta}_C > I_{(Li^+)}$ and $\bar{\delta}_V^* \gtrsim I_{(Li)}$ and defer further discussion of $\bar{\delta}$'s until Sec. IV.

In Eq. (21), $\bar{\delta}_V^*$ represents a small fraction of $\bar{\delta}_C$; moreover, the single excitation terms in Eqs. (17a) and (17b) are small as was mentioned earlier. Thus neglecting the absence of $\bar{\delta}_V^*$ in Eq. (19) [compare Eq. (20)] all the energy denominators may be equated and Eqs. (17a) and (18a) combined into one "series" electron-core correlation energy. For the ground state of Li

$$-E_{CV}^{(2)}(3) = -E_0^{(2)}(23) - E_0^{(2)}(13)$$
$$\approx [\bar{\delta}_C + \bar{\delta}_V(3)]^{-1}[\sum_{l>k\geq 3} \langle \det'(23), g_{12} \det'(kl)\rangle^2 + \sum_{l>m\geq 3} \langle \det'(13), g_{12} \det'(ml)\rangle^2]. \quad (22)$$

For convenience, so far we have considered only the ground state [det (123)] of the Li atom and in Eqs. (9) and (10) analyzed the various types of virtual transitions that are possible from this state. Since, however, one of our objectives is to examine the validity of deriving an effective potential for the outer electron, before giving closed expressions for the sums in Eq. (22) it is necessary to consider the excited states of Li, [det'(12n)] where now the "series" electron occupies an orbital (n) different from $2s_a$.

With a different state of Li, the second-order sum in Eq. (6) again involves the same complete set of "ordered configurations," except that whereas before, det'(123) had been excluded and singled out as the zero-order wave function, now the sum includes this determinant but instead excludes det'(12n), the new zero-order wave function. $E^{(2)}$ in Eq. (6), or in operator form

$$-E_N^{(2)} = \langle N, \{H \sum_{M\neq N} M\rangle (H_{NN} - H_{MM})^{-1} \langle M, H\} N\rangle$$
$$= \langle N, Q_N^{(2)} N\rangle, \quad (23)$$

where N denotes det'(12n), can be put also in the form of an expectation value over the "series" electron orbital n. Denoting

$$N = \det'(12n) = \mathcal{A}\{nu_c(12)\}$$

where

$$u_c(12) = (1/\sqrt{2}!)\ \det(12),$$

and $\mathcal{A}$ is the operator antisymmetrizing n with the two core electrons, we obtain

$$-E_N^{(2)} = \langle n\{u_c(12), \mathcal{A}H \sum_{M\neq N} M\rangle (H_{NN} - H_{MM})^{-1} \times \langle M, H\mathcal{A}u_c(12)\}n\rangle$$
$$= \langle n, t_{cn}^{(2)} n\rangle. \quad (24)$$

The curly brackets in the second term have been placed to indicate that integrations over the coordinates in n are to be performed last. As it stands the formal core "series" electron interaction operator $t_{cn}^{(2)}$ is far from being a potential energy for n. First, the summation over M includes all double virtual excitations of the core orbitals, (12); thus the part corresponding to Eq. (16a), the correlation energy of the core itself, has not yet been separated. As we have mentioned earlier, this part actually depends on n, due to the "exclusion" principle and it will be taken up later. In addition if an arbitrary one-electron basis set were to be used, $t_{cn}^{(2)}$ would depend on which N had been excluded from the sum in Eqs. (23) or (24). On the other hand, with an SCF H.F. basis or the basis $\{k\}$ we have chosen above, this type of dependence is eliminated, because the "series" electron orbitals satisfy Eq. (11). Thus in $E_0^{(2)}$ single virtual excitations from det'(123), i.e., the first of the Eqs. (9), would include

$$1, 2, 3 \rightarrow 1, 2, n,$$

whereas in $E_N^{(2)}$, the same type of excitations from det'(12n) would exclude 1, 2, n but include

$$1, 2, n \rightarrow 1, 2, 3.$$

But, both of these virtual transitions have zero matrix elements by Eq. (11) and, hence, are without effect on $t_{cn}^{(2)}$. The rest of Eqs. (9) and (10) can be generalized to any state of Li, det'(12n), keeping in mind the ordering of configurations in Eq. (2) by $k>l>m$ ($m=1$ to ∞). Some transitions that were single core transitions for one state become "core"-n double transitions for another state and vice versa, as, for example, in

$$1, 2, 3 \rightarrow 1, 5, 3$$
$$1, 2, n \rightarrow 1, 3, 5 \qquad (n\neq 3, 5);$$

otherwise the *totality* of the virtual transitions involving either a single core orbital or a single core orbital and the outer one, n, are unchanged. Thus, after making the same approximations in the energy denominators, the core-valence electron correlation energy in Eq. (22) can be written for any "series" state of Li as

$$-E_{CV}^{(2)}(n) = -E_N^{(2)}(2n) - E_N^{(2)}(1n)$$
$$\approx [\bar{\delta}_C + \bar{\delta}_V(n)]^{-1}[\sum_{l>k\geq 3} \langle \det'(2n), g_{12} \det'(kl)\rangle^2 + \sum_{l>m\geq 3} \langle \det'(1n), g_{12} \det'(ml)\rangle^2], \quad (25)$$

where $n>2$. The independence of the indices in the above sums, from n, is the biggest advantage of the way the basis set $\{k\}$ was chosen previously. [See Eqs. (12) and (7)]. If the orbitals 1, 2, 3 had been taken as the completely SCF solutions of Li, the first terms in Eqs. (17a) and (18a) would have vanished and both the core orbitals 1, 2 and the summing indices in Eq. (25) would have been made to depend on the particular outer orbital. We can now anticipate putting the sums appearing in Eq. (24) into closed forms and hope to obtain the desired potential (independent of n) were it

not for the appearance of $\bar{\delta}_V(n)$ in the denominator. $\bar{\delta}_V(n)$ as in Eqs. (21) and (22) represents the "mean *virtual* excitation" energy of the outer orbital n. For $n>3$, in some terms such as

$$1, 2, n \rightarrow 1, 3, 5 \qquad (n>3, 5),$$

of the equations corresponding to Eqs. (17a) and (18a), $n\rightarrow 5$ would actually be a "deexcitation" and make a negative contribution to $\bar{\delta}_V(n)$. However, there are only a few such terms for low lying n, and the weight of any one term to the sum, e.g., in Eq. (17a), is small. As mentioned earlier, $\bar{\delta}_V(n)$ represents a small fraction of $\bar{\delta}_C$, so that it can either be neglected in comparison with $\bar{\delta}_C$ or replaced by a reasonable average,[7] δ_S, for the few states $\det'(12n)$ of interest. Since $\bar{\delta}_V(n)$ is small, the errors made by replacing it by δ_S will be even smaller. Assuming for the moment that the sums could be put in the suitable form, the requirement $(\bar{\delta}_V(n)/\bar{\delta}_C)<1$ is necessary if any "core-polarization" potential derived from Eq. (25) is to be independent of n. Notice that this requirement is similar to the necessity of having the outer electron move slowly compared to the core electrons in the adiabatic approximation, except that here it does not enter in a fundamental way.

The summations in Eq. (25) can now be carried out. Since the core $(1s_\alpha 1s_\beta)$ is a closed shell, it is necessary to discuss only those n that have either all α or all β spin. Take all n to be odd, i.e., with spin α, and in Eq. (25) consider first the pair involving opposite spins, i.e., $\det'(2n)$. Then

$$\sum_{l>k\geq 3}\langle \det'(2n), g_{12}\det(kl)\rangle^2 = \langle \det'(2n), g_{12}^2\det'(2n)\rangle - \sum_{l>2,k=2}\langle \det'(2n), g_{12}\det'(2l)\rangle^2 - \sum_{l>1,k=1}\langle \det'(2n), g_{12}\det'(1l)\rangle^2 \quad (26)$$

This follows from a matrix multiplication relation of the type

$$\sum_{L=1}^{\infty}\langle M, AL\rangle\langle L, BN\rangle = \langle M, (AB)N\rangle, \quad (27)$$

where A and B are operators acting on the space for which the set of orthonormal vectors $\{L\}=1, 2, 3, \cdots\infty$ form a complete basis. In Eq. (26) the set of all normalized two-electron determinants corresponding to the ordered configurations $l>k\geq 1$, as in Eq. (2), form a complete orthonormal basis for the space of two-electron coordinates (including spin) on which g_{12} acts. The spins of 2 and n being opposed, the determinantal matrix elements on the right-hand side of Eq. (26) reduce to the direct integrals only; e.g., for the ground state of Li,

$$\langle \det'(23), g_{12}^2\det'(23)\rangle = \langle 1s2s, g_{12}^2 1s2s\rangle. \quad (28)$$

Similarly,

$$\sum_{l>2}\langle \det'(2n), g_{12}\det(2l)\rangle^2 = \sum_{l>2,(l=\text{odd})}\langle 2n, g_{12}2l\rangle^2, \quad (29)$$

where to conserve spin, l must have spin α, i.e., be odd. The last sum can also be evaluated by carrying out the integrations in each matrix element over one set of the electron coordinates and, thus, obtaining a function $(W_{2,2})$ of the coordinates of the other electron; i.e.,

$$\langle 2n, g_{12}2l\rangle^2 = \langle n, W_{2,2}l\rangle^2, \quad (30)$$

where

$$W_{2,2}\equiv\int |\,1s(1)\,|^2 r_{12}^{-1}d\tau_1.$$

Then, making use of Eq. (27) we get

$$\sum_{l>2,(l=\text{odd})}\langle 2n, g_{12}2l\rangle^2 = \sum_{l>2,(l=\text{odd})}\langle n, W_{2,2}l\rangle^2 = \langle n, (W_{2,2})^2 n\rangle - \langle n, W_{2,2}1\rangle^2, \quad (31)$$

since $l=1, 3, 5, \cdots$ odd $\cdots\infty$ form a complete *one-electron* basis set and $W_{2,2}$ of Eq. (30) is a function of the coordinates of a single electron. In the same way, in Eq. (26)

$$\sum_{l>1}\langle \det'(2n), g_{12}\det'(1l)\rangle^2 = \sum_{l>1,(l=\text{even})}\langle 2n, g_{12}l1\rangle^2 = \sum_{l>1,(l=\text{even})}\langle 2, W_{n,1}l\rangle^2 = \langle 2, (W_{n,1})^2 2\rangle, \quad (32)$$

since now to conserve spin, l must be even (spin β) and $l=2, 4, 6, \cdots$ even $\cdots\infty$ form a complete basis set for functions of the spatial coordinates of one electron.

Similarly for the parallel spin pair $(1n)$ in Eq. (25), the use of Eq. (27) leads to

$$\sum_{l>m>3}\langle \det'(1n), g_{12}\det'(ml)\rangle^2 = \langle \det'(1n), g_{12}^2\det'(1n)\rangle - \sum_{l>2}\langle \det'(1n), g_{12}\det'(2l)\rangle^2 - \sum_{l>1}\langle \det'(1n), g_{12}\det'(1l)\rangle^2. \quad (33)$$

Now both of the spin orbitals 1 and n have spin α, so that

$$\langle \det'(1n), g_{12}^2\det'(1n)\rangle = \langle 1n, g_{12}^2 1n\rangle - \langle 1n, g_{12}^2 n1\rangle. \quad (34)$$

Also, since 2 has spin β,

$$\sum_{l>2}\langle \det'(1n), g_{12}\det'(2l)\rangle^2 = 0. \quad (35)$$

The last term of Eq. (33)

$$\sum_{l>1}\langle \det'(1n), g_{12}\det'(1l)\rangle^2 = \sum_{l>1,(l=\text{odd})}[\langle 1n, g_{12}1l\rangle - \langle 1n, g_{12}1l\rangle]^2 = \sum_{l>1,(\text{odd})}\langle n, W_{1,1}l\rangle^2 + \sum_{l>1,(\text{odd})}\langle 1, W_{n,1}l\rangle^2 - 2\sum_{l>1,(\text{odd})}\langle n, W_{1,1}l\rangle\langle l, (W_{n,1})1\rangle \quad (36)$$

defining the one electron functions as in Eq. (30). Then, using Eq. (27) in each term of the last expression,

$$\sum_{l>1}\langle \det'(1n), g_{12}\det'(1l)\rangle^2 = \langle n, (W_{1,1})^2 n\rangle + \langle 1, (W_{n,1})^2 1\rangle - 2\langle n, (W_{1,1})(W_{n,1})1\rangle, \quad (37)$$

and, from Eq. (33),

$$\sum_{l>m\geq 3}\langle \det'(1n), g_{12}\det'(ml)\rangle^2 = \langle 1n, g_{12}^2 1n\rangle - \langle 1n, g_{12}^2 n1\rangle - \langle n, (W_{1,1})^2 n\rangle - \langle 1, (W_{n,1})^2 1\rangle + 2\langle n, (W_{1,1})(W_{n,1})1\rangle. \quad (38)$$

Before going into the correlation energy of the core itself and deriving expressions for it similar to those given above, let us examine the meaning of the various terms in the results for $E_{CV}^{(2)}(n)$, Eq. (25). The major part of the core-valence electron correlation energy is due to the pair with opposing spins, i.e., $E_N^{(2)}(2n)$, since the other $\alpha\alpha$ pair electrons are already kept apart by the Pauli exclusion principle. By Eqs. (26), and (29) through (32), the $\alpha\beta$-pair energy for some state $\det'(12n)$ of Li is given by

$$-E_N^{(2)}(2n) \approx (\bar{\delta}_C+\delta_S)^{-1}[\langle 2n, g_{12}^2 2n\rangle - \langle n, (W_{2,2})^2 n\rangle + \langle n, (W_{2,2})1\rangle^2 - \langle 2, (W_{n,1})^2 2\rangle]. \quad (39)$$

Or, for the ground state of Li with $n=3$, replacing $1=(1s)_\alpha$, $2=(1s)_\beta$ and $3=(2s)_\alpha$,

$$-E_0^{(2)}[(1s)_\beta(2s)_\alpha] \approx (\bar{\delta}_C+\delta_S)^{-1} \times[\langle (2s), F_{(1s)}(2s)\rangle - R_{(1s_\beta)(2s_\alpha)}], \quad (40)$$

where we have defined

$$\langle (2s), F_{(1s)}(2s)\rangle \equiv \langle (2s)(1s), g_{12}^2(2s)(1s)\rangle - \langle (2s), (W_{(1s)(1s)})^2(2s)\rangle \quad (41a)$$

and

$$R_{(1s_\alpha)(1s_\beta)} \equiv \langle (1s), (W_{(2s),(1s)})^2(1s)\rangle - \langle 1s2s, g_{12}1s1s\rangle^2. \quad (41b)$$

Clearly $F_{(1s)}$ represents a true potential acting on the outer electron, and depends solely on the core orbital $(1s)$; it is given by

$$F_{(1s)}(\mathbf{r}_2) = \left\{\int |1s(\mathbf{r}_1)|^2[1/(|\mathbf{r}_2-\mathbf{r}_1|^2)]d\tau_1\right\} - \left\{\int |1s(\mathbf{r}_1)|^2[1/(|\mathbf{r}_2-\mathbf{r}_1|)]d\tau_1\right\}^2, \quad (42)$$

where $\mathbf{r}_2$ and $\mathbf{r}_1$ are the position coordinates in $(2s)$ and $(1s)$, respectively, and the potential acting at $\mathbf{r}_2$ is obtained by integration over all $\mathbf{r}_1$. $F_{(1s)}(\mathbf{r}_2)$ in Eq. (42) can be identically written as

$$F_{(1s)}(\mathbf{r}_2) = \langle (1s), [(1/r_{12}^2) - \langle (1s), (1/r_{12})(1s)\rangle_1^2](1s)\rangle_1 = \langle (1s), [(1/r_{12}) - \langle (1s), (1/r_{12})(1s)\rangle_1]^2(1s)\rangle_1 = \langle (g_{12} - \langle g_{12}\rangle_{N,1s})^2\rangle_{N,1s}, \quad (43)$$

where $\langle\ \rangle_1$ means that all integrations in Eq. (43) are over the same coordinates $\mathbf{r}_1$ as in Eq. (42). In the last term we have denoted the quantum mechanical averages of the "source point" $\mathbf{r}_1$ over $(1s)$ with the symbol, $\langle\ \rangle_N$. It will be noticed that $(g_{12}-\langle g_{12}\rangle_{N,1s})$ simply represents the "instantaneous" (in the virtual sense) deviation of the electrostatic potential, produced at the point $\mathbf{r}_2$ by the electronic charge at $\mathbf{r}_1$, from the orbital average [i.e., the expectation value over $1s(\mathbf{r}_1)$] potential of the electron $(\mathbf{r}_1)$ produced at r_2. Thus as we have done in the theory of Van der Waals' interactions between molecules and solid surfaces,[29] $F_{(1s)}(\mathbf{r}_2)/\bar{\delta}_C$ may be called the fluctuation potential since $F_{(1s)}(\mathbf{r}_2)$ is simply the mean square fluctuation of the coulombic potential of the orbital $(1s)$ at the point $\mathbf{r}_2$.

In Eq. (40), there still exists a remainder term $R_{(1s)_\beta(2s)_\alpha}$ which cannot be put in the form of an expectation value of a potential. A close examination of the Eqs. (26) through (32) leading to Eq. (40) shows that $R_{(1s)_\beta(2s_\alpha)}$ arises because the closed inner shell $(1s_\alpha 1s_\beta)$ of Li prevents the outer electron occupying $2s_\alpha$ from making virtual transitions to the already occupied inner levels. This is one of the exclusion effects that were mentioned in the introduction and represents the nonpairwise additive effect of $(1s_\alpha)$ on the pair $(1s_\beta 2s_\alpha)$. $R_{(1s_\beta)(n)}$ has been neglected in the previous treatments of core-polarization for nonpenetrating orbitals.[7-9,13,14] However, especially for the ground state, its magnitude requires examination (See Sec. IV).

Likewise, the correlation energy of the $\alpha\alpha$ pair $(1s_\alpha 2s_\alpha)$ of the ground state of Li in Eq. (25) is derived from Eqs. (38), (40), and (41) by

$$-E_0^{(2)}(1s_\alpha 2s_\alpha) \cong (\bar{\delta}_C+\delta_S)^{-1}[\langle (2s), F_{(1s)}(2s)\rangle - \langle (2s), F_{(1s)}{}^{ex}(2s)\rangle - R_{1s_\alpha 2s_\alpha}{}^{ex}] \quad (44)$$

[29] O. Sinanoğlu, Ph.D. thesis, Part I, University of California, August, 1959; O. Sinanoğlu and K. S. Pitzer, J. Chem. Phys. 32, 1279 (1960).

where

$$\langle (2s), F_{(1s)}{}^{ex}(2s)\rangle \equiv \langle 2s1s, g_{12}{}^{2}1s2s\rangle - \langle 2s, (W_{1s,1s})(W_{1s,2s})1s\rangle \quad (45a)$$

and

$$R_{1s_\alpha 2s_\alpha}{}^{ex} \equiv \langle 1s, (W_{2s,1s})^{2}1s\rangle - \langle 2s, (W_{1s,1s})(W_{1s,2s})1s\rangle. \quad (45b)$$

Comparison of the Eqs. (38) and (44) with (39) and (40) shows that $E_0{}^{(2)}(1s_\alpha 2s_\alpha)$, in addition to the fluctuation potential of $E_0{}^{(2)}(1s_\beta 2s_\alpha)$ also contains $F_{(1s)}{}^{ex}/(\bar{\delta}_C+\delta_S)$ or what may be called the "exchange fluctuation potential." Note that the latter is a "potential" only in exactly the same sense[2] as the exchange part of the Hartree-Fock field [see Eq. (8)] is. The "exclusion" term in Eq. (45b) is similar to that in Eq. (41b). Combining Eqs. (6), (7), (14), (15), (40), and (44), the total energy of Li in any state, $N \equiv \det'(12n)$, is given as

$$E_N(12n) \cong H_{NN} + E_N{}^{(2)} \cong \epsilon_{core}{}^{0}(12) + \langle n, h_{core}{}^{eff} n\rangle + E_N{}^{(2)}(12) + \langle n, U_f n\rangle + Q_n = E_N(\text{core}) + \langle n, (h_{core}{}^{eff} + U_f)n\rangle + Q_n, \quad (46)$$

where

$$U_f = (2F_{(1s)} - F_{(1s)}{}^{ex})/(\bar{\delta}_C+\delta_S)$$

and

$$Q_n = (R_{1s_\beta n} + R_{1s_\alpha n}{}^{ex})/(\bar{\delta}_C+\delta_S).$$

E_N (core) contains the H.F. energy [Eq. (14)] of the *free* ion Li^+, and, in addition, the correlation energy $E_N{}^{(2)}(12)$ [given for the ground state by Eq. (16a)] which refers not to free Li^+ but to the core as it exists in state N of Li. The dependence of $E_N{}^{(2)}(12)$ on the outer orbital n through the "exclusion" principle is discussed in Sec. III. Q_n constitutes the rest of the "exclusion" effect. It depends upon the exchange charge density of n with $(1s)$, so that it will be small for excited states of Li, i.e., "nonpenetrating" n. U_f is the desired correlation (fluctuation) potential. With a larger atom, similar results can easily be written down. In general, there will be a contribution from each electron of the core to U_f and Q_n. After estimating the "exclusion" effects, U_f can be determined semiempirically (see e.g., Douglas[11]) for instance, by leaving $(\bar{\delta}_C+\delta_S)$ as a parameter. Aside from the "exclusion" effects, Eq. (46) has the variational form for the outer electron with an effective "core-Hamiltonian." It is important to realize however that in this form n cannot be varied to improve the energy even when $Q_n \sim 0$ and $E_N(\text{core}) \sim$ constant, because the result was derived for a specific choice of orbitals for n, namely, those satisfying the H.F. condition, Eq. (11). With any other choice, the single virtual transitions of n as in Eq. (9) would lead to nonvanishing matrix elements and make a new contribution to Eq. (46). This point brings out the connection between the present treatment and the recent nuclear manybody theory.[19,30] In fact, Eq. (46) corresponds to a starting approximation of that theory with the neglect of higher-order correlations (Sec. VI) as can be seen, e.g., in the work of Bethe[31] and Rodberg.[32] Improved choices for n can be made and perhaps restrictions, as in Eq. (11), removed by going to higher orders of perturbation, but such generalizations will be deferred to a future date.

III. "EXCLUSION" EFFECT OF AN OUTER ELECTRON ON THE CORE ENERGY

The dependence of the core correlation energy $E_N{}^{(2)}(12)$ of Eq. (46) on the outer orbital n in Li can be examined by a careful classification of all the "ordered configurations" entering Eq. (6) and generalization of Eq. (16a) to any n. In Eq. (10) some of the configurations that correspond to double virtual transitions from the core $(1s_\alpha 1s_\beta)$ when n was 3 (i.e., $2s_\alpha$) become triple transitions from another initial state $\det'(12n)$ with $n>3$, and vice versa. Including all such configurations in $E^{(2)}$, one obtains the expected result that

$$-E_N{}^{(2)}(12) = \sum_{k>m\geq 3,(k,m\neq n)} \frac{\langle \det'(12), g_{12}\det'(mk)\rangle^2}{\Delta(1,2,n\rightarrow m,k,n)}; \quad (47)$$

i.e., all the double core transitions $1,2\rightarrow m,k$ are missing when m or k is the already occupied orbital n. This may be compared with the second-order energy of the *free* ion core Li^+ using the same one-electron basis set $\{k\}$ that was defined previously for Li:

$$-E_{Li^+}{}^{(2)}(12) = \sum_{k>m>2} \frac{\langle \det'(12), g_{12}\det'(mk)\rangle^2}{\Delta(1,2\rightarrow m,k)}. \quad (48)$$

The energy denominator in Eq. (47) differs from that in Eq. (48) by the presence of n [See Eq. (19)]. Nevertheless a semiquantitative estimate of the variation of $E_N{}^{(2)}(12)$ with n and its difference from the energy of Li^+ can be obtained by replacing both Δ's by one average, $\bar{\Delta}_{core}[\bar{\Delta}_{core} > (I_{Li^+}+I_{Li^{2+}})]$. Then comparing Eqs. (47) and (48),

$$(E^{(2)})_{Li\ core}(n) \equiv E_N{}^{(2)}(12) \sim E_{Li^+}{}^{(2)}(12) + \bar{\Delta}_{core}{}^{-1}\sum_{k\geq 3}^{\infty}\langle \det'(12), g_{12}\det'(nk)\rangle^2, \quad (49)$$

or using Eq. (27) as in Eq. (32),

$$E_N{}^{(2)}(12) \sim E_{Li^+}{}^{(2)} + \bar{\Delta}_{core}{}^{-1}[\langle (1s), (W_{(1s),n'})^2(1s)\rangle - \langle (1s)(n'), g_{12}(1s)(1s)\rangle^2], \quad (50a)$$

---

[30] K. A. Brueckner, C. A. Levinson, and H. M. Mahmoud, Phys. Rev. **95**, 217 (1954); for later references see H. Yoshizumi, Advances in Chem. Phys. **2**, 323 (1959).

[31] H. A. Bethe, Phys. Rev. **103**, 1353 (1956).

[32] L. S. Rodberg, Ann. Phys. **2**, 199 (1957).

with $n'\alpha=n$, and from Eq. (46),

$$E_N(\text{core})\cong E_{\text{Li}^+}+\bar{\Delta}_{\text{core}}^{-1}[\langle(1s),(W_{1s,n'})^2(1s)\rangle - \langle(1s)n',g_{12}(1s)(1s)\rangle^2] \equiv E_{(\text{Li}^+)}+(R_{\text{core}-n}/\bar{\Delta}_{\text{core}}). \quad (50b)$$

Thus, the *total* energy of the core in the Li atom is given by the total energy of the *free* Li^+ ion including its correlation energy plus the last term which is the desired "exclusion" effect of n' on the core. With any larger system, the evaluation of all such "exclusion" effects is similarly possible from a classification of ordered configurations and the use of Eq. (27) for summations.

IV. MAGNITUDES FOR THE GROUND STATE OF LITHIUM

In Sec. II, Eq. (46) we have obtained an expression for the total energy of the Li atom in any one of its "series" states. That derivation shows, that aside from the "exclusion" effects, U_f is the desired "core-polarization" potential including exchange and it may be regarded as the mean-square fluctuation of the Hartree-Fock potential of the core per unit of "mean excitation energy." Notice that U_f is a complete potential and is *not* dependent on a multipole expansion of g_{12}. In the previous treatments[7–9,13,14] of "core polarization" (a) the "exclusion" effects, (b) the exchange part of U_f, i.e., $F_{1s}^{ex}[\delta_C+\delta_S)$, has been neglected (see, however, Ludwig[7b]) and (c) after making a multipole expansion of g_{12}, as

$$g_{12}=1/r_{12}=1/r_>+(r_</r_>^2)(\cos\omega)+(r_<^2/2r_>^3)\times(3\cos^2-1)+\cdots \quad (51)$$

mainly the dipole term (with estimates of quadrupole terms) has been considered and the first part $r_>^{-1}$ dropped. In Eq. (51) $r_>$ denotes the greater of the two distances r_1 and r_2, and ω is the angle between the radius vectors of the two electrons. For highly excited states, i.e., with larger n, assumptions *a* to *c* approach validity. For instance, as the portion of the outer orbital that is inside the core becomes negligible, we get $r_>=r_2$ only, so that the $r_>^{-1}$ part of g_{12} no longer contributes to U_f [See Eqs. (41) and (45)]. For "penetrating" orbitals, however, such is not the case. To get an idea of the magnitudes of the previously neglected penetration and "exclusion" terms, we shall consider here the ground state of Li for which the effects should be largest. We take for $2s$ the orthogonalized Slater orbital,

$$2s^0=1.0148(\delta_2^5/3\pi)^{\frac{1}{2}}r\exp(-\delta_2 r)-0.1742(\delta_1^3/\pi)^{\frac{1}{2}}\times\exp(-\delta_1 r) \quad (52a)$$

with $\delta_1=2.65$ and $\delta_2=0.65$, which sufficiently approximates the Hartree-Fock ($2s$) orbital of Fock and Petrashen,[33] and for $1s$,

$$1s=(\delta_1^3/\pi)^{\frac{1}{2}}\exp(-\delta_1 r) \quad (52b)$$

with $\delta_1=2.65$. The "exclusion" terms in Eqs. (41b), (45b), and (50b) involve g_{12} in the W integrals. These are like the usual atomic integrals[34]; upon substitution of Eq. (51) for g_{12}, only the $r_>^{-1}$ term contributes due to the spherical symmetry of $1s$ and $2s$. The first parts of $F_{(1s)}$ and $F_{(1s)}^{ex}$ in U_f on the other hand, contain g_{12}^2. U_f can be obtained completely, without any expansions, from Eqs. (43) and (46). However, in this article we shall consider only the penetration terms.

To compare the penetration effects with the previously considered dipole terms on an equivalent basis, we must also expand g_{12}^2 and not consider higher multipoles. g_{12}^2 can be conveniently expanded in terms of the Gegenbauer[35] polynomials, $C_n^{(1)}(\cos\omega)$.

$$g_{12}^2=1/r_{12}^2=(1/r_>^2)\sum_{n=0}^{\infty}(r_</r_>)^n C_n^{(1)}(\cos\omega). \quad (53)$$

These polynominals are analogous to the Legendre polynominals and have similar addition theorems. The first term of Eq. (53) is $r_>^{-2}$, neglected previously. It is responsible for most of the penetration effects of $2s$, as can be seen e.g., from the fact that only $r_>^{-1}$ contributes to the "exclusion" terms and will be calculated here.

With the orbitals of Eq. (52), the desired integrations can be performed analytically and yield

$$\langle 2s^0,(W_{1s,1s})^2 2s^0\rangle=\left\langle 2s^0,\left(\int|1s(r_1)|^2 r_>^{-1}d\tau_1\right)^2 2s^0\right\rangle =0.16144(\text{a.u.})^2$$
$$\langle 1s,(W_{2s^0,1s})^2 1s\rangle=0.018537(\text{a.u.})^2$$
$$\langle 1s2s^0,g_{12}1s1s\rangle^2=\langle 1s2s^0,r_>^{-1}1s1s\rangle^2=0.013855(\text{a.u.})^2$$
$$\langle 2s^0,(W_{1s,1s})(W_{2s^0,1s})1s\rangle=0.029806(\text{a.u.})^2$$
$$\langle 2s^0 1s,r_>^{-2}2s^0 1s\rangle=0.17385(\text{a.u.})^2$$
$$\langle 2s^0 1s,r_>^{-2}1s2s^0\rangle=0.053256(\text{a.u.})^2 \quad (54a)$$

where 1(a.u.) = 27.202 ev and, e.g.,

$$(1/4\pi)\int|1s(r_1)|^2 r_>^{-2}d\tau_1=(1/r_2^2)\int_0^{r_2}|1s(r_1)|^2 r_1^2 dr_1 + \int_{r_2}^{\infty}|1s(r_1)|^2 dr_1. \quad (55)$$

As it was mentioned in Sec. II, ionization potentials provide lower limits to the "mean excitation energies,"

[33] V. Fock and M. J. Petrashen, Physik. Z. Sowjetunion, 8, 547 (1935).

[34] E. U. Condon and G. H. Shortley, *The Theory of Atomic Spectra* (Cambridge University Press, New York, 1957), p. 174.

[35] For a quite detailed account of these polynominals, see I. Prigogine *et al.*, *Molecular Theory of Solutions* (North-Holland Publishing Company, Amsterdam, 1957), p. 265.

and therefore, we write

$$\bar{\delta}_C+\delta_S\equiv\mathcal{K}_{CS}[I_{(\mathrm{Li})}+I_{(\mathrm{Li}^+)}]\cong 3\mathcal{K}_{CS}(\text{a.u.}) \quad (54b)$$

and

$$\bar{\Delta}_{\text{core}}\equiv\mathcal{K}_{\text{core}}[I_{(\mathrm{Li}^+)}+I_{(\mathrm{Li}^{2+})}]=7.24\mathcal{K}_{\text{core}}(\text{a.u.}),$$

where $\mathcal{K}_{\text{core}}>\mathcal{K}_{CS}>1$. Estimates show that in the (Li^+) ion, where two electrons are in the same orbital, $\mathcal{K}_{\text{core}}$ is approximately four due to the large contribution of the continuum in this case. On the other hand, when two electrons are in different orbitals $\mathcal{K}$ may be about two. We will take $\mathcal{K}_{CS}\sim 2$. For results more quantitative than we are aiming at here, it is also possible to obtain $\mathcal{K}$ values for each of the pair sums in Eqs. (16a) to (18a), e.g., by a procedure devised by Kessler.[36]

We may also remark that, once the total correlation energy of a large system has been separated into those of pairs of electrons, the $E^{(2)}$ of each pair can be obtained in a number of ways. Here we have emphasized the semiempirical approach. One may also formulate "variation-perturbation" methods for each pair as has been possible for He^7[a].

Substituting the foregoing results, Eqs. (54a, b), into Eqs. (41b), (45b), and (50b), we obtain

$$(\bar{\delta}_C+\delta_S)^{-1}R_{1s_\beta 2s_\alpha}=0.04245\mathcal{K}_{cs}^{-1}\text{ ev}, \quad (56a)$$

$$(\bar{\delta}_C+\delta_S)^{-1}R_{1s_\alpha 2s_\alpha}=-0.1022\mathcal{K}_{cs}^{-1}\text{ ev}, \quad (56b)$$

and

$$(\bar{\Delta}_{\text{core}})^{-1}R_{\text{core}-2s_\alpha}=0.0176\mathcal{K}_{\text{core}}^{-1}\text{ ev}. \quad (56c)$$

Using only the first terms of g_{12} and g_{12}^2 from Eqs. (51) and (53) in Eqs. (40) and (44) and denoting the corresponding parts of $F_{(1s)}$ and $F_{(1s)}^{\text{ex}}$ by

$$\langle 2s^0, F_{r>}2s^0\rangle\equiv\langle 2s^0 1s, r_>^{-2}2s^0 1s\rangle-\langle 2s^0, (W_{1s,1s})^2 2s^0\rangle$$

$$\langle 2s^0, F_{r>}^{\text{ex}}2s^0\rangle\equiv\langle 2s^0 1s, r_>^{-2}1s2s^0\rangle$$

$$-\langle 2s^0, (W_{1s,1s})(W_{1s,2s})1s\rangle \quad (57)$$

we get

$$(\bar{\delta}_C+\delta_S)^{-1}\langle 2s^0, F_{r>}2s^0\rangle=0.1125\mathcal{K}_{cs}^{-1}\text{ ev}. \quad (58a)$$

$$(\bar{\delta}_C+\delta_S)^{-1}\langle 2s^0, F_{r>}^{\text{ex}}2s^0\rangle=0.2126\mathcal{K}_{cs}^{-1}\text{ ev}. \quad (58b)$$

Essentially the same values are obtained by the use of $\delta_1=2.70$ instead of 2.65 in $2s^0$ and $1s$ so that the results are not very sensitive to our specific choice of the orbital parameters in Eqs. (52).

Most of the "penetration" effects of $2s$ are included in Eqs. (56) to (58). Callaway[13] has obtained a "core-polarization" potential in Li using only the dipole part of g_{12}, equivalent to taking the second term of Eq. (53) in $F_{(1s)}$ and neglecting $F_{(1s)}^{\text{ex}}$. He finds a contribution of 0.1 ev to $\langle 2s, U_f 2s\rangle$. Actually the results of Ludwig[7b] suggest that the exchange term in the dipole part may be negligible. By comparison, several interesting conclusions follow from the Eqs. (56)–(58). First, the "exclusion" effect of the outer orbital on the core correlation energy is only 0.0176 $\mathcal{K}_{\text{core}}^{-1}$ ev with $\mathcal{K}_{\text{core}}^{-1}<1$, hence negligible even for $2s$. In Eq. (50) we can then take $E_N(\text{core})\approx E_{(\mathrm{Li}^+)}$. Secondly, the total contribution to the correlation energy of the $1s_\beta 2s_\alpha$ pair from the $r_>^{-1}$ terms is $(\bar{\delta}_C+\delta_S)^{-1}(\langle 2s^0, F_{r>}2s^0\rangle-R_{1s_\beta 2s_\alpha})$ or $(0.1125-0.0423=0.0702)\mathcal{K}_{CS}^{-1}$ ev. With $\mathcal{K}_{CS}^{-1}\sim\frac{1}{2}$, this is still appreciable compared to 0.1 ev, the dipole contribution from both of the core electrons.[13] Also the "orbital average polarization" effect of the orbital $2s$ appears only in the $r_>^{-1}$ part of g_{12} due to the spherical symmetry of $1s$ and $2s$. This effect, however. as was mentioned earlier, is not strictly a correlation effect since it results in converting the Li^+ H.F. SCF orbitals to the completely H.F. SCF orbitals in Li. The term, $F_{r>}$, which we have calculated previously, on the other hand, corresponds to the fluctuation of $r_>^{-1}$ i.e., $\langle r_>^{-2}-\langle r_>^{-1}\rangle_1^2\rangle_1$, and, hence, to the inclusion of the "dispersion" effect. It is much larger than the "orbital average polarization" energy (see Sec. II). Thirdly, combining all the $r_>$ or "penetration" terms for the $1s_\alpha 2s_\alpha$ pair we find that

$$(\bar{\delta}_C+\delta_S)^{-1}(\langle 2s^0, F_{r>}2s^0\rangle-\langle 2s^0, F_{r>}^{\text{ex}}2s^0\rangle-R_{1s_\alpha 2s_\alpha}^{\text{ex}})$$

$$=0.00208\mathcal{K}_{CS}^{-1}\text{ ev},$$

an entirely negligible value. Thus the "Fermi hole" is very effective in keeping the electrons of the $\alpha\alpha$ pair apart and not necessitating a "Coulomb hole." Hence to obtain the over-all "core-polarization" potential we need to add the $r_>^{-1}$ terms only for the $1s_\beta 2s_\alpha$ pair. Then neglecting exchange in dipole and higher-order terms, U_f in Li may be taken as

$$U_f\sim(\bar{\delta}_C+\delta_S)^{-1}[F_{r>}+2(F_{(1s)}-F_{r>})]. \quad (59)$$

V. MOLECULES

The treatment that was given in previous sections and demonstrated in detail for the case of the Li atom can be applied to any N-electron system whose zero-order wave function is a single Slater determinant of H.F. orbitals. Thus, the second-order energy of most molecules can be separated into "pair correlations" and nonpairwise additive "exclusion" effects by taking the H.F. SCF molecular orbitals (MO) as the one-electron basis set $\{k\}$. These orbitals are obtainable by Roothaan's procedure.[37] Each energy component can be obtained in closed form by taking out the denominators as "mean excitation energies" for *each* electron pair. Although rather crude, this procedure has the advantage that the various energy components can then be estimated using only the *same* H.F. orbitals as in the initial single determinant. Contrary to the use of an average energy denominator for the over-all second order energy[36] here each "mean excitation energy" has

[36] P. Kessler, Compt. rend., **242**, 350 (1955).

[37] C. C. J. Roothaan, Revs. Modern Phys. **23**, 69 (1951).

a more physical basis and can be left as a semiempirical parameter especially for those electron groups that are relatively unchanged in going from one atom or molecule to another. [See also the discussion following Eq. (54b)].

More directly, two specific applications are suggested by this approach as was mentioned in the Introduction. Both of them may be demonstrated with reference to the Li_2 molecule, for convenience. In this molecule, the first four MO's of the one electron basis $\{k\}$ are $(\sigma_g 1s)^2(\sigma_u 1s)^2$. When the atomic orbitals (AO) that make up such inner shells do not overlap appreciably as in Li_2, we can perform a unitary transformation on the $(\sigma_g 1s)^2(\sigma_u 1s)^2$ part of the basis *only* and convert the MO determinant $\det'[(\sigma_g 1s)^2(\sigma_u 1s)^2]$ into the ion core description $\det'[(1s_a)^2(1s_b)^2]$, i.e., $K_a K_b$, where a and b refer to the two nuclei, assuming that admixture of other AO's is negligible. Then taking $(1s_a)^2(1s_b)^2$ equivalently, as the first four spin-orbitals of $\{k\}$ with the rest of the MO's unchanged, a classification of all "ordered configurations" as in Eqs. (9) and (10) into various types of virtual transitions leads to a separation of the correlation energy as in Eqs. (16)–(18). We get the *total* energy of the molecule separated as in Eq. (46) into the energy of two *free* Li^+'s (including their individual $E^{(2)}$'s), the energy of the two H.F. MO valence electrons $(\sigma_g 2s)^2$, each in the field of both cores including the core "fluctuation potentials" [the effective "core-hamiltonian" from one Li^+ is $(h_{\text{core}}{}^{eff}+U_f)_a$] the energy of the two valence electrons (as in H_2), $(E^{(2)})_{(\sigma_g 2s)^2}$, and finally the correlation energy between the two cores K_a and K_b. There are also the "exclusion" terms associated with each of these components.

The first application concerns the "core-polarization" energy between a valence electron and the ion-cores. When these cores can be assumed quite unchanged, the expectation value of the potential, U_f determined from Eq. (59) in conjunction with the "series" levels of the atom, may be calculated over the ground or an excited state valence MO in the molecule. Thus the calculation of the contribution of "core polarization" to the already small binding energy of a diatomic alkali molecule is possible. Callaway[13] has made such calculations on alkali metals and found appreciable values even with just the dipole part (see Sec. IV) of U_f. In this type of application the change in the "exclusion" energy $(\bar{\delta}_C+\delta_S)R_{1s_a 1s_a}$ [Eq. (56a)] may also need to be estimated.

The second application, although a small effect in the case of Li_2, concerns the correlation energy between the two cores, K_a and K_b themselves. This energy which can be written in the "fluctuation" form similar to that in Eq. (41) and including the exchange part, is just the "dispersion" (plus "orbital average polarization") energy which on making a multipole expansion [or more conveniently, Gegenbauer expansion[35] as in Eq. (53) but now for two centers] for $g_{12}{}^2$ and taking the second term would simply lead to London's formula.[3] Aside from not requiring such an expansion, the approach presented here now includes the exchange terms as well as the "exclusion" effects similar to those in Eq. (50), but with the appropriate orbitals. It is particularly important to recognize that the discussion given here does *not* require the two cores to occupy completely isolated spaces, each with its own distinct basis set as has been considered necessary in previous discussions of London forces.[38] We have started from a complete set of MO's and have made assumptions only about the first four MO's, $(\sigma_g 1s)^2(\sigma_u 1s)^2$. The assumption that only the AO's, $(1s_a)$, $(1s_b)$, should not overlap appreciably is necessary so that we get into the $K_a K_b$ description. In general, such an assumption is much more plausible (and may even be improved on by considering some overlap) than the requirement of essentially complete localization of the core electrons around different centers, each group with its own distinct set of eigenfunctions.

Finally we observe that the second-order method which has been presented in detail in Sec. II, not only provides an approximate but very convenient way of estimating the energy of a many electron system, but also allows one to discuss many of the correlation effects in simple physical terms.

VI. HIGHER-ORDER CORRELATION EFFECTS

For simplicity the treatment presented in this article has been so far confined to the second order. Here, correlations among more than two particles at a time are introduced only by the "exclusion" terms. For three and more body "Coulomb" correlations it is necessary to go to higher orders of perturbation.[39] In the system of a single electron outside closed shells, some third-order correlation effects influencing the "core-polarization" energy (e.g., in Na) can be introduced into U_f as an additional potential by methods similar to those in Sec. II, or by letting the mean-excitation energy, $\bar{\delta}_C$, absorb the higher order effects semiempirically. (A similar situation usually occurs in various Van der Waals forces[10,39].)

An interesting case where higher-order correlations deserve further examination is a nondegenerate system of two electrons outside large closed shells as in Ca. Here, aside from the "exclusion" effects, there would be a U_f from the core acting on each of the $4s$ electrons, and a "fluctuation potential" $(r_{12}{}^{-2}-\langle r_{12}{}^{-1}\rangle^2_{4s,4s})/\bar{\Delta}$ [as in Eq. (41)] acting between the two $(4s)$ electrons [similar to the correlation of $(1s)^2$ in He]. However, the presence of a large polarizable core inside introduces additional effective interactions between the two outer electrons in higher orders. This can be seen by a crude

[38] See, e.g., H. C. Longuet-Higgins, Proc. Roy. Soc. (London) **A235**, 537 (1956).

[39] Actually, at least for the light atoms, the empirical work of Arai and Onishi suggests that the pairwise additivity of correlation effects may turn out to be a quite good description. See T. Arai and T. Onishi, J. Chem. Phys. **26**, 70 (1957).

but suggestive classical argument: Consider the core as a charge sphere with polarizability α and assume the two outer electrons to be momentarily at rest [see Eq. (1)] at distances r_1 and r_2 from the nucleus with an angle θ_{12} between them. Then, each electron induces a dipole moment of α/r_i^2 at the core with which it interacts to yield an energy $-\alpha/2r_i^4$. This is the limiting form of U_f in Eq. (46) as r_i approaches infinity. But, in addition, the dipole induced by the electron at r_1 acts on the electron at r_2 giving

$$[t_{12}^{(3)} \sim -\alpha \cos\theta_{12}/r_1^2 r_2^2].$$

The introduction of such effective interactions between two electrons to account for the influence of a "medium" (the core in this case) is possible quite generally by essentially an extension of the methods given for only the second order in Sec. II. It is also interesting to note the similarity of the additional interaction, $t_{12}^{(3)}$, to the new third-order Van der Waals interaction that is introduced by a solid surface between two inert molecules adsorbed on it[39] (the new force is in addition to the London force between the two molecules alone).

In general, the correlation energy *between* two groups of electrons will be influenced by the *internal* correlation of each group, as in the example just mentioned, where the $(4s^2)$ shell and the core in Ca could be considered as the two groups. The resulting higher order correlation energy can also be treated very simply for the special class of problems pointed out in the introduction. These were the cases where the two groups could be assumed to be totally separated and localized individually, each group with its own set of eigenfunctions. To see how "many electron group functions" can be used in such cases, consider, for instance, two many-electron atoms A and B far apart, and their mutual Van der Waals attraction. Here we can use ordinary second-order Schrödinger perturbation theory. Let ψ_A^k or ψ_B^l be the complete set of exact many electron eigenfunctions for each of the unperturbed "independent" systems A and B, respectively. Then the unperturbed Hamiltonian H_0 equals H_A+H_B, the composite basis set $\psi_{kl}=\psi_A^k\psi_B^l$ and the perturbation is the total interaction between A and B given by

$$V_{AB}=G_{AB}+U_{AB}, \tag{60}$$

where

$$U_{AB}\equiv\sum_{i,j}[1/(|\,\mathbf{r}_i^A-\mathbf{r}_j^B\,|)]=\sum_{i,j}(1/r_{ij}^{AB}),$$

and

$$G_{AB}\equiv\sum_{I,J}[Z_IZ_J/(|\,\mathbf{R}_I^A-\mathbf{R}_J^B\,|)].$$

G_{AB} refers to the interaction between the nuclei in A and the nuclei in B. U_{AB} is the electrostatic potential between pairs of electrons, one in A (at $\mathbf{r}_i^A$) and the other in B (at $\mathbf{r}_j^B$). ψ_A^k and ψ_B^l, being the set of exact eigenfunctions of the isolated systems A and B, include the coordinates of all the electrons and even the nuclei localized at A or B, respectively.[29] Then the intergroup "dispersion" energy is given by

$$E_{\text{disp}}^{(2)}(AB)=-\sum_{k\neq0,\,l\neq0}\frac{\langle\psi_A^0\psi_B^0,\,V_{AB}\psi_A^k\psi_B^l\rangle^2}{\delta_A^{0k}+\delta_B^{0l}}$$

$$\equiv-\sum_{k\neq0,\,l\neq0}\frac{\langle 00,\,V_{AB}kl\rangle^2}{\delta_A^{0k}+\delta_B^{0l}}, \tag{61}$$

where $\delta_A^{0k}=E_A^k-E_A^0$ and $H_A\psi_A^k=E_A^k\psi_A^k$. Replacing the denominators by mean excitation energies and using Eq. (27) we get

$$E_{\text{disp}}^{(2)}(AB)\approx(\bar{\delta}_A+\bar{\delta}_B)^{-1}(\langle 00,\,V_{AB}^2 00\rangle-\langle 0,\,W_A^2 0\rangle$$

$$-\langle 0,\,W_B^2 0\rangle+\langle 00,\,V_{AB}00\rangle^2) \tag{62}$$

where

$$\langle 0,\,W_A^2 0\rangle=\langle\psi_B^0,\,W_A^2(\mathbf{R}_B)\psi_B^0\rangle$$

and

$$W_A(\mathbf{R}_B)=\int|\,\psi_A^0(\mathbf{R}_A)\,|^2U_{AB}d\tau_A, \tag{63}$$

with $\mathbf{R}_A$ denoting all $\mathbf{r}_i^A$ and $\mathbf{R}_I^A$. If A and B are neutral systems, the last three terms of Eq. (62) may be negligible since they depend on the static charge distributions of A and B. Then Eq. (62) takes on the form of the "fluctuation potential" of one system acting on the other; i.e.,

$$E_{\text{disp}}^{(2)}(AB)\approx-\langle 00,\,V_{AB}^2 00\rangle/(\bar{\delta}_A+\bar{\delta}_B). \tag{64}$$

This description of the Van der Waals forces, that they are the result of the mean-square fluctuation of the electrostatic potential between two systems, is the generalization of the usual fluctuating dipoles picture (Sec. I). Note also that the form of Eq. (64) is the same as the potential in the core polarization problem. Similar considerations, of course, apply to the scattering of electrons[40] by atoms as well.

Now, consider only the U_{AB} part of V_{AB} [Eq. (60)] and in Eq. (64) write U_{AB}^2 in detailed form as

$$U_{AB}^2=\left(\sum_{i,j}\frac{1}{r_{ij}^{AB}}\right)^2=\sum_{i,j}\left(\frac{1}{r_{ij}^{AB}}\right)^2+\sum_{i,j\neq r,s}\left(\frac{1}{r_{ij}^{AB}r_{rs}^{AB}}\right). \tag{65}$$

Here i and r designate any two electrons in A and j and s any two electrons in B. The $(r_{ij}^{AB})^2$ terms in Eq. (65) involve the coordinates of only one electron at a time from each group. Their contribution to Eq. (64) can be written in terms of the first-order density matrices of A and B. On the other hand, two electrons i and r from A enter along with one or two electrons (j and s) from B into the $(r_{ij}^{AB}r_{rs}^{AB})$ terms and their contribution is in terms of the second-order density matrices of A and B.[29,41] Now ψ_A^0 and ψ_B^0 were exact many-electron eigenfunctions and included the *internal* correlations of each group, respectively. Thus the preceeding examination of Eq. (65) along with Eqs. (60)

[40] See A. Temkin, Phys. Rev. **107**, 1004 (1957).
[41] J. Bardeen, Phys. Rev. **58**, 727 (1940).

and (64) brings out the desired result, i.e., the effect of the internal correlations of A and B on the "*inter*-group" correlation energy has been taken into account in $E_{\text{disp}}^{(2)}(AB)$.

If, instead of the special case considered, we now have any two groups that cannot be assumed to be separately localized, the treatment of higher-order correlations by the use of many-electron group functions is no longer straight-forward. The difficulty is again mainly due to the exclusion principle (see Introduction). To circumvent this difficulty, previous treatments have been restricted to the use of very special many electron group functions, [17,18] i.e., those satisfying "generalized orthogonality conditions." However, the subdivision of a one-electron basis set into mutually exclusive subsets, apparently implied by these conditions, is too restrictive. The degree of restriction becomes particularly apparent if we consider the Be atom as a two-shell system ($1s^2$ and $2s^2$) with correlated group functions for each shell, instead of the "sigma-pi" problem. In the former case where there is no nominal symmetry difference between the two groups, it is more evident that both groups would have to use the same spin-orbital set. On the other hand, it seems that a treatment based on a single complete basis set can be given not only for two, but also for many-body correlation effects, by going to higher orders of perturbation and classifying all possible virtual excitations as in Sec. II. Some of these excitations will now involve more than two electrons at a time.

ACKNOWLEDGMENTS

The author wishes to thank Professor W. T. Simpson and Professor K. S. Pitzer for various helpful discussions. This research was carried out under the auspices of the U.S. Atomic Energy Commission.

THE JOURNAL OF CHEMICAL PHYSICS VOLUME 33, NUMBER 4 OCTOBER, 1960

Charge Transfer between Atomic Hydrogen and N^+ and O^+†

R. F. STEBBINGS, WADE L. FITE, AND DAVID G. HUMMER*

John Jay Hopkins Laboratory for Pure and Applied Science, General Atomic Division of General Dynamics Corporation, San Diego, California

(Received June 13, 1960)

The cross sections for charge transfer in collisions between atomic hydrogen and singly charged atomic ions of nitrogen and oxygen have been measured within the energy range from 400 to 10 000 ev, using modulated-beam techniques. The results are compared with recent calculations.

I. INTRODUCTION

THE cross sections for resonant charge transfer in collisions between atomic hydrogen and positive and negative atomic ions of hydrogen within the energy range from a few hundred ev to about 40 kev were presented in previous papers.[1] In the present work, measurements of a similar nature were made for the singly charged ions of atomic nitrogen and oxygen. These two charge-transfer processes are of particular interest, as they characterize nonresonant and almost exactly energy-resonant collisions. Since the colliding particles are all atomic in nature, no complication is introduced through dissociation. On the basis of the near-adiabatic theory[2–4] the transfer cross section between O^+ and H (for which the energy defect $\Delta E=0.019$ ev) should show a maximum value at a near-threshold energy, while for collisions between N^+ and H($\Delta E=0.94$ ev) the cross section should be small at low energies and should rise to a maximum value in the region of a few thousand ev.

II. APPARATUS

The apparatus used in these experiments was basically the same as that used in the earlier ion experiments and is shown schematically in Fig. 1. An arbitrarily highly dissociated beam of hydrogen issued from a tungsten furnace in the first of three differentially pumped vacuum chambers and was modulated at 100 cps by a mechanically driven, toothed chopper wheel located in the second chamber. On entering the third chamber, the beam passed between two deflector plates, between which an electrostatic field swept out any charged particles accompanying the neutral beam, and

† This research was supported by the Advanced Research Projects Agency through the United States Office of Naval Research.

* Present address: Department of Physics, University College, London, England.

[1] W. L. Fite, R. F. Stebbings, D. G. Hummer, and R. T. Brackmann, Phys. Rev. **119**, 663 (1960); and D. G. Hummer, R. F. Stebbings, W. L. Fite, and L. M. Branscomb, *ibid.* **119**, 668 (1960).

[2] D. R. Bates and H. S. W. Massey, Phil. Mag. **45**, 111 (1954).

[3] J. B. H. Stedeford and J. B. Hasted, Proc. Roy. Soc. (London) **A227**, 466 (1955).

[4] H. B. Gilbody and J. B. Hasted, Proc. Roy. Soc. (London) **A238**, 334 (1956).

then passed through an aperture in the mass-spectrometer repeller plate into the collision region.

A dc beam of the ions under investigation passed through the collision region in a direction normal to the atom beam, care being taken to ensure that all the ions passed through the atom beam. The slow ions formed in transfer collisions were detected by either of two detectors. One of these was a simple magnetic mass spectrometer, and the other was one of two plates located respectively above and below the interaction region of the two beams. With either of these detectors, the signal associated with the atom beam was distinguishable from that arising from the background gas, since it occurred at the modulation frequency and in a specified phase. The signal associated with the residual gas was dc, together with some noise at the modulation frequency.

When the mass spectrometer was used, the slow ions were swept out of the collision region by means of a weak electrostatic field established between the repeller and the extractor. They were than focused electrostatically into the mass spectrometer and were subsequently collected in a Faraday cage. Voltage signals were generated by passing the ion currents through the 10^{10}-ohm input resistances of the plate-follower preamplifiers that were used as impedance converters. The low-impedance output signals were than fed through vacuum seals to a narrow-band amplifier and a phase-sensitive detector, whose reference signal was generated from a light and photocell that monitored the chopper wheel. An oscilloscope was used to observe the output of the phase-sensitive detector and to ensure correct phasing of the reference signal. The output of the phase-sensitive detector was integrated and displayed on one pen of a two-pen recorder, the other pen of which simultaneously displayed the fast-ion current.

The ion source used in these experiments was that developed for the proton and H^- experiments.[1] Basically, it was a hot-cathode, low-voltage arc source similar to the duoplasmatron of von Ardenne[5] but differing primarily in that the magnetic field was produced by permanent magnets rather than by an electromagnet. The power dissipation was sufficiently low that forced-air cooling was satisfactory. The ion source was mounted on the end of an arm extending from the main vacuum chamber, and 45° mass analysis of the ions was provided in their passage through this side arm by means of an external electromagnet. On entering the main experimental chamber, the ions passed axially through six cylinders, between the fourth and fifth of which the neutral-atom beam crossed the ion beam. A voltage difference between the first and second cylinders provided a weak lens for final focusing of the ion beam, which was then collimated by a small rectangular orifice in the third cylinder. Through

[5] M. von Ardenne, *Tabellen der Elektronenphysik, Ionenphysik, und Übermikroskopie* (Deutscher Verlag der Wissenschaften, Berlin, 1956).

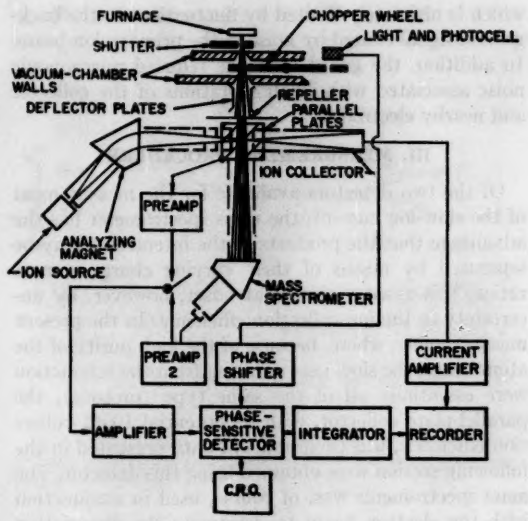

FIG. 1. Schematic diagram of the experiment.

maintenance of this cylinder at a somewhat higher potential than the fourth cylinder, in which a larger rectangular orifice had been cut, secondary electrons ejected from the third cylinder by the primary ion beam were prevented from entering the collision region. The fifth cylinder contained an aperture whose height was less than that of the atom beam The sixth cylinder was the ion collector, which was biased to suppress secondary-electron emission. A grounded cylindrical shield was maintained around the ion collector to prevent the arrival at its external surface of stray electrons or ions. The currents to both the fifth and the sixth cylinders were measured, and the alignment was considered satisfactory when the current to the fifth cylinder was of the order of 1% of that to the ion collector. This ensured that the ion current measured at the ion collector represented sufficiently accurately the current which had traversed the neutral beam.

Certain features of the apparatus are not shown in Fig. 1. The first is a filament located in the fast-ion collector. A beam of electrons from this filament was used to ionize the neutral beam, and mass-spectrometric analysis of the resulting ions enabled the degree of dissociation of the hydrogen beam to be determined. Typically, this was about 95%. The second omission is a pair of Helmholtz coils that provided at the collision region a magnetic field parallel to the direction of the electrostatic collecting field. The third is a guard ring that surrounded the collector of the parallel-plate detector and was maintained at the same potential as the collector. The guard ring was used to limit the path length over which collection was made of the slow ions formed in collisions of the primary ions with the residual gas. This reduction in dc background ion signal gave considerable improvement in the signal-to-noise ratio,

which is ultimately limited by fluctuations in the background signal caused by noise in the primary-ion beam. In addition, the guard electrode reduced microphonic noise associated with small vibrations of the collector and nearby electrodes.

III. MEASUREMENT PROCEDURE

Of the two detectors available for the measurement of the slow-ion current, the mass spectrometer has the advantage that the products of the interaction may be separated by means of their varying charge-to-mass ratios; this asset is somewhat offset, however, by uncertainty in the ion collection efficiency. In the present measurements, where, because of the high purity of the atom beam, the slow ions resulting from the interaction were essentially all of the same type (protons), the parallel-plate collector, with its potential 100% collection efficiency, was preferred. All data presented in the following section were obtained using this detector. The mass spectrometer was, of course, used in conjunction with the electron beam to determine the dissociation of the hydrogen beam. The procedure here was to operate with the collision region at 180 v positive with respect to ground. With the filament at ground potential, electrons entered the collision region with 180 ev energy and gave rise to ionization. The ions were swept towards the mass spectrometer by a small electrostatic field maintained between the repeller and extractor and were then focused into the mass-spectrometer magnet. This magnet and the ion collector were operated at ground potential, so that the ions were accelerated to 180 ev for passage through the mass-spectrometer magnet.

With the parallel-plate collector, the magnetic field was used to prevent electrons that were ejected from the fifth cylinder by the primary ions from penetrating to the interaction region. Saturation curves of the slow positive-ion current were made as a function of this magnetic field and of the electrostatic collecting field. These curves led to the adoption of 30 oe and 30 v/cm, respectively, as the standard operating values for these quantities.

In collecting data, the conditions affecting the neutral hydrogen-atom beam were kept unchanged, while the energy of the ion beam was varied. The signal per unit ion current was then observed as a function of the energy of the primary ion beam. The relative cross-section data obtained in this way were then normalized by determining the ratio of the measured cross section to that for charge transfer between protons and hydrogen atoms. From knowledge of the latter cross section obtained from earlier measurements,[1] the absolute cross section for the process under investigation could be determined. The oxygen and nitrogen data were accumulated using oxygen and air, respectively, as the source gas. In both cases it was possible to extract a sufficiently large beam of protons from residual water vapor in the source to permit comparison of the proton cross section with that for the ion under investigation without substituting hydrogen in the source for the gas under investigation. Thus, to obtain absolute measurements it was necessary only to compare the signals per unit current for the protons with those for the ions being studied as each in turn was selected for observation by adjustment of the current in the analyzing magnet. When O^+ ions were being studied, the oxygen admitted to the source was first dried by passage through a trap immersed in an acetone-dry-ice mixture. Comparison of the N^+ and O^+ cross sections when both ions were drawn from a discharge in air confirmed the values obtained by comparing each cross section separately with that for protons.

It is evident that any positive ions produced from the ionization of atomic hydrogen by the primary ions would contribute additionally to the current of slow charge-transfer ions arriving at the collector. To investigate this effect, the sign of the collecting field was reversed, and the electrons liberated in ionizing collisions were measured. At low primary-beam energies, when ionization was undoubtedly small, the absence of a measurable negative signal was noted. This gave confirmation that secondary emission from the negative plate by the slow charge-transfer ions could be ignored. At the higher beam energies, when ionization might be expected to play a more significant role, the electron current observed on reversing the sign of the collection field was still less than 5% of the slow positive-ion current. The error introduced into the charge-transfer measurements from ionizing collisions was therefore also less than 5%. Since the experimental uncertainties were of the order of 10%, no correction was made to the observations for ionization.

IV. RESULTS

The charge-transfer cross sections for nitrogen and oxygen ions in atomic hydrogen over the energy range from 400 to 10 000 ev are shown in Fig. 2, with the experimental uncertainties given at a number of energies. Figure 3 shows the comparison of these experimental data with the calculations of Rapp and Ortenburger,[6] which pertain only to charge transfer where both the initial and the final particles are in the ground state.

While the experimental and theoretical results are clearly similar with respect to both magnitude and energy dependence, any detailed comparison of theory with experiment must of necessity consider the fact that these experiments were subject to uncertainties in (1) the state of the incident ions and (2) the state of the neutral products. The ion-source conditions were such that both atomic ions in metastable excited states and doubly charged molecular ions, as well as ground-state atomic ions, could have been present in the magnetically analyzed incident ion beam. Detecting

[6] D. Rapp and I. B. Ortenburger, J. Chem. Phys. **33**, 000 (1960).

the reaction by observing the production of slow protons provided no information on the state of the neutral products of the reaction. A quantitative comparison of theory and experiment is therefore not possible.

It is of interest, however, to consider qualitatively the effects which might be expected from the occurrence of charge transfer involving low-lying excited ionic and atomic states in the present experiments. For these considerations, the near-adiabatic theory of charge transfer may be used.

The near-adiabatic theory predicts that a charge-transfer cross section will have its maximum value when the incident-ion velocity approaches the value $a\Delta E/h$, where a is a length of the order of atomic dimensions, ΔE is the energy defect in the reaction, and h is Planck's constant. Hasted and his collaborators[3,4] have examined a considerable number of charge-transfer reactions and have found that for a large fraction of these reactions, involving a wide variety of ion-neutral combinations, a log-log plot of $V_{max}^{\frac{1}{2}}$ vs $m^{\frac{1}{2}}\Delta E$, where V_{max} is the energy at which the cross-section maximum occurs and m is the ion mass, is rather close to a straight line. Assuming that the charge-transfer reactions involving excited ions and atoms of concern in the present experiments also fit into this pattern, the following deductions may be made:

Oxygen

(a) If the primary beam comprised only ground-state atomic ions, two reactions were possible. The increase in the cross section observed at low energies was clearly due to the near energy-resonant reaction

$$O^+(^4S)+H(^2S)\rightarrow H^+ + O(^3P) + 0.019 \text{ ev} (V_{max}\sim 1 \text{ ev}), \quad (1)$$

which has by far the smallest energy defect. At the higher energies some additional slow-ion production

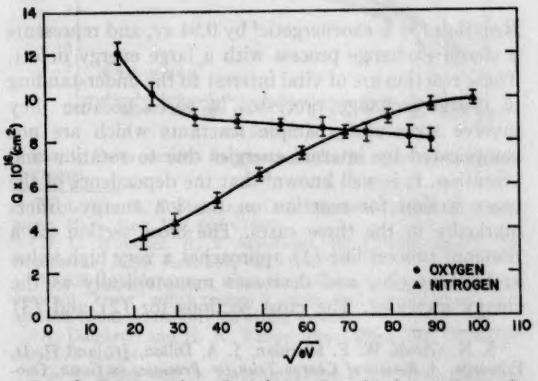

FIG. 2. Cross sections for charge transfer between atomic hydrogen and ions of nitrogen and oxygen.

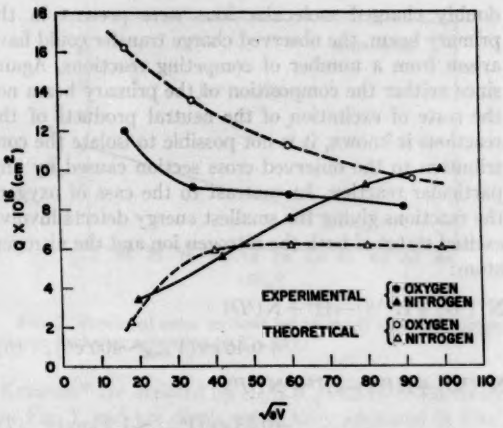

FIG. 3. Charge transfer between atomic hydrogen and ions of nitrogen and oxygen, compared with the theoretical predictions of Rapp and Ortenburger.

may have arisen from the reaction

$$O^+(^4S)+H(^2S)\rightarrow H^+ + O(^1D) \quad -1.94 \text{ ev} (V_{max}\sim 10 \text{ kev}), \quad (2)$$

and the observed cross section would then exceed that for reaction (1) alone.

(b) If, in addition to the ground-state ions, some excited ions were present in the primary beam, the following reactions may also have been operative:

$$O^+(^2D)+H(^2S)\rightarrow H^+ + O(^1D) + 1.37 \text{ ev} (V_{max}\sim 5 \text{ kev}); \quad (3)$$

$$O^+(^2D)+H(^2S)\rightarrow H^+ + O(^1S) - 0.84 \text{ ev} (V_{max}\sim 2 \text{ kev}); \quad (4)$$

$$O^+(^2P)+H(^2S)\rightarrow H^+ + O(^1S) + 0.85 \text{ ev} (V_{max}\sim 2 \text{ kev}). \quad (5)$$

These excited primary ions, although giving rise to few slow charge-transfer ions at near-threshold energies, would nevertheless contribute to the primary ion current. The observed cross section would therefore be less than that for reaction (1) alone at low energies, although at the higher energies the reverse may be true.

(c) Doubly charged molecular ions, which could have been present as a further impurity, would not be expected to undergo appreciable charge transfer over the entire range of the measurements. Their contribution to the primary ion beam would nevertheless reduce the size of the apparent cross section without modifying its shape.

Nitrogen

Similar qualitative reasoning again leads to the conclusion that if excited atomic ions (^1D or ^1S) and

doubly charged molecular ions were present in the primary beam, the observed charge transfer could have arisen from a number of competing reactions. Again, since neither the composition of the primary beam nor the state of excitation of the neutral products of the reactions is known, it is not possible to isolate the contribution to the observed cross section caused by any particular reaction. In contrast to the case of oxygen, the reactions giving the smallest energy defects involve excited states of both the nitrogen ion and the nitrogen atom:

$$N^+(^1D)+H(^2S)\rightarrow H^++N(^2D)$$
$$+0.46\text{ ev}(V_{max}\sim 400\text{ ev}), \quad (6)$$

$$N^+(^1D)+H(^2S)\rightarrow H^++N(^2P)$$
$$-0.73\text{ ev}(V_{max}\sim 1.2\text{ kev}); \quad (7)$$

while for the reaction in which all particles are in their ground states,

$$N^+(^3P)+H(^2S)\rightarrow H^++N(^4S)+0.94\text{ ev}(V_{max}\sim 2\text{ kev}). \quad (8)$$

Again referring to Fig. 3, in which the experimental results are plotted together with those recent calculations of Rapp and Ortenburger which relate only to the reactions (1) and (8), it is clear that it is not possible to say to what extent the discrepancy between theory and experiment is due to some deficiency in the calculations or to the fact that the observations possibly represent the aggregate of several collision processes. In the case of oxygen, the variation of the cross section with energy is obtained similarly by theory and experiment, and the difference in absolute magnitude may be due to the presence in the beam of ions, other than $O^+(^4S)$, having a small cross section within the energy range of these measurements. In the case of nitrogen, the differing shapes of the experimental and theoretical curves suggest that more than one charge-transfer process was operative throughout the range of the measurements, although the close agreement between the predicted magnitudes of the cross section suggests that reaction (8) was dominant throughout most of the energy range.

ACKNOWLEDGMENTS

The authors wish to thank D. Rapp and I. B. Ortenburger for communicating the results of their recent calculations prior to publication.

THE JOURNAL OF CHEMICAL PHYSICS VOLUME 33, NUMBER 4 OCTOBER, 1960

Interchange of Charge between Gaseous Molecules

DONALD RAPP AND IRENE B. ORTENBURGER

Lockheed Missiles and Space Division, Palo Alto, California

(Received June 13, 1960)

The theoretical methods for calculation of charge-exchange cross sections of Gurnee and Magee [J. Chem. Phys. **26**, 1237 (1957)] have been applied to the reactions of H atoms with H^+, O^+, and N^+. The agreement with experiment [Fite, *et al.*, Phys. Rev. **119**, 663 (1960); Hummer, *et al.*, Phys. Rev. **119**, 668 (1960)] is excellent considering the approximations involved in the theory.

THIS work consists of the application of the theoretical methods of Gurnee and Magee[1] to the calculation of charge exchange cross sections for the reactions

$$H^++H\rightarrow H+H^+ \quad (1)$$

$$O^++H\rightarrow O+H^+ \quad (2)$$

$$N^++H\rightarrow N+H^+. \quad (3)$$

Reaction (1) is resonant. Reaction (2) has three final states[1a,2] and represents a "near-resonant" process. Reaction (3) is exoenergetic[2] by 0.94 ev, and represents a charge-exchange process with a large energy defect. These reaction are of vital interest to the understanding of charge-exchange processes in gases because they involve structurally simple reactants which are not complicated by internal energies due to rotation and vibration. It is well known[3] that the dependence of the cross section for reaction on the ion energy differs markedly in the three cases. The cross section for a resonant process like (1) approaches a very high value at low energies, and decreases monotonically as the energy increases. The cross sections for (2) and (3)

[1] E. F. Gurnee and J. L. Magee, J. Chem. Phys. **26**, 1237 (1957).

[1a] The reactions producing oxygen atoms in the P_2, P_1, and P_0 states are 0.019 ev, 0.001 ev, and −0.009 ev exoenergetic, respectively.

[2] The ionization potentials of H, $O(P_2)$, $O(P_1)$, $O(P_0)$, and N are 13.595, 13.614, 13.596, 13,586, and 14.54 ev, respectively (Atomic Energy Levels, 1952 Circular 467, Natl. Bur. Standards).

[3] S. N. Ghosh, W. F. Sheridan, J. A. Dillon, Jr., and H. D. Edwards, *A Review of Charge Transfer Processes in Gases*, Geophysics Research Paper No. 48 (Air Force Cambridge Research Center, Bedford, Massachusetts, July 1955).

decrease to essentially zero at low energies, increase to a maximum at some finite energy, and then decrease monotonically with further increase of energy. Because (2) is nearly resonant, the maximum will be approached at a very low energy. Reaction (3) will have its maximum cross section at a much higher energy. In a series of recent experiments,[4,5] cross sections for these reactions have been obtained over wide ranges of ion energies. It was, therefore, decided that the previous work of Gurnee and Magee[1] ought to be applied to these processes in detail as a further test of the theory.

The required relations for the cross section of (1) are derived in footnote reference 1 by an impact parameter treatment. Equation (14) of footnote reference 1 gives the charge-exchange probability $P(R_0)$ as a function of the impact parameter R_0. The cross section for the reaction is then found from Eq. (7) of footnote reference 1. It is shown in footnote reference 1 that the function $P(R_0)$ oscillates between 0 and 1 for small R_0, but eventually decays from 1 to a final 0 at sufficiently large R_0. In their calculations,[6] they computed $P(R_0)$ from 0 to 0.5 along this decay portion of the curve, and took $P(R_0)$ as the average value 0.5 for all smaller R_0. The cross section so obtained will be denoted by $\sigma^{(0)}$. Actually, the oscillations increase in frequency as they approach the origin, so that $\sigma^{(0)}$ is less than the cross section the theory would predict if the oscillations were taken into account. In practice, only the first oscillation makes any notable difference, and we will denote the cross section which takes into account only the first oscillation by $\sigma^{(1)}$. Typical functions $P(R_0)$ are shown in Fig. 2 of footnote reference 1. The results for reaction (1) are shown in Fig. 1 along with the experimental data of Fite.[4] The scattered wave calculations of Dalgarno and Yadav,[7] Bates and Dalgarno,[8] Jackson and Schiff,[9] and Brinkman and

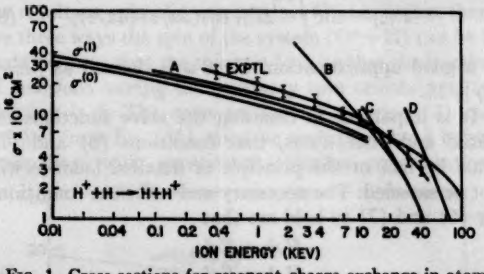

FIG. 1. Cross sections for resonant charge exchange in atomic hydrogen.

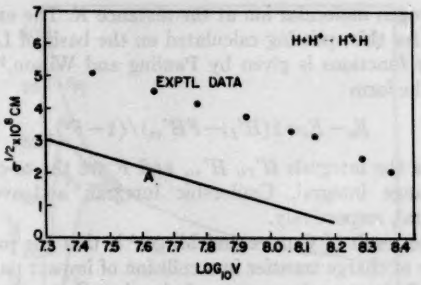

FIG. 2. Predicted cross sections for resonant atomic hydrogen charge exchange according to Eq. (1).

Kramers[10] are denoted by A, B, C, and D, respectively, in Fig. 1, and are displayed as they appeared in Fite's paper. Since curve A is only slightly better than $\sigma^{(1)}$, at the cost of orders of magnitude more calculational effort, the advantages of the impact parameter treatment are apparent. The modified Born approximations of B, C, and D are much more approximate.

The theory of Popescu Iovitsu and Ionescu-Pallas[11] gives the result

$$\sigma^{\frac{1}{2}}=[10^{-13}/(\pi I)^{\frac{1}{2}}]\ln[(\pi I)^{\frac{1}{2}}e^{31}/v], \qquad (1)$$

where σ is the cross section in cm^2, I is the ionization potential in ergs, and v is the velocity in cm/sec. In order to derive this equation, the authors had to assign a value to an undetermined parameter. They chose a value that gave a best fit to the data for resonant charge exchange in rare gases. It turned out that, with a single value of this parameter, an extremely good correlation of the rare gas charge exchange cross sections was obtained. We have applied this equation to reaction (1) and compared the results (curve A) with Fite's experimental data in Fig. 2. The agreement is poor using the value of the parameter they assumed; the experimental and theoretical cross sections differ by more than 400%.

In a recent article on charge exchange in doubly charged ions,[12] the result of Firsov[13] was described, which when applied to reaction (1) gives the result that the cross section for charge exchange is given by $\sigma=\frac{1}{2}\pi R_0^2$, where R_0 is the value necessary to satisfy the equality

$$(1/2\hbar v)\int_{-\infty}^{+\infty}(E_a-E_s)\,dx=\pi, \qquad (2)$$

where $x^2=R^2-R_0^2$, R is the internuclear distance of ion and atom, and E_a-E_s is the resonance splitting of the antisymmetric and symmetric states of the

[4] W. L. Fite, R. F. Stebbings, D. G. Hummer, and R. T. Brackmann, Phys. Rev. **119**, 663 (1960).

[5] D. G. Hummer, R. F. Stebbings, W. L. Fite, and L. M. Branscomb, Phys. Rev. **119**, 668 (1960).

[6] In colloquial language, when the collision is direct the electron does not "know" which proton it originally belonged to and ends up with equal probability on either proton.

[7] A. Dalgarno and H. N. Yadav, Proc. Phys. Soc. (London) **A66**, 173 (1953).

[8] D. R. Bates and A. Dalgarno, Proc. Phys. Soc. (London) **A66**, 972 (1953).

[9] J. D. Jackson and H. Schiff, Phys. Rev. **89**, 359 (1953).

[10] H. C. Brinkman and H. A. Kramers, Proc. Acad. Sci. Amsterdam **33**, 973 (1930).

[11] I. Popescu Iovitsu and N. Ionescu-Pallas, Soviet Phys. (Tech. Phys.) **4**, 781 (January 1960).

[12] I. K. Fetisov and O. B. Firsov, Soviet Phys. JETP **37**, 67 (1960).

[13] O. B. Firsov, Soviet Phys. JETP **21**, 1001 (1951).

hydrogen molecular ion at the distance R. The expression for this splitting calculated on the basis of LCAO wave functions is given by Pauling and Wilson,[14] and has the form

$$E_a - E_s = 2(H'_{fi} - FH'_{ii})/(1-F^2), \qquad (3)$$

where the integrals H'_{fi}, H'_{ii}, and F are the so-called exchange integral, Coulombic integral, and overlap integral, respectively.

The result of Gurnee and Magee[1] is that the probability of charge transfer in a collision of impact parameter R_0 is given by square of the sine of the integral on the left side of Eq. (2).

Pauling and Wilson[15] pointed out that in any system having two equivalent states (when unperturbed), the effect of a perturbation is to make the energy levels of the stationary states split. They also showed that if the system was initially in one unperturbed state, the effect of the perturbation over a period of time is to make the system oscillate between the two unperturbed states with frequency $\omega = (E_a - E_s)/2\hbar$ where $E_a - E_s$ is as before, the splitting of the levels. They found that when a constant perturbation is applied from time 0 to t, the probability of transition from the initial unperturbed state to the final unperturbed state is

$$P_{i\to f} = \sin^2\{[(E_a - E_s)/2\hbar]t\}. \qquad (4)$$

Gurnee and Magee[1] treated the case where $(E_a - E_s)$ is time-dependent, and found that $(E_a - E_s)t$ must be replaced by

$$\int_{-\infty}^{+\infty} (E_a - E_s)\,dt.$$

By assuming $dx = v\,dt$, one obtains Eq. (12) of footnote reference 1

$$P_{i\to f} = \sin^2\left\{\int_{-\infty}^{+\infty} [(E_a - E_s)/2\hbar](dx/v)\right\}. \qquad (5)$$

The relationship between (5) and (2) is obvious. Equation (2) may be said to be an approximation to (5) which sets $P_{i\to f} = 0.5$ for R_0 less than that which satisfied (2), and $P_{i\to f} = 0$ for all larger R_0.

Because of the less specific treatment of the details of the dependence of the transition probability on R_0, Firsov's method appears less "rigorous" than the method of Gurnee and Magee to the present authors. Yet Firsov and Fetisov[12] claim their method is "more rigorous."

The word "rigorous" has many connotations which are somewhat nebulous. One way to define the term is to compare with experiment. One must in this case hope that a fortunate cancellation of errors is not responsible for a fortuitous agreement. It is obvious from Eq. (2) that Firsov's method will predict much lower cross sections than Gurnee and Magee's method, because the last half oscillation and the exponential tail (see Fig. 2 of footnote reference 1) of the $P(R_0)$ vs R_0 curve has been neglected. Since Fig. 1 shows that the predicted cross sections of Gurnee and Magee's method applied to reaction (1) are lower than the experimental results, it may be concluded that Firsov's predictions will be still lower. In the case of double charge-exchange, Fetisov and Firsov[12] have pointed out that Gurnee and Magee's calculation gives results which are too high by about a factor of two. Since Firsov's method gives lower cross sections, it is not surprising that his prediction is in much better agreement with experiment. The exact significance of these applications is difficult to ascertain.

In their treatment of nonresonant charge-exchange, Gurnee and Magee[1] assumed $H'_{fi} = H'_{if}$ and $H'_{ii} = H'_{ff}$, in order to solve the time-dependent Schroedinger equation. The nature of this assumption becomes clearer from considerations like those given by Schiff.[16] In the nonresonant case, it turns out that

$$H'_{fi} - H'_{if} = (E_f - E_i)F, \qquad (6)$$

where E_f and E_i are the energy eigenvalues of the final and initial states, respectively. It can also be shown that

$$H'_{if} \gg H'_{ii} \qquad (7)$$

at moderate internuclear separations. Thus, even in the case of an "accidental" resonance (i.e. when the initial and final states are different even though they have equal energies), $H'_{fi} = H'_{if}$. For near-resonant systems where the right side of (6) is small, this condition will be nearly fulfilled. Explicit calculation in specific cases indicates that when $|E_i - E_f|$ is small compared to E_i and E_f, the solution obtained by Gurnee and Magee,

$$P_{i\to f} = \sin^2\int_{-\infty}^{+\infty} H'_{fi}\cos(\omega x/v)\,(dx/v), \qquad (8)$$

is a good approximation. Here ω is defined as $|E_i - E_f|/2\hbar$.

It is important in choosing the wave functions for initial and final states, that conditions (6) and (7) must be met or the principle of detailed balance will not be satisfied. The necessary and sufficient conditions for (6) and (7) to hold are that

$$H_i\psi_i = E_i\psi_i, \qquad H_f\psi_f = E_f\psi_f, \qquad (9)$$

where $H_i = -(\hbar^2/2m)\nabla^2 + V_i$, and $H_f = -(\hbar^2/2m)\nabla^2 + V_f$, where V_i and V_f are the effective potential energies binding the electron to the initial and final nuclei, respectively. If V is represented by $-Ze^2/r$, where Z is the effective nuclear charge, then hydrogenlike orbitals[17] can be employed. The advantages of using these orbitals are that they can be arranged easily to

[14] L. Pauling and E. B. Wilson, Jr., *Introduction to Quantum Mechanics* (McGraw-Hill Book Company, Inc., New York, 1935), pp. 326–330.

[15] Footnote reference 14, pp. 314–325.

[16] L. I. Schiff, *Quantum Mechanics* (McGraw-Hill Book Company, Inc., New York, 1955), pp. 236–239.

[17] Footnote reference 14, pp. 138–139.

give the correct energy eigenvalues, and they automatically satisfy the virial theorem, thus ensuring that the orbitals have the correct energy and the correct "size." The approximate wave functions described by Gurnee and Magee[1] do not satisfy these criteria.

In the case of reactions (2) and (3) the orbitals for H are known exactly, but approximations must be made for oxygen and nitrogen. Since the orbitals for O and N have nearly the same energies as a hydrogenic $1s$ electron, but have principle quantum number 2, one must choose $Z=2$ because the energy of a hydrogen-like orbital is proportional to Z^2/n^2. One then obtains the wave function for N and O

$$\psi_f=\pi^{-1}(1-r)e^{-r} \tag{10}$$

instead of the nodeless orbital proposed by Gurnee and Magee, Nre^{-r}, which does not have the correct energy and does not satisfy the virial theorem for $Z=1$. Their wave function leads to values of H'_{fi} and H'_{if} which differ by a factor of 3, an obvious absurdity. The use of Eq. (10) makes these integrals equal. Using Eq. (10) in Eq. (8) leads to the result that the probability of charge transfer for a collision of velocity v (cm/sec), and impact parameter R_0 (in units of Bohr radii), with E_i-E_f in ev, is

$$P_{i\to f}=\sin^2\left[1.83\times10^8 v^{-1}R_0^{5/2}\times\exp\left\{-R_0\left(1+\frac{3.28\times10^{13}\,|\,E_i-E_f\,|}{v^2}\right)\right\}\right]. \tag{11}$$

Gurnee and Magee[1] did not treat any cases that had non-unit spin factors. However, one must be careful to include the effect of statistical weights in reactions (2) and (3). In reaction (2), assuming ground states, O^+ has a spin of $\frac{3}{2}$ and H has a spin of $\frac{1}{2}$. The product O has a spin of 1, so that only collision complexes having a net resultant spin of 1 can produce O atoms. But there are three ways the spin of the system (O^++H) can be 1, and five ways that the spin can be 2, so that the fraction of collisions having the necessary spin orientations for reaction is $\frac{3}{8}$. The cross section for reaction (2) calculated from Eq. (11) must be multiplied by $\frac{3}{8}$ before comparing with experiment. Similar considerations

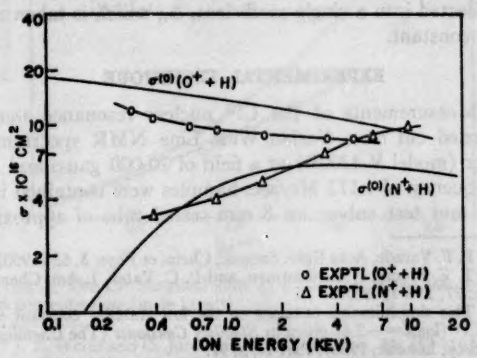

FIG. 3. Nonresonant charge exchange cross sections.

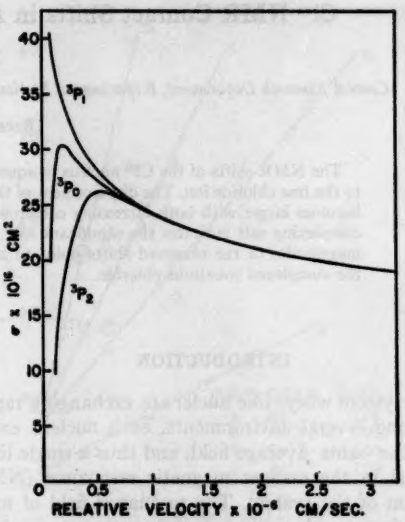

FIG. 4. Nonresonant charge exchange cross sections for $O^++H\to O+H^+$.

in the case of angular momentum show that in the reverse reaction $(O+H^+\to O^++H)$ there is a factor of $\frac{1}{3}$ because O is a p state and H^+ and O^+ are S states. Only in $\frac{1}{3}$ of all collisions is the component of angular momentum along the O—H axis zero. The equilibrium constant for the reaction is thus $\frac{9}{8}$. In reaction (3) the spin factor is $\frac{3}{4}$ and the momentum factor is $\frac{1}{3}$ in the forward direction. Thus the cross section calculated with Eq. (11) for reaction (3) must be multiplied by $\frac{2}{9}$ before comparing with experiment[18]. The results are shown in Figs. 3 and 4 together with the data of footnote reference 5.

Hertzberg[19] has pointed out that if excited O^+ and N^+ ions were formed in the ion sources of the experiments, in some instances they could react to form excited O and N atoms with significant cross sections. The fair agreement of the calculation for ground states with experiment in Fig. 3 indicate that the ground state reactions are probably accounting for at least about half the observed cross section.

ACKNOWLEDGMENT

The authors wish to acknowledge the importance of interesting discussions held with Dr. J. L. Magee, Dr. M. Hertzberg, Dr. W. B. Hanson, and Dr. L. I. Schiff. They also wish to thank R. F. Stebbings for communicating the data in the accompanying paper prior to its publication.

[18] At low velocities, the production of oxygen atoms with various total angular momenta, having zero angular momenta about the O—H axis, splits the calculated cross-section curves as shown in Fig. 4. This is due to the different ionization potentials of the P_2, P_1, and P_0 states. In this case one should multiply the calculated cross section for each state by 1/8, and sum over the three. Since the cross sections in Fig. 4 have already been multiplied by 3/8, one merely has to take the arithmetic mean of the three values presented there.

[19] M. Hertzberg, Lockheed Missiles and Space Division, Palo Alto, California, private communication.

Cl^{35} NMR Contact Shifts in Aqueous Cobaltous Chloride Solutions*

D. B. CHESNUT

Central Research Department, Experimental Station, E. I. du Pont de Nemours and Company, Wilmington, Delaware

(Received April 27, 1960)

The NMR shifts of the Cl^{35} nucleus in aqueous cobaltous chloride solutions have been measured relative to the free chloride ion. The displacement of the Cl^{35} resonance to lower applied fields at constant frequency becomes larger with both increasing cobaltous and chloride ion concentrations. The effect of added non-complexing salt indicates the significant role hydration plays in the complex equilibria taking place. The magnitudes of the observed shifts point to an isotropic electron-spin-nuclear-spin contact interaction in the complexed cobaltous chloride.

INTRODUCTION

IN A system where like nuclei are exchanging rapidly among several environments, each nucleus experiences the same average field, and thus a single line is observed in the nuclear magnetic resonance (NMR) spectrum of the system. The resonance field of nuclei undergoing rapid environmental exchange is determined by the relative concentrations of the nuclei in the separate environments and accordingly can be used to study equilibrium reactions.[1] A particularly interesting situation arises when one of the environments of the nuclei is near a paramagnetic ion. In such a situation the nucleus will experience a very sizeable internal field which should result in a correspondingly large shift. This effect has recently been investigated by Shulman[2] in concentrated solutions of complexed paramagnetic ions. Bloembergen[3] has pointed out that an isotropic contact interaction may well be the dominant factor in the nuclear shifts of such systems and Shulman's work indicates that this is the case for chlorine in ferric chloride complexes. The present investigation was undertaken to study this effect in a system where the shift is more variable, where the initial effects of the paramagnetic-ion-induced shift can be observed, and where the observed shift appears to be due to an isotropic contact interaction between electron and nuclear spins.

Aqueous $CoCl_2$ was chosen as the system to investigate since chloride ion is known to complex with cobalt[4] and since it has been shown[5] that cobaltous ion is relatively ineffective in relaxing nuclear spins.

Cobaltous salts are strong and stable electrolytes. The ion is usually pink in the more, and blue in the less, hydrated states; Co^{++} forms a chloride complex in sufficiently concentrated chloride solutions, the complex being dark blue.[4] Surprisingly little is known quantitatively about the principal species present in such solutions; there is evidence for the existence of the tetrahedral cobalt complex $CoCl_4^{--}$ [6] and for the species $CoCl_2(H_2O)_4$ as well.[7] Undoubtedly, both species are present along with other intermediates.

A quantitative treatment of the present system is practically impossible because of the complications presented by a multicomponent system. One can understand at least qualitatively the origin of some of our observations by considering the general "equation of state" of our solution in an approximate form which, as indicated later, appears to be valid in the present situation. Under the conditions of fast exchange, the chlorine shift is given by

$$\sigma_{obs}=\sum_i f_i\sigma_i^0 \qquad (\sigma_{Cl^-}^0=0), \qquad (1)$$

where σ_i^0 is the shift of species i and f_i is the fraction of the total chloride content present as this species; the shift of the free chloride ion is arbitrarily taken as zero. If it is assumed[8] that relatively little complex species is formed—that is to say, the dominant species are $Co(H_2O)_6^{++}$ and Cl^-—and that reactions proceed via the successive displacement of water by chloride on the cobaltous ion, Eq. (1) can be written as

$$\sigma_{obs}=[Co(H_2O)_6^{++}]\sum_i \alpha_i[Cl^-]^{i-1}\sigma_i^0. \qquad (2)$$

Since a quantitative analysis has not been made, all equilibrium constants, activity coefficients, and other factors necessary to define the system have been collected into a single coefficient, α_i, which is taken to be constant.

EXPERIMENTAL TECHNIQUE

Measurements of the Cl^{35} nuclear resonance were carried out on a Varian Wide Line NMR spectrometer (model V-4200B) at a field of 10 000 gauss and a frequency of 4.172 Mc/sec. Samples were contained in 15 mm test tubes; an 8 mm sealed tube of approxi-

* Contribution No. 616.

[1] H. S. Gutowsky and A. Saika, J. Chem. Phys. **21**, 1688 (1953).

[2] R. G. Shulman, J. Chem. Phys. **29**, 945 (1958).

[3] N. Bloembergen, J. Chem. Phys. **27**, 595 (1957).

[4] N. V. Sidgwick, *Chemical Elements and Their Compounds* (Oxford University Press, London, 1950), Vol. II, pp. 1376–1392.

[5] W. D. Phillips, C. E. Looney, and C. K. Ikeda, J. Chem. Phys. **27**, 1435 (1957).

[6] P. F. Varade, Acta Univ. Szeged., Chem. et Phys. **3**, 62 (1950).

[7] T. E. Moore, E. A. Gostman, and P. C. Yates, J. Am. Chem. Soc. **77**, 298 (1955).

[8] This simplification is based on the low stability constant of $CoCl^+$ ($\log K=-2.4$) given in *Stability Constants* (The Chemical Society, London, 1958), Part II, p. 97.

mately 5 *M* NaCl was placed within the sample tubes to serve as a reference, all shifts being measured relative to the sharp chloride line of the 5*M* NaCl solution. Since susceptibility and demagnetizing effects were very small compared to the shift observed, no attempt was made to correct for these effects.

RESULTS AND DISCUSSION

In this paper, shifts, δH, are related to the "fractional" shifts, σ, by

$$\delta H = \sigma H_{ref} = H_{ref} - H$$

$$H_{ref} \simeq 10\,000 \text{ gauss.} \qquad (3)$$

All the chlorine shifts were paramagnetic—i.e., to lower field at constant frequency—with respect to the standard (Cl^- as aqueous NaCl). In general, as the chloride shift increased, the line width also increased. As the chloride complexes with the cobalt, the cobalt electron relaxation will tend to reduce the lifetime of the chlorine nuclear spin states. Also, the complex formation will tend to distort the charge distribution about the chloride ion from its free ion spherical symmetry, giving rise to an additional quadrupole induced broadening of the resonance line.[9]

Figure 1 shows the Cl^{35} shift as a function of $[Co^{++}]$ in two types of solution. In the first case $CoCl_2$ was diluted, resulting in a shift nearly linear in $[Co^{++}]$. The slope of 4.2 gauss mole^{-1} liter versus the expected susceptibility shift of 0.13 gauss mole^{-1} liter[5] indicates that the observed shifts are due to a much stronger interaction than would result from bulk susceptibility effects. At relatively low concentrations of chloride, the observed shift is independent of the chloride concentration (see Fig. 3); thus, this curve indicates a linear variation in $[Co^{++}]$ of the shift as Eq. (2) would predict. The second curve of Fig. 1 shows the variation

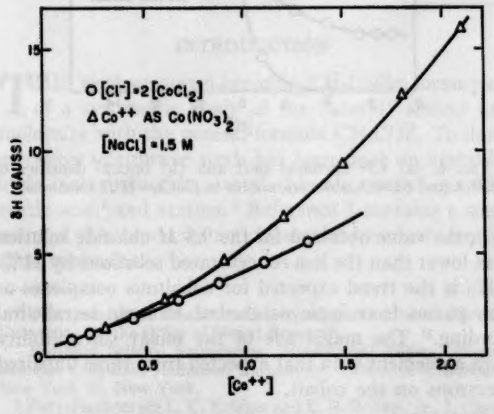

FIG. 1. The Cl^{35} chemical shift as a function of the cobaltous ion concentration (mole liter^{-1}).

[9] J. E. Wertz and O. Jardetzky, J. Chem. Phys. **25**, 357 (1956).

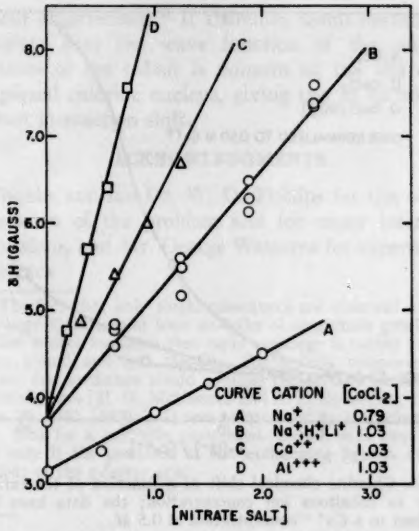

FIG. 2. Effect of added nitrate salts on the Cl^{35} chemical shift.

of δH versus $[Co^{++}]$ with a constant chloride concentration.

The departure from approximate linearity of this latter curve and its divergence from the previous curve was traced to the presence of excess salt—present here as $NaNO_3$—in this system. Experiments were carried out on solutions of constant $CoCl_2$ content and varying salt content. The results are shown in Fig. 2. In all cases the presence of excess salt caused an increase in the paramagnetic shift, the increase being proportional to the salt concentration and being larger as the cationic charge increases.[10] Since no nitrate complex with Co^{++} is expected,[4] the salt effect would appear to be due to a dehydration of the cobalt ion by the salt cations. This competition for water of hydration would favor the complex formation of the cobalt with chloride and thus lead to an increased paramagnetic shift.

A similar dehydration effect can be observed in temperature studies in which one passes reversibly from red to blue colored solutions and increasing paramagnetic shifts with increasing temperature. A solution of 0.9 mole liter^{-1} $Co(NO_3)_2$ and 1.5 mole liter^{-1} NaCl showed a shift approximately linear in $1/T$ in the range 26°–100°, the shifts being 4.7 and 10.9 gauss at the lower and upper temperatures, respectively.

Figure 3 shows the chloride shift as a function of the ratio of chloride to cobalt concentration (R). Since at low chloride concentrations the shift varies approximately linearly with $[Co^{++}]$, the data used in this figure, which came from separate experiments, were

[10] The $Al(NO_3)_3$ solutions were acidified with HNO_3 to prevent hydrolysis; the shift due to the $Al(NO_3)_3$ was then calculated by subtracting from the $Al(NO_3)_3+HNO_3$ shift the contribution from the acid as determined from curve B.

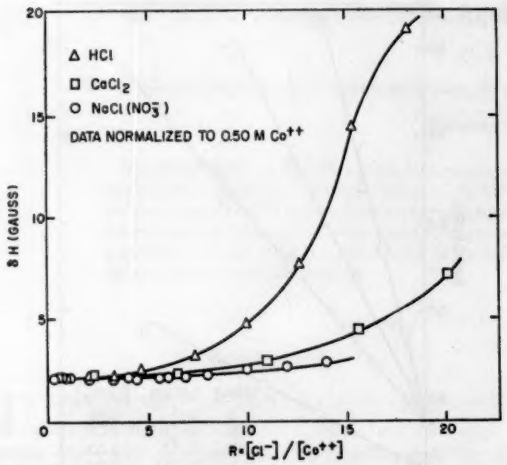

FIG. 3. Chlorine chemical shift as a function of the ratio of chloride to cobaltous ion concentration; the data have been normalized to a Co^{++} concentration of 0.5 *M*.

"normalized" to a Co^{++} concentration of 0.5 *M*. As noted, the shift is essentially independent of $[Cl^-]$ at low concentrations, while quite sizeable changes occur at higher concentrations. From the divergence of several of the sets of data at large *R*, it is apparent that in this region the normalization procedure is no longer valid. The general dependence of the shift on $[Cl^-]$ is difficult to analyze. However, the independence of σ_{obs} and $[Cl^-]$ at low chloride concentrations does suggest, as one might expect, that the primary species of chloride present in this range are free chloride and the monochloro-cobaltous complex (probably as $CoCl(H_2O)_5^+$) since, as seen from Eq. (2), the contribution to σ_{obs} of these species is not a function of the chloride content.

An experiment with concentrated HCl was particularly striking. Figure 4(A) shows the variation of the shift with chloride content and Fig. 4(B) the observed change of the optical densities of "red" 5150 A and "blue" 6250 A lines of the absorption spectra of the solution. As the concentration becomes greater than 6 *M* chloride, the shift increases rapidly as do the intensities of the blue lines of the absorption spectra.

The spectral work was undertaken in hopes of determining relative concentrations of the dominant species. Unfortunately, the band overlap and the large difference in extinction coefficients prevent any quantitative treatment. It can be noted, however, that the lack of change of the optical density of the 5150 A line indicates that a relatively small percentage of complex is formed, the assumption that has been made in this discussion. This assumption is also supported by susceptibility measurements on this system. Susceptibility measurements on solutions of total chloride concentration equal to 1.0, 2.4, and 3.8, and 6.5 molar agree to within

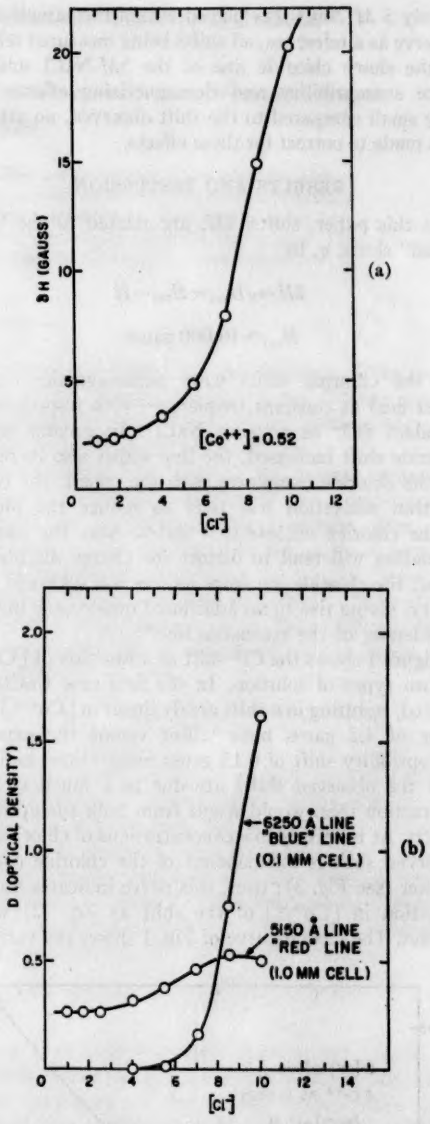

FIG. 4. (a) Cl^{35} chemical shift and (b) optical densities of 5150 A and 6250 A absorption lines in $CoCl_2$—HCl solutions.

1%; the value obtained for the 9.3 *M* chloride solution was lower than the less concentrated solutions by 11%. This is the trend expected for cobaltous complexes as one passes from ionic octahedral to ionic tetrahedral binding.[11] The magnitude of the molar susceptibility is in agreement with that expected from three unpaired electrons on the cobalt.

[11] R. S. Nyholm, Proc. 10th Solvay Congress, Brussels, 1956, pp. 225–287.

CONCLUSIONS

Chlorine nuclear resonance shifts can be sizeable; for example, Phillips[12] finds the resonance in pure $TiCl_4$ to be shifted some 10 gauss (at 10 kilogauss external field) to lower field with respect to an aqueous solution of NaCl. However, for the $CoCl_2$ solutions the shift is attributed to a relatively small concentration of complex so that the shift of the $CoCl^+$ and higher complexes must be very large and an explanation based on diamagnetic shielding or second-order paramagnetic effects is apparently ruled out. Although dipole interactions will not average to zero for a rapidly tumbling paramagnetic species with an anisotropic g factor,[13,14] this effect also appears to be too small to account for the present observations.[15] It therefore seems necessary to postulate that the wave function of the unpaired electrons of the cobalt is nonzero at the site of the complexed chloride nucleus, giving rise to an isotropic contact interaction shift.

[12] W. D. Phillips (private communication).
[13] H. M. McConnell and D. B. Chesnut, J. Chem. Phys. **28**, 107 (1958).
[14] N. Bloembergen and W. D. Dickinson, Phys. Rev. **79**, 179 (1950).

ACKNOWLEDGMENTS

Thanks are due Dr. W. D. Phillips for the original suggestion of the problem and for many interesting discussions, and Mr. George Watunya for experimental assistance.

[15] The fact that only single resonances are observed and that the range of shifts is at least an order of magnitude greater than the line widths indicates that rapid exchange is taking place between bound and free chloride. For a fully complexed axial species, fast exchange would average the dipolar interaction to essentially zero [H. M. McConnell and R. E. Robertson, J. Chem. Phys. **29**, 1361 (1958)]. It was pointed out by the referee, however, that for a partially complexed species, such need be the case only if the positions of the exchanging ligands are independent of the g-factor axis.

THE JOURNAL OF CHEMICAL PHYSICS VOLUME 33, NUMBER 4 OCTOBER, 1960

Microwave Spectrum, Barrier to Internal Rotation, and Quadrupole Coupling of Acetyl Bromide*

LAWRENCE C. KRISHER†

Mallinckrodt Chemical Laboratory, Harvard University, Cambridge 38, Massachusetts

(Received May 27, 1960)

The microwave spectra of the two acetyl bromide species, CH_3COBr^{79} and CH_3COBr^{81}, have been investigated in the region 12 000 to 33 000 Mc.

The bromine nuclear quadrupole hyperfine splittings were analyzed to give values for the quadrupole coupling constants. The observed coupling constants indicate a considerable deviation from cylindrical symmetry of the electric field gradient about the C—Br bond.

Several of the rotational transitions were further split into doublets due to the hindered internal rotation of the methyl group. The quadrupole hyperfine and internal rotation splittings were found to be essentially independent, and analysis of the latter gives a barrier to internal rotation of 1305±30 cal/mole.

INTRODUCTION

THIS work on acetyl bromide, CH_3COBr, forms part of a systematic study of the "acetyl" series,[1] i.e., molecules with the general formula CH_3COZ. To date, extensive microwave work has been done on acetaldehyde, acetyl fluoride, acetyl chloride, acetyl cyanide, acetic acid,[1] and acetone.[2] Reference 1 contains a summary of the structures and internal barriers of some of these molecules.

For this series, the potential barriers hindering the internal rotation of the methyl group fall in a range which allows their precise determination from frequency measurements in the microwave region. The splittings in the rotational spectrum of acetyl bromide proved to be typical in this respect.

The CH_3COBr spectrum is further complicated by the two nearly equally abdundant bromine species, Br^{79} and Br^{81}, and by the fact that these nuclei possess large quadrupole moments. The rotational spectrum exhibits a hyperfine structure due to the interaction of the quadrupole moment with the electric field gradient at the quadrupolar nucleus. Analysis of these hyperfine splittings affords a determination of the quadrupole coupling constants[3] for this molecule, and indicates the

* This research was made possible by support extended Harvard University by the Office of Naval Research.

† National Science Foundation Postdoctoral Fellow. Present address: Columbia Radiation Laboratory, Columbia University, New York 27, New York.

[1] For references see L. C. Krisher and E. B. Wilson, Jr., J. Chem. Phys. **31**, 882 (1959).

[2] J. D. Swalen and C. C. Costain, J. Chem. Phys. **31**, 1562 (1959).

[3] C. H. Townes and A. L. Schawlow, *Microwave Spectroscopy* (McGraw-Hill Book Company, Inc., New York, 1955), Chap. 6.

TABLE I. Observed spectra of acetyl bromide (Mc/sec).[a]

Transition	$F \rightarrow F'$	σ	CH_3COBr^{79}	CH_3COBr^{81}
a-Type				
$3_{1,3}$–$4_{1,4}$	9/2–11/2	*b*	20 139.43	19 999.26
	3/2–5/2		20 143.77	20 003.13
	7/2–9/2		20 150.49	20 007.96
	5/2–7/2		20 154.92	20 012.11
$3_{0,3}$–$4_{0,4}$	7/2–9/2	*b*		20 971.00
	9/2–11/2			20 973.66
	5/2–7/2			20 982.43
	3/2–5/2			20 984.47
$3_{1,2}$–$4_{1,3}$	9/2–11/2	*A*	22 787.47	22 606.54[b]
		E	22 786.79	
	3/2–5/2	*b*	22 794.65[d]	22 614.59
	7/2–9/2	*A*	22 797.96	22 616.98
		E	22 797.44	
	5/2–7/2	*A*	22 805.15	22 623.21
		E	22 803.90	
$4_{1,4}$–$5_{1,5}$	11/2–13/2	*b*	25 106.53	24 932.92
	5/2–7/2		25 110.84	24 936.55
	9/2–11/2		25 111.43	24 937.28
	7/2–9/2		25 115.74	24 940.70
$4_{0,4}$–$5_{0,5}$	9/2–11/2	*b*	26 108.30	25 930.24
	11/2–13/2		26 111.40	25 932.46
	7/2–9/2		26 116.67	25 936.96
	5/2–7/2		26 119.37	25 938.87
b-Type				
$0_{0,0}$–$1_{1,1}$	3/2–3/2	*b*	12 433.58	12 426.91
	3/2–5/2		12 502.61	12 484.78
	3/2–1/2		12 558.12	12 531.19
$1_{0,1}$–$2_{1,2}$	3/2–3/2	*b*		17 090.78
	3/2–5/2		17 154.98	17 117.81[f]
	5/2–7/2		17 223.65	17 175.72
$2_{0,2}$–$3_{1,3}$	5/2–7/2	*b*	21 592.05	21 524.02
	7/2–9/2		21 631.72	21 557.11
	3/2–5/2		21 638.05	21 562.60
	1/2–3/2		21 677.89	21 595.04
$3_{0,3}$–$4_{1,4}$	7/2–9/2	*b*	25 756.54	25 662.47
	5/2–7/2		25 778.50	25 680.83
	9/2–11/2		25 783.12	25 684.46
	3/2–5/2		25 805.56	25 703.40
$4_{1,4}$–$5_{0,5}$	11/2–13/2	*b*	21 450.87	21 220.85
	5/2–7/2			
	9/2–11/2		21 471.39	21 238.52
	7/2–9/2			
$4_{0,4}$–$5_{1,5}$	9/2–11/2	*b*		29 628.40
	7/2–9/2			29 638.95
	11/2–13/2			29 644.39
	5/2–7/2			29 655.20
$5_{1,5}$–$6_{0,6}$	13/2–15/2	*b*		27 041.92[d]
	7/2–9/2			
	11/2–13/2			27 053.88[d]
	9/2–11/2			
$7_{0,7}$–$7_{1,6}$	11/2–11/2	*E*	20 171.49	19 966.22
	11/2–11/2	*A*	20 174.67	19 969.09
	17/2–17/2	*E*		
	17/2–17/2	*A*	20 177.63	19 971.96
	13/2–13/2	*E*	20 186.19	19 978.80
	13/2–13/2	*A*	20 189.13	19 981.44
	15/2–15/2	*E*		
	15/2–15/2	*A*	20 192.05	19 984.18
$8_{0,8}$–$8_{1,7}$	13/2–13/2	*E*	24 442.49	24 170.70
	13/2–13/2	*A*	24 445.67	24 174.40
	19/2–19/2	*E*	24 445.67[d]	24 173.27
	19/2–19/2	*A*	24 449.17	24 176.97
	15/2–15/2	*E*	24 458.58	24 184.13
	15/2–15/2	*A*	24 462.07	24 187.65
	17/2–17/2	*E*	24 461.41	24 186.53
	17/2–17/2	*A*	24 464.90	24 190.15
$8_{2,6}$–$8_{3,5}$	17/2–17/2	*b*	32 602.01	32 804.90
	15/2–15/2		32 607.52	32 809.49
	19/2–19/2		32 633.34	32 830.87
	13/2–13/2		32 638.93	32 835.67
$9_{1,8}$–$9_{2,7}$	*c*	*E*	20 621.91[d]	20 541.46[d]
		A	20 623.67[d]	20 543.00[d]
$9_{2,7}$–$9_{3,6}$	19/2–19/2	*b*	31 115.92	31 326.92
	17/2–17/2		31 119.74	31 330.21
	21/2–21/2		31 141.07	31 348.15
	15/2–15/2		31 145.05	31 351.55
$10_{1,9}$–$10_{2,8}$	17/2–17/2	*E*	22 722.86	22 561.01
	17/2–17/2	*A*	22 725.54	22 563.55
	23/2–23/2	*E*	22 723.66	22 561.63
	23/2–23/2	*A*	22 726.34	22 564.33
	19/2–19/2	*E*	22 727.32	22 564.33[d]
	19/2–19/2	*A*	22 729.99	22 566.91
	21/2–21/2	*E*	22 727.85	22 564.77
	21/2–21/2	*A*	22 730.54	22 567.38
$11_{1,10}$–$11_{2,9}$	19/2–19/2	*E*	25 637.62	25 379.89
	19/2–19/2	*A*	25 641.10	25 383.41
	25/2–25/2	*E*	25 638.65	25 380.83
	25/2–25/2	*A*	25 642.22	25 384.32
	21/2–21/2	*E*	25 645.62	25 386.35
	21/2–21/2	*A*	25 649.20	25 389.77
	23/2–23/2	*E*	25 646.50	25 387.14
	23/2–23/2	*A*	25 650.34	25 390.60
$11_{2,9}$–$11_{3,8}$	23/2–23/2	*b*	28 710.85	28 876.40[e]
	21/2–21/2		28 712.58	28 877.80[e]
	25/2–25/2		28 725.02	28 889.0 [e]
	19/2–19/2		28 726.92	28 890.4 [e]
$12_{2,10}$–$12_{3,9}$	25/2–25/2	*b*	28 198.0 [d]	28 305.51[d]
	23/2–23/2			
	27/2–27/2		28 208.0 [d]	28 313.04[d]
	21/2–21/2			

[a] Estimated uncertainty ±0.15 Mc unless otherwise indicated.
[b] Internal rotation (*A*—*E*) splittings not resolved.
[c] Quadrupole splittings not resolved.
[d] Broad unresolved line.
[e] ±0.4 Mc.
[f] ±0.3 Mc.

lack of cylindrical symmetry of the electric field gradient along the C—Br bond.

EXPERIMENTAL

The sample used was commercial reagent-grade acetyl bromide. Care was taken to prevent unnecessary exposure of the sample to light.

The microwave spectrometer used was a Stark-effect type employing 100-kc modulation. Both oscilloscope and recorder display were used. Frequency measurements were made with multiples of a 5-Mc standard which was monitored by the standard signal from the Cruft Laboratories of Harvard University. The Stark cell was kept at dry ice temperature for most of the runs.

Both *a*-type and *b*-type rotational transitions of the two normal species, CH_3COBr^{79} and CH_3COBr^{81}, were observed in the frequency range 12 000 to 33 000 Mc.

At times it proved difficult to maintain a sample of acetyl bromide in the waveguide for more than about 15 min. This proved to be due primarily to an exchange reaction rather than to direct corrosion of the brass. When the Stark cell had been previously used for various chlorine-containing compounds, the acetyl bromide spectrum would be replaced within minutes by the intense acetyl chloride lines.[4] At other times, when the cell had been used previously to run nonexchangeable substances, a sample of acetyl bromide would last for hours.

OBSERVED SPECTRA AND CONSTANTS

The observed transitions with detailed quadrupole and internal rotation assignments are listed in Table I. In general, the principal quadrupole interaction splits each transition into a quartet due to the main selection rules $\Delta F=1$ for *R*-branch transitions and $\Delta F=0$ for *Q*-branch. The internal rotation perturbation leads to a further doubling of these lines, so that the general transition becomes an octet. Since the magnitudes of these perturbations depend on the particular rotational level, a variety of completely or partially resolved patterns were observed, e.g., in some cases the internal rotation splitting leads to overlapping of otherwise resolvable hyperfine components.

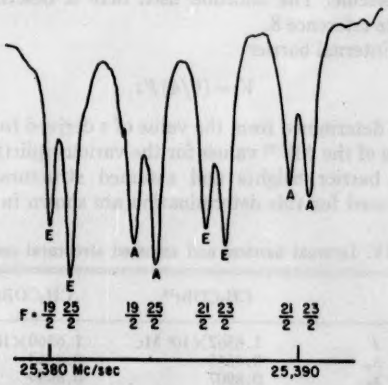

FIG. 1. Recorder tracing of the $11_{1,10}$–$11_{2,9}$ transition of CH_3COBr^{81} with detailed quadrupole hyperfine and internal rotation labeling.

[4] The CH_3COCl spectrum was obtained from Dr. K. M. Sinnott, private communication.

TABLE II. Rotational constants and moments of inertia.

	CH_3COBr^{79}	CH_3COBr^{81}
A	10 126.35 Mc	10 126.11
B	3 027.02	3 001.64
C	2 362.52	2 347.12
I_a	49.9223 amu A²	49.9235
I_b	167.006	168.418
I_c	213.980	215.384

Estimated uncertainty, ±0.15 Mc.

Figure 1 shows a recorder trace of a completely resolved transition, the $11_{1,10}$–$11_{2,9}$ of CH_3COBr^{81}. Notice that in this case, one transition affords four independent internal rotation measurements (*A*–*E* splittings). In each observed case these *A*–*E* splittings were equal, within the accuracy of measurement, indicating that the internal rotation and quadrupole perturbations are additive, and can thus be separately analyzed.

The rotational constants *A* and *C*, listed in Table II, were obtained from the *b*-type low-*J* lines after correcting the observed frequencies for the effect of the hyperfine structure. The rotational constant *B* was then determined from this *A* and *C* and the *a*-type low-*J* transitions.

The moments of inertia listed in Table II were obtained from these rotational constants using the conversion factor 5.05531×10^5 amu A² Mc. The moment of inertia of the methyl group about its symmetry axis can be shown to be, for a rigid model,

$$I_a=I_a+I_b-I_c=2.95 \text{ amu A}^2.$$

However, as has been pointed out by Laurie,[5] this number contains a contribution from the "inertial defect." A reasonable inertial defect for the acetyl series[5] (0.2 amu A²) brings this result into accord with the more conventional value $I_a=3.14$ amu A², which was used in the internal rotation calculations described below.

QUADRUPOLE COUPLING CONSTANTS

The quadrupole coupling constants

$$\chi_{aa}=eQ(\partial^2V/\partial a^2),$$

etc., were obtained by the usual methods,[3] using the low-*J* transitions where the splittings are generally larger. The *b*-type spectrum allows a precise determina-

[5] V. W. Laurie, J. Chem. Phys. 28, 704 (1958).

TABLE III. Quadrupole coupling constants.

	CH_3COBr^{79}	CH_3COBr^{81}
χ_{aa}	460±3 Mc	385±3 Mc
χ_{bb}	−277±1	−232±1
χ_{cc}	−183±3	−153±3
χ_{aa}	464	388
$\chi_{\beta\beta}$	−281	−235
$\chi_{\gamma\gamma}$	−183	−153
	$\eta_{bond}=-0.211$	

tion of χ_{bb}. This value and the observed a-type transitions can then be used to give a good value for χ_{aa}. χ_{cc} follows from the Laplace relation

$$\chi_{aa}+\chi_{bb}+\chi_{cc}=0.$$

The quadrupole coupling constants calculated in this manner are given in Table III.

For certain transitions an anomalous pattern was observed which can be attributed to second-order quadrupole perturbations. Since this effect was always small, ~0.5 Mc, it led to no uncertainty in the assignments, and had a negligible effect on the calculations of the χ's although it does impose the limits of accuracy here. It should be pointed out, however, that if all the χ's were to be calculated from the relatively strong b-type spectrum, without consideration of the second-order effects, serious errors could result, because the calculation of χ_{aa} from the b-type spectrum involves small frequency differences.

It was assumed that a principal axis of the quadrupole tensor coincides with the C—Br bond. The observed quadrupole coupling constants along the inertial axes were transformed to a new system α, β, γ such that the α axis lies along the C—Br bond and the γ axis is perpendicular to the molecular symmetry plane. These bond-system values are listed in Table III, and allow one to determine a value for $\eta_{bond}=(\chi_{\beta\beta}-\chi_{\gamma\gamma})/\chi_{aa}=-0.211$. Using the method described by Goldstein,[6] and assuming that $(eQq)_{atomic}$ for Br^{79} is −770 Mc, this value of η_{bond} suggests about 8% double bond character for the C—Br bond.

BARRIER TO INTERNAL ROTATION

For both CH_3COBr^{79} and CH_3COBr^{81} several of the higher J hyperfine multiplets were further resolved into doublets, resulting from the interaction of internal and over-all rotation. The height of the barrier hindering this internal rotation was determined from these doublet splittings, using the theory of Kilb, Lin, and Wilson[7] and Herschbach.[8] An alternate treatment of this type of data is that of Hecht and Dennison.[9]

[6] J. H. Goldstein, J. Chem. Phys. **24**, 106 (1956).
[7] R. W. Kilb, C. C. Lin, and E. B. Wilson, Jr., J. Chem. Phys. **26**, 1695 (1957).
[8] D. R. Herschbach, J. Chem. Phys. **31**, 91 (1959).
[9] K. T. Hecht and D. M. Dennison, J. Chem. Phys. **26**, 31 (1957).

The analysis assumes a molecular model consisting of a rigid asymmetric framework (here the COBr group) attached to a symmetric internal rotor (CH_3 group). The threefold potential barrier hindering the internal rotation of these groups is taken to be

$$V=V_3/2(1-\cos 3\alpha),$$

where α is the angle describing the relative orientation of the framework and the internal rotor.

For acetyl bromide, the "high barrier approximation" is applicable, i.e., only second-order perturbation corrections are necessary. For an infinite barrier each torsional level is triply degenerate. As the barrier is lowered, the quantum mechanical tunnel effect partially splits this degeneracy giving a nondegenerate A level and a doubly degenerate E level. The rotational energies for the two levels are slightly different and in the high barrier case, follow pseudorigid rotor patterns, with slightly different effective rotational constants. The various A–E assignments are listed in Table I. This A–E splitting is a very sensitive function of the barrier height.

For the ground torsional state of acetyl bromide these differences in effective rotational constant are very small, ~0.2 Mc. It is thus more convenient to find a value of V_3 (actually $\Delta W^{(2)}$) from the separation of each A–E doublet. The rotational energy level differences are expanded according to Eq. (13) through Eq. (16) of Swalen and Herschbach.[10] The frequency separation of a particular doublet is thus given as

$$\nu_A-\nu_E=\Delta\nu_{J',\tau',J,\tau}=(hI_a/8\pi^2r)\Delta W^{(2)}\times[(\lambda_a^2/I_a^2)\{(\partial W_{J,\tau}/\partial A)-(\partial W_{J',\tau'}/\partial A)\}+(\lambda_b^2/I_b^2)\{(\partial W_{J,\tau}/\partial B)-(\partial W_{J',\tau'}/\partial B)\}]$$

and is thus simply $\Delta W^{(2)}$ times a factor depending on the particular transition and the structural parameters of the molecule. The notation used here is described in footnote reference 8.

The internal barrier

$$V_3=(9/4)Fs$$

is then determined from the value of s derived from the average of the $\Delta W^{(2)}$ values for the various splittings.

The barrier heights and assumed structural constants used for this determination are shown in Table

TABLE IV. Internal barriers and assumed structural constants.

	CH_3COBr^{79}	CH_3COBr^{81}
F	1.6562×10^5 Mc	1.6560×10^5
λ_a	0.4545	0.4543
λ_b	0.8907	0.8909
I_a	3.14 amu A²	3.14
V_3	1306 cal/mole	1304

[10] J. D. Swalen and D. R.Herschbach, J. Chem. Phys. **27**, 100 (1957).

IV. Although the two acetyl bromide species studied provide only limited information about the molecular structure, previous work on the CH_3COZ series indicates that many of the structural parameters are relatively constant.[1] In the calculation of F and the λ_g values for CH_3COBr, the structural parameters of CH_3COCl given in reference 1 were used,[11] with the additional assumption that the C—Br bond length is 1.96 A. This rather long C—Br bond is necessary in order to get a good fit to the observed moments of inertia, which were found to be relatively insensitive to the CCBr angle. Any reasonable change in this structure has a negligible effect on the internal barrier value, compared to the effect due to the uncertainty in I_a. Thus a reasonable value for the barrier is 1305±30 cal/mole.

DISCUSSION

The molecular structures of the CH_3COZ molecules show certain regularities as pointed out in footnote reference 1. We might thus expect that the structure of CH_3COBr would be very similar to CH_3COCl, with the exception of the C—Z bond. It has also been pointed out[1] that the C=O distances correlate well with the carbonyl stretching frequencies in the infrared near 1800 cm^{-1}. These frequencies are nearly identical for acetyl bromide and chloride. It is thus unusual, in view of the large value of η_{bond} for CH_3COBr that, using the "normal" CH_3CO structure, a rather long C—Br bond (1.96 A) is necessary in order to get a reasonable fit to the observed moments of inertia. We are aware, however, of the dangers in attempting to extract structural information from a limited amount of isotopic data.

It is interesting to compare the quadrupole coupling data for acetyl bromide with the values given by Cornwell[12] for vinyl bromide, since the C—Br bond in both of these molecules has an adjacent pi-electron system. The value of $\eta_{bond}=-0.093$ for vinyl bromide (adjacent ethylenic system) is considerably less than $\eta_{bond}=-0.211$ for acetyl bromide (adjacent carbonyl system), and the percent double bond characters, calculated by Goldstein's[12] method, are 4% and 8%, respectively.

Perhaps the most interesting result of this study is the essentially exact agreement of the internal barriers of acetyl bromide and acetyl chloride[11] (1300 cal/mole). This is a rather striking further confirmation of Wilson's statement[13] that these barriers do not arise primarily from either steric repulsions or electrostatic interactions.

ACKNOWLEDGMENTS

The author is indebted to Professor E. Bright Wilson, Jr., and to the members of his research group for the use of the Harvard spectrometer on a number of occasions after formal connections there had come to an end.

[11] K. M. Sinnott, private communication.

[12] C. D. Cornwell, J. Chem. Phys. 18, 1118 (1950); see also J. A. Howe and J. H. Goldstein, J. Chem. Phys. 27, 831 (1957).

[13] E. B. Wilson, Jr., Proc. Natl. Acad. Sci. U. S. 43, 811 (1957).

Vibrational Spectra of Penta-Deutero-Fluoro-Benzene

D. STEELE,* E. R. LIPPINCOTT, AND J. XAVIER

Department of Chemistry, University of Maryland, College Park, Maryland

(Received April 11, 1960)

The infrared and Raman spectra of penta-deutero-fluoro-benzene have been measured and a set of assignments for the vibrational fundamentals is proposed. These are shown to be consistent with the present assignments of C_6H_5F, C_6D_6, and C_6D_5H by application of the product and inequality rules.

INTRODUCTION

IT HAS been shown that the vibrational spectra of biphenyl can be considered as due to two mono-substituted aromatic rings which vibrate almost independently.[1,2] By considering the mono-substituted group as a point mass the inequality rule of Whiffen and Steele[3] may be applied to the vibrational frequencies of biphenyl and those of any other mono-substituted benzene. This rule, which is an extension of Rayleigh's rule,[4] may be defined as follows. Consider two molecules, RX and RY, the mass of the substituent X being greater than that of the substituent Y. Then in any given symmetry class of RX containing "a" modes associated with the RX group the jth highest frequency lies between the jth and $(j+a)$th highest frequencies of the equivalent symmetry class of RY. The application of this rule to biphenyl has proved to be very useful and hence the extension of its use to biphenyl-d-10 seemed desirable. C_6D_5F was chosen as a compound suitable for comparison with the deuterated biphenyl because its moments of inertia are such as should give distinctive type band shapes, and the C–F stretching frequency is close to the inter-ring stretching frequency of biphenyl.

EXPERIMENTAL

C_6D_5F was prepared by a Friedel Crafts type reaction by bubbling DCl through fluoro-benzene in the presence of aluminum chloride catalyst.[5] The course of the reaction was studied by taking the infrared spectra of samples of the deuterated material. When the C–H stretching band was no longer visible and no further changes were observed to be occurring in the spectrum, the reaction was stopped and the isotopic purity of the product measured by mass spectroscopy. Due to coincidences of the high peaks with the mercury lines near mass number 100, the interpretation could not be made unambiguously, but suggested an isotopic purity of about 97%. The very weak infrared absorptions in the C–H stretching region and in the C–H out-of-plane deformation region suggest that the purity is much higher than this.

The infrared spectra were run in the vapor and liquid phases on a Beckmann IR4 and a Perkin Elmer 12C from 5000 to 250 cm^{-1} using LiF, NaCl, and CsBr optics.

Raman spectra and qualitative depolarization data were obtained using a two prism Huet spectrograph (aperture $f/8$) with a dispersion of 18 A/mm at 4358 A. Excitation was accomplished with a low-pressure water-cooled Toronto type arc using the 4358 A Hg line with KNO_2 and rhodamine dye as optical filters for radiations above and below this wavelength, respectively. Standard techniques were employed in the recording and the reading of the spectra. The observed Raman and infrared frequencies are listed in Table I, and the infrared spectra are illustrated in Figs. 1 and 2. For consistency the observed infrared frequencies in the liquid phase will be used throughout the text unless otherwise specified.

GENERAL DISCUSSION

There is little doubt that C_6D_5F is planar. The vibrational spectra of most of the fluoro-benzenes have now been studied and no evidence of nonplanarity has been obtained, even for the fully fluorinated molecule.[3] Consequently the symmetry must be taken as C_{2v}, in which case the fundamental vibrations separate between the symmetry classes as $11a_1+10b_2+6b_1+3a_2$. In naming the symmetry classes the recommendations of Mulliken[6] have been followed taking the x axis as perpendicular to the plane of the ring and the z axis as colinear with the C_2 axis. Using the data of Badger and Zumwalt,[7] the infrared band shapes of the active classes have been calculated taking the bond lengths as $r_{CF}=1.29$ A, $r_{CC}=1.40$ A, and $r_{CH}=1.08$ A. These are given in Table II along with the activities and Raman characteristics of the classes. In several cases in the infrared vapor spectrum, bands belonging to different symmetry classes are overlapping, and the calculated band contours proved very useful in identifying the component bands.

* National Science Foundation Post-Doctoral Fellow.

[1] J. E. Katon and E. R. Lippincott, Spectrochim. Acta No. 9, 627 (1959).

[2] E. R. Lippincott and D. Steele, J. Mol. Spectroscopy (to be published).

[3] D. Steele and D. H. Whiffen, Trans. Faraday Soc. **55**, 369 (1959).

[4] Lord Rayleigh, *Theory of Sound* (The Macmillan Company, London, 1894), 2nd ed., Vol. 1, p. 110.

[5] B. Bak, J. N. Schoolery, and Y. A. Williams, J. Mol. Spectroscopy **2**, 525 (1958).

[6] R. Mulliken, J. Chem. Phys. **23**, 1997 (1955).

[7] R. M. Badger and L. R. Zumwalt, J. Chem. Phys. **6**, 711 (1938).

TABLE I. Observed vibrational spectra.

Raman	Infrared		Assignment
	Vapor	Liquid	
229 ms			b_1 fundamental
~350 vvw			a_2 fundamental
391 vvw		388 ms	b_2 fundamental
428 vw	427 C ms	438 s	b_1 fundamental
450 vvw			2×229
505 m	504 A or B m	505 ms	a_1 fundamental
553 w	556 C s	563 s	b_1 fundamental
587 m		590 vvw	b_2 fundamental
618 m	622 m	627 ms	b_1 fundamental
639 m			1311−682
	662 vw	662 w	229+438
	678 A or B vvw		?
687 vvw		682 m	a_2 fundamental
721 vvw	717 C vvw		b_1 fundamental or 229+505
750 ms(p)	756 A s	753 s	a_1 fundamental
767 vw			2×388
	808 B? ms	806 m	b_2 fundamental
820 ms(p)	818 A? w	817 m	a_1 fundamental
849 ms	844 vw	843 w	b_2 fundamental
860 ms			2×438
885 ms(p)	878 A w	880 w	a_1 fundamental
	892 w	892 w	505+388
905 vw	916 C vw	922 w	590+350 or C_6D_4HF
956 s(p)	959 A vw	959 w	a_1 fundamental
976 w	980 B vvw	981 vvw	627+350
1031 vw	1034 B w	1035 m	b_2 fundamental
	1065 B vw	1071 vw	563+505 or 627+438
		1080 vvw	590+505
		1127 vw	2×563
	1139 A vw	1139 vw	789+350
1155 m(p)	1163 A vs	1163 vs	a_1 fundamental
1186 vw	1201 A m	1193 ms	806+388
1215 vw	1228 A m	1222 ms	388+843 or 664+563
1244 vw		1244 vw	805+438
1283 vw	1281 vvw	1281 vvw	b_2 fundamental
		1289 vw	664+627
	1311 B w	1311 m	b_2 fundamental
1378 w	1391 A vs	1389 vs	a_1 fundamental
		1414 vvw	590+817 or 627+789
	1417 A w	1418 m	1035+388
	1423 w	1424 vw	789+627
1464 vw	1465 A w	1473 w	789+682 or 959+505
	1510 vw		
	1566 B s	1564 s	b_2 fundamental
1574 m	1577 A w	1578 vs	a_1 fundamental
	1617 A? w	1618 w	2×806 or 1035+590 or 817+806
		1639 vw	825+817 or 2×817 or 843+789
		1660 vvw	1311+350 or 1163+505 or 843+817
	1680 w	1680 w, 1685 vvw	880+806 or 959+717 or 2×843
	1729 w	1724 m	1035+682 or 843+880
	1797 C? w	1793 w	1035+753 or 1163+627 or 959+825
		1827 w	505+1311 or 1035+789
	1846 A w	1857 w	806+1035
	1929 w	1913 w	1564+350 or 1035+880
	1995 m	1985 m	1311+682 or 1163+817
2054 vw	2065 vw	2061 w	1281+789 or 1311+753
	2160 w	2140 w	1578+563 or 1311+843 or 1564+590
	2238 B vw		1389+843 or 1281+959
2295 ms(p)	2292 A ms	~2320 ms	a_1 fundamental
	2393	~2370	1578+806 or 1564+817 or 1564+806
	2428 A vw		1564+843
	2460 vvw		1578+880 or 1281+1163
	2566 A w	~2550 w	1389+1163 or 2×1281 (or 1311+1281)
	2584 A vw	~2570 w	
	2680 B vvw	~2680 w	2295+388 or 1389+1281
2750 w	2746 vvw	2750 w	1578+1163 or 3120−438
	2890 w	2890 w	1578+1311 or 2295+590 or 1564+1311
	2922 B vvw		2295+627
	2970 vvw	2950 vw	1389+1564 or 1389+1578 or 2276+682 or 2266+682

TABLE I.—*Continued.*

Raman	Infrared		Assignment
	Vapor	Liquid	
3049 w	3080 w	3060 s	2276+789 or 2266+806 or 2270+806
		3110 w	2270+843 or 2275+843 or 2295+806 or 2295+817 or 2276+843
	3162 B vw		1578+1564 or 2266+880
	3256 w	3270 w	2295+959
	3500 w	3480 w	2295+1163
	3750 vw	3748 vw	
	3930 vw	3830 vw	2266+1564 or 2276+1564 or 2270+1564
	4090 vw	4090 vw	
	4590 m	4595 m	2×2295

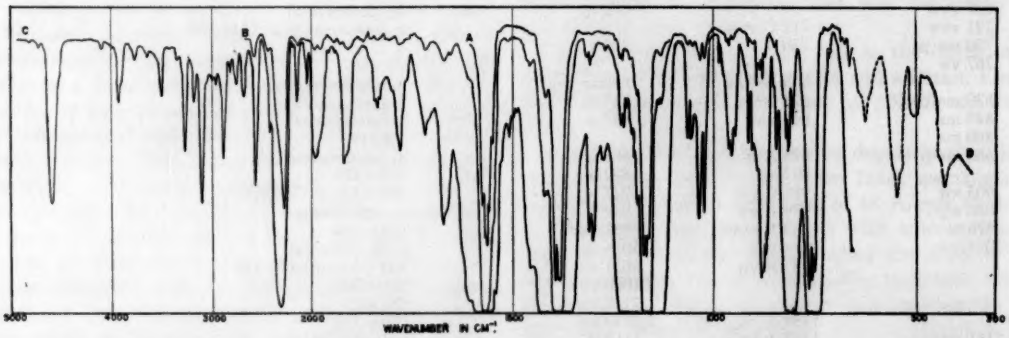

FIG. 1. Vapor phase spectrum of C_6D_5F. A. 10 cm cell, 2 mm pressure; B. 10 cm cell, 60 mm pressure; C. 1 meter cell, 60 mm pressure; D. 10 cm cell, 60 mm pressure—using CsBr prism.

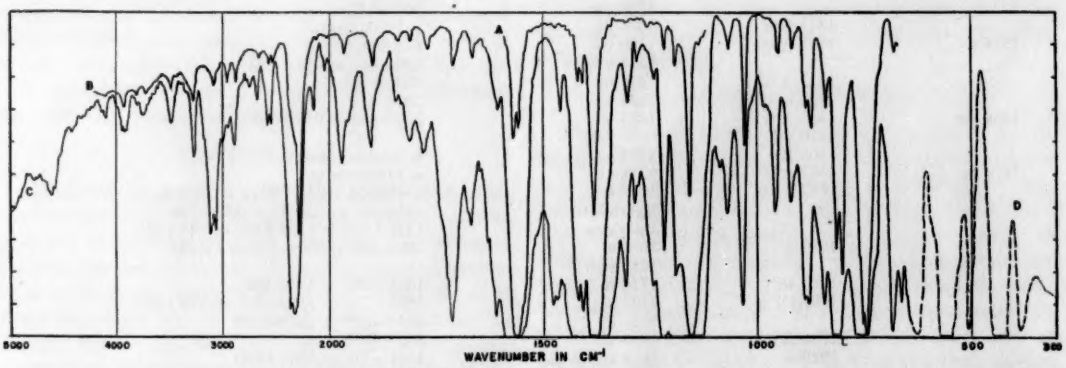

FIG. 2. Liquid phase spectrum of C_6D_5F. A. Very thin film between salt plates; B. Thin film between salt plates; C. 0.004 cm AgC cell; D. 0.004 cm AgCl cell—using CsBr prism.

TABLE II. C_{2v} selection rules.

Symmetry class	Number of fundamentals	Raman activity	Infrared band shapes
a_1	11	pol.	Type *A PR* sep. 13 cm^{-1} medium *Q* branch
a_2	3	dp.	Forbidden
b_1	6	dp.	Type *C PR* sep. 9–10 cm^{-1} prominent *Q* branch
b_2	10	dp.	Type *B PR* sep. 9 cm^{-1}

IN-PLANE VIBRATIONS

a_1 Class

The vibrations of this class are infrared active vibrations of type *A* and give polarized Raman bands. Strong polarized Raman bands at 2295, 1155, 956, 885, 820, and 750 cm^{-1} and strong type *A* infrared bands at 2292, 1577, 1391, 1163, and 756 cm^{-1} must therefore be identified as a_1 fundamental bands. The weakness of the infrared bands at 959 and 880 cm^{-1} corresponding to the Raman shifts at 956 and 885 cm^{-1} is understandable since both are essentially ring modes and are derived from infrared inactive bands of C_6D_6 at 970 $cm^{-1}(b_{1u})$ and 945 $cm^{-1}(a_{1g})$. (All C_6H_6 and C_6D_6 frequencies quoted are from the paper by Broderson and Langseth.[8])

Two of the three C–D stretching bands belonging to this class could not be observed because of band overlapping, but application of the inequality rule to C_6D_6 and C_6D_5F indicates their frequencies to be about 2275 and 2270 cm^{-1}. The remaining a_1 fundamental is that derived from the e_{2g} ring deformation mode of C_6D_6 at 579 cm^{-1}. Although the frequency of this mode drops only from 606 cm^{-1} in C_6H_6 to 579 cm^{-1} in C_6D_6 and although there is no CX deformation in the a_1 class, the frequency appears to be very sensitive to the mass of X since in C_6H_5F it drops to 520 cm^{-1}.[9,10] The C_6D_5F fundamental must lie below its C_6H_5F counterpart and is quite clearly associated with the moderately strong Raman band at 505 cm^{-1} and the infrared band at the same frequency.

The Redlich-Teller product rule ratio for C_6H_5F and C_6D_5F have been evaluated using both the assignments for C_6H_5F given in footnote 9 and those in footnote 10. The assignments differ only in minor details and both lead to acceptable τ values (Table III). Application of the inequality rule to C_6D_6, C_6D_5H,[11] and C_6D_5F (Table IV) indicates consistency between the assignments.

b_2 Class

The only strong infrared band with a type *B* contour in the vapor phase is that at 1564 cm^{-1} which overlaps the a_1 fundamental. All other b_2 bands are surprisingly weak. This weakness of the b_2 absorptions compared with the a_1 is due mainly to the symmetry restrictions on the C–F motions. Since the C–F bond lies on the C_2 axis the C–F stretching motion contributes to the intensities of a_1 bands only, and likewise the CF in-plane deformation contributes to the b_2 intensities only. The dipole gradient associated with a C–F stretching motion is about 6.5 *D*/A whereas the gradient for a C–F bending motion is only about 1.0 *D*/A.[12] Both of these are in turn much larger than the corresponding carbon carbon and carbon hydrogen terms.[13] Consequently those modes in which there is an appreciable admixture of C–F stretching motion will absorb several times more strongly than the others. Such modes are those which are principally a_1 C–D deformations and C–C and C–F stretching modes. The same arguments apply to the in-plane vibrations of

TABLE III. Redlich-Teller product ratios.

Symmetry class	Theoretical	Observed C_6H_5F as footnote 9	Observed C_6H_5F as footnote 10
a_1	5.52	5.26	5.38
b_2	4.97	5.34	5.08
b_1	2.49	2.62	2.66
a_2	1.82	1.7	1.7

TABLE IV.[a] Comparison of vibrational assignments.

C_6D_5H	C_6D_6	C_6D_5F	C_6H_5F[10]	Description of C_6D_5F mode
a_1				
3050	2293	2295	3101	CD stretch
2291	2276	(2275)	3067	CD stretch
2275	2275	(2270)	3044	CD stretch
2275	2266	1578	1596	CC stretch
1564	1553	1389	1499	CC stretch
1341	1330	1163	1220	CF stretch
980	970	959	1157	Ring breathing
950	945	880	1022	CC stretch
859	869	817	1008	β CD deformation
814	812	753	808	β CD deformation
(579)	579	505	519	Ring deformation
b_2				
(2288)	2276	(2276)	3091	CD stretch
(2275)	2266	(2266)	3058	CD stretch
1564	1553	1564	1603	CC stretch
1388	1330	1311	1460	CC stretch
1289	1282	1281	1323	CC stretch
1175	1055	1035	1236	β CD deformation
984	869	843	1157	β CD deformation
840	823	806	1066	β CD deformation
815	812	590	614	Ring deformation
584	579	388	405	CF deformation
b_1				
928	830	(825)	997	γ CD deformation
818	789	717	894	γ CD deformation
711	664	627	754	γ CD deformation
613	599	563	685	Ring deformation
514	497	438	500	Ring deformation
367	351	229	242	γ CF deformation
a_2				
(789)	789	(789)	(970)	γ CD deformation
664	664	682	826	γ CD deformation
(351)	351	350	405	Ring deformation

[a] ( ) estimated; β=in-plane; γ=out-of-plane.

[8] S. Broderson and A. Langseth, Kgl. Danske Videnskab Selskab Mat.-fys. Skr. 1, No. 1 (1956).
[9] D. H. Whiffen, J. Chem. Soc. 1956, 1350.
[10] D. W. Scott *et al.*, J. Am. Chem. Soc. 78, 5457 (1956).
[11] S. Broderson and A. Langseth, Kgl. Danske. Videnskab Selskab Mat.-fys. Skr. 1, No. 7 (1959).
[12] D. Steele and D. H. Whiffen, Trans. Faraday Soc. 8, 177 (1960).
[13] H. Spedding and D. H. Whiffen, Proc. Roy. Soc. (London) A238, 245 (1956).

C_6H_5F and p-$C_6H_4F_2$. A detailed analysis of the vibrations and intensities of the absorption bands of the latter molecule has previously been carried out and confirms the above reasoning.[12,14]

The b_2 band at 806 cm^{-1} is clearly one of the C–D deformation fundamentals. There is one other C–D deformation in this class and this has been taken to be associated with the very weak b_2 band at 843 cm^{-1} and the moderately strong Raman line at 849 cm^{-1}. This assignment is supported by application of the inequality rule which requires, by comparison with C_6D_6 and C_6D_5H, that the fundamental should lie in the interval $869 > b_2 > 823$ cm^{-1}.

The strongest, as yet unassigned, type B bands are the weak pair at 1071 and 1035 cm^{-1}, and the very weak band at 1311 cm^{-1}. The only Raman shifts observed at any of these frequencies was a very weak one at 1031 cm^{-1}, but the identification of two of the infrared bands with a b_2 ring breathing and the highest of the b_2 C–D deformation modes is supported by a comparison with C_6D_6 and C_6D_5H which indicates that the frequencies of these ought to be in the intervals 1330–1289 cm^{-1} and 1055–984 cm^{-1}. The other component of the low-frequency pair is believed to be a combination band in resonance with the fundamental.

By comparison with other fluoro-benzenes the CF deformation frequency is to be expected between 300 and 450 cm^{-1}. The moderately strong absorption band observed in the liquid at 388 cm^{-1} must be due to this mode, the only other active mode expected in this region being a b_1 mode which has a definite assignment of 438 cm^{-1}.

The lowest "e_{2g} like" ring deformation will have a higher frequency than in C_6D_6, where it is 579 cm^{-1}, due to the presence of the C–F deformation mode. No b_2 infrared bands are observable in the expected region, but it seems very probable that one of the two Raman lines at 587 and 639 cm^{-1} is due to this mode. The corresponding vibration in C_6H_5F is at 615 cm^{-1}, thus indicating that 587 cm^{-1} is to be preferred as the fundamental frequency.

In the C–D stretching region the only observable type B band was a very weak one at 2238 cm^{-1}. This has an alternative explanation and seems too low for one of the fundamentals. It seems very unlikely that the C–D stretching frequencies will differ much from the b_2 type frequencies in C_6D_6.

The remaining b_2 fundamental to be assigned is a ring stretching mode. Use of the inequality rule indicates that it is derived essentially from the b_{2u} mode of C_6D_6 at 1282 cm^{-1}, and its frequency should lie between 1282 cm^{-1} and 1175 cm^{-1}. The only absorption above the strong a_1 complex, extending to 1240 cm^{-1}, is an extremely weak band at 1281 cm^{-1} which is proposed as the fundamental.

This set of assignments leads to the Redlich-Teller product ratios given in Table III. The assignments of C_6H_5F by Scott and others and by Whiffen differ appreciably only in their choice of one C–H in-plane deformation frequency; Scott and his co-workers assigning it a value of 1236 cm^{-1}, and Whiffen a value of 1290 cm^{-1}. The former assignment is favored by use of the product rule ratio and the above C_6D_5F assignments. Though one or two of the proposed assignments are open to some doubt, it is thought that none can be altered by more than a few wave numbers. The weakest assignments are those given as 843 cm^{-1} and 1281 cm^{-1}. The former can be no more than 20 cm^{-1} low and it is difficult to understand how the assignment of the ring frequency could be placed much higher than 1281 cm^{-1} when the corresponding frequency of C_6D_5H is only 1289 cm^{-1}. These considerations lead to the conclusion that the a_1 fundamental of C_6H_5F is near 1230 cm^{-1} in agreement with the assignments of Smith[15] and of Scott and their coworkers.

OUT-OF-PLANE VIBRATIONS

b_1 Class

Bands at 627, 563, and 438 cm^{-1} can be assigned as fundamentals of this class on the basis of strength and vapor phase contours. The out-of-plane C–F deformation mode must be identified with the moderately strong Raman shift of 229 cm^{-1}, thus leaving two of the three C–D deformations in this class to be assigned frequencies. According to the inequality rule, the frequencies of these are given by,

$$830 > b_2 > 818 \text{ cm}^{-1}$$

and

$$789 > b_2 > 711 \text{ cm}^{-1}.$$

No type C band could be observed within the upper limits, the band almost certainly being under the b_2 and a_1 fundamentals in that region. A frequency of about 825 cm^{-1} has been assumed for this band. Within the lower limits, only a very weak type C band at 717 cm^{-1} is observable. Taking this value for the b_1 fundamental, a τ value of 2.62 is obtained which is in reasonable agreement with the calculated value.

a_2 Class

Since the G matrix for this class is the same for all C_6D_5X molecules, the vibrational frequencies ought to be the same for C_6D_5H, C_6D_6, and C_6D_5F assuming that the force constants, excluding the C–X constant, remain the same. A very weak Raman shift of 350 cm^{-1} can be assigned to the lowest skeletal out-of-plane deformation mode. No Raman shift close to the other C_6D_6 a_2 values can unambiguously be assigned to this class. However, in changing from the vapor to the liquid phase an infrared band appears at 682 cm^{-1}. It

[14] D. Steele and D. H. Whiffen, Trans. Faraday Soc. **8**, 56 (1960).

[15] D. C. Smith, E. E. Ferguson, R. L. Hudson, and J. Rud Nielsen, J. Chem. Phys. **21**, 1475 (1953).

is almost, if not completely, absent in the vapor spectrum. Since intermolecular interactions can reasonably be expected to have a greater effect on dipole derivative terms such as $\partial^2 U/\partial^2 Q_i^2$ than on cross terms such as $\partial^2 U/\partial Q_i \partial Q_j$ this is felt to be strong evidence for the assignment of 682 cm^{-1} as an a_2 frequency despite the fact that this frequency is appreciably higher than those assigned for C_6D_6 and C_6D_5H. This assignment is given further support by the observation that the corresponding modes of C_6D_6, C_6H_6, and C_6H_5F absorb in the condensed phase although in all cases the vapor selection rules forbid it.

The only Raman band in the region of the highest fundamental is one at 767 cm^{-1} which has alternative acceptable explanations. The exact value of the frequency of this mode cannot be given.

THE JOURNAL OF CHEMICAL PHYSICS VOLUME 33, NUMBER 4 OCTOBER, 1960

Quantitative Relations in the Mass Spectra of *n*-Paraffins

NORMAN D. COGGESHALL

Gulf Research & Development Company, Pittsburgh, Pennsylvania

(Received May 9, 1960)

The mass spectra of *n*-paraffins in the C_6 to C_{30} range have been examined for quantitative relations that must be predicted by any theory of ion formation by electron impact. An ion sum $C(M, n)$ is defined as the sum of the normalized intensities of all ions of n carbon atoms from a *n*-paraffin of M carbon atoms. The molar yield $Y(M, n)$ per unit of ionizing current will be $MC(M, n)$. It has been observed that for large ions from large molecules the yield is independent of M or n but proportional to $(M-n)$. Yields for smaller ions, i.e., n between 3 and 15, are linear with M but not proportional to M. The yields in this region may be expressed as

$$Y(M, n) = An^b e^{-bn}(M-n')$$

where A and b are constants, one set applying for $3 \leqq n \leqq 10$ and another set applying for $10 \leqq n$; the n' values are constants, each depending upon the associated n. The observations indicate that the details of the fragmentation process for *n*-paraffins depend primarily upon the type of molecular skeleton, i.e., straight chain, single valence carbon-carbon linkages and secondarily upon the size of the molecule.

THE statistical theory[1] of mass spectra has been applied to the lower alcohols and alkanes[2,3] with varying degrees of success. It is not believed that this theory in its present form can be effectively used for higher molecular weight compounds. This is based on the disagreements observed between predicted and experimental results[3] and on the computational difficulties of applying it to larger molecules. A simpler theory, even though it might be usable only in a semiquantitative manner, is highly desirable. The present study was conducted to determine the general quantitative relations such a theory would have to predict for the *n*-paraffins. The studies encompass the *n*-paraffins from C_6 to C_{30} inclusive, excepting C_{19} for which no data were available.

SOURCE AND TREATMENT OF DATA

The data used were taken from the mass spectral data issued by the American Petroleum Institute Research Project 44 and from experimental work done in this Laboratory. All data were taken with Consolidated Electrodynamics Model 21-103 type instruments. It is known that a direct comparison of data between such instruments cannot be made because of all the factors that influence sensitivity. However, the normalized patterns obtained from these instruments agree well enough to allow extensive analytical applications.[4,5]

In covering the mass range necessary for the higher molecular weight compounds, it is customary to scan portions at two different magnetic fields. To produce a normalized spectrum from the low and high mass scans means that they must be quantitatively adjusted to agree at a particular mass value or cross-over point. The choice of this point could preferentially weight one end of the spectrum. Discrimination and other effects on pattern can result from the fields used and the magnitude of electron current. The values of these parameters as used for each spectrum are given in Table I.

[1] H. M. Rosenstock, M. B. Wallenstein, A. L. Wahrhaftig, and H. Eyring, Proc. Natl. Acad. Sci. U.S. **38**, 667 (1952).
[2] L. Friedman, F. A. Long, and M. Wolfsberg, J. Chem. Phys. **27**, 613 (1957).
[3] L. Friedman, F. A. Long, and M. Wolfsberg, J. Chem. Phys. **30**, 1605 (1959).
[4] See, for example: American Society for Testing Materials, Committee D-2; Proposed Tentative Method—Hydrocarbon Types in Low Olefinic Gasoline by Mass Spectrometry.
[5] G. F. Crable and N. D. Coggeshall, Anal. Chem. **30**, 310 (1958).

TABLE I. Operating conditions used for spectra employed.

Carbon no.	Laboratory	Electron current in μa	Initial magnet current in ma	Final magnet current in ma	Isatron temperature °C	Cross-over point (C_nH_{2n-1})	API ser. no.
6	GR&DC[a]	19.5	0.7	...	250	...	...
7	GR&DC	19.5	0.7	...	250	...	...
8	GR&DC	19.5	0.7	...	250	...	...
9	GR&DC	19.5	0.7	...	250	...	...
10	GR&DC	19.5	0.7	...	250	...	...
11	GR&DC	19.5	0.7	...	250	...	...
12	NBS	9.0	b	b	245	...	404
13	NBS	9.0	b	b	245	...	523
14	Shell Oil	50.0	0.9	1.3	265	C_5	1255
15	Shell Oil	50.0	0.9	1.3	265	C_5	1318
16	GR&DC	10.5	0.2	0.375	250	C_3	...
17	Shell Oil	50.0	0.9	1.3	265	C_5	1351
18	Shell Oil	13.5	0.6	1.3	250	C_4	574
20	Shell Oil	10.0	0.9	1.3	265	C_4	705
21	Shell Oil	50.0	0.9	1.3	265	C_5	1310
22	Shell Oil	50.0	0.9	1.3	265	C_5	1311
23	Shell Oil	50.0	0.9	1.3	265	C_5	1312
24	Shell Oil	13.5	0.6	1.3	250	C_4	575
25	Shell Oil	50.0	0.9	1.3	265	C_5	1313
26	Atlantic Ref. Co.	9.0	0.56	1.08	250	C_3	PSC 106
27	Shell Oil	50.0	0.9	1.3	265	C_5	1314
28	Shell Oil	10.0	0.9	1.3	265	C_4	886
29	Shell Oil	50.0	0.9	1.3	265	C_5	1315
30	Shell Oil	50.0	0.9	1.3	265	C_5	1316

[a] Gulf Research & Development Company.
[b] Not listed.

The work of Otvos and Stevenson[6] has shown that the total relative ionization cross-section of a compound is a constitutive molecular property, i.e., the sum of the atomic cross sections. Although their work was necessarily done in the lower molecular weight ranges, we are assuming the same results for higher molecular weight compounds. This assumption is somewhat confirmed by the work of Crable and Coggeshall.[5] If we denote the total ionization of a n-paraffin C_MH_{2M+2} by by $T(M)$ we have

$$T(M)=k[M(Q_c+2Q_H)+2Q_H], \qquad (1)$$

where Q_c and Q_H are the relative ionization cross sections for carbon and hydrogen, respectively, and k is a constant depending upon experimental conditions and the units used for $T(M)$. Since, for compounds of interest here, $2Q_H$ will be small compared to $M(Q_c+2Q_H)$, we may with adequate accuracy express $T(M)$ as

$$T(M)=KM, \qquad (2)$$

where K is a constant.

Let us denote by $P_{M,n,j}$ the normalized ion intensity for an ion of stoichiometry C_nH_{2n+2-j}, $n\leq M$ which appears in the normalized mass spectral pattern for a n-paraffin of M carbon atoms. By normalization we mean that the sum of all intensities is equal to unity, or in this case, to 100%, i.e.,

$$\sum_n\sum_j P_{M,n,j}=100.$$

Let us define an ion sum $C(M,n)$ as the summation of intensities of all ions of n carbon atoms appearing in the normalized spectrum. Thus,

$$C(M,n)=\sum_j P_{M,n,j}; \qquad \sum_n C(M,n)=100.$$

Since the total ionization is proportional to M, the product $MC(M,n)$ therefore represents in a manner independent of experimental conditions or units the yield, $Y(M,n)$, per unit of ionizing electron current and per mole, of all ions of n carbon atoms being produced by electron impact on a normal paraffin of M carbon atoms.

$$Y(M,n)=MC(M,n). \qquad (3)$$

Such an approach requires a complete mass spectrum. Many of the API spectra were lacking pattern data for the one and two carbon atom ions. Interpolation and extrapolation were done by utilizing the available data. In Fig. 1 is given a plot of $C(M,1)+C(M,2)$ versus M as obtained from our own and API spectra for which such data were presented. From the curve drawn through these points were obtained the values used for normalizing other spectra.

In Table II are given the $Y(M,n)$ values calculated from the spectra. Note that they are not arranged in a

[6] J. W. Otvos and D. P. Stevenson, J. Am. Chem. Soc. 78, 546 (1956).

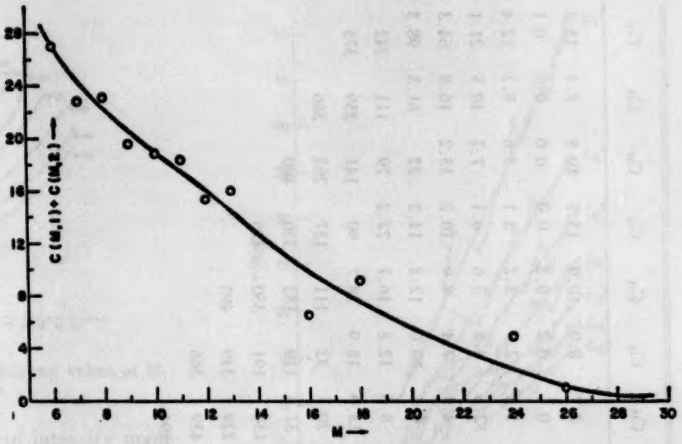

FIG. 1. Plot of $C(M, 1)+C(m, 2)$ used to interpolate for values not obtainable otherwise.

manner to display the variation with n but rather the variation with M and $(M-n)$. Obviously $(M-n)$ represents the number of carbon atoms going into neutral fragments in the process of creating ions of n carbon atoms from a molecule of M carbon atoms.[7]

DISCUSSION OF DATA

Looking across a row, constant $(M-n)$ value, in Table II, we have the yields from different compounds of ions all characterized by leaving behind the same size neutral fragment. In the upper left-hand part of the table, i.e., for the higher molecular weight compounds for $2 \leq (M-n) \leq 11$ (approximately) two surprising observations may be made. One is that, within this region, the probability or yield of ions created by casting off the same size neutral fragment is approximately constant and independent of the mass of the parent molecule. Thus, the yields are about the same for C_{26}^+ ions from C_{30}, for C_{25}^+ ions from C_{29}, for C_{24}^+ ions from C_{28}, etc.

The other observation, which is particularly well seen from the ions from C_{30}, is that, excepting the cases for $M-n=0$ and $M-n=1$, the yields of ions are approximately proportional to the number of carbon atoms $(M-n)$ in the neutral fragment expelled. For C_{30} this proportionality prevails up to a neutral fragment size of C_{15}.

These observations therefore indicate that the processes whereby large ions are created from the higher molecular weight n-paraffins are dominated by the size of the neutral fragment expelled and independent of the total mass of the molecule. This behavior is further demonstrated in Fig. 2 where the yields are plotted versus $(M-n)$ for the higher mass ions for the last eight members of the entire series. The ordinate scale for each successively lighter compound is uniformly shifted upwards to pull the curves apart for display. In this series these curves are generically the same except for C_{26} which shows appreciable deviation. It is not known whether this is a real effect unique to this compound or whether its origin lies in some different experimental conditions. These deviations are also noticeable in Table II.

In contrast to this behavior it is clear from Table II that the yields of the lower mass ions, C_3^+ and C_4^+, for example, depend markedly upon the mass of the parent compound. In Fig. 3 are plotted the yields of several different ions characterized by n versus the mass of the parent molecule. A primary observation is that, excepting for the low ends of the curves and for the pronounced scatter for the C_3^+ ions, the yields are linear with M but not proportional to M.

In Fig. 4 are plotted further yields versus M. The data for such curves are progressively poorer for increasing n and certain points and regions were excluded from the figure to eliminate overlapping of points. Although the scatter is bad, these ion types also display a linear dependence upon M. Despite the scatter, there is evidence for this linear dependence for ions as heavy as C_{24} when the data are plotted in a larger form.

It is clear that the yield may generally be represented as

$$Y(M, n)=f(n)(M-n'), \tag{4}$$

where $f(n)$ represents the slope of the curve for ions of n carbon atoms, and n' is the value of M at the point where the curve intercepts the M axis. We, therefore, have n' as a function of n. In Table III are given the values of $f(n)$ and n' as dependent on n up to $n=15$ as extracted from the data examined.

These values of n' cannot be regarded as very accurate as the value depends critically upon how a straight line is fitted to the data in each case. Excepting for $n=3$ they are of the same order of magnitude as n. This correlates with the behavior observed for the heavy ion

[7] It is assumed in this treatment that during the process of impact and ionization that one ionized and one neutral fragment are created.

TABLE II. $Y(M, n)$ values for the n-paraffins arranged versus $(M-n)$.

$(M-n)$	C_{30}	C_{29}	C_{28}	C_{27}	C_{26}	C_{25}	C_{24}	C_{23}	C_{22}	C_{21}	C_{20}	C_{19}	C_{17}	C_{16}	C_{15}	C_{14}	C_{13}	C_{12}	C_{11}	C_{10}
0	3.8	4.2	8.2	4.7	4.9	5.7	5.3	6.6	7.8	7.2	10.8	33.4	9.3	3.7	8.9	10.9	13.5	10.8	8.3	15.3
1	0.12	0.2	0.1	0.2	0.1	0.2	0.2	0.1	0.6	0.1	0.4	0.1	0.2	0.1	0.2	0.2	0.0	0.0	0.0	0.1
2	2.3	2.5	2.2	2.2	1.8	2.4	2.1	2.3	3.2	2.4	2.3	3.8	2.7	1.4	2.7	3.2	3.1	3.6	5.2	12.4
3	3.4	3.5	3.5	3.4	2.8	3.8	3.3	3.8	5.0	3.9	3.8	6.6	4.7	2.6	4.8	5.6	6.1	7.7	10.5	21.1
4	5.4	5.6	5.4	5.4	4.4	5.9	5.6	6.1	7.8	6.2	6.0	10.3	7.4	4.3	7.4	8.9	10.2	13.2	16.8	64.3
5	6.0	6.0	6.3	6.2	4.9	6.8	6.4	7.2	9.5	7.5	7.5	12.8	9.4	6.3	10.0	12.2	14.2	22	61.5	98.3
6	6.8	6.8	6.7	6.9	5.6	7.5	7.3	8.1	10.0	8.4	9.5	14.9	11.8	8.6	12.8	16.7	22.2	79	111	242
7	7.2	7.5	7.3	7.6	6.4	8.7	8.2	9.5	11.3	10.1	10.8	17.3	14.8	13.0	18.9	28.7	90	141	259	375
8	7.7	7.8	7.8	8.4	7.0	9.3	9.6	10.5	12.2	11.4	13.4	20.6	20	20.7	32	111	157	295	386	
9	8.5	8.8	8.6	9.5	8.2	10.5	11.4	12.0	14.0	13.5	15.1	26.1	29	37.8	119	182	320	400		
10	9.0	9.3	9.6	10.5	9.6	11.9	12.6	13.7	16.0	16.8	18.8	35.5	48	134	191	350	456			
11	9.9	10.3	10.7	11.7	11.3	13.5	14.8	16.6	19.4	21.1	26.5	56.7	158	229	349	495				
12	11.1	11.7	11.5	13.3	13.6	15.7	17.8	20.0	23.8	28.3	40	167	245	439	566					
13	12.3	13.1	13.3	15.0	15.5	18.6	22.1	25.1	33	43	69.1	251	436	594						
14	14.2	15.0	15.3	17.3	21.0	22.2	28.9	34	47	72	208	416	558							
15	15.7	16.6	17.1	20.6	24.9	28.1	40.4	50.2	77.2	219	319	442								
16	18.2	19.2	20.1	27.4	31.9	38.7	60.5	85	229	323	531									
17	20.7	22.2	24.7	31.4	59.5	57.5	99.0	250	337	550	597									
18	24.6	27.2	31.7	43.2	67.2	98.3	276	362	571	660										
19	30.0	34.4	43.5	65.4	117	279	399	605	680											
20	37.3	48.1	66.2	112	294	402	633	702												
21	51.1	74	116	302	428	664	679													
22	78.2	126	284	440	704	747														
23	135	331	472	733	729															
24	354	467	784	783																
25	497	772	810																	
26	806	839																		
27	816																			

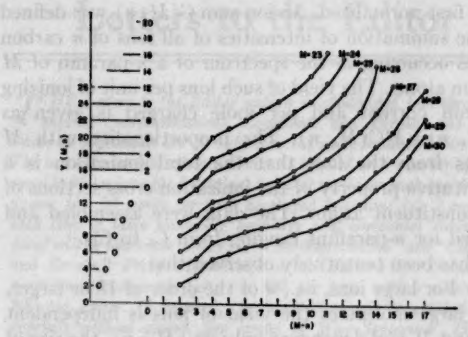

FIG. 2. Yield values versus $(M-n)$ for different values of M. Note the progressively shifted vertical scale.

classes wherein a direct dependence of intensity upon $(M-n)$ was noted.

The conclusions drawn here are based on the assumption that the available mass spectral patterns have absolute significance independent of experimental conditions. The exact status of their absolute significance is not known. It is known that CEC Model 21-103 type instruments give quite reproducible patterns, and this is the basis for extensive analytical applications.[4] On the other hand, the nature of the scatter observable in the above figures indicates that it most likely arises

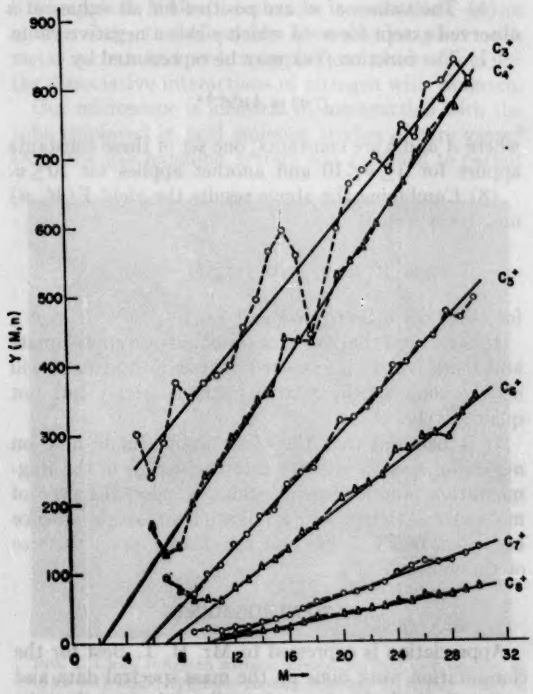

FIG. 3. Plots of yields, $Y(M, n)$ versus M and for different values of n.

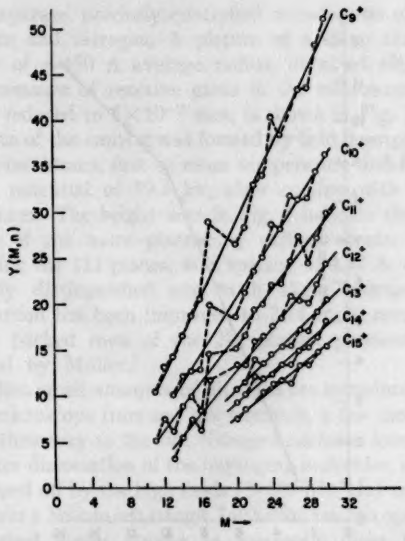

FIG. 4. Further yield plots versus M for the higher values of n.

from experimental conditions rather than unique molecular behavior. Discrimination between ions of different initial kinetic energies can occur in the ion source[8] and between the ion source and the collector.[9] It is not possible to correct the data used here for discrimination; however, it is believed that the data used here are fairly reliable in one sense. The discrimination between ion source and collector is independent of mass and dependent on accelerating voltage.[9] Most investigators generally use about the same range of accelerating and magnetic field values to cover the same mass range. The pattern values used for ions of n carbon atoms will therefore have been obtained with a range of field values independent of M. This condition leads to internally consistent results for the behavior of any $Y(M, n)$ (M variable, n constant). However, the

TABLE III. Values of $f(n)$ and n' as determined from the data examined.

n	$f(n)$	n'
3	23.2	−6.3
4	28.9	2
5	20.6	5.4
6	14.9	6.8
7	6.8	10
8	3.6	10.4
9	2.1	6.0
10	1.6	6.4
11	1.3	6.5
12	0.94	8.5
13	1.1	8.5
14	0.9	8.5
15	0.8	10.0

[8] N. D. Coggeshall, J. Chem. Phys. **12**, 19 (1944).
[9] C. E. Berry, Phys. Rev. **78**, 597 (1950).

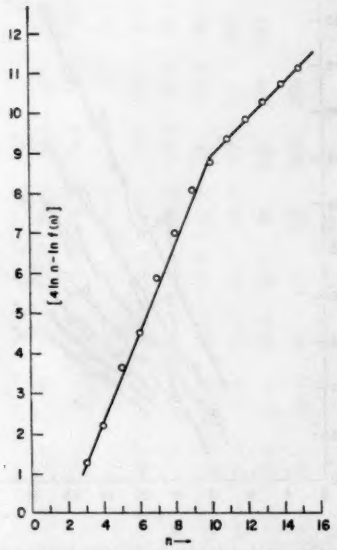

FIG. 5. Plot of $[4\ln n - \ln f(n)]$ versus n.

effects of discrimination undoubtedly attenuate the intensities of the ions in the higher mass range. If correction could be made for discrimination, it is believed that it would change the slopes of the curves but not the nature of the behavior. The quantitative conclusions made here must then be regarded as subject to change when better data are available. It is expected that such changes would affect the numerical results but not the observed qualitative nature of the spectral behavior.

It is interesting to note that the $f(n)$ values as a function of n have the same general characteristics as the mass spectrum for a n-paraffin, i.e., the greatest values for 3 and 4 carbon atoms, a rapid decrease in value down to about 9 carbon atoms and then a more gradual decrease with increasing carbon number. In Fig. 5 is seen a plot of $[4\ln n - \ln f(n)]$ versus n. The straight line behavior shows that $f(n)$ may be represented by

$$f(n) = An^4 e^{-bn}, \tag{5}$$

where A and b are constants. One set of constants applies for $2 < n \leq 10$ and another set applied for $10 \leq n$. No explanation is given for this functional behavior of $f(n)$. From these relations it is clear that yields $Y(M, n)$ may therefore be represented for any n-paraffin in the 3 carbon to 15 carbon ion range by

$$Y(M, n) = An^4 e^{-bn}(M - n'). \tag{6}$$

CONCLUSIONS

In summarizing the observations, it is important to restate the mode of handling the data. The spectra were first normalized. An ion sum $C(M, n)$ was defined as the summation of intensities of all ions of n carbon atoms occurring in the spectrum of a n-paraffin of M carbon atoms. The yield of such ions per unit of ionizing electron current and per mole charged is given as $Y(M, n) = MC(M, n)$. The proportionality with M results from the fact that the total ionization is a constitutive property of the ionization cross sections of the constituent atoms. The data were assembled and studied for n-paraffins ranging from C_6 to C_{30}.

It has been tentatively observed that:

(1) For large ions, i.e., n of the order of 15 or larger, from large molecules the yield of ions is independent of n and M and dependent only on $(M-n)$, the size of neutral fragment created.

(2) The yields of the large ions, as expressed in (1) above, are approximately proportional to $(M-n)$. The extent to which this applies depends, of course, on the size of the molecule; for C_{30} this applies for n between about 15 and 28.

(3) Yields for smaller values of n, for example from 3 to 15, depend upon both M and n.

(4) For any value of n in the region expressed in (3) the yield is linear with M but not proportional to M.

(5) For values of n in this region the yield $Y(M, n)$ can be expressed as

$$Y(M,) = f(n)(M - n').$$

(6) The values of n' are positive for all values of n observed except for $n = 3$ which yields a negative value.

(7) The function $f(n)$ may be represented by

$$f(n) = An^4 e^{-bn}$$

where A and b are constants; one set of these constants applies for $3 \leq n \leq 10$ and another applies for $10 \leq n$.

(8) Combining the above results the yield $Y(M, n)$ may be expressed as

$$Y(M, n) = An^4 e^{-bn}(M - n')$$

for values of n between 3 and 15.

It is realized that these observations are approximate and tentative. It is expected that improved data will change some of the relations quantitatively but not qualitatively.

It is believed that the observations made here on n-paraffin spectra indicate that the details of the fragmentation process depend primarily upon the type of molecular skeleton, i.e., straight-chain, single valence carbon-carbon linkages and secondarily upon the size of the molecule.

ACKNOWLEDGMENTS

Appreciation is expressed to Mr. H. T. Best for the computation work done on the mass spectral data and to Dr. G. F. Crable for various discussions on the subject.

Letters to the Editor

THE Letters to the Editor section is subdivided into three parts entitled Communications, Comments and Errata, and Notes. These three sections are all subject to the same limitations on length. The textual material of each Letter is limited to a number of words equal to 950 minus the following: (a) 200 words for each average-sized figure; (b) 50 words for each displayed equation; (c) 7 words for each line of table including headings and horizontal rulings. No proof will be sent to the authors of "Communications" and "Comments and Errata." Proof will be sent to the authors of "Notes." The publication charge for Letters is $30 per page, with a minimum of $30 per Letter. If honored, the Institution will be entitled to 100 reprints without covers. See issues of May–September, 1957, for descriptions of categories.

Communications

Observation of Adsorption on an Atomic Scale*

GERT EHRLICH AND F. G. HUDDA

General Electric Research Laboratory, Schenectady, New York

(Received August 11, 1960)

THE development of the field ion microscope[1] has for the first time opened the way to the direct observation of atomic events in surface reactions. We have applied Müller's technique to visualize, on an atomic scale, the adsorption of molecular gases on a metal surface and wish to report our observations for the dissociative interactions of nitrogen with tungsten.

Our microscope is identical in construction with the tube employed in field emission studies of rare gases.[2] Only the gas handling system was modified to permit the separate, precisely controlled introduction of both helium and nitrogen. A picture of a clean tungsten point of ~450 A average radius, obtained after the the pressure of reactive gases in the microscope had been reduced to 5×10^{-11} mm, is shown in Fig. 1. The surface of the emitter was formed by field desorption of tungsten atoms, first at room temperature and finally, at a potential of 19.5 kv, after cooling with liquid hydrogen. The bright dots in Fig. 1 indicate the positions of the more protruding surface atoms. These forming the 111 planes, at a spacing of 4.47 A, can be clearly distinguished and with slight changes the resolution has been improved to 2.74 A, to reveal the close packed rows of the 211 planes, previously resolved by Müller.[1]

When small amounts of nitrogen are introduced into the microscope from our gas reservoir, a few molecules find their way to the tip. Nitrogen *adatoms*, formed by surface dissociation of the impinging molecules, are not stripped off by the high fields (>500 Mv/cm) required to form a helium ion image. In the ion microscope these adsorbed atoms appear as scattering disks with a diameter somewhat larger than observed for the tungsten atoms in Fig. 1, presumably because of field enhancement around the protruding adsorbed material.

The arrangement of nitrogen atoms, formed on the tip after a brief exposure to the molecular gas while at 300°K, is shown in Fig. 2. It is immediately apparent that the atoms are not randomly distributed over the surface. In this and similar observations the fairly smooth, close packed planes such as the 110, 211, and 130 are entirely devoid of adsorbed material. Adatoms are found only on the higher index planes. These rougher planes also differ markedly among themselves in the concentration of adatoms and therefore in their ability to promote the dissociation of nitrogen. The

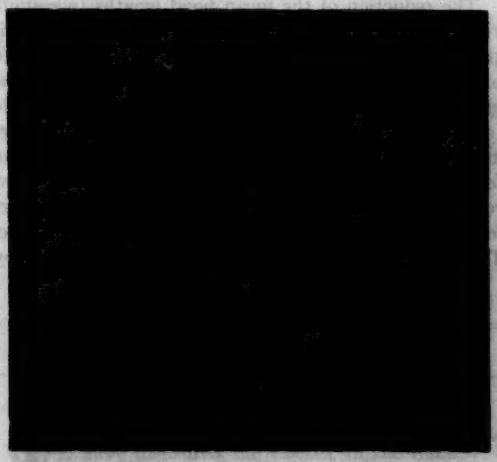

FIG. 1. Clean tungsten surface formed by field evaporation at 19.5 kv with liquid hydrogen cooling. Average tip radius ~450 A. Ion image taken with liquid hydrogen cooled emitter at 14.2 kv and 2×10^{-4} mm helium.

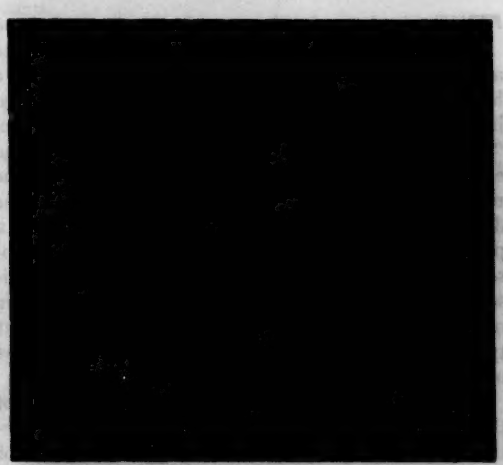

FIG. 2. Tungsten surface (of Fig. 1) after brief exposure to nitrogen while at 300°K. Operating conditions as for Fig. 1. Adatoms appear as large bright dots concentrated on lower left.

region *around* the 130 pole bounded by the 111 zone lines (connecting the 211 planes through the 110) boasts a higher concentration of nitrogen atoms than the area of and around the 111 pole, bounded by the same zone lines.

This non-uniform distribution arises from differences in the dissociation rate and *not* from non-uniformities in the gas supply or the selective effect of the high field on the adsorbed material, since after adsorption on a liquid hydrogen cooled surface we find a uniform distribution of adatoms. The regions around the 130 poles, which in Fig. 2 show the highest nitrogen concentration, are made up of heavily jogged edges of 110 planes, and our observations therefore establish that at 300°K rapid dissociation of nitrogen molecules requires not just lattice steps,[3] but kinked steps at which the nitrogen molecules make the largest number of nearest neighbor contacts with exposed surface atoms.

* This research was supported by the United States Air Force through the Air Force Office of Scientific Research of the Air Research and Development Command.

[1] E. W. Müller, *Proceedings 4th International Conference on Electron Microscopy*, (Springer-Verlag, Berlin, 1960), Vol. I, p. 820.

[2] G. Ehrlich and F. G. Hudda, J. Chem. Phys. **30**, 493 (1959).

[3] G. Ehrlich, J. Phys. Chem. Solids **1**, 3 (1956).

Equilibrium Bond Lengths in Methane and Deuteromethane as Determined by Electron Diffraction and Spectroscopic Methods*

L. S. Bartell, Kozo Kuchitsu,† and R. J. deNeui

Department of Chemistry and Institute for Atomic Research, Iowa State University, Ames, Iowa

(Received July 29, 1960)

THE absolute significance of experimental bond lengths reported for polyatomic molecules is often appreciably obscured by zero-point effects. In only a handful of spectroscopic studies has sufficiently detailed information been obtained to permit reduction of "effective" lengths, r_0, to equilibrium lengths, r_e. In no electron diffraction investigations heretofore have the results been accurately reduced to r_e, even though the diffraction averaging problem, being essentially a purely vibrational one, is simpler than the spectroscopic problem. A really critical experimental comparison of the electron diffraction and spectroscopic methods, properly taking into account the different types of averaging over the zero-point motions, has never been made.

It seemed crucial to make a definitive comparison of the two methods, now that the precision of the diffraction method, properly applied, has approached that of the spectroscopic method. It is particularly important to examine molecules in which zero-point effects are large, as for example, molecules containing hydrogen atoms which exhibit unusually large and asymmetric vibrational motions because of their small mass. Methane, then, affords an especially suitable test.

Preliminary analyses have been made of diffraction patterns of CH_4 and CD_4 taken with the new electron diffraction apparatus of Iowa State University. Diffraction photographs were taken using 40 kv electrons and an r^3 sector on Kodak 4- × 5-in. Process plates. Molecular diffraction features of CD_4 were observed to $q=140$, whereas those of the more energetically vibrating CH_4 damped out at about $q=130$. The data were analyzed by the radial distribution method as described elsewhere,[1] and reduced to molecular parameters by the method of steepest ascents, taking into consideration the asymmetry of vibration. Small corrections were made for the failure of the Born approximation[2] and for the measured delocalization of the noncondensable gas sample. The resulting mean distances, r_g, and root-mean-square amplitudes of vibration, l, are presented in Table I. Standard errors for the bonded distances appear to be not much greater than 0.001 A. For comparison are listed amplitudes calculated from spectroscopic data, including effects of anharmonicity.

It should be noted that the experimental differences between hydrogen and deuterium parameters are significant. This represents the first demonstration by electron diffraction of an isotope effect on molecular parameters. The effect of anharmonicity in the intramolecular vibrations was shown to be present as a uniformly increasing phase shift of the molecular intensity features, and as a deviation from a symmetrical Gaussian shape in the radial distribution curve. The asymmetry constant[3] of the stretching potential derived from the intensity curve agreed well with the predicted constant, $a\sim 2.3A^{-1}$, and represents the first such value measured by electron diffraction.

The reduction of the mean bond lengths to equilibrium bond lengths requires the quadratic and cubic potential constants of the molecule. These were deduced as described elsewhere[4] by representing the potential energy by a modified, anharmonic Urey-Bradley field in which stretching and nonbonded potentials were assumed to have the Lippincott and Buckingham forms, respectively. Several lines of evidence allow reasonable estimates to be made of potential parameters for which insufficient spectroscopic data are available. The required difference, r_g-r_e, was then calculated by

Table I. Structural parameters (angstrom units).

	CH_4		CD_4	
	C—H	H—H	C—D	D—D
r_g	1.107_0	1.811	1.102_3	1.805
l	0.076_0	0.121	0.066_0	0.104
l (calc)	0.075_5	0.121_8	0.064_9	0.102_4

TABLE II. Correction of electron diffraction and spectroscopic bond lengths to r_e.

	C—H in CH_4	C—D in CD_4
Electron diffraction		
r_g (exp)[a]	1.107_0	1.102_3
$r_g - r_e$ (calc)[b]	0.022_1	0.016_5
r_e	1.084_9	1.085_8
Spectroscopy		
r_0 (exp)	1.094_1[c]	1.092_3[d]
$r_0 - r_e$ (calc)[b]	0.009_1	0.006_9
r_e	1.085_0	1.085_4

[a] This investigation.
[b] Footnote reference 5.
[c] B. P. Stoicheff (private communication); K. T. Hecht (private communication).
[d] G. G. Sheppard and H. L. Welsh, J. Mol. Spectroscopy 1, 277 (1957).

a perturbed normal coordinate treatment. The results are given in Table II.

No reliable derivation of r_e from the spectroscopically measured r_0 is available for comparison. Therefore, we have used the potential constants derived before to deduce the equilibrium distance, using the methods of Wilson and Howard,[5] and of Hecht.[6] The results, shown in Table II, indicate that the uncorrected spectroscopic and diffraction parameters differ appreciably from each other and from r_e. The excellent agreement between the equilibrium distances derived by the two methods lends weight to the present interpretation of the absolute significance of the parameters of each.

* This research was supported in part by a grant from the Petroleum Research Fund administered by the American Chemical Society. Grateful acknowledgment is hereby made to the donors of said fund.
† On leave from Department of Chemistry, Faculty of Science, University of Tokyo, Japan.
[1] R. A. Bonham and L. S. Bartell, J. Chem. Phys. **31**, 702 (1959).
[2] V. Schomaker and R. Glauber, Phys. Rev. **89**, 667 (1953); J. A. Ibers and J. A. Hoerni, Acta Cryst. **7**, 405 (1954).
[3] L. S. Bartell, J. Chem. Phys. **23**, 1219 (1955).
[4] K. Kuchitsu and L. S. Bartell, Abstract R7, Symposium on Molecular Structure and Spectroscopy, Columbus, Ohio, 1960.
[5] E. B. Wilson and J. B. Howard, J. Chem. Phys. **4**, 260 (1936).
[6] K. T. Hecht (private communication).

Dipole Moment of Lithium Hydride

LENNARD WHARTON,* L. PETER GOLD,† AND WILLIAM KLEMPERER‡

Department of Chemistry, Harvard University, Cambridge 38, Massachusetts

(Received August 8, 1960)

WE have measured the electric dipole moment of lithium hydride by the molecular beam electric resonance method.[1] Our apparatus utilizes electric quadrupole A and B fields for state selection and space focusing of the beam.[2] The uniform electric C field transition region is 15 cm long. The transition observed is the rotational angular-momentum reorientation $J=1, m_J=0 \rightarrow J=1, |m_J|=1$. For Li^7H in the ground-vibrational-state this transition was observed at about 3.2 Mc in an electric field of 730 v/cm, 22.7 Mc at 1920 v/cm, and 63.6 Mc at 3280 v/cm. The lines arising from the hyperfine structure of this transition extend over a range of 240 kc and the minimum width of these lines is 7 kc at optimum rf power. The hyperfine line pattern is identical at the three observed frequencies, with each line showing the expected strong field behavior

$$\nu_i(E) = \nu_{\text{STARK}}(E) + \alpha_i,$$

where $\nu_{\text{STARK}}(E)$ is the unperturbed Stark frequency and α_i is the voltage-independent displacement of a line from this frequency.

The electric dipole moments of Li^7H and Li^6H are[3]

$$Li^7H \quad V=0 \quad \mu=5.882\pm0.003D$$
$$V=1 \quad \mu=5.990\pm0.003D$$
$$Li^6H \quad V=0 \quad \mu=5.884\pm0.003D.$$

This research has been aided by support from the Atomic Energy Commission and the Research Corporation.

* Junior Fellow, Society of Fellows.
† National Science Foundation Predoctoral Fellow.
‡ Alfred P. Sloan Fellow.
[1] N. F. Ramsey, *Molecular Beams* (Oxford University Press, New York, 1956); P. Kusch and V. Hughes, *Encyclopedia of Physics*, (Springer-Verlag, Berlin, Vienna, 1959) Vol. 37.
[2] G. Bennewitz, W. Paul, and C. Schlier, Z. Physik **141**, 6 (1955); J. P. Gordon, H. J. Zeiger, and C. H. Townes, Phys. Rev. **99**, 1264 (1955).
[3] The rotational constants of Li^7H, $V=0$ and $V=1$, are the effective values of F. H. Crawford and T. Jorgensen, Phys. Rev. **47**, 932 (1935), while that of Li^6H is calculated from these constants.

Comments and Errata

Energy Levels of a Slightly Asymmetric Top

JOHN E. BEAM AND H. L. DAVIS

Physical Sciences Research Department, Sandia Corporation, Albuquerque, New Mexico

(Received July 25, 1960)

IT is the purpose of this comment to correct a table given by Norris and Laurie[1] for certain coefficients C_6 in the expansion

$$w = K^2 + \sum_{n=1}^{\infty} C_n b_p^n, \qquad (1)$$

for the reduced energy levels of a slightly asymmetric prolate rotor.[2] The present authors have been recently

TABLE I. Sixth-order coefficients in the expansion of energy levels of the asymmetric rotor.

J	$K=0$	$K=2$	$\times 10^n$
5	−0.1298858	0.1298880	06
6	−0.1010301	0.1010369	07
7	−0.5782829	0.5783392	07
8	−0.2642748	0.2643054	08
9	−0.1016009	0.1016139	09
10	−0.3405496	0.3405958	09
11	−0.1020965	0.1021109	10
12	−0.2790172	0.2790576	10
13	−0.7052294	0.7053337	10
14	−0.1667336	0.1667587	11
15	−0.3720686	0.3721251	11
16	−0.7894026	0.7895234	11
17	−0.1601961	0.1602208	12
18	−0.3124980	0.3125464	12
19	−0.5884408	0.5885323	12
20	−0.1073401	0.1073569	13
21	−0.1902595	0.1902893	13
22	−0.3285454	0.3285970	13
23	−0.5539867	0.5540739	13
24	−0.9139532	0.9140972	13
25	−0.1477850	0.1478083	14
26	−0.2345803	0.2346174	14
27	−0.3660206	0.3660785	14
28	−0.5620897	0.5621789	14
29	−0.8504919	0.8506268	14
30	−0.1269197	0.1269399	15
31	−0.1869696	0.1869993	15
32	−0.2721120	0.2721552	15
33	−0.3915424	0.3916047	15
34	−0.5573859	0.5574747	15
35	−0.7854990	0.7856242	15
36	−0.1096458	0.1096633	16
37	−0.1516768	0.1517010	16
38	−0.2080339	0.2080671	16
39	−0.2830265	0.2830717	16
40	−0.3820980	0.3821590	16

engaged in obtaining general formulas for C_6 and C_7 in the expansion (1) using a form of perturbation theory based on the adiabatic theorem.[3] When comparing our work with the table given by Norris and Laurie, discrepancies were found to exist; furthermore, our work was also found to disagree with that of Polo.[4] It was then decided to explicitly check some of the entries of the table of footnote reference 1 using Eqs. (3) of Nielsen[5]; e.g., for the level $5_{2,3}$ we found that $C_6=[(C_2)^3-16C_2C_4-528C_4]/48$. Using known values[6] of C_2 and C_4, we obtain $C_6=0.1298880\times10^6$ which agrees with our general formula for C_6 for the $J_{2,J-2}$ level; however, both footnote references 1 and 4 give $C_6=0.1300071\times10^6$ for the $5_{2,3}$ level. Hence, one must conclude that the work of both footnote references 1 and 4 is in error; in fact, not one entry of the table of footnote reference 1 is found to agree with our general formulas. However, we have found minor errors in the work of Polo, which, when accounted for, make his and our results agree. We have calculated the values of C_6 for the levels $J_{0,J}$ and $J_{2,J-2}$ for $J=5$ through 40 using our general formulas; the results are given in Table I under the headings $K=0$ and $K=2$. The coefficients appearing in Table I are to be multiplied by the power of 10 given in the last column. Details of the method used to obtain general formulas for C_6 and C_7 and the formulas themselves will be submitted for publication in the near future.

[1] J. A. Norris and V. W. Laurie, J. Chem. Phys. **32**, 1591 (1960).
[2] See footnote reference 6 for the relation between the reduced energy levels and the actual energy levels of an asymmetric rotor.
[3] M. Gell-Mann and F. Low, Phys. Rev. **84**, 350 (1951).
[4] S. R. Polo, Can. J. Phys. **35**, 880 (1957).
[5] H. H. Nielsen, Phys. Rev. **38**, 1432 (1931). Corrections to Eqs. (3) of Nielsen's paper are found in H. M. Randall, D. M. Dennison, N. Ginsburg, and L. R. Weber, Phys. Rev. **52**, 160 (1937).
[6] C. H. Townes and A. L. Schawlow, *Microwave Spectroscopy* (McGraw-Hill Book Company, Inc., New York, 1955).

Erratum: Energy Levels of a Slightly Asymmetric Top

[J. Chem. Phys. **32**, 1591 (1960)]

JAMES A. NORRIS AND VICTOR W. LAURIE

Department of Chemistry, University of California, Berkeley 4, California

(Received August 5, 1960)

IT has been pointed out to us by Dr. J. E. Beam and Dr. H. L. Davis of Sandia Corporation that the formulas of Polo[1] which were the basis for the calculation of our tables contain minor errors, and that therefore the tables are not quite correct. The absolute magnitude of all entries is too large. For $J>25$, the largest error is $<0.01\%$. For $K=0$, $J=5$–10, however, errors of $\sim1\%$ are present. Corrected tables will be published by Beam and Davis elsewhere in this issue.[2]

[1] S. R. Polo, Can. J. Phys. **35**, 880 (1957).
[2] J. E. Beam and H. L. Davis, J. Chem. Phys. **33**, 1256 (1960).

Analysis of High-Resolution NMR Spectra by Iterative Methods

RAGNAR A. HOFFMAN

Department of Physics, University of Uppsala, Uppsala, Sweden

(Received July 18, 1960)

IN a recent paper, Reilly and Swalen[1] have advanced some iterative procedures for analyzing NMR spectra. The schemes denoted[2] ABK and $AA'K$ will be found useful for analyses of certain types of three-spin systems. The iterative procedure derived for ABC-cases is applicable also for systems of more than three spins, and the purpose of the present note is to compare this method (I) with a closely related method (II), which is based[3] on perturbation theory.

A problem generally encountered in spectroscopy is to determine from a number of observed transition energies and intensities a set of parameters $(a, b, c, \cdots)$ of the Hamiltonian $H(a, b, c, \cdots)$, which describes the

system studied. The energy eigenvalues (λ_i) are analytic functions of these parameters. Thus, granted that approximate values (a^0, b^0, c^0, $\cdots$) of the parameters are known, the corrections to the approximate eigenvalues $\lambda_i^{(0)}=\lambda_i(a^0, b^0, c^0, \cdots)$, derived from the approximate Hamiltonian $H^{(0)}=H(a^0, b^0, c^0, \cdots)$, can be given the form of a power series in $(a-a^0)$, $(b-b^0)$, etc. The general derivation of such expansions has been discussed by Löwdin[4] and others. However, for an analysis of NMR spectra, these series can be obtained by conventional perturbation methods because here the number of possible wave functions (spin states) is limited.

In method II one starts by decomposing the NMR-Hamiltonian according to[3]

$$H=H^{(0)}+H^{(1)}. \qquad (1)$$

Here, $H^{(0)}=H(h_A^0, h_B^0 \cdots J_{AB}^0, J_{AC}^0 \cdots)$ is the approximate Hamiltonian, derived from estimated values of the NMR parameters.[5] H depends linearly on these parameters, and the decomposition is trivial.

Approximate estimations of shift values (h_i^0) and coupling constants (J_{ik}^0) can be obtained in a number of ways. If the spins are not too strongly coupled, the perturbation expressions derived by Anderson[6a] are usable. As illustrated in footnote reference 1, the ABX-approximation[7] can often be used for three-spin systems. In principle, the moment method[8] will always be applicable. Recently, it has been shown[9] that the average of the midpoint and the center of gravity for a multiplet is a good first approximation of the shift of the hydrogen assigned to this multiplet. Finally, the information from structurally similar molecules may be used.

If the estimated h_i^0 and J_{ij}^0 are good approximations to the quantities h_i, J_{ij}, etc., the trial Hamiltonian $H^{(0)}$ in (1) nearly equals H, and $H^{(1)}$ may be treated as a perturbation. First-order perturbation theory gives[3] for energy level number k: $\lambda_k=\lambda_k^{(0)}+H_{kk}^{(1)}$. The first-order corrections to the *transition* energies (which are to be compared with the observed line positions) are given by differences of the form $H_{kk}^{(1)}-H_{ll}^{(1)}$.

$H_{kk}^{(1)}$ is the diagonal element number k of the matrix $\mathbf{U}^{-1}\mathbf{H}^{(1)}\mathbf{U}$. The relation between methods I and II is obvious. To terms of the first order, the method described herein (II), uses the similarity transformation, which diagonalizes $H^{(0)}$ also in transforming the remainder $[H^{(1)}]$ of the correct Hamiltonian. In method I, the *inverse* transformation is used[1] to transform the *experimental* energy matrix. In both cases only the diagonal elements are retained.

Some further comments can be made:

(1) Both methods have the attractive feature that once approximate values of the NMR parameters are found, one obtains *linear* equations relating the corrected values of these parameters to observed quantities.

(2) In method II, there is an obvious way of incorporating higher-order correction terms by means of second and higher-order perturbation theory. However, the linear dependence on the NMR parameters is now lost, and the formulas will not be very useful for the interpretation of a particular spectrum. On the other hand, for a study of several molecules having similar shifts and coupling constants, the inclusion of higher-order terms may suffice to render *one* approximate Hamiltonian $H^{(0)}$ applicable for analysis of *several* spectra. Also, for some studies of solvent effects,[10] this method may be preferable.

(3) The expressions[1] for the diagonal elements of the matrix $\mathbf{U}\Lambda\exp\mathbf{U}^{-1}$ in method I are simpler than those for the elements[3] $H_{kk}^{(1)}$ in method II. However, the setting up of an experimental energy-level scheme (a process perhaps not so conveniently programed for a computer) is unnecessary in method II. Therefore, method II will be effective also in cases where the number of lines initially assigned to specified transitions is not large enough to allow the setting up of a level scheme, as illustrated[3] by the case of thiophene (at 40 Mc).

[1] C. A. Reilly and J. D. Swalen, J. Chem. Phys. **32**, 1378 (1960).
[2] The notations of footnote reference 1 are used throughout.
[3] R. A. Hoffman and S. Gronowitz, Arkiv Kemi **15**, 45 (1959).
[4] P. O. Löwdin, *Technical Notes from the Uppsala Quantum Chemistry Group, 1959*. The author is indebted to Professor Löwdin and to Dr. A. Fröman for valuable discussions of this problem.
[5] It should be noted that the division defined by (1) of the total Hamiltonian differs from that usually[6a,b, 8] encountered.
[6] (a) W. A. Anderson, Phys. Rev. **102**, 151 (1956). (b) H. M. McConnell, A. D. McLean, and C. A. Reilly, J. Chem. Phys. **23**, 1152 (1955).
[7] H. J. Bernstein, J. A. Pople, and W. G. Schneider, Can. J. Chem. **35**, 65 (1957).
[8] W. A. Anderson and H. M. McConnell, J. Chem. Phys. **26**, 1496 (1957).
[9] R. A. Hoffman and S. Gronowitz, Arkiv Kemi (to be published).
[10] For example, S. Clough, Mol. Phys. **2**, 349 (1959).

On The Analysis of High-Resolution NMR Spectra by Iterative Methods

C. A. Reilly and J. D. Swalen
Shell Development Company, Emeryville, California

(Received July 25, 1960)

In view of the preceding comments by R. A. Hoffman we should like to clarify and emphasize some points in our method for analyzing complex NMR spectra.[1] A more detailed discussion will appear shortly.[2]

As Hoffman points out, his method and ours are closely related. Both depend upon making at least a partial assignment of the spectral lines. In the spectra that we have so far analyzed (up to five spins) we have always been able to derive the experimental energy-level matrix from a partial assignment. The complete

assignment follows directly from this matrix. An additional advantage in this technique is that uncertainties in the energy levels tend to be less than in the individual line positions. Hence, the energy levels are more satisfactory for iterative purposes.

Further, the traces of the energy-level submatrices can often be used to obtain improved values for the NMR parameters[3] and thus to reduce the number of iterations required to reach a consistent solution. An exact solution is even possible if the molecule has sufficient symmetry (e.g., the A_2B_3 case).

[1] C. A. Reilly and J. D. Swalen, J. Chem. Phys. **32**, 1378 (1960).
[2] C. A. Reilly and J. D. Swalen, J. Chem. Phys. (to be published).
[3] L. L. Van Reijen, private communication.

Notes

Electronegativities from Comparison of Bond Lengths in AH and AH^+

HENRY A. BENT

School of Chemistry, Institute of Technology, University of Minnesota, Minneapolis, Minnesota

(Received May 2, 1960)

LINNETT and co-workers have established a correlation among the difference in bond lengths in a radical AH (such as CH, NH, OH) and the corresponding hydride AH_n (CH_4, NH_3, OH_2) and the signs, and to a lesser extent the magnitudes, of the crossterms in the potential energy function of AH_n.[1] They have found, for example, that when the change in bond length in going from AH to AH_2 is negative, the bond-bond crossterm constant k_{12} is also negative.

We have observed a correlation between the difference in bond length in a radical (or molecule) AH and the corresponding ion AH^+, and the electronegativity of A. It is found that in going from AH to AH^+ the bond length increases when A is electronegative and decreases when A is electropositive. It is therefore possible to estimate the electronegativity χ_A of A from the interatomic distances in AH and AH^+; or, conversely, to estimate the interatomic distance $R(AH^+)$ in AH^+ from $R(AH)$ and χ_A. One reason for the correlation between χ_A and the difference $R(AH)-R(AH^+)$ may be stated as follows:

We assume that atom A has two or more valence electrons; this ensures that the molecule or radical AH will contain at least one unshared valence-shell electron. In abbreviated notation, the structure of AH may be indicated as $\cdot A-H$. Removal of an electron from this structure gives the ion AH^+. A convenient approximation of the structure of this ion is to regard the ion as a resonant hybrid of two extreme structures which we shall abbreviate as $A-H$ and $\cdot A\cdot H$. $A-H$ represents in qualitative terms the structure that would be obtained if the electron that is removed from $\cdot A-H$ were to come from a predominantly non- or anti-bonding orbital localized about A. $\cdot A\cdot H$ represents the hypothetical structure obtained when ionization occurs from a predominantly bonding orbital, i.e., one localized between A and H. An approximate wave function for the actual molecule AH^+ may be compounded from the wave functions for these two idealized structures.

$$\psi(AH^+)\cong N[\psi(A-H)+\lambda\psi(\cdot A\cdot H)],$$

where the proper value of λ is that value which minimizes the energy. The dependence of the value of λ on the electronegativity of A is suggested by the following argument.

The formal charge[2] on A in the structure $A-H$ is $+1$; and, in $\cdot A\cdot H$, $+\frac{1}{2}$. It is inferred[3] from this that the importance of the latter structure probably increases as the electronegativity of A increases; i.e., it seems reasonable to suppose that

$$\partial\lambda/\partial\chi_A>0.$$

Also, it seems reasonable to suppose that $R(\cdot A\cdot H)>R(\cdot A-H)$ and that the difference $\Delta\equiv R(AH)-R(AH^+)$ becomes smaller (i.e., more negative) as λ increases; in short, that

$$\partial\Delta/\partial\lambda<0.$$

Hence, it follows that

$$\partial\Delta/\partial\chi_A=(\partial\Delta/\partial\lambda)\cdot(\partial\lambda/\partial\chi_A).$$
$$<0.$$

The data in Table I follow this pattern. With an increase in electronegativity of A, there follows a monotonic decrease in Δ.

The fact that Δ is actually positive for the more electropositive elements listed implies that $R(A-H)<R(\cdot A-H)$. Plausible reasons for this inequality may be found by combining information gained from studies of the role of $s-p$ hybridization in the bonding of diatomic hydrides[4] with the generally accepted fact that bonds become shorter with increasing s content[5] and the plausible assumption that ionization of an unshared electron leads to second-order[6] or isovalent[7]

TABLE I. Bond lengths of AH and AH^+, their difference, and χ_A (bond lengths in Å).

Hydride, AH	$R(AH)$[a]	$R(AH^+)$[a]	$\Delta\equiv R_A(H)-R(AH^+)$	χ_A[b]
OH	0.9706	1.0289	−0.0583	3.5
NH	1.038	1.084	−0.046	3.0
HCl	1.27460	1.3153	−0.0407	3.0
HBr	1.414	(1.459)	$-(0.04_5)$	2.8
CH	1.1198	1.1308	−0.0110	2.5–2.6
BH	1.2325	(1.2146)	$+(0.01_8)$	1.8–2.0
BeH	1.3431	1.3121	+0.0310	1.4–1.5
AlH	1.64_7	1.60_1	$+0.04_5$	1.5
MgH	1.7306	1.649	+0.082	1.2–1.3

[a] *Tables of Interatomic Distances and Configuration in Molecules and Ions*, edited by L. E. Sutton, Special Publ. No. 11 (The Chemical Society, Burlington House, W.1, London, 1958); G. H. Herzberg, *Spectra of Diatomic Molecules* (D. Van Nostrand Company, Inc., Princeton, New Jersey, 1950).
[b] H. O. Pritchard and H. A. Skinner, Chem. Revs. **55**, 745 (1955).

rehybridization of A in a direction such as to increase the s content of the bonding orbital.

It is seen from the data in Table I that an electronegativity scale based on changes in bond length caused by the removal of an electron from diatomic hydrides shows promise of comparing well with scales based on the partial[8] or complete[9] removal of a hydrogen atom. From the accepted value for the electronegativity of fluorine (3.9–4) and the near linearity of Δ with χ_A (Table I), it is inferred that the interatomic distance in HF^+ is probably 0.98 ± 0.02 A.

[1] D. F. Heath and J. W. Linnett, Trans. Faraday Soc. **44**, 556 (1947); J. W. Linnett and M. F. Hoare, *ibid.* **45**, 844 (1949); D. F. Heath, J. W. Linnett, and P. J. Wheatley, *ibid.* **46**, 137 (1950).
[2] G. N. Lewis, J. Chem. Phys. **1**, 17 (1933).
[3] See L. Pauling, *Victor Henri Commemoratif Volume* (Maison Desoer, Liége, 1947–1948), p. 1; J. Chem. Soc. **1948**, 1461; J. Phys. Chem. **56**, 361 (1952).
[4] D. Z. Robinson, J. Chem. Phys. **17**, 1022 (1949); W. Moffitt, Proc. Roy. Soc. (London) **A202**, 548 (1950), Repts. Progr. in Phys. **17**, 173 (1954); R. S. Mulliken, J. Chem. Phys. **19**, 900 (1951); J. Phys. Chem. **56**, 295 (1952); A. C. Hurley, Proc. Roy. Soc. (London) **A248**, 119 (1958); A. J. Freeman, J. Chem. Phys. **28**, 230 (1958).
[5] M. G. Brown, Trans. Faraday Soc. **55**, 694 (1959); C. A. Coulson, *Victor Henri Commemoratif Volume* (Maison Desoer, Liege, 1947–1948), p. 15. Also, G. R. Somayajulu, J. Chem. Phys. **31**, 919 (1959); and C. C. Costain and B. P. Stoicheff, J. Chem. Phys. **30**, 777 (1959).
[6] W. Moffitt, Proc. Roy. Soc. (London) **A202**, 534 (1950).
[7] R. S. Mulliken, J. Phys. Chem. **56**, 295 (1952).
[8] A. D. Walsh, Proc. Roy. Soc. (London) **A207**, 13 (1951).
[9] L. Pauling, *Nature of the Chemical Bond* (Cornell University Press, Ithaca, New York, 1960), Chap. 3.

Correlation of Bond Shortening by Electronegative Substituents with Orbital Hybridization

HENRY A. BENT
School of Chemistry, Institute of Technology
University of Minnesota, Minneapolis, Minnesota

(Received April 25, 1960)

IT seems well established that in the absence of marked steric requirements, replacement in the structure $X-A-Y$ of Y by an atom more electronegative than Y causes the adjacent $X-A$ bond to become shorter. This effect is particularly noticeable when fluorine is introduced into a molecule[1] (C–F distances in $F-CH_3$ and $F-CF_3$, for example, are 1.391 A and 1.323 A, respectively),[2] but occurs also on further halogen substitution in the chlorinated and brominated silanes, the methyltin chlorides, bromides, and iodides, and in the methylarsenic chlorides.[3] Several other examples have been cited.[4] It is the purpose of the present note to suggest a possible explanation for this phenomenon.

Often the changes in bond lengths, which are in the opposite direction from what one would expect, were repulsions between nonbonded atoms, the important effect operating. Explanations that invoke participation of double-bonded structures have been criticized by Skinner and Sutton[3] and Wells.[5] It is suggested here that the observed changes in bond lengths are in a direction compatible with present knowledge concerning second-order[6] or isovalent[7] hybridization. These terms have been introduced to describe nonintegral states of hybridization. Evidence for such states may be inferred from bond angles (neither 90° or 109°28′ in NH_3 and H_2O, for example, nor exactly 120° in C_2H_4[8]) and from the effects of electronegative substituents on bond angles, chemical reactivity, and proton-C^{13} coupling constants.

To illustrate, replacement of the methyl groups in CH_3OCH_3 by hydrogen atoms causes the valence angle about oxygen to decrease from 111° to 105°; replacement of the hydrogen by fluorine causes a further decrease to 103.2°.[2] The corresponding angles about nitrogen in the series $N(CH_3)_3$, NH_3, NF_3 are 109°, 106°46′, and 102°30′, respectively.[2] Further evidence of the effect of electronegative substituents on interbond angles has been cited by Mellish and Linnett.[9] While several different explanations have been offered for these changes in geometry,[9,10] it is sufficient here to observe that in nearly every instance the observed changes seem compatible with the view that an increase in electronegativity of Y in the structure $X-A-Y$ causes atom A to divert s character *from* the bond to Y *to* the orbital toward X (a pair of unshared electrons in the examples cited above). Rehybridization of A in this manner is consistent with present views of the inductive effect and the hypothesis tendered many years ago by Mulliken,[11] and more recently by Walsh,[12] that the more s character there is in an atomic valency, the more electronegative is the atom in that valency.[13] Recent data on proton-C^{13} coupling constants may be interpreted in a similar manner. Coupling constants[14] for methane, benzene, and methyl acetylene are 125, 159, and 248 sec^{-1}; this suggests, in agreement with theory, that the greater the s character in a carbon valency toward hydrogen (and, hence the greater the probability of finding the bonding electrons at the C^{13} nucleus), the greater the interaction constant. Accordingly, from the coupling constants for the series CH_3Cl, CH_2Cl_2, $CHCl_3$ of 150, 178, 209 sec^{-1}, respectively,[14] one infers that there is more carbon s character in the orbital toward hydrogen in $CHCl_3$ than in CH_2Cl_2, and more in the latter than in CH_3Cl, in agreement with the view already expressed that an atom tends to concentrate its s character in orbitals toward electropositive groups[15] (unshared electrons may be viewed as electrons in a bond to an atom of vanishing electronegativity). This rule describes the effect of electronegative substituents on orbital hybridization.

The effect of orbital hybridization on bond lengths seems to be already well established.[16] Bonds become shorter with increasing s content. The carbon-carbon single bond, for example, decreases in length with increasing s content in the series sp^3-sp^3 (ethane, propane, diamond), sp^3-sp^2 (acetaldehyde, propene), sp^3-sp (methyl acetylene, methyl cyanide) sp^2-sp (vinyl cyanide), sp-sp (cyanoacetylene, diacetylene,

cyanogen) in approximately the following manner: 1.54, 1.50, 1.46, 1.42, 1.38 A. Other bonds have been discussed from a similar point of view.[16,17]

Together, the effect of electronegative substituents on orbital hybridization and the effect of the latter on bond lengths form a scheme for predicting the effect of electronegative substituents on bond lengths. The three empirical observations that: (i) *s* character tends to concentrate in orbitals toward electropositive groups, (ii) bonds become shorter with increasing *s* content, and (iii) bonds become shorter with the introduction of electronegative substituents are, thus, internally consistent. Any one of the three may be inferred from the other two.

[1] L. S. Bartell and L. O. Brockway, J. Chem. Phys. **23**, 1860 (1955); L. O. Brockway, J. Phys. Chem. **41**, 185 (1937).
[2] *Tables of Interatomic Distances and Configuration in Molecules and Ions*, edited by L. E. Sutton, Special Publ. No. 11 (The Chemical Society, London, England, 1958).
[3] T. L. Cottrell and L. E. Sutton, Quart. Revs. (London) **2**, 260 (1948); H. A. Skinner and L. E. Sutton, Trans. Faraday Soc. **40**, 164 (1944).
[4] H. A. Bent, J. Chem. Phys. (to be published).
[5] A. F. Wells, J. Chem. Soc. 55 (1959).
[6] W. Moffitt, Proc. Roy. Soc. (London) **A202**, 534 (1950).
[7] R. S. Mulliken, J. Phys. Chem. **56**, 295 (1952).
[8] L. S. Bartell and R. A. Bonham, J. Chem. Phys. **27**, 1414 (1957); H. C. Allen and E. K. Plyler, J. Am. Chem. Soc. **80**, 2673 (1958).
[9] C. E. Mellish and J. W. Linnett, Trans. Faraday Soc. **50**, 657 (1954).
[10] V. Schomaker and C. Lu, J. Am. Chem. Soc. **72**, 1182 (1950).
[11] R. S. Mulliken, J. Phys. Chem. **41**, 318 (1937).
[12] A. D. Walsh, Trans. Faraday Soc. **43**, 60 (1947); see also W. Moffitt, Proc. Roy. Soc. (London) **A202**, 548 (1950).
[13] Experimental confirmation of this may be found in the inductive constants given by R. W. Taft, Jr., in *Steric Effects in Organic Chemistry*, edited by M. S. Newman (John Wiley & Sons, Inc., New York, 1956), Chap. 13, and in the bond moments calculated by A. J. Petro, J. Am. Chem. Soc. **80**, 4230 (1958); see also I. M. Mills and H. W. Thompson, Proc. Roy. Soc. (London) **A228**, 287 (1955).
[14] N. Muller and D. E. Pritchard, J. Chem. Phys. **31**, 768, 1471 (1959).
[15] Compare A. D. Walsh, Discussions, Faraday Soc. **2**, 18 (1947).
[16] M. G. Brown, Trans. Faraday Soc. **55**, 694 (1959), see also C. C. Costain and B. P. Stoicheff, J. Chem. Phys. **30**, 777 (1959); and C. A. Coulson, *Victor Henri Commemorative Volume* (Maison Desoer, Liege, 1947–1948), p. 15.
[17] I. Lindquist, J. Inorg. & Nuclear Chem. **6**, 159 (1958); I. Lindquist and M. Mörtsell, Acta Cryst. **10**, 406 (1957).

Bond Shortening by Electronegative Substituents

HENRY A. BENT

School of Chemistry, Institute of Technology, University of Minnesota, Minneapolis, Minnesota

(Received April 4, 1960)

THE systematic effect of electronegative substituents on bond angles has been summarized and discussed by Mellish and Linnett.[1] There exists, also, a systematic effect of electronegative substituents on bond lengths. The noticeable foreshortening of bond lengths that occurs when fluorine atoms are introduced

TABLE I. Effects of electronegative groups on bond lengths (bond lengths in angstroms).

Single bonds

1. Bond: C—F. Substitution: F for H.

		Reference
CH_3F	1.391	a
	1.385	b
CH_2F_2	1.358	c
CHF_3	1.332	d
	1.326	c
CF_4	1.323	a

2. Bond: C—Cl. Substitution: Cl for H.

		Reference
CH_3Cl	1.784	a
	1.781	e
CH_2Cl_2	1.772	c
$CHCl_3$	1.767	f
	1.761	g
CCl_4	1.766	a
	1.760	h

3. Bond: C—Br. Substitution: Br for H.

		Reference
CH_3Br	1.939	f
$CHBr_3$	1.930	f

4. Bond: C—Cl. Substitution: F for H.

		Reference
CH_2Cl	1.783	a, e
CF_3Cl	1.751	i

5. Bond: C—Cl. Substitution: F for Cl.

		Reference
CCl_2F_2	1.77$_5$	i
CF_3Cl	1.751	i

6. Bond: C—C. Substitution: F for H.

		Reference
C_2H_6	1.536	j
C_2F_6	1.51	k

7. Bond: N—Cl. Substitution: Cl for CH_3.

		Reference
$N(CH_3)_2Cl$	1.77	l
$N(CH_3)Cl_2$	1.74	l

Double bonds

8. Bond: C=C. Substitution: F for H.

		Reference
C_2H_4	1.335	m
C_2F_4	1.313	n

9. Bond: C=O in $X\overset{\displaystyle O}{\overset{\|}{C}}Y$.

X	Y	C=O distance	Reference
H	CH_3	1.226	o
H	H	1.225	p
H	C≡CH	1.216	q
H	F	1.192	r
F	F	1.17	s

[a] L. O. Brockway, Acta. Cryst. 7, 682 (1954).
[b] W. Gordy, Phys. Rev. 75, 1014 (1949).
[c] D. R. Lide, Jr., J. Am. Chem. Soc. 74, 3548 (1952); R. L. Livingston and D. H. Lyon, J. Chem. Phys. 24, 1283 (1956).
[d] S. N. Ghosh, R. Trambarulo, and W. Gordy, J. Chem. Phys. 20, 605 (1952).
[e] S. L. Miller, L. C. Aamodt, G. Dousmanis, and C. H. Townes, J. Chem. Phys. 20, 1112 (1952).
[f] C. H. Townes and A. L. Schawlow, *Microwave Spectroscopy* (McGraw-Hill Book Company, Inc., New York, 1955).
[g] R. R. Unterberger, R. Trambarulo, and W. V. Smith, J. Chem. Phys. 18, 565 (1950).
[h] L. S. Bartell, L. O. Brockway, and R. H. Schwendeman, J. Chem. Phys. 23, 1854 (1955).
[i] Livingston and Lyon, *loc. cit.*
[j] K. Hedberg and V. Schomaker, J. Am. Chem. Soc. 73, 1482 (1951).
[k] J. L. Brandt and R. L. Livingston, J. Am. Chem. Soc. 76, 2096 (1954).
[l] V. Schomaker and D. P. Stevenson, J. Am. Chem. Soc. 63, 37 (1941).
[m] L. S. Bartell and R. A. Bonham, J. Chem. Phys. 27, 1414 (1957); H. C. Allen, Jr., and E. K. Plyler, J. Am. Chem. Soc. 80, 2673 (1958).
[n] I. Karle and J. Karle, J. Chem. Phys. 18, 963 (1950).
[o] C. C. Lin and R. W. Kilb, J. Chem. Phys. 24, 631 (1956).
[p] G. H. Herzberg, *Infrared and Raman Spectra of Polyatomic Molecules* (D. Van Nostrand Company, Inc., Princeton, New Jersey, 1945), p. 440.
[q] J. R. Morton, Symposium on Molecular Structure and Spectroscopy, Ohio State, June 1958, Abstract F10.
[r] M. E. Jones, K. Hedberg, and V. Schomaker, J. Am. Chem. Soc. 77, 5278 (1955).
[s] T. T. Broun and R. L. Livingston, J. Am. Chem. Soc. 74, 6084 (1952).

into molecules has already been commented upon.[2] It is the purpose of this note to show that bond shortening by electronegative substituents is of wide occurrence. Table I summarizes some of the recent data that illustrate the foreshortenings which occur in adjacent bonds when an atom of relatively low electronegativity, such as hydrogen, is replaced by an atom of greater electronegativity, such as fluorine or some other halogen. Data for such molecules as CBr_4 and CI_4 in which steric effects are probably very large are not included in this table.

The effects described here are next-nearest neighbor effects; i.e., they involve the effect of an atom on a bond one atom removed. As such, they are closely related to the inductive effect of organic chemistry. It may be mentioned, also, that these variations in bond lengths are not those predicted by the Schomaker-Stevenson rule:[3] they are, in fact, opposite in direction from what one would expect from a logical extension of this rule. It is interesting to note, too, that the variations in bond length are usually in the reverse direction from what one would expect were repulsive interactions between nonbonded atoms the important effect operating.

[1] C. E. Mellish and J. W. Linnett, Trans. Faraday Soc. 50, 657 (1954).
[2] L. S. Bartell and L. O. Brockway, J. Chem. Phys. 23, 1860 (1955).
[3] V. Schomaker and D. P. Stevenson, J. Am. Chem. Soc. 63, 37 (1941).

Number of 3*d* Electrons in Iron

S. K. Joshi

Physics Department, The University, Allahabad 2, U. P., India

(Received June 20, 1960)

RECENTLY there has been much controversy over the number of 3*d* electrons in iron.[1,2] Weiss and DeMarco,[1] from their measurements of absolute intensities of Bragg reflections from an iron crystal, and after applying necessary corrections to them, computed the atomic-scattering factor. They then deduce (2.3 ± 0.3) as the number of 3*d* electrons in iron. This unexpected result was challenged by Batterman[2] who from his x-ray measurements on powdered Fe estimates the number of the effective 3*d* electrons in iron at 6.3 ± 1.0. He also finds that the use of scattering factors calculated from the nonexchange wave functions yields 7.5 as the number of 3*d* electrons.

The number of free electrons in iron can be estimated on the basis of the lattice theory of elastic constants. In an iron crystal a tightly bound *d* electron contributes a strong, but primarily central, force to the cohesive energy and elastic constants. These central forces follow the Cauchy relation, $c_{12}=c_{44}$. The discrepancy in the Cauchy relation will be just equal to the bulk modulus K_e of the electron gas and one can write after de Launay[3]

$$K_e=c_{12}-c_{44}=\tfrac{2}{3}(Nn_0\zeta_0/V). \quad (1)$$

Here N is Avogadro's number, V is atomic volume, and n_0 is the number of free electrons per atom. ζ_0, the Gibbs' potential per electron, is given by

$$\zeta_0=(h^2/2m)(3Nn_0/8\pi V)^{\frac{2}{3}}. \quad (2)$$

where h is Planck's constant and m is electronic mass. Combining (1) and (2) we get

$$n_0=(8\pi/3)^{2/5}(3m/h^2)^{3/5}(V/N)(c_{12}-c_{44})^{3/5}.$$

In the case of iron, $V=7.1$ cc, $c_{12}=1.41$, and $c_{44}=1.16$ in units of 10^{12} dynes cm^{-2} (as cited by de Launay[3]). This gives $n=0.57$. With this value of the number of free electrons per atom and 18 as the number of electrons in the inner core, we find 7.4 to be the number of rather compactly bound 3*d* electrons of iron. This number is in close agreement with Batterman's findings.

The author is deeply indebted to Professor K. Banerjee for his interest and to Dr. B. K. Agrawal for discussion.

[1] R. J. Weiss and J. J. DeMarco, Revs. Modern Phys. 30, 59 (1958); Phys. Rev. Letters 2, 148 (1959).
[2] B. W. Batterman, Phys. Rev. Letters 2, 47 (1959), Phys. Rev. 115, 81 (1959).
[3] J. de Launay, *Solid State Physics*, edited by F. Seitz and D. Turnbull (Academic Press, Inc., New York, 1956), Vol. 2, pp. 219.

Absorption Spectrum of Chlorine in the Vacuum Ultraviolet

Raymond P. Iczkowski, John L. Margrave and John W. Green

Department of Chemistry, University of Wisconsin Madison, Wisconsin

(Received June 24, 1960)

THE absorption spectrum of chlorine in the region 1350 A–1100 A of the vacuum ultraviolet has been observed at a dispersion of 17.5 A/mm. Walsh[1]

TABLE I. Band heads in the absorption spectrum of chlorine.

System	λ(A)	ν(K)	Intensity
A_2	1343.4	74 437	3
	1332.5	75 047	9
	1321.8	75 652	5
A_3	1200.1	83 325	2
	1191.5	83 926	5
B_3	1189.2	84 092	5
	1180.4	84 718	10
	1172.0	85 324	10
	1164.8	85 853	6
A_4	1140.8	87 659	10
B_4	1148.2	87 093	2
	1138.9	87 801	10
A_5	1125.5	88 849	7
	1118.4	89 415	10
B_5	1123.7	88 996	7
	1115.6	89 638	10
A_6	1103.9	90 592	8
Others	1160.8	86 148	2
	1154.6	86 609	6
	1143.6	87 447	7
	1134.5	88 143	9
	1129.1	88 564	6

has reported on the bands from 1870 A−1300 A but his results at low wavelengths were obscured by contamination with HCl produced by reaction of the chlorine with the hydrogen carrier gas. By using the same apparatus as was used previously[2] to study F_2, it was possible in this work to mitigate the effect of contamination by HCl which was experienced by Walsh and extend the region studied sufficiently that a Rydberg series and the ionization potential are established.

The wavelengths, wave numbers, relative intensities, and designations of the strongest bands are given in Table I. Many more bands are observed at higher pressures but are not reported here. The bands are designated and analyzed by analogy with the corresponding bands observed in the previous work on F_2. The progressions labeled "A" have a fundamental frequency of approximately 610 K, are shaded toward the x rays, and probably represent the transition

$$\cdots(2\pi_u)^4(2\pi_g)^3 m\pi_u,\ A\ {}^2\Sigma_{0u}{}^+ \leftarrow \cdots(2\pi_u)^4(2\pi_g)^4,\ X\ {}^1\Sigma_g{}^+.$$

The first vibrationally excited bands in this series are the most intense and they can be arranged in a Rydberg series

$$\nu_m = 93\,200 - 109\,736/(m+0.46)^2.$$

A comparison of calculated and observed band frequencies is given in Table II. Agreement is good except for ν_5, where the deviation is outside of experimental error. The ionization potential to the ground state of $Cl_2{}^+$ is obtained by subtracting from 93 200 K the fundamental frequency of $Cl_2{}^+$, which yields the value 92 550 K, or 11.47 ev.

TABLE II. Rydberg series in chlorine. $\nu_m = 93200 - R/(m+0.46)^2$

m	2	3	4	5	6
ν_{obs} (K)	75 047	83 926	87 659	89 415	90 592
ν_{calc} (K)	75 060	83 980	87 680	89 520	90 570
$\nu_{obs}-\nu_{calc}$	−13	−54	−21	−105	22

In the past, many attempts to interpret ionization potentials for the purpose of gaining insight into the bonding character of a molecule have been rendered valueless because the experimental values were incorrect. Therefore if Cl_2 is to be compared with F_2, it is very necessary to have accurate, and preferably also precise, values of these molecular ionization potentials. A low value of the ionization potential of F_2 was previously obtained from spectroscopic studies, 15.71 ev,[2] and later confirmed by electron impact work, 15.83 ev.[3] The value of the ionization potential of Cl_2 obtained in this work, 11.47 ev, is in agreement with the value obtained from photoionization, 11.48 ev[4] but not with those obtained from electron impact, 11.64 ev[5] and 11.80 ev.[5]

Pitzer[6] pointed out that the first row single bonds, N—N, O—O, and F—F, are much weaker than the corresponding higher row single bonds. In particular, the question of why the bond in F_2 is much weaker than the bond in Cl_2 has been the subject of much speculation. On the basis of the geometry of the orbitals involved, Pitzer suggested that the difference in bond strength between F_2 and Cl_2 was the result of strong repulsions in the π-orbitals of F_2 and a lack of such repulsions in the outer π-orbitals of Cl_2.

If this were true, then in F_2 there would be formed an antibonding π-orbital with a term value appreciably less than that of the p-orbital in the fluorine atom, while in Cl_2, the corresponding difference would be slight. Actually the ionization potentials are changed to the same appreciable extent in the process of molecule formation for both Cl_2 and F_2, and therefore strong interactions are present to the same degree in the π-orbitals of both Cl_2 and F_2.

If there exists any simple explanation of the relationship of the bond energies of the first row elements to those of higher rows, it probably involves the possibility of 3d-orbital hybridization for the higher rows[7] or else the effects of interactions with the inner shells.[6–8] However, 3d-orbital hybridization could not be said to make chlorine more stable than fluorine by effecting less $p\pi$ repulsion[9] in chlorine than exists in F_2.

[1] J. Lee and A. Walsh, Trans. Faraday Soc. **55**, 1281 (1959).
[2] R. P. Iczkowski and J. L. Margrave, J. Chem. Phys. **30**, 403 (1959).
[3] J. T. Herron and V. H. Dibeler, J. Chem. Phys. **32**, 1884 (1960).
[4] K. Watanabe, J. Chem. Phys. **26**, 542 (1957).
[5] J. Morrison and A. Nicholson, J. Chem. Phys. **20**, 1021 (1952).
[6] K. S. Pitzer, J. Am. Chem. Soc. **70**, 2140 (1948).
[7] R. S. Mulliken, J. Am. Chem. Soc. **77**, 884 (1955).
[8] R. S. Mulliken, J. Phys. Chem. **56**, 295 (1952).
[9] L. Pauling, *The Nature of the Chemical Bond* (Cornell University Press, Ithaca, New York, 1960), p. 143.

Comment on Dynamical Theory of Electrosedimentation

C. J. MacCallum

Sandia Corporation, Albuquerque, New Mexico

(Received June 9, 1960)

RECENT papers by Peterlin and Ribarič[1] and by Prock and McConkey[2] discuss the measurement of very large molecular weights via the capacitance change induced in a cylinder of solution by applied electrostatic voltage. This note reports a numerical solution of the time dependence of the capacitance change, valid for all times and voltages, which demonstrates that measurement of the time dependence alone yields only one quantity: a (roughly logarithmic) average diffusion constant. If the diffusion constant is separately determined for the weight average mass present, the width of the mass spectrum present may possibly be estimated.

Using notation from reference 2 (except that $\tau \equiv tD/a^2$), we solve the cylindrical diffusion equation with $m(x, 0) = \exp(\eta/x^2) - 1$ where η is the dimensionless ratio $\alpha E_0/2kT$ which may take any value (positive or negative). The fractional capacitance change is

$$F(\eta,\tau) = \int_1^\infty m(x,\tau)\,dx/x \Big/ \int_1^\infty m(x,0)\,dx/x$$

$$= \int_1^\infty m(x,\tau)\,dx/x \Big/ \sum_1^\infty \eta^n/(2n!). \qquad (1)$$

The right hand denominator will be called $g(\eta)$. Note we have let $\beta \equiv b/a \to \infty$, introducing errors of order β^{-2}. When $\beta \to \infty$ the solution $m(x, \tau)$ can be expressed as a double integral[3] involving $m(x, 0)$. Insertion in Eq. (1) and expansion of $m(x, 0)$ in powers of η yields, after some manipulation,

$$F(\eta,\tau) = \frac{16}{\pi^2 g(\eta)} \int_0^\infty \frac{\exp(-\lambda^2\tau)\lambda^{-1}d\lambda}{|H_1(\lambda)|^2} S_{-2,1}(\lambda)$$

$$\times \sum_1^\infty \frac{\eta^n \lambda^{2n}}{(n-1)!} S_{-2n,1}(\lambda), \quad (2)$$

where the S's are Lommel functions,[4] the first defined by power series and successive ones by recurrence formulas.

An asymptotic series in $\tau^{\frac{1}{2}}$ can be developed yielding

$$g(\eta)(1-F) \sim 4\tau\eta g''(\eta) - (32/3\pi^{\frac{1}{2}})\tau^{\frac{1}{2}}\eta \exp(\eta) + \cdots,$$

but the numerical solution shows that is not useful except when $1-F$ is too small to be experimentally useful. An expression for large τ is

$$8\tau g(\eta) F/\eta \sim (\ln 4\tau + f(\eta) - \gamma)^2 + \pi^2/6 - f^2$$

where γ is the Euler constant $0.577\cdots$ and $f(\eta) = \sum \eta^n/2n(n+1)!$ This is shown by dotted lines in the figure. Since the outer cylinder radius is finite, F must eventually decrease exponentially with τ; this does not occur until $\tau \gtrsim (\beta/2\pi)^2$ by which time F is experimentally zero.

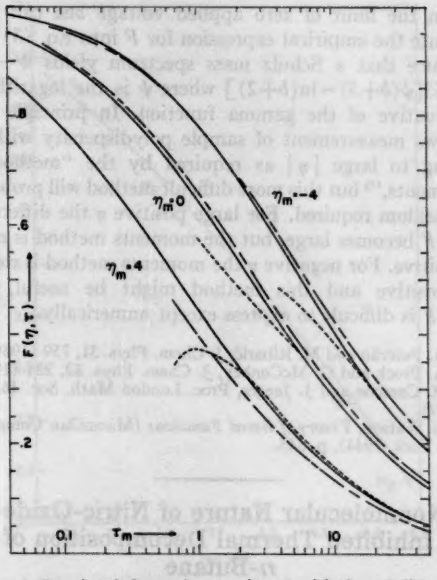

FIG. 1. Fractional change in capacitance with time. Solid curves represent monodisperse systems. Dotted curves represent asymptotic approximation. Dashed curves represent polydisperse systems characterized by Schulz spectrum with $b=0(\eta_m=0, -4)$ and $b=5(\eta_m=+4)$.

Equation (2) can be evaluated numerically by hand for small η; for large η Sandia Corporation's IBM 704 computer was used. Some results are shown as solid lines in Fig. 1. In the region $0.25 < F < 0.75$, $\eta^2 < 20$, the results can be empirically represented as $F = 0.641 - 0.357 \log\tau - 0.0419\eta - 0.0017\eta^2$.

The fractional capacitance change induced in a polydisperse sample is

$$\Phi = \int_0^\infty W(P)\,dP g(\eta) F(\eta,\tau) \Big/ \int_0^\infty W(P)\,dP g(\eta), \quad (3)$$

where $W(P)$ is the differential weight distribution and $\eta = \eta_m(P/P_m)$, $\tau = \tau_m(P/P_m)^{-\delta}$, $(1/3 < \delta < 1)$. Subscript m refers to values for the weight average molecular weight. Φ has been calculated by computer as a function of η_m and τ_m for various δ and various $W(P)$; dashed curves in the figure are for $\delta = 0.5$ and a very broad ($b=0$) Schulz distribution[2] for $W(P)$. Numerical data for other cases are available from the author. As all the curves have virtually identical *shape* even for grossly differing η_m and $W(P)$, the only quantity which can be deduced from a single experimental curve is an effective diffusion constant which, except for large $|\eta|$, is not very different from the value for the weight average.

In the limit of zero applied voltage one can substitute the empirical expression for F into Eq. (3) and deduce that a Schulz mass spectrum yields $\Phi - F = 0.155[\psi(b+3) - \ln(b+2)]$ where ψ is the logarithmic derivative of the gamma function. In principle this allows measurement of sample polydispersity without going to large $|\eta|$ as required by the "method of moments,"[2] but this more difficult method will probably be seldom required. For large positive η the difference $\Phi - F$ becomes large, but the moments method is more sensitive. For negative η the moments method is rather insensitive and this method might be useful, but $\Phi - F$ is difficult to express except numerically.

[1] A. Peterlin and M. Ribarič, J. Chem. Phys. **31**, 759 (1959).
[2] A. Prock and G. McConkey, J. Chem. Phys. **32**, 224 (1960).
[3] H. Carslaw and J. Jaeger, Proc. London Math. Soc. **46**, 383 (1939).
[4] G. Watson, *Theory of Bessel Functions* (Macmillan Company, New York, 1944), p. 345.

Nonmolecular Nature of Nitric-Oxide-Inhibited Thermal Decomposition of *n*-Butane

ARON KUPPERMANN AND JOHN G. LARSON

Noyes Chemical Laboratory, University of Illinois, Urbana, Illinois

(Received June 13, 1960)

THE thermal decomposition of most organic molecules is generally accepted to occur at least in part via a free radical chain process. Since Hinshelwood and Staveley[1] discovered that small additions of nitric oxide reduced the rate of thermal decomposition, there has been much controversy[2] concerning the nature of the "residual" reaction remaining after further additions of inhibitor produce no further decrease in rate. Jach, Stubbs, and Hinshelwood[3] have shown this limiting rate to be independent of the inhibitor used and attribute this residual reaction to a nonchain molecular process in which the parent molecule breaks up, in a single step, into stable products.

Wall and Moore[4] and later Rice and Varnerin[5] studied isotopic exchange in the thermal decomposition of ethane and ethane-d_6 and found extensive mixing in both the inhibited and normal decompositions. In building a case for concluding that the limiting rate corresponds to the complete surpression of chains and hence to a unimolecular split into stable molecules, Hinshelwood[6] discounts the results of Wall and Moore for not using sufficient inhibitor to produce complete inhibition, and the results of Rice and Varnerin on the grounds that the mixing they observe may result from a secondary process involving the methylene radical formed in the split-off of methane from ethane. He suggests that methylene may not be easily scavenged by NO and thus that the isotopic mixing may be due to this atypical decomposition in which one product is a stable molecule and the other a diradical.

Semenov,[7] in quoting work by Voedvodsky, explains complete inhibition as the using up of free valencies on the surface of the reaction vessel which would normally produce a higher gas-phase-radical concentration. Voedvodsky[8] has suggested that two heterogeneous initiation processes, a reversible and an irreversible one, satisfactorily explain experimental observations.

If this limiting rate corresponds to a unimolecular process, then there exists a good set of unimolecular reactions for study. If the residual reaction is of the chain variety, then inhibition may shed some light on the mechanism of chain initiation. In either case, it is important to clearly establish the nature of this residual reaction.

In order to obtain uniquivocal information about this residual reaction, we have investigated the thermal decomposition of a mixture of *n*-butane and *n*-butane-d_{10} in the absence and presence of NO. About 10 cm Hg pressure of an equimolar mixture of these butanes was decomposed in a 100-ml pyrex reaction vessel to extents varying from about 1% to 5%. A temperature of about 430°C was selected so that the reaction could be stopped at small percentages of decomposition. The product-reactant mixture was analyzed with the help of a mass spectrometer. The ratio of ion currents at m/e values 20 and 68 (after a small contribution from the unreacted mixture to the current at m/e 20 was subtracted) was taken as a measure of the extent of decomposition. The latter was also determined by the pressure change in the reaction vessel. The CD_3H/CD_4 ratio was determined from a liquid nitrogen non-condensible fraction of the reacted mixture. This ratio was found not to change as the fractional decomposition varied from 5% down to 1%, which was the lowest value for which reliable measurements could be made. It was further found that this ratio did not change if the reaction was inhibited by initially adding NO to the reaction mixture in amounts variable between 13.4 and 27.6 mole-percent, although this added NO decreased the decomposition-rate-constant by a factor of 3.4. The average CD_3H/CD_4 ratio was 2.38 ± 0.04 for fifteen uninhibited runs and 2.36 ± 0.04 for fifteen inhibited runs. Conditioning of the vessel by twelve successive runs with pure *n*-butane did not, within the accuracy of the experiments, change the rate constants or the CD_3H/CD_4 ratios. A sixty fold increase in the surface to volume ratio, obtained by packing the vessel with pyrex wool, had no detectable effect on the rate-constant or the CD_3H/CD_4 ratio of the uninhibited runs.

In order to eliminate the possibility that the formation of isotopically mixed methanes in the inhibited reaction might be due to secondary processes, mixtures of 5.15% CD_4 and 94.85% C_4H_{10} were reacted in the absence of NO and in the presence of 15.4% of NO, under the same experimental conditions described above, until about 5% of the C_4H_{10} decomposed. No formation of CD_3H whatsoever was detected. This

entirely excludes the possibility of mixing of molecularly formed CD_4 by any subsequent secondary processes, whether heterogeneous or gas phase, under these experimental conditions.

If the inhibited reaction were entirely molecular, the corresponding CD_3H/CD_4 ratio should be zero. Since, within experimental error, it was actually the same as in the uninhibited one, it may be clearly concluded that practically no (i.e., less than 2%) methane is formed by a direct split mechanism in the NO-inhibited thermal decomposition of *n*-butane. This casts very serious doubts on the validity and consequences of the conclusions previously reached[3,6,9] that inhibited reactions of this type were entirely molecular. The results of the present experiments are, furthermore, not inconsistent with a heterogeneous initiation mechanism.[7,8]

[1] L. A. K. Staveley and C. N. Hinshelwood, Proc. Roy. Soc. (London) **A154**, 335 (1936).
[2] E. W. R. Steacie, *Atomic and Free Radical Reactions* (Reinhold Publishing Corporation, New York, 1954), p. 99.
[3] J. Jach, F. J. Stubbs, and C. Hinshelwood, Proc. Roy. Soc. (London) **A224**, 283 (1954).
[4] L. A. Wall and W. J. Moore, J. Am. Chem. Soc. **73**, 2840 (1951).
[5] F. O. Rice and R. E. Varnerin, J. Am. Chem. Soc. **76**, 324 (1954).
[6] C. Hinshelwood, Chem. Soc. (London), Spec. Publ. No. **9**, (1957), 49.
[7] N. N. Semenov, *Some Problems of Chemical Kinetics and Reactivity* (Pergamon Press, New York, 1958), p. 248.
[8] V. V. Voedvodsky, Trans. Faraday Soc. **55**, 65 (1959).
[9] J. Jach and C. Hinshelwood, Proc. Roy. Soc. (London) **A229**, 143 (1955); *ibid.* **A231**, 145 (1955).

Estimation of the Ionization Potential and Dissociation Energy of Molecular Astatine

ROBERT W. KISER

Department of Chemistry, Kansas State University, Manhattan, Kansas

(Received July 7, 1960)

THERE does not exist in the literature any directly measured value for the ionization potential or the dissociation energy of astatine. The ionization potential of At has been found to be 9.5 ev.[1] By using empirical correlations one may arrive at estimations of these values.

The values of ω_e of 892, 565, 323, and 215 cm^{-1} for F_2, Cl_2, Br_2, and I_2[2] allow the estimation of $\omega_e \cong 160$ cm^{-1} for At_2. By using the relation

$$\log\omega_e = a - b\log n^2 I \qquad (1)$$

given by Varshni[3] for XX molecules, one estimates $I(At_2) = 8.3$ ev, as shown in Fig. 1. n = principal quantum number and a and b are constants (or nearly so). Values of $I(X_2)$ are 15.83, 11.48, 10.55, and 9.28, for F_2, Cl_2, Br_2, and I_2, respectively.[4,5]

The relation given by Mitra for XX molecules,

$$\log D = c + d\log I, \qquad (2)$$

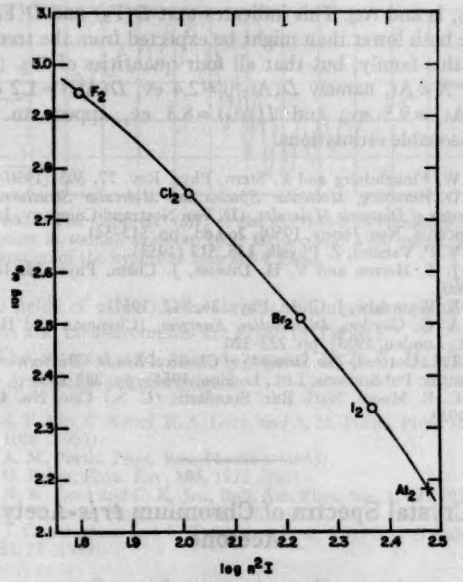

FIG. 1. Plot of the Varshni relation for the halogen molecules.

may be used to estimate the dissociation energy, D, of At_2. The curve of Eq. (2) is shown in Fig. 2, and is found to be remarkably linear, except for the data for F_2 which have been omitted. Values of $D(X_2)$ are 1.59, 2.47, 1.97, and 1.54 ev for F_2, Cl_2, Br_2, and I_2, respectively.[6,7] From Fig. 2, $D(At_2) = 1.2$ ev.

The thermochemical cycle

$$D(X_2^+) = D(X_2) + I(X) - I(X_2) \qquad (3)$$

may be used to calculate values of $D(X_2^+)$. Taking $I(X)$ equal to 17.42, 13.01, 11.84, and 10.45 ev for X = F, Cl, Br, and I, respectively,[8] we find that $D(X_2^+)$ is 3.18, 4.00, 3.26, 2.71, and 2.4 ev for $X_2 = F_2$, Cl_2,

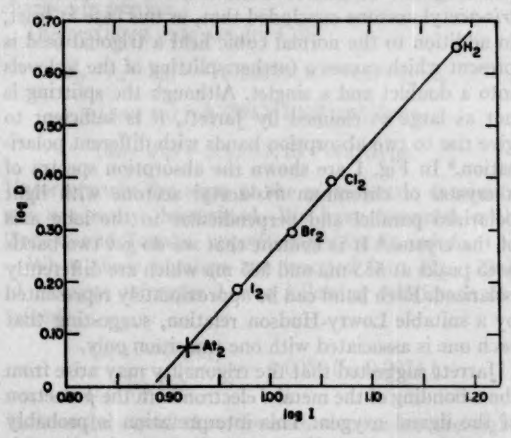

FIG. 2. Plot of the Mitra relation for the halogen molecules.

Br_2, I_2 and At_2. This indicates that $D(F_2)$ and $D(F_2^+)$ are both lower than might be expected from the trends of this family, but that all four quantities of Eq. (3) for $X=At$, namely $D(At_2^+)=2.4$ ev, $D(At_2)=1.2$ ev, $I(At)=9.5$ ev, and $I(At_2)=8.3$ ev, appear to be reasonable estimations.

[1] W. Finkelnburg and F. Stern, Phys. Rev. **77**, 303 (1950).
[2] G. Herzberg, *Molecular Spectra and Molecular Structure. I. Spectra of Diatomic Molecules*, (D. Van Nostrand Company, Inc., Princeton, New Jersey, 1950), 2nd ed., pp. 512–541.
[3] Y. P. Varshni, Z. Physik, **135**, 512 (1953).
[4] J. T. Herron and V. H. Dibeler, J. Chem. Phys. **32**, 1884 (1960).
[5] K. Watanabe, J. Chem. Phys. **26**, 542 (1957).
[6] A. G. Gaydon, *Dissociation Energies*, (Chapman and Hall, Ltd., London, 1953), pp. 222–226.
[7] T. L. Cottrell, *The Strengths of Chemical Bonds*, (Butterworths Scientific Publications, Ltd., London, 1954), pp. 282–288.
[8] C. E. Moore, Natl. Bur. Standards (U. S.) Circ. No. **467**, 3 (1958).

Crystal Spectra of Chromium *tris*-Acetyl Acetone

ANIMESH CHAKRAVORTY AND SADHAN BASU

Department of Chemistry, University College of Science & Technology, Calcutta 9, India

(Received June 2, 1960)

IN chromium *tris*-acetyl acetone the cubic crystal field is expected to split the fivefold degenerate d orbitals into two levels of symmetry, e_g and t_{2g}, respectively, the optical transition between which will give rise to one absorption band. It was observed by Mead[1] that the visible absorption band of hexacoordinated trivalent chromium complexes could be very well represented by Lowry-Hudson's Gaussian curve, suggesting that only one electronic transition is responsible for the absorption band, as expected from the theoretical considerations. Recently Jarrett[2] from the paramagnetic resonance measurements on chromium *tris*-acetyl acetone concluded that, in this case at least, in addition to the normal cubic field a trigonal field is present which causes a further splitting of the t_{2g} levels into a doublet and a singlet. Although the splitting is not as large as claimed by Jarrett, it is sufficient to give rise to two absorption bands with different polarisation.[3] In Fig. 1 are shown the absorption spectra of a crystal of chromium *tris*-acetyl acetone with light polarized parallel and perpendicular to the long axis of the crystal.[4] It is evident that we do get two bands with peaks at 555 mμ and 585 mμ which are differently polarized. Each band can be approximately represented by a suitable Lowry-Hudson relation, suggesting that each one is associated with one transition only.

Jarrett suggested that the trigonality may arise from the π bonding of the metal d electron with the p electron of the ligand oxygen. This interpretation is probably correct because the 275 mμ band of acetyl acetone is

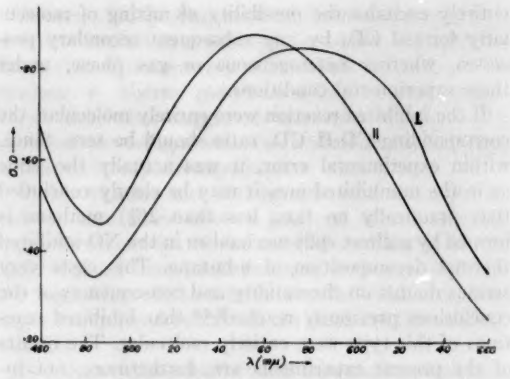

FIG. 1

shifted to 335 mμ in chromium *tris*-acetyl acetone[5] which may be due to mesomeric interaction of the metal-oxygen π bond with the conjugated double bonded system of the ligand molecule.

Sincere thanks are due to Dr. L. E. Orgel, Cambridge, for helpful suggestions.

[1] A. O. Mead, Trans. Faraday Soc. **30**, 1052 (1934).
[2] H. S. Jarrett, J. Chem. Phys. **27**, 1298 (1957).
[3] L. Orgel, private communication.
[4] A. Chakravorty and S. Basu, Nature **184**, 50 (1959); **185**, 681 (1960).
[5] S. Basu and K. K. Chatterjee, Z. physik Chem. **209**, 360 (1958).

Hyperfine Structure of *F*-Center Spin Resonance in Sodium Azide

F. F. CARLSON, G. J. KING, AND B. S. MILLER

Basic Research Group, U. S. Army Engineer Research and Development Laboratories, Fort Belvoir, Virginia

(Received June 14, 1960)

THE electron spin resonance absorption line of an F center is normally a broad, smooth, Gaussian line.[1,2] An important type of broadening which occurs in an F-center resonance is produced by unresolved interactions of the F-center electron with the magnetic hyperfine fields of the nuclei surrounding the F-center site.

The hyperfine structure in the spin resonance line cannot be resolved in the standard electron spin resonance experiment unless special conditions exist. Among these conditions are: the value $|\psi_F|^2$ of the F-center wave function ψ_F at the nuclei of the nearest cations must be large, and the magnetic hyperfine field of these nuclei must be sufficiently strong to overcome competing broadening effects, including the hyperfine fields of other nuclei. Since these conditions are not usually realized, the electron nuclear double-resonance techniques[3] are used to study hyperfine interactions.

On rare occasions, F-center resonances have been observed in which the hyperfine structure has been revolved by standard techniques.[4,5] In this present work we report an ultraviolet irradiation-induced microwave resonance absorption in NaN_3 which we conclude is caused by F centers. The resonance displays the characteristic hyperfine structure of the F center observed by Lord in NaF.[5] The optical absorption data for irradiated NaN_3 corroborates the conclusion that the center is of the F type.[6]

Microcrystalline NaN_3 was sealed in an evacuated fused silica tube and then irradiated at 90°K with an ultraviolet lamp (Hanovia S100). The material turned from white to blue during this treatment. Cunningham and Tompkins[6] have shown that the ultraviolet irradiation of NaN_3 at 90°K produces F-type optical absorption bands but not V-type optical absorption bands.

The sample was examined at 90°K in a Varian EPR spectrometer and an absorption spectrum of 19 evenly spaced lines was found. The shape of the envelope of the lines was Gaussian in nature and showed saturation effects. The g values for the lines were distributed closely above and below $g=2$.

We interpret this spectrum in terms of an N_3^- vacancy model analogous to de Boer's model for an F-center in an alkali halide. Electrons freed during ultraviolet irradiation are trapped at N_3^- vacancies, which are present in large numbers. The immediate environment of the F electron in the N_3^- vacancy consists of six equivalent nearest neighbor sodium ions with nuclear spin $\frac{3}{2}$. The interaction of this F electron with the magnetic field of the six sodium nuclei should split the F resonance into 19 lines. Using broad field sweep and high gain on the EPR spectrometer, 19 lines are actually observed. Figure 1 shows a trace made at lower sweep and gain for presentation purposes.

The analysis of Lord,[5] which assumed that the magnetic hyperfine field effect of the nearest neighbors of the F electron is much greater than that of other ionic shells, is adopted here. The broadening of the individual lines is ascribed in part to the action of nuclear hyperfine fields of other shells of ions. Numerical computations and measurements are given in Table I.

TABLE I. Experimental data and results.

Microwave frequency	≈9000 Mc/sec
Magnetic field	≈3000 gauss
Central g value	2.003±0.001
Separation of hyperfine structure (Hyperfine field of sodium shell)	9.1±0.1 gauss
$\lvert\psi_F\rvert^2$ at sodium nucleus	1.45×10^{23} cm^{-3}
Hyperfine field of next effective shell From linewidth of structure	2.3±0.3 gauss
Crystal structure of NaN_3	Rhombohedral
Temperature of sample during entire experiment	90°K

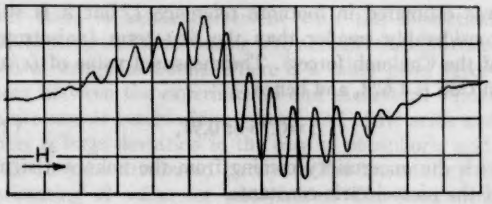

FIG. 1. The slope, dx''/dH, of the electron-spin-resonance absorption in sodium azide at 9000 Mc/sec and 3000 gauss. The separation of the hyperfine lines is 9.1 gauss.

The interest and encouragement of Z. V. Harvalik are gratefully acknowledged.

[1] A. F. Kip, C. Kittel, R. A. Levy, and A. M. Portis, Phys. Rev. **91**, 1066 (1953).
[2] A. M. Portis, Phys. Rev. **91**, 1071 (1953).
[3] G. Feher, Phys. Rev. **105**, 1122 (1957).
[4] N. W. Lord and C. K. Jen, Bull. Am. Phys. Soc. **1**, 12 (1956).
[5] N. W. Lord, Phys. Rev. **105**, 756 (1957).
[6] J. Cunningham and F. Tompkins. Proc. Roy. Soc. (London) **A251**, 27 (1959).

The Effective Ionic Charge in CdS*

FREDERIC KEFFER†

Department of Physics, University of California, Berkeley 4, California

(Received June 20, 1960)

SINCE no precise elastic or piezoelectric data on any of the wurtzite-type binary compounds have been available, a quantitative check of the macroscopic theory of the distortion and polarization of these compounds[1] has not hitherto been possible. Recent measurements of the elastic[2] and piezoelectric[3] constants of CdS, however, now allow a partial verification of the theory and also an estimate of the size of the postulated charge±fe per ion.

The pertinent data are, for CdS,

$$(2s_{13}-s_{11}-s_{12}) = -3.1302\times10^{-12}\ \text{cm}^2/\text{dyne},$$

$$(s_{33}-s_{13}) = 3.2591\times10^{-12}\ \text{cm}^2/\text{dyne},$$

$$(d_{33}-d_{13}) = \pm12.3\times10^{-8}\ \text{esu/dyne}.$$

Unfortunately the signs of the piezoelectric constants are not easily determined. We have assumed, with Tanaka and Tanaka, opposite signs for d_{33} and d_{13}.

When these numbers are inserted into Eq. (21a) of footnote reference 1, the following relation is obtained:

$$\frac{(c/a)-(c_0/a_0)}{(c_0/a_0)} = -0.0089\,\text{f}^2 \pm 0.0014\,\text{f}. \qquad (1)$$

It is to be noted that the second term on the right (piezoelectric distortion) is about ten times larger than

was estimated in footnote reference 1, but it is still considerably smaller than the first term (anisotropy of the Coulomb forces). The measured value of (c/a) in CdS is 1.623, and hence

$$f=0.75 \text{ or } 0.91, \qquad (2)$$

with the uncertainty coming from the unknown signs of the piezoelectric constants.

Thus the c/a distortion can quantitatively be accounted for with a value of f slightly less than 1, i.e., with a lattice slightly less ionic than Cd^+S^-. Roughly the same value of f is required in a quantitative theory of the optical double-refraction.[4] Such an effective ionic charge is very reasonable. Let us imagine, with Goodman,[5] "neutral" Cd^0S^0 brought together into a crystal. Because of the electronegativity difference there will be a shift of electronic charge from Cd to S. This shift will stop short of $Cd^{+}{}^{+}S^{-}{}^{-}$ because of opposing covalent tendencies.

It is to be hoped that elastic and piezoelectric measurements will be made on the other wurtzite like compounds. It might then be possible to establish a semi-empirical relationship between f and electronegativity difference in compounds with the wurtzite structure.

Note added in proof. The elastic and piezoelectric constants of CdS have just been measured by D. Berlincourt, H. Jaffe, H. H. N. Krueger, and L. Shiozawa [Phys. Rev. (to be published)]. They find $d_{33}-d_{13}=+46.5\ 10^{-8}$, in large disagreement with Tanaka and Tanaka. Use of their numbers exclusively in Eq. (1) makes the right side $-0.0187\ f^2+0.00514\ f$, yielding $f=0.73$. Their elastic data differ only slightly from Bolef *et al.*; and it is now evident that the f^2 term, which arises from a subtraction of nearly equal numbers, is extremely sensitive to small changes in the s_{ij}.

* Supported by the National Science Foundation

† On leave from the University of Pittsburgh, Pittsburgh, Pennsylvania.

[1] F. Keffer and A. M. Portis, J. Chem. Phys. **27**, 675 (1957).

[2] D. I. Bolef, N. T. Melamed, and M. Menes, J. Phys. Chem. Solids (to be published). This work is more accurate and more complete than T. Masumi and T. Tanaka, J. Phys. Soc. Japan **14**, 1313 (1959).

[3] T. Tanaka and S. Tanaka, J. Phys. Soc. Japan **15**, 726 (1960).

[4] F. Keffer, J. Chem. Phys. **32**, 62 (1960).

[5] C. H. L. Goodman, J. Electronics **1**, 115 (1955); *ibid.* (to be published).

Molar Sound Velocity in Inorganic Acids

P. R. K. L. Padmini, K. Subba Rao, and B. Ramachandra Rao

Ultrasonic Laboratories, Physics Department, Andhra University Waltair, India

(Received July 8, 1960)

Nomato[1] studied the variation of molar sound velocity in aqueous solutions of weak acids, such as formic, acetic, propionic, and butyric acids and strong acids, such as nitric and sulphuric acids. In all these cases he found a definite linear variation of molar sound velocity with concentration. In the first four acids he computed the theoretical values for R and found that they were always greater than the experimental values. He explained the differences as due to the highly associative nature of the acids and water.

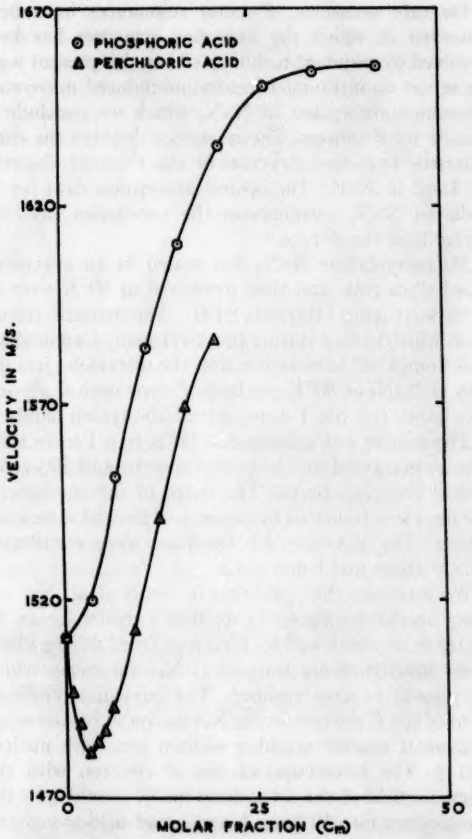

Fig. 1. Variation of ultrasonic velocity with concentration.

In the present investigation, the molar sound velocity in the aqueous solutions of sulphuric, nitric, phosphoric, and perchloric acids is studied. The data for the first two acids is taken from Porosorov's[2] paper and the latter two are studied by the authors. Though there is a significant minimum in the ultrasonic velocity at a concentration of 1.6 mole/liter for perchloric acid as seen from Fig. 1 and similar nonlinear variations in the case of nitric and sulphuric acids as reported by Porosorov, the molar sound velocity exhibited remarkable linear variation with concentration expressed in molar fractions as illustrated in Fig. 2. The results for sulphuric acid are available up to 99% concentration but values up to 50% concentration only are shown in Fig. 2. By extrapolating the graphs shown in Fig. 2 to

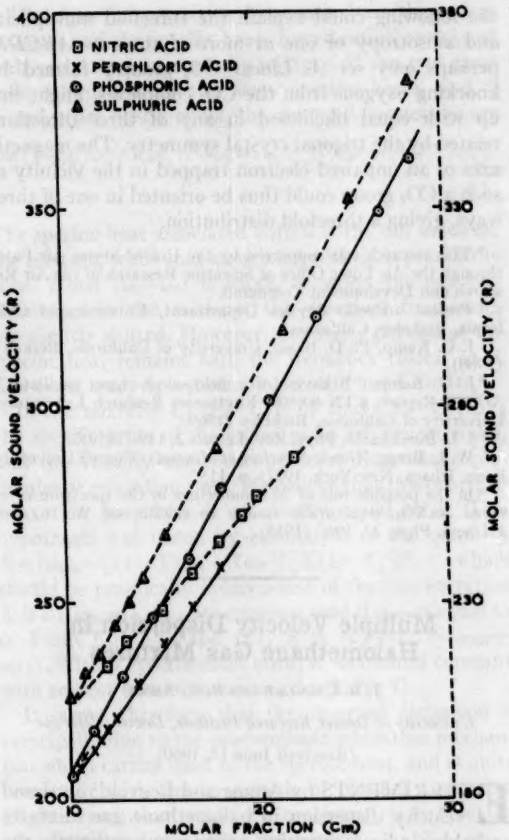

FIG. 2. Variation of Molar sound velocity with concentration.

100% concentration, the molar sound velocity for the pure acid is obtained and these are compared with the theoretical values computed by Rao's atomic-increments method. In this computation due account is taken of the contribution of -25 to semipolar bond as previously estimated.[3] It is well known that sulphuric acid has two, nitric and phosphoric acids, one each, and perchloric acid three semipolar bonds. The experimental values of R thus estimated are presented in the Table I along with the theoretically computed values of R with and without taking into account the contribution of the semipolar bond. It is interesting to note that there is better agreement with the theoretical values computed after taking into account the contribution of semipolar bonds. There is a fairly good agreement between the experimental and theoretical values in the case of perchloric, sulphuric and nitric acids and there is large deviation in the case of phosphoric acid. This may be attributed partly to the uncertainty of estimating R value for phosphorus. The interesting feature of this investigation is the perfect linear variation of R with concentration even in the case of inorganic acids.

TABLE I.

Acid	R Experimental	R Theoretical including semipolar bond	R Theoretical excluding semipolar bond
Nitric acid	410	428.5	453.5
Sulphuric acid	580	626.0	676.0
Perchloric acid	496	540.0	615.0
Phosphoric acid	549	717.0	742.0

The authors are indebted to Council of Scientific & Industrial Research, India for financial assistance of this research project.

[1] O. Nomato, Bull, Kobayaski Inst. Phys. Research 7, 136 (1957).
[2] P. Porosorov, Zhur. Fiz. Khim. 14, 384 (1940).
[3] P. R. K. L. Padmini, K. Subba Rao, and B. Ramachandra Rao, Trans. Faraday Soc. (to be published).

Electron Spin Resonance in Neutron-Irradiated Calcite*

J. C. KEMP†
Electronics Research Laboratory, University of California, Berkeley, California

(Received June 8, 1960)

AN interesting spin resonance spectrum has been observed in single crystals of natural calcite subjected to fast neutrons in a reactor. The lines are extremely narrow (widths of 0.1 gauss were noted) and showed thermal relaxation times T_1 of several seconds at liquid helium temperatures; they have been used to advantage in electron spin echo[1] and pulsed maser[2] experiments. Selected high purity calcite, with only one ppm of manganese and no detected important amount of other impurities, was used; it was believed that impurities played no role in the spectrum reported here. Mn^{++} lines were in all cases much weaker than the principal irradiation-induced lines. Three crystals, designated I, II, and III, weight 900 mg each, were given total dosages of 10^{17}, 10^{18}, and 10^{19} fast neutrons, respectively; a brownish color resulted, sample III being almost opaque. Unlike some short-lived centers in calcite,[3] these centers have not faded during months' storage at room temperature.

The main features of the spectrum, observed at 8700 Mc in sample I at 77°K, were: (a) three strong equal-intensity lines, called the A lines, located within 5 gauss of the free-electron H_0 (Zeeman-splitting) field value; and (b) twelve lines about one-fifth as strong as the A lines, the four threefold sets $BCDX$, located within 50 gauss of the free-electron H_0 value on the low-field ($g>2$) side. Additional lines, mostly much weaker than $BCDX$, were also present. The lines were anisotropic, the sets $ABCDX$ showing certain symmetries, related to the crystal symmetry, under variation of the

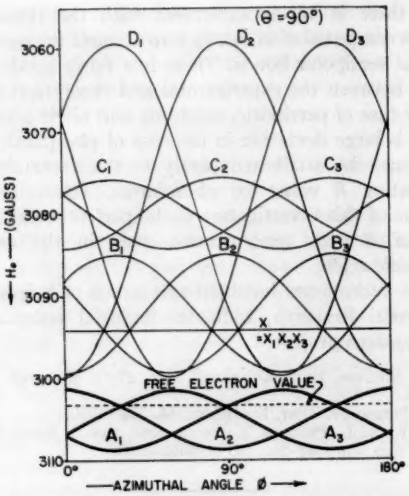

FIG. 1. Behavior of prominent spin resonance lines in neutron-irradiated calcite as function of azimuthal angle ϕ. The Zeeman field (H_0) direction is in a plane normal to the c axis and makes an angle ϕ with a fixed direction in this plane. Constant frequency (8700 Mc) spectra were taken at intervals $\Delta\phi=5°$.

H_0 direction with respect to the crystal axes. Figure 1 shows the behavior of these lines as H_0 was rotated in a plane normal to the c axis, i.e., with the polar angle θ between H_0 and the c axis maintained at 90°. The azimuthal angle ϕ was measured between the plane of H_0 and the c axis, and a twofold axis direction.[4] Lines $X_1X_2X_3$ were coincident for $\theta=0°$ and for $\theta=90°$ for any ϕ, but slightly separated otherwise. For a particular ϕ, as θ was varied from $\theta=90°$ (Fig. 1) to $\theta=0°$ (H_0 along the c axis), the A lines converged to a single line at an H_0 value 5 gauss smaller than their center of gravity in Fig. 1. Sets B, C, and D behaved somewhat similarly, with center of gravity shifts of -7, $+14$, and -30 gauss, respectively. This compact spectrum was well resolved only in sample I and at $T\lesssim 77°$K, but seemed generally the same in samples I and II and over the range 1.5°K—77°K.

The width of all the lines at $T\lesssim 77°$K was 0.12 gauss in sample I, containing $(2\pm1)\times10^{16}$ spins per single A line, and 0.6 gauss in sample II, with 10^{17} spins per A line. Relaxation times for the A lines in sample I, measured during maser and spin echo experiments,[1,2] were $T_1=(5\pm2)$ seconds at 1.5°K and $T_1\sim2$ μsec at 77°K; transverse relaxation time T_2 was 18 μsec at 1.5°K, compared with an inverse line half-width T_2^* of 0.8 μsec. Hyperfine broadening being negligible, the linewidth for $T\lesssim 77°$K was a concentration-dependent spin-spin width; broadening was inhomogeneous and presumably due mostly to nonsecular dipolar interactions between spins in the several lines.

Hyperfine splittings and fine structure (with $S>\frac{1}{2}$ spins) seem unlikely causes of the major multiplicities in this spectrum. Of several structures possibly present, the following could explain the threefold multiplicity and anisotropy of one or more of the sets $ABCDX$, perhaps only set A. Linear CO_2 groups,[5] formed by knocking oxygens from the CO_3 complexes, might line up with equal likelihood in any of three directions related by the trigonal crystal symmetry. The magnetic axes of an unpaired electron trapped in the vicinity of such a CO_2 group could thus be oriented in one of three ways, giving a threefold distribution.

* This research was supported by the United States Air Force through the Air Force Office of Scientific Research of the Air Research and Development Command.

† Present address: Physics Department, University of California, Berkeley, California.

[1] J. C. Kemp, Ph.D. thesis, University of California, Berkeley (1960).

[2] J. C. Kemp, "Behavior of a field-swept maser oscillator," AFOSR Report #TN-60-509, Electronics Research Laboratory, University of California, Berkeley (1960).

[3] J. L. Burckhardt, Phys. Rev. Letters **2**, 149 (1959).

[4] W. L. Bragg, *Atomic Structure of Minerals* (Cornell University Press, Ithaca, New York, 1937), p. 115.

[5] On the possible role of NO_2 molecules in the spectrum of x-rayed $NaNO_3$, structurally similar to calcite, see W. B. Ard, J. Chem. Phys. **23**, 1967 (1955).

Multiple Velocity Dispersion in Halomethane Gas Mixtures

J. B. CALVERT AND R. C. AMME

University of Denver Research Institute, Denver, Colorado

(Received June 13, 1960)

EXPERIMENTS by Amme and Legvold[1] on sound velocity dispersion in halomethane gas mixtures probably indicate multiple dispersion, although the dispersion curves are characteristic of a single relaxation frequency. We shall assume parallel excitation of the vibrational degrees of freedom for the two gases of a mixture. If ω_A, ω_B are the relaxation frequencies in gases A and B, respectively, and ω_{AB}, ω_{BA} are the "interaction" frequencies, the frequencies associated with each gas in the mixture are

$$\omega_1=(1-X)\omega_A+X\omega_{AB}, \qquad \omega_2=X\omega_B+(1-X)\omega_{BA}, \quad (1)$$

where X is the mole fraction of gas B.

TABLE I. Observed relaxation frequencies and the quantity R in halomethane gas mixtures.[a]

conc. X	CCl_3F—$CHCl_2F$ ω_{obs}	R	CF_4—$CHClF_2$ ω_{obs}	R
0.0	4.2	...	1.3	...
0.1	4.6	24	...	...
0.3	10.0	23	3.0	5.2
0.5	16.0	24	4.5	5.7
0.7	24.0	25	6.2	5.8
0.9	...	...	9.2	4.7
1.0	40.0	...	10.5	...

[a] ω_{obs} and R are in units of 10^5 sec^{-1}, data computed from work cited in footnote 1.

The observed relaxation frequencies[2] are dependent on ω_1, ω_2 and the specific heats for vibration associated with each component of the mixture. If the two gases have approximately the same specific heats, and if ω_1 and ω_2 are nearly equal, the observed frequencies are

$$\tilde{\omega}=(1-X)\omega_1+X\omega_2, \qquad \omega_0=(c_0/c_\infty)[X\omega_1+(1-X)\omega_2]. \tag{2}$$

The specific heat associated with $\tilde{\omega}$ is the full value for the mixture, while that associated with ω_0 is practically zero. When $(\omega_1-\omega_2)$ is small, or when one gas predominates in the mixture, the observed frequencies are slightly shifted. However, the major portion of the specific heat remains with the frequency closest to $\tilde{\omega}$. The exact analysis is given by Herzfeld and Litovitz.[3]

In the mixtures $CClF_3$—$CHCl_2F$ and CF_4—$CHClF_2$ the specific heats of the mixed gases are almost equal, and the velocity dispersion occurs with a single predominant relaxation time. We believe that this observed relaxation frequency is practically equal to $\tilde{\omega}$. This hypothesis was tested by calculation of the quantity $R=\{\omega_{obs}-[(1-X)\omega_A+X\omega_B]\}[X(1-X)]^{-1}$, which should be practically independent of the concentration X if $\omega_A, \omega_B, \omega_{AB}, \omega_{BA}$ are constant, and if ω_{obs} is equal to $\tilde{\omega}$. From Eqs. (1) and (2), R is $(\omega_B+\omega_A)-(\omega_{AB}+\omega_{BA})$. Within experimental error, R was found constant with respect to concentration (See Table I).

It seems, therefore, that the observed dispersion is principally due to the predominant relaxation mechanism which carries most of the specific heat, and is quite consistant with the hypothesis of parallel excitation. Higher resolution would be necessary to resolve the contribution of the minor mechanism.

[1] R. C. Amme and S. Legvold, J. Chem. Phys. **26**, 514 (1957).
[2] Throughout this letter, the "observed" frequencies are the inflection-point frequencies multiplied by C_0/C_∞.
[3] K. F. Herzfeld and T. A. Litovitz, *Absorption and Dispersion of Ultrasonic Waves* (Academic Press, Inc., New York, 1959), p. 93ff.

Decomposition of Activated *sec*-Butyl Radicals from Different Sources and Unimolecular Reaction Theory.*

R. E. Harrington and B. S. Rabinovitch

Department of Chemistry, University of Washington, Seattle 5, Washington

AND

H. M. Frey

Department of Chemistry, University of Southampton, England

(Received June 10, 1960)

THE study of the unimolecular decomposition of chemically activated *sec*-butyl radicals[1,2] to give propylene and methyl has been extended here to include radicals formed from H and D atoms with butene-1; these have minimum total excess internal energy, above the critical decomposition energy, of around 8.9 and 10.7 kcal/mole respectively,[3] compared to 8.0[1] and 9.8[2] kcal/mole for radicals formed from H and D+*cis*-butene-2 respectively.

The average experimental rate constants k_a at 25°C are shown in Fig. 1 as functions of S and D, the amounts of radical decomposition D and collisional stabilization S, and are extrapolated to the limits of high and low pressure. In Table I, the results are compared to calculated quantities.[4] The method of calculation and the molecular vibration models used are as given previously.[2] Within the experimental error, reasonable correspondence is obtained in both our present and in earlier work between observed values and those calculated by us under the assumptions that all internal degrees of freedom are active and that rate of reaction varies with total excess internal energy.

In a general way, these findings tend to support the importance of vibrational anharmonicity, and the unimolecular reaction model of coupled vibration modes of O. K. Rice and Kassel. A more specific criterion has been remarked recently by Frey[5]: A molecule may be activated by processes which give rise to characteristically different excitation of the normal modes, e.g., random thermal excitation of 1,1-dimethylcyclopropane, as contrasted with chemical activation by its production from methylene+isobutene; nonrandomization of internal energy during the lifetime of excited molecules should result in different rates of reaction in the two cases (other things being equal or accounted for). Frey concluded, from an observed variation in the relative rates of production of 3-methylbutene-1 and 2-methylbutene-2 in these two cases, that N. B. Slater's model of orthogonality of the normal mode vibrations was supported.

Now formation of activated *sec*-butyl radicals from butene-1 and *cis*-butene-2 involves different processes. With the former, the atom attaches to C_1 of the butene-1 molecule, while the C_3-C_4 bond is later ruptured. With the latter, the atom attaches to C_2, a part of the breaking C_1—C_2 bond. Since the radicals are formed in

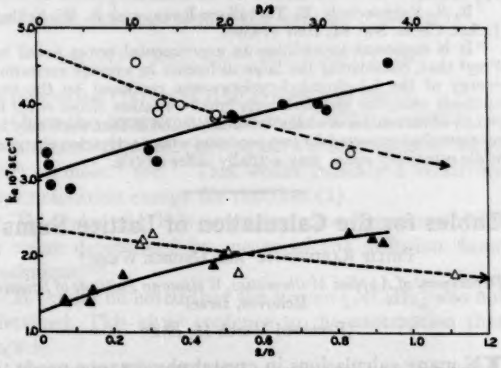

FIG. 1. k_a for *sec*-butyl radicals against S/D, ▲, and D/S, △; k_a for *sec*-butyl-d_1 radicals against S/D, ●, and D/S, ○. 25°C.

TABLE I. Butene-1 k_a values (10^7 sec^{-1}) and butene-1:*cis*-butene-2 k_a ratios at 25°C.

	k_{a00}	k_{a0}	k_{a00}/k_{a0}	k_{a00}	k_{a0}	k_{a00}/k_{a0}
butene-1		hydrogen			deuterium	
obs	2.4	1.3	1.8	4.7	3.1	1.5
calc	2.29	1.57	1.46	4.02	2.92	1.38
butene-1: *cis*-butene-2						
obs	1.60	1.44		1.42	1.41	
calc	1.41	1.47		1.38	1.43	

uniquely different ways (leading to the presumption of significant differences with respect to C—C rupture in the normal mode excitations), but decompose at virtually the same rates, describable by the same model in which only the total excess energy enters, migration of internal energy among the various vibrational modes presumably occurs before decomposition. This conclusion weighs against the orthogonality assumption of Slater's theory, and supports Butler and Kistiakowsky who recently found evidence for migration of energy in their studies of methylcyclopropane energized in several ways.[6] Our data[7] on the relative rates of geometric and structural isomerization of cyclopropane-d_2, excited in characteristically different ways, also supports this conclusion.[8]

* Abstracted from the Ph.D. Thesis, University of Washington, 1960, of R.E.H., which contains a fuller account. This work was supported by the ONR.

[1] B. S. Rabinovitch and R. W. Diesen, J. Chem. Phys. **30**, 735 (1959).

[2] R. E. Harrington, B. S. Rabinovitch, and R. W. Diesen, J. Chem. Phys. **32**, 1245 (1960).

[3] The estimated activation energy for addition of an atom to butene-1 is ~0.6 kcal/mole less than for butene-2, as inferred from the results of M. D. Scheer and R. Klein, J. Phys. Chem. **63**, 1517 (1959).

[4] The data for butene-1 are somewhat complicated by a small amount (~5%) of *n*-butyl radical formation by nonterminal addition, evidenced particularly by its observed decomposition product ethylene and small amounts of stabilization product *n*-pentane (from *n*-butyl+methyl).

[5] H. M. Frey, Trans. Faraday Soc. **56**, 51 (1960).

[6] J. N. Butler and G. B. Kistiakowsky, J. Am. Chem. Soc. **82**, 759 (1960).

[7] B. S. Rabinovitch, E. Tschuikow-Roux, and E. W. Schlag, J. Am. Chem. Soc. **81**, 1081 (1959).

[8] It is suggested in addition to experimental errors noted by Frey[5] that, considering the large difference in average excitation energy of the 1,1-dimethyl-cyclopropane produced by the two methods used, the comparatively small variation (from ~1.0 to ~1.6) of rate ratios of olefin formation found in that work may be no more than expected for two processes whose activation energies, while ostensibly equal, may actually differ a little.

Tables for the Calculation of Lattice Sums*

PHILIP RABINOWITZ* AND GEORGE WEISS†

Department of Applied Mathematics, Weizmann Institute of Science, Rehovot, Israel

(Received March 11, 1960)

IN many calculations in crystal physics, one needs to evaluate sums of the form

$$S_p^{kmn}(x_1, x_2, x_3) = \sum_{j_1,j_2,j_3=-\infty}^{\infty} [j_1^k j_2^m j_3^n/(j_1^2+j_2^2+j_3^2)^p] \times \exp[i\pi(j_1x_1+j_2x_2+j_3x_3)] \quad (1)$$

where the term with $j_1=j_2=j_3=0$ is omitted. This summation might be over all integers, all odd integers, or all even integers. By means of the representation

$$z^{-p} = \{\Gamma(p)\}^{-1}\int_0^\infty t^{p-1}\exp(-zt)\,dt,$$

the sum in Eq. (1) can be written:

$$S_p^{kmn}(x_1, x_2, x_3) = \{\Gamma(p)\}^{-1}\int_0^\infty t^{p-1} \times U(x_1, t)U(x_2, t)U(x_3, t)\,dt \quad (2)$$

where, for example,

$$U(x_1, t) = \sum_{r=-\infty}^{\infty} r^k \exp[i\pi r x_1 - r^2t^2], \quad (3)$$

where the sum may be over all integers, all odd integers, or all even integers. In the present method for evaluating $S_p^{kmn}(x_1, x_2, x_3)$ by means of Eq. (2), we tabulate values of the U functions at values of t suitable for 16-point Laguerre integration. That is, we approximate

$$\int_0^\infty t^n f(t)\,dt \sim \sum_{k=0}^{16} a_k(n) f(x_{kn}) \quad (4)$$

where the x's are roots of generalized Laguerre polynomials and the U's are obtained from derivatives of these polynomials.[1]

We have tabulated six types of functions

$$G_k(x, t) = \sum_{j=1}^{\infty} j^k \exp(-j^2t)\cos\pi jx$$

$$\tilde{G}_k(x, t) = \sum_{j=1}^{\infty} (2j)^k \exp(-(2j)^2t)\cos\pi 2jx$$

$$\underline{G}_k(x, t) = \sum_{j=1}^{\infty} (2j-1)^k \exp(-(2j-1)^2t)\cos\pi(2j-1)x$$

$$H_k(x, t) = \sum_{j=1}^{\infty} j^k \exp(-j^2t)\sin\pi jx$$

$$\tilde{H}_k(x, t) = \sum_{j=1}^{\infty} (2j)^k \exp(-(2j)^2t)\sin 2\pi jx$$

$$\underline{H}_k(x, t) = \sum_{j=1}^{\infty} (2j-1)^k \exp(-(2j-1)^2t)\sin\pi(2j-1)x. \quad (5)$$

The tables contain an x range of $x=0(.05)1.0$ and are good to six significant figures. Tables IIa and IIIa are valid for $k=0$, IIb and IIIb for $k=2$, and IIc and IIIc for $k=4$. Table I facilitates evaluation of the integrals for other values of k by presenting the Laguerre abscissas and various powers of these abscissas. The tables

were prepared by direct summation of all terms less than 10^{-35} in magnitude. The calculations were done on WEIZAC, the digital computer at the Weizmann Institute of Science.

As an example of the use of these tables we cite the representation of $S_{5/2}{}^{110}(x, x_2, x_3)$:

$$S_{5/2}{}^{110}(x_1, x_2, x_3) = [4/3(\pi)^4]\int_0^\infty t^3 [H_1(x_1, t)H_1(x_2, t) + 2H_1(x_1, t)H_1(x_2, t)G_0(x_3, t)]dt, \quad (6)$$

in which form the numerical integration formulas can be applied.

These tables have been deposited as Document number 6393 with the ADI Auxiliary Publications Photoduplication Service, Library of Congress, Washington 25, D.C. A copy may be secured by citing the document number and by remitting for photoprints or for 35-mm microfilm. Advance payment is required. Make checks or money orders payable to Chief, Photoduplication Service, Library of Congress.

* This research was partially supported by the United States Air Force through the Air Force Office of Scientific Research.

† Present address: Institute for Fluid Dynamics and Applied Mathematics, University of Maryland, College Park, Maryland.

[1] P. Rabinowitz and G. Weiss, Math Tables and Other Aids to Comp. *XIII*, 285 (1959).

Rate of Reaction of Nitrogen Atoms with Ethylene*

JOHN T. HERRON

Mass Spectrometry Section, National Bureau of Standards, Washington, D. C.

(Received June 15, 1960)

SOME preliminary results have been obtained on a mass spectrometric study of the reaction of nitrogen atoms with ethylene.

The reaction was studied in a simple flow system. Nitrogen gas was partially dissociated in a 2450-Mc electrodeless discharge. The products flowed through a 0.7-cm tube, across the 1-mil glass sampling leak of the mass spectrometer, and then to the pump. Reactant gas was added through a concentric tube 18 cm upstream of the leak. Normal operating conditions were 2.8 mm of Hg total pressure, 50 cc/min N_2 flow, and 10^{-2} sec reaction time. The reaction zone could be heated to 350°C, as measured by a glass-encased thermocouple.

Changes in the concentrations of stable materials were observed by means of conventional mass spectrometric techniques, using 70-v ionizing electrons. Relative nitrogen atom concentrations were similarly measured, except that nominal ionizing energies of 17.5 v were used.

Absolute N atom concentrations were determined using the NO titration technique.[1,2]

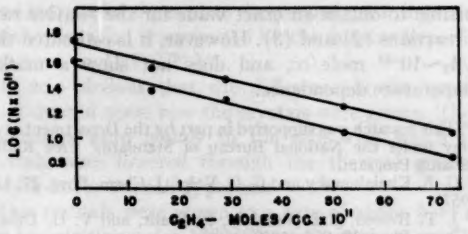

FIG. 1. Log (N) vs (C_2H_4) at 328°C.

The reaction was studied from 27°C to 327°C. Both initial C_2H_4 and N atom concentrations were varied. Initial C_2H_4 concentration was varied from about 10^{-9} mole/cc to 10^{-10} mole/cc. Two different initial N atom concentrations were used, approximately 6×10^{-10} mole/cc, and 4×10^{-10} mole/cc. Over the temperature range covered, most of the nitrogen atoms were destroyed without equivalent decomposition of ethylene. The disappearance of N atoms was found to be first order in both N and C_2H_4 at temperatures greater than 150°C. A reaction mechanism compatible with these observations is

$$N + C_2H_4 \xrightarrow{k_1} [NC_2H_4], \quad (1)$$

followed by either catalytic recombination,

$$N + [NC_2H_4] \xrightarrow{k_2} N_2 + C_2H_4, \quad (2)$$

or dissociation,

$$[NC_2H_4] \xrightarrow{k_3} \text{products}. \quad (3)$$

This mechanism is identical to that proposed by Evans, Freeman, and Winkler[3] in their unified mechanism for the reaction of nitrogen atoms with organic molecules.

The products of reaction (3) are probably HCN and CH_3.[4,5]

If reaction (2) is considerably faster than (1), and the concentration of C_2H_4 is taken to be constant, the rate of disappearance of N atoms reduces to a simple first-order rate expression, the solution of which is

$$\log(N) = \log(N_0) - (2k_1t/2.303)(C_2H_4).$$

A plot of log (N) vs (C_2H_4) is shown in Fig. 1.

Over the temperature interval 200°C to 330°C, k_1 was almost constant, having an average value of 5.8×10^{10} cc mole^{-1} sec^{-1}. This would indicate a relatively low activation energy for reaction (1).

This value of k_1 is in surprisingly good agreement with a value determined by means of the diffusion flame technique.[4,5]

It should be noted that the species $[NC_2H_4]$ was not detected. This gives credence to the assumption that $k_2 \gg k_1$.

Because of the difficulty encountered in accurately measuring the amount of ethylene consumed, it was not

possible to obtain an exact value for the relative rates of reactions (2) and (3). However, it is estimated that $k_3/k_2 \sim 10^{-11}$ mole/cc, and does not show a marked temperature dependence.

* This research was supported in part by the Department of the Army under the National Bureau of Standards' Free Radical Research Program.

[1] G. B. Kistiakowsky and G. G. Volpi, J. Chem. Phys. **27**, 1141 (1957).
[2] J. T. Herron, J. L. Franklin, P. Bradt, and V. H. Dibeler, J. Chem. Phys. **30**, 879 (1959).
[3] H. G. V. Evans, G. R. Freeman, and C. A. Winkler, Can. J. Chem. **34**, 1271 (1956).
[4] J. H. Greenblatt and C. A. Winkler, Can. J. Research **B27**, 721 (1949).
[5] J. Versteeg and C. A. Winkler, Can. J. Chem. **31**, 1 (1953).

Condensation Coefficient of Arsenic Trioxide Glass

A. B. Bestul and D. H. Blackburn
National Bureau of Standards, Washington 25, D. C.

(Received May 13, 1960)

THE condensation coefficient for a surface is defined as the fraction of the molecules striking the surface which condense there. The condensation rate on a surface in equilibrium with its vapor is equal to the maximum rate at which molecules can vaporize from the surface at the prevailing temperature. Only for a small number of substances is it accepted that the condensation coefficient is substantially less than unity.[1] It has been demonstrated that for some substances, low values reported as condensation coefficients may be spurious because limitations on the heat supply to the vaporizing surfaces may have lowered their temperatures below the values indicated.[2] There are reported here the results of some preliminary measurements which indicate that vaporization from arsenic trioxide glass occurs at a rate consistent only with an extremely low value for the condensation coefficient. A value of $<10^{-7}$ is already accepted for the condensation coefficient of monoclinic arsenic trioxide crystals directly on the basis of condensation studies.[3] Without giving the details of the measurements, Stranski reports[4] that the super-cooled liquid has also been observed to have evaporation rates low enough to indicate a condensation coefficient appreciably less than unity. The term "super-cooled liquid" designates uncrystallized matter at temperatures below its freezing point, but above its glass transformation region. In this interval it is in equilibrium with respect to liquidlike states and its properties are unique functions of temperature, which are smooth extrapolations of relations between properties and temperature for the liquid above the melting point. The term "glass" designates uncrystallized matter at temperatures below the glass transformation region. In cooling through this region the relations between properties and temperature deviate from smooth extrapolations of the relations at higher temperatures, and become no longer unique for a given substance. The glass transformation region for arsenic trioxide is estimated to be above 200°C. The temperature of the experimental sample which Stranski refers to as a "super-cooled liquid" is not known.

The maximum rate of vaporization from arsenic trioxide glass at 194°C has been determined by measurement of weight loss in vacuum. The principal specimen used had a surface area of 2.07 cm² and was roughly a cube. The glass was prepared from Baker Analyzed Reagent Primary Standard arsenic trioxide powder by melting at 575°C and recooling, both in an evacuated sealed Pyrex tube.

The specimen was suspended in a thermostatted high speed vacuum chamber jacketed by refluxing *cis*-decalin, of which the boiling point was measured as 194°C. The suspension was 0.0014 in. diam. tungsten wire looped once around the specimen. The calculated rate of heat loss from the specimen through this wire under the experimental conditions is 1.6×10^{-6} cal sec^{-1}. This figure is a factor of 10^{-4} less than the latent heat requirement of the smallest rate of vaporization mentioned in this note. The specimen and the wire were weighed with an analytical balance before and after such exposure to vacuum. The results of Littlewood and Rideal[2] demonstrate that reliable measurements of the maximum rate of vaporization can be obtained without a cold spot near the specimen to serve as a sink for the vapor species. The experimental temperature was determined by separate measurements using a calibrated thermocouple fixed firmly against the surface of a specimen. However, it is not these measurements, but arguments given later, which are relied on to eliminate the possibility of dismissing the results reported here on the basis of surface cooling. Three determinations varying from about 2 to 19 hours of exposure to vacuum, respectively, gave an average value of $1.3\pm 0.2\times10^{-8}$ g cm^{-2} sec^{-1} for the rate of vaporization.

Since the vitreous state is metastable with respect to the crystalline, the vapor pressure of the crystal may be taken as a lower limit for that of a glass of the same composition. The value for monoclinic arsenic trioxide, which is the stable form, at 194°C is 0.11 mm Hg.[5] According to the kinetic theory of gases, a surface surrounded by gaseous As_4O_6 molecules (the vapor species) at this pressure and temperature would be struck by them at the rate of 5.9×10^{-3} g cm^{-2} sec^{-1}. This rate divided into the experimentally determined rate of vaporization reported above gives a ratio of 2.2×10^{-6} as an upper limit for the value of a condensation coefficient for arsenic trioxide glass.

Using the Stefan-Boltzmann radiation law and an arbitrary emissivity coefficient of 0.7, calculations have been made as a function of surface temperature of the maximum rate of vaporization which can be supplied by net radiation from a surrounding heat source at 194°C. Also as a function of temperature, calculations

have been made of the maximum vaporization rate (corresponding to a condensation coefficient of unity) consistent with the vapor pressure of monoclinic arsenic trioxide. These two functions intersect at 155°C at a vaporization rate of 2.3×10^{-4} g cm^{-2} sec^{-1}. These values are taken as approximations to the corresponding values for the glass. Accordingly, if the condensation coefficient of arsenic trioxide glass were in fact unity, undetected surface cooling could not lower the observed rate of vaporization below the above value, which would correspond to an apparent condensation coefficient of 0.04. Since the value reported in this note is lower than this by four orders of magnitude, the entire deviation from unity can hardly be dismissed on the basis of undetected surface cooling. The latent heat for vaporization of monoclinic arsenic trioxide at the experimental rate reported for the glass can be supplied by net radiation alone with a surface temperature lowering of about 0.001°C. This would depress the vaporization rate of the monoclinic form to 0.9999 times the value at the nominal temperature. In order to depress the vapor pressure of monoclinic arsenic trioxide to a value which would yield the reported vaporization rate for the glass with a condensation coefficient of unity, the temperature of the vaporizing surface would have to be lowered to 69°C.

The fact that the super-cooled liquid and the glass both have low condensation coefficients is consistent with the view of the vitreous condition as a non-equilibrium condition of liquidlike molecular configuration.

[1] L. Brewer and J. S. Kane, J. Phys. Chem. **59**, 105 (1955).
[2] R. Littlewood and E. Rideal, Trans. Faraday Soc. **52**, 1598 (1956).
[3] O. Knacke and I. N. Stranski, *Progress in Metal Physics*, edited by B. Chalmers and R. King (Pergamon Press, New York, 1956), Vol. 6, p. 209.
[4] I. N. Stranski and G. Wolff, Research (London) **4**, 15 (1951).
[5] J. A. Schulman and W. C. Schumb, J. Am. Chem. Soc. **65**, 878 (1943).

Effect of Thermal Treatment of Paramagnetic Resonance Spectra of Rare Earth Impurities in Calcium Fluoride*

E. FRIEDMAN AND W. LOW
Department of Physics, The Hebrew University, Jerusalem, Israel
(Received May 27, 1960)

DURING the last few years we have reported paramagnetic resonance spectra of rare earth ions in calcium fluoride.[1-4] These spectra show that trivalent rare-earth ions are substituted for the calcium ions and that the majority of the ions are situated at a site of cubic point-symmetry. On the other hand, the Oxford group has published paramagnetic resonance data on similar rare-earth ions in calcium fluoride indicating axial symmetry.[5-7] They conclude that charge compensation is probably obtained by a fluorine ion situated in an interstitial site next to the paramagnetic impurity. This explanation is supported by the fluorine hyperfine structure in CaF_2:U^{3+}.[5,8]

It was obvious that the difference in the spectra must depend upon how the crystals were grown. These differences were mainly in the rate with which the crystals were lowered through the thermal gradient and/or in the annealing process.

Our crystals were grown at a rate of about $\frac{1}{2}\rightarrow1$ in. per hr (melting point 1380°C), whereas those used by the Oxford group were grown at a very slow rate.[9] We should like to report here supporting evidence that the annealing process is one of the main factors in accounting for the difference between these two types of crystals. We are now able to transform the point-symmetry about the paramagnetic trivalent ion from axial to cubic symmetry or vice versa with relative ease.

Most of the experiments were made on calcium fluoride containing $0.01\%\rightarrow0.001\%$ gadolinium. This paramagnetic impurity was chosen because of the ease with which the paramagnetic resonance spectra can be detected. The results, however, are not limited to this particular ion, since similar effects were observed with Ce^{3+} and U^{3+}.

The annealing procedure was as follows. The crystals were contained in a graphite crucible surrounded by PbF_2 as a scavenger. A constant flow of helium was maintained through the inside tube of the furnace so as to exclude the presence of air. The furnace was heated to 1000°C at a rate of 200°C per hour, and kept at 1000°C for one hour until all the PbF_2 vapor had been driven off. The temperature was increased to 1200°C in one to two hours and kept at this temperature for 18 hours. If a crystal, containing predominantly gadolinium in cubic sites, was cooled slowly at a rate of 100° per hour one obtained a crystal in which the gadolinium showed axial symmetry. The ratio of the number of sites with axial to cubic symmetry was in excess of 50:1. This crystal was then given the same heat treatment except that it was quenched from 1200°C to room temperature in one to two hours. The axial symmetry spectrum nearly disappeared and the cubic spectrum became stronger by a factor of thirty. It has also been found that the conversion from one point-symmetry to the other depends on the length of time the crystal is held at 1200°C. A crystal heated at 1200° from two to four hours gives only a partial conversion, the amount of cubic and axial sites being of the same order of magnitude. Also, if the crystal is held at a lower temperature the conversion is less efficient.

These data indicate that the excess F^- is not tightly bound to the cube nearest to the trivalent impurity ion at high temperatures. If the crystal is quenched, the excess fluorine has no time to diffuse to the energetically more stable sites near the trivalent ion.

The partial conversion from one point-symmetry to another will no doubt effect the ionic conductivity

in doped calcium fluoride crystals. The results of conductivity measurements as a function of temperature by Ure[10] should be, therefore, reinterpreted taking into account the different activation energies of F^- randomly distributed and those located near the trivalent ion.

We are investigating the change of the optical absorption spectrum of a number of rare earth ions as function of a change of the point-symmetry from axial to cubic symmetry. Similarly the effects of the change of point-symmetry on the color centers in irradiated crystals is being planned.

* Supported in part by the U. S. Air Force, Air Research, and Development Command, through its European Office.

[1] W. Low, Phys. Rev. **109**, 275 (1958).
[2] W. Low, Phys. Rev. **118**, 1608 (1960).
[3] M. Dvir and W. Low, Proc. Phys. Soc. (London) **75**, 136 (1960).
[4] W. Low, Proc. Phys. Soc. (London) (to be published).
[5] B. Bleaney, P. M. Llewellyn, and D. A. Jones, Proc. Phys. Soc. (London) **B69**, 858 (1956).
[6] J. M. Baker, W. Hayes, and D. A. Jones, Proc. Phys. Soc. (London) **73**, 942 (1959).
[7] J. M. Baker, B. Bleaney, and W. Hayes, Proc. Roy. Soc. (London) **A247**, 141 (1958).
[8] J. M. Baker, W. Hayes, and M. C. M. O'Brien, Proc. Roy. Soc. (London) **A254**, 273 (1960).
[9] The crystals used by the Oxford group were grown by Dr. D. A. Jones and Dr. R. W. H. Stevenson of the University of Aberdeen. We are grateful to Dr. Stevenson for sending us a sample of his CaF_2:Gd^{3+} crystals.
[10] R. W. Ure, Sr., J. Chem. Phys. **26**, 1363 (1957).

Size Effects Among Isotopic Molecules*

HUBERT W. JOY AND W. F. LIBBY
Department of Chemistry, University of California, Los Angeles

(Received June 22, 1960)

AS Bartel[1] has stated recently, the amplitudes of the zero point vibrations of isotopic molecules will differ by as much as 0.05 A (for hydrogen and deuterium bonded to a heavy atom.) The molal volumes of the solid methanes at low temperatures[2] differ by 6% for the two isotopic forms CH_4 and CD_4—30.94 cc vs 29.2 cc for the molal volumes at the melting points 90.66 and 89.79°K, respectively—in good agreement with the different amplitudes of the stretching mode for methane,[3,4]

$$\{(2912-2085)\cdot[hc/(2\cdot5\cdot10^5)]\}^{\frac{1}{2}} \text{ or } 0.041 \text{ A vs } 1.9 \text{ A}$$

as the mean carbon-carbon distance in solid CH_4, corresponding to an expected $3(.041/1.9)\times100$ or 6.4% increase.

It has long been recognized[5,6] that the equilibrium constants for isotopic reactions will be temperature dependent due to the energy differences in zero point energy. Less well recognized, however, is the possibility of a pressure effect due to the volume differences in the zero point state. Thus a reaction such as

$$H_2O^{18}+CaCO_{3\ \text{calcite}}=H_2O+CaCO_3{}^{18}{}_{\text{calcite}}$$

may have a net change in volume. Assuming that the fractional volume change on isotopic substitution is about equal to the cube of the fractional change in distance from the center of the molecule to the furthermost position of any constituent atom in the course of the normal vibrations in the lowest energy state—

$$\frac{3}{V^{\frac{1}{3}}}\left(\frac{\Delta\omega_{\text{stretching}}\,hc}{2k_{\text{stretching}}}\right)^{\frac{1}{3}},$$

where $\Delta\omega$ is the frequency shift (in cm^{-1} units) on isotopic substitution and V is the average volume per molecule in the state at the temperature considered, then

$$-\Delta V/(hc)^{\frac{1}{3}}=3(\Delta\omega_{CO_3}/2k_{CO_3})^{\frac{1}{3}}V_{CaCO_3}{}^{\frac{1}{3}}-3(\Delta\omega_{H_2O}/2k_{H_2O})^{\frac{1}{3}}V_{H_2O}{}^{\frac{1}{3}}$$

or[4]

$$-\Delta V=(hc)^{\frac{1}{3}}3\left\{\frac{1063\{1-[80/84]^{\frac{1}{3}}\}}{2\cdot10.65\cdot10^5}\right\}^{\frac{1}{3}}1.62\cdot10^{-15}$$

$$=-0.24\cdot10^{-24}\text{ cc/molecule}$$

$$=-0.14\text{ cc/mole},$$

since isotopic substitution of the centrally symmetric oxygen atom in water can to a first approximation cause no volume change. Therefore, if we assume that V for a single O^{18} substitution is $\frac{1}{3}$ of that for the fully substituted ion

$$\partial \ln k/\partial P=+1.9\cdot10^{-6}\text{ atm}^{-1}\text{ (at 298°K)}$$

and at a depth in the ocean of about 3000 feet k is increased by 0.0019. This corresponds to −1° C on the Urey temperature scale.[5,7] This effect should be directly measurable in the laboratory at high pressures, and effects of similar magnitude should apply to the phosphate[8] and silicate oxygen isotopic equilibria with water.

Bartel[1] and Leffels, Llewellyn, and Robertson[9] recently have made a similar explanation for the effects on the rates of certain reactions of the substitution of protium by deuterium in key positions in the reacting molecules. It thus seems likely that isotopic size effects exist for both equilibria and reaction kinetics and that these effects although small may be important in their diagnostic usefulness. They will be enhanced at high pressures, of course.

* This research was supported by the United States Air Force through the Air Force Office of Scientific Research of the Air Research and Development Command.

[1] L. S. Bartel, Tetrahedron Letters No. 6, 13 (1960).
[2] K. Clusius and K. Weigand, Z. physik. Chem. (Leipzig) **B46**, 1 (1940).
[3] Eyring, Walter and Kimbal, *Quantum Chemistry* (John Wiley & Sons, Inc., New York, 1944), p. 79.
[4] Herzberg, *Infrared and Roman Spectra* (D. Van Nostrand and Company, Inc., Princeton, New Jersey, 1945).
[5] H. C. Urey, J. Chem. Soc. **1947**, 562.
[6] H. C. Urey, Science **108**, 489 (1948).
[7] J. M. McCrea, J. Chem. Phys. **18**, 849 (1950).
[8] A. P. Tudge, Geochim. et Cosmochim. Acta **18**, 81 (1960).
[9] K. T. Leffels, J. A. Llewellyn, and R. E. Robertson, Chem. & Ind. (London), **1960**, 588.

Mercury Photosensitized Decomposition of Cyclohexane at High Temperatures

S. Arai, S. Sato, and S. Shida

Laboratory of Physical Chemistry, Tokyo Institute of Technology, Ookayama, Meguro-ku, Tokyo, Japan

(Received March 7, 1960)

Low pressure gas chromatographic technique[1] has been employed for the analysis of products in the mercury photosensitized decomposition of cyclohexane at high temperatures. The observed products were propylene, ethylene, methane, ethane, butadiene, and propane as well as hydrogen, dicyclohexyl, and cyclohexene. At temperatures lower than 200°C only the last three compounds were observed. Gunning *et al.*[2] studied this reaction at room temperature and proposed a reaction mechanism which is consistent with our present data.

In Fig. 1 is shown the time dependence of the relative rate of formation of the main products and in Table I the pressure dependence of the amounts of the main products formed.

It is known that some normal hydrocarbon radicals decompose into olefins and smaller radicals at high temperatures.[3] In the same manner, the cyclohexyl radical produced in the initial process of the reaction may isomerize and decompose at temperatures higher than 200°C. The experimental results suggest the following reaction mechanism.

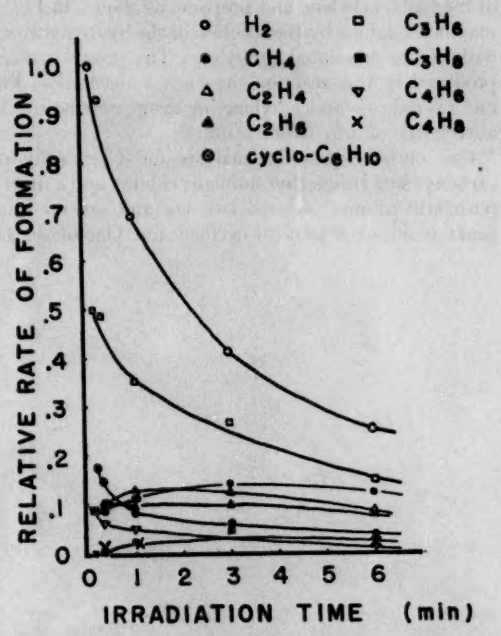

Fig. 1. Time dependence of the relative rates of formation of products in the mercury photosensitized decomposition of cyclohexane at 400°C. The rate of formation of hydrogen in 10 sec is taken as unity. The initial cyclohexane pressure is 50 mm Hg.

$$\text{cyclo } C_6H_{11}\begin{cases}\dot{C}H_2CH_2CH_2CH_2CH{=}CH_2 \rightarrow C_2H_4 + CH_2CH_2CH{=}CH_2 & \text{(a)}\\ CH_3\dot{C}HCH_2CH_2CH{=}CH_2 \rightarrow C_3H_6 + CH_2CH{=}CH_2 & \text{(b)}\\ CH_3CH_2CH_2\dot{C}HCH{=}CH_2 \rightarrow C_2H_5 + CH_2{=}CHCH{=}CH_2 & \text{(c)}\\ CH_3CH_2\dot{C}HCH_2CH{=}CH_2 \rightarrow CH_3 + CH_2{=}CHCH_2CH{=}CH_2 & \text{(d)}\end{cases}$$

Radicals produced here may abstract hydrogen atoms from cyclohexane, may recombine or disproportionate, or may add to the olefins produced.

Of these four reactions, (b) is presumed to be the most important and explains the large formation of propylene. The initial increase of the rates of formation

Table I. Pressure dependence of the amounts of products formed in the mercury photosensitized decomposition of cyclohexane. Reaction temperature, 400°C. Irradiation time, 1 min.

Initial pressure mm Hg	Products (μ mole)									
	H_2	CH_4	C_2H_6	C_2H_4	C_2H_2	C_3H_8	C_3H_6	C_4H_8[b]	C_4H_6	c—C_6H_{10}
15	7.9	1.9	0.9	2.2	nd[a]	nd	nd	0.6	0.6	1.4
25	10	2.6	0.9	2.6	nd	0.5	5.7	nd	nd	nd
35	12	2.1	1.5	2.5	nd	nd	nd	0.5	0.8	nd
48	14	2.3	2.0	2.7	0.2	0.5	8.0	0.5	1.0	1.8
63	15	2.6	2.5	2.9	nd	nd	nd	0.6	1.3	3.3
74	15	2.2	2.7	2.5	trace	0.6	9.4	0.5	1.3	3.2

[a] nd=not determined.
[b] Mainly butene-1.

of methane, ethylene and propane, as shown in Fig. 1, may be explained by the reaction of the hydrogen atoms with the accumulated propylene. The propyl radicals produced in this reaction may either decompose into methyl radicals and ethylene, or form propane by the abstraction of a hydrogen atom.

Gas chromatographic analysis for C_5-C_6 hydrocarbons using a dimethyl sulfolane column and a dioctyl phthalate column[1] showed two big and several small peaks besides the peak of cyclohexane. One of the big peaks is assigned to cyclohexene and the other to methyl cyclopentane, the formation of which may result from the recyclization of the radical, $\dot{C}H_2CH_2CH_2CH_2CH{=}CH_2$, followed by abstraction of a hydrogen atom.

[1] A. B. Callear and R. J. Cvetanović, Can. J. Chem. **33**, 1256 (1955). S. Sato, T. Terao, and S. Shida, J. Chem. Soc. Japan (to be published).

[2] P. W. Bech, D. V. Kniebes, and H. E. Gunning, J. Chem. Phys. **22**, 672 (1954).

[3] E. W. R. Steacie, *Atomic and Free Radical Reactions* (Reinhold Publishing Corporation, New York, 1954).